Divisive Normalization as a Mechanism for Stable and Efficient Recurrent Neural Computation

by

Shivang Rawat

A dissertation submitted in partial fulfillment

of the requirements for the degree of

Doctor of Philosophy

Department of Mathematics

New York University

August, 2025

Dr. Stefano Martiniani

© Shivang Rawat

All rights reserved, 2025

"All stable processes we shall predict. All unstable processes we shall control."

— John von Neumann

Dedication

To my mother, whose countless sacrifices made this journey possible.

Acknowledgements

I would like to express my deepest gratitude to my advisor, Stefano Martiniani, whose constant support and guidance have significantly shaped my growth as a scientist. Stefano provided me with academic freedom to explore diverse scientific interests and has been a wonderful advisor and friend, offering invaluable mentorship throughout my doctoral journey. I am proud to be one of his first PhD students. My sincere thanks also go to David Heeger, my unofficial co-advisor, for introducing me to and guiding me through the field of neuroscience, a domain entirely new to me. His consistent encouragement and support throughout my PhD journey have been immensely helpful.

I extend my appreciation to my thesis committee members, Brent Doiron, Adam Kohn, and Lai-Sang Young, for their constructive critiques and insightful suggestions that greatly enhanced the quality of this work. Special thanks to my friend and office mate, Flaviano Morone, with whom I collaborated on the work presented in Chapter 3. Our discussions, both scientific and otherwise, and collaborative problem-solving sessions have been tremendously enjoyable. Thanks also to Lyndon Duong, Ruben Coen-Cagli, and Jonathan Winawer for their valuable feedback and engaging discussions, which substantially contributed to my research. I am grateful to the National Institute of Mental Health (NIMH) and the National Eye Institute (NEI) for their generous funding. My thanks also extend to NYU IT for providing the essential computational resources required for my research.

A special thank you to Praharsh Suryadevara for being a supportive friend and office mate

through most of my PhD journey. I also thank Satyam Anand, Asit Pal, Gaurav Mitra and Aaron Shih for their friendship and camaraderie, making the PhD experience more enjoyable. To Mathias Casiulis, Guanming Zhang, and the other members of the Martiniani lab, thank you for fostering a collaborative and stimulating environment. Your support and openness to discussions significantly enriched my academic experience. Thank you to my cherished friends from the University of Minnesota: Tushar Rathi, Mayank Tanwar, Anshur Chawla, and Akshit Goyal, for the shared laughter and memorable experiences.

Heartfelt thanks to my family, Manju Lata, Dinesh Rawat, and Aayushi Rawat, for their unwavering love, support, and patience. To my late grandfather, Rajendra Rawat, thank you for your belief in my potential and being a constant source of inspiration. Finally, my deepest gratitude goes to Laure Briol for her enduring love, motivation, and encouragement, all of which have been vital sources of strength throughout my doctoral studies.

Preface

Parts of this thesis are included in work that has either been published or is to be published:

- Shivang Rawat, David Heeger, and Stefano Martiniani. "Unconditional stability of a recurrent neural circuit implementing divisive normalization". In: *Advances in Neural Information Processing Systems* 37 (2024), pp. 14712–14750.
- Flaviano Morone*, Shivang Rawat*, David Heeger, and Stefano Martiniani. "Stabilization of recurrent neural networks through divisive normalization". In: *bioRxiv* (2025), pp. 2025–05.
- Shivang Rawat and Stefano Martiniani. "Element-wise and recursive solutions for the power spectral density of biological stochastic dynamical systems at fixed points". In: *Physical Review Research* 6.4 (2024), p. 043179.
- Shivang Rawat, Flaviano Morone, David Heeger, and Stefano Martiniani. "Exact Variance and Fano Factor for Arbitrary Level Crossings in Stationary Gaussian Processes". (2025).

In particular, results from "Unconditional stability of a recurrent neural circuit implementing divisive normalization" can be found in Chapters 2 and 4; results from "Stabilization of recurrent neural networks through divisive normalization" can be found in Chapter 3; results from "Element-wise and recursive solutions for the power spectral density of biological stochastic dynamical systems at fixed points" can be found in Chapter 5; and results from "Exact Variance and Fano Factor for Arbitrary Level Crossings in Stationary Gaussian Processes" can be found in Chapter 6.

Abstract

This dissertation develops a unified theoretical framework for understanding the dynamics, stability, and variability of recurrent neural circuits in both biological and artificial systems. We focus on a family of analytically tractable models known as ORGaNICs (Oscillatory Recurrent Gated Neural Integrated Circuits), which inherently implement the canonical computation of divisive normalization (DN). We investigate the consequences of embedding DN within recurrent neural circuits, with particular emphasis on its impact on circuit stability. First, we prove that high-dimensional ORGaNICs are unconditionally stable and can be mapped to a system of coupled damped harmonic oscillators under constrained recurrent connections. We then characterize the dynamics of ORGaNICs with arbitrary recurrent connections via perturbation theory. We find that the transition to instability is preceded by critical slowing down in the neural dynamics, the onset of which co-occurs with the breakdown of normalization in the neural responses. This stability property enables us to train ORGaNICs on RNN benchmarks, achieving performance competitive with the state of the art. Finally, we develop a large-scale retinotopic model of the primary visual cortex (V1) based on stochastic ORGaNICs. We also derive closed-form solutions for the power spectral density of stochastic linear time-invariant systems driven by Gaussian white noise. Finally, we extend the theory of level crossings of stationary Gaussian processes by deriving closed-form expressions for the variance and Fano factor of *arbitrary* level *up*-crossings, previously only known for the mean level. Collectively, this thesis offers novel analytical tools and a cohesive perspective for exploring how neural circuits process information reliably.

Contents

Dedication iv

Acknowledgments v

Preface vii

Abstract viii

List of Figures xvi

List of Tables xx

List of Appendices xxi

1 Introduction 1

1.1 Divisive Normalization . . . 3

1.2 Introduction to ORGaNICs . . . 5

1.2.1 Two-neuron ORGaNICs: Modeling Response Saturation . . . 5

1.2.2 Three-neuron ORGaNICs: Modeling Response Suppression . . . 6

1.2.3 Arbitrary Dimensional ORGaNICs . . . 8

1.3 Thesis Organization . . . 12

2 Unconditional Stability of ORGaNICs with Identity Recurrence 14

2.1 Overview . . . 14

2.2 Main Result . . . 15
2.3 Discussion . . . 19

3 Critical Slowing down in ORGaNICs with Arbitrary Recurrence 21
3.1 Overview . . . 21
3.2 Definition of the model . . . 22
3.3 Numerical Solution of the Fixed Point . . . 25
3.4 Loss of Normalization Predicts Critical Slowing Down . . . 29
3.5 Oscillatory Activity . . . 34
3.6 E-I Imbalanced Recurrent Networks . . . 36
3.7 Discussion . . . 39

4 ORGaNICs as a Machine Learning Architecture 41
4.1 Overview . . . 41
4.2 Introduction . . . 42
4.3 ORGaNICs with Rectification in the Recurrence Term . . . 43
4.4 Related Work . . . 46
4.5 Experiments . . . 48
4.5.1 Static Input Classification Task . . . 48
4.5.2 Time Varying Input . . . 51
4.6 Discussion . . . 55

5 Element-wise and Recursive Solutions for the Power Spectral Density of Biological Stochastic Dynamical Systems at Fixed Points 57
5.1 Overview . . . 57
5.2 Introduction . . . 58
5.3 Preliminary Examples . . . 61

5.4 Element-wise Solution . . . 65
5.4.1 2-D Solution . . . 67
5.4.2 3-D Solution . . . 68
5.4.3 4-D Solution . . . 69
5.5 Recursive Solutions . . . 70
5.6 Applications . . . 72
5.6.1 Hindmarsh-Rose . . . 73
5.6.2 Wilson-Cowan Model . . . 76
5.6.3 Stabilized Supralinear Network (SSN) . . . 78
5.6.4 Rock-Paper-Scissors . . . 81
5.6.5 Hawkes Model . . . 88
5.7 Discussion . . . 91

6 Exact Variance and Fano Factor for Arbitrary Level Crossings in Stationary Gaussian Processes 93

6.1 Overview . . . 93
6.2 Introduction . . . 94
6.3 Description of the Problem . . . 96
6.3.1 Mean of the Counting Processes . . . 97
6.3.2 Variance of the Counting Processes . . . 99
6.4 Main Result . . . 102
6.5 Applications . . . 112
6.5.1 Stochastic Damped Harmonic Oscillator . . . 112
6.5.2 Mean Reverting Process with Ornstein-Uhlenbeck Noise . . . 117
6.5.3 Process with Rational Quadratic Correlation Function . . . 119
6.6 Discussion . . . 121

7 A Large-scale Model of the Primary Visual Cortex (V1) 123

7.1 Overview . . . 123

7.2 A Three-Neuron ORGaNICs Model of V1 . . . 124

7.3 LFP Power Spectra and Coherence . . . 127

7.4 A Gaussian-Rectification Model for Spiking Statistics . . . 129

7.4.1 Derivation of the Analytical Fano Factor . . . 129

7.4.2 Effective Time Constant . . . 131

7.4.3 Results . . . 132

7.5 Discussion . . . 134

8 Discussion 135

8.1 Key Contributions and Implications . . . 135

8.1.1 Normalization Stabilizing Recurrent Neural Networks . . . 135

8.1.2 ORGaNICs as a Machine Learning Architecture . . . 136

8.1.3 Analytical Tools for Stochastic Processes . . . 138

8.1.4 Broader Implications for Neuroscience . . . 138

8.1.5 Methodological Advances . . . 139

8.2 Future Work . . . 140

8.2.1 Experimental Validation . . . 140

8.2.2 Expanding Machine Learning Applications . . . 140

8.2.3 From Phenomenological to Mechanistic Models of Neural Activity . . . 141

8.3 Concluding Remarks . . . 142

A ORGaNICs with Identity Recurrence 144

A.1 Derivation of ORGaNICs . . . 144

A.2 Proof of the Stability Theorem . . . 149

A.2.1 Positive Definite Block Matrices (Schur Complement) . . . 153

A.2.2 Lyapunov Stability Criteria . . . 154
A.3 Convergent Theorem . . . 155
A.4 Analytical Eigenvalue for the Fully Normalized Circuit . . . 157
A.5 Energy of ORGaNICs . . . 159

B ORGaNICs with Arbitrary Recurrence 164
B.1 Linear Stability Analysis of the Two-dimensional Model . . . 164
B.1.1 Contractive Constraint on Recurrence ($0 < w_r \leq 1$) . . . 167
B.1.2 Expansive Constraint on Recurrence ($w_r > 1$) . . . 168
B.2 Numerical Study of ORGaNICs' Fixed-point . . . 170
B.3 Analytical Calculation of the Threshold for Loss of Normalization . . . 172
B.3.1 Delocalized Input Drive . . . 176
B.3.2 Localized Input Drive . . . 177
B.4 Effect of Critical Slowing Down on Neural Variability . . . 181

C ORGaNICs as an ML Architecture 184
C.1 Analysis of the Rectified Model . . . 184
C.1.1 Stability of the High-dimensional System . . . 184
C.1.2 Analytical Eigenvalue for Fully Normalized Circuit . . . 187
C.1.3 Linear Stability Analysis of the Two-dimensional Model . . . 188
C.1.3.1 Contractive Constraint on Recurrence ($0 < w_r \leq 1$) . . . 189
C.1.3.2 Expansive Constraint on Recurrence ($w_r > 1$) . . . 189
C.2 Iterative Algorithm for Fixed-point of ORGaNICs . . . 190

D Power Spectral Density 193
D.1 Spectral Density Matrix for a Linear SDE / Non-linear SDE Near Stable Fixed Points 193
D.2 Recursive Algorithm Solutions . . . 202

D.2.1 Spectral Density Solution . . . 202
D.2.1.1 Coefficient Matrices of the Numerator . . . 204
D.2.1.2 Coefficients of the Denominator . . . 207
D.2.2 Auxiliary Spectral Matrix . . . 215
D.2.3 Integrated Covariance Matrix . . . 220
D.3 Element-wise Solution . . . 223
D.3.1 Denominator and Newton's Identities . . . 224
D.3.2 Numerator . . . 230
D.3.2.1 Auto-spectrum . . . 232
D.3.2.2 Cross-spectrum . . . 236
D.3.2.3 Coherence as a Rational Function . . . 240
D.4 Detailed Function Definitions . . . 241
D.4.1 $d(\omega; \mathbf{A})$ . . . 241
D.4.2 $g(\omega; \mathbf{A}, \mathbf{B})$ . . . 242
D.4.3 $h(\omega; \mathbf{A}, \mathbf{B})$ . . . 244
D.4.4 $f(\omega; \mathbf{A}, \mathbf{e}_\beta)$ . . . 246
D.4.5 $s(\omega; \mathbf{A}, \mathbf{B}, \mathbf{e}_\beta)$ . . . 248
D.4.6 $t(\omega; \mathbf{A}, \mathbf{B}, \mathbf{e}_{\beta_1}, \mathbf{e}_{\beta_2})$ . . . 250
D.5 Basic Identities . . . 252

E Upcrossings **255**

E.1 Theory for the Upcrossing Process . . . 255
E.1.1 Mean Number of Upcrossings . . . 256
E.1.2 Variance of Upcrossings . . . 257
E.1.2.1 Central Limit Theorem for Variance . . . 263
E.1.3 Fano Factor . . . 263

E.2 Theory for the Crossing Process . . . 264
E.2.1 Mean Number of Crossings . . . 264
E.2.2 Variance and Fano Factor of Crossings . . . 265
E.3 Explicit Formulae for Level Crossings . . . 267
E.4 Special Formulae for Zero Level Upcrossings and Crossings . . . 269
E.4.1 Upcrossings . . . 269
E.4.2 Crossings . . . 270
E.5 Note About the Dimensionality . . . 271
E.6 Additional Theorems . . . 273

Bibliography **295**

List of Figures

1.1 The divisive normalization model. . . . 4
1.2 Normalization via ORGaNICs. . . . 6
1.3 Response suppression via ORGaNICs. . . . 7
1.4 Schematic of the general ORGaNICs circuit. . . . 10

2.1 Phase portraits for 2D ORGaNICs for different time constants. . . . 19

3.1 Phase portraits for 2D ORGaNICs with a positive input drive z. . . . 23
3.2 Illustration of the model. . . . 24
3.3 Numerical solution to the ORGaNICs' fixed point equations. . . . 25
3.4 Definition of critical slowing down. . . . 27
3.5 Distribution of the Jacobian's largest eigenvalue (λ) for different system sizes (n). . . . 28
3.6 Finite size scaling analysis. . . . 30
3.7 Neuronal trajectories for different recurrent synaptic strength Δ. . . . 31
3.8 Definition of loss of normalization. . . . 32
3.9 Loss of normalization predicts the onset of critical slowing down. . . . 33
3.10 Phase diagram and oscillation frequencies in ORGaNICs. . . . 35
3.11 Effect of E-I imbalanced recurrence on stability. . . . 37
3.12 Effect of E-I imbalanced recurrence on oscillation frequency. . . . 38

4.1 Phase portraits for 2D rectified ORGaNICs with a positive input drive z. . . . 44
4.2 Effect of rectification on network stability. . . . 45

4.3 Fast convergence of the iterative algorithm. 49
4.4 Histogram for the eigenvalue with the largest real part. 52
4.5 Eigenvalue with the largest real part while training on static input (MNIST) classification task. 53
4.6 Trajectories of the hidden states ($\mathbf{y}$). 54

5.1 Power spectral density of the membrane potential for the Fitzhugh-Nagumo model. 63
5.2 Power spectral density of the membrane potential for the Fitzhugh-Nagumo model with large noise. 64
5.3 Definitions of $\mathbf{O}_{ij}$ matrices. 66
5.4 Power spectrum of the Hindmarsh-Rose model. 74
5.5 Wilson-Cowan 4D model. 77
5.6 Spectral density (auto and cross) and coherence for the Wilson-Cowan model. . . 77
5.7 SSN circuit. 78
5.8 Spectral density (auto and cross) and coherence for the SSN circuit. 79
5.9 31-D Rock-Paper-Scissors model. 82
5.10 Spectral density (auto and cross) and coherence for the Rock-Paper-Scissors-Lizard-Spock model. 83
5.11 Coefficients of the rational function for the auto-spectrum of Paper population in the Rock-Paper-Scissors-Lizard-Spock model. 84
5.12 Rational function solution for the spectral density in the Rock-Paper-Scissors-Lizard-Spock ($n = 5$) model. 86
5.13 Spectral density (auto and cross) and coherence using different methods for a 31-dimensional Rock-Paper-Scissors type model. 87
5.14 Population covariance of spiking neural networks. 89

6.1 Illustration of level crossing events for a stationary Gaussian process. 95

6.2 Variable transform visualized. . . . 101
6.3 Mean rate, variance rate, and Fano factor of upcrossings for the stochastic damped harmonic oscillator as functions of level u and damping ratio ζ. . . . 115
6.4 Comparison of analytical formulae with numerical simulations for the stochastic damped harmonic oscillator. . . . 116
6.5 Fano factor landscapes for the stochastic damped harmonic oscillator across different parameter regimes. . . . 117
6.6 Mean rate, variance rate, and Fano factor of upcrossings for a mean-reverting process driven by Ornstein-Uhlenbeck noise. . . . 118
6.7 Fano factor for a stationary Gaussian process with a rational quadratic correlation function. . . . 120

7.1 Schematic of the large-scale V1 model. . . . 124
7.2 Power spectral density of LFP in the V1 model for a grating stimulus of varying contrast. . . . 127
7.3 Power spectral of LFP in the V1 model for different stimuli. . . . 128
7.4 The Gaussian-Rectification (GR) model for spike generation. . . . 130
7.5 Quenching of the Fano factor upon stimulus presentation. . . . 132
7.6 Fano factor as a function of stimulus contrast and attention. . . . 133

B.1 Numerical exploration of ORGaNICs' fixed-point statistics. . . . 172
B.2 Loss of normalization. . . . 177
B.3 Numerical solution of the ORGaNICs' fixed point equations for localized input drive. 178
B.4 Loss of normalization for localized input drive. . . . 179
B.5 Loss of normalization predicts the onset of critical slowing down for localized input drive. . . . 180

D.1 Time complexity of the recursive algorithm. . . . 214

D.2 Time complexity of the element-wise algorithm. 240

E.1 Variable transform visualized. 261

E.2 Splitting of $\mathbb{R}^2$ into two disjoint regions. 283

E.3 Splitting of $\mathcal{R}_+$ into two disjoint regions. 284

List of Tables

4.1 Test accuracy on MNIST dataset 50

4.2 Autoencoder architecture 50

4.3 ORGaNICs parametrization for static MNIST classification 51

4.4 ORGaNICs architecture for static MNIST classification 51

4.5 Hyperparameters 52

4.6 ORGaNICs parametrization for sequential MNIST classification 54

4.7 Test accuracy on sequential pixel-by-pixel MNIST and permuted MNIST 55

List of Appendices

A ORGaNICs with Identity Recurrence 144
B ORGaNICs with Arbitrary Recurrence 164
C ORGaNICs as an ML Architecture 184
D Power Spectral Density 193
E Upcrossings 255

1 Introduction

The human brain, a vast network of interconnected neurons, performs complex computations with remarkable efficiency and robustness. A central challenge in neuroscience remains the elucidation of the principles that govern these neural computations. Individual neurons, the brain's fundamental computational units, continuously process signals through an intricate web of synaptic interactions [1]. From a systems perspective, the brain functions as a high-dimensional dynamical system, where collective neuronal activity gives rise to sophisticated cognitive and behavioral functions. Despite microscopic variability, the brain's structural and functional architectures exhibit significant consistency across individuals of a species, suggesting shared underlying blueprints.

To navigate this complexity, the theory of canonical microcircuits offers a valuable conceptual framework. This theory posits that modular computational motifs are replicated across diverse neural systems, executing operations that support a wide range of cognitive functions [2–5]. Substantial evolutionary and anatomical evidence supports this modular view, suggesting that complex brain functions arise from the systematic deployment of a limited set of fundamental computational principles [6, 7]. Prominent examples include: linear filtering, that is, the weighted summation of inputs, crucial for sensory processing [8]; thresholding mechanisms that govern neuronal firing [1]; and divisive normalization [5]. However, integrating these canonical computations into a single unified theoretical model that can comprehensively explain neural activity across multiple systems, while maintaining biological plausibility, analytical tractability, and

stability, presents an ongoing and significant challenge.

Among these fundamental operations, divisive normalization stands out for its pervasiveness and functional importance. Initially proposed to explain nonlinear neuronal response properties in the primary visual cortex [9], divisive normalization describes how a neuron's response is modulated by the integrated activity of a surrounding population. This principle has since been identified in numerous sensory modalities, cortical regions, and species, and has been implicated in a wide array of cognitive processes, including attention, decision-making, sensory adaptation, and efficient coding [5]. By modulating neuronal responses relative to ensemble activity, divisive normalization is pivotal for functions like gain control [10] and redundancy reduction [11].

Despite its widespread relevance, effectively incorporating divisive normalization into analytically tractable and dynamically stable models of recurrent neural circuits has proven difficult. Conventional excitatory-inhibitory (E-I) models, such as the Wilson-Cowan model [12] (see Section 5.6.2) or Stabilized Supralinear Networks (SSNs) [13] (see Section 5.6.3), only approximate divisive normalization-like behavior under specific parameter constraints [14]. Furthermore, rigorous mathematical analysis of these models, especially regarding stability in high-dimensional settings or when trained for complex tasks, often encounters substantial hurdles. Given the ubiquity and functional significance of divisive normalization, its explicit integration into neurodynamical circuit models is essential for advancing our theoretical grasp of neural processing.

This thesis focuses on a recently introduced class of recurrent neural circuits known as ORGaNICs (Oscillatory Recurrent Gated Neural Integrator Circuits) [15, 16]. A core characteristic of ORGaNICs is that they inherently implement divisive normalization as an integral component of their dynamics. A key advantage of the ORGaNICs framework, and a recurring theme in this research, is its analytical tractability and robust dynamical stability. These properties hold even when the circuits are scaled to high dimensions and subjected to strong recurrent interactions, differentiating them from previous models of neural dynamics.

1.1 Divisive Normalization

Divisive normalization is a form of multiplicative neuronal modulation occurring in the brain whereby the response of an individual neuron is divided by the summed activity of other similarly tuned neurons [9]. Simply put, normalization explains how the response of a given neuron, which is selective for a specific stimulus, is suppressed by different stimuli that would elicit a weaker or no response if they were presented alone, as illustrated in Fig. 1.1. In its simplest form, normalization works by dividing a neuron's total input by the sum of all inputs to n neurons in the normalization pool [9], akin to normalizing the length of a vector, expressed mathematically by the formula:

$$y_i^+ = \frac{z_i^2}{\sigma^2 + \sum_{j=1}^{n} z_j^2}, \tag{1.1}$$

where y_i^+ is the firing rate of neuron i; z_i is its input drive, defined as a weighted sum of the responses of a population of presynaptic neurons; and σ is the semisaturation constant, whose experimental value in primary visual cortex (V1) is $\sigma \sim 0.1$ [17]. For simplicity, we assume that the input drive $z_i \geq 0$. We will consider the case where $z_i \in \mathbb{R}$ in Section 1.2.3. Two important implications of the normalization equation (1.1) as applied to the primary visual cortex are response saturation and cross-orientation suppression, illustrated in Fig. 1.1.

Divisive normalization was introduced in the 1990s to explain nonlinearities in the responses of neurons in the primary visual cortex (V1) [9, 18–20]. It was later invoked to interpret a larger body of physiological data in the olfactory [21] and auditory [11] cortical areas. Subsequently, its application has been extended to diverse cognitive processes such as attention, working memory, and value-based decision making [5, 22–32]. Divisive normalization models various neural processes, including adaptation [33, 34], attention [22], automatic gain control [35], decorrelation, and statistical whitening [36]. Therefore, it has been proposed as a canonical neural computation [5] that is linked to many well-documented physiological [37, 38] and psychophysical [39, 40]

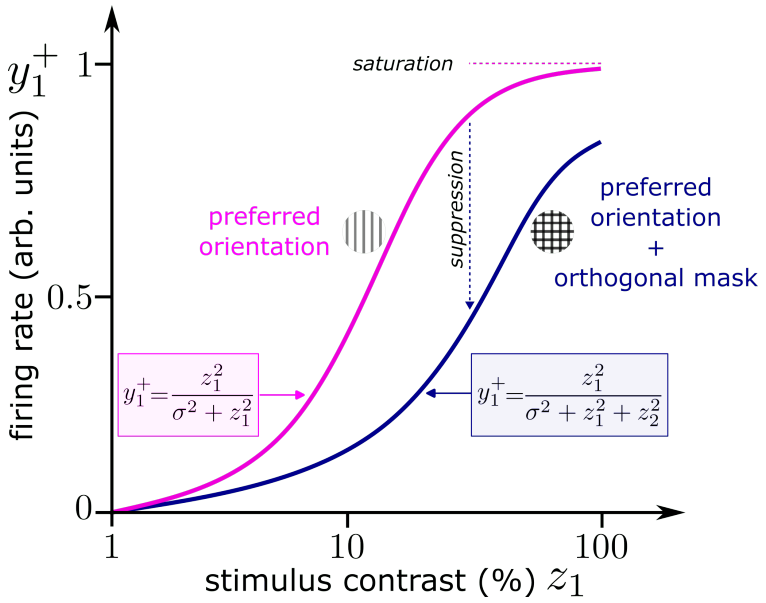


Figure 1.1: The divisive normalization model. An orientation selective principal neuron y_1 in primary visual cortex (V1) fires only when the stimulus orientation matches its preferred orientation (pink curve). The larger the stimulus contrast z_1, the greater the strength of the response. The firing rate of this neuron y_1^+ can be modeled by a nonlinear response function that saturates at high contrast. When a second grating stimulus z_2 with orientation perpendicular to the preferred one (*viz.* an orthogonal mask) is presented simultaneously with stimulus z_1, there is a rightward shift of the response function y_1^+ (blue curve). The suppressive effect of the orthogonal mask can be modeled by an extra term z_2^2 in the denominator of the response function. This phenomena is known as cross-orientation suppression.

phenomena. Due to its wide applicability, we argue that divisive normalization should be central to any neurodynamical model.

Notwithstanding the general character of this neural computation, different biophysical mechanisms may perform normalization in different neural systems. These include intracortical shunting inhibition [18, 41], thalamocortical synaptic depression [42], pre-synaptic inhibition [21], and recurrent amplification (i.e., amplifying weak inputs more than strong inputs) [43–47], to name the most prominent ones.

Since Eq. (1.1) describes a neural process that is static, it is natural to ask how the output responses $y_i^+(t)$ evolve in time towards the normalized state. That is: how does a neural circuit accomplish normalization? It has been proposed that divisive normalization is achieved via a recurrent circuit [9, 15, 18, 42, 48–50]. Therefore, we consider a recurrent neural circuit that is

designed to implement divisive normalization dynamically.

1.2 Introduction to ORGaNICs

A way to achieve normalization dynamically is to couple the output responses of the principal neurons, $y_i^+(t)$, to a secondary neuronal population represented by a single variable $a(t)$, which acts as a multiplicative inhibitory modulator, as illustrated in Fig. 1.2 & 1.3. This circuit achieves normalization via amplification of the recurrent input; the gain of this amplification is controlled by the modulator $a(t)$, whose activity increases with the strength of normalization. The class of dynamical systems implementing divisive normalization in this way is known as ORGaNICs (Oscillatory Recurrent Gated Neural Integrator Circuits) [15, 51].

ORGaNICs are much like the linear recurrent circuits introduced in the 1980s [52], but with a multiplicative gain on the recurrent term that implements normalization. While other neurodynamical models like the Wilson-Cowan and Stabilized Supralinear Network (SSN) models have been shown to approximate divisive normalization responses [13, 14], they do so only approximately in certain parameter regimes. This makes ORGaNICs unique as they are designed to achieve normalization by imposing Eq. (1.1) as the fixed-point (see Appendix A.1 for the derivation).

1.2.1 Two-neuron ORGaNICs: Modeling Response Saturation

The simplest ORGaNICs involves only two neurons and is described by the following dynamical equations:

$$\begin{cases} \tau_y \dot{y} = -y + z + (1 - a^+)y \\ \tau_a \dot{a} = -a + \sigma^2 + y^+ a \,, \end{cases} \tag{1.2}$$

where $y(t)$ and $a(t)$ represent the membrane potentials (relative to an arbitrary threshold potential that we take to be 0) of the excitatory (E) and inhibitory (I) neurons, respectively, and y^+ and a^+ are the corresponding firing rates. The firing rate of the E neuron y^+ is related to the membrane

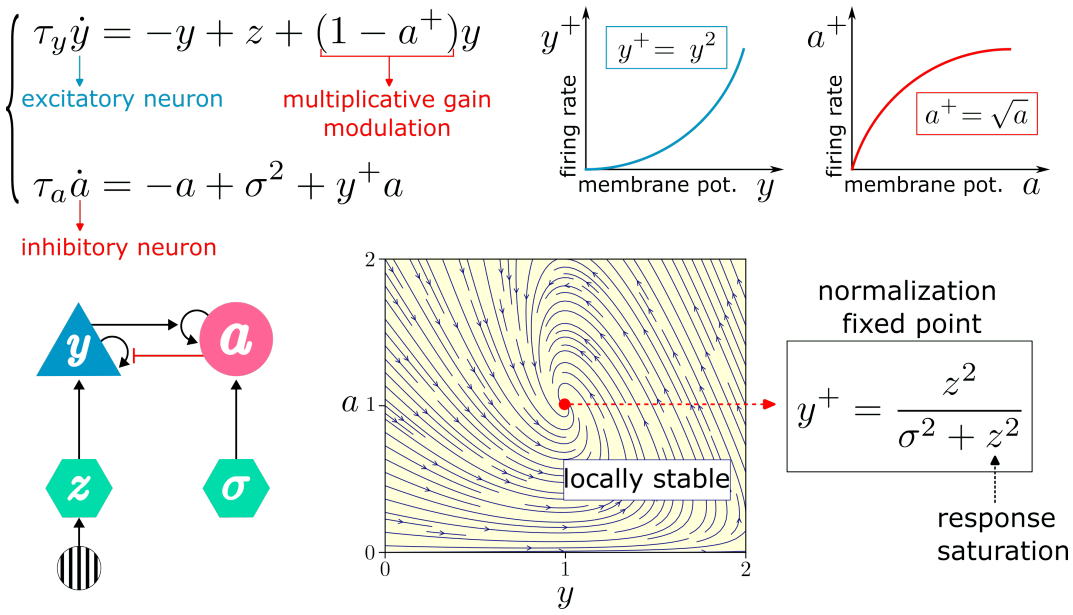


Figure 1.2: Normalization via Oscillatory Recurrent Gated Neural Integrator Circuits (ORGaNICs). The saturation of the firing rate y^+ at high contrast z (Fig. 1.1 pink curve) can be obtained as the fixed point of the 2-neuron circuit in Eq. (1.2) involving the principal neuron y and a secondary inhibitory neuron a that acts on y as a multiplicative gain modulator. This fixed point is locally stable for any value of input drive z, the time constants τ_y, τ_a, and the semisaturation constant σ.

potential by rectification and squaring [53–55], $y^+ = k\lfloor y \rfloor^2$ (henceforth we set the dimensional proportionality factor $k = 1$), while the firing rate of the I neuron is given by $a^+ = \sqrt{\lfloor a \rfloor}$; and $\tau_y > 0$, $\tau_a > 0$ are the neurons' time constants. The 2-neuron circuit described by Eq. (1.2) is depicted in Fig. 1.2 and models, for example, the response of a neuron in the primary visual cortex with z proportional to stimulus contrast.

At the fixed point, the principal neuron y follows the normalization equation (1.1) for $n = 1$, i.e., $y^+ = \frac{z^2}{\sigma^2 + z^2}$, which explains the *saturation* of the firing rate at large contrast z. As we will show in Chapter 2, this normalization fixed point is always locally stable.

1.2.2 Three-neuron ORGaNICs: Modeling Response Suppression

To account for the *suppression* of the firing rate when a second stimulus is presented concomitantly with the preferred one (as shown by the blue curve in Fig. 1.1), it suffices to consider an

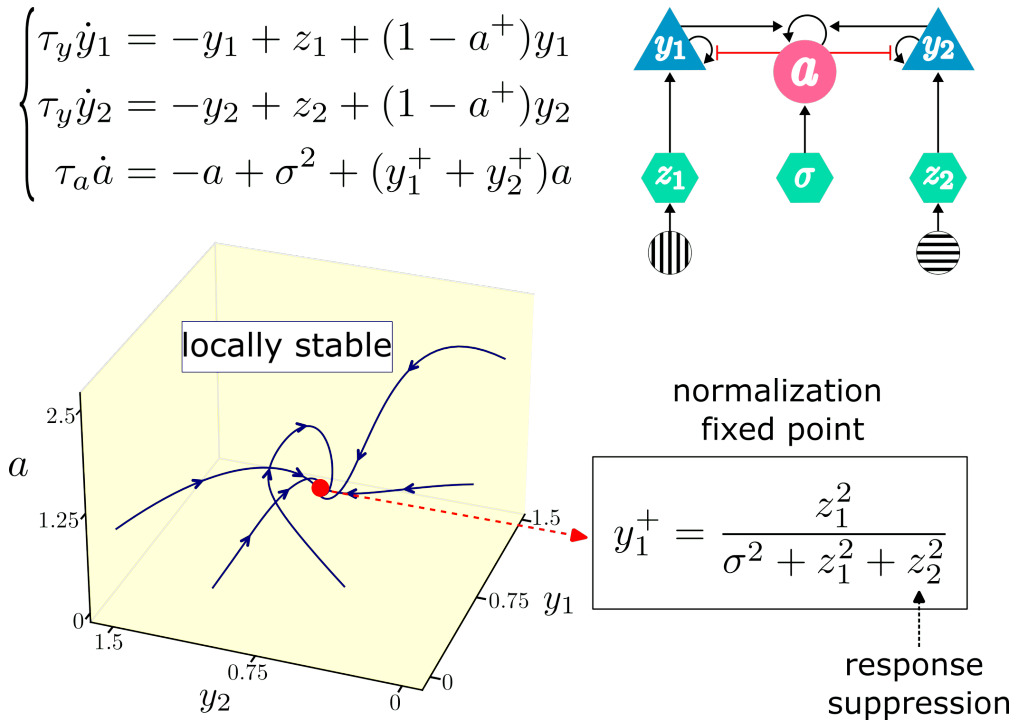


Figure 1.3: Response suppression via ORGaNICs. The suppressive effect of the orthogonal mask (Fig. 1.1 blue curve) can be modeled by the fixed point of the 3-neuron circuit, where y_1 and y_2 respond selectively to the vertical and horizontal orientations, respectively, and a performs the multiplicative gain modulation on both y_1 and y_2. This fixed point is locally stable for any value of the parameters. Notice that neurons y_1 and y_2 do not interact directly, but only through neuron a, i.e., there are no recurrent connections between the principal neurons in this simplistic model.

ORGaNICs with 3 neurons (two E neurons y_1, y_2 and one I neuron a) given by:

$$\begin{cases} \tau_y \dot{y}_1 = -y_1 + z_1 + (1 - a^+) y_1 \\ \tau_y \dot{y}_2 = -y_2 + z_2 + (1 - a^+) y_2 \\ \tau_a \dot{a} = -a + \sigma^2 + (y_1^+ + y_2^+) a \,, \end{cases} \tag{1.3}$$

and shown in Fig. 1.3. Again, the fixed point of this 3-neuron circuit is given by the normalization equation (1.1) (with $n = 2$) and is locally unconditionally stable.

1.2.3 Arbitrary Dimensional ORGaNICs

To generalize ORGaNICs beyond circuits with only a few neurons, we first extend the model to an arbitrary number, n, of principal neurons y_i whose activity is modulated by a single, shared inhibitory neuron a. The dynamics of such a system are described by:

$$\begin{cases} \tau_y \dot{y}_i = -y_i + z_i + (1 - a^+)\, y_i \\ \tau_a \dot{a} = -a + \sigma^2 + \left(\sum_{i=1}^{n} y_i^+ \right) a \,. \end{cases} \tag{1.4}$$

At its fixed point, this circuit precisely implements divisive normalization for each principal neuron, such that $y_i^+ = \frac{z_i^2}{\sigma^2 + \sum_{j=1}^{n} z_j^2}$. As will be demonstrated in Chapter 2, ORGaNICs of this form are locally unconditionally stable.

The model's capacity to represent complex neural computations is significantly enhanced by introducing lateral (recurrent) connections among the principal neurons. These connections are characterized by the weight matrix W_{rij}, which describes the influence of neuron y_j on neuron y_i. With these recurrent connections, the dynamics of the n principal neurons and the single inhibitory neuron are given by:

$$\begin{cases} \tau_y \dot{y}_i = -y_i + z_i + (1 - a^+) \sum_{j=1}^{n} W_{rij} y_j \\ \tau_a \dot{a} = -a + \sigma^2 + \left(\sum_{i=1}^{n} y_i^+ \right) a \,. \end{cases} \tag{1.5}$$

The inclusion of these arbitrary recurrent connections brings forth several critical questions that this thesis explores: Does the ORGaNICs framework still achieve divisive normalization under these conditions? What are the constraints on the recurrent weights and input stimuli for maintaining stability, particularly when recurrent amplification is substantial? We will discuss and answer these questions in Chapter 3.

Furthermore, the canonical form of the divisive normalization equation, Eq. (1.1), can be generalized. The term in the denominator representing the normalization pool, $\sum_{j=1}^{n} z_j^2$, can be formulated as a weighted sum, $\sum_{j=1}^{n} W_{ij} z_j^2$ [5, 38, 56–61]. This leads to the following normalization equation:

$$y_i^+ = \frac{z_i^2}{\sigma^2 + \sum_{j=1}^{n} W_{ij} z_j^2}, \tag{1.6}$$

Moreover, so far, we have assumed that the input drive $z_i \geq 0$. To handle negative inputs, we define y_i^+ and y_i^- as the firing rates of neurons with complementary receptive fields, encoding positive and negative components of the input drive, respectively. Such complementary (ON/OFF or anti-phase) receptive fields are observed, for instance, in the visual cortex [62], where they contribute to each other's normalization pool. We hypothesize that complementary neuron pairs are a common motif throughout the neocortex. Further, allowing for neuron-specific semisaturation constants σ, we get the general normalization equation:

$$y_i^{\pm} \equiv \lfloor \pm y_i \rfloor^2 = \frac{\lfloor \pm z_i \rfloor^2}{\sigma_i^2 + \sum_{j=1}^{n} W_{ij} \left(\lfloor z_j \rfloor^2 + \lfloor -z_j \rfloor^2 \right)}. \tag{1.7}$$

Note that only one of the complementary neurons fires at a given time. Therefore, in ORGaNICs, these neurons have a single dynamical equation for their membrane potentials, where the sign of y_i dictates which neuron is active. The term $\lfloor z_j \rfloor^2 + \lfloor -z_j \rfloor^2$ in the denominator is equal to z_j^2, representing the contrast energy of the input stimulus.

Taken together, to dynamically achieve the normalization specified in Eq. (1.7), we now consider a system with n inhibitory neurons a_i, each associated with a principal neuron y_i. The dynamical

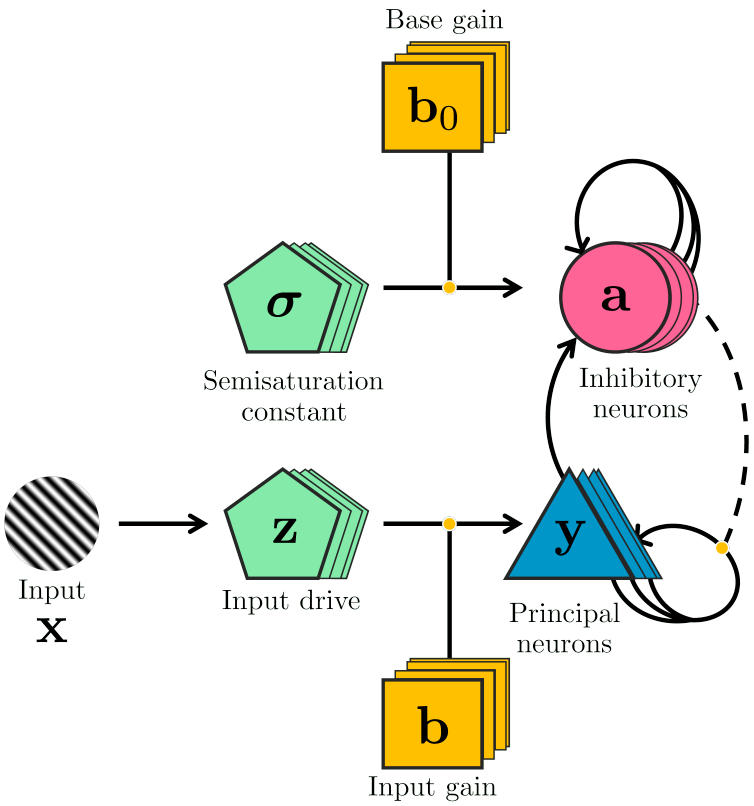


Figure 1.4: Schematic of the general ORGaNICs circuit. The input drive $\mathbf{z}$ is a weighted sum of the input $\mathbf{x}$. The input drive is modulated by the input gain $\mathbf{b}$. $\mathbf{b} \odot \mathbf{z}$ forms the external input to the principal neurons $\mathbf{y}$. The principal neurons also receive recurrent inputs from other principal neurons. This recurrent input is modulated by the inhibitory neurons $\mathbf{a}$. The activity of inhibitory neurons $\mathbf{a}$ is driven by the principal neurons and the semisaturation constant $\boldsymbol{\sigma}$ multiplied by the base input gain $\mathbf{b}_0$. Solid lines with arrows indicate excitatory influence, while the dashed line from inhibitory neurons to principal neurons indicates inhibitory influence. The stacked shapes represent populations of neurons or different constants.

equations are given by:

$$\begin{cases} \tau_{y_i} \dot{y}_i = -y_i + z_i + (1 - a_i^+)\, y_i \\ \tau_{a_i} \dot{a}_i = -a_i + \sigma_i^2 + \sum_{j=1}^{n} W_{ij} (y_j^+ + y_j^-)\, \lfloor a_j \rfloor \,. \end{cases} \tag{1.8}$$

We have allowed the time constants to be different for different neurons. As shown in Appendix A.1, the fixed-point solution of this dynamical system (Eq. (1.8)) is indeed given by Eq. (1.7).

Finally, we incorporate recurrent connections between the y-neurons, via the matrix $\mathbf{W}_r$ and

input gain parameters, $\mathbf{b}$ and $\mathbf{b}_0$ to present the most general form of ORGaNICs considered in this thesis. A schematic of this general circuit is shown in Fig. 1.4. The dynamical system, expressed in vector notation, is:

$$\begin{aligned} \boldsymbol{\tau}_y \odot \dot{\mathbf{y}} &= -\mathbf{y} + \mathbf{b} \odot \mathbf{z} + \left(\mathbf{1} - \mathbf{a}^{+}\right) \odot \left(\mathbf{W}_r \left(\sqrt{\mathbf{y}^{+}} - \sqrt{\mathbf{y}^{-}}\right)\right) \\ \boldsymbol{\tau}_a \odot \dot{\mathbf{a}} &= -\mathbf{a} + \mathbf{b}_0^2 \odot \boldsymbol{\sigma}^2 + \mathbf{W} \left(\left(\mathbf{y}^{+} + \mathbf{y}^{-}\right) \odot \mathbf{a}^{+2}\right) . \end{aligned} \tag{1.9}$$

In these equations:

- $\mathbf{y}, \mathbf{a} \in \mathbb{R}^n$ are vectors representing the membrane potentials of the excitatory ($\mathbf{y}$) and inhibitory ($\mathbf{a}$) neuron populations, respectively.
- The symbol $\odot$ denotes element-wise (Hadamard) multiplication. Division, squaring, and square-root operations are also performed element-wise.
- $\mathbf{z} \in \mathbb{R}^n$ is the input drive to the circuit, which is a weighted sum of external sensory inputs $\mathbf{x} \in \mathbb{R}^m$, i.e., $\mathbf{z} = \mathbf{W}_{zx}\mathbf{x}$.
- The firing rates are rectified power functions of the membrane potentials: $\mathbf{y}^{\pm} = \lfloor \pm \mathbf{y} \rfloor^2$ for the principal neurons and $\mathbf{a}^{+} = \sqrt{\lfloor \mathbf{a} \rfloor}$ for the inhibitory neurons. The term $\sqrt{\mathbf{y}^{+}} - \sqrt{\mathbf{y}^{-}}$ serves to reconstruct the signed membrane potential signal from these non-negative firing rates.
- $\boldsymbol{\tau}_y$, $\boldsymbol{\tau}_a \in \mathbb{R}_*^{+n}$ are vectors of time constants for the respective neuron types. $\mathbb{R}_*^{+}$ is the set of positive real numbers.
- $\mathbf{b}$, $\mathbf{b}_0 \in \mathbb{R}_*^{+n}$ are vectors of input gains, providing a potential mechanism for phenomena such as attentional modulation.
- $\boldsymbol{\sigma} \in \mathbb{R}_*^{+n}$ is a vector of semisaturation constants that contribute to the depolarization of the $\mathbf{a}$ neurons.
- $\mathbf{1}$ represents an n-dimensional vector where all entries are equal to 1.

- Recurrent interactions among the principal $\mathbf{y}$ neurons are captured by the recurrent weight matrix $\mathbf{W}_r \in \mathbb{R}^{n \times n}$. This recurrent input is crucially gated by the activity of the inhibitory $\mathbf{a}$ neurons through the term $(\mathbf{1} - \mathbf{a}^+)$.

- The non-negative matrix $\mathbf{W} \in \mathbb{R}_*^{n \times n}$ is the normalization weight matrix, where $\mathbb{R}_*$ is the set of nonnegative real numbers. It defines how the activity of the principal neurons (both $\mathbf{y}^+$ and $\mathbf{y}^-$) contributes to the activation of their corresponding inhibitory $\mathbf{a}$-neurons, which in turn provide the divisive normalization signal.

1.3 Thesis Organization

This thesis is structured as follows: Chapter 2 investigates the unconditional stability of high-dimensional ORGaNICs when the recurrent weight matrix is the identity matrix. We demonstrate that the system's stability can be analyzed via a quadratic eigenvalue problem; consequently, ORGaNICs act as a system of coupled damped harmonic oscillators in the vicinity of their fixed point. In Chapter 3, we extend the stability analysis of ORGaNICs to scenarios with generic recurrent weight matrices, such as those drawn from the Gaussian Orthogonal Ensemble. We find that ORGaNICs remain stable even when the spectral radius of the recurrent weight matrix is larger than 1. The transition to instability is preceded by critical slowing down of the neural dynamics, which coincides with a loss of normalization. In Chapter 4, we showcase the practical utility of ORGaNICs as a versatile machine learning architecture. The model's inherent stability facilitates straightforward training of ORGaNICs both as multi-layer perceptrons (MLPs) and recurrent neural networks (RNNs), enabling competitive performance.

Chapter 5 presents novel analytical and recursive solutions for computing the power spectral density (PSD) of stochastic dynamical systems operating near stable fixed points. We illustrate these methods with applications to various neurodynamical and biological systems models. Chapter 6 focuses on the statistics of level crossings in stochastic processes. We derive exact analytical

expressions for the variance and Fano factor of arbitrary level crossings in smooth, stationary Gaussian processes, validating these expressions across diverse models. In Chapter 7, we apply the ORGaNICs framework to develop a large-scale model of the primary visual cortex, demonstrating that it can reproduce a wide range of physiological phenomena, including stimulus-dependent gamma oscillations and the statistics of spiking variability. We conclude with Chapter 8, which summarizes the key findings, discusses their implications, and suggests potential avenues for future research.

2 | Unconditional Stability of ORGaNICs with Identity Recurrence

2.1 Overview

In this chapter, we prove the exceptional property of unconditional local stability of ORGaNICs when the recurrent weight matrix $\mathbf{W}_r$ is identity, i.e., the recurrent connections between all the principal neurons $\mathbf{y}$ are only self-excitatory. The core findings discussed herein have been published in [51].

We employ the indirect method of Lyapunov, analyzing the stability of the dynamical system linearized about its unique fixed point. This analysis demonstrates that the system's stability is governed by a quadratic eigenvalue problem, equivalent to assessing the stability of the linear second-order system $\mathbf{I}\ddot{\mathbf{x}} + \mathbf{B}\dot{\mathbf{x}} + \mathbf{K}\mathbf{x} = \mathbf{0}$. This crucial link allows us to interpret ORGaNICs as a system of coupled damped harmonic oscillators and derive the circuit's energy function, offering a normative principle for what the circuit and its neurons aim to accomplish. To do this, we derive novel results on the quadratic eigenvalue problem of gyroscopically stabilized systems with indefinite damping.

2.2 Main Result

Consider the general high-dimensional ORGaNICs (Eq. (1.9)) when the recurrent weight matrix is identity, $\mathbf{W}_r = \mathbf{I}$. We first simplify the dynamical system by noting that $\sqrt{\mathbf{y}^+} - \sqrt{\mathbf{y}^-} = \mathbf{y}$ and $\mathbf{y}^+ + \mathbf{y}^- = \mathbf{y}^2$ yielding the following coupled nonlinear dynamical system,

$$\begin{aligned} \boldsymbol{\tau}_y \odot \dot{\mathbf{y}} &= -\sqrt{\lfloor \mathbf{a} \rfloor} \odot \mathbf{y} + \mathbf{b} \odot \mathbf{z} \\ \boldsymbol{\tau}_a \odot \dot{\mathbf{a}} &= -\mathbf{a} + \mathbf{b}_0^2 \odot \boldsymbol{\sigma}^2 + \mathbf{W} \left(\mathbf{y}^2 \odot \lfloor \mathbf{a} \rfloor\right) \end{aligned} \tag{2.1}$$

For identity recurrent weight matrix, we have a unique fixed point, given by,

$$\mathbf{y}_s = \frac{\mathbf{b} \odot \mathbf{z}}{\sqrt{\mathbf{b}_0^2 \odot \boldsymbol{\sigma}^2 + \mathbf{W}\left(\mathbf{b}^2 \odot \mathbf{z}^2\right)}}; \quad \mathbf{a}_s = \mathbf{b}_0^2 \odot \boldsymbol{\sigma}^2 + \mathbf{W}\left(\mathbf{b}^2 \odot \mathbf{z}^2\right) \tag{2.2}$$

Since the normalization weights in the matrix $\mathbf{W}$ are nonnegative, at steady-state we have $\mathbf{a}_s > \mathbf{0}$, so that $\sqrt{\lfloor \mathbf{a}_s \rfloor} = \sqrt{\mathbf{a}_s}$, and the corresponding firing rates at steady-state are,

$$\mathbf{y}_s^{\pm} = \frac{\lfloor \pm \mathbf{b} \odot \mathbf{z} \rfloor^2}{\mathbf{b}_0^2 \odot \boldsymbol{\sigma}^2 + \mathbf{W}\left(\mathbf{b}^2 \odot \mathbf{z}^2\right)}; \quad \mathbf{a}_s^+ = \sqrt{\mathbf{b}_0^2 \odot \boldsymbol{\sigma}^2 + \mathbf{W}\left(\mathbf{b}^2 \odot \mathbf{z}^2\right)} \tag{2.3}$$

Note that we recover the normalization equation, Eq. (1.7), if $\mathbf{b} = \mathbf{b}_0 = b_0 \mathbf{1}$. Since the fixed points of $\mathbf{y}$ and $\mathbf{a}$ neurons are known analytically, to prove that this fixed point is *locally asymptotically stable* (i.e., the responses converge asymptotically to the fixed point), we apply the *indirect method of Lyapunov* at this fixed point [63]. This method allows us to analyze the stability of the nonlinear system in the vicinity of the fixed point by studying the corresponding linearized system. The Jacobian matrix $\mathbf{J} \in \mathbb{R}^{2n \times 2n}$ about $(\mathbf{y}_s, \mathbf{a}_s)$, defining the linearized system, is given by,

$$\mathbf{J} = \begin{bmatrix} -\mathbf{D}\left(\frac{\sqrt{\mathbf{a}_s}}{\boldsymbol{\tau}_y}\right) & -\mathbf{D}\left(\frac{\mathbf{y}_s}{2 \odot \sqrt{\mathbf{a}_s} \odot \boldsymbol{\tau}_y}\right) \\ \mathbf{D}\left(\frac{2}{\boldsymbol{\tau}_a}\right) \mathbf{W}\, \mathbf{D}\left(\mathbf{a}_s \odot \mathbf{y}_s\right) & \mathbf{D}\left(\frac{1}{\boldsymbol{\tau}_a}\right)\left(-\mathbf{I} + \mathbf{W}\, \mathbf{D}\left(\mathbf{y}_s^2\right)\right) \end{bmatrix} \tag{2.4}$$

where $\mathbf{D}(\mathbf{x})$ is a diagonal matrix of appropriate size with the elements of the vector $\mathbf{x}$ on the diagonal. A necessary and sufficient condition for local stability is that the real parts of all eigenvalues of this matrix are negative. We thus proceed by computing the characteristic polynomial for the Jacobian, $p_{\mathbf{J}}(\lambda) \equiv \det(\mathbf{J} - \lambda\mathbf{I})$. The roots of this polynomial, found by setting $p_{\mathbf{J}}(\lambda) = 0$, are the eigenvalues of the system. Consider the block matrix,

$$\mathbf{J} - \lambda\mathbf{I} = \begin{bmatrix} \mathbf{A}_{11} & \mathbf{A}_{12} \\ \mathbf{A}_{21} & \mathbf{A}_{22} \end{bmatrix} = \begin{bmatrix} -\mathbf{D}\left(\frac{\sqrt{\mathbf{a}_s}}{\boldsymbol{\tau}_y}\right) - \lambda\mathbf{I} & -\mathbf{D}\left(\frac{\mathbf{y}_s}{2\odot\sqrt{\mathbf{a}_s}\odot\boldsymbol{\tau}_y}\right) \\ \mathbf{D}\left(\frac{2}{\boldsymbol{\tau}_a}\right)\mathbf{W}\,\mathbf{D}\left(\mathbf{a}_s \odot \mathbf{y}_s\right) & \mathbf{D}\left(\frac{1}{\boldsymbol{\tau}_a}\right)\left(-\mathbf{I} + \mathbf{W}\,\mathbf{D}\left(\mathbf{y}_s^2\right)\right) - \lambda\mathbf{I} \end{bmatrix} \tag{2.5}$$

Notice that $\mathbf{A}_{11}$ and $\mathbf{A}_{12}$ are diagonal and therefore they commute, i.e., $\mathbf{A}_{11}\mathbf{A}_{12} = \mathbf{A}_{12}\mathbf{A}_{11}$, so we have that $\det(\mathbf{J} - \lambda\mathbf{I}) = \det(\mathbf{A}_{22}\mathbf{A}_{11} - \mathbf{A}_{21}\mathbf{A}_{12})$ which is a property of the determinant of block matrices with commuting blocks [64]. Therefore, the characteristic polynomial of the linearized system after expansion of the terms and simplification is given by,

$$\det(\mathbf{J} - \lambda\mathbf{I}) = \det\left(\lambda^2\mathbf{I} + \lambda\left[\mathbf{D}\left(\frac{\mathbf{1}}{\boldsymbol{\tau}_a}\right) + \mathbf{D}\left(\frac{\sqrt{\mathbf{a}_s}}{\boldsymbol{\tau}_y}\right) - \mathbf{D}\left(\frac{\mathbf{1}}{\boldsymbol{\tau}_a}\right)\mathbf{W}\mathbf{D}\left(\mathbf{y}_s^2\right)\right] + \mathbf{D}\left(\frac{\sqrt{\mathbf{a}_s}}{\boldsymbol{\tau}_y \odot \boldsymbol{\tau}_a}\right)\right) \tag{2.6}$$

Finding the roots of this polynomial is thus a quadratic eigenvalue problem of the form $\mathcal{L}(\lambda) \equiv \det(\lambda^2\mathbf{I} + \lambda\mathbf{B} + \mathbf{K}) = 0$, which has been studied extensively [65–68]. $\mathcal{L}(\lambda)$ can be interpreted as the characteristic polynomial associated with a system of linear second-order differential equations with constant coefficients of the form $\mathbf{I}\ddot{\mathbf{x}} + \mathbf{B}\dot{\mathbf{x}} + \mathbf{K}\mathbf{x} = \mathbf{0}$. Therefore, proving the stability of our system (i.e., $\mathbf{Re}(\lambda) < 0$ for $\{\lambda : \mathcal{L}(\lambda) = 0\}$), is equivalent to proving the asymptotic stability of $\mathbf{I}\ddot{\mathbf{x}} + \mathbf{B}\dot{\mathbf{x}} + \mathbf{K}\mathbf{x} = \mathbf{0}$.

Tisseur et al. [66] and Kirillov et al. [68] list a set of constraints on the damping matrix, $\mathbf{B}$, and stiffness matrix, $\mathbf{K}$, that yield a stable system, but they are *not* directly applicable to our system. In the context of a high-dimensional mechanical system, our system falls under the category of *gyroscopically stabilized systems with indefinite damping*. Few results are known about the conditions leading to the stability of such systems. By constructing a Lyapunov function, we

prove the following stability theorem (Appendix A.2) that is directly applicable to our system, following an approach similar to Kliem et al. [69].

Theorem 2.1. *For a system of linear differential equations with constant coefficients of the form,*

$$\mathbf{I}\ddot{\mathbf{x}} + \mathbf{B}\dot{\mathbf{x}} + \mathbf{K}\mathbf{x} = \mathbf{0} \tag{2.7}$$

where $\mathbf{B} \in \mathbb{R}^{n\times n}$ *and* $\mathbf{K} \in \mathbb{R}^{n\times n}$ *is a positive diagonal matrix (hence* $\mathbf{K}$ *is positive definite), the dynamical system is globally asymptotically stable if* $\mathbf{B}$ *is Lyapunov diagonally stable.*

Since the stiffness matrix,

$$\mathbf{K} = \mathbf{D}\left(\frac{\sqrt{\mathbf{a}_s}}{\boldsymbol{\tau}_y \odot \boldsymbol{\tau}_a}\right) = \mathbf{D}\left(\frac{\sqrt{\mathbf{b}_0^2 \odot \boldsymbol{\sigma}^2 + \mathbf{W}\left(\mathbf{b}^2 \odot \mathbf{z}^2\right)}}{\boldsymbol{\tau}_y \odot \boldsymbol{\tau}_a}\right), \tag{2.8}$$

is a positive diagonal matrix, a sufficient condition for stability of the dynamical system is that the damping matrix, $\mathbf{B}$, given by,

$$\begin{aligned}\mathbf{B} =& \mathbf{D}\left(\frac{\mathbf{1}}{\boldsymbol{\tau}_a}\right) + \mathbf{D}\left(\frac{\sqrt{\mathbf{a}_s}}{\boldsymbol{\tau}_y}\right) - \mathbf{D}\left(\frac{\mathbf{1}}{\boldsymbol{\tau}_a}\right)\mathbf{W}\mathbf{D}\left(\mathbf{y}_s^2\right) \\ =& \underbrace{\mathbf{D}\left(\frac{\mathbf{1}}{\boldsymbol{\tau}_a}\right)}_{\mathbf{B}_1} + \underbrace{\mathbf{D}\left(\frac{\sqrt{\mathbf{b}_0^2 \odot \boldsymbol{\sigma}^2 + \mathbf{W}\left(\mathbf{b}^2 \odot \mathbf{z}^2\right)}}{\boldsymbol{\tau}_y}\right)}_{\mathbf{B}_2} - \underbrace{\mathbf{D}\left(\frac{\mathbf{1}}{\boldsymbol{\tau}_a}\right)\mathbf{W}\mathbf{D}\left(\frac{\mathbf{b}^2 \odot \mathbf{z}^2}{\mathbf{b}_0^2 \odot \boldsymbol{\sigma}^2 + \mathbf{W}\left(\mathbf{b}^2 \odot \mathbf{z}^2\right)}\right)}_{\mathbf{B}_3},\end{aligned} \tag{2.9}$$

is *Lyapunov diagonally stable*, i.e., there exists a positive definite diagonal matrix $\mathbf{T}$, such that $\mathbf{T}\mathbf{B} + \mathbf{B}^\top\mathbf{T}$ is positive definite [70].

Since all of the parameters are positive, and the weights in the matrix $\mathbf{W}$ are nonnegative, we can conclude the following: $\mathbf{B}_1$ and $\mathbf{B}_2$ are positive diagonal matrices, and $\mathbf{B}_3$ is a matrix with all positive entries (that may or may not be symmetric). Therefore, $\mathbf{B}$ is a *Z-matrix*, meaning that its off-diagonal entries are nonpositive. Further, a *Z-matrix* is *Lyapunov diagonally stable* if and only

if it is a nonsingular *M-matrix*. Intuitively, *M-matrices* are matrices with non-positive off-diagonal elements and "large enough" positive diagonal entries. Berman & Plemmons [70] list 50 equivalent definitions of nonsingular *M-matrices*. We use the one that is best suited for our problem,

Theorem 2.2. *(Chapter 6, Theorem 2.3 from [70]) A Z-matrix matrix* $\mathbf{B} \in \mathbb{R}^{n\times n}$ *is Lyapunov diagonally stable if and only if there exists a convergent regular splitting of the matrix, that is, it has a representation of the form* $\mathbf{B} = \mathbf{M} - \mathbf{N}$*, where* $\mathbf{M}^{-1}$ *and* $\mathbf{N}$ *have all nonnegative entries, and* $\mathbf{M}^{-1}\mathbf{N}$ *has a spectral radius smaller than 1.*

We now show that, indeed, $\mathbf{B}$ has a *convergent regular splitting* for all combinations of the circuit parameters and for all inputs. We have already shown that $\mathbf{B}$ is a *Z-matrix*, therefore, the first condition of the theorem is satisfied. Next, we consider the following splitting $\mathbf{B} = \mathbf{M} - \mathbf{N}$ with $\mathbf{M} = \mathbf{B}_1 + \mathbf{B}_2$ and $\mathbf{N} = \mathbf{B}_3$. Since $\mathbf{B}_1$ and $\mathbf{B}_2$ are positive diagonal matrices, $\mathbf{M}^{-1}$ is nonnegative, while $\mathbf{N}$ is also nonnegative because $\mathbf{B}_3$ has all positive entries. Therefore, the only condition left to satisfy is that the spectral radius of $\mathbf{M}^{-1}\mathbf{N}$ is smaller than 1, or that the matrix is convergent.

The matrix $\mathbf{S} = \mathbf{M}^{-1}\mathbf{N} = (\mathbf{B}_1 + \mathbf{B}_2)^{-1}\mathbf{B}_3$ can be written as,

$$\mathbf{S} = \mathbf{D}\left(\frac{\mathbf{1}}{\mathbf{1} + (\boldsymbol{\tau}_a/\boldsymbol{\tau}_y) \odot \sqrt{\mathbf{b}_0^2 \odot \boldsymbol{\sigma}^2 + \mathbf{W}\,(\mathbf{b}^2 \odot \mathbf{z}^2)}}\right)\mathbf{W}\mathbf{D}\left(\frac{\mathbf{b}^2 \odot \mathbf{z}^2}{\mathbf{b}_0^2 \odot \boldsymbol{\sigma}^2 + \mathbf{W}\,(\mathbf{b}^2 \odot \mathbf{z}^2)}\right) \tag{2.10}$$

We prove the following theorem (Appendix A.3) which directly applies to $\mathbf{S}$,

Theorem 2.3. *A matrix* $\mathbf{A}$ *of the form* $\mathbf{A} = \mathbf{D}(\mathbf{t})\,\mathbf{W}\,\mathbf{D}\,(\mathbf{u}/(\mathbf{v} + \mathbf{W}\mathbf{u}))$ *is convergent (i.e., its spectral radius is less than 1), if* $\mathbf{W} \in \mathbb{R}^{n\times n}$ *and* $\mathbf{t}, \mathbf{u}, \mathbf{v} \in \mathbb{R}^n$ *satisfy* $0 < t_i < 1$, $u_i \geq 0$, $v_i > 0$ *and* $w_{ij} \geq 0$ *for all* i, j.

Defining $\mathbf{t} \rightarrow \mathbf{1}/(\mathbf{1}+(\boldsymbol{\tau}_a/\boldsymbol{\tau}_y)\odot\sqrt{\mathbf{b}_0^2 \odot \boldsymbol{\sigma}^2 + \mathbf{W}\,(\mathbf{b}^2 \odot \mathbf{z}^2)})$, $\mathbf{u} \rightarrow \mathbf{b}^2 \odot \mathbf{z}^2$ and $\mathbf{v} \rightarrow \mathbf{b}_0^2 \odot \boldsymbol{\sigma}^2$, it can be seen that they satisfy the constraints of the theorem, and thus $\mathbf{S}$ is convergent. This implies that $\mathbf{B}$ has a *convergent regular splitting* and, as a result, the linearized dynamical system is unconditionally

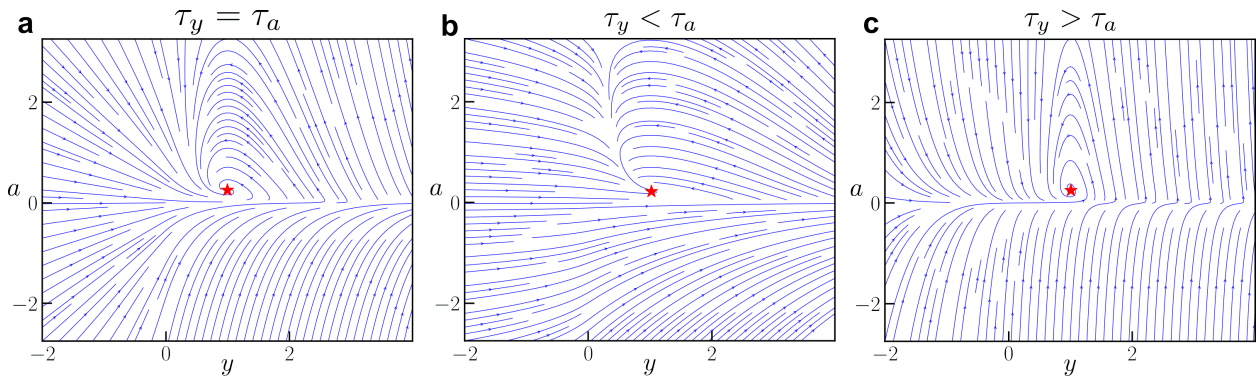


Figure 2.1: Phase portraits for 2D ORGaNICs for different time constants. Red stars indicate stable fixed points. The parameters for all plots are: $w_r = 1.0$, $b_0 = 0.5$, $b = 0.5$, $\sigma = 0.1$, $w = 1.0$, and $z = 1.0$. For **(a)**, the time constants are $\tau_a = 2$ ms, $\tau_y = 2$ ms; for **(b)**, $\tau_a = 10$ ms, $\tau_y = 2$ ms; for **(c)**, $\tau_a = 2$ ms, $\tau_y = 10$ ms.

globally asymptotically stable for all values of parameters and inputs. Further, the global asymptotic stability of linearization implies the local asymptotic stability of the normalization fixed point for ORGaNICs.

2.3 Discussion

This result holds even when the neurons have different time constants, regardless of their type, as no assumptions were made about the time constants. As a demonstration, in Fig. 2.1, we show the phase portraits for a two-dimensional ORGaNICs circuit with the recurrence scalar w_r set to 1. The phase lines change when the time constants τ_y and τ_a are changed, but the fixed points remain stable. This property is maintained for a high-dimensional circuit where the time constants can also be different within the type of neurons. This finding is significant for machine learning, particularly for designing architectures based on ORGaNICs. It allows neurons/units to integrate information at varying time scales while maintaining a stable circuit that performs normalization dynamically.

Moreover, analytical expressions for eigenvalues can be obtained in the following case,

Theorem 2.4. *Let* $\mathbf{W}_r = \mathbf{I}$*, the normalization matrix be given by* $\mathbf{W} = \alpha\mathbf{E}$*, where* $\mathbf{E}$ *is the all-ones*

matrix, and the parameters are scalars, i.e., $\boldsymbol{\tau}_y = \tau_y \mathbf{1}$, $\boldsymbol{\tau}_a = \tau_a \mathbf{1}$, $\mathbf{b}_0 = b_0 \mathbf{1}$, *and* $\boldsymbol{\sigma} = \sigma \mathbf{1}$. *Under these conditions, the eigenvalues of the system admit closed-form solutions (detailed in Appendix A.4).*

This result is particularly useful for neuroscience as it elucidates the connection between ORGaNICs parameters and the strength and frequency of oscillatory activity. Since we followed a direct Lyapunov approach to prove Theorem 2.1 as shown in Appendix A.2, we can derive an *energy* (viz., Lyapunov function) for ORGaNICs as shown in Appendix A.5.

Theorem 2.5. *When* $\mathbf{W}_r = \mathbf{I}$, *the energy (Lyapunov function) minimized by ORGaNICs in the vicinity of the normalization fixed point, is given by,*

$$V(\mathbf{y}, \mathbf{a}) = \sum_{i=1}^{n} t_i \frac{a_{si}}{{y_{s_i}}^2} \left[\frac{\tau_{y_i}}{\tau_{ai}} \sqrt{a_{si}} \left(y_i - y_{si} \right)^2 + \left(\sqrt{a_i} y_i - \sqrt{a_{si}} y_{si} \right)^2 \right]. \tag{2.11}$$

Where t_i *are the diagonal entries of* $\mathbf{T}$ *(a positive diagonal matrix such that* $\mathbf{TB} + \mathbf{B}^\top \mathbf{T}$ *is positive definite) and* y_{s_i} (a_{si}) *are the steady-state values of neurons* y_i (a_i).

Specifically, for a two-dimensional model (one y neuron and one a neuron), this expression simplifies to reveal that ORGaNICs behave like a damped harmonic oscillator with *energy* in the vicinity of the fixed point given by,

$$V(y, a) = \frac{\tau_y}{\tau_a} \sqrt{b_0^2 \sigma^2 + w b^2 z^2} \left(y - \frac{bz}{\sqrt{b_0^2 \sigma^2 + w b^2 z^2}} \right)^2 + \left(\sqrt{a} y - bz \right)^2 \tag{2.12}$$

This result demonstrates that ORGaNICs minimize the residual of the instantaneously reconstructed gated input drive ($\sqrt{a}y - bz$), while also ensuring that the principal neuron's response, y, achieves DN. The balance between these objectives is governed by the parameters and the external input strength. With fixed parameters, weaker inputs, z, cause the model to prioritize input matching over normalization, whereas stronger inputs increasingly engage the normalization objective.

3 | Critical Slowing down in ORGaNICs with Arbitrary Recurrence

3.1 Overview

In this chapter, we explore the extent of stability of ORGaNICs when the recurrent weight matrix $\mathbf{W}_r$ has a spectral radius larger than 1. The core findings discussed herein can also be found in [71].

We elaborate further on the relationship between normalization and stability in the case of a generic recurrent weight matrix, such as a large random matrix drawn from the Gaussian Orthogonal Ensemble (GOE). We find that ORGaNICs models with recurrent weights drawn from the GOE ensemble are stable even when the spectral radius of the recurrent matrix is larger than 1, thanks to the normalization mechanism. Quantitatively, ORGaNICs push the stability limit of linear recurrent models by more than 100% (see phase diagram of stability in Fig. 3.9). More importantly, we find that the transition to an unstable fixed point is preceded by critical slowing down [72, 73] in the neural dynamics (where the circuit is slow to reach the fixed point or to recover from small perturbations), the onset of which co-occurs with the breakdown of normalization in the neural responses. This result has the remarkable implication that loss of normalization can be used as an early warning signal for anticipating the loss of stability of the neural network, a signal we can predict analytically in terms of the recurrent interaction strength

(i.e., the variance of the recurrent weights) and the magnitude of the external input.

3.2 Definition of the model

Here, we relax the constraint that the recurrent weight matrix must be identity (discussed in Chapter 2), allowing $\mathbf{W}_r \neq \mathbf{I}$, and see if the dynamical stability of ORGaNICs is maintained. Upon simplifying Eq. (1.9), we get the following coupled dynamical system,

$$\begin{aligned} \boldsymbol{\tau}_y \odot \dot{\mathbf{y}} &= -\mathbf{y} + \mathbf{b} \odot \mathbf{z} + \left(\mathbf{1} - \sqrt{\lfloor \mathbf{a} \rfloor}\right) \odot (\mathbf{W}_r \mathbf{y}) \\ \boldsymbol{\tau}_a \odot \dot{\mathbf{a}} &= -\mathbf{a} + \mathbf{b}_0^2 \odot \boldsymbol{\sigma}^2 + \mathbf{W} \ \left(\mathbf{y}^2 \odot \lfloor \mathbf{a} \rfloor\right) \end{aligned} \tag{3.1}$$

The linear stability analysis becomes intractable for this dynamical system because we no longer have a closed-form analytical expression for the steady states of $\mathbf{y}$ and $\mathbf{a}$. Nevertheless, for a two-dimensional system,

$$\begin{aligned} \tau_y \dot{y} &= -y + bz + \left(1 - \sqrt{\lfloor a \rfloor}\right) w_r y \\ \tau_a \dot{a} &= -a + b_0^2 \sigma^2 + w y^2 \lfloor a \rfloor, \end{aligned} \tag{3.2}$$

we can prove the following, with a detailed analysis provided in Appendix B.1.

Theorem 3.1. *Given that the recurrence is contractive, i.e.,* $0 < w_r \leq 1$*, when* $z > 0$ *(*$z < 0$*), there exists a unique fixed point with* $y_s > 0$ *(*$y_s < 0$*) and* $a_s > 0$*, and it is asymptotically stable.*

Theorem 3.2. *Given that the recurrence is expansive, i.e.,* $w_r > 1$*, there are either 1 or 3 fixed points of which at least one is asymptotically stable. When* $z > 0$ *(*$z < 0$*) there exists exactly 1 fixed point with* $y_s > 0$ *(*$y_s < 0$*) and* $a_s > 0$*, and it is asymptotically stable. If* $b_0\sigma > 1 - 1/w_r$*, there are no additional fixed points. If* $b_0\sigma < 1 - 1/w_r$*, there exist either* 0 *or* 2 *additional fixed points with* $y_s < 0$ *(*$y_s > 0$*) and* $a_s > 0$ *whose stability cannot be guaranteed.*

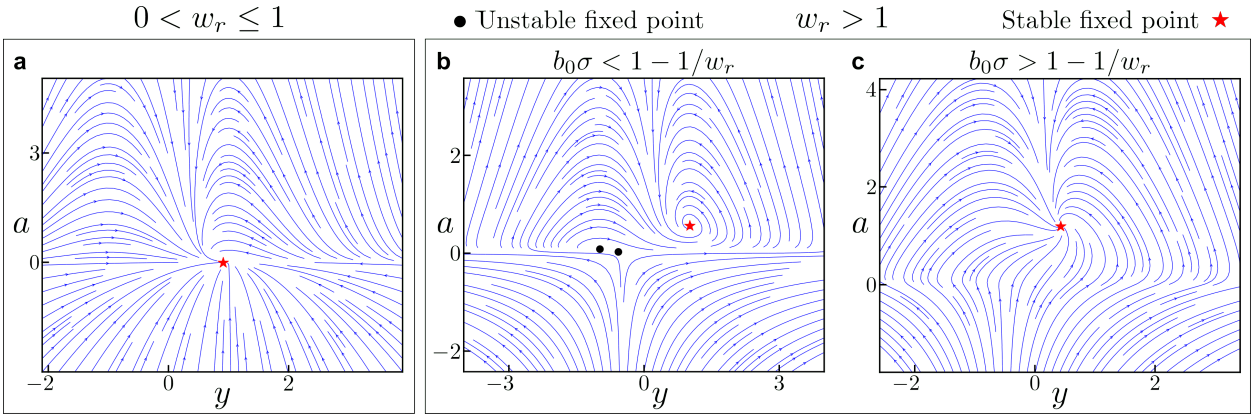


Figure 3.1: Phase portraits for 2D ORGaNICs with a positive input drive z. We plot the phase portraits of 2D ORGaNICs (Eq. (3.2)) in the vicinity of the stable fixed points for contractive (**a**) and expansive (**b, c**) recurrence scalar w_r. Red stars and black circles indicate stable and unstable fixed points, respectively. The parameters for all plots are: $b = 0.5$, $\tau_a = 2$ ms, $\tau_y = 2$ ms, $w = 1.0$, and $z = 1.0$. For **(a)**, the parameters are $w_r = 0.5$, $b_0 = 0.5$, $\sigma = 0.1$; for **(b)**, $w_r = 2.0$, $b_0 = 0.5$, $\sigma = 0.1$; and for **(c)**, $w_r = 2.0$, $b_0 = 1.0$, $\sigma = 1.0$. We find that a stable fixed point always exists across all parameter values.

We plot the phase portraits for these different cases in Fig. 3.1. The key takeaway is that there is always a fixed point (y_s, a_s) with $a_s > 0$ and y_s having the same sign as z. This fixed point is asymptotically stable regardless of the value of w_r. Based on these results and the proven stability of arbitrary dimensional ORGaNICs when $\mathbf{W}_r = \mathbf{I}$ (as shown in Chapter 2), we conjecture that

Conjecture 3.3. *Consider high-dimensional ORGaNICs with an arbitrary recurrent weight matrix* $\mathbf{W}_r$ *and no constraints on the remaining parameters. If the norm of the input drive satisfies* $||\mathbf{z}|| \leq 1$, *and the spectral radius of* $\mathbf{W}_r$ *is constrained to be less than 1, then the system possesses at least one asymptotically stable fixed point.*

This conjecture is supported by empirical evidence showing consistent stability, as ORGaNICs initialized with random parameters and inputs under these constraints have exhibited stability in 100% of the trials.

The central questions we answer in this chapter are: What happens when arbitrary recurrent connections are included in the circuit and the spectral radius of $\mathbf{W}_r$ is larger than 1? Does ORGaNICs still accomplish normalization? Is the stability preserved? To answer these questions,

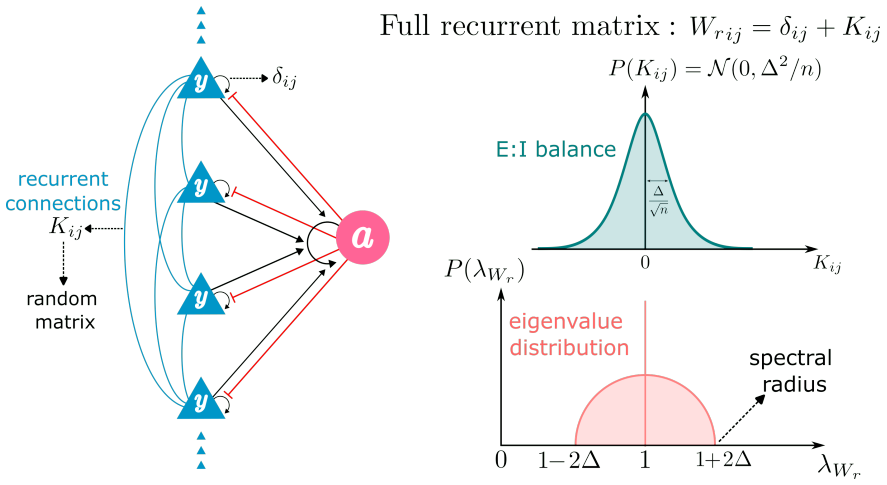


Figure 3.2: Illustration of the model. We consider an ORGaNICs circuit with recurrent connections included via the weight matrix $\mathbf{W}_r$ composed of the identity $\mathbf{I}$ plus a random matrix $\mathbf{K}$ modeling lateral synaptic connections between the principal neurons. The weights K_{ij} are E:I balanced (i.e., mean 0) and sampled from a symmetric Gaussian distribution such that the spectral radius of $\mathbf{W}_r$ is equal to $1 + 2\Delta$ in the limit where the number of neurons n goes to infinity.

we include recurrent connections between the principal neurons; set the time constants to be the same across neurons of the same type; set the gain parameters $\mathbf{b} = \mathbf{b}_0 = \mathbf{1}$ and set all of the entries in the normalization weight matrix $\mathbf{W}$ equal to 1 (broad normalization pool), which gives us a single representative a neuron. Under these assumptions, Eq. (3.1) can be written as,

$$\begin{cases} \tau_y \dot{y}_i = -y_i + z_i + \left(1 - \sqrt{\lfloor a \rfloor}\right) \sum_{j=1}^{n} W_{rij} y_i \\ \tau_a \dot{a} = -a + \sigma^2 + \left(\sum_{i=1}^{n} y_i^2 \right) \lfloor a \rfloor \,, \end{cases} \tag{3.3}$$

where the recurrent weight matrix $\mathbf{W}_r$ captures the lateral connections between the principal neurons, as shown in Fig. 3.2.

Our goal is twofold: first, we determine the conditions on $\mathbf{W}_r$ and $\mathbf{z}$ such that normalization still approximately holds for the circuit in Eq. (3.3); second, we investigate the consequences of the breakdown of normalization, due to substantial recurrent amplification, for the stability of the whole neural network.

3.3 Numerical Solution of the Fixed Point

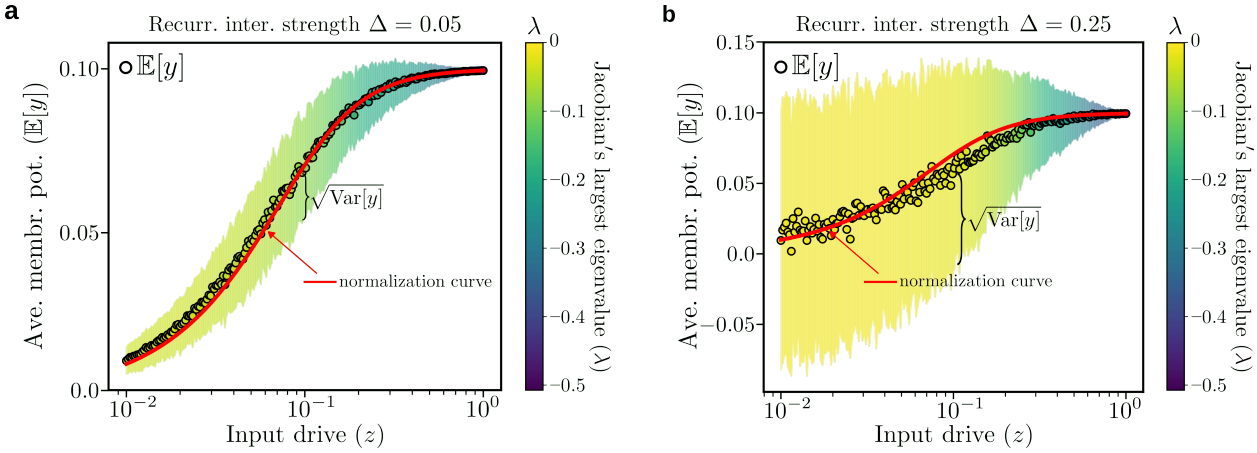


Figure 3.3: Numerical solution to the ORGaNICs' fixed point equations. (**a**), Fixed-point average membrane potential $\mathbb{E}[y]$ (open circles) as a function of the input drive z (here we use $n = 100$ neurons and $z_i = z/\sqrt{n}$, called *delocalized* input drive) for an E:I balanced recurrent network $\mathbf{K}$ with zero mean and std. dev. $\Delta = 0.05$, obtained by solving numerically Eq. (3.3) using the explicit Euler method with time step $dt = 0.05 \times \tau_y$. The semisaturation constant is $\sigma = 0.1$ and the neurons' time constants τ_y and τ_a are equal. Each point is an average over 1000 realizations of the synaptic weight matrix $\mathbf{K}$. The neural response still follows, on average, the normalization Eq. (1.1) (solid red curve), but picks up a variance across different random samples of recurrent synaptic weights, represented by the shaded area around the data points. The color code of the shaded area represents the real part of the largest eigenvalue of the Jacobian at the fixed point averaged over samples, whose value is well below 0 for all z. (**b**), For $\Delta = 0.25$ the average response is still normalized, but the variance (across random samples of the recurrent weights) is bigger than in (**a**) (see Fig. B.1 for more Δ values). For sufficiently small input drives, the largest eigenvalue of the Jacobian at the fixed point becomes very small ($\lambda \sim 0$). As a consequence, convergence to the fixed point occurs on time scales much longer than the time constant τ_y of individual neurons, a phenomenon known as critical slowing down (see also Fig. 3.4c).

We start with a numerical study of the stability of the fixed-point of Eq. (3.3) and then we derive our analytical solution perturbatively, supported by the exact numerical result. We express the recurrent matrix as the sum of the identity plus a perturbation as

$$\mathbf{W}_r = \mathbf{I} + \mathbf{K}\,, \tag{3.4}$$

where $\mathbf{K}$ is a symmetric GOE random matrix [74] whose entries K_{ij} are independent and identically

distributed Gaussian random variables with zero mean and variance Δ^2/n if $i = j$ or $\Delta^2/2n$ if $i \neq j$, corresponding to balanced excitation and inhibition. The scaling of the variance by $1/n$ ensures that the spectral radius $\rho(\mathbf{K})$ does not grow with the number of neurons n, but is controlled only by Δ (specifically, $\rho(\mathbf{K}) = 2\Delta$, hence $\rho(\mathbf{W}_r) = 1 + 2\Delta$, see Fig. 3.2). The choice of a random matrix to study the stability of large systems of differential equations can be traced back to the seminal work of May on the stability of complex ecosystems [75], that initiated a new field in theoretical ecology [76, 77] as well as the famous diversity-stability debate [78–80]. Methods based on random matrix theory are also well-suited to model very large neural circuits whose experimental parametrization would be otherwise unfeasible [81]. Here, we follow a similar approach with the goal of deriving a condition on the recurrent interaction strength Δ such that the output responses y_i still approximately satisfy the normalization equation (1.1), and then study the consequences of the breakdown of normalization on the system's stability. We note, *en passant*, that a linear model (i.e. a model where $a \equiv 0$) would become unstable as soon as the spectral radius of $\mathbf{W}_r$ gets larger than 1, i.e. a soon as $\Delta > 0$ (see Fig. 3.9). In contrast, the nonlinear model described by Eq. (3.3) can be stable even when $\mathbf{W}_r$ has spectral radius larger than 1, as we show next.

In Figure 3.3a,b we show the numerical solution of the fixed point of Eq. (3.3) (see Appendix B.2 for details on the numerical methods). We plot the mean and variance of the fixed point membrane potentials, y_i, over the ensemble of random recurrent matrices $\mathbf{K}$, as a function of the input drive z for $\Delta = 0.05$ and $\Delta = 0.25$. We find that the output responses, on average, still follow the normalization curve, i.e. $\mathbb{E}[y_i] \sim z_i/\sqrt{\sigma^2 + ||\mathbf{z}||^2}$ (noting that membrane potential in this model is the square root of firing rate), but pick up a variance that increases with increasing Δ. For sufficiently large Δ we observe that the circuit's convergence to its fixed point, as measured by the real part of the largest eigenvalue λ of the Jacobian evaluated at the fixed point [82], becomes very slow (i.e. $\lambda \sim 0$ corresponding to a convergence time $t_{conv} = \frac{1}{|\lambda|} \gg 1$), as seen in Fig. 3.3b. This phenomenon, called **critical slowing down**, is widely considered to be an important early

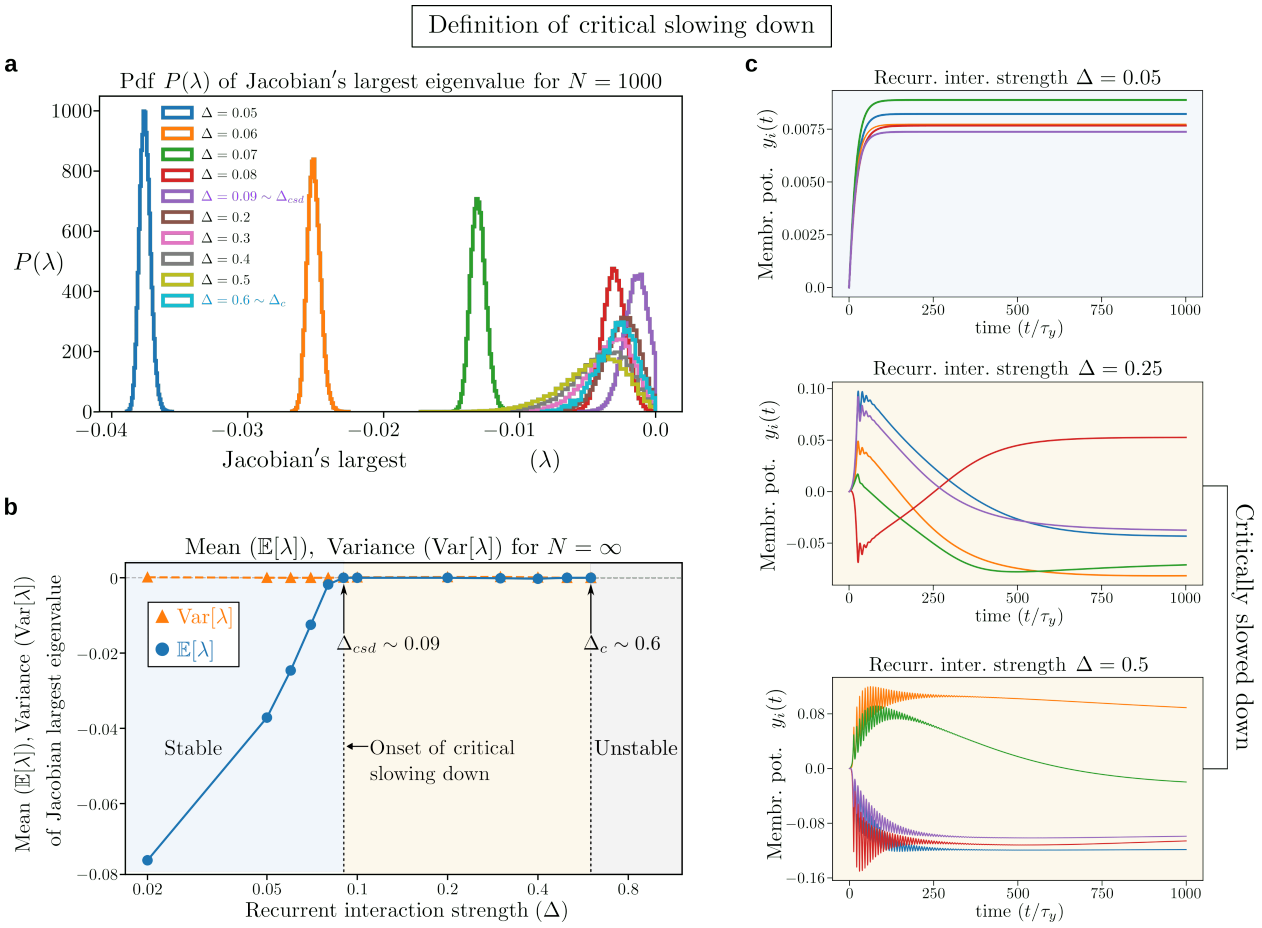


Figure 3.4: Definition of critical slowing down. (**a**), Probability distribution of the largest eigenvalue of the Jacobian at the fixed point for a network with $n = 1000$ neurons (see Fig. 3.5 for different sizes); input drive $z_i = 0.01/\sqrt{n}$ (very weak input drive); semisaturation constant $\sigma = 0.1$; and several values of the recurrent interaction strength Δ. For small Δ the distribution $P(\lambda)$ is gapped from 0 and, as a consequence, the neural responses converge quickly to their fixed points. When Δ increases, the gap shrinks and then closes at $\Delta = \Delta_{csd}$, signaling the onset of critical slowing down. For $\Delta_{csd} \leq \Delta \leq \Delta_c$ the neural responses converge slowly to their fixed points. For $\Delta \geq \Delta_c$ the neural circuits do not have stable fixed points, but exhibit limit cycles and, for even larger Δ, they eventually become unstable (see Fig. 3.9). (**b**), Mean, $\mathbb{E}[\lambda]$, and variance, $\mathrm{Var}(\lambda)$, of the largest eigenvalue of the Jacobian extrapolated to $n \to \infty$ as a function of Δ (see Fig. 3.6 for details on the extrapolation). The model parameters' values are as in (**a**). Since the variance is zero in the $n \to \infty$ limit, $P(\lambda)$ tends to a delta function $\delta(\lambda - \mathbb{E}[\lambda])$, thus making the determination of Δ_{csd} well defined as the value at which the mean $\mathbb{E}[\lambda]$ goes to zero. Slowing down persists up to the critical value Δ_c, beyond which there are no stable fixed points (see Fig. 3.9). (**c**), Representative trajectories of the neural responses $y_i(t)$ in the stable phase ($\Delta = 0.05$) and in the critically slowed down phase ($\Delta = 0.25, 0.5$), showing the slowness of the dynamics in reaching the fixed point. (see Fig. 3.7 for trajectories of all the neurons and Figs. 3.10, 3.12 for the analysis of the frequency of oscillations).

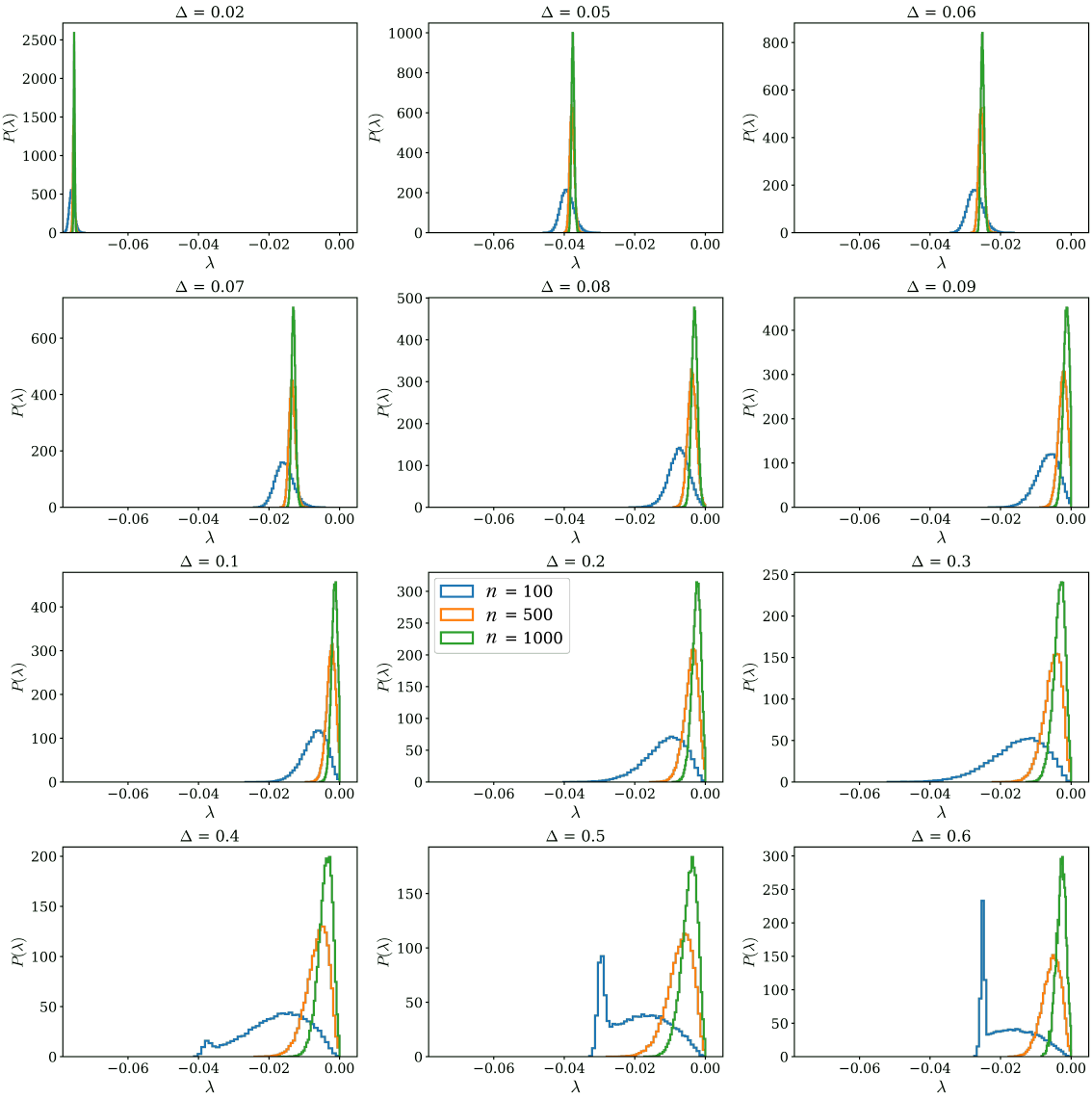


Figure 3.5: Distribution of the Jacobian's largest eigenvalue (λ) for different system sizes (n). Distribution of the largest eigenvalue of the Jacobian at the fixed point computed several values of Δ for different system sizes ($n = 100,\ 500$ and 1000). The input drive, simulation parameters, and the parameters of ORGaNICs are the same as those used for generating Fig. 3.4 in the main text. Each panel plots the distribution for different values of Δ. As system size increases, finite-size fluctuations narrow, sharpening the gap edge and more clearly revealing the approach of the rightmost eigenvalue toward zero at $\Delta \approx 0.09$. For $\Delta < \Delta_{csd}$, all sizes exhibit a clear gap from zero; for $\Delta \geq \Delta_{csd}$ the largest-n curve touches zero most sharply.

warning signal that anticipates the system's tipping point [72, 73, 83].

To identify the onset of critical slowing down we plot in Fig. 3.4a the probability distribution

$P(\lambda)$ of the real part of the largest eigenvalue of the Jacobian at the fixed point for circuits with $n = 1000$ neurons, weak input drive $z = 0.01$, and different values of the recurrent interaction strength Δ. At small Δ, $P(\lambda)$ has a gap from 0, which closes when Δ approaches the critical value $\Delta = \Delta_{csd}$, signaling the onset of critical slowing down. To get a more precise estimate of Δ_{csd}, we extrapolate the mean and variance of $P(\lambda)$ in the limit $n \to \infty$ via finite size scaling analysis, yielding the asymptotic mean and variance shown in Fig. 3.4b (see Fig. 3.6 for details on the finite size scaling analysis). In Fig. 3.5 we show $P(\lambda)$ for several values of n and Δ. The variance goes to zero in the large n limit, meaning that $P(\lambda)$ becomes a δ-function sharply peaked around its mean. The mean vanishes at $\Delta = \Delta_{csd}$ and remains zero in the whole interval $\Delta_{csd} \leq \Delta \leq \Delta_c$ (Fig. 3.4b). In this interval the neural dynamics are very slow (compared to the neuron's intrinsic time scale τ_y) to reach the fixed point, as illustrated by some representative trajectories shown in Fig. 3.4c. Eventually, for $\Delta \geq \Delta_c$, the circuits enter first into limit cycles and then become unstable (see Fig. 3.9).

Next, we demonstrate that the onset of critical slowing down occurs precisely when normalization of the neural responses breaks down.

3.4 Loss of Normalization Predicts Critical Slowing Down

To quantify the loss of normalization, we look at the mean and variance (across many instances of the recurrent matrix $\mathbf{K}$) of the neural responses. As seen in Figure 3.3, the neural response y_i can be described by its expected value plus the standard deviation: the expected value follows the normalization equation and the standard deviation quantifies the departure from normalization. Therefore, neuron i loses normalization as soon as the standard deviation of its response is equal to its mean value, as given by the formula

$$\sqrt{\mathrm{Var}[y_i]} = \mathbb{E}[y_i] \quad \text{(loss of normalization)}\,, \tag{3.5}$$

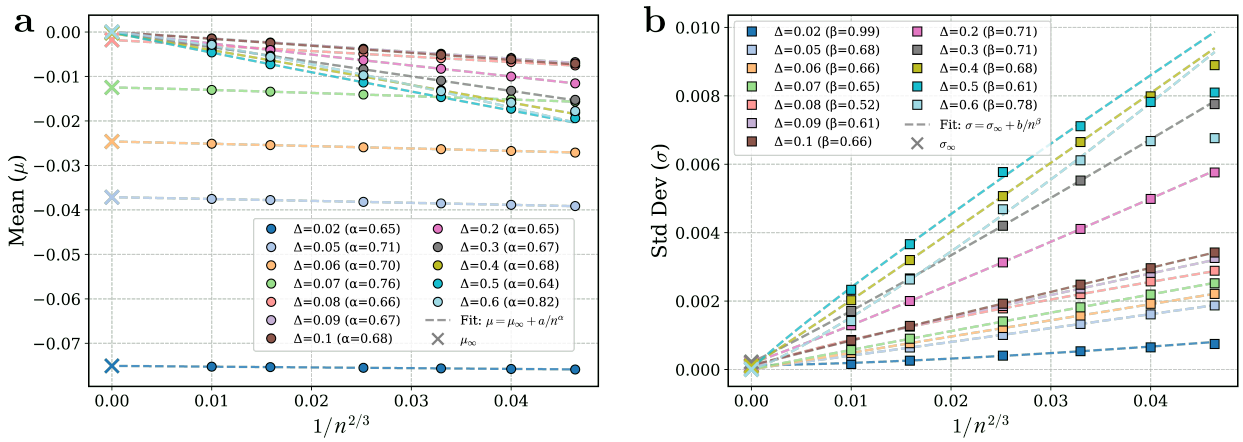


Figure 3.6: Finite size scaling analysis. The mean and standard deviation of the largest eigenvalue of the Jacobian are shown. The input drive, simulation parameters, and the parameters of ORGaNICs are the same as those used for generating Fig. 3.4. (**a**), The mean μ of the largest eigenvalue λ of the Jacobian matrix at the fixed point as a function of $1/n^{2/3}$ for several values of Δ. Dashed lines represent fits following the functional form $\mu = \mu_\infty + a/n^\alpha$, where μ_∞, a, and α are fitting parameters and the fits are performed using the four largest system sizes. The 'x' markers correspond to the extrapolated mean for the infinite system size (μ_∞). The values α in the legend correspond to the fitted slopes and they are close to $2/3$ for nearly all values of Δ. μ_∞ vanishes for all values of Δ where we observe critical slowing down ($\Delta \gtrsim 0.09$). (**b**) The standard deviation σ of the largest eigenvalue λ of the Jacobian matrix at the fixed point as a function of $1/n^{2/3}$ for several values of Δ. Dashed lines represent fits following the functional form $\sigma = \sigma_\infty + b/n^\beta$, where σ_∞, b, and β are fitting parameters, and fits are performed using the four largest system sizes. The fits extrapolate to a vanishing standard deviation for the infinite system size ($\sigma_\infty \approx 0$), indicating that fluctuations of λ vanish in the thermodynamic limit.

and illustrated in Fig. 3.8a,b. Equation (3.5) defines implicitly a threshold $\Delta_{loss}(z)$ marking the boundary between the phase in which responses are normalized and the phase where they are not. We compare the loss of normalization threshold $\Delta_{loss}(z)$ with the critical slowing down threshold $\Delta_{csd}(z)$ in Fig. 3.9, showing excellent agreement between the two at all values of the input drive z, thus demonstrating that the onset of critical slowing down co-occurs with the loss of normalization of the neural responses, which represents our most important result.

An immediate consequence of this correspondence is that we can predict theoretically the onset of critical slowing down by calculating $\Delta_{loss}(z)$, which is a simpler quantity to estimate analytically, as explained next. To compute the mean and variance entering in equation (3.5), we must first find the fixed point of the dynamical system in Eq. (3.3), which, unfortunately, cannot be

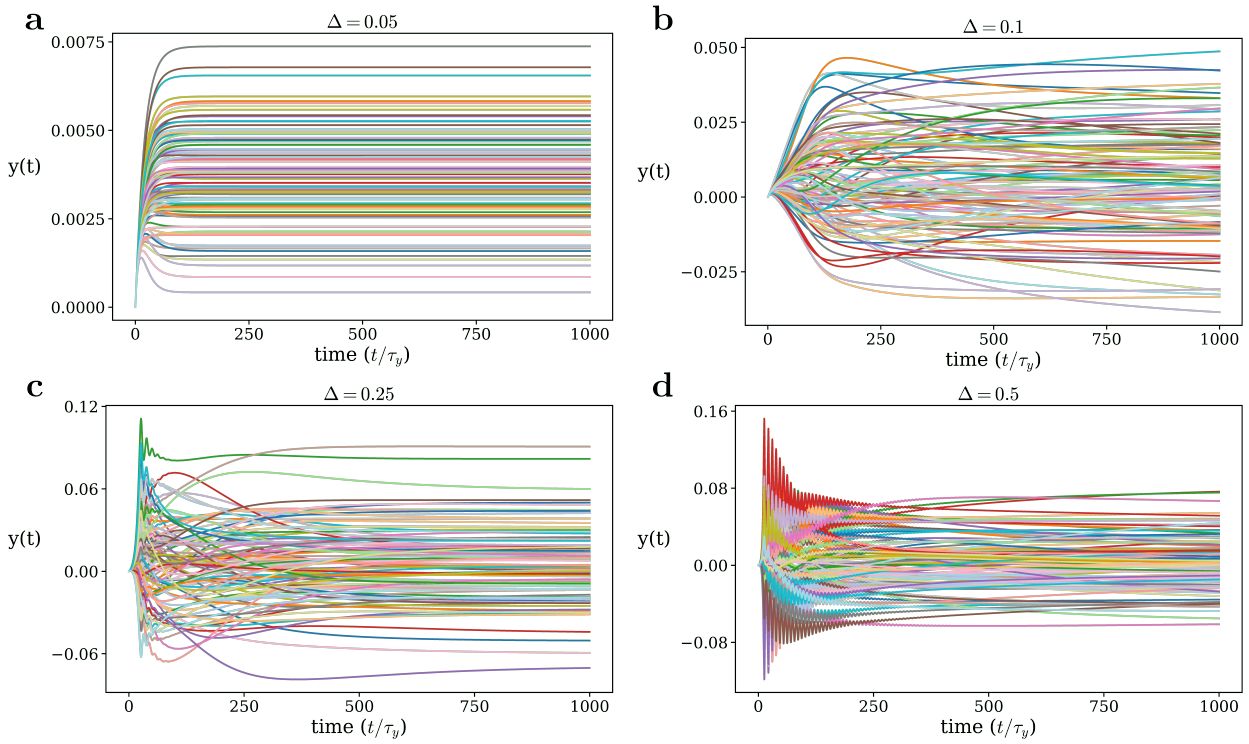


Figure 3.7: Neuronal trajectories for different recurrent synaptic strength Δ**.** Each curve traces the time evolution of a distinct principal neuron's response for a given value of Δ (recurrent interaction strength). The input type and the parameters of ORGaNICs are the same as those used for generating Fig. 3.4. We plot the trajectories for 100 neurons selected randomly from the 1000. In the stable regime ($\Delta = 0.05$), trajectories converge rapidly, whereas in the critical-slowing regime ($\Delta = 0.10$, 0.25, and 0.50) convergence is markedly slower.

expressed in closed form. To overcome this obstacle, we use perturbation theory to approximate the exact solution. We look for a solution to the fixed point equations in the form of a series $y_i = y_i^{(0)} + y_i^{(1)} + ...$, where $y_i^{(0)}$ is given by the normalization equation (1.1), and $y_i^{(1)}$ is of the same order of magnitude as the perturbation $\mathbf{K}$. Inserting this expansion in Eq. (3.3) we find the approximate fixed point solution (see details in Appendix B.3):

$$y_i \approx \frac{z_i}{\sqrt{\sigma^2 + ||\mathbf{z}||^2}} + \left(\sum_j K_{ij} z_j - z_i \frac{\mathbf{z}^\top \mathbf{K} \mathbf{z}}{\sigma^2 + ||\mathbf{z}||^2} \right) G(||\mathbf{z}||) \,, \tag{3.6}$$

where $G(z) = \frac{1-\sqrt{\sigma^2+z^2}}{\sigma^2+z^2}$ and $||\mathbf{z}||^2 = \mathbf{z}^\top \mathbf{z}$. The last term on the right hand side of Eq. (3.6) quantifies

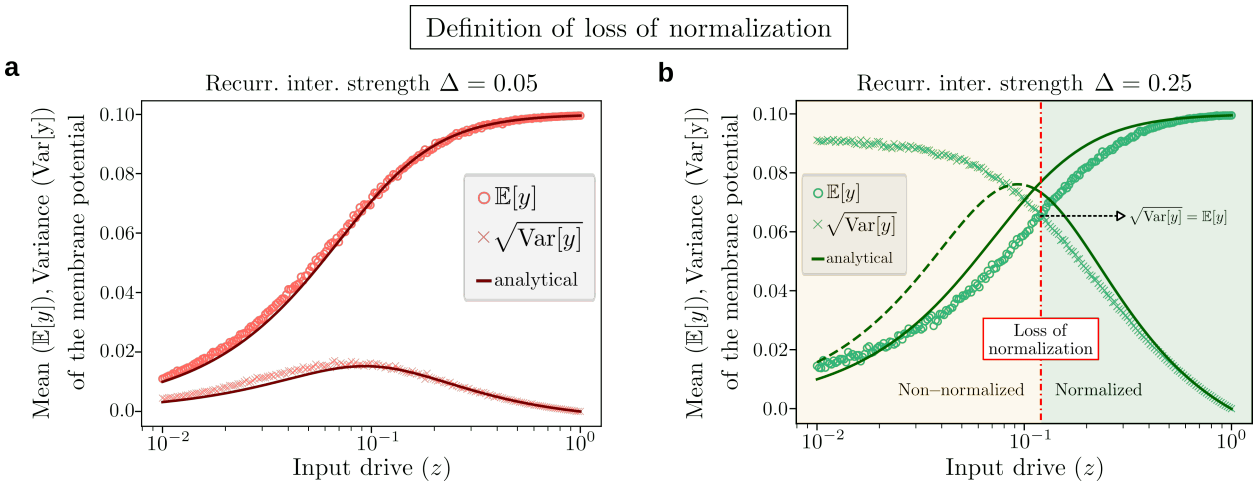


Figure 3.8: Definition of loss of normalization. (**a**), Mean, $\mathbb{E}[y]$, (circles) and standard deviation, $\sqrt{\mathrm{Var}[y]}$, (crosses) of the fixed point membrane potential as a function of the norm z of the input drive $z_i = z/\sqrt{n}$ for an E:I balanced recurrent network $\mathbf{K}$ with zero mean and std. dev. $\Delta = 0.05$. We used $n = 100$ neurons and averaged over 10^4 realizations of $\mathbf{K}$. The standard deviation is smaller than the mean for all values of z, so the neural responses are always normalized. The analytical approximations (solid curves) for the mean and standard deviation Eq. (3.7) of the response, computed with perturbation theory, show a good agreement with the exact numerical solutions. (**b**), Same as in (**a**), but using $\Delta = 0.25$. The standard deviation is smaller than the mean ($\sqrt{\mathrm{Var}[y]} < \mathbb{E}[y]$) at large z, but it is larger than the mean ($\sqrt{\mathrm{Var}[y]} > \mathbb{E}[y]$) at small z. The value of z where the two curves cross each other, given by Eq. (3.5), defines the threshold at which the neural responses lose normalization (dashed red line). The analytical approximations are in good agreement with numerical simulations for almost all values of the input drive (notice the log scale on the abscissa), but become less accurate at small z where the responses are non-normalized and perturbation theory breaks down, another indication of a major shift in the circuit's behavior.

the impact of the recurrent interactions on the normalization fixed point. Taking the expectation on both sides, and using the fact that the K_{ij}'s have zero mean, we find $\mathbb{E}[y_i] \approx \frac{z_i}{\sqrt{\sigma^2+||\mathbf{z}||^2}}$, meaning that the neural responses still follow, on average, the normalization equation, as seen in Figure 3.8a,b. Departure from normalization is quantified by the variance of y_i. The calculation of $\mathrm{Var}[y_i]$ yields the following general expression (see Appendix B.3 for details)

$$\mathrm{Var}[y_i] \approx \frac{\Delta^2}{2n}\left[||\mathbf{z}||^2 - z_i^2 + \frac{2z_i^2\sigma^4}{\left(\sigma^2 + ||\mathbf{z}||^2\right)^2}\right] G^2(||\mathbf{z}||)\,, \tag{3.7}$$

which depends on the magnitude $||\mathbf{z}||$ and shape z_i of the input drive. For example, we consider

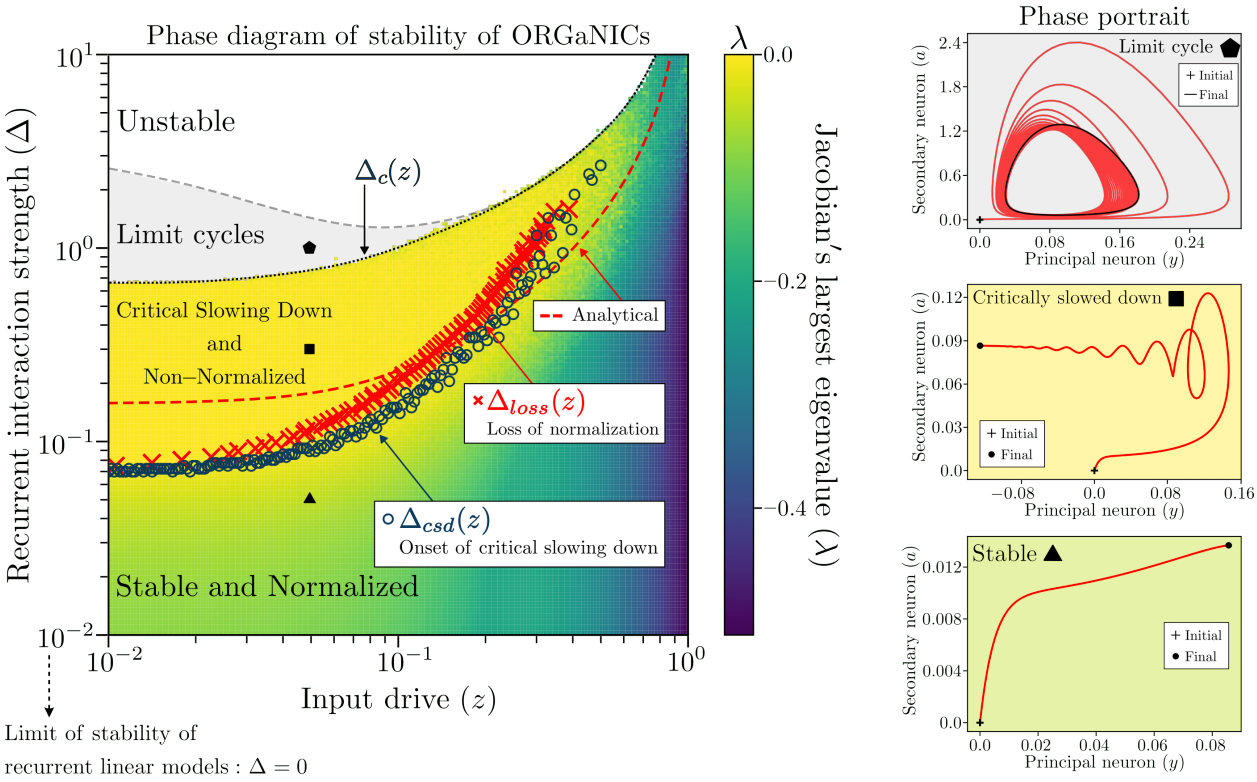


Figure 3.9: Loss of normalization predicts the onset of critical slowing down. Real part of the largest eigenvalue λ of the Jacobian at the fixed point in the (z, Δ) plane obtained by solving numerically Eq. (3.3) for E-I balanced networks with $n = 100$ neurons; delocalized input drive $z_i = z/\sqrt{n}$; semisaturation constant $\sigma = 0.1$; neurons' time constants $\tau_y = \tau_a$; using a mesh of 200×200 values of z and Δ. Color represents the maximum value of λ across 100 random samples of the recurrent synaptic weights. Circuits with small Δ are stable at any value of the input drive z and converge quickly to their fixed point, as indicated by a strictly negative eigenvalue $\lambda < 0$ and by the *Stable* phase portrait in the (y, a) plane (where a is the inhibitory neuron). Conversely, for $\Delta_{csd} \leq \Delta < \Delta_c$, the circuits exhibit critical slowing down, in that they approach the fixed point very slowly, as indicated by $\lambda \sim 0$ and by the spiral attractor in the *Critically slowed down* phase portrait. The points marking the onset of critical slowing down (open blue circles) are determined by the closing of the gap in the distribution $P(\lambda)$ (see Fig. 3.4), which define the curve $\Delta_{csd}(z)$. The points defining $\Delta_{loss}(z)$ (red crosses) represent the boundary between the normalized and non-normalized phases and are determined via Eq. (3.5) (see Fig. 3.8). Loss of normalization predicts well the onset of critical slowing down, i.e. $\Delta_{loss}(z) \approx \Delta_{csd}(z)$, thus providing a good early warning indicator of neurodynamical tipping points. For sufficiently large Δ the neural circuits exhibit limit cycles, as shown in the *Limit cycle* phase portrait, and for even larger Δ they become unstable. Notice, however, that simple linear recurrent models would become unstable as soon as $\Delta > 0$, while adding normalization pushes the stability limit much further.

a *delocalized* input drive, i.e. $z_i = \frac{z}{\sqrt{n}}$, (the opposite case of a *localized* input drive is discussed in Appendix B.3.2 and Figs B.3, B.4, B.5, leading to qualitatively similar results) and find that

$\mathrm{Var}[y_i] \approx \frac{\Delta^2 z^2}{2n} G^2(z)$, independent of i. In Figure 3.8a,b we plot the mean and variance of the neural response for two values of Δ, showing that the analytical approximations agree well with the exact numerical solution (see Fig. B.2 for more values of Δ). Finally, by equating the mean and the standard deviation of the response, we find the threshold $\Delta_{loss}(z)$ marking the boundary between the normalized and non-normalized phases as

$$\Delta_{loss}(z) = \frac{\sqrt{2(\sigma^2 + z^2)}}{1 - \sqrt{\sigma^2 + z^2}}, \tag{3.8}$$

The analytical approximation given by Eq. (3.8) for the function $\Delta_{loss}(z)$, shown in Fig. 3.9, is in good agreement with the exact numerical estimate. Since $\Delta_{loss}(z) \approx \Delta_{csd}(z)$, Eq. (3.8) can be used to predict the onset of critical slowing down in the neural dynamics from the magnitude of the *external* input and the strength of the *internal* recurrent weights. On the one hand, when $z \longrightarrow 1 - \sigma^2 \approx 1$ normalization is enganged robustly and the range of stability of the circuit extends indefinitely. On the other hand, when $z \longrightarrow 0$ the range of stability is narrowest.

3.5 Oscillatory Activity

To understand how the interplay between external stimuli and recurrent drive affects the dynamics of ORGaNICs, we investigated the system's propensity to oscillate under varying conditions. Specifically, we explored the influence of the overall input drive z and the recurrent interaction strength Δ. We systematically varied these two parameters and computed the average oscillation frequency of the network activity as the mean imaginary part of the Jacobian eigenvalues $\mathrm{Im}(\lambda_J)/(2\pi)$ evaluated at the system's fixed point. Oscillatory dynamics (spiralling fixed points) are indicated by complex eigenvalues. Fig. 3.10 shows the resulting heat map in the (z, Δ) plane, where we plot the mean oscillation frequency for a network of $n = 100$ neurons with time constants $\tau_y = \tau_a = 2$ ms, considering both delocalized (Fig. 3.10a) and localized input drives (Fig. 3.10b).

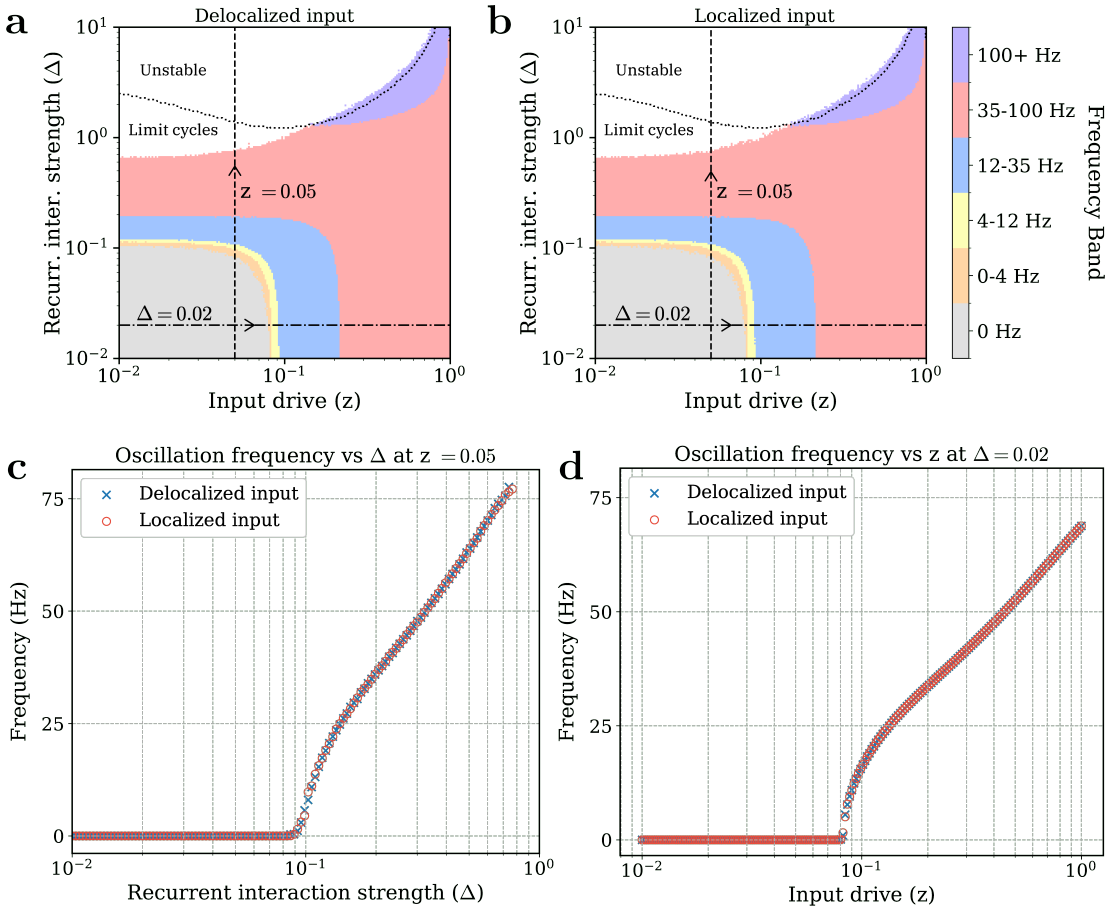


Figure 3.10: Phase diagram and oscillation frequencies in ORGaNICs. (**a**, **b**), Phase diagrams depicting the average oscillation frequency for ORGaNICs as a function of input drive (z) and recurrent interaction strength (Δ). Frequency is color-coded according to standard bands (see color bar: 0 Hz, 0-4 Hz, 4-12 Hz, 12-35 Hz, 35-100 Hz, 100+ Hz), calculated as the mean imaginary part of the Jacobian eigenvalues $\mathrm{Im}(\lambda_J)/(2\pi)$ across trials. Results are shown for delocalized (**a**) and localized (**b**) inputs in a system with $n = 100$ neurons, semisaturation constant $\sigma = 0.1$, and time constants $\tau_y = \tau_a = 2$ ms. Dotted curves indicate the transition from limit cycles to an unstable regime, where instability is defined as trajectories diverging in at least 50% of trials. (**c**), Oscillation frequency vs recurrent interaction strength (Δ) at a fixed input drive $z = 0.05$. (**d**), Oscillation frequency vs input drive (z) at a fixed recurrent interaction strength $\Delta = 0.02$. Plots (**c**) and (**d**) compare delocalized (blue circles) and localized (red circles) inputs, showing minimal difference between the two input types.

We find distinct dynamical regimes. When the input drive and the synaptic strength are weak, i.e., $z \lesssim 0.1$ and $\Delta \lesssim 0.1$, the circuits settle into a stable, non-oscillating fixed point. However, as the input drive increases ($z \gtrsim 0.1$), the fixed point becomes a spiral attractor, leading to oscillations falling within the gamma frequency range (30-100 Hz). Within this regime, the frequency of these

input-driven oscillations scales positively with the input drive z (Fig. 3.10d). A different scenario unfolds when the recurrent synaptic strength is increased (Fig. 3.10c). For low input drive ($z \lesssim 0.1$), damped oscillations emerge beyond $\Delta \approx 0.1$. In this recurrence-driven regime, the oscillation frequency increases monotonically with Δ from 0 Hz to 80 Hz, before the attractor ultimately turns into limit cycles at higher Δ. These findings highlight the dual roles of external input and internal recurrent drive in shaping the frequency of the oscillatory behavior in ORGaNICs.

3.6 E-I Imbalanced Recurrent Networks

We investigate the impact of excitation-inhibition (E-I) imbalance in the recurrent weight matrix $\mathbf{W}_r$ on the stability of ORGaNICs. We introduce E-I imbalance by setting a non-zero mean μ for the entries of the recurrent connectivity matrix $\mathbf{K}$, such that $K_{ii} \sim \mathcal{N}(\mu/n, \Delta^2/n)$ and $K_{ij} \sim \mathcal{N}(\mu/n, \Delta^2/2n)$ for $i \neq j$. This introduces net inhibition (for $\mu < 0$) or net excitation ($\mu > 0$) in $\mathbf{K}$. We generated phase diagrams, shown in Fig. 3.11, analogous to Fig. 3.9 for different values of $\mu = [0.0,\ 0.05,\ 0.1,\ 0.25,\ 0.5,\ 1.0,\ -0.1,\ -0.5,\ -1.0]$, using a delocalized input drive $z_i = z/\sqrt{n}$ and network parameters $n = 100$, $\sigma = 0.1$, $\tau_y = \tau_a$. We observe three main things:

1. increasing excitation (larger positive μ) shifts the onset of critical slowing down towards larger values of the recurrent interaction strength Δ. For strong excitatory imbalance (e.g., $\mu = 1.0$), the network transitions from the stable regime to the limit cycle regime at small input drive z without undergoing critical slowing down;

2. increasing inhibition (larger negative μ) makes the circuit operate in the critically slowed down regime for a larger range of values of Δ at any input drive z. For strong inhibitory imbalance (e.g., $\mu = -1.0$), the circuit remains stable across all z without entering into limit cycles at small z;

3. most importantly, the loss of normalization is still a good predictor of the onset of critical

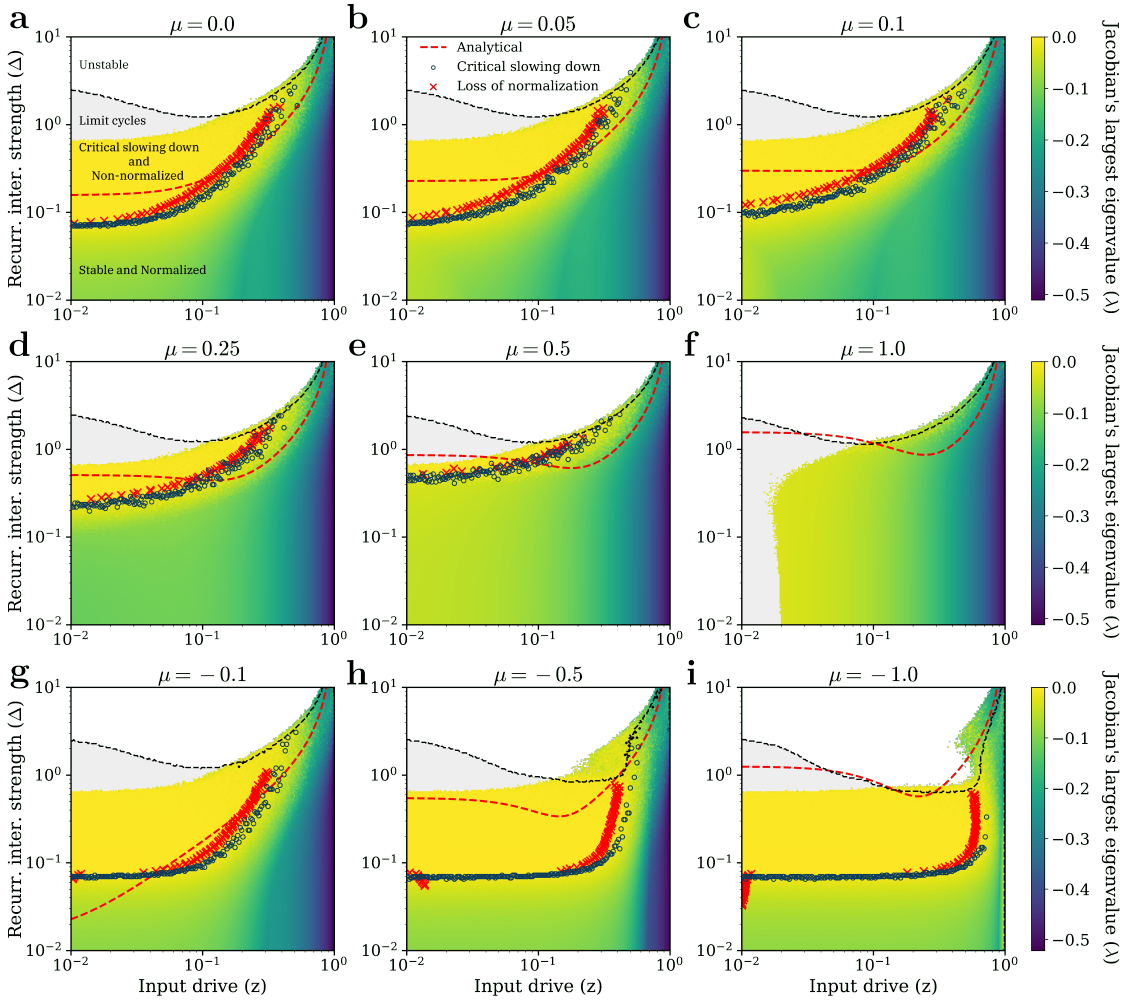


Figure 3.11: Effect of E-I imbalanced recurrence on stability. Phase diagrams showing the real part of the largest eigenvalue λ of the Jacobian at the fixed point in the (z, Δ) plane for varying levels of E-I imbalance, controlled by the mean μ of the recurrent weights K_{ij}. Each panel corresponds to a different value of μ (see discussion in the text): (**a**), $\mu = 0.0$ (balanced, identical to Fig. 3.9); excess excitation: (**b**), $\mu = 0.05$, (**c**), $\mu = 0.1$, (**d**), $\mu = 0.25$, (**e**), $\mu = 0.5$, (**f**), $\mu = 1.0$; excess inhibition: (**g**), $\mu = -0.1$, (**h**), $\mu = -0.5$, (**i**), $\mu = -1.0$. Color represents the maximum λ across 100 trials (for $n = 100$, $\sigma = 0.1$, $\tau_y = \tau_a$, delocalized input $z_i = z/\sqrt{n}$). Blue open circles mark the numerically determined onset of critical slowing down, while red crosses indicate the numerically determined loss of normalization. The dashed red curves show the analytical prediction for loss of normalization. Dashed black curves delineate boundaries between the limit cycle (gray region) and the unstable (white region) regimes, where instability is defined as trajectories diverging in at least 50% of trials.

slowing down across all values of μ.

We also examined how E-I imbalance affects the oscillation frequencies in ORGaNICs (Fig. 3.12). Upon increasing excitation ($\mu > 0$), the region exhibiting high-frequency oscillations (gamma

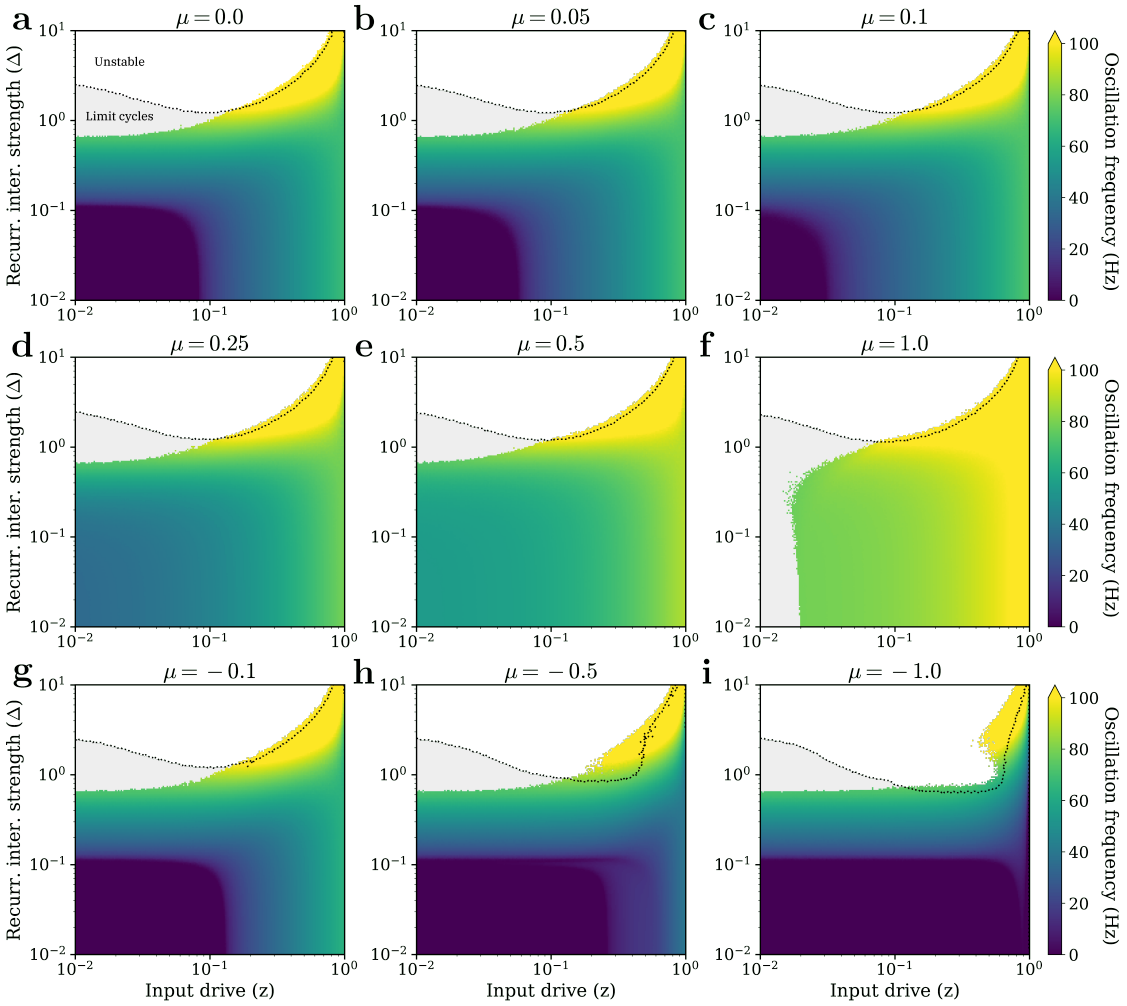


Figure 3.12: Effect of E-I imbalanced recurrence on oscillation frequency. Phase diagrams depicting the average oscillation frequency (calculated as mean of $\mathrm{Im}(\lambda_J)/(2\pi)$ across trials) as a function of input drive z and recurrent interaction strength Δ for varying levels of E-I imbalance μ. Parameters are $n = 100$, $\sigma = 0.1$, $\tau_y = \tau_a = 2$ ms, delocalized input $z_i = z/\sqrt{n}$. Panels correspond to: (**a**), $\mu = 0.0$; excess excitation: (**b**), $\mu = 0.05$, (**c**), $\mu = 0.1$, (**d**), $\mu = 0.25$, (**e**), $\mu = 0.5$, (**f**), $\mu = 1.0$; excess inhibition: (**g**), $\mu = -0.1$, (**h**), $\mu = -0.5$, (**i**), $\mu = -1.0$. Dotted black curves delineate boundaries between the limit cycle (gray region) and the unstable (white region) regimes, where instability is defined as trajectories diverging in at least 50% of trials. Overall, increasing excitation ($\mu > 0$) generally promotes higher oscillation frequencies, especially at small input drives. While increasing inhibition ($\mu < 0$) promotes lower oscillation frequencies, especially at large input drives.

band and higher) expands. For strong excitation (e.g., $\mu = 1.0$), the network tends to oscillate at high frequencies across a wider range of Δ and z values. This suggests that net excitation in the recurrent connections promotes faster oscillations. On the contrary, increasing inhibition

(Fig. 3.12g,h,i) ($\mu < 0$) promotes slower oscillations, especially at large input drives.

3.7 Discussion

We have established, via numerical experiments and analytical calculation, that: *(i)* the nonlinear modulation of recurrent interactions via inhibitory neurons implementing divisive normalization makes neural networks more stable than unmodulated recurrent linear models; *(ii)* the breakdown of normalization, due to substantial recurrent amplification which is not compensated by an equally strong input drive, occurs concomitantly with the onset of critical slowing down in a broad class of random neural networks.

Our results demonstrate that, at low input drives, increasing the recurrent synaptic strength turns the fixed point into a spiral attractor, as indicated by the damped oscillations in Fig. 3.4c and Fig. 3.10. Crucially, the oscillations begin at the same parameter conditions where we observe the loss of normalization and onset of critical slowing down. This suggests a strong link between these phenomena. Consequently, the detection of such recurrence-driven oscillations under a weak input drive could provide an experimental signature of a non-normalized neural circuit nearing a critical transition. For example, experimental evidence suggests that neural circuits in individuals with autism spectrum disorder exhibit both failure of normalization [84, 85] and excess variability (i.e., near the tipping point of instability) [86, 87]. Hence, we predict that such neural circuits will also exhibit critical slowing down, which can be measured as the elapsed time to reach steady state. Increased neural variability and noise correlations, measured across trials of the same stimulus presentation, are also characteristic markers of critical slowing down (see Appendix B.4 for discussion).

We noticed that, in the whole phase of critical slowing down, the spectrum of the Jacobian contains a large number of zero eigenvalues in the large n limit, corresponding to the emergence of multiple long time scales. Recently, it has been noted [88] that generating many long time

scales in linear models requires fine tuning of the recurrent weights. In our model, many long time scales emerge for a broad range of values of the recurrent interaction strength, hence without fine tuning, suggesting that normalization (or other similar forms of multiplicative inhibitory modulation) might be the key mechanism to generate a full spectrum of slow modes in brain dynamics.

4 | ORGaNICs as a Machine Learning Architecture

4.1 Overview

This chapter demonstrates the utility of ORGaNICs as a versatile machine learning architecture, showcasing its application as both multi-layer perceptrons (MLPs) and recurrent neural networks (RNNs). The key results presented are based on findings published in [51].

Stability in recurrent neural models poses a significant challenge, particularly in developing biologically plausible neurodynamical models that can be seamlessly trained. Traditional cortical circuit models often prove difficult to train due to their complex nonlinear dynamics, which translate into optimization problems with nonlinear stability constraints that are challenging to enforce. Conversely, recurrent neural networks (RNNs) excel in tasks involving sequential data but lack biological plausibility and interpretability. We posit that the inherent stability and emergent slow timescales of ORGaNICs facilitate straightforward training; address the problems of exploding, vanishing, and oscillating gradients; and enable competitive performance against traditional RNNs. Consequently, we demonstrate that ORGaNICs can be trained effectively using backpropagation through time without the need for gradient clipping or scaling. Furthermore, by evaluating the model's performance on RNN benchmarks, we find that ORGaNICs outperform alternative neurodynamical models on static image classification tasks and achieve performance

comparable to LSTMs on sequential tasks.

4.2 Introduction

Deep neural networks (DNNs) have found widespread use in modeling tasks from experimental systems neuroscience. The allure of DNN-based models lies in their ease of training and the flexibility they offer in architecting systems [89–91]. In contrast, neurodynamical models like the Wilson-Cowan [12] or the Stabilized Supralinear Network (SSN) [13] are more biologically plausible than DNNs, but these models confront considerable training challenges due to the lack of stability guarantees for high-dimensional problems. Training recurrent neural networks (RNNs), by comparison, is more straightforward thanks to ad hoc regularization techniques like layer normalization, batch normalization, and gradient clipping/scaling, which help stabilize training without imposing strict stability constraints. Conversely, neurodynamical models require enforcing hard stability constraints while maintaining biological plausibility. In lower dimensions, it is relatively straightforward to derive constraints on model parameters that ensure a dynamically stable system [92, 93]. However, for high-dimensional systems, integrating these hard constraints into the optimization problem is significantly more complex [94, 95]. Stability is generally advantageous in DNNs, as it is linked to improved generalization, mitigation of exploding gradient problems, increased robustness to input noise, and simplified training techniques [96].

Normalization techniques have been extensively adopted for training DNNs, demonstrating their ability to stabilize, accelerate training, and enhance generalization [97–99]. Divisive normalization can be viewed as a comprehensive normalization strategy, with batch and layer normalization being specific instances [100]. Models implementing DN have shown superior performance compared to common normalization methods (Batch [97], Layer [98], Group [101]) in tasks such as image recognition with convolutional neural networks (CNNs) [102] and language modeling with RNNs [100, 103]. Despite the foundational role of these techniques in deep learning

algorithms, their implementation is ad hoc, limiting their conceptual relevance. They serve as practical solutions addressing the limitations of current machine learning frameworks rather than offering principled insights derived from understanding cortical circuits.

ORGaNICs can be viewed as biophysically plausible extensions of Long Short Term Memory units (LSTMs) [91] and Gated Recurrent Units (GRUs) [104], RNN architectures that have been widely used in ML applications [91, 105–108]. The main differences are that ORGaNICs operate in continuous time and have built-in dynamic normalization (via recurrent gain modulation) and built-in attention (via input gain modulation). Thus, we expect that ORGaNICs should be able to solve relatively sophisticated tasks [15]. Here, we demonstrate (Section 4.5) that by virtue of their intrinsic stability, ORGaNICs can be trained on sequence modeling tasks by Backpropagation Through Time (BPTT), in the same manner as traditional RNNs (unlike SSN that instead requires costly specialized training strategies [109]), despite implementing power-law activations [13]. Moreover, we show that ORGaNICs trained by naive BPTT (i.e., without gradient clipping/scaling or other ad hoc strategies) achieve performance comparable to LSTMs on the tasks that we consider, despite no systematic hyperparameter tuning.

4.3 ORGaNICs with Rectification in the Recurrence Term

We investigate the impact of including only *principal neurons with positive receptive fields*, i.e., we set $\mathbf{y}^- = \mathbf{0}$ in Eq. (1.9). This yields the following dynamical system:

$$\begin{aligned} \boldsymbol{\tau}_y \odot \dot{\mathbf{y}} &= -\mathbf{y} + \mathbf{b} \odot \mathbf{z} + \left(\mathbf{1} - \mathbf{a}^+\right) \odot \left(\mathbf{W}_r \lfloor \mathbf{y} \rfloor\right) \\ \boldsymbol{\tau}_a \odot \dot{\mathbf{a}} &= -\mathbf{a} + \mathbf{b}_0^2 \odot \boldsymbol{\sigma}^2 + \mathbf{W} \left(\mathbf{y}^+ \odot \lfloor \mathbf{a} \rfloor\right) \end{aligned} \tag{4.1}$$

While a linear stability analysis for this high-dimensional system is intractable, the special case of $\mathbf{W}_r = \mathbf{I}$ becomes analytically tractable and can be shown to be unconditionally stable (Appendix C.1), exhibiting properties similar to the model in Chapter 2 (Eq. (2.1)).

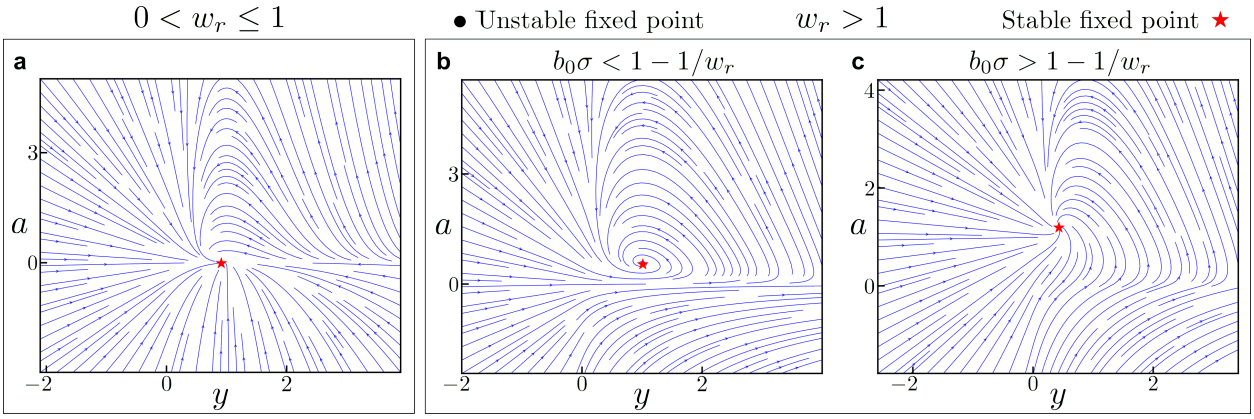


Figure 4.1: Phase portraits for 2D rectified ORGaNICs with a positive input drive z. We plot the phase portraits of 2D rectified ORGaNICs (Eq. (4.2)) in the vicinity of the stable fixed points for contractive (**a**) and expansive (**b, c**) recurrence scalar w_r. Red stars and black circles indicate stable and unstable fixed points, respectively. The parameters for all plots are: $b = 0.5$, $\tau_a = 2$ ms, $\tau_y = 2$ ms, $w = 1.0$, and $z = 1.0$. For **(a)**, the parameters are $w_r = 0.5$, $b_0 = 0.5$, $\sigma = 0.1$; for **(b)**, $w_r = 2.0$, $b_0 = 0.5$, $\sigma = 0.1$; and for **(c)**, $w_r = 2.0$, $b_0 = 1.0$, $\sigma = 1.0$. We find that a stable fixed point always exists across all parameter values.

Furthermore, for the two-dimensional model:

$$\begin{aligned} \tau_y \dot{y} &= -y + bz + \left(1 - \sqrt{\lfloor a \rfloor}\right) w_r \lfloor y \rfloor \\ \tau_a \dot{a} &= -a + b_0^2 \sigma^2 + w \lfloor y \rfloor^2 \lfloor a \rfloor, \end{aligned} \tag{4.2}$$

we prove its unconditional stability even when $w_r \neq 1$ (see Appendix C.1.3 for the proof). This result shares similarities with the model discussed in Chapter 3 (Eq. (3.2)), but with a crucial distinction: for a positive input drive z, while both models are unconditionally stable, the model in Eq. (4.2) admits only stable fixed points (Fig. 4.1). In contrast, the model in Eq. (3.2) can admit both stable and unstable fixed points for certain values of w_r (Fig. 3.1). This inherent stability in the rectified model is highly advantageous for the design of Recurrent Neural Networks (RNNs) based on ORGaNICs, as it reduces the presence of undesirable diverging trajectories within the dynamical system.

To understand the stability of the high-dimensional system (Eq. (4.1)), we use specific parameter

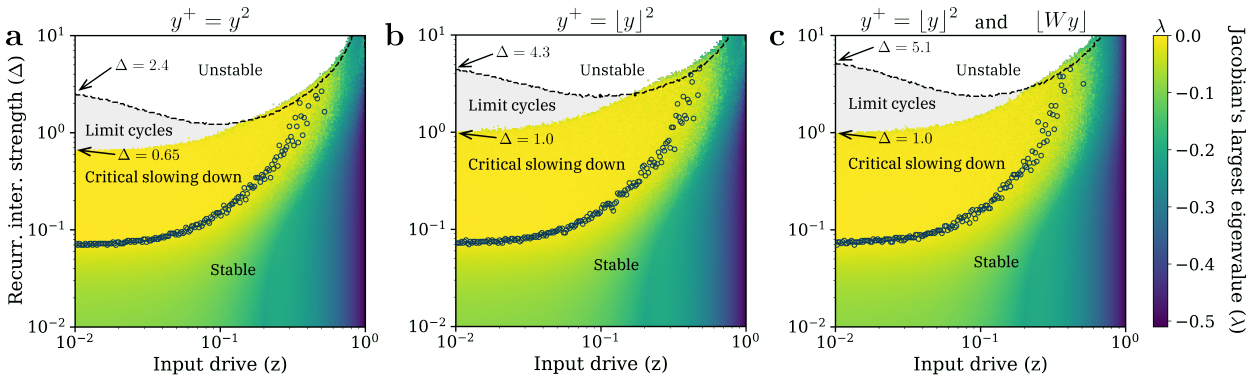


Figure 4.2: Effect of rectification on network stability. Phase diagram in the parameter space of input drive z and recurrent interaction strength Δ (mesh size 200×200). Color represents the maximum value (across 100 trials) of the Jacobian's eigenvalue with the largest real part (λ). The input type and the parameters of ORGaNICs are the same as those used for generating Fig. 3.9. The panels correspond to: **a**, Model with quadratic activation ($y^+ = y^2$), identical to the phase diagram in Fig. 3.9. **b**, Model with rectification in the activation function ($y^+ = \lfloor y \rfloor^2$, Eq. (4.3)). **c**, Model with rectification applied in both the activation function and after the recurrent summation ($y^+ = \lfloor y \rfloor^2$ and $\lfloor Wy \rfloor$ term, Eq. (4.4)). We observe that the boundaries marking the transition from critical slowing down to limit cycles, and from limit cycles to unstable dynamics (indicated by dashed curves), shift upwards in going from **a** to **b** to **c**.

choices (consistent with Eq. (3.3)), resulting in the following dynamical system:

$$\begin{cases} \tau_y \dot{y}_i = -y_i + z_i + \left(1 - \sqrt{\lfloor a \rfloor}\right) \sum_{j=1}^{n} W_{rij} \lfloor y \rfloor_i \\ \tau_a \dot{a} = -a + \sigma^2 + \left(\sum_{i=1}^{n} \lfloor y \rfloor_i^2 \right) \lfloor a \rfloor. \end{cases} \tag{4.3}$$

We analyze the stability of this system by examining its phase diagram (similar to Fig. 3.9) in the parameter space of input drive (z) and recurrent interaction strength (Δ), as shown in Fig. 4.2b. We also investigated an alternative placement for rectification: applying it *after* the weighted recurrent inputs are summed in the dynamical equation for y. This leads to the following dynamical system (with its corresponding phase diagram in Fig. 4.2c):

$$\begin{cases} \tau_y \dot{y}_i = -y_i + z_i + \left(1 - \sqrt{\lfloor a \rfloor}\right) \left\lfloor \sum_{j=1}^{n} W_{rij} y_i \right\rfloor \\ \tau_a \dot{a} = -a + \sigma^2 + \left(\sum_{i=1}^{n} \lfloor y \rfloor_i^2 \right) \lfloor a \rfloor \,, \end{cases} \tag{4.4}$$

Our findings indicate that these alternative forms of rectification do not qualitatively alter the network's phase diagram. However, the boundaries that mark the transition from critical slowing down to limit cycles, and from limit cycles to unstable dynamics, shift towards larger values of Δ when moving from panel (a) to (b) to (c) in Fig. 4.2. This means that introducing rectification increases the range of parameters for which the neuron's trajectories remain bounded (including the limit cycle regime). This is crucial for designing RNN architectures based on ORGaNICs, as our goal is to maximize the parameter space that admits stable dynamics. Numerical evidence strongly suggests that applying rectification *after* the summation of weighted recurrent inputs (Eq. (4.4)) yields a model with more favorable stability properties, described by:

$$\begin{aligned} \boldsymbol{\tau}_y \odot \dot{\mathbf{y}} &= -\mathbf{y} + \mathbf{b} \odot \mathbf{z} + \left(\mathbf{1} - \sqrt{\lfloor \mathbf{a} \rfloor}\right) \odot \lfloor \mathbf{W}_r \mathbf{y} \rfloor \\ \boldsymbol{\tau}_a \odot \dot{\mathbf{a}} &= -\mathbf{a} + \mathbf{b}_0^2 \odot \boldsymbol{\sigma}^2 + \mathbf{W} \left(\lfloor \mathbf{y} \rfloor^2 \odot \lfloor \mathbf{a} \rfloor \right). \end{aligned} \tag{4.5}$$

Consequently, we adopt this set of coupled differential equations for designing an RNN based on ORGaNICs in Section 4.5.2.

4.4 Related Work

Trainable biologically plausible neurodynamical models: There have been several attempts to develop neurodynamical models that mimic the function of biological circuits and that can be trained on cognitive tasks. Song et al. [110] incorporated Dale's law into the vanilla RNN architecture, which was successfully trained across a variety of cognitive tasks. Building on this, Soo et al. [111] developed a technique for such RNNs to learn long-term dependencies

by using skip connections through time. ORGaNICs is a model that is already built on biological principles and can learn long-term dependencies intrinsically by tuning the (intrinsic or effective) time constants, therefore, it does not require the method used in [111]. Soo et al. [109] introduced a novel training methodology (dynamics-neural growth) for SSNs and demonstrated its utility for tasks involving static (time-independent) stimuli. However, this training approach is costly and difficult to scale (because high-dimensional SSNs with randomly sampled weights, unlike ORGaNICs, are not stable), and its applicability to tasks with dynamically changing inputs remains unclear.

Dynamical systems view of RNNs: The stability of continuous-time RNNs has been extensively studied and discussed in a comprehensive review by Zhang et al. [112]. Recent advancements have focused on designing architectures that address the issues of vanishing and exploding gradients, thereby enhancing trainability and performance. A central idea in these designs is to achieve better trainability and generalization by ensuring the dynamical stability of the network. Moreover, to avoid the problem of vanishing gradients, the key idea is to constrain the real part of the eigenvalues of the linearized dynamical system to be close to zero, which facilitates the propagation and retention of information over long durations of time. Chang et al. [113] and Erichson et al. [114] achieve this by imposing an antisymmetric constraint on the recurrent weight matrix. Meanwhile, Rusch et al. [115, 116] propose an architecture based on coupled damped harmonic oscillators, resulting in a second-order system of ordinary differential equations that behaves similarly to how ORGaNICs behave in the vicinity of the normalization fixed point, as shown in Chapter 2. Despite their impressive performance on various sequential data benchmarks, these models lack biological plausibility due to their use of saturating nonlinearities (instead of normalization) and unrealistic weight parameterizations.

4.5 Experiments

We now demonstrate that ORGaNICs can serve as efficient and high-performing ML architectures, trainable via naïve BPTT on two distinct tasks: 1) static classification of MNIST, and 2) sequential classification of pixel-by-pixel MNIST. Given that these specific ML tasks do not directly pertain to neurobiological or cognitive processes, we relax one aspect of ORGaNICs' biological plausibility by allowing arbitrary (learned) non-negative values for the intrinsic time constants.[1]

4.5.1 Static Input Classification Task

We first show that we can train ORGaNICs on the MNIST handwritten digit dataset [117] presented to the circuit as a static input. This setting corresponds to evolving the responses of the neurons dynamically until they reach a fixed point solution and using the steady-state firing rates of the principal neurons to predict the labels, akin to deep equilibrium models [118]. While the fixed point of the circuit (Eq. (3.1)) is known when $\mathbf{W}_r = \mathbf{I}$, we allow $\mathbf{W}_r$ to be learnable and parameterize it to have a maximum singular value of 1. This constraint allows us to find the fixed point responses of all the neurons without simulation, using a fixed point iteration scheme (Algorithm 1) that converges with great accuracy in a few (less than 5) steps, see Fig. 4.3. The rationale for this algorithm's efficacy, supported by empirical evidence of its rapid convergence, is detailed in Appendix C.2.

We trained ORGaNICs on this task and compared its performance to SSN [13] trained by dynamics-neutral growth [109]. We found that ORGaNICs perform better than SSN with the same model size, and on par with an MLP (Table 4.1).

For training, we performed a random split of 57,000 training samples and 3,000 validation samples and picked the model with the largest validation accuracy for testing. To make a direct comparison to SSN [109], we use the same architecture structure as theirs. First, we train an

[1] Python code for this study is available at https://github.com/martiniani-lab/dynamic-divisive-norm.

Algorithm 1 Iterative scheme for the fixed point when the maximum singular value of $\mathbf{W}_r$ is 1

Input: ORGaNICs parameters, input $(\mathbf{z})$, tolerance (ϵ), maximum iterations (N)
Output: Approximation to the fixed point $(\mathbf{y}_s, \mathbf{a}_s)$
$\mathbf{a} \leftarrow \boldsymbol{\sigma}^2 \odot \mathbf{b}_0^2 + \mathbf{W}\ (\mathbf{W}_r\ (\mathbf{b} \odot \mathbf{z}))^2$ // initial approximation for a neurons
$\mathbf{y} \leftarrow (\mathbf{W}_r\ (\mathbf{b} \odot \mathbf{z}))\ /\sqrt{\mathbf{a}}$ // initial approximation for y neurons
$k \leftarrow 0$
while $||\mathbf{y} - \mathbf{b} \odot \mathbf{z} - \left(1 - \sqrt{\mathbf{a}}\right) \odot (\mathbf{W}_r \mathbf{y})\ || > \epsilon$ and $k < N$ **do**
    $\mathbf{y} \leftarrow \left(\mathbf{I} - \mathbf{W}_r + \mathbf{D}\left(\sqrt{\mathbf{a}}\right) \mathbf{W}_r\right)^{-1} (\mathbf{b} \odot \mathbf{z})$ // y neurons update
    $\mathbf{a} \leftarrow \mathbf{b}_0^2 \odot \boldsymbol{\sigma}^2 + \mathbf{W}\ \left(\mathbf{y}^2 * \mathbf{a}\right)$ // a neurons update
    $k \leftarrow k + 1$
end while
return $(\mathbf{y}, \mathbf{a})$

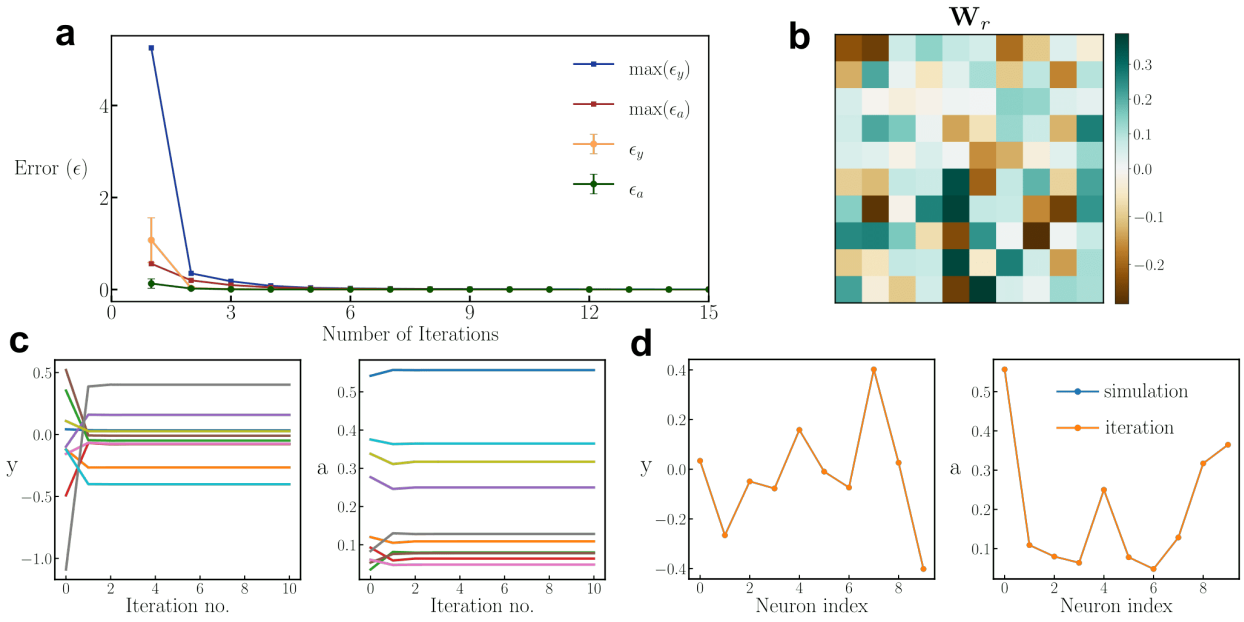


Figure 4.3: Fast convergence of the iterative algorithm. The results are for 20-dimensional ORGaNICs (10 y and 10 a neurons) with random parameters and inputs with the additional constraint of the maximum singular value of $\mathbf{W}_r$ equal to 1 and $||\mathbf{z}|| < 1$. **(a)**, Mean (with error bars representing 1-sigma S.D.) and maximum errors (ϵ) as a function of number of iterations. ϵ is calculated as the norm of the difference between the true solution (found by simulation starting with random initialization) and the iteration solution. **(b)**, An example of a randomly sampled $\mathbf{W}_r$. **(c)**, Steady-state approximation as a function of iteration number. Different lines represent different neurons. **(d)**, Overlap between the iteration solution (after 15 iterations) and the true solution.

autoencoder (Table 4.2) to reduce the dimensionality of MNIST images to 40 by using a mean-squared loss function. Then, we use this 40-dimensional vector as input to ORGaNICs and train it

Table 4.1: Test accuracy on MNIST dataset

Model	Accuracy
SSN (50:50)	94.9%
SSN (80:20)	95.2%
MLP (50)	98.2%
ORGaNICs (50:50)	98.1%
ORGaNICs (80:80)	98.2%
ORGaNICs (two layers)	98.1%

using the cross-entropy loss function. We additionally make the input gain $\mathbf{b}$ dependent on the input $\mathbf{x}$, $\mathbf{b} = f(\mathbf{W}_{bx}\mathbf{x})$, where f is sigmoid. A layer of ORGaNICs is then given by,

$$\begin{aligned} \boldsymbol{\tau}_y \odot \dot{\mathbf{y}} &= -\mathbf{y} + f(\mathbf{W}_{bx}\mathbf{x}) \odot (\mathbf{W}_{zx}\mathbf{x}) + \left(\mathbf{1} - \sqrt{\lfloor \mathbf{a} \rfloor}\right) \odot (\mathbf{W}_r \mathbf{y}) \\ \boldsymbol{\tau}_a \odot \dot{\mathbf{a}} &= -\mathbf{a} + \mathbf{b}_0^2 \odot \boldsymbol{\sigma}^2 + \mathbf{W}\ \left(\mathbf{y}^2 \odot \lfloor \mathbf{a} \rfloor\right) \end{aligned} \tag{4.6}$$

The "output" of a layer is the steady-state firing rate of the neuron with the positive receptive field, i.e., $\mathbf{y}_s^+ = \lfloor \mathbf{y}_s \rfloor^2$. Details about the parameters are given in Table 4.3; kaiming uniform initialization is used from [119]. Additional hyperparameters are given in Table 4.5. We train ORGaNICs in a single-layer setting (i.e., one hidden layer) with the number of $\mathbf{y}$ neurons encoding the input, $N_1 = 50, 80$. We also train two-layer ORGaNICs (Table 4.4) with $N_1 = 120$ and $N_2 = 60$ neurons in each layer. The model is trained using backpropagation and takes approximately 10 min to fully train.

Table 4.2: Autoencoder architecture

Layer	**Shape**	**Nonlinearity**
Input ⟶ encoder (layer-1)	784×360	ReLU
encoder (layer-1) ⟶ encoder (layer-2)	360×120	ReLU
encoder (layer-2) ⟶ embedding	120×40	sigmoid
embedding ⟶ decoder (layer-1)	40×120	ReLU
decoder (layer-1) ⟶ decoder (layer-2)	120×360	ReLU
decoder (layer-2) ⟶ output	360×784	sigmoid

Table 4.3: ORGaNICs parametrization for static MNIST classification

Parameter	Shape	Learned	Initialization
$\mathbf{W}_{zx}$	$N \times M$	yes	kaiming uniform
$\mathbf{W}_{bx}$	$N \times M$	yes	kaiming uniform
$\mathbf{W}_r$	$N \times N$	yes	identity
$\mathbf{W}$	$N \times N$	yes	ones
$\mathbf{b}_0$	N	yes	random normal
$\boldsymbol{\sigma}$	N	no	ones

Table 4.4: ORGaNICs architecture for static MNIST classification

Layer	Shape	Nonlinearity
Input $\longrightarrow$ ORGaNICs (layer-1)	$40 \times N_1$	None
ORGaNICs (layer-1) $\longrightarrow$ ORGaNICs (layer-2)	$N_1 \times N_2$	None
ORGaNICs (layer-2) $\longrightarrow$ fully-connected	$N_2 \times 10$	None

We analyzed the eigenvalues of the Jacobian matrix of the trained model and consistently found the largest real part to be negative (Fig. 4.4), indicating stability. Moreover, we found that stability was maintained during training (Fig. 4.5).

4.5.2 Time Varying Input

We trained unconstrained ORGaNICs, i.e., we set all parameters (including $\mathbf{W}_r$) to be trainable, by naïve BPTT on a classification task of sequential MNIST (sMNIST), proposed by Le et al. [120]. This is a challenging task because it involves long-term dependencies and requires the architecture to maintain and integrate information over long timescales. Briefly, the task involves the presentation of pixels of MNIST images sequentially (one pixel for each timestep) in scanline order, and at the end of the input, the model has to predict the digit that was presented. There is a more complicated version of this task, permuted sequential MNIST, in which the pixels of all images are permuted in some random order before being presented sequentially.

We train ORGaNICs with different hidden layer sizes (number of $\mathbf{y}$ neurons) on these two tasks by discretizing the rectified ORGaNICs with arbitrary recurrence, Eq. (4.5). The hidden states of

Table 4.5: Hyperparameters

Hyperparameter	Static MNIST	Sequential MNIST
Batch size	256	256
Initial Learning rate	0.001	0.01
Weight decay	10^{-5}	10^{-5}
Step size (StepLR)	None	30 epochs
Gamma (StepLR)	None	0.8

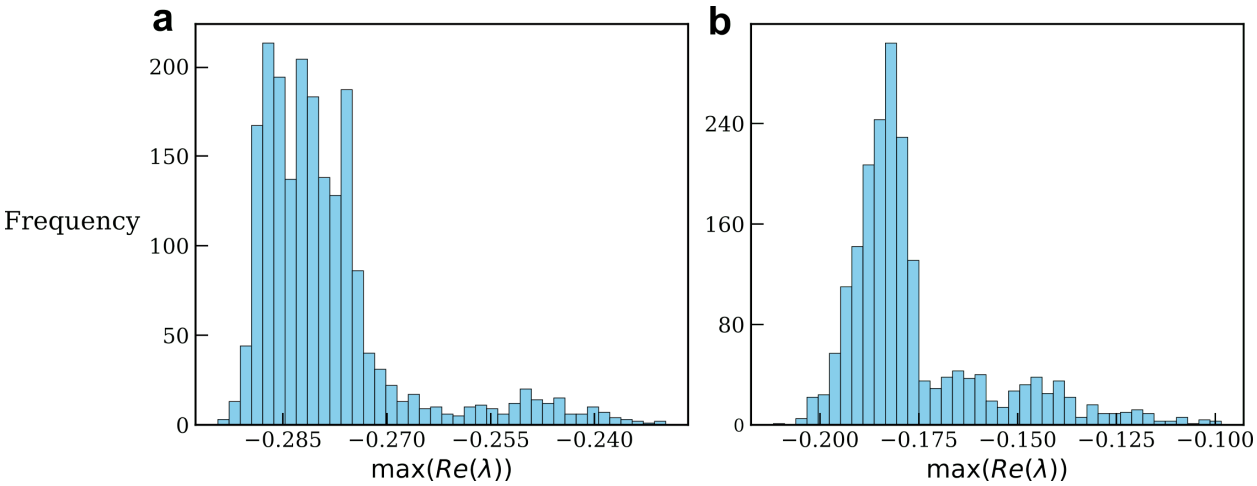


Figure 4.4: Histogram for the eigenvalue with the largest real part. We train two-layer ORGaNICs ($\tau_a = \tau_y = 2$ ms) with a static MNIST input where $\mathbf{W}_r$ is constrained to have a maximum singular value of 1. We plot the histogram of eigenvalues of the Jacobian matrix with the largest real part, for inputs from the test set. We find that all the eigenvalues of the Jacobian have negative real parts, implying asymptotic stability. **(a)**, histogram for the first layer. **(b)**, histogram for the second layer. Note that since this is implemented in a feedforward manner, this is a cascading system with no feedback, hence, we can perform the stability analysis of the two layers independently.

the neurons are initialized with a uniform random distribution. Additionally, we make the input gains $\mathbf{b}$ and $\mathbf{b}_0$ dynamical with their ODEs given by,

$$\begin{aligned} \boldsymbol{\tau}_b \odot \dot{\mathbf{b}} &= -\mathbf{b} + f(\mathbf{W}_{bx}\mathbf{x} + \mathbf{W}_{by}\mathbf{y} + \mathbf{W}_{ba}\mathbf{a}) \\ \boldsymbol{\tau}_{b_0} \odot \dot{\mathbf{b}_0} &= -\mathbf{b}_0 + f(\mathbf{W}_{b_0x}\mathbf{x} + \mathbf{W}_{b_0y}\mathbf{y} + \mathbf{W}_{b_0a}\mathbf{a}), \end{aligned} \tag{4.7}$$

where f is sigmoid. We performed a random split of 57,000 training samples and 3,000 validation samples and picked the model with the largest validation accuracy for testing. The unpermuted

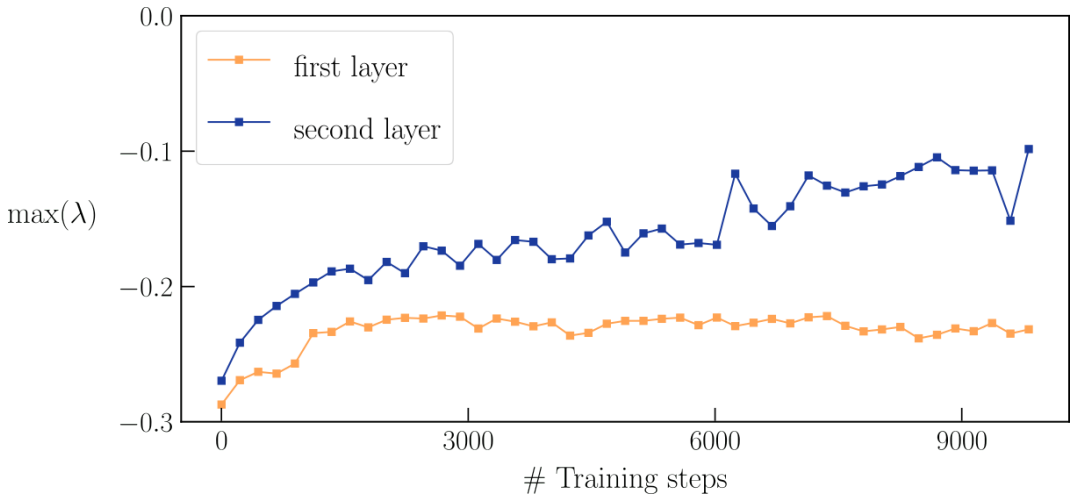


Figure 4.5: Eigenvalue with the largest real part while training on static input (MNIST) classification task. This plot shows the largest real part of eigenvalues across all test samples as training progresses. The fact that the largest real part consistently remains below zero indicates that the system maintains stability throughout training.

sequential MNIST task is defined as follows: for a given 28×28 image, we flatten it to get a one-dimensional, 784 timestep-long input. Then these pixels are presented as an input ($\mathbf{x}_i$, one pixel at each time-step i) to the Euler discretized rectified ORGaNICs model with rectified input drive, given by the following equations,

$$\begin{aligned}
\mathbf{y}_{i+1} &= \mathbf{y}_i + \frac{\Delta t}{\boldsymbol{\tau}_y} \odot \left(-\mathbf{y}_i + \mathbf{b}_i \odot \lfloor \mathbf{W}_{zx}\mathbf{x}_i \rfloor + \left(1 - \sqrt{\lfloor \mathbf{a}_i \rfloor}\right) \odot \lfloor \mathbf{W}_r \mathbf{y}_i \rfloor\right) \\
\mathbf{a}_{i+1} &= \mathbf{a}_i + \frac{\Delta t}{\boldsymbol{\tau}_a} \odot \left(-\mathbf{a}_i + \mathbf{b}_{0,i}^2 \odot \boldsymbol{\sigma}^2 + \mathbf{W}\ \left(\lfloor \mathbf{y}_i \rfloor^2 \odot \lfloor \mathbf{a}_i \rfloor\right)\right) \\
\mathbf{b}_{i+1} &= \mathbf{b}_i + \frac{\Delta t}{\boldsymbol{\tau}_b} \odot \left(-\mathbf{b}_i + f(\mathbf{W}_{bx}\mathbf{x}_i + \mathbf{W}_{by}\mathbf{y}_i + \mathbf{W}_{ba}\mathbf{a}_i)\right) \\
\mathbf{b}_{0,i+1} &= \mathbf{b}_{0,i} + \frac{\Delta t}{\boldsymbol{\tau}_{b_0}} \odot \left(-\mathbf{b}_{0,i} + f(\mathbf{W}_{b_0 x}\mathbf{x}_i + \mathbf{W}_{b_0 y}\mathbf{y}_i + \mathbf{W}_{b_0 a}\mathbf{a}_i)\right)
\end{aligned} \tag{4.8}$$

Upon completion of the pixel sequence presentation, the final hidden state, $\mathbf{y}_{784}$, is used for prediction. To further evaluate the model on a more demanding task, we also trained ORGaNICs on permuted sMNIST, where pixels across all images are first permuted according to a fixed random order, with other task aspects remaining unchanged. Instead of directly parametrizing

Table 4.6: ORGaNICs parametrization for sequential MNIST classification

Parameter	Shape	Learned	Initialization
$\mathbf{W}_{zx}$	$N \times 1$	yes	kaiming uniform
$\mathbf{W}_{bx}$	$N \times 1$	yes	kaiming uniform
$\mathbf{W}_{by}$	$N \times N$	yes	kaiming uniform
$\mathbf{W}_{ba}$	$N \times N$	yes	kaiming uniform
$\mathbf{W}_{b_0x}$	$N \times 1$	yes	kaiming uniform
$\mathbf{W}_{b_0y}$	$N \times N$	yes	kaiming uniform
$\mathbf{W}_{b_0a}$	$N \times N$	yes	kaiming uniform
$\mathbf{W}_r$	$N \times N$	yes	identity
$\mathbf{W}$	$N \times N$	yes	ones
$\boldsymbol{\sigma}$	N	no	ones

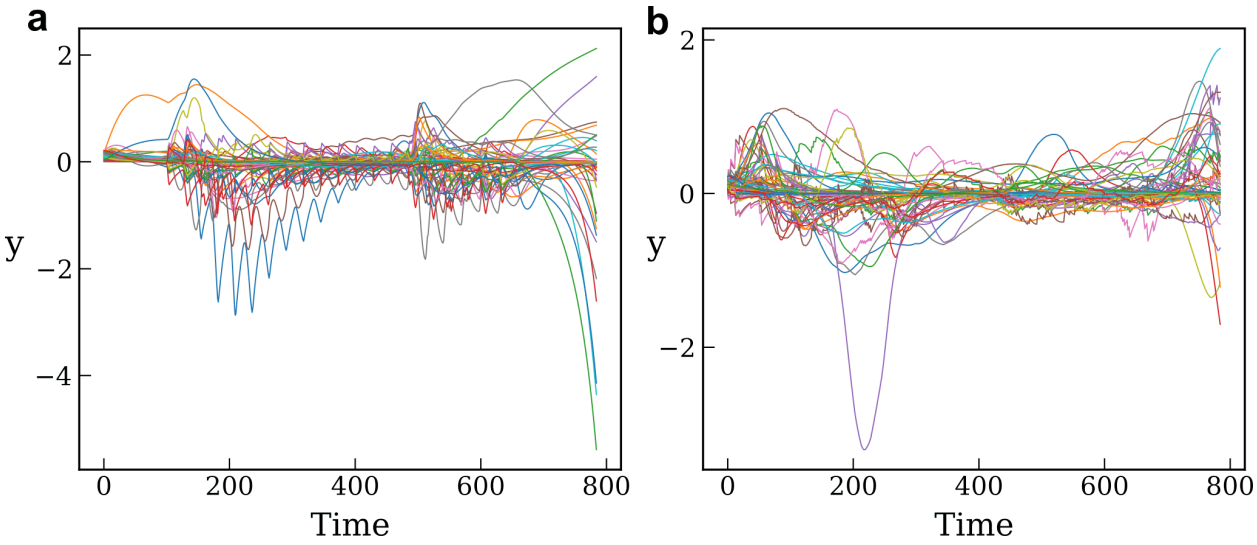


Figure 4.6: Trajectories of the hidden states (y). This plot shows the dynamics of the hidden state as the input is being presented sequentially. We train ORGaNICs (128 units) as an RNN on **(a)**, unpermuted sequential MNIST and **(b)**, permuted sequential MNIST. The inputs are picked randomly from the test set. The hidden state trajectory remains bounded, indicating stability.

$\boldsymbol{\tau}$, we parametrize $\Delta t/\boldsymbol{\tau}_y = 0.05 * f(\mathbf{p}_y)$, $\Delta t/\boldsymbol{\tau}_a = 0.01 * f(\mathbf{p}_a)$ and $\Delta t/\boldsymbol{\tau}_b = 0.1 * f(\mathbf{p}_b)$ and $\Delta t/\boldsymbol{\tau}_{b_0} = 0.1 * f(\mathbf{p}_{b_0})$, where $\mathbf{p}_i$ represent the free parameters, enabling control over dimensionless relative time constants. Empirically, we observed that rendering the **a** neurons more sluggish compared to **y** improved performance, a heuristic supported by the two-dimensional phase portraits for varying relative time constants (Fig. 2.1). All parameters, including $\mathbf{W}_r$, were unconstrained

Table 4.7: Test accuracy on sequential pixel-by-pixel MNIST and permuted MNIST

Model	sMNIST	psMNIST	# units	# params
LSTMs [121]	97.3%	92.6%	128	68k
AntisymmetricRNN [113]	98.0%	95.8%	128	10k
coRNN [115]	99.3%	96.6%	128	34k
Lipschitz RNN [114]	99.4%	96.3%	128	34k
ORGaNICs (fixed time constants)	90.3%	80.3%	64	26k
ORGaNICs (fixed time constants)	94.8%	84.8%	128	100k
ORGaNICs	97.7%	89.9%	64	26k
ORGaNICs	97.8%	90.7%	128	100k

for this task, with initializations specified in Table 4.6. Due to the inherent stability of ORGaNICs, gradient clipping—a common requirement for training LSTMs was unnecessary. The model was trained using a StepLR learning rate scheduler (parameters in Table 4.5) via BPTT, requiring approximately 30 hours for full training.

We achieved slightly better performance than LSTMs on sMNIST with a smaller model size and comparable performance on permuted sMNIST, without hyperparameter optimization and without gradient clipping/scaling (Table 4.7). We found that the trajectories of $\mathbf{y}$ are bounded when it is trained on the sequential task (Fig. 4.6), indicating stability. We also show that the training of ORGaNICs is stable and does not require gradient clipping when the intrinsic time constants of the neurons are fixed (Table 4.7).

4.6 Discussion

While extensive research has been aimed at identifying highly expressive RNN architectures that can model complex data, there has been little advancement in developing robust, biologically plausible recurrent neural circuits that are easy to train and perform comparably to their artificial counterparts. Regularization techniques such as batch, group, and layer normalization have been developed and are implemented as ad hoc add-ons making them biologically implausible. Further,

these strategies can only be applied between layers and do not influence the computation within the layers. In this work, we bridge these gaps by leveraging the recently proposed ORGaNICs model, which implements divisive normalization (DN) dynamically in a recurrent circuit. Since ORGaNICs remain stable for a wide range of parameter values and inputs, we do not need to resort to techniques that are restrictive in parameter space or that require designing unrealistic structures for weight matrices. ORGaNICs' intrinsic stability mitigates the issues of exploding and oscillating gradients, enabling the use of "vanilla" BPTT without the need for gradient clipping, which is instead required when training LSTMs. ORGaNICs also effectively tackle the vanishing gradient problem prevalent in RNN training. This is facilitated by their capacity to process information across diverse slow timescales—effectively creating a mix of information-preserving and selectively lossy pathways—all while maintaining overall system stability. The model's effectiveness in overcoming vanishing gradients is further evidenced by its competitive performance against architectures specifically designed to address this issue, such as LSTMs.

It is important to note that while the stability property pertains to a continuous-time system of nonlinear differential equations, typical implementations for tasks involving sequential data utilize an Euler discretization of these equations for training. This discretization can potentially lead to a stiff dynamical system, which may cause numerical instabilities and explosive dynamics. Therefore, careful parameterization of time constants and the selection of a sufficiently small time step are crucial for maintaining stable dynamics. Regarding the model's architecture, in its current form, the weight matrices of the input gain modulators, $\mathbf{W}_{by}$, $\mathbf{W}_{ba}$, $\mathbf{W}_{b_0y}$, and $\mathbf{W}_{b_0a}$, are each $n \times n$. Consequently, the number of parameters grows more rapidly with the hidden state size compared to other RNNs. To mitigate this, a recommended approach is the use of compact and/or convolutional weights. This strategy can prevent a significant increase in the number of parameters as the hidden state size expands, offering a path towards more scalable implementations.

5 Element-wise and Recursive Solutions for the Power Spectral Density of Biological Stochastic Dynamical Systems at Fixed Points

5.1 Overview

This chapter presents analytical solutions for the power spectral density (PSD) of stochastic dynamical systems operating near stable fixed points. The core findings discussed herein have been published in [82].

Stochasticity plays a central role in nearly every biological process, and the noise power spectral density (PSD) is a critical tool for understanding variability and information processing in living systems. In steady-state, many such processes can be described by stochastic linear time-invariant (LTI) systems driven by Gaussian white noise, whose PSD is a complex rational function of the frequency that can be concisely expressed in terms of their Jacobian, dispersion, and diffusion matrices, fully defining the statistical properties of the system's dynamics at steady-state. Here, we arrive at compact element-wise solutions of the rational function coefficients for the auto- and cross-spectrum that enable the explicit analytical computation of the PSD in

dimensions $n = 2, 3, 4$. We further present a recursive Leverrier-Faddeev-type algorithm for the exact computation of the rational function coefficients. Crucially, both solutions are free of matrix inverses. We illustrate our element-wise and recursive solutions by considering the stochastic dynamics of neural systems models, namely Fitzhugh-Nagumo ($n = 2$), Hindmarsh-Rose ($n = 3$), Wilson-Cowan ($n = 4$), and the Stabilized Supralinear Network ($n = 22$), as well as an evolutionary game-theoretic model with mutations ($n = 5, 31$). We extend our approach to derive a recursive method for calculating the coefficients in the power series expansion of the integrated covariance matrix for interacting spiking neurons modeled as Hawkes processes on arbitrary directed graphs.

5.2 Introduction

Unlike in an abstract painting by Mondrian [122], the world is not made of perfect forms. Rather, we are surrounded by imperfect, yet regular patterns emerging from the randomness of microscopic processes that collectively give rise to statistically predictable phenomena. A point in case is the derivation of the diffusion equation from the random (Brownian) motion of microscopic particles [123, 124]. This is but one example of the many processes that can be recapitulated in terms of ordinary differential equations driven by random processes, known as stochastic differential equations (SDEs). For instance, the effect of thermal fluctuations on synaptic conductance (linked to the stochastic opening of voltage-gated ion channels) and on the voltage of an electrical circuit (Johnson's noise), or the fluctuations of a neuron's membrane potential driven by stochastic spike arrival, can all be modeled as SDEs. Alternatively, SDEs are commonly adopted to model processes for which the exact dynamics are not known, and it is thus appropriate to express the model in terms of random variables encoding our uncertainty about the state of the system. Examples are the trajectory of an aircraft as modeled by navigation systems, or the evolution of stock prices subject to market fluctuations [125].

Among stochastic models, linear time-invariant (LTI) SDEs play a special role because (i) they

are amenable to analytical treatment and (ii) the linear response of many nonlinear systems (e.g., around a fixed point of the dynamics) can be reduced to LTI SDEs. To make this point explicit, let us consider a non-linear autonomous dynamical system driven by additive white noise with finite variance, namely

$$\mathrm{d}\mathbf{x} = \mathbf{f}(\mathbf{x})\mathrm{d}t + \mathbf{L}\mathrm{d}\mathbf{W} \tag{5.1}$$

where $\mathbf{x} \in \mathbb{R}^n$ is the state vector, $\mathbf{f} : \mathbb{R}^n \to \mathbb{R}^n$ is a nonlinear drift function encoding the deterministic dynamics, $\mathbf{L} \in \mathbb{R}^{n\times m}$ is the *dispersion* matrix defining how noise enters the system, and $\mathrm{d}\mathbf{W} \in \mathbb{R}^m$ is a vector of mutually independent Gaussian increments satisfying $\mathbb{E}[\mathrm{d}\mathbf{W}\mathrm{d}\mathbf{W}^\top] = \mathbf{D}\mathrm{d}t$ where $\mathbf{D}$ is the *diffusion* matrix (or spectral density matrix) with entries $D_{ij} = \delta_{ij}\sigma_i^2$, where δ_{ij} is the Kronecker delta [125].

We are interested in the power spectral density of the system's response, $\mathbf{x}(t)$, near a stable fixed point, $\mathbf{x}_0$, so we proceed by linearizing the drift function about this point, yielding the following LTI system

$$\mathrm{d}\mathbf{x} = \mathbf{J}\mathbf{x}\mathrm{d}t + \mathbf{L}\mathrm{d}\mathbf{W} \tag{5.2}$$

where we have redefined $\mathbf{x}(t) \equiv \mathbf{x}(t) - \mathbf{x}_0$ such that $\mathbf{x}(t_0) = \mathbf{0}$, and $\mathbf{J} = |\mathrm{d}\mathbf{f}/\mathrm{d}\mathbf{x}|_{\mathbf{x}_0} \in \mathbb{R}^{n\times n}$ is the Jacobian evaluated at the fixed point, that we take to be Hurwitz (real part of all eigenvalues less than zero) to assure stability. The solution to this linear SDE is given by the stochastic integral $\mathbf{x}(t) = \int_{-\infty}^{t} e^{\mathbf{J}(t-s)}\mathbf{L}\mathrm{d}\mathbf{W}(s)$ which is a zero-mean stationary process with covariance $\boldsymbol{\mathcal{R}}(\tau)$.

The PSD of this stochastic process is known to be expressed in terms of the following matrix product[1] (see [126] and Appendix D.1),

$$\boldsymbol{\mathcal{S}}_{\mathbf{x}}(\omega) = (i\omega\mathbf{I} + \mathbf{J})^{-1}\,\mathbf{L}\,\mathbf{D}\,\mathbf{L}^\top(-i\omega\mathbf{I} + \mathbf{J})^{-\top} \tag{5.4}$$

[1]The power spectral density of the LTI SDE described in Eq. (5.2) can alternatively be written as the inverse of the Hermitian positive definite matrix (see Appendix D.1), assuming that $\mathbf{C} \equiv \mathbf{L}\,\mathbf{D}\,\mathbf{L}^\top$ is positive definite,

$$\mathrm{S}(\omega) = \left[\mathbf{J}^\top\mathbf{C}^{-1}\mathbf{J} + \omega^2\mathbf{C}^{-1} + i\omega(\mathbf{J}^\top\mathbf{C}^{-1} - \mathbf{C}^{-1}\mathbf{J})\right]^{-1} \tag{5.3}$$

This enables us to efficiently compute the matrix inverse by Cholesky decomposition.

For the sake of brevity, from now on we refer to $\boldsymbol{\mathcal{S}}_{\mathbf{x}}(\omega)$ as $\boldsymbol{\mathcal{S}}(\omega)$, whose i, j^{th} entry is denoted $\mathcal{S}^{ij}(\omega)$. $\boldsymbol{\mathcal{S}}(\omega)$ is a product of the spectral factors (the transfer function matrix) of the dynamical system and can be expressed as a rational function of the following form [127, 128],

$$\boldsymbol{\mathcal{S}}(\omega) = \frac{\text{adj}(\mathbf{J} + i\omega\mathbf{I})\,\mathbf{L}\,\mathbf{D}\,\mathbf{L}^{\top}\,\text{adj}^{\top}(\mathbf{J} - \imath\omega\mathbf{I})}{\det(\mathbf{J} + i\omega\mathbf{I})\det(\mathbf{J} - \imath\omega\mathbf{I})} = \frac{\mathbf{Z}(\omega)}{Q(\omega)} \tag{5.5}$$

Here, $\mathbf{Z}(\omega)$ is a complex polynomial matrix representing the numerator of the solution, and $Q(\omega)$ is an even-powered polynomial of degree $2n$ representing the denominator of the solution. When we express the adjugate of the matrices in terms of the corresponding cofactor matrices, it is apparent that $\mathbf{Z}(\omega)$ contains complex polynomials of degree $2n-2$ with even powers of ω being real and odd powers of ω being imaginary. We can further, split the numerator into the real and imaginary parts,

$$\boldsymbol{\mathcal{S}}(\omega) = \frac{\mathbf{P}(\omega) + i\omega\mathbf{P}'(\omega)}{Q(\omega)} = \frac{\sum_{\alpha=0}^{n-1}\mathbf{P}_{\alpha}\omega^{2\alpha} + i\omega\sum_{\alpha=0}^{n-2}\mathbf{P}'_{\alpha}\omega^{2\alpha}}{\sum_{\alpha=0}^{n} q_{\alpha}\omega^{2\alpha}} \tag{5.6}$$

and the corresponding PSD matrix elements are of the form,

$$\mathcal{S}^{ij}(\omega) = \frac{P^{ij}(\omega) + i\delta_{ij}\omega P^{ij\prime}(\omega)}{Q(\omega)} \tag{5.7}$$

where $P^{ij}(\omega) = \sum_{\alpha=0}^{n-1} p_{\alpha}^{ij}\omega^{2\alpha}$, $P^{ij\prime}(\omega) = \sum_{\alpha=0}^{n-2} p_{\alpha}^{ij\prime}\omega^{2\alpha}$ and $Q(\omega) = \sum_{\alpha=0}^{n} q_{\alpha}\omega^{2\alpha}$ are even powered polynomials with real coefficients (p_{α}^{ij}, $p_{\alpha}^{ij\prime}$ and q_{α}).

In this work, we derive closed-form expressions for the individual coefficients of the rational function of a given element of $\boldsymbol{\mathcal{S}}(\omega)$, i.e., $\mathcal{S}^{ij}(\omega)$. In Section 5.4 we provide the formulae for the auto-spectrum of 2, 3, and 4-dimensional systems expressed in terms of elementary trace operations applied to the submatrices of $\mathbf{J}$. The element-wise solutions for the auto- and cross-spectrum of a generic n-dimensional system are presented in the Appendix D.3, and they can be

obtained directly in symbolic form through our software[2].

In Section 5.5, we derive a recursive algorithm (Theorem D.1) to calculate the coefficient matrices $\mathbf{P}_\alpha$ and $\mathbf{P}'_\alpha$ and the coefficients of the denominator, q_α. We follow an approach similar to the one adopted by Hou [129] to derive the Leverrier-Faddeev (LF) method, which is a recursive approach to find the characteristic polynomial of a matrix in $O(n^4)$ operations, where n is the dimensionality of the system [130, 131]. Note that unlike Eq. (5.4), our solutions are free of matrix inverses, which is numerically advantageous when the system is ill-conditioned. To demonstrate the wide applicability of the recursive algorithm, we derive a recursive solution for the rational function of an auxiliary spectral matrix, Theorem D.5. Using this solution, we develop a recursive method (Theorem 5.2) to find the power series expansion of the integrated covariance matrix of the Hawkes process [132] with arbitrary connectivity (Section 5.6).

In Section 5.6 we apply our solutions to several stochastic nonlinear models from neuroscience and evolutionary biology, providing model-specific solutions for the auto-spectrum when appropriate. In practice, readers seeking analytical expressions for the auto-spectrum of specific models (e.g., Fitzhugh-Nagumo [133–135], or Hindmarsh-Rose [136]), can refer directly to Section 5.3 and 5.6.

5.3 Preliminary Examples

Before presenting the general solutions, it is instructive to review concrete 1- and 2-dimensional cases that are commonly encountered in the literature, for which we can derive the coefficients analytically with little effort, without resorting to our sophisticated solutions. To this end, let us consider the simplest and most common case: the auto-spectrum of an LTI system with mutually independent additive noise (i.e., $\mathbf{L} = \mathbf{I}$). For the $d = 1$ case, also known as the Ornstein-Uhlenbeck

[2] https://github.com/martiniani-lab/spectre

process, we have

$$\mathrm{d}x = -\tau_r^{-1} x \mathrm{d}t + \mathrm{d}W \tag{5.8}$$

with $\mathrm{d}W^2 = \sigma^2 \mathrm{d}t$. It can be seen from Eq. (5.4) that

$$\mathcal{S}(\omega) = \frac{\sigma^2}{\tau_r^{-2} + \omega^2} \tag{5.9}$$

so that the coefficients in Eq. (5.7) are $p_0^{11} = \sigma^2$, $q_0 = \tau_r^{-2}$ and $q_1 = 1$. [3]

A slightly more sophisticated example is the stochastic Fitzhugh-Nagumo model [133–135], which amounts to a simplification of the Hodgkin-Huxley equations for action potential generation [137]. We simulate the dynamical evolution of a neuron's membrane potential in response to an input current by the following set of SDEs:

$$\begin{aligned} \frac{\mathrm{d}v}{\mathrm{d}t} &= \left(v - \frac{v^3}{3} - w + I\right) + h_1(v)\eta_1 \\ \frac{\mathrm{d}w}{\mathrm{d}t} &= \epsilon(v + \alpha - \beta w) + h_2(w)\eta_2. \end{aligned} \tag{5.10}$$

Here, v represents the difference between the membrane potential and the resting potential, w is the variable associated with the recovery of the ion channels after the generation of an action potential, and I is the external current input. The parameters α and β are related to the activation threshold of the fast sodium channel and the inactivation threshold of the slow potassium channels, respectively. $\epsilon \ll 1$ sets the time scale for the evolution of the activity, making the dynamics of v much faster than those of w. In the subthreshold regime, the fixed point, (v_e, w_e), can be found analytically as a function of the parameters of the model and the input current. We set the RHS of Eq. (5.10) equal to 0. Therefore, v_e is the solution to the cubic equation,

$$v^3 + 3\left(\frac{1}{\beta} - 1\right)v + 3\left(\frac{\alpha}{\beta} - I\right) = 0 \tag{5.11}$$

[3] Note that Eq. (5.9) readily leads us to the correlation function $R(\tau) = \mathcal{F}^{-1}(S(\omega)) = \frac{\tau_r}{2}\sigma^2 e^{-|\tau|/\tau_r}$

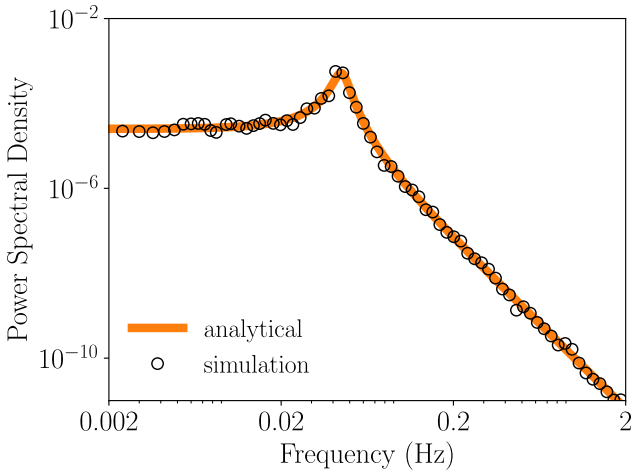


Figure 5.1: Power spectral density of the membrane potential for the Fitzhugh-Nagumo model. A comparison of the PSD of the membrane potential (v) calculated via simulation and the analytical rational function solution. The parameters used to simulate the system are $I = 0.265$, $\alpha = 0.7$, $\beta = 0.75$ and $\epsilon = 0.08$ that yields a fixed point solution $v_e = -1.00125$, $w_e = -0.401665$. Here, we plot the auto-spectrum for the case of multiplicative noise, i.e., $h_1(v) = 0$ and $h_2(w) = \sigma w$, where $\sigma = 0.001$.

and $w_e = (v_e + \alpha)/\beta$. The sign of the discriminant, $\Delta = (1/\beta - 1)^3 + \frac{9}{4}(\alpha/\beta - I)^2$, of the cubic equation determines if the system admits one or more fixed points. We pick the parameters such that $\Delta > 0$, yielding a system with a global attractor. Since the solution to v_e is from a depressed cubic, it can be analytically expressed in terms of Δ using Cardano's formula,

$$v_e = \sqrt[3]{-\frac{3}{2}\left(\frac{\alpha}{\beta} - I\right) - \sqrt{\Delta}} + \sqrt[3]{-\frac{3}{2}\left(\frac{\alpha}{\beta} - I\right) + \sqrt{\Delta}}. \tag{5.12}$$

The stochasticity in v and w is represented by two uncorrelated Gaussian white noise sources, η_1 and η_2, with a standard deviation of 1. We consider the case of multiplicative noise which is realized by setting $h_1(v)$ and $h_2(w)$ proportional to the respective function variables. Specifically, we set $h_1(v) = 0$ and $h_2(w) = \sigma w$. We choose the variance of the noise small enough that we are always in the vicinity of the fixed point. Then, upon linearizing Eq. (5.10) around the fixed point,

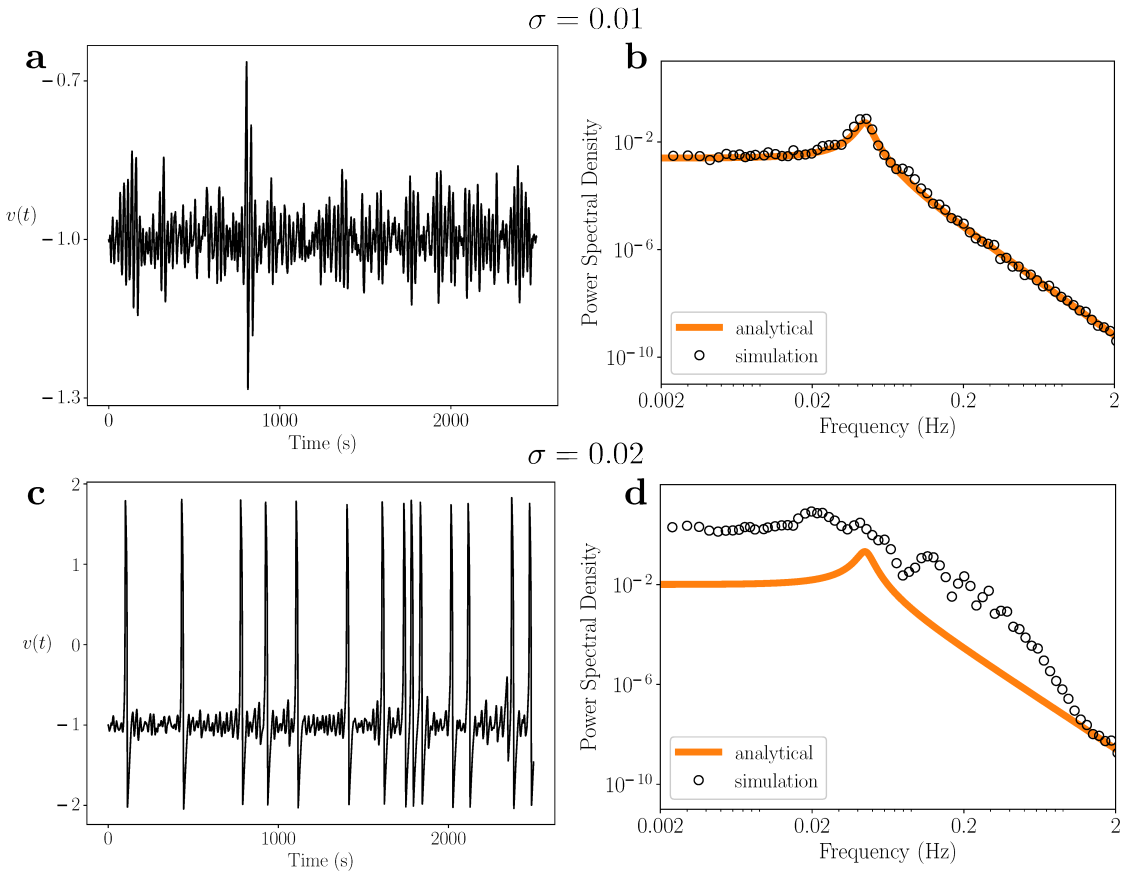


Figure 5.2: Power spectral density of the membrane potential for the Fitzhugh-Nagumo with large noise. A comparison of the PSD of the membrane potential (v) calculated via simulation and the analytical rational function solution (**b** and **d**). The parameters (except for σ) used to simulate the system are the same as those used in Fig. 5.1. We consider two different strengths of noise $\sigma = 0.01$ (**a** and **b**) and $\sigma = 0.02$ (**c** and **d**). We also plot sample stochastic trajectories (**a** and **c**) for the different noise strengths.

(v_e, w_e), we arrive at the following LTI SDEs,

$$\begin{bmatrix} \dot{v} \\ \dot{w} \end{bmatrix} = \begin{bmatrix} 1 - v_e^2 & -1 \\ \epsilon & -\beta\epsilon \end{bmatrix} \begin{bmatrix} v - v_e \\ w - w_e \end{bmatrix} + \sigma \begin{bmatrix} 0 & 0 \\ 0 & w_e \end{bmatrix} \begin{bmatrix} \eta_1 \\ \eta_2 \end{bmatrix} \tag{5.13}$$

Plugging the Jacobian and noise matrices into Eq. (5.4), we obtain the PSD of the membrane potential, v, as

$$\mathcal{S}_v(\omega) = \frac{w_e^2 \sigma^2}{(\epsilon + (v_e^2 - 1)\beta\epsilon)^2 + ((v_e^2 - 1)^2 - 2\epsilon + \beta^2\epsilon^2)\omega^2 + \omega^4} \tag{5.14}$$

so that in Eq. (5.7) we have $p_0^{11} = w_e^2\sigma^2$, $p_1^{11} = 0$, $q_0 = (\epsilon + (v_e^2 - 1)\beta\epsilon)^2$, $q_1 = ((v_e^2 - 1)^2 - 2\epsilon + \beta^2\epsilon^2)$ and $q_2 = 1$.

We verify the accuracy of this solution, Eq. (5.14), by comparison with the PSD obtained numerically by simulating the nonlinear model, Eq. (5.10), with multiplicative noise, and find excellent agreement as shown in Fig. 5.1. We note that the approximation works well even when the strength of the noise is increased (Fig. 5.2b), but breaks down if the noise strength is increased even further (Fig. 5.2d).

This laborious approach works well for systems with dimensions $n = 1, 2$, but it becomes infeasible in higher dimensions. This is due to the multiplication of inverses of two matrices with complex entries, $(i\omega\mathbf{I} + \mathbf{J})^{-1}$ and $(-i\omega\mathbf{I} + \mathbf{J})^{-\top}$.

5.4 Element-wise Solution

We now introduce element-wise solutions for the auto-spectrum of 2, 3, and 4-dimensional systems. The general n-dimensional solutions for both auto- and cross-spectrum can be found in the Appendix D.3 alongside their derivations, and can be conveniently obtained in symbolic form for any dynamical system through our software[4]. This method relies on expressing the rational function expression of Eq. (5.4) in terms of elementary matrix operations on submatrices of the Jacobian, $\mathbf{J}$. Although this approach requires roughly $O(n^4 \log n)$ Fig. D.2, operations for each element of the PSD matrix, i.e., $O(n^6 \log n)$ total, it is particularly valuable to arrive at analytical closed-form solutions for the auto- or cross-spectra of specific dynamical variables, yielding greater insight into the dependence of the power spectral density on the model's functional form and its parameters. For simplicity, we consider the auto-spectrum of an LTI system driven by uncorrelated white noise (see Appendix D.3 for the most general case of correlated noise and/or the cross-spectrum).

[4] https://github.com/martiniani-lab/spectre

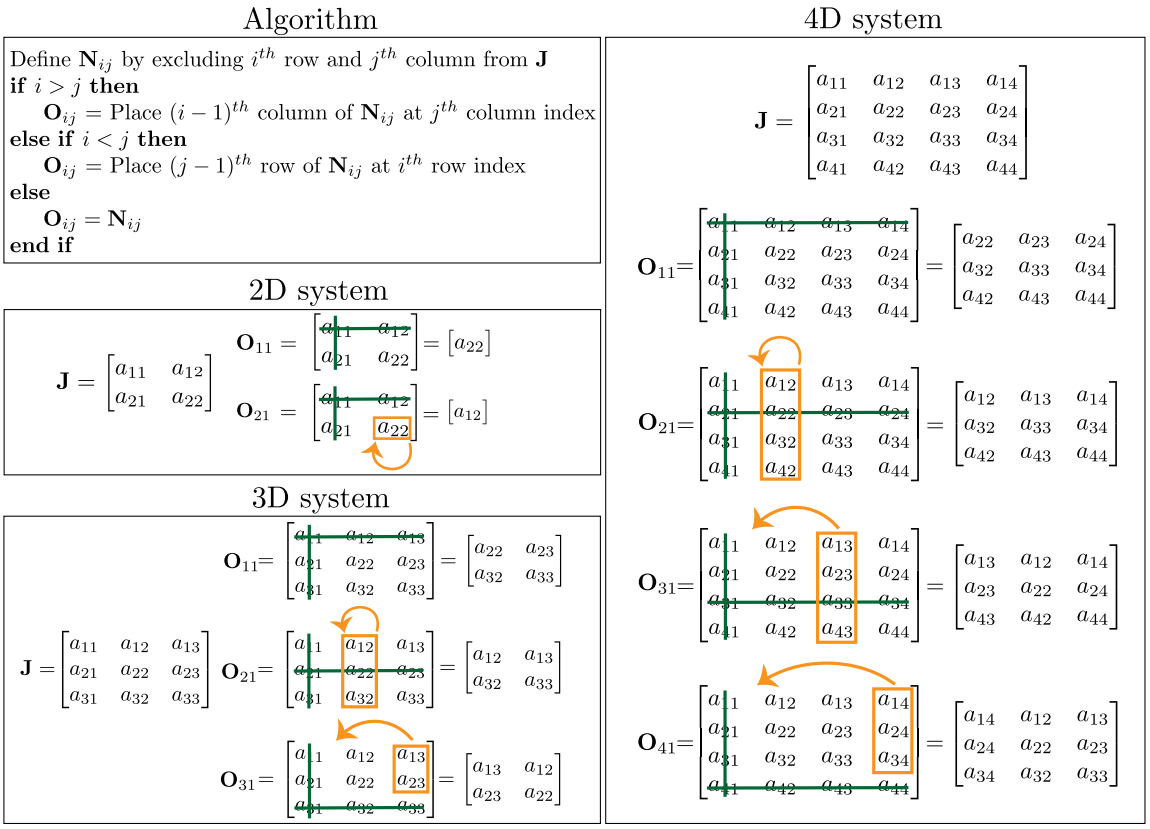


Figure 5.3: Definitions of $\mathbf{O}_{ij}$ matrices. We show the algorithm to generate the $\mathbf{O}_{ij}$ matrices with examples for the 2, 3 and 4D systems. To find $\mathbf{O}_{ij}$, we have to first find the excluded matrix by removing the i^{th} row and j^{th} column (denoted by green lines) from the Jacobian matrix and then perform the row/column change operations, denoted by orange arrows.

We start by noting that the denominator in Eq. (5.7) is independent of the type of noise driving the system, and it can be written as an even-powered expansion in ω with real coefficients. Similarly, the numerator of the auto-spectrum is an even-powered expansion in ω with real coefficients, but they depend directly on how the noise is added via the dispersion matrix, $\mathbf{L}$, whose elements we denote l_{ij}. For the particular case of independent noise, i.e., $l_{ij} = 0$ for $i \neq j$, the coefficient of $\omega^{2\alpha}$ in the numerator of the rational function for the i^{th} variable takes the simplified form,

$$p_\alpha^{ii} = \sigma_i^2 \, l_i^2 \, d^\alpha(\mathbf{O}_{ii}) + \sum_{\substack{j=1 \\ j\neq i}}^{n} \sigma_j^2 \, l_j^2 \, f^\alpha(\mathbf{O}_{ji}, \mathbf{e}_{\min(i,j)}) \tag{5.15}$$

where $d^\alpha(\mathbf{O}_{ii})$ and $f^\alpha(\mathbf{O}_{ji})$ are functions of the Jacobian submatrices, $\mathbf{O}_{ij}$, defined according to

the algorithm in Fig. 5.3. The functions themselves can be expressed in terms of Bell polynomials [138], and are defined in Appendix D.4. $\mathbf{e}_\beta \in \{0,1\}^{n-1\times 1}$ is the standard unit vector equal to 1 at index $\beta = \min(i,j)$ and 0 everywhere else. $\sigma_i^2 \equiv \sigma_{ii}^2$ is the i-th diagonal entry of the noise matrix $\mathbf{D}$, and, since $\mathbf{L}$ is diagonal, we also use the notation $l_i \equiv l_{ii}$.

Here, we only provide the solution for the auto-spectrum of the first variable, i.e., $i = 1$. This solution can be generalized for any variable $i \neq 1$, as shown in Appendix D.3. Alternatively, one can simply interchange the rows and columns of the LTI system so that the variable of interest appears at index $i = 1$, and directly use the solution reported in this section.

Since the coefficients of the denominator are the same for all dimensions, n, we define them first,

$$\begin{aligned}
q_{n-4} &= \frac{1}{24}\left[\operatorname{Tr}^4\left(\mathbf{J}^2\right) - 6\operatorname{Tr}^2\left(\mathbf{J}^2\right)\operatorname{Tr}\left(\mathbf{J}^4\right) + 8\operatorname{Tr}\left(\mathbf{J}^2\right)\operatorname{Tr}\left(\mathbf{J}^6\right) + 3\operatorname{Tr}^2\left(\mathbf{J}^4\right) - 6\operatorname{Tr}\left(\mathbf{J}^8\right)\right] \\
q_{n-3} &= \frac{\operatorname{Tr}^3\left(\mathbf{J}^2\right) - 3\operatorname{Tr}\left(\mathbf{J}^2\right)\operatorname{Tr}\left(\mathbf{J}^4\right) + 2\operatorname{Tr}\left(\mathbf{J}^6\right)}{6} \\
q_{n-2} &= \frac{\operatorname{Tr}^2\left(\mathbf{J}^2\right) - \operatorname{Tr}\left(\mathbf{J}^4\right)}{2} \\
q_{n-1} &= \operatorname{Tr}\left(\mathbf{J}^2\right) \\
q_n &= 1
\end{aligned} \tag{5.16}$$

Note that for each n we will only need to consider the coefficients q_α with $\alpha \geq 0$.

5.4.1 2-D Solution

For a 2D system, we can write the auto-spectrum of the first variable as,

$$\mathcal{S}^{11}(\omega) = \frac{p_0 + p_1\omega^2}{q_0 + q_1\omega^2 + q_2\omega^4} \tag{5.17}$$

where the coefficients of the numerator are given by the equations

$$\begin{aligned} p_0 &= l_1^2\sigma_1^2\,\mathrm{Tr}(\mathbf{O}_{11}^2) + l_2^2\sigma_2^2\,\mathrm{Tr}(\mathbf{O}_{21}^2) \\ p_1 &= l_1^2\sigma_1^2 \end{aligned} \tag{5.18}$$

Here, the matrices $\mathbf{O}_{11} = [a_{22}]$ and $\mathbf{O}_{21} = [a_{12}]$ are found from the 2D Jacobian using the algorithm summarized in Fig. 5.3 (*n.b.*, we denote a_{ij} the i, j^{th} entry of the Jacobian). The coefficients of the denominator are given by the last three entries of Eq. (5.16).

5.4.2 3-D Solution

For a 3D system, the auto-spectrum of the first variable takes the form,

$$\mathcal{S}^{11}(\omega) = \frac{p_0 + p_1\omega^2 + p_2\omega^4}{q_0 + q_1\omega^2 + q_2\omega^4 + q_3\omega^6} \tag{5.19}$$

where the coefficients of the numerator are given by the equations

$$\begin{aligned} p_0 =& \frac{1}{2}\left[l_1^2\sigma_1^2\left(\mathrm{Tr}^2\left(\mathbf{O}_{11}^2\right) - \mathrm{Tr}\left(\mathbf{O}_{11}^4\right)\right) + \sum_{j=2}^{3} l_j^2\sigma_j^2\left(\mathrm{Tr}^2\left(\mathbf{O}'_{j1}{}^2\right) - \mathrm{Tr}\left(\mathbf{O}'_{j1}{}^4\right) + \mathrm{Tr}^2\left(\mathbf{O}_{j1}^2\right) - \mathrm{Tr}\left(\mathbf{O}_{j1}^4\right)\right)\right] \\ p_1 =& l_1^2\sigma_1^2\,\mathrm{Tr}\left(\mathbf{O}_{11}^2\right) + \sum_{j=2}^{3} l_j^2\sigma_j^2\left(-2\,\mathrm{Tr}\left(\mathbf{O}'_{j1}\right)\mathrm{Tr}\left(\mathbf{O}_{j1}\right) + \mathrm{Tr}\left(\mathbf{O}'_{j1}{}^2\right) + \mathrm{Tr}^2\left(\mathbf{O}_{j1}\right)\right) \\ p_2 =& l_1^2\sigma_1^2 \end{aligned} \tag{5.20}$$

Here, the matrices $\mathbf{O}_{11}$, $\mathbf{O}_{21}$ and $\mathbf{O}_{31}$ are found from the 3D Jacobian matrix using the algorithm summarized in Fig. 5.3. Furthermore, the matrices $\mathbf{O}'_{ij}$ are found by excluding the k^{th} row and column from the corresponding $\mathbf{O}_{ij}$ matrix, where $k = \min(i, j)$. Since we are interested in the spectrum of the first variable ($j = 1$), $k = \min(i, 1) = 1$. Thus, $\mathbf{O}'_{21}$ and $\mathbf{O}'_{31}$ are found by removing the first row and column from the matrices $\mathbf{O}_{21}$ and $\mathbf{O}_{31}$, respectively. The coefficients of the denominator are given by the last four entries of Eq. (5.16).

If the variance of the noise is the same for all the variables, i.e., $l_1^2\sigma_1^2 = l_2^2\sigma_2^2 = l_3^2\sigma_3^2 = \sigma^2$, we can further simplify the coefficients of the numerator, which become

$$\begin{aligned} p_0 &= \sigma^2 \det(\mathbf{A}^\top \mathbf{A}) \\ p_1 &= \sigma^2 \operatorname{Tr}(\mathbf{A}_1^\top \mathbf{A}_1 + \mathbf{A}_2^2) \\ p_2 &= \sigma^2 \end{aligned} \tag{5.21}$$

where, $\mathbf{A} \in \mathbb{R}^{3\times 2}$ is the submatrix of $\mathbf{J}$ obtained by removing its first column. Then, $\mathbf{A}_1 \in \mathbb{R}^{1\times 2}$ is the submatrix obtained by isolating the first row of $\mathbf{A}$, and $\mathbf{A}_2 \in \mathbb{R}^{2\times 2}$ is the submatrix obtained by removing the first row of $\mathbf{A}$.

5.4.3 4-D Solution

For a 4D system, the auto-spectrum of the first variable becomes

$$\mathcal{S}^{11}(\omega) = \frac{p_0 + p_1\omega^2 + p_2\omega^4 + p_3\omega^6}{q_0 + q_1\omega^2 + q_2\omega^4 + q_3\omega^6 + q_4\omega^8} \tag{5.22}$$

where the coefficients of the numerator are given by Eq. (5.23). Here, the matrices $\mathbf{O}_{11}$, $\mathbf{O}_{21}$, $\mathbf{O}_{31}$ and $\mathbf{O}_{41}$ are found from the 4D Jacobian matrix using the algorithm summarized in Fig. 5.3. Using an argument similar to the 3D case, $\mathbf{O}'_{21}$, $\mathbf{O}'_{31}$ and $\mathbf{O}'_{41}$ can be found by removing the first row and column from the matrices $\mathbf{O}_{21}$, $\mathbf{O}_{31}$ and $\mathbf{O}_{41}$, respectively. The coefficients of the denominator are

given by Eq. (5.16).

$$
\begin{aligned}
p_0 =& \frac{1}{6}\Bigg[l_1^2\sigma_1^2\big(\mathrm{Tr}^3\left(\mathbf{O}_{11}^2\right) - 3\,\mathrm{Tr}\left(\mathbf{O}_{11}^2\right)\mathrm{Tr}\left(\mathbf{O}_{11}^4\right) + 2\,\mathrm{Tr}\left(\mathbf{O}_{11}^6\right)\big) + \sum_{j=2}^{4} l_j^2\sigma_j^2\Bigg(\mathrm{Tr}^3\left(\mathbf{O}'_{j1}{}^2\right) \\
& - 3\,\mathrm{Tr}\left(\mathbf{O}'_{j1}{}^2\right)\mathrm{Tr}\left(\mathbf{O}'_{j1}{}^4\right) + 2\,\mathrm{Tr}\left(\mathbf{O}'_{j1}{}^6\right) + \mathrm{Tr}^3\left(\mathbf{O}_{j1}^2\right) - 3\,\mathrm{Tr}\left(\mathbf{O}_{j1}^2\right)\mathrm{Tr}\left(\mathbf{O}_{j1}^4\right) + 2\,\mathrm{Tr}\left(\mathbf{O}_{j1}^6\right)\Bigg)\Bigg] \\
p_1 =& \frac{1}{6}\Bigg[3l_1^2\sigma_1^2\big(\mathrm{Tr}^2\left(\mathbf{O}_{11}^2\right) - \mathrm{Tr}\left(\mathbf{O}_{11}^4\right)\big) + \sum_{j=2}^{4} l_j^2\sigma_j^2\Bigg(-3\big(\mathrm{Tr}^2\left(\mathbf{O}'_{j1}\right) - \mathrm{Tr}\left(\mathbf{O}'_{j1}{}^2\right)\big) \\
& \times \big(\mathrm{Tr}^2\left(\mathbf{O}_{j1}\right) - \mathrm{Tr}\left(\mathbf{O}_{j1}^2\right)\big) + 3\,\mathrm{Tr}^2\left(\mathbf{O}'_{j1}{}^2\right) + 2\,\mathrm{Tr}\left(\mathbf{O}'_{j1}\right)\big(\mathrm{Tr}^3\left(\mathbf{O}_{j1}\right) - 3\,\mathrm{Tr}\left(\mathbf{O}_{j1}\right)\mathrm{Tr}\left(\mathbf{O}_{j1}^2\right) \\
& + 2\,\mathrm{Tr}\left(\mathbf{O}_{j1}^3\right)\big) - 3\,\mathrm{Tr}\left(\mathbf{O}'_{j1}{}^4\right) + 3\,\mathrm{Tr}^2\left(\mathbf{O}_{j1}^2\right) - 3\,\mathrm{Tr}\left(\mathbf{O}_{j1}^4\right)\Bigg)\Bigg] \\
p_2 =& l_1^2\sigma_1^2\,\mathrm{Tr}\left(\mathbf{O}_{11}^2\right) + \sum_{j=2}^{4} l_j^2\sigma_j^2\big(\mathrm{Tr}^2\left(\mathbf{O}'_{j1}\right) + \mathrm{Tr}^2\left(\mathbf{O}_{j1}\right) - 2\,\mathrm{Tr}\left(\mathbf{O}'_{j1}\right)\mathrm{Tr}\left(\mathbf{O}_{j1}\right)\big) \\
p_3 =& l_1^2\sigma_1^2
\end{aligned}
\tag{5.23}
$$

5.5 Recursive Solutions

We derive an alternative approach to computing the polynomial coefficients of the auto- and cross-spectrum based on a recursive algorithm. By this method, we can obtain coefficients for all entries of the power spectral matrix simultaneously in $O(n^4)$ operations Fig. D.1. To make our solution compact, we denote the noise covariance matrix $\mathbf{C} \equiv \mathbf{L}\,\mathbf{D}\,\mathbf{L}^\top$. We specify the algorithm in the following theorem and provide a proof in Appendix D.2. Note that the algorithm can alternatively be derived by leveraging the Barnett-Leverrier recursive formula [139].

Theorem 5.1. *The noise power spectral density matrix of an LTI system is a complex-valued rational*

function of the form

$$\begin{aligned}\boldsymbol{\mathcal{S}}(\omega) &= (i\omega\mathbf{I}+\mathbf{J})^{-1}\,\mathbf{C}\,(-i\omega\mathbf{I}+\mathbf{J})^{-\top} \\ &= \frac{\sum_{\alpha=0}^{n-1}\mathbf{P}_\alpha\omega^{2\alpha} + i\omega\sum_{\alpha=0}^{n-2}\mathbf{P}'_\alpha\omega^{2\alpha}}{\sum_{\alpha=0}^{n} q_\alpha\omega^{2\alpha}}\end{aligned}$$

The numerator's matrix coefficients are given by the recursive equations,

$$\begin{aligned}\mathbf{P}'_{\alpha-1} &= \mathbf{J}\mathbf{P}_\alpha - \mathbf{P}_\alpha\mathbf{J}^\top - \mathbf{J}\mathbf{P}'_\alpha\mathbf{J}^\top \\ \mathbf{P}_{\alpha-1} &= q_\alpha\mathbf{C} + \mathbf{P}'_{\alpha-1}\mathbf{J}^\top - \mathbf{J}\mathbf{P}'_{\alpha-1} - \mathbf{J}\mathbf{P}_\alpha\mathbf{J}^\top\end{aligned} \tag{5.24}$$

for $\alpha \in \{1,\ldots,n\}$*, starting from* $\alpha = n$ *with* $\mathbf{P}_n = \mathbf{P}'_n = \mathbf{0}$*. The scalar coefficients of the denominator can be recursively calculated using,*

$$q_\alpha = \frac{1}{n-\alpha}\left[\mathrm{Tr}\left(\mathbf{J}\mathbf{Q}'_{\alpha-1}\right) + \mathrm{Tr}\left(\mathbf{J}\mathbf{Q}_\alpha\mathbf{J}^\top\right)\right] \tag{5.25}$$

if $\alpha < n$*, and* $q_n = 1$*. The coefficients* $\mathbf{Q}'_{\alpha-1}$ *and* $\mathbf{Q}_\alpha$ *are given in turn by the recursive equations,*

$$\begin{aligned}\mathbf{Q}'_{\alpha-1} &= \mathbf{J}\mathbf{Q}_\alpha - \mathbf{Q}_\alpha\mathbf{J}^\top - \mathbf{J}\mathbf{Q}'_\alpha\mathbf{J}^\top \\ \mathbf{Q}_{\alpha-1} &= q_\alpha\mathbf{I} + \mathbf{Q}'_{\alpha-1}\mathbf{J}^\top - \mathbf{J}\mathbf{Q}'_{\alpha-1} - \mathbf{J}\mathbf{Q}_\alpha\mathbf{J}^\top\end{aligned} \tag{5.26}$$

for $\alpha \in \{0,1,\ldots,n\}$*, starting from* $\alpha = n$ *with* $\mathbf{Q}_n = \mathbf{Q}'_n = \mathbf{0}$ *and* $\mathbf{Q}_{-1} = \mathbf{Q}'_{-1} = \mathbf{0}$*.*

Note that Eq. (D.42) is the same as Eq. (D.81) for $\mathbf{C} = \mathbf{I}$, and that the $\mathbf{P}'_\alpha$ ($\mathbf{Q}'_\alpha$) matrices are anti-symmetric, whereas the $\mathbf{P}_\alpha$ ($\mathbf{Q}_\alpha$) matrices are symmetric.

The approach used to derive the recursive solution for $\boldsymbol{\mathcal{S}}(\omega)$ is broadly applicable to matrices of similar forms. In Theorem D.5, we provide an example of one such recursive algorithm for the

similarly defined matrix

$$\mathcal{T}(\omega) = (\omega \mathbf{I} - \mathbf{G})^{-1} \, \mathbf{Y} \, (\omega \mathbf{I} - \mathbf{G}^\top)^{-1} \tag{5.27}$$

We use this result to prove the following Theorem (proof in Appendix D.2),

Theorem 5.2. *Let* $\mathbf{G}$ *be a convergent matrix, i.e., with a spectral radius less than 1,* $\mathbf{Y}$ *be a positive definite matrix, and* $\mathbf{R}$ *be a matrix with the following series expansion:*

$$\begin{aligned} \mathbf{R} &= (\mathbf{I} - \mathbf{G})^{-1} \, \mathbf{Y} \left(\mathbf{I} - \mathbf{G}^\top\right)^{-1} \\ &= \sum_{m=0}^{\infty} \sum_{\substack{j+k=m \\ j \geq 0,\, k \geq 0}} \mathbf{G}^j \, \mathbf{Y} \, \left(\mathbf{G}^\top\right)^k \end{aligned} \tag{5.28}$$

$\mathbf{S}_m \coloneqq \sum_{\substack{j+k=m \\ j \geq 0,\, k \geq 0}} \mathbf{G}^j \, \mathbf{Y} \, \left(\mathbf{G}^\top\right)^k$ *can be found by the following recursive algorithm,*

$$\begin{aligned} t_m &= \frac{2}{m} \left[\mathrm{Tr}\left(\mathbf{Y}^{-1} \mathbf{G} \mathbf{U}_{m-2} \mathbf{G}^\top\right) - \mathrm{Tr}\left(\mathbf{Y}^{-1} \mathbf{G} \mathbf{U}_{m-1}\right) \right] \\ \mathbf{U}_m &= t_m \mathbf{Y} + \mathbf{G} \mathbf{U}_{m-1} + \mathbf{U}_{m-1} \mathbf{G}^\top - \mathbf{G} \mathbf{U}_{m-2} \mathbf{G}^\top \\ \mathbf{S}_m &= \mathbf{U}_m - \sum_{k=0}^{m-1} t_{m-k} \, \mathbf{S}_k \end{aligned} \tag{5.29}$$

starting with $m = 0$ *until* $m = 2n$ *and the initial values* $t_0 = 1$ *and* $\mathbf{U}_{-2} = \mathbf{U}_{-1} = \mathbf{0}$.

We will use this result in Section 5.6.5 to recursively find the terms of various orders in the power series expansion of the integrated covariance matrix of a network of spiking neurons modeled by Hawkes processes [132].

5.6 Applications

We now apply the rational function solutions of Sections 5.4 and 5.5 to compute the power spectra of a range of nonlinear models exhibiting fixed point solutions and, where appropriate,

we provide analytical closed-form expressions[5]. We consider four models: (i) The stochastic Hindmarsh-Rose model simulating the subthreshold activity of a neuron subject to an input current [136, 140]; (ii) a 4D Wilson-Cowan model simulating the activity of excitatory and inhibitory neuronal populations in the cortex [12, 141]; (iii) the stochastic Stabilized Supralinear Network (SSN) model [13, 93], which is a neural circuit model for the sensory cortex approximating divisive normalization [5, 9]; (iv) an evolutionary game-theoretic model which involves a population of agents playing a generalized version of the rock-paper-scissors game in n dimensions [142]. Additionally, we apply the recursive solution described in Theorem 5.2 to analyze the correlation structure of a network of spiking neurons, in random and ring networks, modeled by the Hawkes process [132].

5.6.1 Hindmarsh-Rose

Hindmarsh-Rose [136, 140] is a phenomenological 3D neuron model that can be considered a simplification of the Hodgkin-Huxley equations [137] or a generalization of the Fitzhugh-Nagumo model [133, 135]. We consider a stochastic version of the model based on the implementation by Storace et al. [140]. The system of SDEs defining the model is given by

$$\begin{aligned} \frac{\mathrm{d}x}{\mathrm{d}t} &= y - x^3 + bx^2 + I - z + \sigma\eta_1 \\ \frac{\mathrm{d}y}{\mathrm{d}t} &= 1 - 5x^2 - y \\ \frac{\mathrm{d}z}{\mathrm{d}t} &= \mu\big(s(x - x_{rest}) - z\big) \end{aligned} \tag{5.30}$$

Here, x represents the membrane potential of the neuron, y is a recovery variable, and z is a slow adaptation variable. I represents the synaptic current input to the neuron; $\mu \ll 1$ controls the relative timescales between the fast subsystem (x, y) and the slow z variable; x_{rest} is the resting

[5]The code for the general solutions of the auto- and cross-spectrum along with descriptions of the various dynamical systems (including the Hawkes model) considered in the manuscript can be found at https://github.com/martiniani-lab/spectre.

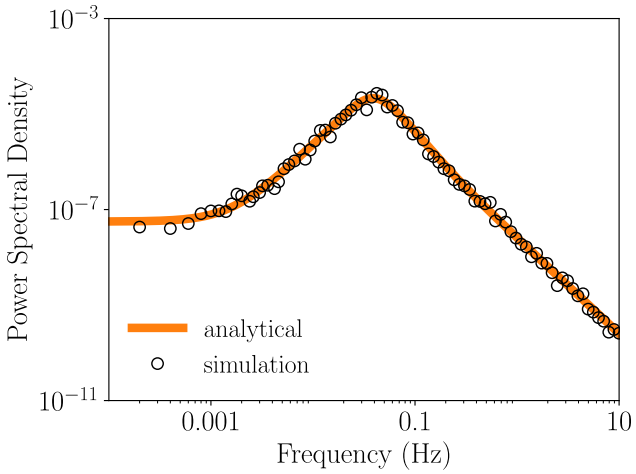


Figure 5.4: Power spectrum of the Hindmarsh-Rose model. The power spectral density of the membrane potential x, is calculated via simulation and our analytical (element-wise) solution. We use the following parameters to simulate the model: $I = 5.5$, $b = 0.5$, $\mu = 0.01$, $x_{rest} = -1.6$, and $s = 4$. We consider the case of additive Gaussian white noise with standard deviation $\sigma = 0.001$.

state of the membrane potential of the neuron; s governs adaptation, and b controls the transition of the activity to different dynamical states (quiescent, spiking, regular bursting, irregular bursting and so on) [140]. We add Gaussian white noise, $\sigma\eta_1$, with standard deviation σ, to the membrane potential and choose the model parameters so that the system is in a quiescent (subthreshold) state with a single stable equilibrium, namely $I = 5.5$, $b = 0.5$, $\mu = 0.01$, $x_{rest} = -1.6$, $s = 4$ and $\sigma = 0.001$ [6].

Since the system is in a quiescent state, it exhibits a single fixed-point solution. Assuming that the deterministic steady-state is given by the triplet (x_e, y_e, z_e), we can linearize the system about the fixed point and write Eq. (5.30) as the LTI system

$$\begin{bmatrix} \dot{x} \\ \dot{y} \\ \dot{z} \end{bmatrix} = \begin{bmatrix} 2bx_e - 3x_e^2 & 1 & -1 \\ -10x_e & -1 & 0 \\ \mu s & 0 & -\mu \end{bmatrix} \begin{bmatrix} x - x_e \\ y - y_e \\ z - z_e \end{bmatrix} + \begin{bmatrix} \sigma\eta_1 \\ 0 \\ 0 \end{bmatrix} \tag{5.31}$$

To show how our element-wise solution leads to a closed-form expression for the power

[6] We choose parameters in the pale cyan region of the bifurcation diagram in Fig. 1 of [140]

spectrum of the membrane potential, we use the general analytical solution for a 3D system given by Eq. (5.19),

$$\mathcal{S}_x(\omega) = \frac{Z(\omega)}{Q(\omega)} = \frac{p_0 + p_1\omega^2 + p_2\omega^4}{q_0 + q_1\omega^2 + q_2\omega^4 + q_3\omega^6}.$$

From the application of Eq. (5.16), we obtain the coefficients of the denominator, $Q(\omega)$, as

$$\begin{aligned}
q_0 =& \mu^2(x_e(3x_e - 2b + 10) + s)^2 \\
q_1 =& \mu^2\left((x_e(3x_e - 2b) + s)^2 - 20x_e + 1\right) + x_e^2(3x_e - 2b + 10)^2 - 2\mu s + 20\mu s x_e \\
q_2 =& x_e\left(x_e(3x_e - 2b)^2 - 20\right) + \mu^2 - 2\mu s + 1 \\
q_3 =& 1
\end{aligned} \tag{5.32}$$

Similarly, the coefficients of the numerator, $Z(\omega)$, can be found from Eq. (5.20): using the fact that $\sigma_1 = \sigma_2 = \sigma_3 = \sigma$, $l_1 = 1$, and $l_2 = l_3 = 0$, we obtain

$$\begin{aligned}
p_0 =& \frac{1}{2}\sigma^2\left(\mathrm{Tr}^2\left(\mathbf{O}_{11}^2\right) - \mathrm{Tr}\left(\mathbf{O}_{11}^4\right)\right) \\
p_1 =& \sigma^2\,\mathrm{Tr}\left(\mathbf{O}_{11}^2\right) \\
p_2 =& \sigma^2
\end{aligned} \tag{5.33}$$

Now, plugging $\mathbf{O}_{11}$ given by

$$\mathbf{O}_{11} = \begin{bmatrix} -1 & 0 \\ 0 & -\mu \end{bmatrix} \tag{5.34}$$

into the equation above, yields the polynomial expansion of the numerator as,

$$Z(\omega) = \mu^2\sigma^2 + \left(\mu^2 + 1\right)\sigma^2\omega^2 + \sigma^2\omega^4 \tag{5.35}$$

We simulate the 3D system and verify that the simulated spectrum matches with the analytical element-wise solution we just derived, shown in Fig. 5.4. Furthermore, we calculate and plot the power spectral density for the membrane potential x, and the absolute cross-power spectral

density and coherence between the fast variables x and y, using Welch's method [143] (simulation), the recursive and element-wise rational function solutions, and the "matrix solution" given by Eq. (5.4) (*n.b.*, this relies on a numerical inverse). We confirm that all the solutions match across the entire range of frequencies, see Fig. 5.4.

5.6.2 Wilson-Cowan Model

The Wilson-Cowan model is a rate-based model that simulates the activity of Excitatory (E) and Inhibitory (I) populations of neurons and has been shown to exhibit gamma oscillations (30-120 Hz) for an appropriate choice of time constants [12]. Specifically, we consider a stochastic 4-dimensional version of the model introduced by Keeley et al. [141], which includes dynamical variables describing the synaptic activation and the firing rate of the E and I populations, see Fig. 5.5 for an illustration. The stochastic dynamical system is defined by the following set of equations,

$$\begin{aligned}
\tau_{\mathrm{E}} \frac{\mathrm{d}r_{\mathrm{E}}}{\mathrm{d}t} &= -r_{\mathrm{E}} + f((I_{\mathrm{E}} + w_{\mathrm{EE}} s_{\mathrm{E}} - w_{\mathrm{EI}} s_{\mathrm{I}} - \theta_{\mathrm{E}})/\kappa_{\mathrm{E}}) + \sigma_r \eta_1 \\
\tau_{\mathrm{I}} \frac{\mathrm{d}r_{\mathrm{I}}}{\mathrm{d}t} &= -r_{\mathrm{I}} + f((I_{\mathrm{I}} + w_{\mathrm{IE}} s_{\mathrm{E}} - w_{\mathrm{II}} s_{\mathrm{I}} - \theta_{\mathrm{I}})/\kappa_{\mathrm{I}}) + \sigma_r \eta_2 \\
\tau_{s_{\mathrm{E}}} \frac{\mathrm{d}s_{\mathrm{E}}}{\mathrm{d}t} &= -s_{\mathrm{E}} + \gamma_{\mathrm{E}} r_{\mathrm{E}} (1 - s_{\mathrm{E}}) + s_{\mathrm{E}}^0 + \sigma_s \eta_3 \\
\tau_{s_{\mathrm{I}}} \frac{\mathrm{d}s_{\mathrm{I}}}{\mathrm{d}t} &= -s_{\mathrm{I}} + \gamma_{\mathrm{I}} r_{\mathrm{I}} (1 - s_{\mathrm{I}}) + s_{\mathrm{I}}^0 + \sigma_s \eta_4
\end{aligned} \tag{5.36}$$

These equations describe the activity of E and I neurons at a population level, with r_{E} and r_{I} representing their firing rates, and s_{E} and s_{I} representing the corresponding synaptic activations. $w_{\alpha\beta}$, where α and $\beta \in \{\mathrm{E}, \mathrm{I}\}$, are the synaptic weights, and $f(x) = 1/(1 + e^{-x})$ is a sigmoid nonlinearity.

The input to the sigmoid is a weighted sum of the synaptic responses plus the external drives I_α, which are offset by θ_α and scaled by κ_α. The synaptic activity (s_α) for E and I populations evolves with time and depends on the firing rate of the corresponding population (r_α), scaled by

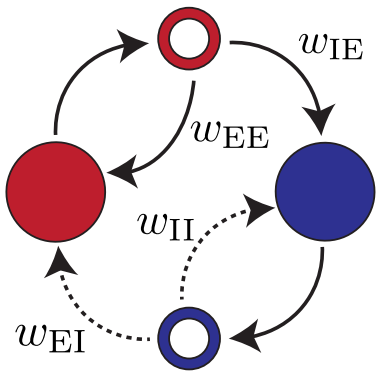


Figure 5.5: Wilson-Cowan 4D model. The mean-field circuit consists of 4 variables modeling excitatory activity (solid red), inhibitory activity (solid blue), excitatory synaptic activity (hollow red), and inhibitory synaptic activity (hollow blue). The solid and dashed arrows indicate excitatory and inhibitory connections, respectively. w_{ij}, with $i, j \in \{\mathrm{E}, \mathrm{I}\}$, represents the weight associated with the connections from j to i.

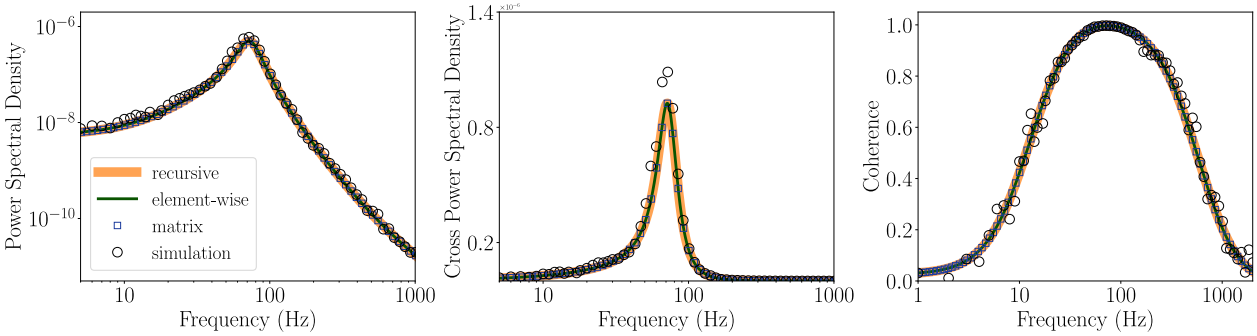


Figure 5.6: Spectral density (auto and cross) and coherence for the Wilson-Cowan model. We plot the power spectral density (left), the absolute cross-power spectral density (middle), and the coherence (right) for a given stimulus, each calculated via simulation, the rational function solutions (recursive and element-wise), and the matrix solution (Eq. (5.4)). The PSD is calculated for the firing rate of the excitatory population. The cross-PSD and coherence are calculated between the firing rates of the excitatory and inhibitory populations. We use the following parameters for simulations and analytical calculations. Time constants: $\tau_{\mathrm{E}} = 2$ ms, $\tau_{\mathrm{I}} = 8$ ms, $\tau_{s_{\mathrm{E}}} = 10$ ms and $\tau_{s_{\mathrm{I}}} = 10$ ms. Strength of the weights: $w_{\mathrm{EE}} = 5$, $w_{\mathrm{EI}} = 5$, $w_{\mathrm{IE}} = 3.5$ and $w_{\mathrm{II}} = 3$. Offset of the input: $\theta_{\mathrm{E}} = 0.4$ and $\theta_{\mathrm{I}} = 0.4$. Scaling of the input: $\kappa_{\mathrm{E}} = 0.2$ and $\kappa_{\mathrm{I}} = 0.02$. Scaling of the population synaptic activity: $\gamma_{\mathrm{E}} = 1$ and $\gamma_{\mathrm{I}} = 2$. External inputs to the system: $I_{\mathrm{E}} = 1$, $I_{\mathrm{I}} = 0.5$, $s_{\mathrm{E}}^0 = 0.2$ and $s_{\mathrm{I}}^0 = 0.05$. We consider additive Gaussian white noise with standard deviations $\sigma_r = 0.001$, and $\sigma_s = 0.002$.

γ_α, as well as on the corresponding background synaptic inputs s_α^0. The time constants controlling the rise/decay times are τ_α. The variables evolve stochastically on account of the uncorrelated Gaussian additive white noise, $\sigma\eta_i$, with standard deviations σ_r and σ_s, added to the firing rates and the synaptic activity, respectively.

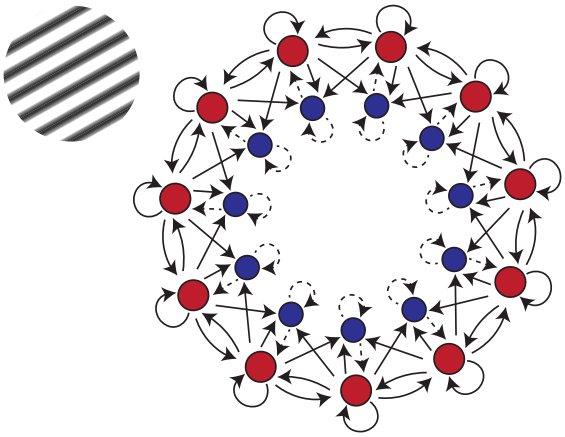


Figure 5.7: SSN circuit. The circuit consists of 11 excitatory (red) and 11 inhibitory neurons (blue) and receives a sinusoidal grating input shown on the left. The arrows schematize the connections between the different neurons. E-E and I-E connections are excitatory (solid arrows) fully connected, whereas E-I and I-I connections are self-inhibitory (dashed arrows).

We perform a simulation of the 4-dimensional system and generate power spectral density plots for the firing rate of the E population, r_{E}, the absolute cross-power spectral density between the firing rate of the E and I populations, and the coherence

$$K_{ij} = \frac{|\mathcal{S}_{ij}|^2}{|\mathcal{S}_{ii}||\mathcal{S}_{jj}|} \tag{5.37}$$

between the firing rates of the E and I populations using Welch's method [143] for simulation, the recursive and element-wise rational function solutions, and the matrix solution (Eq. (5.4)). Our results demonstrate that all the solutions match across the entire range of frequencies, as confirmed in Fig. 5.6.

5.6.3 Stabilized Supralinear Network (SSN)

The Stabilized Supralinear Network (SSN) [13, 93] is a neural circuit model reproducing divisive normalization approximately [5, 9] that has been used to simulate neuronal activity in the sensory cortex [13, 93, 144–146]. We implement an SSN for simulating the activity of the primary visual cortex (V1) as described in [13]. We consider a 11-dimensional spatial input which is a sinusoidal

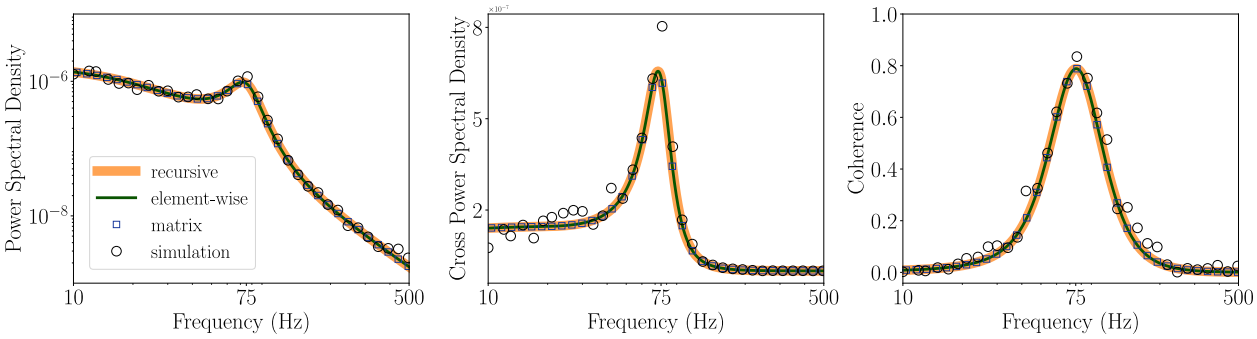


Figure 5.8: Spectral density (auto and cross) and coherence for the SSN circuit. We plot the power spectral density (left), the absolute cross-power spectral density (middle), and the coherence (right) for a given stimulus each calculated via simulation, the rational function solutions (recursive and element-wise), and the matrix solution (Eq. (5.4)). The PSD is calculated for the excitatory neuron with the highest preference for the stimulus (i.e., exhibiting maximum firing rate). The cross-PSD and coherence are calculated between the two excitatory neurons with the highest firing rates. We use the following parameters for simulating the model: Contrast $c = 50$, stimulus length $l = 9$, $\Delta x = 3.0$, $\sigma_{RF} = 0.125\Delta x$. Time constants of $\tau_{\mathrm{E}} = 6$ ms and $\tau_{\mathrm{I}} = 4$ ms. Supralinear activation parameters $n = 2.2$ and $k = 0.01$. We add zero-mean Gaussian noise to the SDEs describing the activity of the E and I neurons with standard deviation $\sigma = 0.01$.

grating of a fixed orientation and a given contrast (*n.b.*, the response of V1 neurons is tuned to specific positions, orientations, size, etc., of the visual stimulus [147]) and varies with Michelson contrast, $c = (I_{\max} - I_{\min})/(I_{\max} + I_{\min})$, where $I_{\min,\max}$ are the minimum and maximum luminance in the stimulus. The input evaluated at a set of discrete points $\mathbf{x}$, is taken to be proportional to the contrast, $\mathbf{h}(\mathbf{x}) \propto c$, and decays with distance from the origin.

Specifically, the input is centered at 0 with the distance between any two consecutive points $\Delta x = 3$. The input at a given location x is given by,

$$\mathbf{h}(x) = c\left(\frac{1}{1+e^{-\frac{x+l/2}{\sigma_{RF}}}}\right)\left(1 - \frac{1}{1+e^{-\frac{x-l/2}{\sigma_{RF}}}}\right) \tag{5.38}$$

where $l = 9$ is the length of the stimulus, and $\sigma_{RF} = 0.125\Delta x$ defines the width of the edges of the input. We operate in a regime where the circuit exhibits a fixed point solution with damped oscillations (for parameters see Fig. 5.8).

The dynamical equations for the firing rates of the excitatory neurons, $\mathbf{r}_{\mathrm{E}}(\mathbf{x})$, and the inhibitory

neurons, $\mathbf{r}_{\mathrm{I}}(\mathbf{x})$, are given by

$$\begin{aligned}\tau_{\mathrm{E}}\frac{\mathrm{d}\mathbf{r}_{\mathrm{E}}(\mathbf{x})}{\mathrm{d}t} &= -\mathbf{r}_{\mathrm{E}}(\mathbf{x}) + \mathbf{r}_{\mathrm{E}}^{ss}(\mathbf{x}) + \sigma\eta_{\mathrm{E}}(\mathbf{x}) \\ \tau_{\mathrm{I}}\frac{\mathrm{d}\mathbf{r}_{\mathrm{I}}(\mathbf{x})}{\mathrm{d}t} &= -\mathbf{r}_{\mathrm{I}}(\mathbf{x}) + \mathbf{r}_{\mathrm{I}}^{ss}(\mathbf{x}) + \sigma\eta_{\mathrm{I}}(\mathbf{x})\end{aligned} \tag{5.39}$$

where τ_{E} and τ_{I} are the time constants of the excitatory and inhibitory neurons, $\sigma\eta_{\mathrm{E}}(\mathbf{x})$ and $\sigma\eta_{\mathrm{I}}(\mathbf{x})$ are zero-mean uncorrelated Gaussian noise vectors with standard deviation σ, and $\mathbf{r}_{\mathrm{E}}^{ss}$ and $\mathbf{r}_{\mathrm{I}}^{ss}$ are the steady-state responses of the excitatory and inhibitory neurons, given by the equations

$$\begin{aligned}\mathbf{r}_{\mathrm{E}}^{ss}(\mathbf{x}) &= k([\mathbf{h}(\mathbf{x}) + \mathbf{W}_{\mathrm{EE}}\mathbf{r}_{\mathrm{E}}(\mathbf{x}) - \mathbf{W}_{\mathrm{EI}}\mathbf{r}_{\mathrm{I}}(\mathbf{x})]_+)^n \\ \mathbf{r}_{\mathrm{I}}^{ss}(\mathbf{x}) &= k([\mathbf{h}(\mathbf{x}) + \mathbf{W}_{\mathrm{IE}}\mathbf{r}_{\mathrm{E}}(\mathbf{x}) - \mathbf{W}_{\mathrm{II}}\mathbf{r}_{\mathrm{I}}(\mathbf{x})]_+)^n\end{aligned} \tag{5.40}$$

Here, $[z]_+ = \max(z, 0)$ denotes a ReLU activation. In the SSN, the steady-state responses depend on a supralinear activation ($n = 2.2$ and $k = 0.01$) of the input to the neurons, which is a sum of the stimulus input and feedback from the neurons in the population.

The E-E (excitatory to excitatory) and I-E (inhibitory to excitatory) connections are given by a Gaussian function. The i, j entry of the weight matrix is defined as follows,

$$\mathbf{W}_{\alpha\mathrm{E}}(j,k) = J_{\alpha\mathrm{E}}e^{-\frac{(x_j - y_k)^2}{2\sigma_{\alpha\mathrm{E}}^2}}, \quad \alpha \in \{\mathrm{E}, \mathrm{I}\} \tag{5.41}$$

where x_i and y_j are the locations of the i^{th} and j^{th} neurons, respectively. $J_{\mathrm{EE}} = 2.0$, $J_{\mathrm{IE}} = 2.25$ define the magnitude of the weights, and $\sigma_{\mathrm{EE}} = 4$ and $\sigma_{\mathrm{IE}} = 8$ are the parameters of the Gaussians determining the spatial extent of the connections between E-E and I-E populations, respectively. The E-I and I-I connections are not fully connected but self-inhibitory with the weights $J_{\mathrm{EI}} = 0.9$, $J_{\mathrm{II}} = 0.5$.

We simulate a 22-dimensional system, see Fig. 5.7 for an illustration. In Fig. 5.8, we show the power spectral density for the excitatory neuron with the highest preference for the stimulus (viz.,

that is maximally firing); the absolute cross-power spectral density and the coherence between the two excitatory neurons with the highest firing rates, each using Welch's method [143] (simulation), our recursive and element-wise rational function solutions, and the matrix solution (Eq. (5.4)). We confirm that all the solutions match across the entire range of frequencies.

5.6.4 Rock-Paper-Scissors

The game of Rock-Paper-Scissors, where rock smashes scissors, scissors cut paper, and paper wraps rock has been employed by evolutionary biologists to investigate the interactions between competing populations of species, where one species has an advantage over only one of its opponents. The game dynamics that describe the evolution of the populations following a particular strategy can be examined with the use of evolutionary game theory [142]. We explore the evolution of this dynamical system in accordance with a sociological model [148, 149], where each population, following a unique strategy, seeks to minimize the difference between the average payoff of the population and the individual payoff.

Mathematically, we can represent the system as follows: Let $\mathbf{x} = [x_1, x_2, ..., x_n]$ be the n-dimensional system comprising the fractional populations corresponding to different strategies. The sociological model dictates that these fractional populations evolve according to a metric given by $\dot{x_i} \propto (f_{x_i} - \phi)$, where f_{x_i} is the individual payoff for choosing a strategy corresponding to the population x_i, and ϕ is the average payoff of the population given by $\phi = \sum_{i=1}^{n} x_i f_{x_i}$. It is important to note that the dynamical system is effectively $n - 1$ dimensional due to the mass conservation equation $\sum_{i=1}^{n} x_i = 1$.

We consider a high-dimensional version of the Rock-Paper-Scissors game, consisting of n populations each following a unique strategy, described by the pay-off matrix, $\mathbf{P}$. For an n-

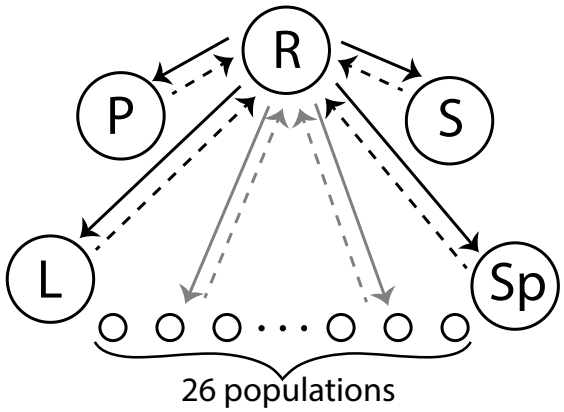


Figure 5.9: 31-D Rock-Paper-Scissors model. Circles represent the different strategies ($n = 31$) in the evolutionary game theoretic model. Shown in the figure are 5 of the 31 strategies: Rock (R), paper (P), Scissors (S), Spock (Sp), and Lizard (L). We consider a model with global mutations, i.e., each population associated with a strategy mutates into every other population with the same rate μ. Depicted in the figure are mutations to (dashed arrows) and from (solid arrows) the Rock population.

dimensional version of the game, the payoff matrix (P_{ij}) can be summarized as,

$$P_{ij} = \begin{cases} (-1)^{i+j+1} & i > j \\ 0 & i = j \\ (-1)^{i+j} & i < j. \end{cases} \tag{5.42}$$

Here, 1 indicates a win against the opponent, -1 indicates a loss and 0 indicates neither a win nor a loss (a draw). Therefore, the individual payoff for a given strategy is given in terms of $\mathbf{P}$ as, $f_{x_i} = \sum_{j=1}^{n} P_{ij} x_j$.

In addition to the populations evolving according to the sociological strategy, we also consider the effects of global mutations and fluctuations in population. For the global mutations, we introduce a parameter μ such that each population mutates into every other population with constant rate μ, as illustrated in Fig. 5.9. This results in a stochastic dynamical system where the deterministic part evolves according to replicator-mutator dynamics [142, 150]. Furthermore, we model the noise as multiplicative Gaussian white noise, $\sigma x_i \eta_i$, with standard deviation σ small enough that the population stays close to the fixed point. Thus, for the n-dimensional system, we

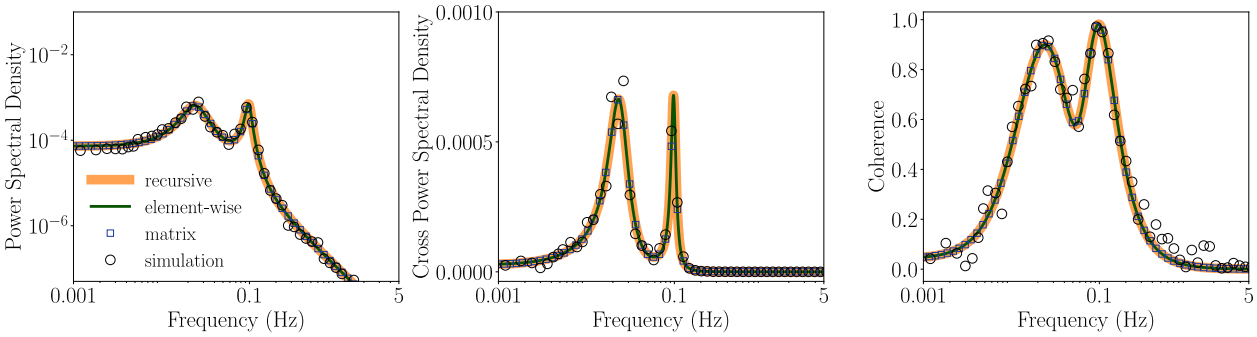


Figure 5.10: Spectral density (auto and cross) and coherence for the Rock-Paper-Scissors-Lizard-Spock model. We plot the power spectral density (left), the absolute cross power spectral density (middle), and the coherence (right) for a fixed mutation parameter ($\mu = 0.01$) each calculated via simulation, the rational function solutions, and the matrix solution. The PSD is calculated for the Paper population. The cross-PSD and coherence are calculated between the Rock and Paper populations.

can represent the set of differential equations for all $i \leq n$ as follows:

$$\frac{\mathrm{d}x_i}{\mathrm{d}t} = x_i(f_{x_i} - \phi) + \mu\left(-(n-1)x_i + \sum_{\substack{j=1 \\ j\neq i}}^{n} x_j\right) + \sigma x_i \eta_i \tag{5.43}$$

To ensure that mass conservation is followed, we define the system according to the replicator-mutator differential equation (Eq. (5.43)) for $i \leq n-1$, and compute the n-th population from the constraint $\sum_{i=1}^{n} x_i = 1$. Recall that the individual payoff is $f_{x_i} = \sum_{i=1}^{n} P_{ij} x_j$, and the average payoff of the population is $\phi = \sum_{i=1}^{n} x_i f_{x_i} = 0$. The dynamical system has a fixed point at $x_i^{ss} = 1/n$, for all $i \leq n$. Additionally, the elements of the Jacobian, J_{ij}, for the dynamical system evaluated at the fixed point can be defined as a function of the mutation rate parameter μ,

$$J_{ij} = \begin{cases} \begin{cases} 0 & j \text{ is even} \\ (-1)^i \times 2/n & j \text{ is odd} \end{cases} & i > j \\ (-1)^i/n - \mu n & i = j \\ \begin{cases} (-1)^i \times 2/n & j \text{ is even} \\ 0 & j \text{ is odd} \end{cases} & i < j. \end{cases} \tag{5.44}$$

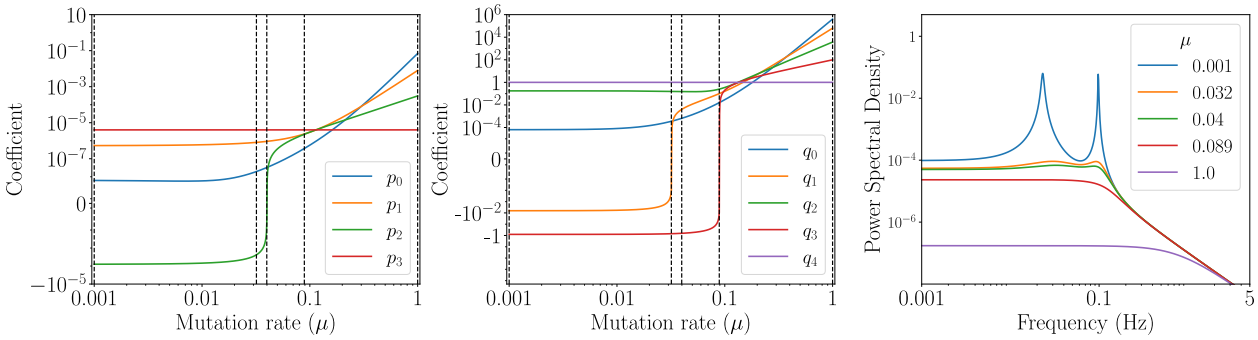


Figure 5.11: Coefficients of the rational function for the auto-spectrum of Paper population in the Rock-Paper-Scissors-Lizard-Spock model. We plot the coefficients of the numerator (left) and the denominator (middle) of the rational function of the auto-spectrum of the Paper population for a range of mutation rates μ. We identify the mutation rates at which the various coefficients change sign (plotted as vertical dotted lines in the left and middle plots) and plot the corresponding power spectral density. The analysis is done for the Paper population.

We first simulate a 5-dimensional Rock-Paper-Scissors-Lizard-Spock model. This game can be described by the pay-off matrix (**P**) given below. Note that the player and the opponent choose their strategies from the rows and the columns of the table, respectively. 1 indicates you win against your opponent, -1 indicates you lose, and 0 indicates you neither win nor lose against your opponent.

	R	P	S	Sp	L
R	0	-1	1	-1	1
P	1	0	-1	1	-1
S	-1	1	0	-1	1
Sp	1	-1	1	0	-1
L	-1	1	-1	1	0

The equations describing the evolution of populations following a certain strategy with global mutations ($\mu = 0.01$) and multiplicative Gaussian white noise (with standard deviation $\sigma = 0.01$)

are defined as follows,

$$\begin{aligned}
\dot{x_1} &= x_1(-x_2 + x_3 - x_4 + x_5 - \phi) + \mu(-4x_1 + x_2 + x_3 + x_4 + x_5) + \sigma x_1 \eta_1 \\
\dot{x_2} &= x_2(x_1 - x_3 + x_4 - x_5 - \phi) + \mu(-4x_2 + x_1 + x_3 + x_4 + x_5) + \sigma x_2 \eta_2 \\
\dot{x_3} &= x_3(-x_1 + x_2 - x_4 + x_5 - \phi) + \mu(-4x_3 + x_1 + x_2 + x_4 + x_5) + \sigma x_3 \eta_3 \\
\dot{x_4} &= x_4(x_1 - x_2 + x_3 - x_5 - \phi) + \mu(-4x_4 + x_1 + x_2 + x_3 + x_5) + \sigma x_4 \eta_4 \\
x_1 + x_2 + x_3 + x_4 + x_5 &= 1
\end{aligned} \tag{5.45}$$

The fixed point solution of the equations above is $x_1^{ss} = x_2^{ss} = x_3^{ss} = x_4^{ss} = 1/5$. Therefore, the effective standard deviation of the noise at steady-state is $\sigma_e = \sigma/5$. Further, the Jacobian matrix is given by,

$$\mathbf{J} = \begin{bmatrix} -1/5 - 5\mu & -2/5 & 0 & -2/5 \\ 2/5 & 1/5 - 5\mu & 0 & 2/5 \\ -2/5 & 0 & -1/5 - 5\mu & -2/5 \\ 2/5 & 0 & 2/5 & 1/5 - 5\mu \end{bmatrix} \tag{5.46}$$

Using our analytical solution, we have access to the coefficients of ω in the numerator and the denominator. Therefore, we can write the rational function for the auto-spectrum of the Paper population as,

$$\mathcal{S}^{22}(\omega) = \frac{p_0 + p_1\omega^2 + p_2\omega^4 + p_3\omega^6}{q_0 + q_1\omega^2 + q_2\omega^4 + q_3\omega^6 + q_4\omega^8} \tag{5.47}$$

with the coefficients for the numerator given by,

$$\begin{aligned}
p_0 &= \left(15625\mu^6 + 1250\mu^5 + 575\mu^4 + 28\mu^3 + \frac{79\mu^2}{25} - \frac{6\mu}{125} + \frac{1}{625}\right)\sigma_e^2 \\
p_1 &= \left(1875\mu^4 + 100\mu^3 + 18\mu^2 + \frac{36\mu}{25} + \frac{83}{625}\right)\sigma_e^2 \\
p_2 &= \left(75\mu^2 + 2\mu - \frac{1}{5}\right)\sigma_e^2 \\
p_3 &= \sigma_e^2
\end{aligned} \tag{5.48}$$

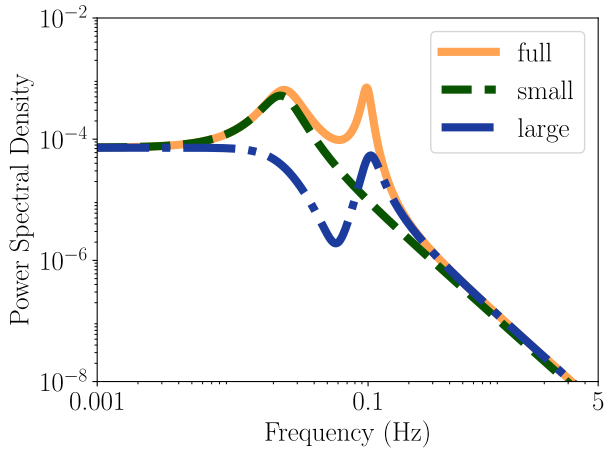


Figure 5.12: Rational function solution for the spectral density in the Rock-Paper-Scissors-Lizard-Spock ($n = 5$) model. We plot the full rational function for the power spectral density of the "paper" population, and its analytical approximations isolating the low-frequency peak, $\mathcal{S}^{22}_{\text{small}}(\omega) = (p_0 + p_1\omega^2)/(q_0+q_1\omega^2+q_2\omega^4)$ and the high-frequency peak, $\mathcal{S}^{22}_{\text{large}}(\omega) = (p_0+p_2\omega^4+p_3\omega^6)/(q_0+q_2\omega^4+q_3\omega^6+q_4\omega^8)$.

and for the denominator given by,

$$\begin{aligned} q_0 &= 390625\mu^8 + 12500\mu^6 + 110\mu^4 + \frac{4\mu^2}{25} + \frac{1}{15625} \\ q_1 &= 62500\mu^6 + 500\mu^4 + \frac{28\mu^2}{5} - \frac{4}{625} \\ q_2 &= 3750\mu^4 - 20\mu^2 + \frac{22}{125} \\ q_3 &= 100\mu^2 - \frac{4}{5} \\ q_4 &= 1 \end{aligned} \tag{5.49}$$

Similarly, we can write the coefficients for the rational function for the cross-spectrum (between the Rock and Paper populations). These coefficients (for auto/cross-spectrum) define the spectral density over the entire frequency domain. Since the elements of the Jacobian matrix depend on the mutation rate μ and on the noise standard deviation σ, the coefficients p_i and q_i are also a function of μ and σ. We first confirm that the solutions for the auto-spectrum (for the paper population), cross-spectrum, and coherence (between the Rock and the Paper populations) match across the range of frequencies for the different methods (Fig. 5.10). We then plot (Fig. 5.11) the

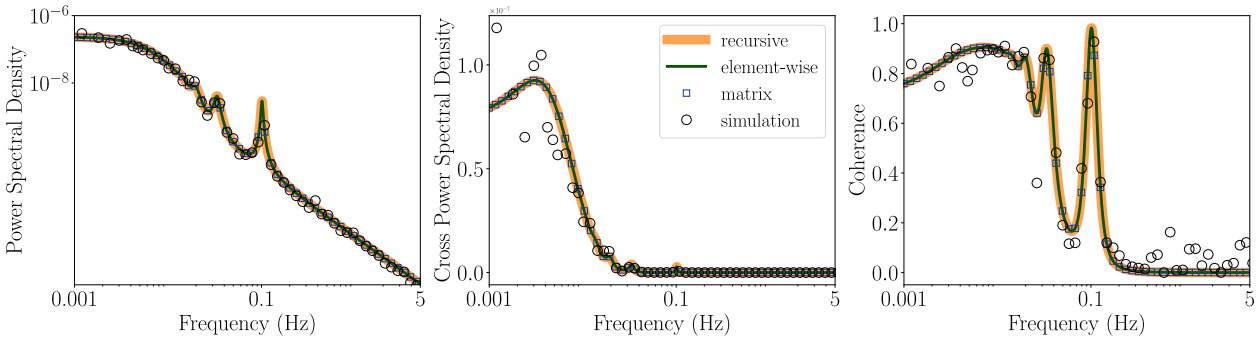


Figure 5.13: Spectral density (auto and cross) and coherence using different methods for a 31-dimensional Rock-Paper-Scissors type model. We plot the power spectral density (left), the absolute cross-power spectral density (middle), and the coherence (right) for a fixed mutation parameter ($\mu = 0.0005$) each calculated via simulation, the rational function solutions, and the matrix solution. The PSD is calculated for the Rock population. The cross-PSD and coherence are calculated between the Rock and Paper populations. We consider the case of multiplicative noise, σx_j, added to each population, with standard deviation $\sigma = 10^{-4}$.

coefficients p_i and q_i for varying mutation rates and find the values of μ for which the sign of any of the coefficients changes. We also plot the PSD corresponding to those mutation rates and find that these values of μ correspond to the emergence of oscillations (marked by the appearance of a peak in the PSD). For this system, it is possible to leverage the analytical coefficients obtained by our rational function solution to derive analytical approximations that isolate the different features of the model (Fig. 5.12).

We also simulate a 31D system with a fixed mutation parameter, $\mu = 0.0005$, and the scaling factor of the noise, $\sigma = 10^{-4}$, that is the same for all the populations. In Fig. 5.13, we show the power spectral density for the Rock population (viz., the first strategy), the absolute cross-power spectral density and the coherence between the Rock and Paper populations (viz., the first and second strategy), each using Welch's method [143] (simulation), our recursive and element-wise rational function solutions, and the matrix solution (Eq. (5.4)). Our solutions match across the entire range of frequencies, verifying their correctness.

5.6.5 Hawkes Model

Our final example shows how we can use Theorem 5.2 to find the connectivity-dependent correlation structure of spiking neurons connected in an arbitrary network. We consider the Hawkes model [132] describing recurrently connected linearly interacting spiking neurons, as in Ref. [151]. The network consists of linearly interacting point processes with recurrent connectivity given by the kernel matrix, $\mathbf{G}(t)$. The firing rates vector, $\mathbf{y}(t)$, evolves according to the Hawkes process, given by the following equation,

$$\mathbf{y}(t) = \mathbf{y}_0 + \int_{-\infty}^{t} \mathbf{G}(t-u) d\mathbf{N}(u) \tag{5.50}$$

where $\mathbf{N}(t)$ is the vector of point processes and $\mathbf{y}_0$ is a biasing vector encoding a constant external drive. Assuming a stationary state, the covariance matrix is defined by the following self-consistent equation,

$$\mathbf{R}(\tau) = \mathbf{G}(\tau)\mathbf{Y} + (\mathbf{G} * \mathbf{R})(\tau) \tag{5.51}$$

where $\mathbf{Y}$ is the diagonal matrix containing the entries of $\mathbf{y}_0$ on its diagonal and $*$ denotes convolution. The spectral density matrix of the Hawkes process is then given by [132],

$$\boldsymbol{\mathcal{S}}(\omega) = \left(\mathbf{I} - \hat{\mathbf{G}}(\omega)\right)^{-1} \mathbf{Y} \left(\mathbf{I} - \hat{\mathbf{G}}^{\top}(\omega)\right)^{-1} \tag{5.52}$$

where $\hat{\mathbf{G}}(\omega)$ is the Fourier transform of $\mathbf{G}(\tau)$. Then, the integrated covariance matrix $\mathbf{R} \coloneqq \int_{-\infty}^{\infty} \mathbf{R}(\tau) \mathrm{d}\tau = \boldsymbol{\mathcal{S}}(0)$ is given by,

$$\mathbf{R} = (\mathbf{I} - \mathbf{G})^{-1} \mathbf{Y} \left(\mathbf{I} - \mathbf{G}^{\top}\right)^{-1} \tag{5.53}$$

where $\mathbf{G} \coloneqq \int_{-\infty}^{\infty} \mathbf{G}(\tau) \mathrm{d}\tau = \hat{\mathbf{G}}(0)$.

We consider the problem of how the connectivity pattern influences the correlation structure

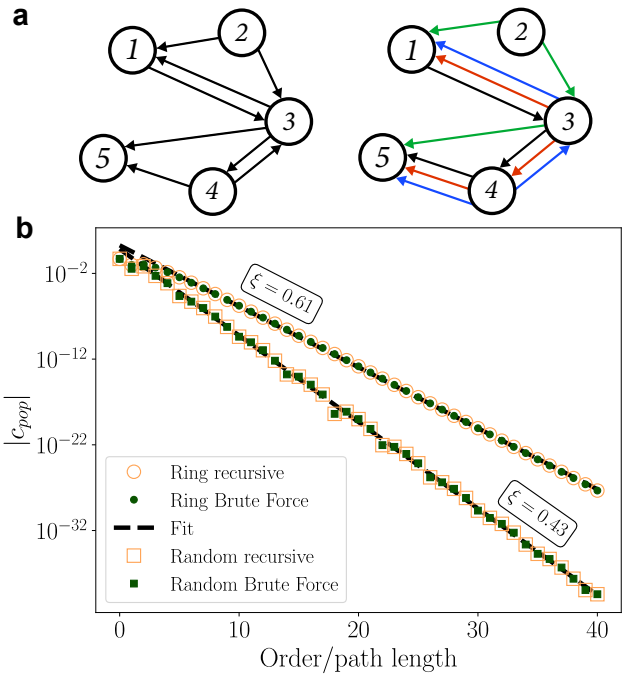


Figure 5.14: Population covariance of spiking neural networks. a: (Left) Directed graph representing the connectivity structure of a spiking network model. (Right) Third-order paths contributing to the $(a = 1, b = 5)$ entry of $\mathbf{S}_3$ in the integrated covariance, Eq. (5.54). $c = 2, 3, 4$ are the intermediary nodes in the graph. Colored arrows represent the path between nodes $a = 1$ and $b = 5$ via (green) $c = 2$ and (red) $c = 3$ due to the term $\mathbf{G}\,\mathbf{Y}\,(\mathbf{G}^\top)^2$; (blue) via $c = 4$ due to the term $\mathbf{G}^2\,\mathbf{Y}\,(\mathbf{G}^\top)$; (black) direct path between nodes $a = 1$ and $b = 5$ due to the term $\mathbf{Y}\,(\mathbf{G}^\top)^3$. **b**: Absolute average pairwise population covariance, $|c_{pop}|$, as a function of path length m, found by calculating the mean of the matrix elements $\mathbf{S}_m$ in Eq. (5.54), for a directed cycle graph (circles), and a directed random graph (squares). The contributions $\mathbf{S}_m$ are computed by the recursive algorithm in Theorem 5.2, and by a brute force approach. The Hawkes models are defined by the following parameters: $N_E = 16$ (#E neurons), $N_I = 4$ (#I neurons), $g_E = 0.015$, $g_I = -0.075$. For the model on a random graph, the probability of drawing a directed edge between any two nodes (i, j) is 0.45.

in networks of spiking neurons, as studied in [151–153]. In particular, when the spectral radius of $\mathbf{G}$ is less than 1, we can expand the covariance matrix as the following infinite sum,

$$\mathbf{R} = \left(\sum_{j=0}^{\infty} \mathbf{G}^j\right) \mathbf{Y} \left(\sum_{k=0}^{\infty} (\mathbf{G}^\top)^k\right) = \sum_{j,k=0}^{\infty} \mathbf{G}^j\,\mathbf{Y}\,(\mathbf{G}^\top)^k = \sum_{m=0}^{\infty} \mathbf{S}_m \tag{5.54}$$

where $\mathbf{S}_m \coloneqq \sum_{\substack{j+k=m \\ j\geq 0,\, k\geq 0}} \mathbf{G}^j\,\mathbf{Y}\,(\mathbf{G}^\top)^k$ accounts for the contributions of *paths* of order (length) m to the integrated covariance matrix. Note that for the $(a, b)^{th}$ entry of $\mathbf{G}^j\,\mathbf{Y}\,(\mathbf{G}^\top)^k$, $\mathbf{G}^j$ represents the sum over all paths towards a from driving nodes c that are distance j from a; while $(\mathbf{G}^\top)^k$

encodes the sum over all paths towards b from nodes c that are distance k from b. Then the total length of the paths between a and b through driving nodes c is $m = j + k$ (see Fig. 5.14a for an example). Therefore, this quantity provides a way of quantifying how graph connectivity influences correlations in a network of spiking neurons modeled as a Hawkes process.

We demonstrate how the recursive algorithm in Theorem 5.2 allows us to compute $\mathbf{S}_m$ in $O(n^4)$ compared to $O(n^5)$ by a brute force solution. We consider two different types of networks, both described in detail in [151]. The first network has neurons (both E & I) in a ring structure with only connections between nearest neighbors allowed (i.e., in a bidirectional directed cycle graph). The second is a randomly connected network of E and I neurons (i.e., a random directed graph). The total number of neurons is 20, with 16 E and 8 I neurons, each receiving a constant input of 10Hz, i.e., $y_0 = 10$Hz. The kernels in matrix $\mathbf{G}(\tau)$ are exponentially decaying with a time constant of 10 ms and an amplitude of 1.5Hz/-7.5Hz for E/I spikes. This corresponds to the entries of the matrix $\mathbf{G}$ being 0.015 for E presynaptic neurons and -0.075 for I presynaptic neurons. For the randomly connected network, the oriented edge between neurons i and j is added with a probability 0.45, chosen so that the total number of connections for the ring model and the random model are equal.

Fig. 5.14 shows the absolute average pairwise population covariance, $|c_{pop}|$, as a function of path length m, found by calculating the mean of the matrix elements of $\mathbf{S}_m$, and confirms that the recursive solution (Theorem 5.2) matches the brute force solution. Moreover, since $|c_{pop}|$ decays exponentially as a function of the order m, we estimate the typical order/path (correlation) length (ξ) by assuming the relation, $|c_{pop}| \propto e^{-m/\xi}$. Clearly, the network topology influences the characteristic path length, so that $\xi_{ring} > \xi_{random}$, despite both networks having the same number of connections.

5.7 Discussion

In this work, we presented two approaches for computing explicitly the rational function solution of the power spectral density matrix for stochastic linear time-invariant systems driven by Gaussian white noise. In one approach, we derived element-wise solutions (valid for arbitrary n-dimensional LTI systems) for the rational function coefficients of any given entry of the PSD matrix, computable in roughly $O(n^4 \log n)$ operations. Each coefficient is expressed in terms of Bell polynomials [138] evaluated on submatrices of the Jacobian, defined according to the algorithm summarized in Fig. 5.3. Our element-wise solution is particularly useful to gain insights into the dependence of the PSD on the model's functional form and its parameters, especially when the model is fairly low dimensional. Therefore, we provide explicit solutions for the auto-spectra of a general $n = 2, 3$ and 4 dimensional system driven by uncorrelated Gaussian noise increments. A similar, albeit longer, symbolic expression can be obtained for any dimensional system and noise correlation structure via our software package (or working through the general solution in Appendix D.3). We also showed that the polynomial matrix coefficients in the numerator and the polynomial coefficients in the denominator can be obtained recursively by means of a Faddeev-Leverrier-type algorithm in $O(n^4)$ operations, see Theorem D.1.[7]. Since the algorithm involves simple matrix multiplication and trace operations, it should be possible to further optimize it to achieve better time complexity. Crucially, both our solutions are free of matrix inverses, in addition to being more revealing than the simpler matrix solution given by Eq. (5.4).

Finally, we applied our approaches for the derivation of analytical (i.e., closed form) PSD of stochastic nonlinear dynamical models of neural systems, namely Fitzhugh-Nagumo ($n = 2$), Hindmarsh-Rose ($n = 3$), Wilson-Cowan ($n = 4$), and the Stabilized Supralinear Network ($n = 22$), as well as of an evolutionary game-theoretic model with mutations ($n = 5, 31$).

[7]Note that since we perform our numerical calculations with arbitrary precision our implementation scales $O(n^5)$, see Appendix D.3

To showcase the power of the recursive approach and its broad applicability, we used it to find a recursive solution for an auxiliary spectral matrix of similar form, Theorem D.5. This enabled us to derive a recursive algorithm (Theorem 5.2) for the terms of varying order in an expansion of the integrated covariance matrix for a network of linearly interacting spiking neurons modeled by Hawkes processes. The recursive nature of the solution not only leads to a faster algorithm ($O(n^4)$ vs the $O(n^5)$ of the brute force approach) but also provides deeper insights into the structure of the covariance matrix.

Since ω appears in different powers in both the numerator and denominator of the rational function of the power spectral density, we can neglect certain terms when they are small within the relevant range of ω. For example, in Fig. 5.12, we demonstrated how setting these small terms to zero in specific frequency regimes, both small and large, enables us to isolate the two peaks observed in the spectra of the paper population within the 5D Rock-Paper-Scissor-Lizard-Spock model. The analytical tractability of these solutions may enable us to rule out certain models, identify simpler ones (e.g., by providing insight into how model parameters contribute to spectral features) or to establish constraints on model parameters that ensure the presence of a peak in the spectra within a specified frequency range.

Overall, our solutions should find broad applicability in the analysis of the dynamics of stochastic biological systems exhibiting fixed point solutions, as well as in the broader context of dynamical systems and control theory.

6 Exact Variance and Fano Factor for Arbitrary Level Crossings in Stationary Gaussian Processes

6.1 Overview

Understanding the statistics of level crossings in stochastic processes is crucial across many scientific disciplines. While exact results for mean-level crossings exist, this work provides the exact analytical expressions for the variance and the Fano factor of arbitrary level *up*/*down*-crossings and bidirectional crossings in smooth, stationary Gaussian processes. To demonstrate the generality of our findings, these analytical solutions are validated across a diverse set of stochastic processes: the classic stochastic damped harmonic oscillator, a mean-reverting process driven by Ornstein-Uhlenbeck (OU) noise, and a stochastic process with a rational quadratic correlation function. For each model, we first confirm our analytical results and then elucidate how the variance and Fano factors depend on process parameters, revealing the influence of the correlation structure on crossing statistics. These results offer versatile tools for inference and parameter estimation across a broad class of correlation structures, particularly in fields like environmental science and biophysics where Gaussian processes are prevalent.

6.2 Introduction

The study of level crossings in stochastic processes is of fundamental importance across a range of scientific and engineering disciplines, including signal processing, neuroscience [154–157], and financial mathematics [158, 159]. While the renowned Kac-Rice formula [160, 161] provides a powerful tool for quantifying the mean number of level crossings (the first moment), a deeper understanding often necessitates the study of higher-order moments. Higher-order statistical properties of these crossing events, including their variability, can yield critical insights into the intrinsic dynamics and underlying mechanisms of the systems being modeled.

In this work, we focus on the statistics of level crossings for a smooth, stationary Gaussian process X_t. As illustrated in Fig. 6.1, an *up*-crossing of a given level u occurs when the process X_t intersects the threshold u with a positive slope (i.e., $X_t = u$ and $\dot{X}_t > 0$). We denote the number of such events within a time interval $[0, T]$ as $N_u^{\uparrow}(T)$. Similarly, *down*-crossings, where $X_t = u$ and $\dot{X}_t < 0$, are denoted by $N_u^{\downarrow}(T)$. The total number of crossings, encompassing both directions, is $N_u(T) = N_u^{\uparrow}(T) + N_u^{\downarrow}(T)$. Our primary objective is to derive exact analytical expressions for the variance of these counting processes, specifically $\mathrm{Var}[N_u^{\uparrow}(T)]$ and $\mathrm{Var}[N_u(T)]$. Furthermore, we investigate the Fano factor, a key dimensionless metric that characterizes the variance of the crossing counts relative to their mean, providing a measure of their regularity.

The study of higher-order moments of level crossings has a rich history [162], with general expressions for these moments often formulated as multiple integrals involving the process's derivatives. For the specific case of the variance of *mean-level* upcrossings (i.e., $u = 0$), exact analytical solutions, expressed as a single integral over time whose integrand depends on the autocorrelation function and its derivatives, have been known since the early 1950s [163]. However, extending such a compact single-integral form to the variance of upcrossings for an *arbitrary* level u has remained a more challenging problem. While some progress has been made, for instance, by deriving expressions involving a time integral combined with an integral over the process

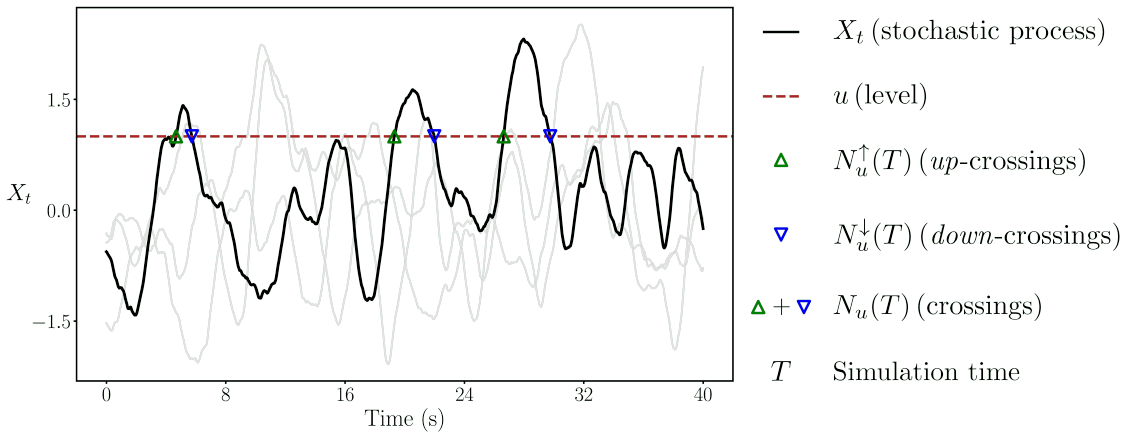


Figure 6.1: Illustration of level crossing events for a stationary Gaussian process. We plot the sample paths of a stationary Gaussian stochastic process X_t generated by the stochastic damped harmonic oscillator model, which is detailed in Section 6.5.1. The model parameters are set to $\omega_0 = 1.0$, $\vartheta = 1.0$, and $\zeta = 0.5$, yielding a process variance $r(0) = \vartheta/\omega_0^2 = 1.0$. One prominent realization of X_t is shown as a black curve, with other realizations depicted in gray, all over the time interval $[0, T]$. The horizontal dashed red line indicates the constant threshold level $u = 1.0$. Upcrossings, defined as instances where $X_t = u$ and its time derivative $\dot{X}_t > 0$, are denoted by $N_u^{\uparrow}(T)$ and marked with green upward triangles. Downcrossings, where $X_t = u$ and $\dot{X}_t < 0$, are denoted by $N_u^{\downarrow}(T)$ and marked with blue downward triangles. The total number of crossings, $N_u(T)$, is the sum of $N_u^{\uparrow}(T)$ and $N_u^{\downarrow}(T)$.

derivative [164, 165], the present work seeks to provide a direct counterpart to the mean-level solution for arbitrary u, expressed solely as a single integral over time.

This chapter is structured as follows: Section 6.3 provides a precise mathematical formulation of the level-crossing problem for stationary Gaussian processes and briefly reviews established results for the mean and variance of the number of upcrossings. In Section 6.4, we present our central contribution: exact analytical formulae for the variance and Fano factor of arbitrary level upcrossings and total crossings, applicable for both finite time intervals and in the asymptotic long-time limit. Simplified expressions for the special case of mean-level crossings are detailed in Appendix E.4. Finally, Section 6.5 demonstrates the utility and generality of our findings by applying them to several relevant examples of Gaussian stationary processes. We explore how the parameters of these processes influence their correlation functions and, consequently, shape the resulting level-crossing statistics.

6.3 Description of the Problem

Let $\{X_t;\ t \in [0,T]\}$ denote a smooth (i.e., differentiable), stationary, zero-mean, Gaussian process characterized by the autocorrelation function $r(t)$, defined as

$$r(t) \coloneqq R_X(s, s+t) = \mathbb{E}\left[X_s X_{s+t}\right]. \tag{6.1}$$

The function $r(t)$ is real-valued for all $t \in (-\infty, \infty)$ and satisfies the following properties:

- $|r(t)| < r(0)$ for all $t \notin \{0\}$,
- $0 < r(0) < \infty$,
- $r(t) \to 0$ as $t \to \infty$.

Due to stationarity, $r(t)$ depends only on the time difference t and satisfies the symmetry property $r(-t) = r(t)$. Additionally, we assume that X_t is smooth, i.e., $r(t)$ is twice-differentiable ($r''(t)$ exists).

In this work, we find explicit expressions for the variance of the counting processes $N_u^{\uparrow}(T)$, $N_u^{\downarrow}(T)$, and $N_u(T)$, which represent the number of upcrossings, downcrossings, and the total number of crossings, respectively, of a specified level u by the process X_t within the interval $t \in (0,T]$. All results derived for $N_u^{\uparrow}(T)$ also hold for $N_u^{\downarrow}(T)$. Therefore, to avoid redundancy, we will primarily focus on $N_u^{\uparrow}(T)$, with the corresponding results for $N_u^{\downarrow}(T)$ implied. The total number of crossings is simply given by the sum $N_u(T) = N_u^{\uparrow}(T) + N_u^{\downarrow}(T)$. Additionally, we explore the Fano factors for these counting processes, a crucial metric that quantifies the dispersion, defined as the ratio between the variance and the mean of the counting process in the long-time limit. Formally, we have,

$$\mathrm{F}^{\uparrow} = \lim_{T\to\infty} \frac{\mathrm{Var}[N_u^{\uparrow}(T)]}{\mathbb{E}[N_u^{\uparrow}(T)]} \text{ and } \mathrm{F} = \lim_{T\to\infty} \frac{\mathrm{Var}[N_u(T)]}{\mathbb{E}[N_u(T)]}. \tag{6.2}$$

The counting processes $N_u^{\uparrow}(T)$ and $N_u(T)$ can be expressed as integrals of the underlying generator stochastic process X_t:

$$\begin{aligned} N_u^{\uparrow}(T) &= \int_0^T \delta\left(X_{t_1} - u\right)\, \mathrm{H}\left(\dot{X}_{t_1}\right) \dot{X}_{t_1}\, \mathrm{d}t_1, \\ N_u(T) &= \int_0^T \delta\left(X_{t_1} - u\right) \left|\dot{X}_{t_1}\right|\, \mathrm{d}t_1. \end{aligned} \tag{6.3}$$

Here, $\dot{X}_{t_1}$ denotes the derivative of the stochastic process, $\delta(x)$ represents the Dirac delta function, and $\mathrm{H}(x)$ is the Heaviside step function. The term $\delta\left(X_{t_1} - u\right)$ ensures that only the crossings of level u are counted. The presence of $\mathrm{H}(\dot{X}_{t_1})$ restricts the count to upward crossings, while $|\dot{X}_{t_1}|$ accounts for both upward and downward crossings.

Since the autocorrelation function $r(t)$ is assumed to be twice differentiable, the expected values of $N_u^{\uparrow}(T)$ and $N_u(T)$ remain finite over a bounded interval T [166, 167]. Furthermore, Geman [168] established that a necessary and sufficient condition for the variance of zero-level crossings, $\mathrm{Var}\left[N_0(T)\right]$, to be finite in a bounded interval T is given by:

$$\int_0^{\epsilon} \frac{r''(t) - r''(0)}{t}\, \mathrm{d}t \; < \infty; \qquad \text{for some } \epsilon > 0. \tag{6.4}$$

Later, Kratz [169] demonstrated that this condition remains both necessary and sufficient for ensuring a finite variance of crossings at an arbitrary level, i.e., for $\mathrm{Var}\left[N_u(T)\right]$ to be finite over a bounded interval T. Consequently, this also guarantees a finite $\mathrm{Var}[N_u^{\uparrow}(T)]$. Throughout this work, we assume that this condition is satisfied by the correlation function.

6.3.1 Mean of the Counting Processes

Taking the expectation on both sides of Eq. (6.3), we get

$$\mathbb{E}\left[N_u^{\uparrow}(T)\right] = \int_0^T \mathbb{E}\left[\delta\left(X_{t_1} - u\right) \mathrm{H}\left(\dot{X}_{t_1}\right) \dot{X}_{t_1}\right] \mathrm{d}t_1. \tag{6.5}$$

To proceed, we define the random vector $\mathbf{P} = [X_{t_1}, \dot{X}_{t_1}]^\top$, which has the probability density function (p.d.f.) given by $f_{\mathbf{P}}(x, y)$. Since X_{t_1} is a stationary process, the distribution of $\mathbf{P}$ does not depend on t_1, implying that we can write $\mathbf{P} = [X_0, \dot{X}_0]^\top$. Therefore, $f_{\mathbf{P}}(u, y)$ is independent of time t_1 and we can rewrite Eq. (6.5) as

$$\begin{aligned}\mathbb{E}\left[N_u^{\uparrow}(T)\right] &= \int_0^T \int_{\mathbb{R}^2} \delta(x-u)\,\mathrm{H}(y)\,y\,f_{\mathbf{P}}(x,y)\,\mathrm{d}x\,\mathrm{d}y\,\mathrm{d}t_1 \\ &= \int_0^T \int_0^\infty y\,f_{\mathbf{P}}(u,y)\,\mathrm{d}y\,\mathrm{d}t_1 \\ &= T\int_0^\infty y\,f_{\mathbf{P}}(u,y)\,\mathrm{d}y,\end{aligned} \tag{6.6}$$

This result is known as the Kac-Rice formula [161].

Furthermore, because X_{t_1} is a zero-mean Gaussian process, $\mathbf{P}$ has a zero-mean multivariate Gaussian distribution with the correlation matrix (see Appendix E.1.1 for details)

$$\Sigma_{\mathbf{P}} = \begin{bmatrix} \mathbb{E}[X_0X_0] & \mathbb{E}\left[X_0\dot{X}_0\right] \\ \mathbb{E}\left[\dot{X}_0X_0\right] & \mathbb{E}\left[\dot{X}_0\dot{X}_0\right] \end{bmatrix} = \begin{bmatrix} r(0) & 0 \\ 0 & -r''(0) \end{bmatrix}, \tag{6.7}$$

and the p.d.f. $f_{\mathbf{P}}(x, y)$ is given by,

$$\begin{aligned} f_{\mathbf{P}}(x,y) &= \frac{1}{2\pi\sqrt{|\Sigma_{\mathbf{P}}|}} \exp\left(-\frac{1}{2}[x,y]\,\Sigma_{\mathbf{P}}^{-1}\,[x,y]^\top\right) \\ &= \frac{1}{2\pi\sqrt{r(0)\,(-r''(0))}} \exp\left(-\frac{1}{2}\left(\frac{x^2}{r(0)} + \frac{y^2}{(-r''(0))}\right)\right). \end{aligned} \tag{6.8}$$

Substituting the expression for $f_{\mathbf{P}}(x, y)$ into the integral in Eq. (6.6) yields

$$\mathbb{E}\left[N_u^{\uparrow}(T)\right] = T\,\frac{1}{2\pi}\sqrt{\frac{-r''(0)}{r(0)}}\,e^{-\frac{u^2}{2r(0)}}. \tag{6.9}$$

Since $\mathbb{E}\left[N_u(T)\right]$ accounts for both upward and downward crossings, it is simply given by $2\,\mathbb{E}[N_u^{\uparrow}(T)]$:

$$\mathbb{E}\left[N_u(T)\right] = T\,\frac{1}{\pi}\sqrt{\frac{-r''(0)}{r(0)}}\,e^{-\frac{u^2}{2r(0)}}. \tag{6.10}$$

6.3.2 Variance of the Counting Processes

We now derive the integral expression for the variance of $N_u^{\uparrow}(T)$ and $N_u(T)$. This derivation follows the approach outlined in [170], pg. 59. However, we note that the final result for the variance, Eq. (3.17) in [170] is incorrect. Using the definition in Eq. (6.3), it can be shown that the second factorial moment of $N_u^{\uparrow}(T)$, defined as $M_2 \coloneqq \mathbb{E}[N_u^{\uparrow}(T)\,(N_u^{\uparrow}(T)-1)]$, can be expressed as [171] (see Appendix E.1.2 for a detailed derivation),

$$M_2 = \int_0^T \int_0^T \mathbb{E}\Big[\mathrm{H}\left(\dot{X}_{t_1}\right)\mathrm{H}\left(\dot{X}_{t_2}\right)\delta\left(X_{t_1}-u\right)\delta\left(X_{t_2}-u\right)\dot{X}_{t_1}\dot{X}_{t_2}\Big]\mathrm{d}t_1\,\mathrm{d}t_2 \tag{6.11}$$

To proceed, we define the random vector $\mathbf{Q} = [X_{t_1},\, X_{t_2},\, \dot{X}_{t_1},\, \dot{X}_{t_2}]^{\top}$ with p.d.f. given by $f_{\mathbf{Q}}(x_1,\, x_2,\, y_1,\, y_2;\, t_1,\, t_2)$. Since X_t is a stationary process, $\mathbf{Q}$ only depends on t_1 and t_2 only through their difference, i.e., $f_{\mathbf{Q}}(x_1,\, x_2,\, y_1,\, y_2;\, t_2 - t_1)$. Furthermore, as X_t is a zero-mean Gaussian process, $\mathbf{Q}$ is a zero-mean multivariate Gaussian stationary process with the correlation matrix:

$$\Sigma_{\mathbf{Q}}(t) = \begin{bmatrix} r(0) & r(t) & 0 & r'(t) \\ r(t) & r(0) & -r'(t) & 0 \\ 0 & -r'(t) & -r''(0) & -r''(t) \\ r'(t) & 0 & -r''(t) & -r''(0) \end{bmatrix}, \tag{6.12}$$

where $t = t_2 - t_1$. Due to the symmetry property of $r(t)$ about the origin, we have $r(-t) = r(t)$, $r'(-t) = -r'(t)$ and $r''(-t) = r''(t)$, which are used in constructing the covariance matrix above.

Using the p.d.f., the second factorial moment M_2 from Eq. (6.11) can be rewritten as:

$$M_2 = \int_0^T \int_0^T \int_0^\infty \int_0^\infty y_1 y_2 \, f_{\mathbf{Q}}(u, u, y_1, y_2; t_2 - t_1) \, \mathrm{d}y_1 \, \mathrm{d}y_2 \, \mathrm{d}t_1 \, \mathrm{d}t_2 \tag{6.13}$$

The variance of $N_u^{\uparrow}(T)$ is then given by:

$$\mathrm{Var}[N_u^{\uparrow}(T)] = M_2 - \mathbb{E}[N_u^{\uparrow}(T)]^2 + \mathbb{E}[N_u^{\uparrow}(T)]. \tag{6.14}$$

Using Eq. (6.6), we express $\mathbb{E}\left[N_u^{\uparrow}(T)\right]^2$ as:

$$\mathbb{E}\left[N_u^{\uparrow}(T)\right]^2 = \int_0^T \int_0^T \int_0^\infty \int_0^\infty y_1 y_2 \, f_{\mathbf{P}}(u, y_1) \times f_{\mathbf{P}}(u, y_2) \, \mathrm{d}y_1 \, \mathrm{d}y_2 \, \mathrm{d}t_1 \, \mathrm{d}t_2 \tag{6.15}$$

Thus, $M_2 - \mathbb{E}[N_u^{\uparrow}(T)]^2$ is given by,

$$\begin{aligned} M_2 - \mathbb{E}\left[N_u^{\uparrow}(T)\right]^2 = \int_0^T \int_0^T \int_0^\infty \int_0^\infty y_1 y_2 \, \big(& f_{\mathbf{Q}}(u, u, y_1, y_2; t_2 - t_1) \\ & - f_{\mathbf{P}}(u, y_1) \, f_{\mathbf{P}}(u, y_2) \big) \, \mathrm{d}y_1 \, \mathrm{d}y_2 \, \mathrm{d}t_1 \, \mathrm{d}t_2 \end{aligned} \tag{6.16}$$

Applying the variable transformation $t = t_2 - t_1$ and $s = t_2$, the integration region in Fig. 6.2a transforms into the one shown in Fig. 6.2b. It can be shown that the integral contributes equally over regions I and II (see Appendix E.1.2 for details), leading to:

$$\begin{aligned} \mathrm{Var}[N_u^{\uparrow}(T)] = \mathbb{E}\left[N_u^{\uparrow}(T)\right] + 2\,T \int_0^T \int_0^\infty \int_0^\infty \left(1 - \frac{t}{T}\right) y_1 y_2 \, \big(& f_{\mathbf{Q}}(u, u, y_1, y_2; \, t) \\ & - f_{\mathbf{P}}(u, y_1) \, f_{\mathbf{P}}(u, y_2) \big) \, \mathrm{d}y_1 \, \mathrm{d}y_2 \, \mathrm{d}t \end{aligned} \tag{6.17}$$

It can be further shown that $\lim_{T\to\infty} \mathrm{Var}\left[N_u^{\uparrow}(T)\right]/T$ is finite if $\int_0^\infty t \, (|r(t)| + |r'(t)| + |r''(t)|) \, \mathrm{d}t$ is finite [170], pg. 60. This leads to the following expressions for the asymptotic variance and the

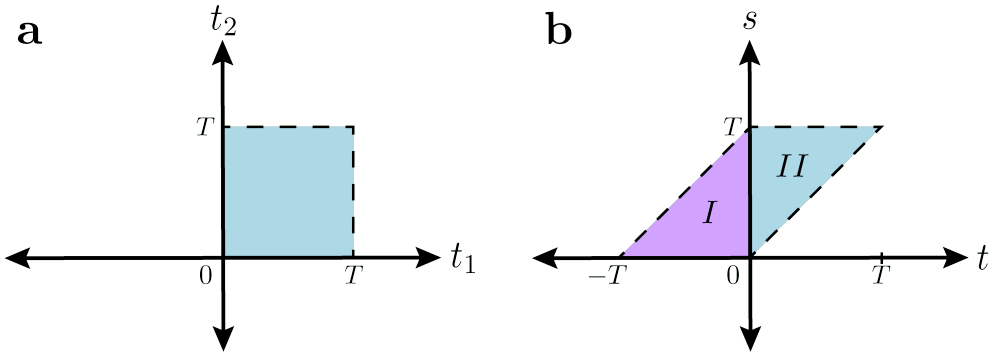


Figure 6.2: Variable transform visualized. (**a**), The area under which the integral is performed for t_1 and t_2. (**b**), The area under which the integral should be performed upon variable transformation given by $t = t_2 - t_1$ and $s = t_2$. I and II represent further partitioning of this region.

Fano factor:

$$\lim_{T\to\infty} \frac{\mathrm{Var}\left[N_u^{\uparrow}(T)\right]}{T} = \lim_{T\to\infty} \frac{\mathbb{E}\left[N_u^{\uparrow}(T)\right]}{T} + 2\int_0^\infty \int_0^\infty \int_0^\infty y_1 y_2 \left(f_{\mathrm{Q}}(u,u,y_1,y_2;t) - f_{\mathrm{P}}(u,y_1)\, f_{\mathrm{P}}(u,y_2)\right) \mathrm{d}y_1\, \mathrm{d}y_2\, \mathrm{d}t\,, \tag{6.18}$$

$$\mathrm{F}^{\uparrow} = 1 + \frac{2\int_0^\infty \int_0^\infty \int_0^\infty y_1 y_2 \left(f_{\mathrm{Q}}(u,\,u,\,y_1,\,y_2;\,t) - f_{\mathrm{P}}(u,\,y_1)\, f_{\mathrm{P}}(u,\,y_2)\right)\, \mathrm{d}y_1\, \mathrm{d}y_2\, \mathrm{d}t}{\int_0^\infty y\, f_{\mathrm{P}}(u,\,y)\, \mathrm{d}y}\,. \tag{6.19}$$

Using a similar approach, we can derive these quantities for the crossing process $N_u(T)$ (see Appendix E.2 for details),

$$\mathrm{Var}[N_u(T)] = \mathbb{E}\left[N_u(T)\right] + 2\,T \int_0^T \int_{-\infty}^\infty \int_{-\infty}^\infty \left(1 - \frac{t}{T}\right) |y_1 y_2| \left(f_{\mathrm{Q}}(u,u,y_1,y_2;\,t) - f_{\mathrm{P}}(u,y_1)\, f_{\mathrm{P}}(u,y_2)\right) \mathrm{d}y_1\, \mathrm{d}y_2\, \mathrm{d}t, \tag{6.20}$$

$$\lim_{T\to\infty} \frac{\mathrm{Var}\left[N_u(T)\right]}{T} = \lim_{T\to\infty} \frac{\mathbb{E}\left[N_u(T)\right]}{T} + 2\int_0^\infty \int_{-\infty}^\infty \int_{-\infty}^\infty |y_1 y_2| \left(f_{\mathrm{Q}}(u,u,y_1,y_2;t) - f_{\mathrm{P}}(u,y_1)\, f_{\mathrm{P}}(u,y_2)\right) \mathrm{d}y_1\, \mathrm{d}y_2\, \mathrm{d}t, \tag{6.21}$$

$$\mathrm{F} = 1 + \frac{2\int_0^\infty \int_{-\infty}^\infty \int_{-\infty}^\infty |y_1 y_2| \left(f_{\mathrm{Q}}(u,\, u,\, y_1,\, y_2;\, t) - f_{\mathrm{P}}(u,\, y_1)\, f_{\mathrm{P}}(u,\, y_2) \right) \mathrm{d}y_1\, \mathrm{d}y_2\, \mathrm{d}t}{\int_{-\infty}^\infty |y|\, f_{\mathrm{P}}(u,\, y)\, \mathrm{d}y}\,. \tag{6.22}$$

6.4 Main Result

We first present the main result of this work as a theorem, and prove it subsequently.

Theorem 6.1. *Consider a zero-mean stationary Gaussian stochastic process X_t with the autocorrelation function $r(t)$ satisfying the properties defined in Section 6.3. Let $N_u^{\uparrow}(T)$ denote the number of upcrossings of an arbitrary level u. Denoting $r(t) \to r$, $r(0) \to r_0$, $r'(t) \to p$, $r'(0) \to p_0$, $-r''(t) \to q$, and $-r''(0) \to q_0$. and*

$$\begin{aligned}
\alpha &= -\frac{r + r_0}{2\left(p^2 + (q - q_0)(r + r_0)\right)}, \\
\beta &= -\frac{r_0 - r}{2\left(p^2 + (q + q_0)(r - r_0)\right)}, \\
\gamma &= \frac{\sqrt{2}\, p}{r + r_0}\, u, \\
\delta &= \frac{1}{r + r_0}\,.
\end{aligned} \tag{6.23}$$

The mean of $N_u^{\uparrow}(T)$ is given by:

$$\mathbb{E}\left[N_u^{\uparrow}(T)\right] = T\, \frac{1}{2\pi} \sqrt{\frac{q_0}{r_0}}\, e^{-u^2/(2r_0)}, \tag{6.24}$$

and the finite-time variance of $N_u^{\uparrow}(T)$ is:

$$\mathrm{Var}\left[N_u^{\uparrow}(T)\right] = \mathbb{E}\left[N_u^{\uparrow}(T)\right] + 2T \int_0^T \left(1 - \frac{t}{T}\right) I^{\uparrow} \mathrm{d}t\,, \tag{6.25}$$

where $I^{\uparrow}$ is a function of the time dependent quantities r, α, β, γ, δ given by:

$$I^{\uparrow} = \frac{e^{-\delta u^2}}{4\pi^2\sqrt{r_0^2 - r^2}}\left[\frac{e^{-\alpha\gamma^2}}{2\sqrt{\alpha\beta}}\left(1 + \sqrt{\pi}\,\gamma\sqrt{\alpha+\beta}\,e^{\frac{\alpha^2\gamma^2}{\alpha+\beta}}\,\operatorname{Erf}\left(\frac{\alpha\gamma}{\sqrt{\alpha+\beta}}\right)\right)\right. \\ \left. + \pi\left(\frac{\alpha - \beta - 2\alpha\beta\gamma^2}{\alpha\beta}\right)\mathcal{T}\left(\gamma\sqrt{\frac{2\alpha\beta}{\alpha+\beta}}, \sqrt{\frac{\alpha}{\beta}}\right)\right] - \frac{1}{4\pi^2}\left(\frac{q_0}{r_0}\right)e^{-u^2/r_0}, \tag{6.26}$$

where $\operatorname{Erf}(z)$ is the error function defined as:

$$\operatorname{Erf}(z) = \frac{2}{\sqrt{\pi}}\int_0^z e^{-t^2}\,\mathrm{d}t, \tag{6.27}$$

and $\mathcal{T}(h, a)$ is Owen's T function [172] defined as:

$$\mathcal{T}(h, a) = \frac{1}{2\pi}\int_0^a \frac{e^{-\frac{1}{2}h^2(1+t^2)}}{1+t^2}\,\mathrm{d}t. \tag{6.28}$$

Proof. The result for the mean can be found by using the new notation in Eq. (6.9). For deriving the expression for variance, we take the result derived for $\operatorname{Var}[N_u^{\uparrow}(T)]$, stated in Eq. (6.17), and explicitly evaluate the integrals in y_1 and y_2 for an arbitrary level u. To the best of our knowledge, this has only been done for zero-level, i.e., $u = 0$ [163, 173–176], but not for an arbitrary level u due to the complexity of an asymmetric Gaussian integral involved. We overcome this difficulty by explicitly solving the integral in terms of known functions.

We denote the integral of interest by $I^{\uparrow}$, defined as,

$$I^{\uparrow} = \int_0^{\infty}\int_0^{\infty} y_1 y_2 \left(f_{\mathrm{Q}}(u, u, y_1, y_2; t) - f_{\mathrm{P}}(u, y_1)\, f_{\mathrm{P}}(u, y_2)\right)\mathrm{d}y_1\,\mathrm{d}y_2\,. \tag{6.29}$$

Splitting the integral, we get,

$$I^{\uparrow} = \underbrace{\int_0^\infty \int_0^\infty y_1 y_2 \, f_{\mathbf{Q}}(u,\, u,\, y_1,\, y_2;\, t)\, \mathrm{d}y_1\, \mathrm{d}y_2}_{I_1} - \underbrace{\int_0^\infty \int_0^\infty y_1 y_2 \, f_{\mathbf{P}}(u,\, y_1)\, f_{\mathbf{P}}(u,\, y_2)\, \mathrm{d}y_1\, \mathrm{d}y_2}_{I_2} \,. \quad (6.30)$$

To derive an explicit analytical expression for $I^{\uparrow}$, we use the shorter notations for quantities depending on the correlation function $r(t)$: $r(t) \to r$, $r(0) \to r_0$, $r'(t) \to p$, $r'(0) \to p_0$, $-r''(t) \to q$, and $-r''(0) \to q_0$. Note that since $r(t)$ is a differentiable function with $r(0)$ being its maximum value (by definition), the curvature at $t = 0$ is concave, therefore $-r''(0) > 0$ or $q_0 > 0$. In this new notation, we can write the covariance matrix for the vector $\mathbf{P} = [X_{t_1},\, \dot{X}_{t_1}]^\top$, defined in Eq. (6.7) as,

$$\Sigma_{\mathbf{P}} = \begin{bmatrix} r_0 & 0 \\ 0 & q_0 \end{bmatrix} . \quad (6.31)$$

Further, since $\mathbf{P}$ is a zero-mean Gaussian random vector, its p.d.f. is given by,

$$\begin{aligned} f_{\mathbf{P}}(x, y) &= \frac{1}{2\pi\sqrt{|\Sigma_{\mathbf{P}}|}} \exp\left(-\frac{1}{2}[x, y]\, \Sigma_{\mathbf{P}}^{-1}\, [x, y]^\top\right) \\ &= \frac{1}{2\pi\sqrt{r_0\, q_0}} \exp\left(-\frac{1}{2}\left(\frac{x^2}{r_0} + \frac{y^2}{q_0}\right)\right) . \end{aligned} \quad (6.32)$$

To calculate I_2 (Eq. (6.30)), we substitute the expressions for $f_{\mathbf{P}}(u,\, y_1)$ and $f_{\mathbf{P}}(u,\, y_2)$ using the equation above:

$$\begin{aligned} I_2 &= \int_0^\infty \int_0^\infty y_1 y_2 \, f_{\mathbf{P}}(u, y_1)\, f_{\mathbf{P}}(u, y_2)\, \mathrm{d}y_1\, \mathrm{d}y_2 \\ &= \frac{e^{-u^2/r_0}}{4\pi^2\, r_0 q_0} \int_0^\infty \int_0^\infty y_1 y_2 \exp\left(-\frac{y_1^2 + y_2^2}{2q_0}\right) \mathrm{d}y_1\, \mathrm{d}y_2 \\ &= \frac{1}{4\pi^2}\left(\frac{q_0}{r_0}\right) e^{-u^2/r_0} . \end{aligned} \quad (6.33)$$

Now we evaluate an explicit expression for I_1 (Eq. (6.30)), given by,

$$I_1 = \int_0^\infty \int_0^\infty y_1 y_2 \, f_{\mathbf{Q}}(u,\, u,\, y_1,\, y_2;\, t)\, \mathrm{d}y_1\, \mathrm{d}y_2 \,. \tag{6.34}$$

We first make the following transformation of variables in the integral:

$$z_1 = \frac{y_2 - y_1}{\sqrt{2}} \quad \text{and} \quad z_2 = \frac{y_2 + y_1}{\sqrt{2}}. \tag{6.35}$$

We get the following relations between the old and new variables:

$$\begin{aligned} y_1^2 + y_2^2 &= z_1^2 + z_2^2 \,, \\ y_2 - y_1 &= \sqrt{2}\, z_1 \,, \\ y_1 y_2 &= \frac{z_2^2 - z_1^2}{2} \,. \end{aligned} \tag{6.36}$$

The absolute value of the Jacobian of this transformation is 1 and the area of integration changes as follows,

$$I_1 = \frac{1}{2} \int_{-\infty}^\infty \int_{|z_1|}^\infty \left(z_2^2 - z_1^2\right) f_{\mathbf{Q}}(u, u, z_1, z_2; t)\, \mathrm{d}z_2 \mathrm{d}z_1 \,. \tag{6.37}$$

Now, we find how the p.d.f. changes due to this transformation of variables, i.e., we find the expression for $f_{\mathbf{Q}}(u,\, u,\, z_1,\, z_2;\, t)$. First, in the new notation, the covariance matrix for the vector $\mathbf{Q} = [X_{t_1},\, X_{t_2},\, \dot{X}_{t_1},\, \dot{X}_{t_2}]^\top$, defined in Eq. (6.12) becomes,

$$\Sigma_{\mathbf{Q}}(t) = \begin{bmatrix} r_0 & r & 0 & p \\ r & r_0 & -p & 0 \\ 0 & -p & q_0 & q \\ p & 0 & q & q_0 \end{bmatrix}, \tag{6.38}$$

Further, since $\mathbf{Q}$ is a zero-mean Gaussian random vector, its p.d.f. is given by,

$$f_{\mathbf{Q}}(x_1, x_2, y_1, y_2; t) = \frac{1}{4\pi^2\sqrt{\left|\Sigma_{\mathbf{Q}}(t)\right|}} \exp\left(S\right), \tag{6.39}$$

where,

$$S = -\frac{1}{2}[x_1, x_2, y_1, y_2]\, \Sigma_{\mathbf{Q}}(t)^{-1}\, [x_1, x_2, y_1, y_2]^{\top}. \tag{6.40}$$

We denote the determinant $\left|\Sigma_{\mathbf{Q}}(t)\right|$ by Δ. Calculating the determinant of the matrix above, we find,

$$\Delta = \left(p^2 + (q - q_0)(r + r_0)\right)\left(p^2 + (q + q_0)(r - r_0)\right). \tag{6.41}$$

Since we need the expression for $f_{\mathbf{Q}}(u,\, u,\, y_1,\, y_2;\, t)$ to find I_1, we focus on the expression in the exponential (S), evaluated at $(u,\, u,\, y_1,\, y_2)$. Finding the inverse of the matrix $\Sigma_{\mathbf{Q}}(t)^{-1}$, and upon simplification, we get,

$$S = -\frac{1}{2\Delta}\left(c_0\, u^2 + c_1\left(y_1^2 + y_2^2\right) + c_2\, u\,(y_2 - y_1) + c_3\, y_1 y_2\right), \tag{6.42}$$

where c_0, c_1, c_2 and c_3 are given by,

$$\begin{aligned}
c_0 &= 2\,(q - q_0)\left(p^2 + (q + q_0)\,(r - r_0)\right),\\
c_1 &= q_0 r_0^2 - q_0 r^2 - r_0 p^2,\\
c_2 &= 2\,p\left(p^2 + (q + q_0)\,(r - r_0)\right),\\
c_3 &= 2\left(p^2 r + q r^2 - q r_0^2\right).
\end{aligned} \tag{6.43}$$

Transforming S into new variables defined in Eq. (6.35), using the relations stated in Eq. (6.36), we

get,

$$\begin{aligned} S &= -\frac{1}{2\Delta}\left(c_0\,u^2 + \left(c_1 - \frac{c_3}{2}\right) z_1^2 + \sqrt{2}\,c_2\,u\,z_1 + \left(c_1 + \frac{c_3}{2}\right) z_2^2\right) \\ &= -\frac{1}{2\Delta}\left(\tilde{c}_0\,u^2 + \tilde{c}_1\,z_1^2 + \tilde{c}_2\,u\,z_1 + \tilde{c}_3\,z_2^2\right). \end{aligned} \tag{6.44}$$

where $\tilde{c}_0$, $\tilde{c}_1$, $\tilde{c}_2$ and $\tilde{c}_3$ are given by,

$$\begin{aligned} \tilde{c}_0 &= 2\,(q - q_0)\left(p^2 + (q + q_0)\,(r - r_0)\right), \\ \tilde{c}_1 &= -\,(r + r_0)\left(p^2 + (q + q_0)\,(r - r_0)\right), \\ \tilde{c}_2 &= 2\sqrt{2}\,p\left(p^2 + (q + q_0)\,(r - r_0)\right), \\ \tilde{c}_3 &= -\,(r_0 - r)\left(p^2 + (q - q_0)\,(r + r_0)\right). \end{aligned} \tag{6.45}$$

Now we complete the square in z_1, which gives us,

$$\begin{aligned} S &= -\frac{1}{2\Delta}\left(\left(\tilde{c}_0 - \frac{\tilde{c}_2^2}{4\tilde{c}_1}\right) u^2 + \tilde{c}_1\left(z_1 + \frac{\tilde{c}_2}{2\tilde{c}_1}u\right)^2 + \tilde{c}_3\,z_2^2\right) \\ &= \underbrace{-\frac{1}{2\Delta}\left(\tilde{c}_0 - \frac{\tilde{c}_2^2}{4\tilde{c}_1}\right)}_{\delta} u^2 - \underbrace{\frac{\tilde{c}_1}{2\Delta}}_{\alpha}\left(z_1 - \underbrace{\frac{-\tilde{c}_2}{2\tilde{c}_1}}_{\gamma}u\right)^2 - \underbrace{\frac{\tilde{c}_3}{2\Delta}}_{\beta} z_2^2. \end{aligned} \tag{6.46}$$

In this new notation, S is given simply by the expression,

$$S = -\delta\,u^2 - \alpha\,(z_1 - \gamma)^2 - \beta\,z_2^2, \tag{6.47}$$

where, α, β, γ, and δ are given by the following expressions, found using the definition above and

the definition of Δ from Eq. (6.41),

$$\boxed{\begin{aligned}\alpha &= -\frac{r + r_0}{2\left(p^2 + (q - q_0)(r + r_0)\right)},\\ \beta &= -\frac{r_0 - r}{2\left(p^2 + (q + q_0)(r - r_0)\right)},\\ \gamma &= \frac{\sqrt{2}\,p}{r + r_0}\,u,\\ \delta &= \frac{1}{r + r_0}\,.\end{aligned}} \tag{6.48}$$

Now, we determine the signs of these variables for $t \geq 0$.

- α and β: Strictly positive due to Theorem E.1.
- γ : The sign of γ depends on the sign of the u and p, therefore γ can be negative or nonnegative.
- δ : Since $r_0 \geq |r|\ \forall\ t \geq 0$ and $r_0 > 0$ by definition, $\implies$ $r + r_0 \geq 0\ \forall\ t \geq 0$. Therefore, δ is strictly positive for all $t \geq 0$.

To summarize, $\alpha > 0$, $\beta > 0$, $\delta > 0$ and $\gamma \in \mathbb{R}$ for all $t \geq 0$. Now, we express the determinant in terms of r, α and β. It can be verified using the expressions for α and β in Eq. (6.48) and the expression for the determinant in Eq. (6.41) that,

$$\Delta = \frac{r_0^2 - r^2}{4\alpha\beta}\,. \tag{6.49}$$

Therefore, we get the following expression for $f_{\mathrm{Q}}(u,\, u,\, z_1,\, z_2;\, t)$:

$$\begin{aligned} f_{\mathrm{Q}}(u, u, z_1, z_2; t) &= \frac{1}{4\pi^2\sqrt{\Delta}}\,\exp\left(S\right)\\ &= \frac{1}{2\pi^2}\sqrt{\frac{\alpha\beta}{r_0^2 - r^2}}\,\exp\left(-\delta\,u^2 - \alpha\,(z_1 - \gamma)^2 - \beta\,z_2^2\right), \end{aligned} \tag{6.50}$$

and, the integral I_1 (Eq. (6.37)) can be written as,

$$I_1 = \frac{e^{-\delta u^2}}{4\pi^2}\sqrt{\frac{\alpha\beta}{r_0^2 - r^2}}\int_{-\infty}^{\infty}\int_{|z_1|}^{\infty}\left(z_2^2 - z_1^2\right) \times \exp\left(-\alpha\left(z_1 - \gamma\right)^2 - \beta\, z_2^2\right) \mathrm{d}z_2\, \mathrm{d}z_1\,. \tag{6.51}$$

We derive an explicit analytical formula for this double integral:

Lemma 6.2 (see Theorem E.2 for proof). *Let $\alpha > 0$, $\beta > 0$, and $\gamma \in \mathbb{R}$. The following result holds:*

$$\begin{aligned}\int_{-\infty}^{\infty}\int_{|x|}^{\infty}\left(y^2 - x^2\right) e^{-\alpha(x-\gamma)^2 - \beta y^2}\mathrm{d}y\,\mathrm{d}x = \frac{e^{-\alpha\gamma^2}}{2\alpha\beta}\left(1 + \sqrt{\pi}\,\gamma\sqrt{\alpha+\beta}\, e^{\frac{\alpha^2\gamma^2}{\alpha+\beta}}\,\mathrm{Erf}\left(\frac{\alpha\gamma}{\sqrt{\alpha+\beta}}\right)\right) \\ + \pi\left(\frac{\alpha - \beta - 2\alpha\beta\gamma^2}{(\alpha\beta)^{3/2}}\right)\mathcal{T}\left(\gamma\sqrt{\frac{2\alpha\beta}{\alpha+\beta}}, \sqrt{\frac{\alpha}{\beta}}\right),\end{aligned} \tag{6.52}$$

where $\mathrm{Erf}(z)$ *is the error function defined as*

$$\mathrm{Erf}(z) = \frac{2}{\sqrt{\pi}}\int_0^z e^{-t^2}\mathrm{d}t, \tag{6.53}$$

and $\mathcal{T}(h, a)$ *is Owen's T function [172] defined as*

$$\mathcal{T}(h, a) = \frac{1}{2\pi}\int_0^a \frac{e^{-\frac{1}{2}h^2(1+t^2)}}{1+t^2}\,\mathrm{d}t. \tag{6.54}$$

Since we have already shown that $\alpha > 0$, $\beta > 0$, and $\gamma \in \mathbb{R}$, the result of this integral applies; therefore, we get the following expression for I_1:

$$\begin{aligned}I_1 = \frac{e^{-\delta u^2}}{4\pi^2\sqrt{r_0^2 - r^2}}\left[\frac{e^{-\alpha\gamma^2}}{2\sqrt{\alpha\beta}}\left(1 + \sqrt{\pi}\gamma\sqrt{\alpha+\beta}e^{\frac{\alpha^2\gamma^2}{\alpha+\beta}}\,\mathrm{Erf}\left(\frac{\alpha\gamma}{\sqrt{\alpha+\beta}}\right)\right)\right. \\ \left. + \pi\left(\frac{\alpha - \beta - 2\alpha\beta\gamma^2}{\alpha\beta}\right)\mathcal{T}\left(\gamma\sqrt{\frac{2\alpha\beta}{\alpha+\beta}}, \sqrt{\frac{\alpha}{\beta}}\right)\right].\end{aligned} \tag{6.55}$$

Finally, since $I^{\uparrow} = I_1 - I_2$, using Eq. (6.33) and (6.55) we have,

$$\boxed{I^{\uparrow} = \frac{e^{-\delta u^2}}{4\pi^2\sqrt{r_0^2 - r^2}}\left[\frac{e^{-\alpha\gamma^2}}{2\sqrt{\alpha\beta}}\left(1 + \sqrt{\pi}\,\gamma\sqrt{\alpha+\beta}\,e^{\frac{\alpha^2\gamma^2}{\alpha+\beta}}\,\operatorname{Erf}\left(\frac{\alpha\gamma}{\sqrt{\alpha+\beta}}\right)\right)\right.}$$
$$\boxed{\left. + \pi\left(\frac{\alpha - \beta - 2\alpha\beta\gamma^2}{\alpha\beta}\right)\mathcal{T}\left(\gamma\sqrt{\frac{2\alpha\beta}{\alpha+\beta}}, \sqrt{\frac{\alpha}{\beta}}\right)\right] - \frac{1}{4\pi^2}\left(\frac{q_0}{r_0}\right)e^{-u^2/r_0}\,.} \tag{6.56}$$

From Eq. (6.17), the Var $\left[N_u^{\uparrow}(T)\right]$ depends on $I^{\uparrow}$ as follows:

$$\operatorname{Var}\left[N_u^{\uparrow}(T)\right] = \mathbb{E}\left[N_u^{\uparrow}(T)\right] + 2\,T\int_0^T\left(1 - \frac{t}{T}\right)I^{\uparrow}\,\mathrm{d}t\,, \tag{6.57}$$

where, the $\mathbb{E}\left[N_u^{\uparrow}(T)\right]$ is given by the Rice formula derived in Eq. (6.9),

$$\mathbb{E}\left[N_u^{\uparrow}(T)\right] = T\,\frac{1}{2\pi}\sqrt{\frac{q_0}{r_0}}\,e^{-u^2/(2r_0)}\,. \tag{6.58}$$

□

Corollary 6.3 (to Theorem 6.1)**.** *In the long-time limit, the variance becomes:*

$$\lim_{T\to\infty}\frac{\operatorname{Var}\left[N_u^{\uparrow}(T)\right]}{T} = \frac{1}{2\pi}\sqrt{\frac{q_0}{r_0}}\,e^{-\frac{u^2}{2r_0}} + 2\int_0^{\infty} I^{\uparrow}\mathrm{d}t. \tag{6.59}$$

The corresponding Fano factor is:

$$\mathrm{F}^{\uparrow} = 1 + 4\pi\sqrt{\frac{r_0}{q_0}}\,e^{\frac{u^2}{2r_0}}\int_0^{\infty} I^{\uparrow}\,\mathrm{d}t. \tag{6.60}$$

Proof. In the long-time limit, using the result for variance in Theorem 6.1 and Eq. (6.21), we get:

$$\lim_{T\to\infty}\frac{\operatorname{Var}\left[N_u^{\uparrow}(T)\right]}{T} = \frac{1}{2\pi}\sqrt{\frac{q_0}{r_0}}\,e^{-\frac{u^2}{2r_0}} + 2\int_0^{\infty} I^{\uparrow}\,\mathrm{d}t\,. \tag{6.61}$$

This also gives us an expression for the Fano factor:

$$\mathrm{F}^{\uparrow} = 1 + 4\pi \sqrt{\frac{r_0}{q_0}}\, e^{u^2/(2r_0)} \int_0^{\infty} I^{\uparrow}\, \mathrm{d}t\,. \tag{6.62}$$

□

Theorem 6.4 (see Appendix E.3 for proof)**.** *Consider a zero-mean stationary Gaussian stochastic process X_t with the autocorrelation function $r(t)$ satisfying the properties defined in Section 6.3. Let $N_u(T)$ denote the number of total crossings of an arbitrary level u. The mean of $N_u(T)$ is given by:*

$$\mathbb{E}\left[N_u(T)\right] = T\,\frac{1}{\pi}\sqrt{\frac{q_0}{r_0}}\, e^{-u^2/(2r_0)}, \tag{6.63}$$

and the finite-time variance of $N_u(T)$ is:

$$\mathrm{Var}\left[N_u(T)\right] = \mathbb{E}\left[N_u(T)\right] + 2T \int_0^T \left(1 - \frac{t}{T}\right) I \mathrm{d}t\,, \tag{6.64}$$

where I is a function of the time dependent quantities r, α, β, γ, δ given by:

$$\begin{aligned} I = \frac{e^{-\delta u^2}}{4\pi^2\sqrt{r_0^2 - r^2}} \Bigg[\frac{2e^{-\alpha\gamma^2}}{\sqrt{\alpha\beta}} \left(1 + \sqrt{\pi}\,\gamma\sqrt{\alpha+\beta}\, e^{\frac{\alpha^2\gamma^2}{\alpha+\beta}}\, \mathrm{Erf}\left(\frac{\alpha\gamma}{\sqrt{\alpha+\beta}}\right)\right) \\ + 4\pi \left(\frac{\alpha - \beta - 2\alpha\beta\gamma^2}{\alpha\beta}\right) \left(\mathcal{T}\left(\gamma\sqrt{\frac{2\alpha\beta}{\alpha+\beta}}, \sqrt{\frac{\alpha}{\beta}}\right) - \frac{1}{8}\right)\Bigg] - \frac{1}{\pi^2}\left(\frac{q_0}{r_0}\right) e^{-u^2/r_0}. \end{aligned} \tag{6.65}$$

Corollary 6.5 (see Appendix E.3 for proof)**.** *In the long-time limit, the variance becomes:*

$$\lim_{T\to\infty} \frac{\mathrm{Var}\left[N_u(T)\right]}{T} = \frac{1}{\pi}\sqrt{\frac{q_0}{r_0}}\, e^{-\frac{u^2}{2r_0}} + 2\int_0^{\infty} I \mathrm{d}t \tag{6.66}$$

The corresponding Fano factor is:

$$\mathrm{F} = 1 + 2\pi\sqrt{\frac{r_0}{q_0}}\, e^{\frac{u^2}{2r_0}} \int_0^\infty I \,\mathrm{d}t \tag{6.67}$$

6.5 Applications

In this section, we verify the explicit variance and Fano factor results for upcrossing and crossing of Gaussian stationary processes with different correlation functions.

6.5.1 Stochastic Damped Harmonic Oscillator

The stochastic damped harmonic oscillator is a fundamental model, particularly in statistical physics [177–181], for describing systems that experience inherent random fluctuations while simultaneously relaxing towards an equilibrium state. This model is widely applied across diverse fields because it is not only concise, linear, and often analytically tractable, but also powerful in capturing essential physical phenomena. Its descriptive strength derives from its core components: an underlying *restorative force* pulling the system toward stability, a *damping mechanism* that dissipates the system's energy, and *random fluctuations*, often originating from sources like thermal noise. While analytical solutions for the first-order statistics of upcrossings have been employed in the study of this model [154, 182, 183], we consider the second-order statistics of upcrossings.

The oscillator's dynamics are governed by a second-order stochastic differential equation:

$$\frac{\mathrm{d}^2x}{\mathrm{d}t^2} + 2\zeta\omega_0\frac{\mathrm{d}x}{\mathrm{d}t} + \omega_0^2 x = \sqrt{4\zeta\omega_0(k_B\vartheta)}\,\eta(t), \tag{6.68}$$

where $x(t)$ represents the oscillator's position relative to its stable equilibrium at 0. The parameter $\omega_0 > 0$ is the natural angular frequency of the oscillator in the absence of damping, and $\zeta \geqslant 0$ is the dimensionless damping ratio which determines the rate at which the dynamics decay.

The term $\eta(t)$ represents zero-mean Gaussian white noise, satisfying $\mathbb{E}\left[\eta(t)\,\eta(s)\right] = \delta(t-s)$. The temperature of the heat bath coupled to the oscillator, ϑ, controls the intensity of thermal fluctuations. For simplicity, the Boltzmann constant k_B is set to unity ($k_B = 1$). The coefficient of the noise term, $4\zeta\omega_0(k_B\vartheta)$, is chosen consistent with the fluctuation-dissipation theorem, ensuring that the system reaches thermal equilibrium for $\zeta > 0$.

Equation (6.68) can be recast as a two-dimensional linear stochastic dynamical system:

$$\begin{aligned} \frac{\mathrm{d}x}{\mathrm{d}t} &= v \\ \frac{\mathrm{d}v}{\mathrm{d}t} &= -\omega_0^2 x - 2\zeta\omega_0 v + \sqrt{4\zeta\omega_0\vartheta}\,\eta(t), \end{aligned} \tag{6.69}$$

where $v(t) = \dot{x}(t)$ is the velocity of the oscillator. This system conforms to the general form of a linear stochastic dynamical system:

$$\mathrm{d}\mathbf{x} = \mathbf{J}\mathbf{x}\mathrm{d}t + \mathbf{L}\mathrm{d}\mathbf{W} \tag{6.70}$$

where $\mathbf{x} = [x, v]^\top$ is the state vector, and $\mathrm{d}\mathbf{W} = [\mathrm{d}W_1, \mathrm{d}W_2]^\top$ is a vector of independent standard Wiener increments. The Jacobian matrix $\mathbf{J}$ and the noise diffusion matrix $\mathbf{L}$ are given by:

$$\mathbf{J} = \begin{bmatrix} 0 & 1 \\ -\omega_0^2 & -2\zeta\omega_0 \end{bmatrix} \quad \text{and} \quad \mathbf{L} = \begin{bmatrix} 0 & 0 \\ 0 & \sqrt{4\zeta\omega_0\vartheta} \end{bmatrix}. \tag{6.71}$$

The power spectral density matrix of the state vector $\mathbf{x}$ can be obtained using the formula [82]:

$$\boldsymbol{\mathcal{S}}_{\mathbf{x}}(\omega) = (i\omega\mathbf{I} - \mathbf{J})^{-1}\,\mathbf{L}\,\mathbf{L}^\top(-i\omega\mathbf{I} - \mathbf{J})^{-\top}. \tag{6.72}$$

Extracting the (1,1) component of $\boldsymbol{\mathcal{S}}_{\mathbf{x}}(\omega)$ yields the power spectral density of the position variable $x(t)$:

$$\mathcal{S}_x(\omega) = \frac{4\zeta\omega_0\vartheta}{(\omega_0^2 - \omega^2)^2 + (2\zeta\omega_0\omega)^2}. \tag{6.73}$$

According to the Wiener–Khinchin theorem, the autocorrelation function of the stationary process $x(t)$, denoted by $r_x(t) = \mathbb{E}[x(t')x(t'+t)]$, is the inverse Fourier transform of its power spectral density:

$$r_x(t) = \mathcal{F}^{-1}\left\{\mathcal{S}_x(\omega)\right\}(t). \tag{6.74}$$

Calculating the inverse Fourier transform of Eq. (6.73), provides the correlation function $r_x(t)$, expressed as follows in three distinct damping regimes:

Underdamped ($0 < \zeta < 1$): The system exhibits oscillations with exponentially decaying amplitude. The correlation function is:

$$r_x(t) = \frac{\vartheta}{\omega_0^2} e^{-\zeta\omega_0|t|}\left(\cos\left(\omega_0\sqrt{1-\zeta^2}|t|\right) + \frac{\zeta}{\sqrt{1-\zeta^2}}\sin\left(\omega_0\sqrt{1-\zeta^2}|t|\right)\right). \tag{6.75}$$

Critically Damped ($\zeta = 1$): The system returns to equilibrium as quickly as possible without oscillating. The correlation function takes the form:

$$r_x(t) = \frac{\vartheta}{\omega_0^2} e^{-\omega_0|t|}\left(1 + \omega_0|t|\right). \tag{6.76}$$

Overdamped ($\zeta > 1$): The system returns to equilibrium without oscillating, but slower than in the critically damped case. The correlation function is a sum of two exponentials with different timescales:

$$r_x(t) = \frac{\vartheta}{2\omega_0^2}\left[\left(1 + \frac{\zeta}{\sqrt{\zeta^2-1}}\right)e^{-\omega_0(\zeta-\sqrt{\zeta^2-1})|t|} + \left(1 - \frac{\zeta}{\sqrt{\zeta^2-1}}\right)e^{-\omega_0(\zeta+\sqrt{\zeta^2-1})|t|}\right]. \tag{6.77}$$

Note that $r_x(0) = \vartheta/\omega_0^2$ in all cases, representing the variance of the position $x(t)$.

With the expressions for the correlation function $r_x(t)$ (Eqs. (6.75)-(6.77)), we can now compute the mean, variance, and Fano factor for upcrossings for the stochastic damped harmonic oscillator

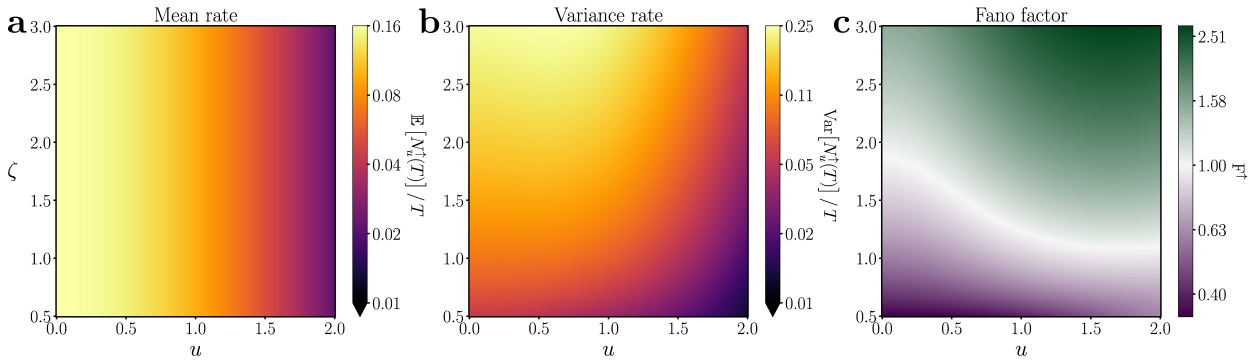


Figure 6.3: Mean rate, variance rate, and Fano factor of upcrossings for the stochastic damped harmonic oscillator as functions of level u and damping ratio ζ. We plot (**a**), the mean rate of upcrossings $\mathbb{E}[N_u^{\uparrow}(T)]/T$; (**b**), the variance rate of upcrossings $\mathrm{Var}[N_u^{\uparrow}(T)]/T$; and (**c**), the upcrossing Fano factor $\mathrm{F}^{\uparrow}$ for the stochastic damped harmonic oscillator across various combinations of threshold (u) and damping constant (ζ). The natural oscillation frequency is fixed at $\omega_0 = 1.0$ and the temperature at $\vartheta = 1.0$, resulting in a process variance $r(0) = \vartheta/\omega_0^2 = 1.0$. Color bars indicate the magnitude of the respective quantities on a logarithmic scale. All plotted values are calculated using the analytical formulae derived in this work. Notably, for a fixed threshold u, the mean rate (**a**) is independent of the damping ratio ζ, while the variance rate (**b**) is ζ-dependent. Consequently, the Fano factor (**c**) spans a broad range, revealing both sub-Poisson and super-Poisson upcrossing statistics depending on the specific (u, ζ) combination.

using the analytical results stated in Theorem 6.1. In Fig. 6.3, we present the mean rate of upcrossings $\mathbb{E}[N_u^{\uparrow}(T)]/T$, the variance rate $\mathrm{Var}[N_u^{\uparrow}(T)]/T$, and the Fano factor $\mathrm{F}^{\uparrow}$ as functions of the threshold level u and the damping ratio ζ. We set the temperature ϑ and the natural frequency of the oscillator ω_0 to unity, such that the process variance $r_x(0) = 1.0$ across all ζ. As depicted in Fig. 6.3a, the mean upcrossing rate for a given u is independent of ζ. This is a direct outcome of Eq. (6.24), since $\mathbb{E}[N_u^{\uparrow}(T)]$ depends only on $r_x(0)$ and $-r_x''(0)$ (i.e., q_0), which are themselves independent of ζ. In contrast, Fig. 6.3b and Fig. 6.3c show that both the variance rate and the Fano factor are strongly dependent on u and ζ. This dependence reveals that the upcrossing statistics can span a wide range, from sub-Poissonian to super-Poissonian. To ensure the validity of our analytical framework, we compared the analytical solutions for the mean, variance, and the Fano factor with results from direct numerical simulations (Fig. 6.4). We find excellent agreement across a wide range of parameters and threshold levels u.

We further investigate the behavior of the upcrossing Fano factors $\mathrm{F}^{\uparrow}$, detailed in Fig. 6.5, by

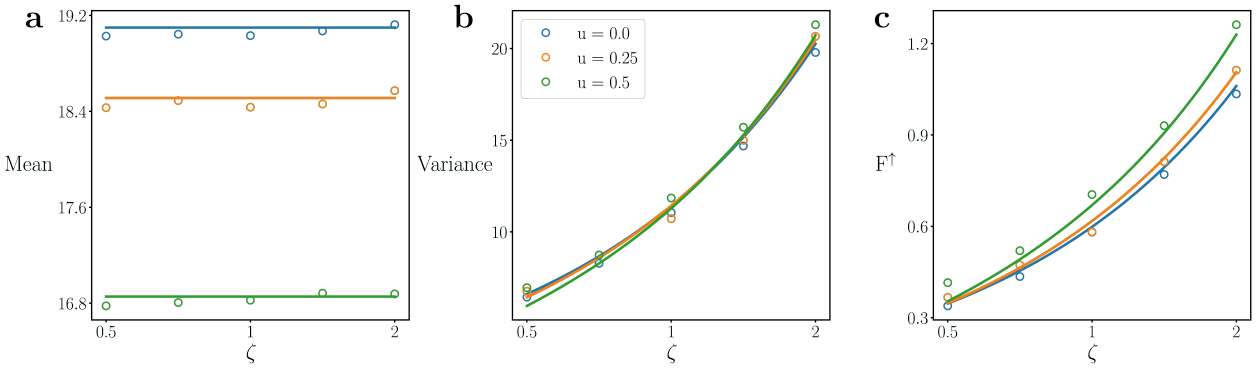


Figure 6.4: Comparison of analytical formulae with numerical simulations for the stochastic damped harmonic oscillator. We plot (**a**), the mean number of upcrossings $\mathbb{E}[N_u^{\uparrow}(T)]$; (**b**), the variance of upcrossings $\mathrm{Var}[N_u^{\uparrow}(T)]$; and (**c**), the upcrossing Fano factor $\mathrm{F}^{\uparrow}$ as a function of the damping ratio ζ for three different threshold level $u = [0.0, 0.25, 0.5]$. Solid lines represent the analytical solutions derived in this work, while circles denote results obtained from numerical simulations. The model parameters were fixed at $\omega_0 = 1.0$ Hz and $\vartheta = 1.0$, for a total simulation time of $T = 120$ s for each trial. For the numerical simulations, we used a discretization time-step $dt = 0.01 \times$ (slowest timescale of the system), and computed the statistics from 5000 independent trials. We find an excellent agreement between the analytical predictions and the simulation results across the explored parameter range.

examining its landscapes across various parameter configurations. First, we set the temperature to unity, i.e., $\vartheta = 1.0$ and compute $\mathrm{F}^{\uparrow}$ as a function of the threshold u and the natural frequency ω_0 for different damping regimes (Fig. 6.5a-c). Then we set the natural frequency ω_0 to unity and compute $\mathrm{F}^{\uparrow}$ as a function of the threshold u and temperature ϑ for the same damping regimes (Fig. 6.5d-f). These heatmaps reveal distinct characteristics of $\mathrm{F}^{\uparrow}$ based on the damping regime:

- In the underdamped ($\zeta = 0.5$; plots **a**, **d**) and critically damped ($\zeta = 1.0$; plots **b**, **e**) regimes, the statistics are predominantly sub-Poissonian ($\mathrm{F}^{\uparrow} < 1$, corresponding to the purple and lighter central regions of the colormap). For the underdamped case (**a**, **d**), $\mathrm{F}^{\uparrow}$ generally exhibits monotonic variations along lines of constant u, ω_0, or ϑ.

- In the overdamped regime ($\zeta = 2.0$; plots **c**, **f**), regions of both sub-Poissonian (purple/light regions) and super-Poissonian ($\mathrm{F}^{\uparrow} > 1$, greener regions) statistics are evident. The specific nature of the statistics depends on the particular combination of the parameters and the level u.

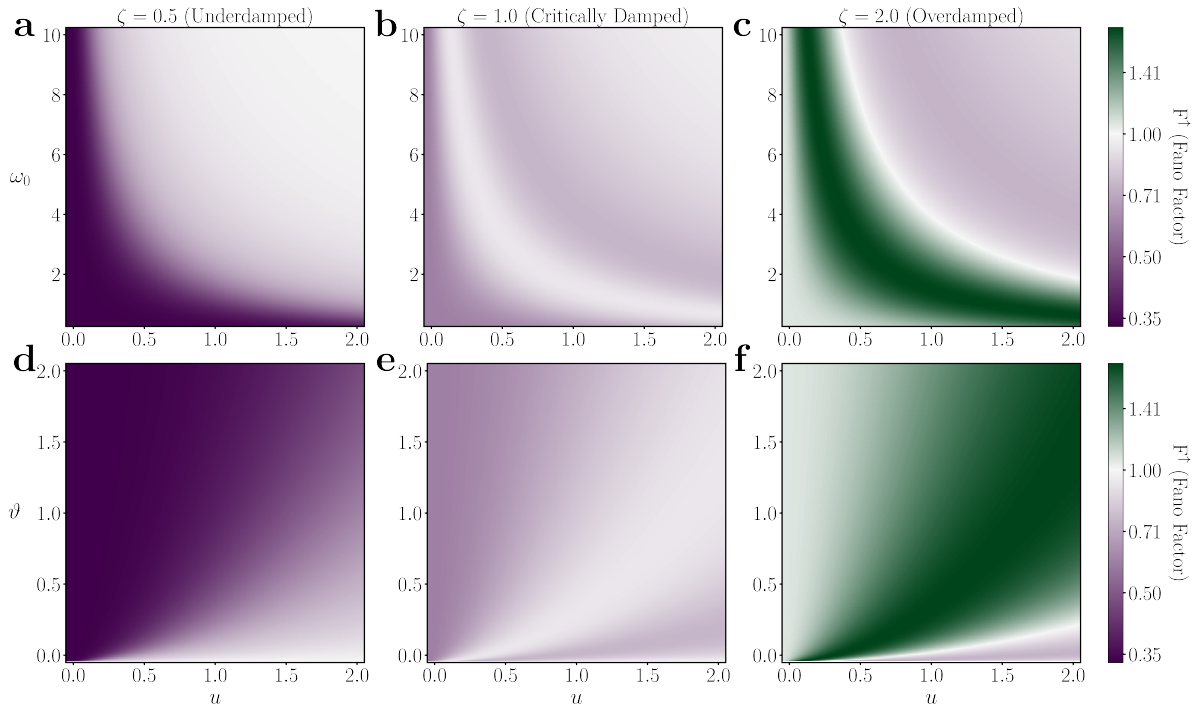


Figure 6.5: Fano factor landscapes for the stochastic damped harmonic oscillator across different parameter regimes. We plot the analytical upcrossing Fano factor ($F^{\uparrow}$) for the stochastic damped harmonic oscillator across various parameter configurations. (**a**-**c**), Fano factor as a function of the natural frequency ω_0 and threshold level u, for a fixed temperature $\vartheta = 1.0$ and different damping ratios: (**a**), Underdamped $\zeta = 0.5$; (**b**), Critically Damped $\zeta = 1.0$; and (**c**), Overdamped $\zeta = 2.0$. (**d**-**f**) Fano factor as a function of the temperature (noise strength parameter) ϑ and threshold level u, for a fixed natural frequency $\omega_0 = 1.0$ and the same damping ratios: (**a**), Underdamped $\zeta = 0.5$; (**b**), Critically Damped $\zeta = 1.0$; and (**c**), Overdamped $\zeta = 2.0$. The color bars indicate the magnitude of the Fano factor on a logarithmic scale, where values near $F^{\uparrow} = 1.0$ are represented by lighter colors, sub-Poisson values by purples, and super-Poisson values by greens.

- Non-monotonic behavior in $F^{\uparrow}$ is frequently observed in the critically damped (plots **b**, **e**) and overdamped (plots **c**, **f**) regimes. For instance, when fixing u and varying ω_0 (in **b**, **c**) or ϑ (in **e**, **f**), $F^{\uparrow}$ exhibits a peak. Similar non-monotonic variations occur when varying u while holding ω_0 or ϑ constant.

6.5.2 Mean Reverting Process with Ornstein-Uhlenbeck Noise

We consider a mean-reverting process driven by Ornstein-Uhlenbeck noise. This model is relevant in various fields, including finance for modeling stochastic volatility and in neuroscience

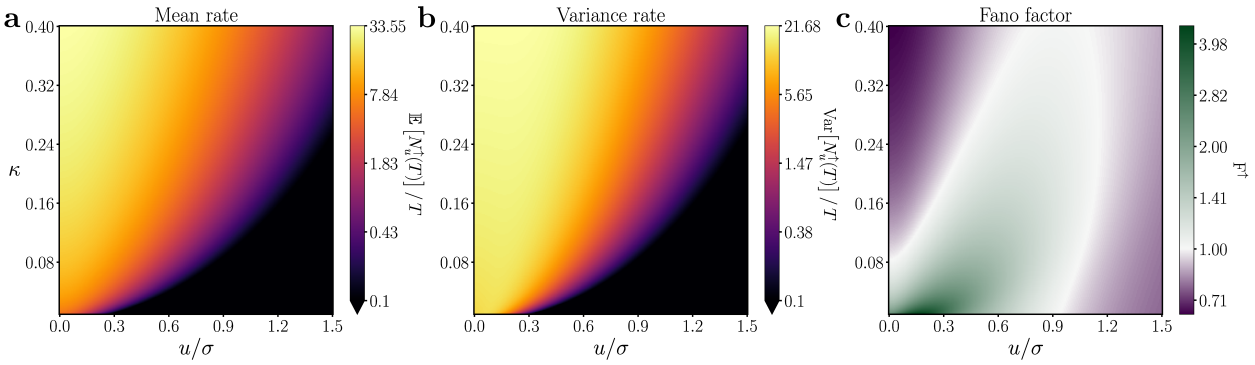


Figure 6.6: Mean rate, variance rate, and Fano factor of upcrossings for a mean-reverting process driven by Ornstein-Uhlenbeck noise. We plot (**a**), the mean rate of upcrossings $\mathbb{E}[N_u^{\uparrow}(T)]/T$; (**b**), the variance rate of upcrossings $\mathrm{Var}[N_u^{\uparrow}(T)]/T$; and (**c**), the upcrossing Fano factor $\mathrm{F}^{\uparrow}$ for a mean-reverting process with characteristic timescale τ_e, driven by Ornstein-Uhlenbeck (OU) noise with correlation time τ_f; this system is described by Eq. (6.78). The plots illustrate the dependence on two dimensionless parameters: the normalized threshold u/σ and the timescale ratio $\kappa = \tau_f/\tau_e$. We set the standard deviation of the input OU noise $\sigma = 1.0$ and its correlation time $\tau_f = 3$ ms. Note that the resulting variance of the observed mean-reverting process $y(t)$ is $r_y(0) = \sigma^2\kappa/(1+\kappa)$. Color bars indicate the magnitude of the respective quantities on a logarithmic scale. All plotted values are computed using the analytical formulae derived in this work. We find that the Fano factor (**c**) spans a broad range, revealing both sub-Poisson and super-Poisson upcrossing statistics depending on the specific $(u/\sigma, \kappa)$ combination.

for describing the membrane equation with filtered synaptic inputs [184]. The dynamics of the system are given by the following set of stochastic differential equations:

$$\begin{aligned} \frac{\mathrm{d}x}{\mathrm{d}t} &= -\frac{x}{\tau_f} + \sqrt{\frac{2\sigma^2}{\tau_f}}\,\eta(t) \\ \frac{\mathrm{d}y}{\mathrm{d}t} &= -\frac{1}{\tau_e}\Big(y - x\Big). \end{aligned} \tag{6.78}$$

Here, $x(t)$ represents an Ornstein-Uhlenbeck process, which is an exponentially low-pass filtered white noise $\eta(t)$ (where $\mathbb{E}\left[\eta(t)\,\eta(s)\right] = \delta(t-s)$) process. The OU process $x(t)$ has a characteristic correlation time τ_f and its fluctuations are scaled by the parameter σ. The process $y(t)$ receives $x(t)$ as its input and exhibits mean-reverting behavior towards 0 with a characteristic timescale τ_e. Since $y(t)$ is a linear transformation of the Gaussian process $x(t)$, it is also a stationary Gaussian process.

To analyze the level-crossing statistics of $y(t)$, we first need its autocorrelation function.

Following a procedure similar to that used for the stochastic damped harmonic oscillator (i.e., by solving the system in the Fourier domain), the autocorrelation function $r_y(t) = \mathbb{E}[y(s)y(s+t)]$ for the process $y(t)$ is found to be:

$$r_y(t) = \frac{\sigma^2 \kappa}{1-\kappa^2}\left(e^{-|t|/\tau_e} - \kappa\, e^{-|t|/(\kappa\tau_e)}\right), \tag{6.79}$$

where $\kappa = \tau_f/\tau_e$ is the dimensionless ratio of the input noise correlation timescale τ_f to the system's relaxation timescale τ_e. The variance of this process is $r_y(0) = \sigma^2\kappa/(1+\kappa)$.

Using this autocorrelation function $r_y(t)$, we can apply Theorem 6.1 to compute the mean per unit time, variance per unit time, and Fano factor for level upcrossings of $y(t)$. Figure 6.6 illustrates these quantities as functions of the normalized threshold level u/σ and the timescale ratio κ. Similar to the damped harmonic oscillator operated in the overdamped regime, the Fano factor for this system (Fig. 6.6c) spans a broad range, indicating that the upcrossing statistics can be sub-Poissonian, Poissonian, or super-Poissonian, depending on the specific combination of the normalized threshold u/σ and the timescale ratio κ. In fact, it can be shown that the correlation function of $y(t)$ in Eq. (6.79) can be mapped to the correlation function of the damped harmonic oscillator operated in the overdamped regime (Eq. (6.77)).

6.5.3 Process with Rational Quadratic Correlation Function

We consider a stationary Gaussian process whose covariance follows the rational-quadratic kernel, a popular choice in Gaussian-process regression [185]. This kernel can be written as a continuous mixture of squared-exponential kernels with different characteristic time-scales, enabling it to capture variability that occurs over a wide range of time-scales. For such a process X_t, its rational quadratic correlation function $r(t)$ is given by:

$$r(t) = \sigma^2\left(1 + \frac{1}{2\alpha}\left(\frac{t}{\tau}\right)^2\right)^{-\alpha} \tag{6.80}$$

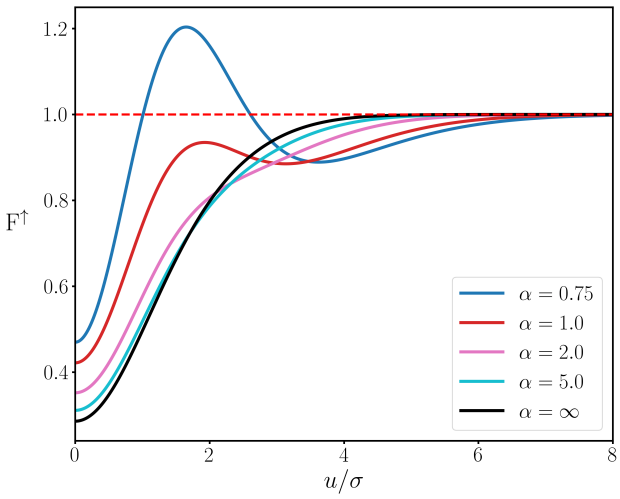


Figure 6.7: Fano factor for a stationary Gaussian process with a rational quadratic correlation function. We plot the upcrossing Fano factor $F^{\uparrow}$ as a function of the normalized threshold level u/σ for a stochastic process with the rational quadratic correlation function, $r(t) = \sigma^2 \left(1 + \frac{1}{2\alpha}\left(\frac{t}{\tau}\right)^2\right)^{-\alpha}$. Each colored line corresponds to a different value of the shape parameter α. The black line represents the $\alpha \to \infty$ limit, where the correlation function simplifies to a squared exponential form, $r(t) = \sigma^2 \exp\left(-t^2/(2\tau^2)\right)$. As the Fano factor is evaluated in the infinite time limit, the results presented are independent of the timescale parameter τ. The behavior of $F^{\uparrow}$ varies markedly with α. For smaller values (e.g., $\alpha = 0.75$), $F^{\uparrow}$ can exceed 1, indicating a regime of super-Poisson statistics for certain u/σ. Conversely, for larger α values $F^{\uparrow}$ remains sub-Poisson ($F^{\uparrow} < 1$) for all u/σ. For all α, the Fano factor approaches the Poisson limit ($F^{\uparrow} \to 1$) as $u/\sigma \to \infty$.

where $\sigma^2 = r(0)$ is the variance of the process, $\tau > 0$ is a characteristic timescale parameter, and $\alpha > 0$ is a shape parameter that dictates the long-range behavior and smoothness of the correlation. As $\alpha \to \infty$, the rational quadratic correlation function approaches the squared exponential correlation function: $r(t) = \sigma^2 \exp\left(-t^2/(2\tau^2)\right)$.

In Fig. 6.7, we plot the upcrossing Fano factor $F^{\uparrow}$ for this process as a function of the dimensionless normalized threshold level u/σ for several different values of the shape parameter α. Since the Fano factor is evaluated in the long-time limit, the results are independent of the specific timescale parameter τ, depending only on α and the normalized threshold. The shape parameter α critically influences the upcrossing statistics: smaller α, associated with longer-range correlations, can lead to super-Poissonian Fano factors, while larger α yields sub-Poissonian upcrossing statistics. Ultimately, for very high thresholds, the Fano factor consistently approaches the Poissonian limit.

This underscores how the correlation function's structure directly shapes these higher-order statistical properties.

6.6 Discussion

In this chapter, we presented exact analytical expressions for the variance and Fano factor of *arbitrary* level crossings in smooth, stationary Gaussian processes. Our formulae, encapsulated in Theorems 6.1 and 6.4, provide a single-integral formulation for the variance, analogous to the well-established result for mean-level upcrossings [163], but now generalized to any level u. This was achieved by explicitly solving the requisite asymmetric Gaussian integrals, expressed in terms of known special functions. We demonstrate the utility and generality of these formulae by applying them to diverse stochastic models: the stochastic damped harmonic oscillator, a mean-reverting process driven by Ornstein-Uhlenbeck noise, and a process characterized by a rational quadratic correlation function. In each case, we elucidated the rich dependence of the variance and Fano factor on the underlying process parameters and the chosen threshold level. These examples underscore how the correlation structure of the process intricately shapes the higher-order statistics of its level crossings, leading to a wide spectrum of behaviors, from sub-Poissonian to super-Poissonian statistics.

The analytical expressions offer versatile tools with several important implications. Firstly, they significantly enhance the toolkit for parameter estimation and inference in systems modeled by stationary Gaussian processes. While the Kac-Rice formula for the mean number of crossings is invaluable, the incorporation of exact second-order statistics can lead to more robust and accurate parameter determination, particularly when the mean rate alone is insufficient or when assessing the uncertainty of estimates [163]. Secondly, they provide a solid foundation for developing and validating simpler, potentially more tractable, upper and lower bounds on the variance of level crossings. Such bounds could extend previous work on mean-crossing statistics [186] to the more

general case of arbitrary level crossings.

Furthermore, the insights gained from the variance and Fano factor can deepen our understanding of the dynamics of various physical, biological, and financial systems where threshold-crossing events are of primary interest. The ability to precisely quantify the variability of these events, beyond just their average frequency, is crucial for characterizing phenomena such as neuronal firing patterns [156, 157], critical transitions in environmental systems, or fluctuations in financial markets [159]. Our results not only fill a theoretical gap but also offer powerful practical tools for analysis, inference, and model validation across a multitude of scientific and engineering disciplines where Gaussian processes and their thresholding behavior play a pivotal role. Future work will be directed towards developing more accurate and robust parameter estimation techniques that directly incorporate the analytical variance of level crossings derived herein.

7 | A Large-scale Model of the Primary Visual Cortex (V1)

7.1 Overview

In this chapter, we develop a large-scale model of the primary visual cortex (V1) using ORGaNICs. The core findings discussed herein were presented in [187].

We construct a retinotopic model of V1 where the dynamics of complex cells are governed by ORGaNICs. The input to these cells is provided by the outputs of a steerable pyramid decomposition of visual stimuli, which effectively captures the retinotopy, spatial frequency selectivity, receptive field size, and orientation tuning of V1 neurons. Using the analytical tools for stochastic LTI systems developed in Chapter 5, we demonstrate that the model reproduces key features of V1 physiology. For grating stimuli, the circuit naturally oscillates in the gamma frequency range and accurately captures the experimentally observed local field potential (LFP) coherence across neuronal populations with different tuning properties. To model spiking statistics, we introduce a Gaussian-Rectification (GR) model that incorporates the temporal correlations of the underlying membrane potentials. This framework allows us to analytically predict how the Fano factor of individual neurons depends on grating stimulus contrast and attention, closely matching experimental data. The model makes predictions for these quantities in response to more complex stimuli like plaids and natural images, offering a powerful tool for dissecting the dynamics of V1.

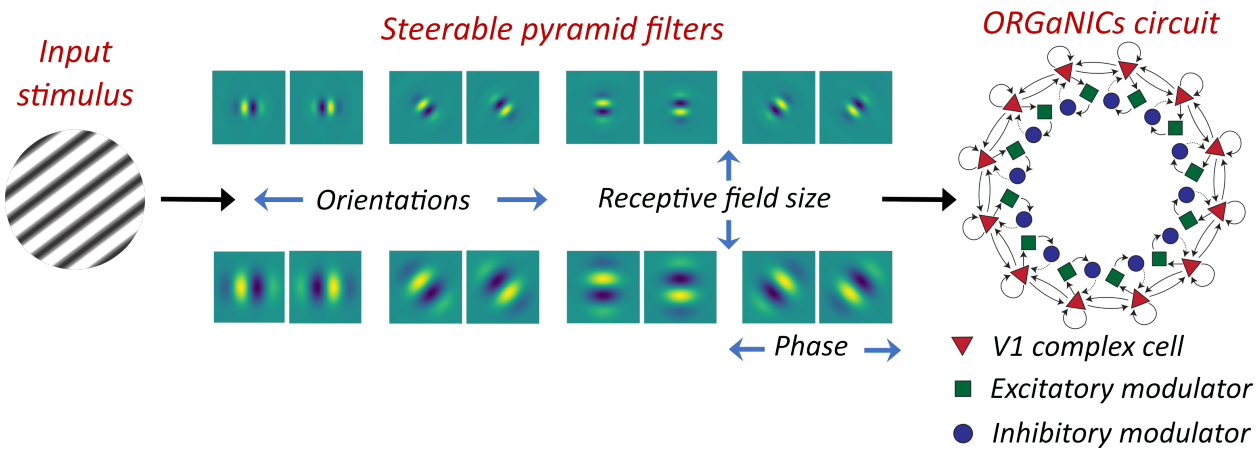


Figure 7.1: Schematic of the large-scale V1 model. An input stimulus (e.g., a sinusoidal grating) is processed by a bank of steerable pyramid filters, which model the responses of V1 simple cells with varying orientations, receptive field sizes, and phases. The energy of these filter outputs (modulus of the complex-valued response) serves as the input drive $\mathbf{z}$ to the ORGaNICs circuit. This circuit is composed of three interconnected populations of neurons: V1 complex cells ($\mathbf{y}$, red triangles), inhibitory modulators ($\mathbf{a}$, blue circles), and excitatory modulators ($\mathbf{u}$, green squares). This three-neuron type ORGaNICs (Eq. (7.1)) is designed to implement the general divisive normalization equation (Eq.(1.7)) at steady-state.

7.2 A Three-Neuron ORGaNICs Model of V1

ORGaNICs has previously been proposed as a framework for modeling V1 responses [16]. Here, we extend that work in two ways: first, by implementing a large-scale dynamical system that explicitly models the retinotopic organization and diverse tuning properties of V1 neurons; and second, by incorporating a biophysically motivated noise model to account for the trial-to-trial variability of spiking activity. We adopt the three-neuron circuit architecture, similar to that in [16], which includes principal excitatory neurons, inhibitory interneurons, and a population of excitatory modulatory neurons.

The dynamics of the circuit (Fig. 7.1) are described by the following set of stochastic differential

equations:

$$\begin{aligned}
\tau_y \dot{\mathbf{y}} &= -\mathbf{y} + b\,\mathbf{z} + \left(\frac{1}{1+\mathbf{a}^+}\right) \odot \mathbf{W}_r \left(\sqrt{\mathbf{y}^+} - \sqrt{\mathbf{y}^-}\right) + \boldsymbol{\eta}_y \\
\tau_a \dot{\mathbf{a}} &= -\mathbf{a} + \alpha\,\dot{\mathbf{u}}^+ + \mathbf{u}^+ + \mathbf{u}^+ \odot \mathbf{a}^+ + \boldsymbol{\eta}_a \\
\tau_u \dot{\mathbf{u}} &= -\mathbf{u} + b_0^2\,\sigma^2 + \mathbf{W}\,\left((\mathbf{y}^+ + \mathbf{y}^-) \odot \mathbf{u}^{+2}\right) + \boldsymbol{\eta}_u
\end{aligned} \tag{7.1}$$

This model is a generalized version of the two-neuron circuit analyzed in previous chapters. The primary difference is the addition of the excitatory modulatory neuron population $\mathbf{u}$, which now computes the normalization signal. In the limit of infinitely fast inhibitory dynamics ($\tau_a \longrightarrow 0$) and with $\alpha = 0$, this three-neuron model converges to the two-neuron model of Eq. (1.9). The components are defined as follows:

- $\mathbf{y}$, $\mathbf{a}$, and $\mathbf{u}$ are vectors representing the membrane potentials of the principal excitatory (V1 complex cells), inhibitory and excitatory modulatory neuron populations, respectively.

- $\mathbf{z}$ is the external input drive to the V1 complex cells. To model the inputs realistically, we process visual stimuli with a steerable pyramid transform [188]. This transform uses a basis of oriented filters at multiple spatial scales and orientations, providing a good model for the receptive fields of V1 simple cells [9]. The complex-valued output of each filter can be seen as the response of a pair of simple cells with complementary receptive fields. The V1 complex cell input $\mathbf{z}$ is then computed as the energy (modulus) of these complex-valued responses. Our model consists of neurons arranged on a 16×16 retinotopic grid, with each location containing populations selective for 6 different orientations and 2 receptive field sizes (spatial frequency), resulting in a total of 3,072 principal neurons.

- $\mathbf{y}^\pm$, $\mathbf{u}^+$, and $\mathbf{a}^+$ represent the firing rates of the corresponding neuron types. They are obtained

by filtering the membrane potentials after rectification and a power-law transformation:

$$\tau_s \dot{\mathbf{x}}^+ = -\mathbf{x}^+ + \lfloor \mathbf{x} \rfloor^\beta , \tag{7.2}$$

where the exponent β is 2 for $\mathbf{y}$ (complex cells), 1 for $\mathbf{a}$, and 0.5 for $\mathbf{u}$.

- $\boldsymbol{\eta}_y$, $\boldsymbol{\eta}_a$, and $\boldsymbol{\eta}_u$ are uncorrelated Gaussian white noise sources modeling stochastic fluctuations in membrane potential. We set their standard deviations to 0.01. Noise in the firing rate dynamics is assumed to be negligible, since synaptic noise is a predominant source of noise in neural circuits [189, 190].

- The terms highlighted in green represent external inputs, while those in blue represent recurrent inputs. $\mathbf{W}_r$ is the recurrent weight matrix among principal neurons, which, for analytical tractability in this chapter, is set to the identity matrix. $\mathbf{W}$ is the normalization weight matrix. To implement surround suppression, we designed $\mathbf{W}$ such that neurons with receptive fields centered at the same location are strongly coupled (weight of 1 across all orientations and receptive field sizes), with connection strength decaying exponentially as a function of retinotopic distance.

- We set the gain parameters $b = b_0 = 0.5$ and $\alpha = 2$. We set the semisaturation constant $\sigma = 0.1$ based on experimental evidence [17] and the time constants $\tau_y = \tau_u = 2.5$ ms and $\tau_a = 1$ ms.

With 3,072 neurons of each of the three types, and a corresponding firing rate variable for each, the full stochastic dynamical system has a dimension of 18,432.

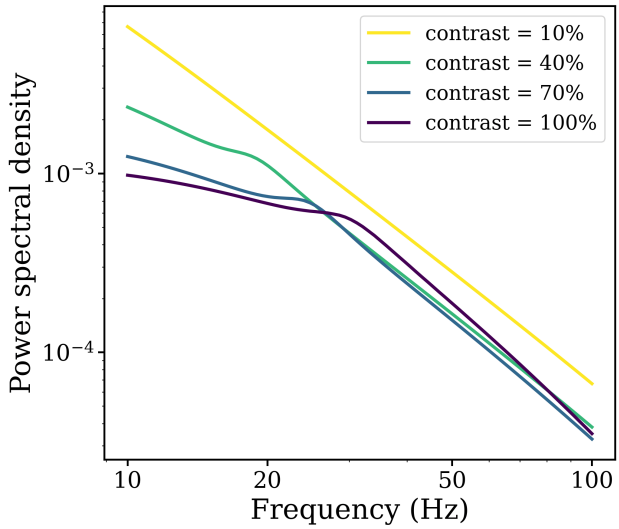


Figure 7.2: Power spectral density of LFP in the V1 model for a grating stimulus of varying contrast. Power spectral density is plotted for the maximally firing principal neuron at the center of the stimulus. The model produces strong gamma-band oscillatory activity for gratings with larger contrast. The peak frequency increases with increasing stimulus contrast.

7.3 LFP Power Spectra and Coherence

A prominent feature of V1 activity is the presence of gamma-band (30-80 Hz) oscillations, whose strength and coherence are modulated by stimulus properties like contrast [191, 192]. We used our model to investigate whether these phenomena emerge from the circuit's dynamics. By linearizing the high-dimensional system (Eq. (7.1)) around its analytically known fixed point, we can compute the full Power Spectral Density (PSD) matrix $\boldsymbol{S}(\omega) = (\imath\omega\mathbf{I} - \mathbf{J})^{-1}\,\mathbf{L}\,\mathbf{D}\,\mathbf{L}^{\top}\,(-\imath\omega\mathbf{I} - \mathbf{J})^{-\top}$ (Chapter 5), where $\mathbf{J}$ is the Jacobian and $\mathbf{L}\,\mathbf{D}\,\mathbf{L}^{\top}$ forms the noise covariance matrix (see Chapter 5). The power spectral density of any neuron is given by the diagonal element of $\boldsymbol{S}(\omega)$. Fig. 7.2 shows the power spectral density of the maximally firing principal neuron in response to a grating stimulus of varying contrast. We observe no oscillatory activity for a grating of small contrast (10%), but gamma oscillations (indicated by peaks in the power spectral density) emerge for larger stimulus contrasts, and the peak frequency increases with increasing contrast. These findings are consistent with experimental measurements [191].

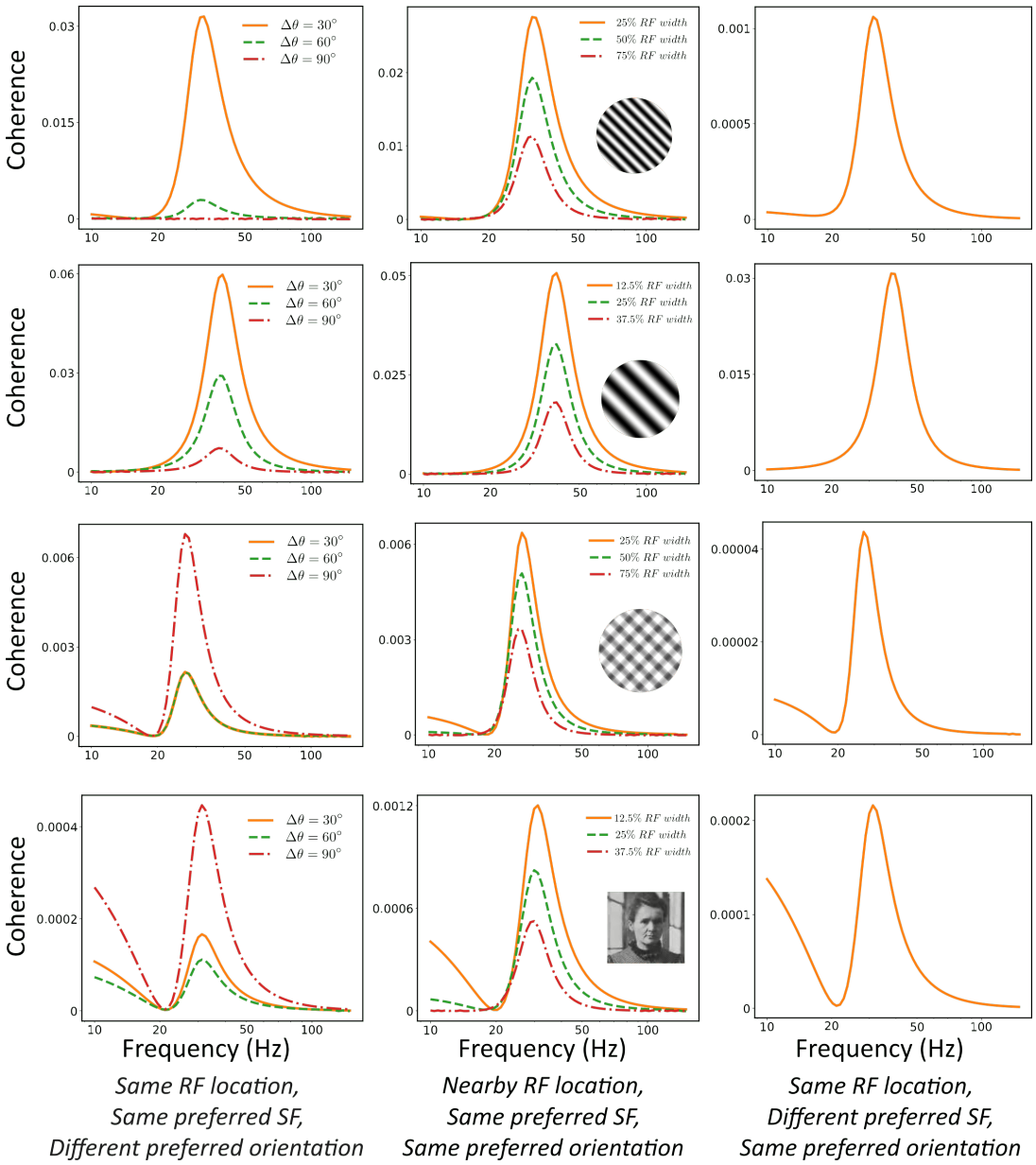


Figure 7.3: Coherence of LFP in the V1 model for different stimuli. Coherence is computed between the maximally firing principal neuron (at the center of the stimulus) and a second principal neuron. The rows correspond to different stimuli: gratings (top two), plaid (third), and a natural image (bottom). The second principal neuron for calculating coherence is picked as follows: **(Left)** same RF location and preferred spatial frequency (SF), but different preferred orientations ($\Delta\theta$); **(Center)** nearby RF location but same preferred SF and orientation; **(Right)** same RF location and orientation but different preferred SF. The model reproduces strong gamma-band coherence for gratings, which diminishes for more complex stimuli. Coherence decreases with increasing differences in neuronal tuning properties, consistent with experimental observations.

The coherence between any two neurons can then be computed from the elements of $\boldsymbol{S}(\omega)$. Specifically, the coherence between neurons at index i and j is given by $\kappa_{ij}(\omega) = \frac{|\mathcal{S}_{ij}(\omega)|^2}{\mathcal{S}_{ii}(\omega)\mathcal{S}_{jj}(\omega)}$. Fig. 7.3 shows the predicted coherence for different visual stimuli. The model correctly predicts that for grating stimuli, coherence peaks in the gamma frequency range. This coherence is strongest between neurons with similar receptive field properties (e.g., same location and preferred orientation) and decreases as the difference in preferred orientation, spatial location, or spatial frequency increases. The model also captures the reduction in gamma coherence for more complex stimuli like plaids, consistent with experimental findings [193].

7.4 A Gaussian-Rectification Model for Spiking Statistics

To bridge the gap between continuous membrane potential dynamics and discrete spike trains, and to account for the observed variability in neuronal firing, we employ a dynamic version of the Gaussian-Rectification (GR) model [53]. This model posits that trial-to-trial variability arises from fluctuations in the membrane potential, which is assumed to follow a Gaussian distribution around its mean (Fig. 7.4). While the standard GR model assumes independent samples, we account for the temporal correlations inherent in the membrane potential dynamics to derive an analytical expression for the Fano factor.

7.4.1 Derivation of the Analytical Fano Factor

Let the spike train be a point process, and let N_T be the number of spikes counted in a time window of duration T. We model N_T as a sum of Bernoulli indicator variables, $N_T = \sum_{i=1}^{n} I_i$, where I_i is 1 if a spike occurs in the i-th small time bin of size Δt (such that $T = n\Delta t$), and 0 otherwise. The probability of a spike in a bin is $P(I_i = 1) = r\Delta t$, where r is the neuron's mean firing rate, given by the steady-state solution of the ORGaNICs model, $r = \mathrm{y}_s^+$.

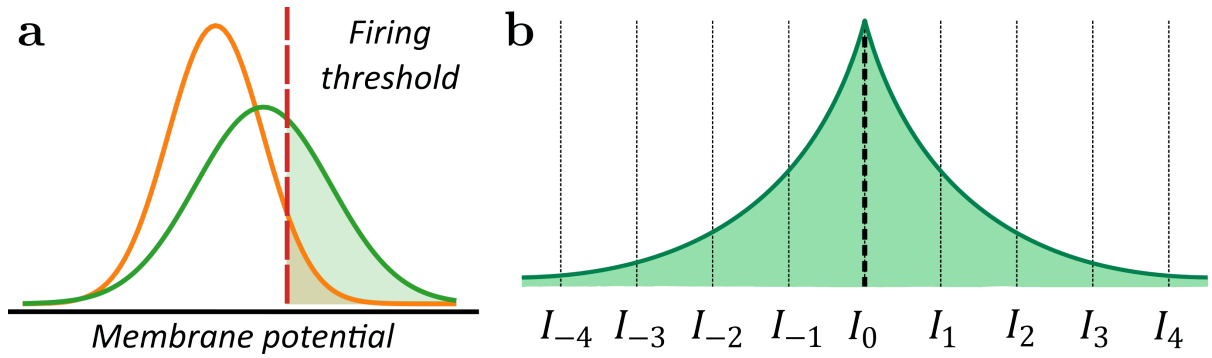


Figure 7.4: The Gaussian-Rectification (GR) model for spike generation. (a) The membrane potential (y) of a neuron is modeled as a stationary Gaussian process. The mean firing rate is proportional to the shaded area under the Gaussian curve. **(b)** Illustration of the indicator random variables generating the spike train. The green envelope displays the exponential decay of the time correlation between a central indicator random variable I_0 and others.

The mean spike count is given by the linearity of expectation:

$$\mathbb{E}[N_T] = \sum_{i=1}^{n} \mathbb{E}[I_i] = n(r\Delta t) = rT \tag{7.3}$$

The variance of the spike count is more complex due to temporal correlations between the indicator random variables:

$$\mathrm{Var}(N_T) = \sum_{i=1}^{n} \mathrm{Var}(I_i) + \sum_{i \neq j} \mathrm{Cov}(I_i, I_j) \tag{7.4}$$

The first term corresponds to the variance of a Poisson process. Since I_i is a Bernoulli variable, $\mathrm{Var}(I_i) = (r\Delta t)(1 - r\Delta t) \approx r\Delta t$ for small Δt. Thus, $\sum_i \mathrm{Var}(I_i) \approx n(r\Delta t) = rT$.

The second term captures the excess variance due to correlations. For a stationary process, the covariance depends only on the time lag $\tau = |t_i - t_j|$. In the limit of a large time window T (i.e., T much greater than the correlation time of the process), the sum can be approximated by an integral:

$$\sum_{i \neq j} \mathrm{Cov}(I_i, I_j) \approx 2n \sum_{k=1}^{\infty} \mathrm{Cov}(I_0, I_k) \approx 2\frac{T}{(\Delta t)^2} \int_0^{\infty} C(\tau) d\tau \tag{7.5}$$

where $C(\tau)$ is the continuous-time covariance density of the spiking process. The dynamics of $C(\tau)$ are governed by the autocorrelation of the underlying membrane potential. Since the

linearized membrane potential follows an Ornstein-Uhlenbeck process, its autocorrelation decays exponentially with an effective time constant τ_e. We approximate the covariance density for the counting process as $C(\tau) \approx \Delta t \cdot k \cdot r \cdot e^{-\tau/\tau_e}$, where k is a constant of proportionality.

The integral of the covariance density is then $\int_0^\infty C(\tau)d\tau = \Delta t k r \tau_e$. Substituting this back into the variance expression gives:

$$\mathrm{Var}(N_T) \approx rT + 2\frac{T}{(\Delta t)^2}(\Delta t k r \tau_e) = rT(1 + 2k\tau_e/\Delta t) \tag{7.6}$$

The Fano factor, $FF = \mathrm{Var}(N_T)/\mathbb{E}[N_T]$, is therefore:

$$FF \approx \frac{rT(1 + 2k\tau_e/\Delta t)}{rT} = 1 + 2k\tau_e/\Delta t = 1 + \gamma\tau_e \tag{7.7}$$

where $\gamma = 2k/\Delta t$ is a constant that absorbs the details of the spike generation process, for example, the refractory period. This crucial result links the Fano factor directly to the effective time constant of the neuron's membrane potential.

7.4.2 Effective Time Constant

The effective time constant, τ_e, which governs the correlation time of membrane potential fluctuations, can be derived analytically for our model. Linearizing the deterministic part of the equation for the $\mathbf{y}$ neurons (Eq. (7.1)) around the fixed point (assuming $\mathbf{W}_r = \mathbf{I}$) gives:

$$\begin{aligned} \tau_y \dot{\mathbf{y}} &\approx -\mathbf{y} + b\,\mathbf{z} + \left(\frac{1}{1 + \mathbf{a}_s^+}\right) \odot \mathbf{y} \\ \implies \frac{\tau_y(1 + \mathbf{a}_s^+)}{\mathbf{a}_s^+}\,\dot{\mathbf{y}} &\approx -\mathbf{y} + \text{const.} \end{aligned} \tag{7.8}$$

Thus, the vector of effective time constants for the principal neurons is:

$$\boldsymbol{\tau}_{\mathbf{y}}^e = \frac{\tau_y(1 + \mathbf{a}_s^+)}{\mathbf{a}_s^+} \tag{7.9}$$

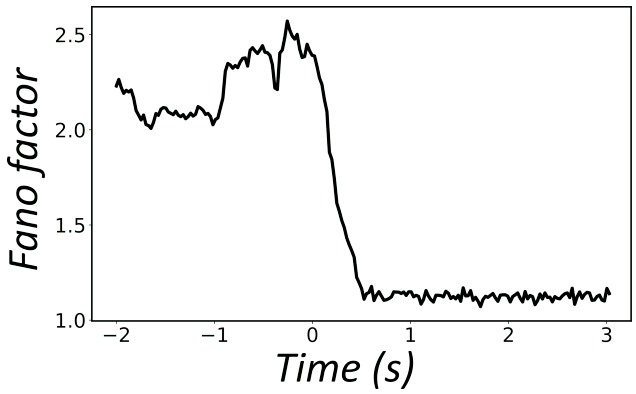


Figure 7.5: Quenching of the Fano factor upon stimulus presentation. The plot shows the Fano factor computed in a sliding window over time. Before stimulus onset ($t < 0$), variability is high (Fano factor > 2). Upon stimulus presentation at $t = 0$, the Fano factor rapidly decreases and stabilizes at a lower value close to 1.

Because the steady-state activity of the inhibitory population, $\mathbf{a}_s^+$, is itself a function of the input drive, the effective time constant becomes stimulus-dependent. Plugging the fixed point solution into Eq. (7.7), we get

$$\tau_{y_i}^e = \frac{\tau_y}{\sqrt{b_0^2\,\sigma^2 + b^2 \sum_j w_{ij} z_j^2}}, \tag{7.10}$$

where w_{ij} are the weights of the normalization weight matrix $\mathbf{W}$.

7.4.3 Results

Plugging the analytical expression for the effective time constants into Eq. (7.7), we arrive at a final analytical expression for the Fano factor of the principal neurons:

$$FF_i \approx 1 + \frac{\gamma \tau_y}{\sqrt{b_0^2\,\sigma^2 + b^2 \sum_j w_{ij} z_j^2}} \tag{7.11}$$

Our model successfully reproduces key experimental findings related to spiking variability. Fig 7.5 demonstrates that upon the presentation of a stimulus at $t = 0$, the Fano factor is rapidly "quenched" from a high baseline value to a lower, sustained level. This stimulus-induced reduction

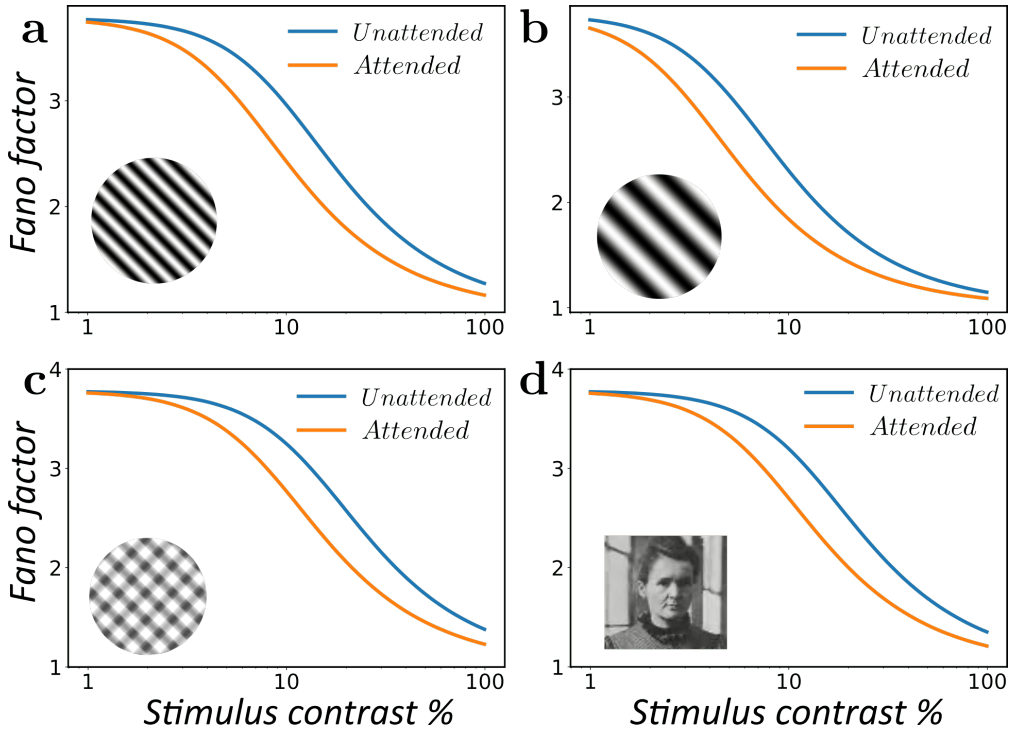


Figure 7.6: Fano factor as a function of stimulus contrast and attention. The Fano factor of the maximally firing V1 complex cell is plotted against stimulus contrast for both an unattended (blue) and an attended (orange) condition. Attention is modeled as an increase in the input gain $b = 1$ while keeping the baseline gain $b_0 = 0.5$. Panels show results for different stimuli: **(a, b)** sinusoidal gratings, **(c)** a plaid stimulus, and **(d)** a natural image. In all cases, the Fano factor decreases with increasing stimulus contrast and is further reduced by attention.

in variability is a ubiquitous phenomenon in the cortex [194].

Furthermore, the model captures the detailed dependence of the Fano factor on stimulus contrast and attention (Fig. 7.6). As predicted by our analytical result in Eq. (7.11), the Fano factor decreases with increasing stimulus contrast ($\propto z_j$) for the grating stimulus, consistent with experimental findings [195]. We also make predictions about the contrast dependence of the Fano factors for different stimuli (plaids and natural images) and the noise quenching effect of attention.

7.5 Discussion

In this chapter, we have demonstrated that a large-scale V1 model built on the ORGaNICs framework can account for a wide range of complex neurophysiological phenomena, from emergent gamma oscillations and stimulus-dependent coherence to the statistics of spiking variability. The Gaussian-Rectification model provided a powerful analytical tool for linking membrane potential dynamics to spiking statistics, yielding accurate predictions for the Fano factor. However, it remains a phenomenological, rather than a fully mechanistic, model of spike generation. A promising avenue for future work is to replace the GR model with a spiking mechanism based on the theory of level upcrossings for stochastic processes, as developed in Chapter 6. This would provide a more principled, first-principles account of how spike trains are generated from continuous, correlated membrane potential fluctuations, and how their statistics are shaped by the underlying normalization dynamics. For analytical tractability, we assumed identity recurrent connections ($\mathbf{W}_r = \mathbf{I}$) among principal cells. While this simplification allowed us to derive closed-form expressions, real cortical circuits possess structured lateral connections. Future iterations of the model should incorporate learned, non-trivial recurrent weights to study the interplay between structured recurrence and dynamic normalization.

A complete model of V1 must account for feedback from higher cortical areas. The current model is purely feedforward. A natural and exciting extension would be to build a hierarchical system with ORGaNICs for deeper cortical areas that receive input from the V1 but also project back, modulating V1 activity. This would allow for the investigation of how feedback signals, potentially carrying attentional or predictive information, interact with the normalization circuitry to shape sensory processing. While our analytical approach to computing coherence and other spectral properties is far more efficient than brute-force simulation, the inversion of very large matrices at each frequency point remains computationally intensive. Scaling up to even larger, multi-area models will necessitate the development of more efficient computational techniques.

8 Discussion

In conclusion, this thesis has extensively analyzed Oscillatory Recurrent Gated Neural Integrator Circuits (ORGaNICs), a class of neurodynamical models that implement divisive normalization (DN), a canonical neural computation. The overarching goal was to develop and understand this framework that is both biologically plausible and computationally powerful, offering insights into brain function and providing a robust neuroscience-inspired machine learning (ML) architecture. We have also developed novel analytical tools for characterizing stochastic dynamical systems, which are broadly applicable but particularly relevant to understanding neural processes.

8.1 Key Contributions and Implications

8.1.1 Normalization Stabilizing Recurrent Neural Networks

A central pillar of this work has been the rigorous examination of ORGaNICs' stability. In Chapter 2, we established the *unconditional* local asymptotic stability of ORGaNICs when the recurrent weight matrix, $\mathbf{W}_r$, is the identity matrix. In the proof of stability, we established a direct connection between ORGaNICs and systems of coupled damped harmonic oscillators, which have long been studied in mechanics and control theory. This analogy enabled us to derive an interpretable energy function for ORGaNICs (Eq. (2.11)), providing a normative principle of what the circuit aims to accomplish: it seeks to maintain a balance between accurate input representation and efficient, normalized coding. This intrinsic stability, stemming from the

dynamic implementation of divisive normalization, sets ORGaNICs apart from many traditional recurrent neural models that often require careful parameter tuning or ad-hoc mechanisms to avoid instabilities.

The extension to generic recurrent weight matrices (Chapter 3) revealed an even more remarkable property: ORGaNICs can remain stable even when the spectral radius of the recurrent matrix exceeds unity, a condition that would lead to instability in linear systems. This enhanced stability is directly attributable to the divisive normalization mechanism. Crucially, we demonstrated that the transition to instability is not abrupt but is preceded by *critical slowing down* in the neural dynamics. Remarkably, the onset of this critical slowing down was found to coincide with the *breakdown of divisive normalization.* This tight coupling suggests that the loss of normalization could serve as an observable early warning signal for impending neurodynamical instability. The implications of this are profound, potentially offering a way to monitor and predict transitions in brain states or the health of neural circuits. Furthermore, our model demonstrated the emergence of multiple long timescales without the need for fine-tuning of parameters, suggesting that normalization could be a fundamental mechanism for generating the rich temporal dynamics observed in the brain. We also explored how E-I imbalance affects stability and oscillatory patterns, finding that increased excitation can promote higher-frequency oscillations and shift the onset of critical slowing down, while increased inhibition tends to stabilize the circuit further, all while the loss of normalization remains a reliable predictor of the onset critical slowing down.

8.1.2 ORGaNICs as a Machine Learning Architecture

Normalization techniques, such as batch and layer normalization, are fundamental in modern ML architectures, significantly enhancing the training and performance of Convolutional Neural Networks (CNNs). However, a principled approach to incorporating normalization directly into the dynamics of Recurrent Neural Networks (RNNs) has remained less explored. While layer normalization is commonly applied to RNNs to stabilize training, it typically acts on the

output activations post-hoc and does not inherently alter the underlying circuit's dynamical stability properties in the same way as a dynamic, intrinsic mechanism. ORGaNICs, unlike RNNs with conventional layer normalization, implement DN dynamically within the recurrent circuit. Building upon the findings of ORGaNICs' stability established in Chapters 2 and 3, we proposed and validated ORGaNICs as an inherently stable and readily trainable ML architecture in Chapter 4. This stability, a direct consequence of dynamic DN, endows ORGaNICs with both output normalization and model robustness. As a result, ORGaNICs can be effectively trained using Backpropagation Through Time (BPTT), achieving performance comparable to LSTMs on RNN benchmarks, without requiring any specialized training techniques like gradient clipping/scaling. The key insight is that the application of DN intrinsically not only enhances training efficiency but also contributes to the overall robustness and stability of the model.

For a relevant ML task, having an analytical expression for an energy function, such as that derived for ORGaNICs (Eq. (2.11)), allows for a degree of interpretability not commonly found in other RNN architectures. It helps quantify the relative contributions of individual neurons to the dynamics in the trained model. For instance, Eq. (2.11) suggests that the ratio of time constants (τ_y/τ_a) for excitatory-inhibitory neuron pairs can determine the weight a neuron assigns to divisive normalization relative to aligning its responses with the input drive $\mathbf{z}$. This insight provides a clearer functional role for different components within the trained model. Moreover, since ORGaNICs are biologically plausible, we can understand how the various components of the dynamical system might be computed within a neural circuit [16], bridging the gap between theoretical models and biological implementation, and offering a means to generate and test hypotheses about neural computation in real biological systems. Therefore, ORGaNICs is a promising, biologically-inspired alternative for building robust, efficient, and more interpretable learning systems.

8.1.3 Analytical Tools for Stochastic Processes

Complementing our primary focus on ORGaNICs, this thesis also contributed to the broader field of computational neuroscience and dynamical systems theory through the development of novel analytical tools. In Chapter 5, we derived element-wise and recursive solutions for computing the power spectral densities (PSDs) of stochastic dynamical systems linearized around stable fixed points. These methods offer computational advantages and can provide deeper insights into how system parameters shape spectral features. Furthermore, in Chapter 6, we addressed a long-standing problem in the study of stochastic processes by deriving exact analytical expressions for the variance and Fano factor of arbitrary level crossings in smooth, stationary Gaussian processes. These results extend the classical Kac-Rice formula for the first moment, providing a more complete statistical description of thresholding phenomena. These solutions have the potential to significantly aid in parameter estimation and model validation across numerous scientific domains where threshold-crossing events are critical.

8.1.4 Broader Implications for Neuroscience

The findings presented in this thesis have several important implications for our understanding of neural computation and brain function. The ubiquity of divisive normalization across diverse neural systems, from sensory pathways to cognitive areas, has long been recognized. Our demonstration of its potent stabilizing effects on recurrent circuit dynamics suggests that normalization may have evolved not only for its known computational benefits (e.g., gain control, redundancy reduction, efficient coding) but also as a fundamental mechanism for ensuring dynamical stability and robustness in the face of strong recurrent interactions. This proposed dual role offers a more comprehensive perspective on why normalization is such a pervasive feature of neural architecture.

ORGaNICs offer a compelling framework for understanding how canonical neural computa-

tions, specifically divisive normalization, contribute to the brain's functional stability and rich dynamics. The model's ability to maintain stability despite strong recurrence, its inherent tendency to produce oscillations under certain conditions, and the observed link between the breakdown of normalization and the onset of critical slowing down provide a suite of testable hypotheses regarding neural circuit function and potential dysfunction. Specifically, the concept of loss of normalization as an early warning signal for dynamical instability could be particularly relevant for investigating neurological or psychiatric disorders characterized by altered neural dynamics, disrupted sensory processing, or transitions between brain states (e.g., seizure initiation).

8.1.5 Methodological Advances

The mathematical techniques developed and employed throughout this thesis also represent methodological contributions to applied mathematics and computational neuroscience. The extension of the Leverrier-Faddeev algorithm (Chapter 5) for computing spectral properties of complex systems provides a valuable and efficient tool for analyzing the spectral properties of high-dimensional linear stochastic dynamical systems and point processes. The approach to solving specific classes of asymmetric Gaussian integrals encountered in the level-crossing problem (Chapter 6), yielding expressions in terms of known special functions like Owen's T function and the error function, advances the mathematical toolkit available for analyzing threshold-crossing phenomena in continuous stochastic processes. Moreover, the systematic approach to stability analysis of ORGaNICs using Lyapunov theory, particularly the connection to the properties of M-matrices when analyzing the quadratic eigenvalue problem (Chapter 2), provides a structured template that could be adapted for analyzing the stability of other classes of nonlinear dynamical systems encountered in biology and engineering.

8.2 Future Work

The research presented in this thesis opens up several promising avenues for future investigation, spanning theoretical extensions, experimental validation, and broader applications.

8.2.1 Experimental Validation

The theoretical predictions made in this thesis, particularly those regarding the relationship between divisive normalization, critical slowing down, and dynamical stability, are ripe for experimental testing in biological neural circuits.

- Measuring the onset of critical slowing down (e.g., by analyzing autocorrelation times or recovery rates from perturbations in neural activity) in neural populations where normalization is known to operate and can be manipulated would provide direct validation of our theoretical framework.

- Developing experimental protocols to modulate normalization strength in vivo, combined with simultaneous multi-electrode recordings to measure neural variability and response timing, could directly test the predicted relationships between normalization efficacy and stability.

- The predicted oscillatory regimes in ORGaNICs, and how they depend on E-I balance and input drive (Chapter 3), could be compared with experimentally observed oscillations (e.g., gamma rhythms) in cortical areas.

8.2.2 Expanding Machine Learning Applications

While Chapter 4 demonstrated the promise of ORGaNICs as an ML architecture, there is considerable scope for further development and application.

- We have primarily explored single-layer ORGaNICs for sequential tasks. Future work should investigate the capabilities of stacked or multi-layer ORGaNICs architectures, potentially with feedback connections inspired by cortical hierarchies [196]. Such architectures could be benchmarked on more complex sequential modeling tasks and cognitive tasks exhibiting long-term dependencies.

- ORGaNICs offer an intrinsic mechanism for modulating effective time constants through the activity of the **a** (inhibitory/normalizing) and **b** (input gain) populations, as suggested by Heeger [15]. Future investigations could focus on training ORGaNICs to explicitly learn to control these modulatory neurons to implement working memory circuits capable of adaptively maintaining and manipulating information across various timescales.

- Benchmarking ORGaNICs on a wider variety of ML tasks is crucial. This includes applications in natural language processing (NLP), robust time-series forecasting in domains such as finance or climate science, and control problems in robotics where continuous-time dynamics and stability are desirable.

- Further exploration of the interpretability of trained ORGaNICs models, leveraging their connection to the energy function and the functional roles of their components, could provide valuable insights into the learned solutions.

8.2.3 From Phenomenological to Mechanistic Models of Neural Activity

A primary motivation for developing the analytical theory of level upcrossings (Chapter 6), was to lay the groundwork for more mechanistic models of neuronal spiking statistics. As demonstrated in the large-scale model of V1 (Chapter 7), phenomenological models like the Gaussian-Rectification (GR) model can be highly effective for analytically capturing spiking variability. However, a central goal for future research is to move beyond such descriptions toward a first-principles account of spike generation.

- A direct next step is to replace the GR model in the V1 circuit with a spiking mechanism based on the level-upcrossing theory. This would allow for the generation of spike trains whose statistics are directly shaped by the underlying normalized dynamics.

- Such a hybrid model could be used to investigate whether ORGaNICs, coupled with threshold upcrossings, can provide a mechanistic explanation for the rich, stimulus-dependent, and super-Poissonian spiking statistics observed across various brain areas. This contrasts with many current models that offer a statistical description (e.g., [197]) without fully elucidating the underlying circuit dynamics generating such statistics.

- Extending the framework to encompass multiple cortical areas (e.g., a V1-V2 circuit) is a crucial next step. Modeling the feedforward and feedback interactions between hierarchically organized ORGaNICs circuits would provide a powerful platform for studying how attentional modulation and predictive signals are integrated within sensory pathways. Initial work toward this goal has been presented in [196].

- The analytical tools for PSD and level-crossing variance could be used to fit these comprehensive models to experimental data, constraining parameters and testing hypotheses about how normalization shapes the neural activity.

8.3 Concluding Remarks

In summary, this thesis has provided a comprehensive analysis of ORGaNICs, highlighting their robust stability conferred by dynamic divisive normalization, their potential as a novel machine learning architecture, and their utility in modeling neural dynamics. The theoretical insights into the interplay between normalization, stability, and critical phenomena, coupled with practical demonstrations in machine learning and the development of new analytical methods for stochastic processes applicable well beyond ORGaNICs, open up numerous avenues for future

research. We hope that the work presented here will stimulate further investigation into the rich interplay between neural dynamics, canonical computations, and learning, ultimately contributing to more powerful and robust models of both biological and artificial intelligence.

A | ORGaNICs with Identity Recurrence

A.1 Derivation of ORGaNICs

Here, we derive a generalized 2-neuron types (excitatory and inhibitory) ORGaNICs model for a high-dimensional input. The system presented in Eq. (1.9) is a special case of this generalized model where $p = 2$ and $\mathbf{a}^+ = \sqrt{\lfloor \mathbf{a} \rfloor}$. Assuming $\mathbf{W}$ is the normalization weight matrix, and $\mathbf{z}$ is the input drive, we can write the normalization equations for principal neurons with complementary receptive fields as,

$$\mathbf{y}_s^+ = \frac{\lfloor \mathbf{z} \rfloor^p}{\boldsymbol{\sigma}^p + \mathbf{W}\left(\lfloor \mathbf{z} \rfloor^p + \lfloor -\mathbf{z} \rfloor^p\right)}; \quad \mathbf{y}_s^- = \frac{\lfloor -\mathbf{z} \rfloor^p}{\boldsymbol{\sigma}^p + \mathbf{W}\left(\lfloor \mathbf{z} \rfloor^p + \lfloor -\mathbf{z} \rfloor^p\right)} \tag{A.1}$$

Note that typically the exponent of the input $p \sim 2$ for cortical neurons. $\lfloor \mathbf{z} \rfloor^p$ and $\lfloor -\mathbf{z} \rfloor^p$ represent the contribution of neurons with complementary receptive fields to the normalization pool. Mathematically, we have, $\lfloor \mathbf{z} \rfloor^p + \lfloor -\mathbf{z} \rfloor^p = |\mathbf{z}|^p$.

Here, we derive, for a general p, the dynamical equations that have the fixed point defined by the normalization equation above. First, it is important to distinguish between the membrane potentials and the firing rates of neurons. The coarse (low-pass filtered) membrane potential of a given type of neuron is denoted by the vector, $\mathbf{y}, \mathbf{a}$, with the corresponding firing rates of $\mathbf{y}^+(\mathbf{y}^-), \mathbf{a}^+$. The instantaneous firing rates of the neurons are obtained from the corresponding coarse membrane potentials by applying rectification, denoted by $\lfloor . \rfloor$, and a power law (sub/supra-

linear) activation for different types of neurons [53–55]. Therefore, for a set of membrane potentials $\mathbf{x}$ the instantaneous firing rates are $\mathbf{x}^+ = \lfloor \mathbf{x} \rfloor^\alpha$. Specifically for principal neurons, we have, $\mathbf{y}^+ = \lfloor \mathbf{y} \rfloor^p$ and $\mathbf{y}^- = \lfloor -\mathbf{y} \rfloor^p$. Combining the firing of principal neurons with the complementary receptive fields, $\mathbf{y}^+$ and $\mathbf{y}^-$, Eq. (A.1) can be alternatively written as,

$$|\mathbf{y}_s|^p = \mathbf{y}_s^+ + \mathbf{y}_s^- = \frac{|\mathbf{z}|^p}{\boldsymbol{\sigma}^p + \mathbf{W}\,|\mathbf{z}|^p} \tag{A.2}$$

Now for the principal neuron y_j receiving an input drive z_j, we can rewrite the normalization equation for each neuron as,

$$|y_j^s|^p = \frac{|z_j|^p}{\sigma_j^p + \sum_k W_{jk}|z_k|^p} \tag{A.3}$$

In the ORGaNICs paradigm [15], the steady-state activity of the principal neurons (single equation for complementary receptive fields) is a weighted sum of input drive and recurrent drive,

$$\tau_{y_j}\frac{\mathrm{d}y_j}{\mathrm{d}t} = -y_j + \underbrace{b_j z_j}_{\text{Weighted input drive}} + \underbrace{\left(1 - a_j^+\right)\sum_k w_{rjk}\left((y_k^+)^{1/p} - (y_k^-)^{1/p}\right)}_{\text{Weighted recurrent drive}} \tag{A.4}$$

Here w_r are the weights of the recurrent weight matrix $\mathbf{W}_r$ encoding the recurrent/lateral connections between the principal neurons $\mathbf{y}$; y_k^+ is the firing rate of the principal neuron k, given by $y_k^+ = \lfloor y_k \rfloor^p$, and $y_k^- = \lfloor -y_k \rfloor^p$ is the firing rate of the complementary principal neuron k. b_j is the gain to the input drive z_j which simulates attention (realized via gain modulation). $(1 - a_j^+)$ is the gain to the recurrent drive which controls the recurrent amplification.

Now, we find the dynamics of the inhibitory neurons a_j with firing rates a_j^+, that yield stable dynamics with the fixed point given by Eq. (A.1). First, we assume that the recurrent weight matrix $\mathbf{W}_r = \mathbf{I}$. Also, note that the following identity holds: $(y_k^+)^{1/p} - (y_k^-)^{1/p} = \lfloor y_k \rfloor - \lfloor -y_k \rfloor = y_k$.

Therefore, Eq. (A.4) can be simplified to,

$$\tau_{y_j} \frac{\mathrm{d}y_j}{\mathrm{d}t} = -y_j + b_j z_j + \left(1 - a_j^+\right) y_j \tag{A.5}$$

At steady-state, the fixed-points (y_j^s, a_j^s), satisfy the following relationship,

$$a_j^{s+} y_j^s = b_j z_j \tag{A.6}$$

Taking modulus and raising both sides to the power p, we get,

$$\left|a_j^{s+} y_j^s\right|^p = \left|b_j z_j\right|^p \tag{A.7}$$

or in vector form,

$$\begin{aligned} \left|\mathbf{a}_s^+ \odot \mathbf{y}_s\right|^p &= |\mathbf{b} \odot \mathbf{z}|^p \\ \left(\mathbf{a}_s^+\right)^p \odot |\mathbf{y}_s|^p &= \mathbf{b}^p \odot |\mathbf{z}|^p \end{aligned} \tag{A.8}$$

From Eq. (A.2), we know that

$$|\mathbf{z}|^p = \boldsymbol{\sigma}^p \odot |\mathbf{y}_s|^p + |\mathbf{y}_s|^p \odot \left(\mathbf{W} |\mathbf{z}|^p\right) \tag{A.9}$$

Since we can write the element-wise product between two vectors $\mathbf{x}_1$ and $\mathbf{x}_2$, $\mathbf{x}_1 \odot \mathbf{x}_2 = \mathbf{x}_2 \odot \mathbf{x}_1 = \mathbf{D}(\mathbf{x}_1)\mathbf{x}_2$. Where $\mathbf{D}(\mathbf{x}_1)$ is a diagonal matrix with elements of the vector $\mathbf{x}_1$ on the diagonal.

Therefore, using this fact, we can rewrite the equation above as,

$$\begin{aligned} |\mathbf{z}|^p &= \boldsymbol{\sigma}^p \odot |\mathbf{y}_s|^p + \mathbf{D}\left(|\mathbf{y}_s|^p\right)\left(\mathbf{W}\,|\mathbf{z}|^p\right) \\ |\mathbf{z}|^p &= \boldsymbol{\sigma}^p \odot |\mathbf{y}_s|^p + \mathbf{D}\left(|\mathbf{y}_s|^p\right)\mathbf{W}\,|\mathbf{z}|^p \\ \left[\mathbf{I} - \mathbf{D}\left(|\mathbf{y}_s|^p\right)\mathbf{W}\right]|\mathbf{z}|^p &= \boldsymbol{\sigma}^p \odot |\mathbf{y}_s|^p \\ |\mathbf{z}|^p &= \left[\mathbf{I} - \mathbf{D}\left(|\mathbf{y}_s|^p\right)\mathbf{W}\right]^{-1}\left(\boldsymbol{\sigma}^p \odot |\mathbf{y}_s|^p\right) \end{aligned} \tag{A.10}$$

Substituting the expression for $|\mathbf{z}|^p$ into Eq. (A.8), we get,

$$\left(\mathbf{a}_s^+\right)^p \odot |\mathbf{y}_s|^p = \mathbf{b}^p \odot \left(\left[\mathbf{I} - \mathbf{D}\left(|\mathbf{y}_s|^p\right)\mathbf{W}\right]^{-1}\left(\boldsymbol{\sigma}^p \odot |\mathbf{y}_s|^p\right)\right) \tag{A.11}$$

We simplify this equation as,

$$\begin{aligned} \left[\mathbf{I} - \mathbf{D}\left(|\mathbf{y}_s|^p\right)\mathbf{W}\right]\left(\frac{\left(\mathbf{a}_s^+\right)^p \odot |\mathbf{y}_s|^p}{\mathbf{b}^p}\right) &= \boldsymbol{\sigma}^p \odot |\mathbf{y}_s|^p \\ \mathbf{D}\left(1/|\mathbf{y}_s|^p\right)\left[\mathbf{I} - \mathbf{D}\left(|\mathbf{y}_s|^p\right)\mathbf{W}\right]\left(\frac{\left(\mathbf{a}_s^+\right)^p \odot |\mathbf{y}_s|^p}{\mathbf{b}^p}\right) &= \mathbf{D}\left(1/|\mathbf{y}_s|^p\right)\left(\boldsymbol{\sigma}^p \odot |\mathbf{y}_s|^p\right) \\ \frac{\left(\mathbf{a}_s^+\right)^p}{\mathbf{b}^p} - \mathbf{W}\left(\frac{\left(\mathbf{a}_s^+\right)^p \odot |\mathbf{y}_s|^p}{\mathbf{b}^p}\right) &= \boldsymbol{\sigma}^p \end{aligned} \tag{A.12}$$

Now we assume that all of the entries of $\mathbf{b}$ are equal to a constant b_0, therefore, we have,

$$\begin{aligned} \left(\mathbf{a}_s^+\right)^p - \mathbf{W}\left(\left(\mathbf{a}_s^+\right)^p \odot |\mathbf{y}_s|^p\right) &= b_0^p \boldsymbol{\sigma}^p \\ \left(\mathbf{a}_s^+\right)^p &= b_0^p \boldsymbol{\sigma}^p + \mathbf{W}\left(\left(\mathbf{a}_s^+\right)^p \odot |\mathbf{y}_s|^p\right) \end{aligned} \tag{A.13}$$

Element-wise multiplying both sides by $\mathbf{a}_s/\left(\mathbf{a}_s^+\right)^p$ on the left, we get,

$$\mathbf{0} = -\mathbf{a}_s + \frac{\mathbf{a}_s}{\left(\mathbf{a}_s^+\right)^p} \odot \left[b_0^p \boldsymbol{\sigma}^p + \mathbf{W}\left(\left(\mathbf{a}_s^+\right)^p \odot |\mathbf{y}_s|^p\right)\right] \tag{A.14}$$

This equation is true at the steady-state, but it is also in a form similar to that of $\mathbf{y}$, such that we have a weighted input drive and a weighted recurrent drive, therefore, we propose the following dynamical equation for $\mathbf{a}$,

$$\boldsymbol{\tau}_a \odot \dot{\mathbf{a}} = -\mathbf{a} + \frac{\mathbf{a}}{(\mathbf{a}^+)^p} \odot \left[b_0^p \boldsymbol{\sigma}^p + \mathbf{W} \left((\mathbf{a}^+)^p \odot |\mathbf{y}|^p \right) \right] \tag{A.15}$$

This equation naturally follows Eq. (A.14) at steady-state and thus also follows the normalization equation Eq. (A.2). Note that the equation above is true for any choice of $\mathbf{a}^+$, but cortical neurons have been experimentally observed to have an exponent close to $p = 2$, i.e., $\mathbf{y}^+ = \lfloor \mathbf{y} \rfloor^2$ and $\mathbf{y}^- = \lfloor -\mathbf{y} \rfloor^2$. Therefore, we get a particularly simple form of the equations when $p = 2$ and $\mathbf{a}^+ = \sqrt{\lfloor \mathbf{a} \rfloor}$. In this case, the equation for $\mathbf{a}$ is given by,

$$\boldsymbol{\tau}_a \odot \dot{\mathbf{a}} = -\mathbf{a} + \left[b_0^2 \boldsymbol{\sigma}^2 + \mathbf{W} \left((\mathbf{a}^+)^2 \odot \mathbf{y}^2 \right) \right] \tag{A.16}$$

We reintroduce the recurrent weight matrix $\mathbf{W}_r$ and to simulate the effect of attention by gain modulation, we define different gains for $\mathbf{y}$ and $\mathbf{a}$ neurons. Additionally, replacing $\mathbf{y}^2 \rightarrow \mathbf{y}^+ + \mathbf{y}^-$ and $\mathbf{y} \rightarrow \sqrt{\mathbf{y}^+} - \sqrt{\mathbf{y}^-}$ yields the dynamical system that we analyze,

$$\begin{aligned} \boldsymbol{\tau}_y \odot \dot{\mathbf{y}} &= -\mathbf{y} + \mathbf{b} \odot \mathbf{z} + (\mathbf{1} - \mathbf{a}^+) \odot \left(\mathbf{W}_r \left(\sqrt{\mathbf{y}^+} - \sqrt{\mathbf{y}^-} \right) \right) \\ \boldsymbol{\tau}_a \odot \dot{\mathbf{a}} &= -\mathbf{a} + \mathbf{b}_0^2 \odot \boldsymbol{\sigma}^2 + \mathbf{W} \left((\mathbf{y}^+ + \mathbf{y}^-) \odot \mathbf{a}^{+2} \right) \end{aligned} \tag{A.17}$$

Finally, in the most general form, i.e., any choice of p and nonlinearity for $\mathbf{a}^+$, the dynamical system of ORGaNICs is given by,

$$\begin{aligned} \boldsymbol{\tau}_y \odot \dot{\mathbf{y}} &= -\mathbf{y} + \mathbf{b} \odot \mathbf{z} + (\mathbf{1} - \mathbf{a}^+) \odot \left(\mathbf{W}_r \left((\mathbf{y}^+)^{1/p} - (\mathbf{y}^-)^{1/p} \right) \right) \\ \boldsymbol{\tau}_a \odot \dot{\mathbf{a}} &= -\mathbf{a} + \frac{\mathbf{a}}{(\mathbf{a}^+)^p} \odot \left[\mathbf{b}_0^p \odot \boldsymbol{\sigma}^p + \mathbf{W} \left((\mathbf{y}^+ + \mathbf{y}^-) \odot (\mathbf{a}^+)^p \right) \right] \end{aligned} \tag{A.18}$$

A.2 Proof of the Stability Theorem

Theorem A.1. *For a system of linear differential equations with constant coefficients of the form,*

$$\mathbf{I}\ddot{\mathbf{x}} + \mathbf{B}\dot{\mathbf{x}} + \mathbf{K}\mathbf{x} = \mathbf{0} \tag{A.19}$$

where $\mathbf{B} \in \mathbb{R}^{n\times n}$ *and* $\mathbf{K} \in \mathbb{R}^{n\times n}$ *is a positive diagonal matrix (hence* $\mathbf{K} \succ 0$*), the dynamical system is globally asymptotically stable if* $\mathbf{B}$ *is Lyapunov diagonally stable.*

Proof. The stability of the system is defined by solving the following associated quadratic eigenvalue problem,

$$\mathbb{L}(\lambda) = \det(\lambda^2\mathbf{I} + \mathbf{B}\lambda + \mathbf{K}) \tag{A.20}$$

The spectrum of $\mathbb{L}(\lambda)$, i.e., $\{\lambda \in \mathbb{C} : \det(\mathbb{L}(\lambda)) = 0\}$ are also known as the eigenvalues of the system. The system defined by Eq. (A.19) is globally asymptotically stable if all of the eigenvalues have negative real parts. We take the direct Lyapunov approach to prove the stability of the linear system. We write Eq. (A.19) in the matrix form as $\dot{\mathbf{z}} = \mathbf{J}\mathbf{z}$, where,

$$\mathbf{z} = \begin{bmatrix} \mathbf{x} \\ \dot{\mathbf{x}} \end{bmatrix} \quad \text{and} \quad \mathbf{J} = \begin{bmatrix} \mathbf{0} & \mathbf{I} \\ -\mathbf{K} & -\mathbf{B} \end{bmatrix} \tag{A.21}$$

We will first prove the Lyapunov stability ($\mathrm{Re}(\lambda_{\mathbf{J}}) \leq 0$) of this system to find the appropriate block diagonal matrices and then we will prove global asymptotic stability ($\mathrm{Re}(\lambda_{\mathbf{J}}) < 0$). To prove Lyapunov stability (Section A.2.2), we propose a Lyapunov function $V(\mathbf{z}) = \mathbf{z}^\top\mathbf{P}\mathbf{z}$, where $\mathbf{P}$ is a block positive definite matrix defined as follows,

$$\mathbf{P} = \begin{bmatrix} \mathbf{A} & \mathbf{0} \\ \mathbf{0} & \mathbf{T} \end{bmatrix} \tag{A.22}$$

where $\mathbf{T} \in \mathbb{R}^{n \times n}$ is a positive diagonal matrix such that $\mathbf{TB} + \mathbf{B}^\top \mathbf{T} \succ 0$ (notation for positive definite matrix) and $\mathbf{A} \in \mathbb{R}^{n \times n}$ a flexible symmetric positive definite matrix that we will find using the second Lyapunov criteria. Note that such a matrix $\mathbf{T}$ exists since $\mathbf{B}$ is defined to be Lyapunov diagonally stable. It can be easily seen that $\mathbf{P} \succ 0$ using the first criteria in Section A.2.1 since $\mathbf{A} \succ 0$ and $\mathbf{T} \succ 0$. Additionally, since $\mathbf{T} \succ 0$, it is invertible.

Now, for Lyapunov stability, we need $\dot{V}(\mathbf{z}) = \mathbf{z}^\top \left(\mathbf{PJ} + \mathbf{J}^\top \mathbf{P}\right) \mathbf{z} \leq 0$. Therefore, we find $\mathbf{A}$ such that $\mathbf{Q} = -\left(\mathbf{PJ} + \mathbf{J}^\top \mathbf{P}\right)$ is positive semi-definite.

$$
\begin{aligned}
\mathbf{Q} &= -\left(\mathbf{PJ} + \mathbf{J}^\top \mathbf{P}\right) \\
&= -\begin{bmatrix} \mathbf{A} & \mathbf{0} \\ \mathbf{0} & \mathbf{T} \end{bmatrix} \begin{bmatrix} \mathbf{0} & \mathbf{I} \\ -\mathbf{K} & -\mathbf{B} \end{bmatrix} - \begin{bmatrix} \mathbf{0} & -\mathbf{K} \\ \mathbf{I} & -\mathbf{B}^\top \end{bmatrix} \begin{bmatrix} \mathbf{A} & \mathbf{0} \\ \mathbf{0} & \mathbf{T} \end{bmatrix} \\
&= \begin{bmatrix} \mathbf{0} & \mathbf{KT} - \mathbf{A} \\ \mathbf{TK} - \mathbf{A} & \mathbf{TB} + \mathbf{B}^\top \mathbf{T} \end{bmatrix}
\end{aligned}
\tag{A.23}
$$

We want to define $\mathbf{A} \succ 0$, such that $\mathbf{Q} \succeq 0$. Using the second criteria from Section A.2.1, we need $\mathbf{TB} + \mathbf{B}^\top \mathbf{T} \succ 0$ and $-(\mathbf{KT} - \mathbf{A})(\mathbf{TB} + \mathbf{B}^\top \mathbf{T})^{-1}(\mathbf{TK} - \mathbf{A}) \succeq 0$. The first condition is satisfied by the definition of $\mathbf{T}$. For the second condition to be satisfied, an obvious candidate for $\mathbf{A}$ is $\mathbf{TK}$. Note that both $\mathbf{T}$ and $\mathbf{K}$ are positive definite and diagonal, therefore, they commute ($\mathbf{KT} = \mathbf{TK}$) and $\mathbf{A}$ is symmetric and positive definite. When $\mathbf{A} = \mathbf{TK}$, the LHS of the second condition becomes $\mathbf{0} \succeq 0$. Therefore, the system is Lyapunov stable.

Now, we prove the global asymptotic stability of the system by again using the direct Lyapunov approach. We propose the Lyapunov function of the same form as before, i.e., $V(\mathbf{z}) = \mathbf{z}^\top \mathbf{P} \mathbf{z}$, where $\mathbf{P}$ is a positive definite matrix. But for global asymptotic stability, we need a more stringent condition on the Lyapunov function, $\dot{V}(\mathbf{z}) = \mathbf{z}^\top \left(\mathbf{PJ} + \mathbf{J}^\top \mathbf{P}\right) \mathbf{z} < 0$. Drawing inspiration from the

previous exercise, we consider the following form of the matrix $\mathbf{P}$,

$$\mathbf{P} = \begin{bmatrix} \mathbf{TK} & \epsilon\mathbf{I} \\ \epsilon\mathbf{I} & \mathbf{T} \end{bmatrix} \tag{A.24}$$

Here, $\epsilon > 0$ is a scalar whose magnitude is to be determined based on the Lyapunov criteria for asymptotic stability. First, we need $\mathbf{P} \succ 0$. Applying the first criteria from Section A.2.1, we want ϵ to satisfy, $\mathbf{TK} - \epsilon^2\mathbf{T}^{-1} \succ 0$. Second, for $\dot{V}(\mathbf{z}) < 0$, we want $\mathbf{Q} = -(\mathbf{PJ} + \mathbf{J}^\top\mathbf{P})$ to be positive definite. $\mathbf{Q}$ is given by,

$$\begin{aligned} \mathbf{Q} &= -\begin{bmatrix} \mathbf{TK} & \epsilon\mathbf{I} \\ \epsilon\mathbf{I} & \mathbf{T} \end{bmatrix}\begin{bmatrix} \mathbf{0} & \mathbf{I} \\ -\mathbf{K} & -\mathbf{B} \end{bmatrix} - \begin{bmatrix} \mathbf{0} & -\mathbf{K} \\ \mathbf{I} & -\mathbf{B}^\top \end{bmatrix}\begin{bmatrix} \mathbf{TK} & \epsilon\mathbf{I} \\ \epsilon\mathbf{I} & \mathbf{T} \end{bmatrix} \\ &= \begin{bmatrix} 2\epsilon\mathbf{K} & \epsilon\mathbf{B} \\ \epsilon\mathbf{B}^\top & \mathbf{TB} + \mathbf{B}^\top\mathbf{T} - 2\epsilon\mathbf{I} \end{bmatrix} \end{aligned} \tag{A.25}$$

Again, we apply the first criterion from Section A.2.1. $\mathbf{Q} \succ 0$ if and only if $\mathbf{TB} + \mathbf{B}^\top\mathbf{T} - 2\epsilon\mathbf{I} \succ 0$ and $2\epsilon\mathbf{K} - \epsilon^2\mathbf{B}\left(\mathbf{TB} + \mathbf{B}^\top\mathbf{T} - 2\epsilon\mathbf{I}\right)^{-1}\mathbf{B}^\top \succ 0$. To simplify notation, we replace $\mathbf{TB} + \mathbf{B}^\top\mathbf{T}$ with a positive definite matrix $\mathbf{M}$. Therefore, we have to prove that there exists an $\epsilon > 0$ which satisfies the following conditions,

- $\mathbf{TK} - \epsilon^2\mathbf{T}^{-1} \succ 0$
- $\mathbf{M} - 2\epsilon\mathbf{I} \succ 0$
- $2\mathbf{K} - \epsilon\mathbf{B}\left(\mathbf{M} - 2\epsilon\mathbf{I}\right)^{-1}\mathbf{B}^\top \succ 0$

Assuming t_i and k_i to be the diagonal values of the positive diagonal matrices $\mathbf{T}$ and $\mathbf{K}$, we get the following two conditions, $\epsilon < \min\left(t_i\sqrt{k_i}\right)$ and $\epsilon < \alpha/2$, where α is the smallest eigenvalue of $\mathbf{M}$, or $\alpha = \min\left(\lambda_{\mathbf{M}}\right)$.

Now, for the third condition, we will use a number of facts about positive definite matrices which are all listed in [131]. We first consider the following matrix inequality, $\mathbf{M} \succeq \alpha\mathbf{I}$. This notation is equivalent to saying that $\mathbf{M} - \alpha\mathbf{I}$ is positive semi-definite or $\mathbf{M} - \alpha\mathbf{I} \succeq 0$. Therefore, we have,

$$\mathbf{M} - 2\epsilon\mathbf{I} \succeq (\alpha - 2\epsilon)\mathbf{I} \tag{A.26}$$

Assuming ϵ is small enough such that the matrices on LHS and RHS are positive definite, we have,

$$\frac{1}{\alpha - 2\epsilon}\mathbf{I} \succeq (\mathbf{M} - 2\epsilon\mathbf{I})^{-1} \tag{A.27}$$

Since $\mathbf{B}$ is nonsingular, it is full rank, therefore, we have,

$$\frac{1}{\alpha - 2\epsilon}\mathbf{B}\mathbf{B}^\top \succeq \mathbf{B}\left(\mathbf{M} - 2\epsilon\mathbf{I}\right)^{-1}\mathbf{B}^\top \tag{A.28}$$

Multiplying both sides by ϵ, we get,

$$\frac{\epsilon}{\alpha - 2\epsilon}\mathbf{B}\mathbf{B}^\top \succeq \epsilon\mathbf{B}\left(\mathbf{M} - 2\epsilon\mathbf{I}\right)^{-1}\mathbf{B}^\top \tag{A.29}$$

Notice that $\mathbf{B}\mathbf{B}^\top$ is a positive definite matrix. Let β be the maximum eigenvalue of $\mathbf{B}\mathbf{B}^\top$, or $\beta = \max\left(\lambda_{\mathbf{B}\mathbf{B}^\top}\right)$. Therefore, we can add an upper-bound matrix to the inequality as follows,

$$\frac{\epsilon\beta}{\alpha - 2\epsilon}\mathbf{I} \succeq \frac{\epsilon}{\alpha - 2\epsilon}\mathbf{B}\mathbf{B}^\top \succeq \epsilon\mathbf{B}\left(\mathbf{M} - 2\epsilon\mathbf{I}\right)^{-1}\mathbf{B}^\top \tag{A.30}$$

Now, we find ϵ such that,

$$2\mathbf{K} \succ \frac{\epsilon\beta}{\alpha - 2\epsilon}\mathbf{I} \tag{A.31}$$

The range of values for which the above inequality is true is,

$$\epsilon < \min\left(\frac{2k_i\alpha}{\beta + 4k_i}\right) \tag{A.32}$$

If ϵ satisfies the inequality above, we have,

$$2\mathbf{K} \succ \frac{\epsilon\beta}{\alpha - 2\epsilon}\mathbf{I} \succeq \frac{\epsilon}{\alpha - 2\epsilon}\mathbf{B}\mathbf{B}^\top \succeq \epsilon\mathbf{B}\left(\mathbf{M} - 2\epsilon\mathbf{I}\right)^{-1}\mathbf{B}^\top \tag{A.33}$$

Therefore, we have, $2\mathbf{K} \succ \epsilon\mathbf{B}\left(\mathbf{M} - 2\epsilon\mathbf{I}\right)^{-1}\mathbf{B}^\top$ and the third condition required for ϵ is satisfied.

This implies that there exists a range of ϵ, given by,

$$0 < \epsilon < \min\left\{\min\left(t_i\sqrt{k_i}\right),\ \frac{\alpha}{2},\ \min\left(\frac{2k_i\alpha}{\beta + 4k_i}\right)\right\} \tag{A.34}$$

for which

$$\mathbf{P} = \begin{bmatrix} \mathbf{T}\mathbf{K} & \epsilon\mathbf{I} \\ \epsilon\mathbf{I} & \mathbf{T} \end{bmatrix} \tag{A.35}$$

is a valid Lyapunov function for asymptotic stability. Therefore, the dynamical system is globally asymptotically stable.

□

A.2.1 Positive Definite Block Matrices (Schur Complement)

For a symmetric block matrix of the form,

$$\mathbf{P} = \begin{bmatrix} \mathbf{A} & \mathbf{B} \\ \mathbf{B}^\top & \mathbf{C} \end{bmatrix} \tag{A.36}$$

with $\mathbf{A} = \mathbf{A}^\top$ and $\mathbf{C} = \mathbf{C}^\top$. If $\mathbf{C}$ is invertible the following two properties hold, [198],

- $\mathbf{P} \succ 0$ if and only if $\mathbf{C} \succ 0$ and $\mathbf{A} - \mathbf{B}\mathbf{C}^{-1}\mathbf{B}^\top \succ 0$.
- If $\mathbf{C} \succ 0$, then $\mathbf{P} \succeq 0$ if and only if $\mathbf{A} - \mathbf{B}\mathbf{C}^{-1}\mathbf{B}^\top \succeq 0$.

A.2.2 Lyapunov Stability Criteria

Consider a non-linear autonomous dynamical system defined as $\dot{\mathbf{x}} = \mathbf{f}(\mathbf{x})$, with a point of equilibrium at $\mathbf{x} = \mathbf{0}$. Where $\mathbf{x} \in \mathcal{D} \subseteq \mathbb{R}^n$ is the system state vector and $\mathbf{f}(\mathbf{x}) : \mathcal{D} \to \mathbb{R}^n$ is a continuous vector field on $\mathcal{D}$ (contains origin). The dynamical system is called Lyapunov stable if there exists a real scalar function $V(\mathbf{x}) : \mathbb{R}^n \to \mathbb{R}$, also known as the Lyapunov function, such that it satisfies the following conditions,

- $V(\mathbf{x}) = 0$, if and only if $\mathbf{x} = \mathbf{0}$.
- $V(\mathbf{x}) > 0$, if and only if $\mathbf{x} \neq \mathbf{0}$.
- $\dot{V}(\mathbf{x}) \leq 0$, $\forall\, \mathbf{x} \neq \mathbf{0}$. Note that for asymptotic stability, we require the strict inequality $\dot{V}(\mathbf{x}) < 0$.

For a linear dynamical system of the form $\dot{\mathbf{x}} = \mathbf{J}\mathbf{x}$, where $\mathbf{J} \in \mathbb{R}^{n \times n}$, with a point of equilibrium at $\mathbf{x} = \mathbf{0}$. Consider a Lyapunov function $V(\mathbf{x})$ of the form $\mathbf{x}^\top \mathbf{P}\mathbf{x}$, such that $\mathbf{P} \succ 0$. By the definition of a positive definite matrix, it satisfies the first two conditions, namely, $V(\mathbf{x}) = \mathbf{x}^\top \mathbf{P}\mathbf{x} = 0$ when $\mathbf{x} = \mathbf{0}$ and $V(\mathbf{x}) = \mathbf{x}^\top \mathbf{P}\mathbf{x} > 0$ when $x \neq \mathbf{0}$. For the third condition, consider $\dot{V}(\mathbf{x})$,

$$\begin{aligned} \dot{V}(\mathbf{x}) &= \frac{\mathrm{d}}{\mathrm{d}t} V(\mathbf{x}) \\ &= \frac{\mathrm{d}}{\mathrm{d}t} \mathbf{x}^\top \mathbf{P}\mathbf{x} \\ &= \mathbf{x}^\top \mathbf{P}\dot{\mathbf{x}} + \dot{\mathbf{x}}^\top \mathbf{P}\mathbf{x} \\ &= \mathbf{x}^\top \left(\mathbf{P}\mathbf{J} + \mathbf{J}^\top \mathbf{P}\right) \mathbf{x} \end{aligned} \tag{A.37}$$

For stability, We need $\dot{V}(\mathbf{x}) = \mathbf{x}^\top \left(\mathbf{P}\mathbf{J} + \mathbf{J}^\top \mathbf{P}\right) \mathbf{x} \leq 0$. This is satisfied when the matrix $\mathbf{P}\mathbf{J} + \mathbf{J}^\top \mathbf{P} \preceq 0$.

In summary, a linear dynamical system $\dot{\mathbf{x}} = \mathbf{J}\mathbf{x}$ is Lyapunov stable if there exists a positive definite matrix $\mathbf{P}$, such that $\mathbf{P}\mathbf{J} + \mathbf{J}^\top\mathbf{P}$ is negative semi-definite.

A.3 Convergent Theorem

Theorem A.2. *A matrix* $\mathbf{A}$ *of the form,*

$$\mathbf{A} = \mathbf{D}(\mathbf{t})\,\mathbf{W}\,\mathbf{D}\left(\frac{\mathbf{u}}{\mathbf{v} + \mathbf{W}\mathbf{u}}\right) \tag{A.38}$$

is convergent, i.e., its spectral radius is less than one, if $\mathbf{W} \in \mathbb{R}^{n\times n}$ *and* $\mathbf{t}, \mathbf{u}, \mathbf{v} \in \mathbb{R}^n$ *with the additional constraints* $0 < t_i < 1$, $u_i \geq 0$, $v_i > 0$ *and* $w_{ij} \geq 0$ *for all* i, j.

Proof. Assuming the constraints mentioned in the theorem, we first notice that,

$$\mathbf{W}\,\mathbf{D}\left(\frac{\mathbf{u}}{\mathbf{v} + \mathbf{W}\mathbf{u}}\right) \tag{A.39}$$

is a nonnegative matrix. Further, because $\mathbf{D}(\mathbf{t})$ is a positive diagonal matrix with all entries less than 1, we notice that the following is true element-wise,

$$\mathbf{D}(\mathbf{t})\,\mathbf{W}\,\mathbf{D}\left(\frac{\mathbf{u}}{\mathbf{v} + \mathbf{W}\mathbf{u}}\right) < \mathbf{W}\,\mathbf{D}\left(\frac{\mathbf{u}}{\mathbf{v} + \mathbf{W}\mathbf{u}}\right) \tag{A.40}$$

We denote the spectral radius of $\mathbf{A}$, $\max\{|\lambda| : \lambda = \sigma(\mathbf{A})\}$, by $\rho(\mathbf{A})$, where $\sigma(\mathbf{A})$ is the spectrum of $\mathbf{A}$ and make use of the following inequality for the spectral radius of nonnegative matrices.,

Theorem A.3. *(Theorem 8.1.18 from [199]) Let* $\mathbf{X}$ *and* $\mathbf{Y}$ *be nonnegative matrices with spectral radius* $\rho(\mathbf{X})$ *and* $\rho(\mathbf{Y})$*, respectively. If* $\mathbf{X} \leq \mathbf{Y}$ *(*$x_{ij} \leq y_{ij}, \forall\ i, j$*), then* $\rho(\mathbf{X}) \leq \rho(\mathbf{Y})$.

Therefore, we have,

$$\rho\left(\mathbf{A}\right) \leq \rho\left(\mathbf{W}\,\mathbf{D}\left(\frac{\mathbf{u}}{\mathbf{v} + \mathbf{W}\mathbf{u}}\right)\right) \tag{A.41}$$

Now the elements of the matrix are given by,

$$\mathbf{W}\,\mathbf{D}\left(\frac{\mathbf{u}}{\mathbf{v}+\mathbf{W}\mathbf{u}}\right) = \begin{bmatrix} w_{11} & w_{12} & \dots \\ w_{21} & w_{22} & \dots \\ \vdots & \vdots & \ddots \end{bmatrix} \begin{bmatrix} \frac{u_1}{v_1+\sum_j w_{1j}u_j} & 0 & \dots \\ 0 & \frac{u_2}{v_2+\sum_j w_{2j}u_j} & \dots \\ \vdots & \vdots & \ddots \end{bmatrix} \tag{A.42}$$

Let s_{ij} be the i, j element of this matrix. Upon multiplication of the matrices above, we find that,

$$s_{ij} = \frac{w_{ij}u_j}{v_j + \sum_k w_{jk}u_k} \tag{A.43}$$

Now we use the following theorem that provides an upper bound for the spectral radius based on the entries of the matrix.

Theorem A.4. *(Theorem 8.1.26 from [199]) Let* $\mathbf{S}$ *be a nonnegative matrix. Then for any positive vector* $\mathbf{x} \in \mathbb{R}^n$ *with entries* x_j*, we have,*

$$\rho(\mathbf{S}) \leq \max_{1\leq i\leq n} \frac{1}{x_i} \sum_{j=1}^{n} s_{ij}x_j \tag{A.44}$$

We pick $x_j = v_j + \sum_k w_{jk}u_k$, which is a positive vector, and apply the theorem to the matrix. Substituting s_{ij} and x_j, we get the following bound for the spectral radius,

$$\rho\left(\mathbf{W}\,\mathbf{D}\left(\frac{\mathbf{u}}{\mathbf{v}+\mathbf{W}\mathbf{u}}\right)\right) \leq \max_{1\leq i\leq n} \frac{1}{v_i + \sum_k w_{ik}u_k} \sum_{j=1}^{n} \frac{w_{ij}u_j}{v_j + \sum_k w_{jk}u_k} \left(v_j + \sum_k w_{jk}u_k\right) \tag{A.45}$$

Upon simplification, we get,

$$\rho\left(\mathbf{W}\,\mathbf{D}\left(\frac{\mathbf{u}}{\mathbf{v}+\mathbf{W}\mathbf{u}}\right)\right) \leq \max_{1\leq i\leq n} \frac{\sum_j w_{ij}u_j}{v_i + \sum_k w_{ik}u_k} = \max_{1\leq i\leq n} \frac{\sum_k w_{ik}u_k}{v_i + \sum_k w_{ik}u_k} < 1 \tag{A.46}$$

The inequality is true because, for all i, the denominator is larger than the numerator because of

the extra positive term v_i. Therefore,

$$\rho\left(\mathbf{A}\right) \leq \rho\left(\mathbf{W}\,\mathbf{D}\left(\frac{\mathbf{u}}{\mathbf{v}+\mathbf{W}\mathbf{u}}\right)\right) < 1 \tag{A.47}$$

and $\mathbf{A}$ is a convergent matrix. □

A.4 Analytical Eigenvalue for the Fully Normalized Circuit

Here we show that when all of the normalization weights in the system are equal, to value α, and the various parameters are scalars, i.e., $\boldsymbol{\tau}_y = \tau_y\mathbf{1}$, $\boldsymbol{\tau}_a = \tau_a\mathbf{1}$, $\mathbf{b}_0 = b_0\mathbf{1}$ and $\boldsymbol{\sigma} = \sigma\mathbf{1}$, we can derive a closed-form analytical expression for all of the eigenvalues. Considering these assumptions, we can break the determinant in Eq. (2.6) into a diagonal and non-diagonal part as follows,

$$\det(\mathbf{J}-\lambda\mathbf{I}) = \det\left(\lambda^2\mathbf{I}+\lambda\left[\frac{\mathbf{I}}{\tau_a}+\frac{\mathbf{D}\left(\sqrt{\mathbf{a}_s}\right)}{\tau_y}\right]+\frac{\mathbf{D}\left(\sqrt{\mathbf{a}_s}\right)}{\tau_y\tau_a}-\lambda\frac{\mathbf{W}\mathbf{D}\left(\mathbf{y}_s{}^2\right)}{\tau_a}\right) \tag{A.48}$$

Consider the non-diagonal part of the matrix in the determinant, $(\lambda/\tau_a)\mathbf{W}\mathbf{D}\left(\mathbf{y}_s^2\right)$. Since $\mathbf{W}$ is a matrix with all entries equal to a positive constant, α, it is rank 1. Therefore, it can be written as the following outer product,

$$\mathbf{W} = \alpha\begin{bmatrix}1\\1\\\vdots\\1\end{bmatrix}\begin{bmatrix}1 & 1 & \dots & 1\end{bmatrix} \tag{A.49}$$

Therefore, the non-diagonal part of the matrix can be written as,

$$\frac{\lambda}{\tau_a}\mathbf{W}\,\mathbf{D}\left(\frac{\mathbf{b}^2\odot\mathbf{z}^2}{\sigma^2b_0^2\mathbf{1}+\mathbf{W}\left(\mathbf{b}^2\odot\mathbf{z}^2\right)}\right) = \frac{\lambda\alpha}{\tau_a}\mathbf{u}\mathbf{v}^\top \tag{A.50}$$

where $\mathbf{u} = [1, 1, ..., 1]^\top$ and $\mathbf{v} = \left(\mathbf{b}^2 \odot \mathbf{z}^2\right) / \left(\sigma^2 b_0^2 \mathbf{1} + \mathbf{W}\left(\mathbf{b}^2 \odot \mathbf{z}^2\right)\right)$. We use the matrix determinant lemma which states that,

$$\det(\mathbf{A} - \gamma \mathbf{u}\mathbf{v}^\top) = (1 - \gamma \mathbf{v}^\top \mathbf{A}^{-1}\mathbf{u}) \det(\mathbf{A}) \tag{A.51}$$

The matrix $\mathbf{A}$ is given by,

$$\begin{aligned}
\mathbf{A} &= \lambda^2 \mathbf{I} + \lambda \left[\frac{\mathbf{I}}{\tau_a} + \frac{\mathbf{D}\left(\sqrt{\mathbf{a}_s}\right)}{\tau_y} \right] + \frac{\mathbf{D}\left(\sqrt{\mathbf{a}_s}\right)}{\tau_y \tau_a} \\
&= \lambda^2 \mathbf{I} + \lambda \left[\frac{\mathbf{I}}{\tau_a} + \frac{\mathbf{D}\left(\sqrt{\sigma^2 b_0^2 \mathbf{1} + \mathbf{W}\left(\mathbf{b}^2 \odot \mathbf{z}^2\right)}\right)}{\tau_y} \right] + \frac{\mathbf{D}\left(\sqrt{\sigma^2 b_0^2 \mathbf{1} + \mathbf{W}\left(\mathbf{b}^2 \odot \mathbf{z}^2\right)}\right)}{\tau_y \tau_a} \\
&= \lambda^2 \mathbf{I} + \lambda \left[\frac{\mathbf{I}}{\tau_a} + \frac{\mathbf{D}\left(\sqrt{\sigma^2 b_0^2 \mathbf{1} + \alpha ||\mathbf{b} \odot \mathbf{z}||^2}\right)}{\tau_y} \right] + \frac{\mathbf{D}\left(\sqrt{\sigma^2 b_0^2 \mathbf{1} + \alpha ||\mathbf{b} \odot \mathbf{z}||^2}\right)}{\tau_y \tau_a} \\
&= \left(\lambda^2 + \lambda \left(\frac{1}{\tau_a} + \frac{\sqrt{\sigma^2 b_0^2 + \alpha ||\mathbf{b} \odot \mathbf{z}||^2}}{\tau_y} \right) + \frac{\sqrt{\sigma^2 b_0^2 + \alpha ||\mathbf{b} \odot \mathbf{z}||^2}}{\tau_y \tau_a} \right) \mathbf{I}
\end{aligned} \tag{A.52}$$

Here, $||x||$, represents the Euclidean norm of x. Therefore, $\mathbf{A} = \delta \mathbf{I}$, where δ is a quadratic scalar polynomial in λ. Now using Eq. (A.51), we can write

$$\begin{aligned}
\det(\mathbf{J} - \lambda \mathbf{I}) &= \left(1 - \frac{\lambda \alpha}{\tau_a} \mathbf{v}^\top \left(\frac{1}{\delta} \mathbf{I} \right) \mathbf{u} \right) \delta^n \\
&= \left(\delta - \frac{\lambda}{\tau_a} \frac{\alpha ||\mathbf{b} \odot \mathbf{z}||^2}{\sigma^2 b_0^2 + \alpha ||\mathbf{b} \odot \mathbf{z}||^2} \right) \delta^{n-1}
\end{aligned} \tag{A.53}$$

Solving for the eigenvalues, $\det(\mathbf{J} - \lambda \mathbf{I}) = 0$, we get $2(n-1)$ repeated solutions by equation $\delta^{n-1} = 0$, where each solution is found by solving $\delta = 0$,

$$\lambda^2 + \lambda \left(\frac{1}{\tau_a} + \frac{\sqrt{\sigma^2 b_0^2 + \alpha ||\mathbf{b} \odot \mathbf{z}||^2}}{\tau_y} \right) + \frac{\sqrt{\sigma^2 b_0^2 + \alpha ||\mathbf{b} \odot \mathbf{z}||^2}}{\tau_y \tau_a} = 0 \tag{A.54}$$

This gives us the following strictly negative eigenvalues,

$$\lambda = -\frac{1}{\tau_a} \quad \& \quad \lambda = -\frac{\sqrt{\sigma^2 b_0^2 + \alpha ||\mathbf{b} \odot \mathbf{z}||^2}}{\tau_y} \tag{A.55}$$

The potentially complex eigenvalues are given by solving for zeros of the first part of the factorized determinant,

$$\lambda^2 + \lambda \left(\frac{\sigma^2 b_0^2}{\tau_a (\sigma^2 b_0^2 + \alpha ||\mathbf{b} \odot \mathbf{z}||^2)} + \frac{\sqrt{\sigma^2 b_0^2 + \alpha ||\mathbf{b} \odot \mathbf{z}||^2}}{\tau_y} \right) + \frac{\sqrt{\sigma^2 b_0^2 + \alpha ||\mathbf{b} \odot \mathbf{z}||^2}}{\tau_y \tau_a} = 0 \tag{A.56}$$

The eigenvalues found by solving this equation have negative real parts (as expected) for all choices of parameters since the coefficient of λ and the constant term of the quadratic equation are positive for all choices of parameters and inputs. Therefore, this solution does admit complex roots (thereby oscillations) for certain choices of the parameters that can be found by solving this quadratic equation.

A.5 Energy of ORGaNICs

Here, we find the *energy* (Lyapunov function) that is minimized by the dynamics of the ORGaNICs in the vicinity of the normalization fixed point. We consider the dynamical system with $\mathbf{W}_r = \mathbf{I}$, which is given by Eq. (2.1). Upon linearizing about the fixed point we get the following linear dynamical system,

$$\begin{bmatrix} \dot{\mathbf{y}} \\ \dot{\mathbf{a}} \end{bmatrix} = \begin{bmatrix} -\mathbf{D}\left(\frac{\sqrt{\mathbf{a}_s}}{\tau_y}\right) & -\mathbf{D}\left(\frac{\mathbf{y}_s}{2 \odot \sqrt{\mathbf{a}_s} \odot \tau_y}\right) \\ \mathbf{D}\left(\frac{2}{\tau_a}\right) \mathbf{W}\, \mathbf{D}\left(\mathbf{a}_s \odot \mathbf{y}_s\right) & \mathbf{D}\left(\frac{1}{\tau_a}\right) \left(-\mathbf{I} + \mathbf{W}\, \mathbf{D}\left(\mathbf{y}_s^2\right)\right) \end{bmatrix} \begin{bmatrix} \mathbf{y} - \mathbf{y}_s \\ \mathbf{a} - \mathbf{a}_s \end{bmatrix} \tag{A.57}$$

This system is dynamically equivalent (admits the same eigenvalues) to a system of coupled

harmonic oscillators with the following equations,

$$\ddot{\mathbf{x}} + \left[\mathbf{D}\left(\frac{\mathbf{1}}{\boldsymbol{\tau}_a}\right) + \mathbf{D}\left(\frac{\sqrt{\mathbf{a}_s}}{\boldsymbol{\tau}_y}\right) - \mathbf{D}\left(\frac{\mathbf{1}}{\boldsymbol{\tau}_a}\right)\mathbf{W}\mathbf{D}\left(\mathbf{y}_s^2\right)\right]\dot{\mathbf{x}} + \mathbf{D}\left(\frac{\sqrt{\mathbf{a}_s}}{\boldsymbol{\tau}_y \odot \boldsymbol{\tau}_a}\right)\mathbf{x} = \mathbf{0}. \tag{A.58}$$

We can rewrite the linear system in terms of the position, $\mathbf{x}$, and the velocity, $\mathbf{v}$,

$$\begin{bmatrix}\dot{\mathbf{x}} \\ \dot{\mathbf{v}}\end{bmatrix} = \begin{bmatrix}\mathbf{0} & \mathbf{I} \\ -\mathbf{D}\left(\frac{\sqrt{\mathbf{a}_s}}{\boldsymbol{\tau}_y \odot \boldsymbol{\tau}_a}\right) & -\left[\mathbf{D}\left(\frac{\mathbf{1}}{\boldsymbol{\tau}_a}\right) + \mathbf{D}\left(\frac{\sqrt{\mathbf{a}_s}}{\boldsymbol{\tau}_y}\right) - \mathbf{D}\left(\frac{\mathbf{1}}{\boldsymbol{\tau}_a}\right)\mathbf{W}\mathbf{D}\left(\mathbf{y}_s^2\right)\right]\end{bmatrix}\begin{bmatrix}\mathbf{x} \\ \mathbf{v}\end{bmatrix} \tag{A.59}$$

Since this system is of the form $\mathbf{I}\ddot{\mathbf{x}} + \mathbf{B}\dot{\mathbf{x}} + \mathbf{K}\mathbf{x} = \mathbf{0}$, Eq. (A.19), the *energy* of this dynamical system is given by $V(\mathbf{z}) = \mathbf{z}^\top \mathbf{P}\mathbf{z}$, or,

$$V(\mathbf{x}, \mathbf{v}) = \begin{bmatrix}\mathbf{x}^\top & \mathbf{v}^\top\end{bmatrix}\begin{bmatrix}\mathbf{T}\mathbf{K} & \epsilon\mathbf{I} \\ \epsilon\mathbf{I} & \mathbf{T}\end{bmatrix}\begin{bmatrix}\mathbf{x} \\ \mathbf{v}\end{bmatrix} = \mathbf{x}^\top(\mathbf{T}\mathbf{K})\,\mathbf{x} + \mathbf{v}^\top\mathbf{T}\mathbf{v} + 2\epsilon\,\mathbf{x}^\top\mathbf{v} \tag{A.60}$$

Here, $\mathbf{T}$ is any positive diagonal matrix such that $\mathbf{T}\mathbf{B} + \mathbf{B}^\top\mathbf{T} \succ 0$ and $\mathbf{K}$ is also a positive diagonal matrix given by $\mathbf{D}\left(\sqrt{\mathbf{a}_s}/\left(\boldsymbol{\tau}_y \odot \boldsymbol{\tau}_a\right)\right)$. Now, for a valid Lyapunov function, we can take ϵ to be arbitrarily small, Eq. (A.34). Therefore, the *energy* minimized by the dynamical system is given by $V(\mathbf{x}, \mathbf{v}) = \mathbf{x}^\top(\mathbf{T}\mathbf{K})\,\mathbf{x} + \mathbf{v}^\top\mathbf{T}\mathbf{v}$. This is a high-dimensional version of the energy of a damped harmonic oscillator. For a single oscillator, we have $V(x, v) = t(kx^2 + v^2)$, which is proportional to the total energy (kinetic + potential) of the oscillator.

We now express this *energy* in terms of the variables relevant to ORGaNICs, i.e., we find $V(\mathbf{y}, \mathbf{a})$. First, we denote the Jacobian matrices in RHS of Eq. (A.57) & (A.59) by $\mathbf{A}$ & $\mathbf{B}$, respectively. We note the simple fact that $\mathbf{A}$ & $\mathbf{B}$ are related by a similarity transformation (a change of basis). This means that there exists an invertible matrix $\mathbf{U}$, such that $\mathbf{A} = \mathbf{U}^{-1}\mathbf{B}\mathbf{U}$ and the corresponding transform is given by $[\mathbf{x}\ \mathbf{v}]^\top = \mathbf{U}[\mathbf{y} - \mathbf{y}_s\ \mathbf{a} - \mathbf{a}_s]^\top$. Assuming that $\mathbf{U}$ is invertible, we can write this equation as $\mathbf{U}\mathbf{A} = \mathbf{B}\mathbf{U}$. To solve this, we consider a block matrix representation of $\mathbf{U}$ and find the

following solution,

$$\mathbf{U} = \begin{bmatrix} \mathbf{D}\left(\frac{\sqrt{\mathbf{a}_s}\odot\boldsymbol{\tau}_y}{\mathbf{y}_s}\right) & \mathbf{0} \\ -\mathbf{D}\left(\frac{\mathbf{a}_s}{\mathbf{y}_s}\right) & -\frac{1}{2}\mathbf{I} \end{bmatrix} \tag{A.61}$$

This change of basis gives us the transformation,

$$\begin{bmatrix} \mathbf{x} \\ \mathbf{v} \end{bmatrix} = \begin{bmatrix} \mathbf{D}\left(\frac{\sqrt{\mathbf{a}_s}\odot\boldsymbol{\tau}_y}{\mathbf{y}_s}\right) & \mathbf{0} \\ -\mathbf{D}\left(\frac{\mathbf{a}_s}{\mathbf{y}_s}\right) & -\frac{1}{2}\mathbf{I} \end{bmatrix} \begin{bmatrix} \mathbf{y}-\mathbf{y}_s \\ \mathbf{a}-\mathbf{a}_s \end{bmatrix} \tag{A.62}$$

or,

$$\begin{aligned} \mathbf{x} &= \frac{\sqrt{\mathbf{a}_s}\odot\boldsymbol{\tau}_y}{\mathbf{y}_s}\odot(\mathbf{y}-\mathbf{y}_s) \\ \mathbf{v} &= -\frac{\mathbf{a}_s}{\mathbf{y}_s}\odot(\mathbf{y}-\mathbf{y}_s) - \frac{(\mathbf{a}-\mathbf{a}_s)}{2} \end{aligned} \tag{A.63}$$

Substituting these expressions into $V(\mathbf{x},\mathbf{v}) = \mathbf{x}^\top(\mathbf{TK})\,\mathbf{x} + \mathbf{v}^\top\mathbf{T}\mathbf{v}$, and assuming the diagonal entries of the matrix $\mathbf{T}$ to be t_i and substituting the diagonal entries of $\mathbf{K}$, $k_i \rightarrow \sqrt{a_{si}}/(\tau_{y_i}\tau_{ai})$, we get the *energy* in terms of $\mathbf{y}$ and $\mathbf{a}$,

$$V(\mathbf{y},\mathbf{a}) = \sum_{i=1}^{n} t_i \left[\frac{\tau_{y_i}}{\tau_{ai}}\frac{{a_{si}}^{3/2}}{{y_{s_i}}^2}\left(y_i-y_{s_i}\right)^2 + \frac{a_{si}}{{y_{s_i}}^2}\left(\sqrt{a_{si}}\left(y_i-y_{s_i}\right) + \frac{y_{s_i}}{2\sqrt{a_{si}}}\left(a_i-a_{si}\right)\right)^2\right] \tag{A.64}$$

We notice that Taylor expanding the term $\sqrt{a_i}y_i$ about $\sqrt{a_{si}}y_{s_i}$ and ignoring the second order terms, we get,

$$\sqrt{a_i}y_i \approx \sqrt{a_{si}}y_{s_i} + \sqrt{a_{si}}\left(y_i-y_{s_i}\right) + \frac{y_{s_i}}{2\sqrt{a_{si}}}\left(a_i-a_{si}\right) \tag{A.65}$$

Therefore the *energy* function, $V(\mathbf{y},\mathbf{a})$, is given by,

$$V(\mathbf{y},\mathbf{a}) = \sum_{i=1}^{n} t_i \frac{a_{si}}{{y_{s_i}}^2}\left[\frac{\tau_{y_i}}{\tau_{ai}}\sqrt{a_{si}}\left(y_i-y_{s_i}\right)^2 + \left(\sqrt{a_i}y_i - \sqrt{a_{si}}y_{s_i}\right)^2\right] \tag{A.66}$$

Notice that $\sqrt{a_{si}}y_{si} = b_i z_i$. This gives us the following expression for the *energy* function,

$$V(\mathbf{y}, \mathbf{a}) = \sum_{i=1}^{n} t_i \frac{a_{si}}{{y_{si}}^2} \left[\frac{\tau_{y_i}}{\tau_{ai}} \sqrt{a_{si}} \left(y_i - y_{si}\right)^2 + \left(\sqrt{a_i} y_i - b_i z_i\right)^2 \right] \tag{A.67}$$

Further, for an ORGaNICs model containing one y and one a neuron, after removing the proportionality constants, the *energy* function is given by,

$$V(y, a) = \frac{\tau_y}{\tau_a} \sqrt{a_s} \left(y - y_s\right)^2 + \left(\sqrt{a} y - b z\right)^2 \tag{A.68}$$

After plugging in the steady-state values, we get,

$$V(y, a) = \frac{\tau_y}{\tau_a} \sqrt{b_0^2 \sigma^2 + w b^2 z^2} \left(y - \frac{b z}{\sqrt{b_0^2 \sigma^2 + w b^2 z^2}} \right)^2 + \left(\sqrt{a} y - b z\right)^2 \tag{A.69}$$

For this system, it is easy to verify that this is a valid Lyapunov function and is minimized by the dynamics of the circuit. We now demonstrate that it has the properties of a Lyapunov function. First, $V(y_s, a_s) = 0$ and $V(y_s, a_s) > 0 \; \forall \; y \neq y_s \; \& \; a \neq a_s$, this can be easily seen from Eq. (A.68). Second, we need to show that, $\dot{V}(y, a) < 0 \; \forall \; y \neq y_s \; \& \; a \neq a_s$. Using Eq. (A.57) & (A.69) $\dot{V}(y, a)$, we can write the total time derivative of the *energy* to be,

$$\begin{aligned} \frac{\mathrm{d}V(y, a)}{\mathrm{d}t} &= \frac{\partial V}{\partial y} \frac{\mathrm{d}y}{\mathrm{d}t} + \frac{\partial V}{\partial a} \frac{\mathrm{d}a}{\mathrm{d}t} \\ &= -\frac{\left(2 y a_s - 3 a_s y_s + a y_s\right)^2 \left(\sqrt{a_s} \tau_a - w y_s^2 \tau_y + \tau_y\right)}{2 a_s \tau_a \tau_y} \end{aligned} \tag{A.70}$$

Since $a_s > 0$ and,

$$\left(\sqrt{a_s} \tau_a - w y_s^2 \tau_y + \tau_y\right) = \left(\sqrt{a_s} \tau_a + \tau_y \left(\frac{b_0^2 \sigma^2}{b_0^2 \sigma^2 + w b^2 z^2} \right) \right) > 0, \tag{A.71}$$

for all the choices of parameters and $\forall \; y \neq y_s, a \neq a_s$, we have $\dot{V}(y, a) < 0$, therefore, it is a valid

Lyapunov function and can be interpreted as the *energy* that decreases with time via the dynamics of ORGaNICs.

B | ORGaNICs with Arbitrary Recurrence

B.1 Linear Stability Analysis of the Two-dimensional Model

Here we consider the dynamical stability of the 2D model containing one neuron each of y and a when the recurrent scalar, w_r can take any positive value. The dynamical system to be analyzed is given by,

$$\begin{aligned}\tau_y \dot{y} &= -y + bz + \left(1 - \sqrt{\lfloor a \rfloor}\right) w_r y \\ \tau_a \dot{a} &= -a + b_0^2 \sigma^2 + w y^2 \lfloor a \rfloor\end{aligned} \tag{B.1}$$

with a positive real constraint on the following set of parameters, $\tau_y, \tau_a, b, b_0, \sigma, w$. We first notice the symmetry in the dynamical system about $y = 0$. Replacing, $\hat{y} \rightarrow -y$, we get the mirrored dynamical system,

$$\begin{aligned}\tau_{\hat{y}} \dot{\hat{y}} &= -\hat{y} + b(-z) + \left(1 - \sqrt{\lfloor a \rfloor}\right) w_r \hat{y} \\ \tau_a \dot{a} &= -a + b_0^2 \sigma^2 + w \hat{y}^2 \lfloor a \rfloor\end{aligned} \tag{B.2}$$

These equations are the same as Eq. (B.1), up to a sign change in z. Therefore, we can derive analogous conditions for stability for $z < 0$ once the conditions for $z > 0$ are known.

The steady-state of Eq. (B.1), (y_s, a_s) satisfies the following equations,

$$y_s = bz + \left(1 - \sqrt{\lfloor a_s \rfloor}\right) w_r y_s \tag{B.3}$$

$$a_s = b_0^2\sigma^2 + w y_s^2 \lfloor a_s \rfloor \tag{B.4}$$

Since the RHS of the second equation is always positive, if a root exists, we have $a_s > 0$. Therefore, we can remove the rectification around a_s and look for positive solutions for a_s. Upon rearranging the terms, we get,

$$\left(1 - w_r + w_r\sqrt{a_s}\right) y_s = bz \tag{B.5}$$

$$\left(1 - w y_s^2\right) a_s = b_0^2\sigma^2 \tag{B.6}$$

Substituting y_s from Eq. (B.5) in Eq. (B.6), we get the following quartic equation in $m = \sqrt{a_s}$,

$$\begin{aligned} {w_r}^2 m^4 + 2(1 - w_r) w_r m^3 + \left((1 - w_r)^2 - w b^2 z^2 - b_0^2\sigma^2 {w_r}^2\right) m^2 \\ - 2(1 - w_r) w_r b_0^2\sigma^2 m - (1 - w_r)^2 b_0^2\sigma^2 = 0 \end{aligned} \tag{B.7}$$

For a valid fixed point (y_s, a_s), i.e., $y_s \in \mathbb{R}$ and $a_s \in \mathbb{R}_*^+$, a necessary condition is that a_s must be positive and real, which in turn implies m must be positive and real.

Theorem B.1. *A fixed point, (y_s, a_s), is valid if and only if it satisfies $\sqrt{a_s} > 0$.*

Proof. Due to Lemma B.2, we have: a fixed point, (y_s, a_s), is valid if and only if it satisfies $m > b_0\sigma$. Further, due to Lemma B.3, we have that the conditions $m > 0$ and $m > b_0\sigma$ are equivalent. Combining these two we get the statement of the theorem. □

Lemma B.2. *A fixed point, (y_s, a_s), is valid if and only if it satisfies $\sqrt{a_s} > b_0\sigma$.*

Proof. $\implies$ Given, $m = \sqrt{a_s} > b_0\sigma$, we have $a_s > b_0^2\sigma^2$, therefore, $a_s \in \mathbb{R}_*^+$; and $y_s = \sqrt{m^2 - b_0^2\sigma^2}/(m\sqrt{w})$, therefore, $y_s \in \mathbb{R}$. $\impliedby$ Given $a_s \in \mathbb{R}_*^+$ and $y_s \in \mathbb{R}$, implies $m \in \mathbb{R}_*^+$. Now, Eq. (B.6) posits that, $m = b_0\sigma/\sqrt{1 - wy_s^2}$, therefore, $m > b_0\sigma$. □

Lemma B.3. *For a positive real root, $m = \sqrt{a_s}$, to the quartic equation (Eq. (B.7)), the condition $m > 0$ is equivalent to the condition $m > b_0\sigma$. Further, no fixed point satisfies $0 < m < b_0\sigma$.*

Proof. $\implies$ Given $m > b_0\sigma$, we have $m > 0$ because $b_0 > 0$ and $\sigma > 0$. $\impliedby$ Since m is a root of the quartic, it also satisfies Eq. (B.6). Therefore, we have $m = b_0\sigma/\sqrt{1 - wy_s^2}$. Since we are given $m > 0$, this implies that $0 < 1 - wy_s^2 < 1$, or $m > b_0\sigma$. Therefore, $m > 0$ is equivalent to $m > b_0\sigma$. This also implies that there exists no fixed point that satisfies $0 < m < b_0\sigma$. □

Further, the Jacobian matrix at the fixed point of the dynamical system, in terms of the parameters and the fixed point is given by,

$$\mathbf{J} = \begin{bmatrix} \frac{w_r - 1 - w_r\sqrt{a_s}}{\tau_y} & -\frac{w_r y_s}{2\sqrt{a_s}\tau_y} \\ \frac{2wa_s y_s}{\tau_a} & \frac{-1 + wy_s^2}{\tau_a} \end{bmatrix} \tag{B.8}$$

From the linear stability theory, we know that a fixed point (y_s, a_s) is asymptotically stable when the real part of the eigenvalues of $\mathbf{J}$ are less than 0, i.e., $\mathrm{Re}(\lambda_\mathbf{J}) < 0$. For a 2D system, this is equivalent to the conditions: $\mathrm{Tr}(\mathbf{J}) < 0$ and $\det(\mathbf{J}) > 0$. The trace of the Jacobian matrix is given by,

$$\begin{aligned} \mathrm{Tr}(\mathbf{J}) &= \frac{w_r - 1 - w_r\sqrt{a_s}}{\tau_y} + \frac{-1 + wy_s^2}{\tau_a} \\ &= -\left(\frac{1 - w_r + w_r\sqrt{a_s}}{\tau_y} + \frac{1 - wy_s^2}{\tau_a}\right) \\ &= -\left(\frac{1 - w_r + w_r\sqrt{a_s}}{\tau_y} + \frac{b_0^2\sigma^2}{a_s\tau_a}\right) \end{aligned} \tag{B.9}$$

The determinant of the Jacobian matrix is given by,

$$\begin{aligned}\det(\mathbf{J}) &= \left(\frac{w_r - 1 - w_r\sqrt{a_s}}{\tau_y}\right)\left(\frac{-1 + wy_s^2}{\tau_a}\right) + \left(\frac{w_r y_s}{2\sqrt{a_s}\tau_y}\right)\left(\frac{2wa_s y_s}{\tau_a}\right) \\ &= \frac{(1-w_r)(1-wy_s^2)}{\tau_a\tau_y} + \frac{w_r\sqrt{a_s}}{\tau_a\tau_y} \\ &= \frac{1}{\tau_y\tau_a}\left(\frac{(1-w_r)b_0^2\sigma^2}{a_s} + w_r\sqrt{a_s}\right)\end{aligned} \tag{B.10}$$

Now we consider the different conditions on w_r and the input drive z for stability and state the various cases as theorems along with their proofs,

B.1.1 Contractive Constraint on Recurrence ($0 < w_r \leq 1$)

- $z > 0$: *There exists a unique fixed point with $y_s > 0$ and $a_s > 0$ and it is asymptotically stable.*

  Proof. The existence and uniqueness of the fixed point, along with its stability properties, are established by Lemma B.4. Additionally, the positivity of a_s (i.e., $a_s > 0$) ensures that the expression $1 - w_r + w_r\sqrt{a_s} > 0$. Consequently, given that $z > 0$, it follows from Eq. (B.5) that $y_s > 0$. □

- $z < 0$: *There exists a unique fixed point with $y_s < 0$ and $a_s > 0$ and it is asymptotically stable.*

  Proof. Since this condition becomes equivalent to $z > 0$, up to a sign change in y (Eq. (B.2)), it is straightforward to see why this is true. □

Lemma B.4. *Given $0 < w_r \leq 1$ and $z \in \mathbb{R}$, there exists a unique fixed point and it is asymptotically stable.*

Proof. We observe that given $0 < w_r \leq 1$, if there exists a valid fixed point, which satisfies $a_s > 0$, $\mathrm{Tr}(\mathbf{J})$ in Eq. (B.9) is less than 0 (since $1 - w_r + w_r\sqrt{a_s} > 0$ for any $\sqrt{a_s} > 0$), and $\det(\mathbf{J})$ in Eq. (B.10)

is greater than 0 for all combinations of parameters and $z \in \mathbb{R}$. Therefore, we need to find the constraints on the parameters that allow for at least one fixed point. The fixed point, $m = \sqrt{a_s}$, satisfies the quartic polynomial in Eq. (B.7). Due to Theorem B.1, for a valid fixed point, we need to find positive real roots that satisfy $m > 0$.

The sequence of signs of the coefficients of the polynomial when $0 \leq w_r < 1$ is given by $(+, +, \pm, -, -)$. We use *Descartes' Rule of Signs*, which states the following: The number of positive real roots of a polynomial $p(x)$ is either equal to the number of sign changes (omitting the zero coefficients) between consecutive non-zero coefficients of $p(x)$, or it is less than this by a multiple of 2. Since there is exactly one sign change from left to right in the sequence, regardless of the sign of the coefficient of m^2, we know that the equation above has exactly one real positive root for m. This further implies that a_s has exactly one positive root and the corresponding fixed point (y_s, a_s), is locally dynamically stable for all of the combinations of parameters and $z \in \mathbb{R}$.

Note that the result also holds for $w_r = 1$. There is exactly one positive fixed point (y_s, a_s) and it is given by, i.e., $y_s = bz/\sqrt{b_0^2\sigma^2 + wb^2z^2}$ and $a_s = b_0^2\sigma^2 + wb^2z^2$. □

B.1.2 Expansive Constraint on Recurrence ($w_r > 1$)

Now we consider the case when $w_r > 1$. We first find an alternative form of the determinant of the Jacobian (Eq. (B.10)) that is more amenable to the case, $w_r > 1$,

$$\begin{aligned} \det(\mathbf{J}) &= \frac{1}{\tau_y \tau_a}\left((1 - w_r)(1 - wy_s^2) + w_r\sqrt{a_s}\right) \\ &= \frac{1}{\tau_y \tau_a}\left(1 - w_r + w_r\sqrt{a_s} + (w_r - 1)wy_s^2\right) \end{aligned} \tag{B.11}$$

Rewriting the trace,

$$\mathrm{Tr}(\mathbf{J}) = -\left(\frac{1 - w_r + w_r\sqrt{a_s}}{\tau_y} + \frac{b_0^2\sigma^2}{a_s\tau_a}\right) \tag{B.12}$$

The properties of stability can be summarized in the following two cases,

- $z > 0$: *There exists exactly one fixed point with $y_s > 0$ and $a_s > 0$ and it is asymptotically stable. Further, if $b_0\sigma > 1 - 1/w_r$, there exist no additional fixed points. But if $b_0\sigma < 1 - 1/w_r$, then there exist either two or no fixed points with $y_s < 0$ and $a_s > 0$, and they may or may not be stable.*

  Proof. Since the fixed point satisfies Eq. (B.5), there are two possibilities, either $1 - w_r + w_r\sqrt{a_s} > 0$ or $1 - w_r + w_r\sqrt{a_s} < 0$. We consider them separately,

  - $1 - w_r + w_r\sqrt{a_s} > 0$: If $z > 0$, we have $y_s > 0$ because y_s satisfies Eq. (B.5). Further, due to Lemma B.5, this fixed point is unique and asymptotically stable for all combinations of parameters.
  - $1 - w_r + w_r\sqrt{a_s} < 0$: If $z > 0$, we have $y_s < 0$ because y_s satisfies Eq. (B.5). Further, if we are given $b_0\sigma > 1 - 1/w_r$, no root exists. We prove this by contradiction, assuming a root exists that satisfies $\sqrt{a_s} < 1 - 1/w_r$, since $b_0\sigma > 1 - 1/w_r$, this root satisfies $0 < \sqrt{a_s} < b_0\sigma$, but due to Lemma B.3 no such root exists, therefore we have a contradiction.

    Now if we have $b_0\sigma < 1 - 1/w_r$, the root for $m = \sqrt{a_s}$ must satisfy $b_0\sigma < m < 1 - 1/w_r$. Since either one or three roots satisfy $m > 0$ (equivalently $m > b_0\sigma$) in Eq. (B.7) and exactly one root satisfies $m > 1 - 1/w_r$ (Lemma B.5), we conclude that the number of roots for m in the interval $(b_0\sigma, 1 - 1/w_r)$ are either two or none.

  □

- $z < 0$: *There exists exactly one fixed point with $y_s < 0$ and $a_s > 0$ and it is asymptotically stable. Further, if $b_0\sigma > 1 - 1/w_r$, there exist no additional fixed points. But if $b_0\sigma < 1 - 1/w_r$, then there exist either two or no fixed points with $y_s > 0$ and $a_s > 0$, and they may or may not be stable.*

Proof. Since this condition becomes equivalent to $z > 0$, up to a sign change in y (Eq. (B.2)), it is straightforward to see why this is true. □

Lemma B.5. *Given $w_r > 1$, there exists a unique fixed point, (y_s, a_s), that satisfies $1 - w_r + w_r\sqrt{a_s} > 0$ and it is asymptotically stable.*

Proof. The fixed point, $m = \sqrt{a_s}$, satisfies the quartic polynomial in Eq. (B.7). Due to Theorem B.1, for a valid fixed point, we need to find positive real roots that satisfy $m > 0$.

The sequence of signs of the coefficients of the polynomial is given by $(+, -, \pm, +, -)$. Regardless of the sign of the coefficient of m^2, using *Descartes' Rule of Signs*, we find that since there are 3 sign changes, there are either 1 or 3 positive real roots for m. Since, we are given $w_r > 1$ and $1 - w_r + w_r\sqrt{a_s} > 0$, these roots are valid only if they satisfy $1 - w_r + w_r m > 0$, or, $m > 1 - 1/w_r$. We make a transformation $m \longrightarrow \hat{m} + (1 - 1/w_r)$ which gives us,

$$\begin{aligned} {w_r}^2\hat{m}^4 - 2(1 - w_r)w_r\hat{m}^3 + \left((1 - w_r)^2 - wb^2z^2 - b_0^2\sigma^2{w_r}^2\right)\hat{m}^2 \\ - 2wb^2z^2(1 - 1/w_r)\hat{m} - wb^2z^2(1 - 1/w_r)^2 = 0 \end{aligned} \tag{B.13}$$

The number of valid roots is given by the number of positive real roots of this polynomial. The signs of the coefficients are given by $(+, +, \pm, -, -)$. There is exactly one sign change, hence there is a unique fixed point that satisfies $1 - w_r + w_r\sqrt{a_s} > 0$.

Now we prove that this fixed point is asymptotically stable. It can be easily seen that $\mathrm{Tr}(\mathbf{J}) < 0$ in Eq. (B.12) and $\det(\mathbf{J}) > 0$ in Eq. (B.11) when $1 - w_r + w_r\sqrt{a_s} > 0$ and $w_r > 1$. Therefore, this unique fixed point is asymptotically stable. □

B.2 Numerical Study of ORGaNICs' Fixed-point

To produce Fig. 3.3 in the main text, we simulated an ORGaNICs network comprising $n = 100$ principal neurons with parameters set to $\sigma = 0.1$ and $\tau_y = \tau_a$. For each chosen value of the

recurrent interaction strength Δ, we generated an ensemble of 10^4 recurrent connectivity matrices $\mathbf{W}_r = \mathbf{I}+\mathbf{K}$. This was achieved by first sampling the entries of an auxiliary matrix $\mathbf{L}$ from a Gaussian distribution $\mathcal{N}(0, \Delta^2/n)$, and then defining the symmetric interaction matrix $\mathbf{K} = (\mathbf{L}+\mathbf{L}^\top)/2$. This prescription yields a symmetric random matrix $\mathbf{K}$, whose entries are normally distributed according to

$$K_{ij} = \begin{cases} \mathcal{N}\left(\frac{\mu}{n}, \frac{\Delta^2}{n}\right), & i = j \\ \mathcal{N}\left(\frac{\mu}{n}, \frac{\Delta^2}{2n}\right), & i \neq j \end{cases} \tag{B.14}$$

The network dynamics were simulated using the explicit Euler method (starting with a zero initial condition for all the neurons) with time step $dt = 0.05 \times \tau_y$, using a delocalized input drive $\mathbf{z}$ where each component $z_i = z/\sqrt{n}$ (ensuring $||\mathbf{z}|| = z$). We analyzed the steady-state behavior, identifying whether trajectories converged to a stable fixed point, diverged (indicating an unstable fixed point), or entered a limit cycle. For instances resulting in a stable fixed point, we computed the trial-averaged mean response $\mathbb{E}[y_i]$ and its standard deviation $\sqrt{\mathrm{Var}(y_i)}$ across the ensemble. Furthermore, we calculated the Jacobian matrix of the dynamical system at each stable fixed point using automatic differentiation [82]. Finally, as shown in Fig. 3.3 and Fig. B.1, we plotted the mean response and its standard deviation as a function of the input drive z for different values of Δ. These plots are colored based on the average real part of the largest eigenvalue (in units of $1/\tau_y$) of the Jacobian matrix across trials, indicating the slowest mode of the dynamics near the fixed point.

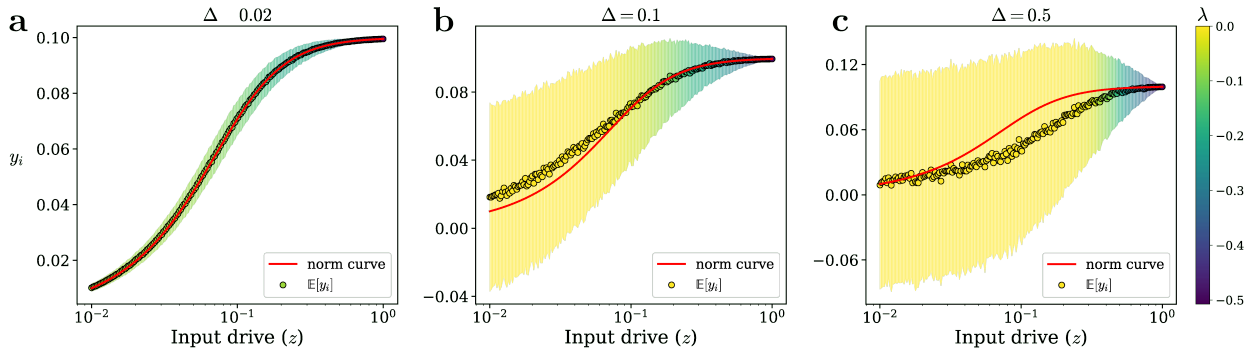


Figure B.1: Numerical exploration of ORGaNICs' fixed-point statistics. For each panel, we plot the fixed-point average response $\mathbb{E}[y]$ (dots) and its std. dev. (shaded area) as a function of the normalized input drive z (with $z_i = z/\sqrt{n}$, $n = 100$), for an E:I balanced recurrence matrix $\mathbf{K}$ of zero mean and standard deviation Δ, with the same parameters as used in Fig. 3.3. The solid red curve indicates the normalization equation Eq. (1.1). The shading color encodes the real part of the largest Jacobian eigenvalue at the fixed point, averaged over samples (always < 0 when convergence is stable). (**a**), $\Delta = 0.02$: recurrent interactions are weak, yielding minimal variance around the normalization curve. (**b**), $\Delta = 0.1$: moderate recurrence induces variability in the responses across random samples of the recurrent weights at small z, but the mean follows the normalization curve. (**c**), $\Delta = 0.5$: strong recurrence dramatically increases the variability at small z; the mean also starts to deviate from the normalization curve.

B.3 Analytical Calculation of the Threshold for Loss of Normalization

Let us consider the ORGaNICs fixed point equations obtained by setting to zero the time derivative in Eq. (3.3) of the main text:

$$\begin{aligned} y_i &= z_i + (1 - \sqrt{a}) \sum_{j=1}^{n} W_{rij} y_j \,, \\ a &= \sigma^2 + a \sum_{j=1}^{n} y_j^2 \,, \end{aligned} \tag{B.15}$$

where we assumed that $a \geq 0$, which can be checked *a posteriori* to always hold true. To expand around the identity matrix we set

$$\mathbf{W}_r = \mathbf{I} + \mathbf{K}\,, \tag{B.16}$$

where $\mathbf{K}$ is a small correction. The conditions under which the perturbation $\mathbf{K}$ can be considered small with respect to the identity will be deduced later on in our calculation. Inserting Eq. (B.16) into Eq. (B.15) we obtain

$$\begin{aligned} \sqrt{a} y_i &= z_i + (1 - \sqrt{a}) \sum_{j=1}^{N} K_{ij} y_j\,, \\ a &= \frac{\sigma^2}{1 - ||\mathbf{y}||^2}\,, \end{aligned} \tag{B.17}$$

where we defined the squared norm as $||\mathbf{y}||^2 = \sum_{j=1}^{n} y_j^2$. We look for a solution to Eq. (B.17) in the form of a series

$$\begin{aligned} y_i &= y_i^{(0)} + y_i^{(1)} + y_i^{(2)} + \cdots\,, \\ a &= a^{(0)} + a^{(1)} + a^{(2)} + \cdots\,, \end{aligned} \tag{B.18}$$

where $y_i^{(1)}, a^{(1)}$ are of the same order of magnitude of the perturbation $\mathbf{K}$, the quantities $y_i^{(2)}, a^{(2)}$ are of second order, and so on. To find the first approximation, we substitute $y_i = y_i^{(0)} + y_i^{(1)}$ and $a = a^{(0)} + a^{(1)}$ in Eq. (B.17) and we keep only terms up to the first order, thus obtaining

$$\begin{aligned} y_i^{(0)} + y_i^{(1)} &= z_i + \left(1 - \sqrt{a^{(0)}}\right) y_i^{(0)} + \left(1 - \sqrt{a^{(0)}}\right)\left(y_i^{(1)} + \sum_j K_{ij} y_j^{(0)}\right) - \frac{y_i^{(0)} a^{(1)}}{2\sqrt{a^{(0)}}}\,, \\ a^{(0)} + a^{(1)} &= \frac{\sigma^2}{1 - ||\mathbf{y}^{(0)}||^2} + 2\sigma^2 \frac{\mathbf{y}^{(0)} \cdot \mathbf{y}^{(1)}}{\left(1 - ||\mathbf{y}^{(0)}||^2\right)^2}\,, \end{aligned} \tag{B.19}$$

where $\mathbf{y}^{(0)} \cdot \mathbf{y}^{(1)} = \sum_i y_i^{(0)} y_i^{(1)}$ is the usual dot product. Equating the terms of order zero on both sides of Eq. (B.19) we obtain

$$\begin{aligned} y_i^{(0)} &= \frac{z_i}{\sqrt{a^{(0)}}}\,, \\ a^{(0)} &= \frac{\sigma^2}{1 - ||\mathbf{y}^{(0)}||^2}\,, \end{aligned} \tag{B.20}$$

which, as it should, is equivalent to the normalization equation

$$\begin{aligned} y_i^{(0)} &= \frac{z_i}{\sqrt{\sigma^2 + ||\mathbf{z}||^2}} \,, \\ a^{(0)} &= \sigma^2 + ||\mathbf{z}||^2 \,. \end{aligned} \tag{B.21}$$

To find the first order corrections $y_i^{(1)}$ and $a^{(1)}$ we equate the terms of order one on both sides of Eq. (B.19) and we get

$$\begin{aligned} y_i^{(1)} \sqrt{a^{(0)}} &= \left(1 - \sqrt{a^{(0)}}\right) \sum_j K_{ij} y_j^{(0)} - \frac{y_i^{(0)} a^{(1)}}{2\sqrt{a^{(0)}}} \,, \\ a^{(1)} &= 2a^{(0)} \frac{\mathbf{y}^{(0)} \cdot \mathbf{y}^{(1)}}{1 - ||\mathbf{y}^{(0)}||^2} \,, \end{aligned} \tag{B.22}$$

where in the equation for $a^{(1)}$ we have used the definition of $a^{(0)}$ given in Eq. (B.20). To solve Eq. (B.22) we multiply the first equation by $y_i^{(0)}$ and, after summing over i, we find

$$\mathbf{y}^{(0)} \cdot \mathbf{y}^{(1)} = \frac{\sigma^2 \left(1 - \sqrt{\sigma^2 + ||\mathbf{z}||^2}\right)}{\left(\sigma^2 + ||\mathbf{z}||^2\right)^{5/2}} \mathbf{z}^\top \mathbf{K} \mathbf{z} \,, \tag{B.23}$$

from which we can compute $a^{(1)}$. Substituting this result into Eq. (B.22) we can express $y_i^{(1)}$ as a function of $\mathbf{z}$ and $\mathbf{K}$ as

$$\boxed{\begin{aligned} y_i^{(1)} &= G(||\mathbf{z}||) \left(\sum_j K_{ij} z_j - z_i \frac{\mathbf{z}^\top \mathbf{K} \mathbf{z}}{\sigma^2 + ||\mathbf{z}||^2} \right) , \\ G(||\mathbf{z}||) &= \frac{1 - \sqrt{\sigma^2 + ||\mathbf{z}||^2}}{\sigma^2 + ||\mathbf{z}||^2} \end{aligned}} \tag{B.24}$$

Having found the general form of the first order correction, we move next to consider the case of a random matrix $\mathbf{K}$ sampled from the so-called Gaussian Orthogonal Ensemble (GOE).

We consider the ensemble of symmetric random matrices $\mathbf{K}$, whose entries are normally

distributed according to

$$K_{ij} = \begin{cases} \mathcal{N}\left(\frac{\mu}{n}, \frac{\Delta^2}{n}\right), & i = j \\ \mathcal{N}\left(\frac{\mu}{n}, \frac{\Delta^2}{2n}\right), & i \neq j \end{cases} \tag{B.25}$$

We can compute the average of $y_i^{(1)}$ in Eq. (B.24) straightforwardly and find

$$\mathbb{E}\left[y_i^{(1)}\right] = \frac{\mu}{n} G(||\mathbf{z}||) \left[\sum_j z_j - \frac{z_i}{\sigma^2 + ||\mathbf{z}||^2} \Big(\sum_j z_j \Big)^2 \right]. \tag{B.26}$$

A little bit of algebra yields the following expression for the second moment

$$\begin{aligned} \mathbb{E}\left[\left(y_i^{(1)}\right)^2\right] &= G^2(||\mathbf{z}||) \left[Q_i - \frac{2z_i}{\sigma^2 + ||\mathbf{z}||^2} P_i + \frac{z_i^2}{\left(\sigma^2 + ||\mathbf{z}||^2\right)^2} R \right], \\ Q_i &= \frac{\Delta^2}{2n}\left(z_i^2 + ||\mathbf{z}||^2\right) - \frac{\mu^2}{n^2}\left[||\mathbf{z}||^2 - \Big(\sum_j z_j \Big)^2 \right], \\ P_i &= \frac{\Delta^2}{n} z_i ||\mathbf{z}||^2 - \frac{\mu^2}{n^2}\left[2z_i ||\mathbf{z}||^2 - z_i^3 - \Big(\sum_j z_j \Big)^3 \right], \\ R &= \frac{\Delta^2}{n} ||\mathbf{z}||^4 - \frac{\mu^2}{n^2}\left[2||\mathbf{z}||^4 - \Big(\sum_j z_j^4 \Big) - \Big(\sum_j z_j \Big)^4 \right]. \end{aligned} \tag{B.27}$$

Having found the general expressions for the first and second moments of $y_i^{(1)}$, next we discuss the case $\mu = 0$ (E:I balance), corresponding to having an equal number (on average) of positive and negative synaptic weights. Mathematically, this is obtained by setting to zero the mean ($\mu = 0$) of the random matrix entries K_{ij}. The mean and variance of the perturbation $y_i^{(1)}$ simplify considerably and read

$$\begin{aligned} \mathbb{E}\left[y_i^{(1)}\right] &= 0\,, \\ \mathbb{E}\left[\left(y_i^{(1)}\right)^2\right] &= G^2(||\mathbf{z}||) \left[\frac{\Delta^2}{2n}\left(z_i^2 + ||\mathbf{z}||^2\right) - \frac{\Delta^2}{n} \frac{2z_i^2 ||\mathbf{z}||^2}{\sigma^2 + ||\mathbf{z}||^2} + \frac{\Delta^2}{n} \frac{z_i^2 ||\mathbf{z}||^4}{\left(\sigma^2 + ||\mathbf{z}||^2\right)^2} \right]. \end{aligned} \tag{B.28}$$

In the following, we will consider two types of input drives, a **delocalized** input drive, character-

ized by a vector $\mathbf{z}$ with all entries z_i equal to

$$z_i = \frac{z}{\sqrt{n}} \quad \text{delocalized input drive} , \tag{B.29}$$

and the case of a **localized** input drive where all entries are equal to zero but one, for example z_1, and denoted

$$z_i = z\delta_{i1} \quad \text{localized input drive} . \tag{B.30}$$

B.3.1 Delocalized Input Drive

When the input drive is delocalized, the variance of the perturbation becomes

$$\mathbb{E}\left[\left(y_i^{(1)}\right)^2\right] = \frac{\Delta^2 z^2}{2n} G(||\mathbf{z}||)^2 + O(n^{-2}) . \tag{B.31}$$

The threshold $\Delta_{loss}(z)$ separating the phase where responses are normalized from the phase where they are not is obtained by equating the mean of the response $\mathbb{E}[y_i]$ to its standard deviation $\sqrt{\text{Var}[y_i]}$, yielding

$$1 = \frac{\mathbb{E}[y_i]}{\sqrt{\text{Var}[y_i]}} = \frac{y_i^{(0)}}{\sqrt{\mathbb{E}\left[\left(y_i^{(1)}\right)^2\right]}} \quad \rightarrow \quad \frac{z}{\sqrt{n}} \frac{1}{\sqrt{\sigma^2 + z^2}} = \frac{\Delta z}{\sqrt{2n}} G(||\mathbf{z}||) , \tag{B.32}$$

from which we obtain

$$\frac{\Delta_{loss}(z)}{\sqrt{2}} = \frac{\sqrt{\sigma^2 + z^2}}{1 - \sqrt{\sigma^2 + z^2}} , \tag{B.33}$$

which is Eq. (3.8) in the main text. In Fig. B.2 we compare the analytical approximations for the mean and variance of the responses with the exact numerical values. The agreement is excellent at small Δ, since the neural responses are always normalized, i.e. normalization always holds. For larger Δ, the analytical and numerical results also agree well at large input drive, where the responses are normalized. At small z, normalization breaks down as well as the analytical

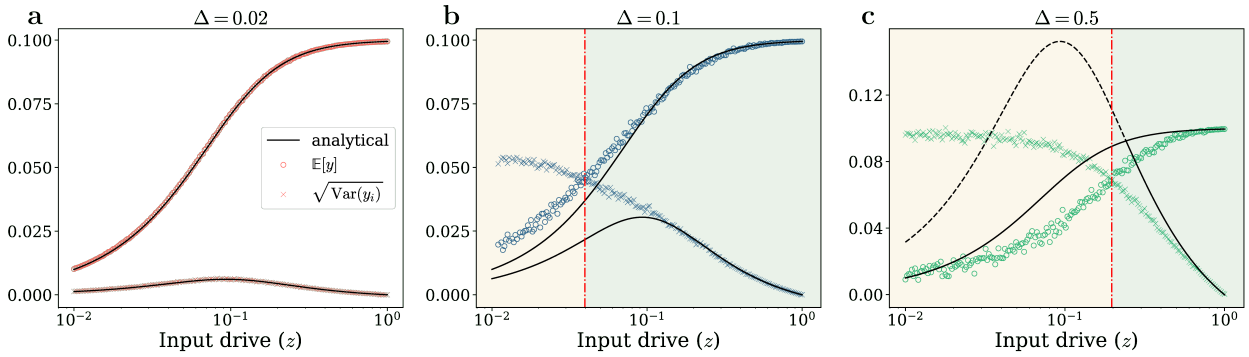


Figure B.2: Loss of normalization. Following the analysis presented in Fig. 3.8, this figure illustrates the mean (circles) and standard deviation (crosses) of the fixed point neural responses versus the input norm z for three additional values of the recurrent interaction strength: $\Delta = 0.02$, $\Delta = 0.1$, and $\Delta = 0.5$. The network consists of $n = 100$ neurons, and each point is found using 1000 realizations. (**a**), $\Delta = 0.02$, the std. dev. remains below the mean across all input drives, indicating preserved normalization. (**b**), $\Delta = 0.1$ and **c,** $\Delta = 0.5$, the std. dev. exceeds the mean at small z, demonstrating loss of normalization, defined by the crossing point (dashed red line). The theoretical predictions from perturbation theory (black curves) match the numerical simulations well in the normalized regime (mean > std. dev.). Discrepancies increase at small z for larger Δ, where normalization is lost.

approximation.

B.3.2 Localized Input Drive

In this section, we show that our results and conclusions are the same for the localized input. We consider the extreme case where $\mathbf{z}$ is a one-hot vector with

$$z_i = z\delta_{i1} \ . \tag{B.34}$$

Since the fixed point y_i depends on i we consider the sum over all responses y_{pop} defined as

$$y_{pop} = \sum_{i=1}^{N} y_i \approx \sum_{i=1}^{N} y_i^{(0)} + y_i^{(1)} \ . \tag{B.35}$$

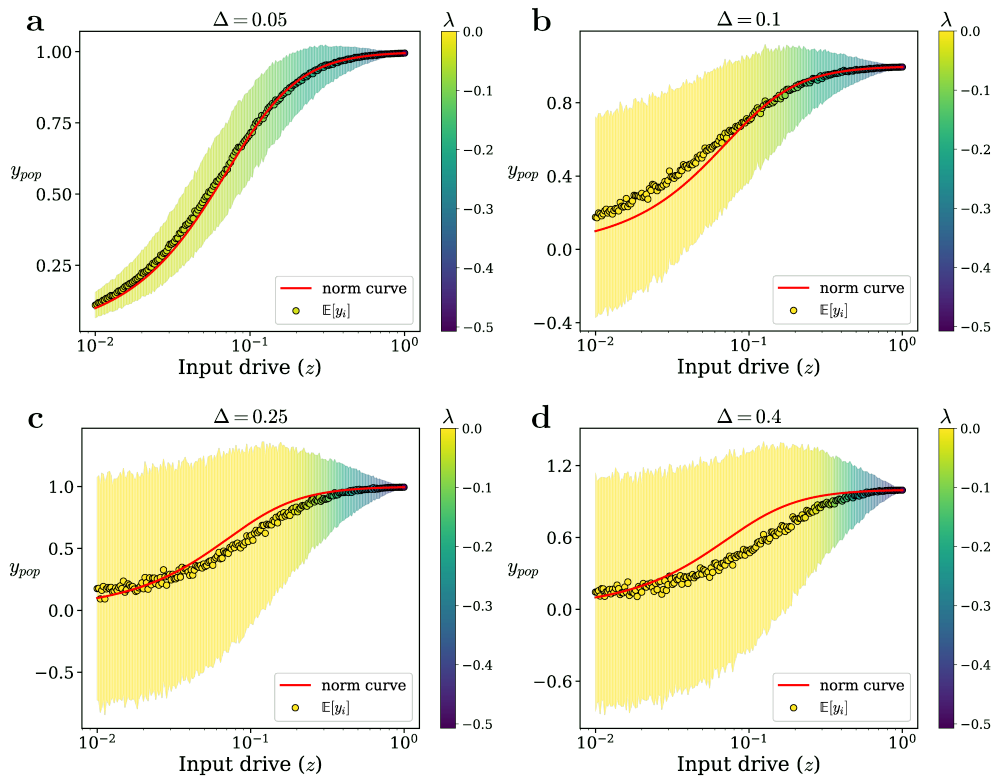


Figure B.3: Numerical solution of the ORGaNICs' fixed point equations for localized input drive. (**a**), Fixed-point average response $\mathbb{E}[y_{pop}]$, defined in Eq. (B.35), as a function of the input drive z (chosen as $z_i = z\delta_{1i}$) for an E:I balanced recurrence matrix $\mathbf{K}$ with zero mean and recurrent interaction strength $\Delta = 0.05$ and $n = 100$ neurons, obtained by solving numerically Eq. (3.3) using the explicit Euler method with time step $dt = 0.05 \times \tau_y$. The semisaturation constant is $\sigma = 0.1$ and the time constants $\tau_y = \tau_a$. Each point is an average over 1000 realizations of the synaptic weights K_{ij}. The neural responses still follow, on average, the normalization Eq. (1.1) (solid red curve), but pick up a variance in presence of recurrent connections, represented by the shaded area around the data points. The color code of the shaded area represents the real part of the largest eigenvalue of the Jacobian at the fixed point averaged over samples, whose value is well below 0 for all z. (**b, c, d**), For $\Delta = 0.1,\ 0.25,\ 0.4$ the average response is still normalized, but the variance is bigger than in (**a**). For sufficiently small input drives, the largest eigenvalue of the Jacobian at the fixed point vanishes and, as a consequence, convergence to the fixed point occurs on long time scales, a phenomenon known as critical slowing down.

The mean of y_{pop} is simply

$$\mathbb{E}[y_{pop}] = \frac{z}{\sqrt{\sigma^2 + z^2}}\,. \tag{B.36}$$

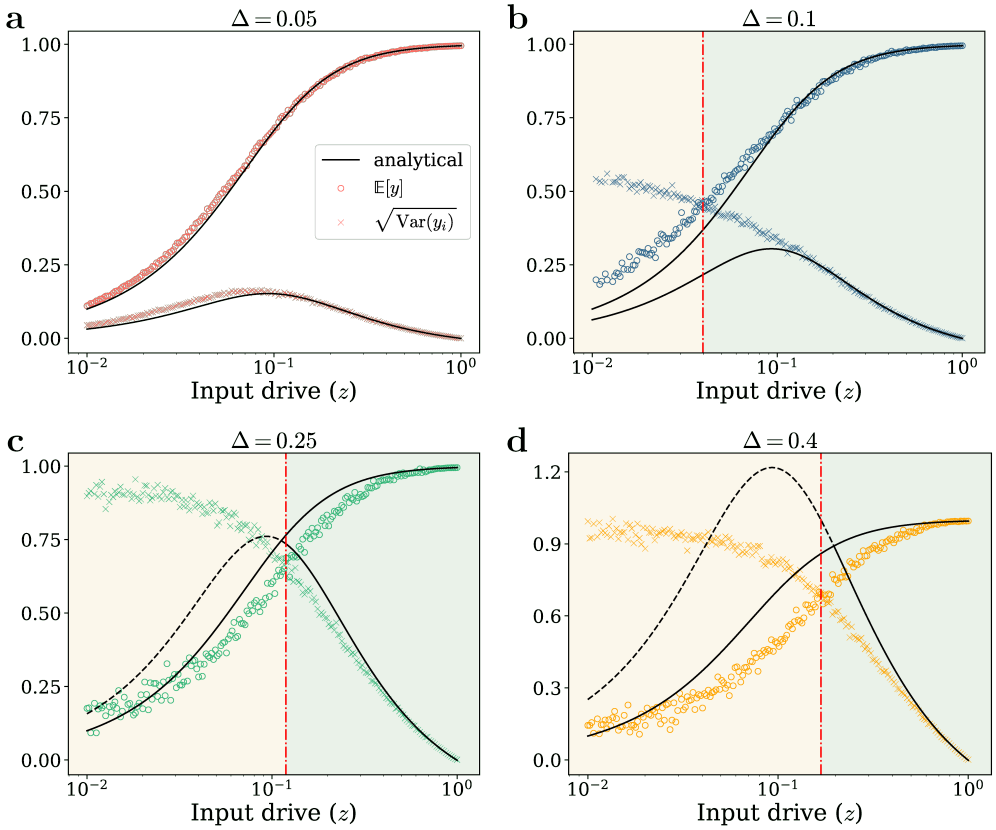


Figure B.4: Loss of normalization for localized input drive. (**a**), Mean (circles) and standard deviation (crosses) of the fixed point response y_{pop}, defined in Eq. (B.35), as a function of the norm z of the localized input drive $z_i = z\delta_{1i}$ for an E:I balanced recurrence matrix $\mathbf{K}$ with zero mean and recurrent interaction strength $\Delta = 0.05$. We used $n = 100$ neurons and averaged over 10^3 realizations of the random matrix $\mathbf{K}$. The analytical approximations (solid curves) for the mean Eq. (B.36) and standard deviation Eq. (B.37) of the response, computed with perturbation theory, show a good agreement between the theoretical and numerical solutions. In this case the standard deviation is smaller than the mean for all values of z, so the neural responses are always normalized. (**b, c, d**), Same as in (**a**), but using $\Delta = 0.1, 0.25, 0.4$. The standard deviation is smaller than the mean at large input drive, but gets bigger than the mean at a small input drive. The value of z where the two curves cross each other, given by Eq. (B.40), defines the point at which the neural responses lose normalization. The analytical approximations are in good agreement with numerical simulations for almost all values of the input drive (notice the log scale on the abscissa), but become less accurate at small z where the responses are non-normalized.

The variance is given by

$$\mathrm{Var}[y_{pop}] = \mathbb{E}\left[\left(y_1^{(1)}\right)^2\right] + 2\sum_{i\neq 1}\mathbb{E}\left[y_1^{(1)}y_i^{(1)}\right] + \sum_{i,j\neq 1}\mathbb{E}\left[y_i^{(1)}y_j^{(1)}\right]. \tag{B.37}$$

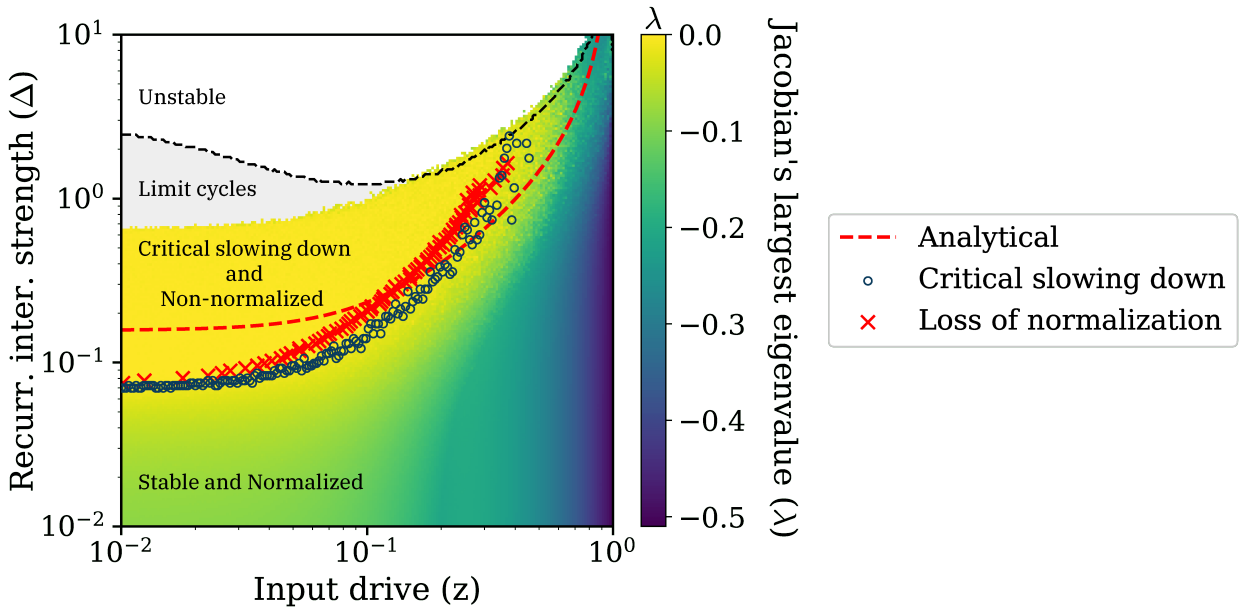


Figure B.5: Loss of normalization predicts the onset of critical slowing down for localized input drive. Real part of the largest eigenvalue of the Jacobian at the fixed point in the (z, Δ) plane obtained by solving numerically Eqs. (3.3) with a localized input drive, i.e., $z_i = z\delta_{i1}$. The parameters of ORGaNICs are the same as those used for generating Fig. 3.9 in the main text. Color represents the maximum value of λ across 100 trials. Circuits with small Δ are stable at any value of the input drive z and converge quickly to their fixed point, as indicated by a strictly negative eigenvalue $\lambda < 0$. Conversely, for $\Delta_{csd} < \Delta < \Delta_c$, the circuits exhibit critical slowing down, in that they approach the fixed point very slowly, as indicated by the zero eigenvalue, $\lambda = 0$. The onset of critical slowing down is defined by the first time the eigenvalue becomes zero, here denoted by the blue empty circle. The onset of slowing down is equally well captured by the red crosses, representing the boundary between the normalized and non-normalized phases. Loss of normalization is a good proxy for critical slowing down even for localized input drives. For sufficiently large Δ the circuits exhibit limit cycles and for even larger Δ they eventually become unstable, where instability is defined as trajectories diverging in at least 50% of trials.

The calculation of the expectation values gives

$$
\begin{aligned}
&\mathbb{E}\left[\left(y_1^{(1)}\right)^2\right] = \frac{\Delta^2 z^2}{n} G^2(||\mathbf{z}||)\left(1 - \frac{z^2}{\sigma^2 + z^2}\right)^2 + O(n^{-2})\,, \\
&\mathbb{E}\left[y_1^{(1)} y_i^{(1)}\right] = 0 \quad \text{for } i \neq 1\,, \\
&\mathbb{E}\left[y_i^{(1)} y_j^{(1)}\right] = \begin{cases} \frac{\Delta^2 z^2}{2n} G^2(||\mathbf{z}||) + O(n^{-2}) & \text{for } i, j \neq 1 \\ 0 & \text{for } i = 1 \text{ or } j = 1\,. \end{cases}
\end{aligned}
\tag{B.38}
$$

Inserting the previous expressions in Eq. (B.37) and keeping only the leading order in n we find

$$\mathrm{Var}[y_{pop}] = \frac{\Delta^2 z^2}{2} G^2(||\mathbf{z}||) \ . \tag{B.39}$$

Equating the mean and standard deviation of y_{pop} we find the $\Delta_{loss}(z)$ as

$$\frac{\mathbb{E}[y_{pop}]}{\sqrt{\mathrm{Var}[y_{pop}]}} = 1 \ \rightarrow \ \frac{\Delta_{loss}(z)}{\sqrt{2}} = \frac{\sqrt{\sigma^2 + z^2}}{1 - \sqrt{\sigma^2 + z^2}} \ , \tag{B.40}$$

which is the same expression as in Eq. (B.33).

B.4 Effect of Critical Slowing Down on Neural Variability

A key marker of critical slowing down is a drastic increase in trial-to-trial neural variability and noise correlations between neurons. To illustrate why this occurs, we consider the ORGaNICs model with additive Gaussian white noise in the dynamical system (Eq. (3.3)):

$$\begin{cases} \tau_y \dot{y}_i = -y_i + z_i + \left(1 - \sqrt{\lfloor a \rfloor}\right) \sum_{j=1}^{n} W_{rij} y_i + \sigma \eta_i(t) \\ \tau_a \dot{a} = -a + \sigma_{ss}^2 + \left(\sum_{i=1}^{n} y_i^2 \right) \lfloor a \rfloor + \sigma \eta_a(t) \ , \end{cases} \tag{B.41}$$

where $\eta_i(t)$ and $\eta_a(t)$ represent uncorrelated Gaussian white noise processes with zero mean and unit variance (i.e., $\mathbb{E}[\eta_k(t)\eta_l(s)] = \delta_{kl}\delta(t-s)$), and σ here denotes the strength of this noise. Note that σ_{ss} is used for the semisaturation constant to avoid confusion with the noise strength σ. This introduction of stochasticity is distinct from the randomness in the recurrent matrix $\mathbf{W}_r$ considered in the main text.

Assuming the dynamical system operates in the vicinity of the stable fixed point (found in both stable and critically slowed-down regimes) and that the noise strength σ is sufficiently small,

we can linearize the system around the fixed point. Let $\mathbf{x}$ be the vector of deviations from the fixed point. The linearized system is:

$$\dot{\mathbf{x}}(t) = \mathbf{J}\mathbf{x}(t) + \sigma\boldsymbol{\eta}(t)\,, \tag{B.42}$$

where $\mathbf{J}$ is the Jacobian matrix evaluated at the fixed point, and $\boldsymbol{\eta}(t)$ is the vector of white noise processes. The steady-state covariance matrix $\mathbf{P} = \mathbb{E}[\mathbf{x}\mathbf{x}^\top]$ (whose diagonal entries capture trial-to-trial variability and off-diagonal entries capture noise correlations) is given by the solution to the continuous-time Lyapunov equation:

$$\mathbf{J}\mathbf{P} + \mathbf{P}\mathbf{J}^\top + \sigma^2\mathbf{I} = \mathbf{0}\,, \tag{B.43}$$

where $\mathbf{I}$ is the identity matrix, and $\sigma^2\mathbf{I}$ is the covariance matrix of the noise term $\sigma\boldsymbol{\eta}(t)$.

Assuming that $\mathbf{J}$ is diagonalizable, we can write its eigendecomposition as $\mathbf{J} = \mathbf{V}\boldsymbol{\Lambda}\mathbf{V}^{-1}$, where $\boldsymbol{\Lambda}$ is a diagonal matrix whose entries λ_i are the eigenvalues of $\mathbf{J}$, and $\mathbf{V}$ is the matrix whose columns are the corresponding eigenvectors. We can transform the coordinates to the eigenbasis of $\mathbf{J}$ by defining $\mathbf{y} = \mathbf{V}^{-1}\mathbf{x}$. The covariance matrix of $\mathbf{y}$ is $\mathbf{M} = \mathbb{E}[\mathbf{y}\mathbf{y}^\top] = \mathbf{V}^{-1}\mathbf{P}(\mathbf{V}^{-1})^\top = \mathbf{V}^{-1}\mathbf{P}\mathbf{V}^{-\top}$. Left-multiplying Eq. (B.43) by $\mathbf{V}^{-1}$ and right-multiplying by $\mathbf{V}^{-\top}$, we obtain:

$$\mathbf{V}^{-1}\mathbf{J}\mathbf{V}(\underbrace{\mathbf{V}^{-1}\mathbf{P}\mathbf{V}^{-\top}}_{\mathbf{M}}) + (\underbrace{\mathbf{V}^{-1}\mathbf{P}\mathbf{V}^{-\top}}_{\mathbf{M}})\mathbf{V}^\top\mathbf{J}^\top\mathbf{V}^{-\top} + \sigma^2\mathbf{V}^{-1}\mathbf{V}^{-\top} = \mathbf{0} \tag{B.44}$$

Using $\mathbf{V}^{-1}\mathbf{J}\mathbf{V} = \mathbf{V}^\top\mathbf{J}^\top\mathbf{V}^{-\top} = \boldsymbol{\Lambda}$ and defining $\mathbf{B} = \mathbf{V}^{-1}\mathbf{V}^{-\top}$, Eq. (B.44) becomes:

$$\boldsymbol{\Lambda}\mathbf{M} + \mathbf{M}\boldsymbol{\Lambda} + \sigma^2\mathbf{B} = \mathbf{0}\,. \tag{B.45}$$

This is the Lyapunov equation for the transformed coordinates $\mathbf{y}$. Since $\boldsymbol{\Lambda}$ is diagonal, we can

solve for the entries of $\mathbf{M}$ element-wise:

$$M_{ij}(\lambda_i + \lambda_j) + \sigma^2 B_{ij} = 0 \implies M_{ij} = -\frac{\sigma^2 B_{ij}}{\lambda_i + \lambda_j} \,. \tag{B.46}$$

Therefore, if the real part of an eigenvalue, say $\mathrm{Re}(\lambda_k)$, approaches zero (which characterizes critical slowing down), the denominator $2\mathrm{Re}(\lambda_k)$ for the diagonal term M_{kk} becomes very small. Assuming B_{kk} (which depends on the eigenvectors) is non-zero, M_{kk} will become very large:

$$M_{kk} = -\frac{\sigma^2 B_{kk}}{2\lambda_k} \,. \tag{B.47}$$

As $\mathrm{Re}(\lambda_k) \to 0$, the magnitude of M_{kk} tends to infinity. Since the original covariance matrix entries P_{mn} are linear combinations of M_{ij} (as $\mathbf{P} = \mathbf{V}\mathbf{M}\mathbf{V}^\top$), a large M_{kk} will typically lead to large entries P_{mn}. This implies increased trial-to-trial variability (large diagonal elements of $\mathbf{P}$) and large noise correlations (large off-diagonal elements of $\mathbf{P}$) when the system is in the critically slowed-down regime compared to the stable and normalized regime.

C | ORGaNICs as an ML Architecture

C.1 Analysis of the Rectified Model

Here, we present the stability results for the model with only the positive part of the complementary receptive fields present. The model is given by the following dynamical equations,

$$\begin{aligned} \boldsymbol{\tau}_y \odot \dot{\mathbf{y}} &= -\mathbf{y} + \mathbf{b} \odot \mathbf{z} + \left(\mathbf{1} - \mathbf{a}^{+}\right) \odot \lfloor \mathbf{W}_r \mathbf{y} \rfloor \\ \boldsymbol{\tau}_a \odot \dot{\mathbf{a}} &= -\mathbf{a} + \mathbf{b}_0^2 \odot \boldsymbol{\sigma}^2 + \mathbf{W} \left(\mathbf{y}^{+} \odot \mathbf{a}^{+2}\right) \end{aligned} \tag{C.1}$$

We will follow the same procedure for stability analysis as we did for the main model (Appendix A) and state the key steps in the various derivations for stability.

C.1.1 Stability of the High-dimensional System

We analyze the stability of the system when $\mathbf{W}_r = \mathbf{I}$. Upon substituting $\mathbf{y}^{+} \rightarrow \lfloor \mathbf{y} \rfloor^2$ and $\mathbf{a}^{+} \rightarrow \sqrt{\lfloor \mathbf{a} \rfloor}$, we get the following dynamical system,

$$\begin{aligned} \boldsymbol{\tau}_y \odot \dot{\mathbf{y}} &= -\mathbf{y} + \mathbf{b} \odot \mathbf{z} + \left(\mathbf{1} - \sqrt{\lfloor \mathbf{a} \rfloor}\right) \odot \lfloor \mathbf{y} \rfloor \\ \boldsymbol{\tau}_a \odot \dot{\mathbf{a}} &= -\mathbf{a} + \mathbf{b}_0^2 \odot \boldsymbol{\sigma}^2 + \mathbf{W} \left(\lfloor \mathbf{y} \rfloor^2 \odot \lfloor \mathbf{a} \rfloor\right) \end{aligned} \tag{C.2}$$

The fixed point is given by,

$$\begin{aligned}\mathbf{y}_s &= \frac{\lfloor \mathbf{b} \odot \mathbf{z} \rfloor}{\sqrt{\mathbf{b}_0^2 \odot \boldsymbol{\sigma}^2 + \mathbf{W}\lfloor \mathbf{b} \odot \mathbf{z} \rfloor^2}} - \lfloor -\mathbf{b} \odot \mathbf{z} \rfloor \\ \mathbf{a}_s &= \mathbf{b}_0^2 \odot \boldsymbol{\sigma}^2 + \mathbf{W}\lfloor \mathbf{b} \odot \mathbf{z} \rfloor^2\end{aligned} \tag{C.3}$$

Also, $\lfloor \mathbf{y}_s \rfloor$ is given by,

$$\lfloor \mathbf{y}_s \rfloor = \frac{\lfloor \mathbf{b} \odot \mathbf{z} \rfloor}{\sqrt{\mathbf{b}_0^2 \odot \boldsymbol{\sigma}^2 + \mathbf{W}\lfloor \mathbf{b} \odot \mathbf{z} \rfloor^2}} \tag{C.4}$$

The Jacobian matrix, $\mathbf{J}$, about this fixed point is given by,

$$\mathbf{J} = \begin{bmatrix} -\mathbf{D}\left(\frac{\sqrt{\mathbf{a}_s} \odot \mathbf{1}_{\mathbf{z}\geq 0} + \mathbf{1}_{\mathbf{z}<0}}{\tau_y}\right) & -\mathbf{D}\left(\frac{\lfloor \mathbf{y}_s \rfloor}{2 \odot \sqrt{\mathbf{a}_s} \odot \tau_y}\right) \\ \mathbf{D}\left(\frac{2}{\tau_a}\right)\mathbf{W}\,\mathbf{D}\left(\mathbf{a}_s \odot \lfloor \mathbf{y}_s \rfloor\right) & \mathbf{D}\left(\frac{1}{\tau_a}\right)\left(-\mathbf{I} + \mathbf{W}\,\mathbf{D}\left(\lfloor \mathbf{y}_s \rfloor^2\right)\right) \end{bmatrix} \tag{C.5}$$

Here $\mathbf{1}_{\mathbf{z}\geq 0}$ is an indicator function that returns a vector the size of $\mathbf{z}$ with 1 at locations where $z_i \geq 0$ and 0 elsewhere. Similarly, $\mathbf{1}_{\mathbf{z}<0}$ returns a vector the size of $\mathbf{z}$ with 1 at locations where $z_i < 0$ and 0 elsewhere. Further $\mathbf{J} - \lambda\mathbf{I}$ is given by,

$$\begin{aligned}\mathbf{J} &= \begin{bmatrix} \mathbf{A}_{11} & \mathbf{A}_{12} \\ \mathbf{A}_{21} & \mathbf{A}_{22} \end{bmatrix} \\ &= \begin{bmatrix} -\mathbf{D}\left(\frac{\sqrt{\mathbf{a}_s} \odot \mathbf{1}_{\mathbf{z}\geq 0} + \mathbf{1}_{\mathbf{z}<0}}{\tau_y}\right) - \lambda\mathbf{I} & -\mathbf{D}\left(\frac{\lfloor \mathbf{y}_s \rfloor}{2 \odot \sqrt{\mathbf{a}_s} \odot \tau_y}\right) \\ \mathbf{D}\left(\frac{2}{\tau_a}\right)\mathbf{W}\,\mathbf{D}\left(\mathbf{a}_s \odot \lfloor \mathbf{y}_s \rfloor\right) & \mathbf{D}\left(\frac{1}{\tau_a}\right)\left(-\mathbf{I} + \mathbf{W}\,\mathbf{D}\left(\lfloor \mathbf{y}_s \rfloor^2\right)\right) - \lambda\mathbf{I} \end{bmatrix}\end{aligned} \tag{C.6}$$

Since $\mathbf{A}_{11}$ and $\mathbf{A}_{12}$ commute, we can write, $\det(\mathbf{J} - \lambda\mathbf{I}) = \det(\mathbf{A}_{22}\mathbf{A}_{11} - \mathbf{A}_{21}\mathbf{A}_{12})$. Upon simplification,

we get,

$$\begin{aligned}\det(\mathbf{J}-\lambda\mathbf{I}) =&\det\Bigg(\lambda^2\mathbf{I}+\lambda\Bigg[\mathbf{D}\left(\frac{1}{\boldsymbol{\tau}_a}\right)+\mathbf{D}\left(\frac{\sqrt{\mathbf{a}_s}\odot\mathbf{1}_{\mathbf{z}\geq 0}+\mathbf{1}_{\mathbf{z}<0}}{\boldsymbol{\tau}_y}\right)\\&-\mathbf{D}\left(\frac{1}{\boldsymbol{\tau}_a}\right)\mathbf{W}\mathbf{D}\left(\lfloor\mathbf{y}_s\rfloor^2\right)\Bigg]+\mathbf{D}\left(\frac{\sqrt{\mathbf{a}_s}\odot\mathbf{1}_{\mathbf{z}\geq 0}+\mathbf{1}_{\mathbf{z}<0}}{\boldsymbol{\tau}_y\odot\boldsymbol{\tau}_a}\right)\Bigg)\end{aligned} \tag{C.7}$$

Note that here we used the fact that $\mathbf{y}_s$ has the same sign as $\mathbf{z}$, as seen from Eq. (C.3). The dynamical system is stable if all eigenvalues of this characteristic polynomial have negative real parts. Just like the main model, we map this to a quadratic eigenvalue problem of the form $\mathcal{L}(\lambda)=\det(\lambda^2\mathbf{I}+\lambda\mathbf{B}+\mathbf{K})=0$. Now, we see if the conditions of Theorem 2.1 are met. The stiffness matrix is given by,

$$\mathbf{K}=\mathbf{D}\left(\frac{\sqrt{\mathbf{a}_s}\odot\mathbf{1}_{\mathbf{z}\geq 0}+\mathbf{1}_{\mathbf{z}<0}}{\boldsymbol{\tau}_y\odot\boldsymbol{\tau}_a}\right)=\mathbf{D}\left(\frac{\sqrt{\mathbf{b}_0^2\odot\boldsymbol{\sigma}^2+\mathbf{W}\lfloor\mathbf{b}\odot\mathbf{z}\rfloor^2}\odot\mathbf{1}_{\mathbf{z}\geq 0}+\mathbf{1}_{\mathbf{z}<0}}{\boldsymbol{\tau}_y\odot\boldsymbol{\tau}_a}\right) \tag{C.8}$$

Clearly, $\mathbf{K}$ is a positive diagonal matrix for all choices of parameters and input. Now we check if the $\mathbf{B}$ is a Lyapunov diagonally stable matrix, which is implied when $\mathbf{B}$ admits a *regular convergent splitting*, i.e., it has a representation of the form $\mathbf{B}=\mathbf{M}-\mathbf{N}$, where $\mathbf{M}^{-1}$ and $\mathbf{N}$ have all nonnegative entries and $\mathbf{M}^{-1}\mathbf{N}$ has a spectral radius smaller than 1.

$$\mathbf{B}=\underbrace{\mathbf{D}\left(\frac{1}{\boldsymbol{\tau}_a}\right)+\mathbf{D}\left(\frac{\sqrt{\mathbf{a}_s}\odot\mathbf{1}_{\mathbf{z}\geq 0}+\mathbf{1}_{\mathbf{z}<0}}{\boldsymbol{\tau}_y}\right)}_{\mathbf{M}}\underbrace{-\mathbf{D}\left(\frac{1}{\boldsymbol{\tau}_a}\right)\mathbf{W}\mathbf{D}\left(\lfloor\mathbf{y}_s\rfloor^2\right)}_{\mathbf{N}} \tag{C.9}$$

Since $\mathbf{M}$ is a positive diagonal matrix, all the entries of $\mathbf{M}^{-1}$ are nonnegative. Also, since all the matrices involved in the definition of $\mathbf{N}$ are nonnegative; therefore, their product $\mathbf{N}$ is nonnegative. We are only left to prove that $\mathbf{M}^{-1}\mathbf{N}=\mathbf{S}$ has a spectral radius smaller than 1. Consider the matrix $\mathbf{S}$,

$$\mathbf{S}=\mathbf{D}\left(\frac{\mathbf{1}}{\mathbf{1}+(\boldsymbol{\tau}_a/\boldsymbol{\tau}_y)\odot\left(\sqrt{\mathbf{a}_s}\odot\mathbf{1}_{\mathbf{z}\geq 0}+\mathbf{1}_{\mathbf{z}<0}\right)}\right)\mathbf{W}\mathbf{D}\left(\frac{\lfloor\mathbf{b}\odot\mathbf{z}\rfloor^2}{\mathbf{b}_0^2\odot\boldsymbol{\sigma}^2+\mathbf{W}\lfloor\mathbf{b}\odot\mathbf{z}\rfloor^2}\right) \tag{C.10}$$

Theorem A.3 puts a bound of 1 on the spectral radius of this matrix.

Define $\mathbf{t} \rightarrow \mathbf{1}/\left(\mathbf{1} + (\boldsymbol{\tau}_a/\boldsymbol{\tau}_y) \odot \left(\sqrt{\mathbf{a}_s} \odot \mathbf{1}_{\mathbf{z}\geq 0} + \mathbf{1}_{\mathbf{z}<0}\right)\right)$, $\mathbf{u} \rightarrow \lfloor \mathbf{b} \odot \mathbf{z} \rfloor^2$ and $\mathbf{v} \rightarrow \mathbf{b}_0^2 \odot \boldsymbol{\sigma}^2$, we notice that they follow the constraints of the theorem, therefore, S is convergent. This implies that $\mathbf{B}$ has a *convergent regular splitting*, therefore, the linearized dynamical system is unconditionally globally asymptotically stable (and nonlinear dynamical system is locally asymptotically stable) across all the values of parameters and inputs.

C.1.2 Analytical Eigenvalue for Fully Normalized Circuit

Following a procedure similar to that in Appendix A.4, when all of the normalization weights in the system are equal, to value α, and the various parameters are scalars, i.e., $\boldsymbol{\tau}_y = \tau_y \mathbf{1}$, $\boldsymbol{\tau}_a = \tau_a \mathbf{1}$, $\mathbf{b}_0 = b_0 \mathbf{1}$ and $\boldsymbol{\sigma} = \sigma \mathbf{1}$, we can write the analytical expressions for eigenvalues. The characteristic polynomial is given by,

$$\det(\mathbf{J} - \lambda \mathbf{I}) = \left(1 - \frac{\lambda \alpha}{\tau_a} \mathbf{v}^\top \mathbf{D} \left(\frac{\mathbf{1}}{\delta_1 \mathbf{1}_{\mathbf{z}\geq 0} + \delta_2 \mathbf{1}_{\mathbf{z}<0}}\right) \mathbf{u}\right) \delta_1^{n_1} \delta_2^{n_2} \tag{C.11}$$

where, $\mathbf{u} = [1, 1, ..., 1]^\top$, $\mathbf{v} = \lfloor \mathbf{b} \odot \mathbf{z} \rfloor^2 / \left(\sigma^2 b_0^2 \mathbf{1} + \mathbf{W} \lfloor \mathbf{b} \odot \mathbf{z} \rfloor^2\right)$; n_1 and n_2 are the number of nonnegative and negative values, respectively, in the input drive $\mathbf{z}$; δ_1 and δ_2 are given by,

$$\begin{aligned} \delta_1 &= \lambda^2 + \lambda \left(\frac{1}{\tau_a} + \frac{\sqrt{\sigma^2 b_0^2 + \alpha ||\lfloor \mathbf{b} \odot \mathbf{z} \rfloor||^2}}{\tau_y}\right) + \frac{\sqrt{\sigma^2 b_0^2 + \alpha ||\lfloor \mathbf{b} \odot \mathbf{z} \rfloor||^2}}{\tau_y \tau_a} \\ \delta_2 &= \lambda^2 + \lambda \left(\frac{1}{\tau_a} + \frac{1}{\tau_y}\right) + \frac{1}{\tau_y \tau_a} \end{aligned} \tag{C.12}$$

Simplification of Eq. (C.11) gives us,

$$\det(\mathbf{J} - \lambda \mathbf{I}) = \left(\delta_1 - \frac{\lambda}{\tau_a} \frac{\alpha ||\lfloor \mathbf{b} \odot \mathbf{z} \rfloor||^2}{\sigma^2 b_0^2 + \alpha ||\lfloor \mathbf{b} \odot \mathbf{z} \rfloor||^2}\right) \delta_1^{n_1 - 1} \delta_2^{n_2} \tag{C.13}$$

Since the characteristic polynomial is a product of quadratic polynomials, we can solve them analytically. The strictly negative eigenvalues are given by,

$$\lambda = -\frac{1}{\tau_a}; \quad \lambda = -\frac{1}{\tau_y} \quad \& \quad \lambda = -\frac{\sqrt{\sigma^2 b_0^2 + \alpha ||\lfloor \mathbf{b} \odot \mathbf{z} \rfloor||^2}}{\tau_y} \tag{C.14}$$

The potentially complex eigenvalues are given by the solution to the following quadratic equation,

$$\lambda^2 + \lambda \left(\frac{\sigma^2 b_0^2}{\tau_a (\sigma^2 b_0^2 + \alpha ||\lfloor \mathbf{b} \odot \mathbf{z} \rfloor||^2)} + \frac{\sqrt{\sigma^2 b_0^2 + \alpha ||\lfloor \mathbf{b} \odot \mathbf{z} \rfloor||^2}}{\tau_y} \right) + \frac{\sqrt{\sigma^2 b_0^2 + \alpha ||\lfloor \mathbf{b} \odot \mathbf{z} \rfloor||^2}}{\tau_y \tau_a} = 0 \tag{C.15}$$

C.1.3 Linear Stability Analysis of the Two-dimensional Model

The dynamical system to consider is,

$$\begin{aligned} \tau_y \dot{y} &= -y + bz + \left(1 - \sqrt{\lfloor a \rfloor}\right) \lfloor w_r y \rfloor \\ \tau_a \dot{a} &= -a + b_0^2 \sigma^2 + w \lfloor y \rfloor^2 \lfloor a \rfloor \end{aligned} \tag{C.16}$$

Since a valid fixed point must have $a_s > 0$, the fixed point (y_s, a_s) satisfies,

$$(1 - w_r + w_r \sqrt{a_s}) \lfloor y_s \rfloor - \lfloor -y_s \rfloor = bz \tag{C.17}$$

$$(1 - w \lfloor y_s \rfloor^2) a_s = b_0^2 \sigma^2 \tag{C.18}$$

We divide this into two cases,

- $y_s > 0$: The fixed point is given by the equations,

$$(1 - w_r + w_r \sqrt{a_s}) y_s = bz \tag{C.19}$$

$$(1 - w y_s^2) a_s = b_0^2 \sigma^2 \tag{C.20}$$

A fixed point, (y_s, a_s), is valid only if it satisfies $y_s \in \mathbb{R}_*^+$ and $a_s \in \mathbb{R}_*^+$. The Jacobian matrix is given by,

$$\mathbf{J} = \begin{bmatrix} \frac{w_r - 1 - w_r\sqrt{a_s}}{\tau_y} & -\frac{w_r y_s}{2\sqrt{a_s}\tau_y} \\ \frac{2wa_s y_s}{\tau_a} & \frac{-1+wy_s^2}{\tau_a} \end{bmatrix} \tag{C.21}$$

Note that this is equivalent to the main model, with the additional constraint of $y_s > 0$, whose stability analysis is presented in Appendix B.1.

- $y_s < 0$: Eq. (C.17) & (C.18) yield us a unique fixed point $y_s = bz$ and $a_s = b_0^2\sigma^2$. Since $y_s < 0$ and $y_s = bz$, this is only possible when $z < 0$. The Jacobian matrix about (y_s, a_s) is given by,

$$\mathbf{J} = \begin{bmatrix} -\frac{1}{\tau_y} & 0 \\ 0 & -\frac{1}{\tau_a} \end{bmatrix} \tag{C.22}$$

Since the eigenvalues of $\mathbf{J}$ are $\lambda_\mathrm{J} = -1/\tau_y, -1/\tau_a$ are real and both negative, this fixed point is always stable.

Combining the cases above and results already established in Appendix B.1, we characterize the stability of the system as follows,

C.1.3.1 Contractive Constraint on Recurrence ($0 < w_r \leq 1$)

- $z > 0$: *There exists a unique fixed point with $y_s > 0$ and $a_s > 0$ and it is asymptotically stable.*
- $z < 0$: *There exists a unique fixed point with $y_s < 0$ and $a_s > 0$, given by, $(bz, b_0^2\sigma^2)$, and it is asymptotically stable.*

C.1.3.2 Expansive Constraint on Recurrence ($w_r > 1$)

- $z > 0$: *There exists a unique fixed point with $y_s > 0$ and $a_s > 0$ and it is asymptotically stable.*

- $z < 0$: *There exists exactly one fixed point with $y_s < 0$ and $a_s > 0$ given by, $(bz, b_0^2\sigma^2)$, and it is asymptotically stable. Further, if $b_0\sigma > 1 - 1/w_r$, there exist no additional fixed points. But if $b_0\sigma < 1 - 1/w_r$, then there exist either two or no fixed points with $y_s > 0$ and $a_s > 0$, and they may or may not be stable.*

C.2 Iterative Algorithm for Fixed-point of ORGaNICs

In this section, we present an iterative approach to finding the fixed point for ORGaNICs with an arbitrary recurrent weight matrix. We show that this algorithm converges in a few steps (2-10) with great accuracy. We consider the system given by Eq. (3.1),

$$\begin{aligned} \boldsymbol{\tau}_y \odot \dot{\mathbf{y}} &= -\mathbf{y} + \mathbf{b} \odot \mathbf{z} + \left(\mathbf{1} - \sqrt{\lfloor \mathbf{a} \rfloor}\right) \odot (\mathbf{W}_r \mathbf{y}) \\ \boldsymbol{\tau}_a \odot \dot{\mathbf{a}} &= -\mathbf{a} + \mathbf{b}_0^2 \odot \boldsymbol{\sigma}^2 + \mathbf{W} \left(\mathbf{y}^2 \odot \lfloor \mathbf{a} \rfloor\right) \end{aligned} \tag{C.23}$$

The fixed point of this system ($\mathbf{y}_s$ and $\mathbf{a}_s$) is found by solving the following simultaneous equations,

$$\mathbf{y}_s = \mathbf{b} \odot \mathbf{z} + \left(\mathbf{1} - \sqrt{\mathbf{a}_s}\right) \odot (\mathbf{W}_r \mathbf{y}_s) \tag{C.24}$$

$$\mathbf{a}_s = \mathbf{b}_0^2 \odot \boldsymbol{\sigma}^2 + \mathbf{W} \left(\mathbf{y}_s^2 \odot \mathbf{a}_s\right) \tag{C.25}$$

These equations do not admit a closed-form analytical solution when $\mathbf{W}_r \neq \mathbf{I}$. We first find a good approximation for the initialization of $\mathbf{y}_s$ and $\mathbf{a}_s$ and then define the iterative algorithm. The equation for $\mathbf{y}_s$ can be written in terms of $\mathbf{a}_s$ as,

$$\mathbf{y}_s = \left(\mathbf{I} + \left(\mathbf{D}\left(\sqrt{\mathbf{a}_s}\right) - \mathbf{I}\right) \mathbf{W}_r\right)^{-1} (\mathbf{b} \odot \mathbf{z}) \tag{C.26}$$

Now applying the Woodbury matrix identity, which states that

$$(\mathbf{A}+\mathbf{UCV})^{-1} = \mathbf{A}^{-1} - \mathbf{A}^{-1}\mathbf{U}\left(\mathbf{C}^{-1} + \mathbf{V}\mathbf{A}^{-1}\mathbf{U}\right)^{-1}\mathbf{V}\mathbf{A}^{-1}, \tag{C.27}$$

to the inverse in Eq. (C.26) with $\mathbf{A} = \mathbf{I}$, $\mathbf{U} = \mathbf{I}$, $\mathbf{C} = \mathbf{D}\left(\sqrt{\mathbf{a}_s}\right) - \mathbf{I}$ and $\mathbf{V} = \mathbf{W}_r$, we get,

$$\mathbf{y}_s = \left(\mathbf{I} - \left(\left(\mathbf{D}\left(\sqrt{\mathbf{a}_s}\right) - \mathbf{I}\right)^{-1} + \mathbf{W}_r\right)^{-1}\mathbf{W}_r\right)(\mathbf{b}\odot\mathbf{z}) \tag{C.28}$$

We approximate the above equation by assuming that $\mathbf{W}_r$ is a symmetric matrix with the eigendecomposition given by $\mathbf{Q}\mathbf{\Lambda}\mathbf{Q}^\top$, with $\mathbf{Q}^\top\mathbf{Q} = \mathbf{Q}\mathbf{Q}^\top = \mathbf{I}$ and $\mathbf{\Lambda} = \mathbf{D}(\boldsymbol{\lambda})$ is a diagonal matrix with the eigenvalues as its diagonal entries. This gives us the following approximation,

$$\begin{aligned}
\mathbf{y}_s &\approx \left(\mathbf{I} - \left(\mathbf{Q}\left(\left(\mathbf{D}\left(\sqrt{\mathbf{a}_s}\right) - \mathbf{I}\right)^{-1} + \mathbf{\Lambda}\right)\mathbf{Q}^\top\right)^{-1}\mathbf{Q}\mathbf{\Lambda}\mathbf{Q}^\top\right)(\mathbf{b}\odot\mathbf{z}) \\
&= \left(\mathbf{I} - \mathbf{Q}\mathbf{D}\left(\boldsymbol{\lambda} + \frac{\mathbf{1}}{\sqrt{\mathbf{a}_s} - \mathbf{1}}\right)^{-1}\mathbf{Q}^\top\mathbf{Q}\mathbf{\Lambda}\mathbf{Q}^\top\right)(\mathbf{b}\odot\mathbf{z}) \\
&= \left(\mathbf{I} - \mathbf{Q}\mathbf{D}\left(\frac{\boldsymbol{\lambda} * \sqrt{\mathbf{a}_s} - \boldsymbol{\lambda}}{\mathbf{1} - \boldsymbol{\lambda} + \boldsymbol{\lambda} * \sqrt{\mathbf{a}_s}}\right)\mathbf{Q}^\top\right)(\mathbf{b}\odot\mathbf{z}) \\
&= \left(\mathbf{I} - \mathbf{Q}\left(\mathbf{I} - \mathbf{D}\left(\frac{\mathbf{1}}{\mathbf{1} - \boldsymbol{\lambda} + \boldsymbol{\lambda} * \sqrt{\mathbf{a}_s}}\right)\right)\mathbf{Q}^\top\right)(\mathbf{b}\odot\mathbf{z}) \\
&= \mathbf{Q}\mathbf{D}\left(\frac{\mathbf{1}}{\mathbf{1} - \boldsymbol{\lambda} + \boldsymbol{\lambda} * \sqrt{\mathbf{a}_s}}\right)\mathbf{Q}^\top(\mathbf{b}\odot\mathbf{z}) \\
&= \mathbf{Q}\mathbf{D}\left(\frac{\mathbf{1}}{\boldsymbol{\lambda} - \boldsymbol{\lambda}^2 + \boldsymbol{\lambda}^2 * \sqrt{\mathbf{a}_s}}\right)\mathbf{\Lambda}\mathbf{Q}^\top(\mathbf{b}\odot\mathbf{z})
\end{aligned} \tag{C.29}$$

We approximate the eigenvalues, $\boldsymbol{\lambda}$, by the maximum eigenvalue of the $\mathbf{W}_r$ and assume the entries of $\sqrt{\mathbf{a}_s}$ are identical. This gives us the following initial guess for $\mathbf{y}_s$.

$$\begin{aligned}
\mathbf{y}_s^0 &= \mathbf{D}\left(\frac{\mathbf{1}}{\lambda_m - \lambda_m^2 + \lambda_m^2\sqrt{\mathbf{a}_s^0}}\right)\mathbf{Q}\mathbf{\Lambda}\mathbf{Q}^\top(\mathbf{b}\odot\mathbf{z}) \\
&= \frac{\mathbf{W}_r(\mathbf{b}\odot\mathbf{z})}{\lambda_m - \lambda_m^2 + \lambda_m^2\sqrt{\mathbf{a}_s^0}}
\end{aligned} \tag{C.30}$$

Algorithm 2 Iterative scheme for finding the fixed point

Input: ORGaNICs parameters and input ($\mathbf{z}$), Tolerance ϵ, maximum iterations N
Output: Approximation to the fixed point $(\mathbf{y}_s, \mathbf{a}_s)$
$\mathbf{a} \leftarrow \boldsymbol{\sigma}^2 \odot \mathbf{b}_0^2 + \mathbf{W}\left(\left(\frac{\mathbf{W}_r(\mathbf{b}\odot\mathbf{z})}{\lambda_m - \lambda_m^2 + \lambda_m^2\sqrt{\mathbf{b}_0^2\odot\boldsymbol{\sigma}^2}}\right)^2 \odot \left(\mathbf{b}_0^2 \odot \boldsymbol{\sigma}^2\right)\right)$ // initial approximation for $\mathbf{a}$
$\mathbf{y} \leftarrow \frac{\mathbf{W}_r(\mathbf{b}\odot\mathbf{z})}{\lambda_m - \lambda_m^2 + \lambda_m^2\sqrt{\mathbf{a}}}$ // initial approximation for $\mathbf{y}$
$k \leftarrow 0$
while $||\mathbf{y} - \mathbf{b}\odot\mathbf{z} - \left(1 - \sqrt{\mathbf{a}}\right)\odot(\mathbf{W}_r\mathbf{y})|| > \epsilon$ and $k < N$ **do**
    $\mathbf{y} \leftarrow \left(\mathbf{I} - \mathbf{W}_r + \mathbf{D}\left(\sqrt{\mathbf{a}}\right)\mathbf{W}_r\right)^{-1}(\mathbf{b}\odot\mathbf{z})$ // $\mathbf{y}$ update
    $\mathbf{a} \leftarrow \mathbf{b}_0^2 \odot \boldsymbol{\sigma}^2 + \mathbf{W}\left(\mathbf{y}^2 * \mathbf{a}\right)$ // $\mathbf{a}$ update
    $k \leftarrow k + 1$
end while
return $(\mathbf{y}, \mathbf{a})$

For the initial guess of $\mathbf{a}_s^0$, we use Eq. (C.25) and plug in the following on the RHS $\mathbf{a}_s \to \mathbf{b}_0^2 \odot \boldsymbol{\sigma}^2$ and the corresponding $\mathbf{y}_s$ found by using Eq. (C.30). This gives us the following,

$$\mathbf{a}_s^0 = \boldsymbol{\sigma}^2 \odot \mathbf{b}_0^2 + \mathbf{W}\left(\left(\frac{\mathbf{W}_r\left(\mathbf{b}\odot\mathbf{z}\right)}{\lambda_m - \lambda_m^2 + \lambda_m^2\sqrt{\mathbf{b}_0^2\odot\boldsymbol{\sigma}^2}}\right)^2 \odot \left(\mathbf{b}_0^2 \odot \boldsymbol{\sigma}^2\right)\right) \tag{C.31}$$

Next we update the $\mathbf{y}_s$ and $\mathbf{a}_s$ by performing the following iterations derived using Eq. (C.24) & (C.25). For instance, $(\mathbf{y}_s^1, \mathbf{a}_s^1)$ are given by,

$$\begin{aligned}\mathbf{y}_s^1 &= \left(\mathbf{I} - \mathbf{W}_r + \mathbf{D}\left(\sqrt{\mathbf{a}_s^0}\right)\mathbf{W}_r\right)^{-1}(\mathbf{b}\odot\mathbf{z}) \\ \mathbf{a}_s^1 &= \mathbf{b}_0^2 \odot \boldsymbol{\sigma}^2 + \mathbf{W}\left(\left(\mathbf{y}_s^1\right)^2 * \mathbf{a}_s^0\right)\end{aligned} \tag{C.32}$$

This procedure is summarized in Algorithm 2. Substituting $\lambda_m = 1$ in Eq. (C.30) & (C.31) yields simpler initial conditions and gives us Algorithm 1. Even though we had assumed that $\mathbf{W}_r$ should be symmetric, in practice we find that this algorithm leads to fast convergence even for non-symmetric matrices. The fast convergence is owed to the fact that we have a good initial approximation of the solution.

D | Power Spectral Density

D.1 Spectral Density Matrix for a Linear SDE / Non-linear SDE Near Stable Fixed Points

We begin with describing the system. A general high-dimensional stochastic differential equation (SDE) describing the time evolution of quantities associated with the system can be written as:

$$\mathrm{d}\mathbf{x} = \mathbf{f}(\mathbf{x})\mathrm{d}t + \mathbf{L}\mathrm{d}\mathbf{W} \tag{D.1}$$

Where $\mathbf{x} \in \mathbb{R}^n$ is a vector of variables that evolve with time according to the nonlinear function $\mathbf{f}(\mathbf{x}) \in \mathbb{R}^n$ and an additive noisy drive given by $\mathbf{L}\mathrm{d}\mathbf{W} \in \mathbb{R}^n$. The matrix $\mathbf{L} \in \mathbb{R}^{n\times m}$ is composed of the weights of the different noise sources appearing in the SDE,

$$\mathbf{L} = \begin{bmatrix} l_{11} & l_{12} & \dots & l_{1m} \\ l_{21} & l_{22} & \dots & l_{2m} \\ \vdots & & \ddots & \vdots \\ l_{n1} & l_{n2} & \dots & l_{nm} \end{bmatrix} \tag{D.2}$$

The differential noise vector (Wiener increments) ($d\mathbf{W} = [dW_1 \quad dW_2 \quad \dots \quad dW_m]^\top$) contains infinitesimally small independent Wiener increments with the following properties:

$$\mathbb{E}[dW_i dW_j] = \begin{cases} 0 & i \neq j \\ \sigma_i^2\, dt & i = j \end{cases} \tag{D.3}$$

with $\sigma^i \in \mathbb{R}^+$. Therefore, there is a diagonal diffusion matrix, $\mathbf{D}$, associated with the noise vector $d\mathbf{W}$, such that its diagonal entries contain the variance of the corresponding noise terms. We can express this matrix as the product of two matrices that contain the corresponding standard deviations, σ_i. We call this matrix $\mathbf{S} \in \mathbb{R}^{m \times m}$ defined as follows,

$$\mathbf{S} = \begin{bmatrix} \sigma_1 & & & & \\ & \sigma_2 & & & \\ & & \ddots & & \\ & & & \sigma_{m-1} & \\ & & & & \sigma_m \end{bmatrix} \tag{D.4}$$

Such that the diffusion matrix $\mathbf{D}$ can be written as,

$$\mathbf{D} = \mathbf{S}\,\mathbf{S}^\top \tag{D.5}$$

We want to calculate the Power Spectral Density (PSD) matrix using the responses $\mathbf{x}(t)$, near the stable fixed points (stable node/spiral), when simulated using the dynamical system, Eq. (D.1). To accomplish this, we consider the deterministic part of the SDE and linearize $\mathbf{f}(\mathbf{x})$ around its stable fixed point $\mathbf{x}_{ss}$, such that $\mathbf{f}(\mathbf{x_{ss}}) = \mathbf{0}$. Now, let us consider the linearized system about the stable fixed point $\mathbf{x}_{ss}$,

$$d\mathbf{x} = \mathbf{J}|_{\mathbf{x}_{ss}}\,(\mathbf{x} - \mathbf{x}_{ss})dt + \mathbf{L}d\mathbf{W} \tag{D.6}$$

We make the variable transformation $\boldsymbol{\Delta} = \mathbf{x} - \mathbf{x}_{ss}$ and use a simpler notation for the Jacobian $\mathbf{J}|_{\mathbf{x}_{ss}} \rightarrow \mathbf{J} \in \mathbb{R}^{n \times n}$. The SDE then becomes,

$$\mathrm{d}\boldsymbol{\Delta} = \mathbf{J}\boldsymbol{\Delta}\mathrm{d}t + \mathbf{L}\mathrm{d}\mathbf{W} \tag{D.7}$$

We can solve this LTI SDE analytically by Ito's solution, given by the following sum of a function of the initial condition (we assume that we start at the steady-state such that $\boldsymbol{\Delta}(0) = \mathbf{0}$) and a stochastic integral,

$$\boldsymbol{\Delta}(t) = e^{\mathrm{J}t}\boldsymbol{\Delta}(0) + \int_0^t e^{\mathrm{J}(t-s)}\,\mathbf{L}\mathrm{d}\mathbf{W}(s) = \int_0^t e^{\mathrm{J}(t-s)}\,\mathbf{L}\mathrm{d}\mathbf{W}(s) \tag{D.8}$$

Similarly, we have,

$$\boldsymbol{\Delta}(t+\tau) = \int_0^{t+\tau} e^{\mathrm{J}(t+\tau-s)}\,\mathbf{L}\mathrm{d}\mathbf{W}(s) \tag{D.9}$$

The cross-correlation matrix $\boldsymbol{\mathcal{R}}(t, \tau)$ is defined as follows,

$$\boldsymbol{\mathcal{R}}(t,\tau) = \mathbb{E}\left[\boldsymbol{\Delta}(t)\boldsymbol{\Delta}^{\top}(t+\tau)\right] \tag{D.10}$$

We assume stationary conditions which can be implemented by taking the limit $t \rightarrow \infty$ to make the statistics of the random variable $\boldsymbol{\Delta}(t \rightarrow \infty)$ stationary, such that the correlation matrix is only a function of τ, $\boldsymbol{\mathcal{R}}(\tau)$. Substituting the solution for $\boldsymbol{\Delta}(t)$ and applying the limit, we get,

$$\boldsymbol{\mathcal{R}}(\tau) = \lim_{t\to\infty} \mathbb{E}\left[\boldsymbol{\Delta}(t)\boldsymbol{\Delta}^{\top}(t+\tau)\right] = \lim_{t\to\infty} \mathbb{E}\left[\int_0^t e^{\mathrm{J}(t-s)}\,\mathbf{L}\mathrm{d}\mathbf{W}(s)\left(\int_0^{t+\tau} e^{\mathrm{J}(t+\tau-s)}\,\mathbf{L}\mathrm{d}\mathbf{W}(s)\right)^{\top}\right] \tag{D.11}$$

Now, we calculate the correlation matrix for positive and negative values of τ separately. First, we consider the case when $\tau \geq 0$. Using the Ito isometry, the properties of matrix exponentials, and

the independence of Wiener increments through time, we can write Eq. (D.11) as,

$$\begin{aligned}\boldsymbol{\mathcal{R}}(\tau) &= \lim_{t\to\infty}\int_0^t e^{\mathbf{J}(t-s)}\,\mathbf{L}\,\mathbb{E}\left[\mathrm{d}\mathbf{W}(s)\mathrm{d}\mathbf{W}(s)^\top\right]\mathbf{L}^\top\,e^{\mathbf{J}^\top(t+\tau-s)} \\ &= \lim_{t\to\infty}\int_0^t e^{\mathbf{J}(t-s)}\,\mathbf{L}\,\mathbf{D}\,\mathbf{L}^\top\,e^{\mathbf{J}^\top(t+\tau-s)}\,\mathrm{d}s\end{aligned} \tag{D.12}$$

We use the property described in Eq. (D.3) to make the substitution $\mathbb{E}\left[\mathrm{d}\mathbf{W}(s)\mathrm{d}\mathbf{W}(s)^\top\right] = \mathbf{D}\mathrm{d}s$. We simplify Eq. (D.12) further by changing the variable of integration as $k = t - s$.

$$\begin{aligned}\boldsymbol{\mathcal{R}}(\tau) &= \lim_{t\to\infty}\int_0^t e^{\mathbf{J}k}\,\mathbf{L}\,\mathbf{D}\,\mathbf{L}^\top\,e^{\mathbf{J}^\top(\tau+k)}\,\mathrm{d}k \\ &= \int_0^\infty e^{\mathbf{J}k}\,\mathbf{L}\,\mathbf{D}\,\mathbf{L}^\top\,e^{\mathbf{J}^\top(\tau+k)}\,\mathrm{d}k\end{aligned} \tag{D.13}$$

Next, we consider the case when $\tau < 0$. Again, using the Ito isometry, the properties of matrix exponentials, and the independence of Wiener increments through time, we can write Eq. (D.11) as,

$$\boldsymbol{\mathcal{R}}(\tau) = \lim_{t\to\infty}\int_0^{t+\tau} e^{\mathbf{J}(t-s)}\,\mathbf{L}\,\mathbf{D}\,\mathbf{L}^\top\,e^{\mathbf{J}^\top(t+\tau-s)}\,\mathrm{d}s \tag{D.14}$$

We change the variable of integration to $k = t - s$. The integral above becomes,

$$\begin{aligned}\boldsymbol{\mathcal{R}}(\tau) &= \lim_{t\to\infty}\int_{-\tau}^t e^{\mathbf{J}k}\,\mathbf{L}\,\mathbf{D}\,\mathbf{L}^\top\,e^{\mathbf{J}^\top(\tau+k)}\,\mathrm{d}k \\ &= \int_{-\tau}^\infty e^{\mathbf{J}k}\,\mathbf{L}\,\mathbf{D}\,\mathbf{L}^\top\,e^{\mathbf{J}^\top(\tau+k)}\,\mathrm{d}k\end{aligned} \tag{D.15}$$

Therefore, the correlation matrix can be written as,

$$\mathbf{R}(\tau) = \begin{cases}\int_0^\infty e^{\mathbf{J}k}\,\mathbf{L}\,\mathbf{D}\,\mathbf{L}^\top\,e^{\mathbf{J}^\top(\tau+k)}\,\mathrm{d}k, & \text{for } \tau \geq 0 \\ \int_{-\tau}^\infty e^{\mathbf{J}k}\,\mathbf{L}\,\mathbf{D}\,\mathbf{L}^\top\,e^{\mathbf{J}^\top(\tau+k)}\,\mathrm{d}k, & \text{for } \tau < 0\end{cases} \tag{D.16}$$

Since the correlation matrix is only a function of τ ($\Delta(t)$ is a wide-sense stationary process in the limit $t \to \infty$), we can apply the cross-correlation theorem (a general form of Wiener-Khinchin

theorem) to calculate the analytical PSD matrix. The PSD matrix is defined as the Fourier transform of the correlation matrix:

$$\boldsymbol{\mathcal{S}}(\omega) = \mathcal{F}(\boldsymbol{\mathcal{R}}(\tau)) = \int_{-\infty}^{\infty} \boldsymbol{\mathcal{R}}(\tau) e^{-i\omega\tau} \, \mathrm{d}\tau \tag{D.17}$$

Substituting the analytical integrals for the correlation matrix and simplifying, we get,

$$\begin{aligned} \boldsymbol{\mathcal{S}}(\omega) &= \int_{-\infty}^{0} \boldsymbol{\mathcal{R}}(\tau) e^{-i\omega\tau} \, \mathrm{d}\tau + \int_{0}^{\infty} \boldsymbol{\mathcal{R}}(\tau) e^{-i\omega\tau} \, \mathrm{d}\tau \\ &= \underbrace{\int_{-\infty}^{0} \int_{-\tau}^{\infty} e^{\mathbf{J}k} \, \mathbf{L}\mathbf{D}\mathbf{L}^{\top} \, e^{\mathbf{J}^{\top}(\tau+k)} \, \mathrm{d}k e^{-i\omega\tau} \, \mathrm{d}\tau}_{I} \\ &\quad + \underbrace{\int_{0}^{\infty} \int_{0}^{\infty} e^{\mathbf{J}k} \, \mathbf{L}\mathbf{D}\mathbf{L}^{\top} \, e^{\mathbf{J}^{\top}(\tau+k)} \, \mathrm{d}k e^{-i\omega\tau} \, \mathrm{d}\tau}_{II} \end{aligned} \tag{D.18}$$

We first consider I and try to simplify the integral. On changing the order of integration, we get,

$$\begin{aligned} I &= \int_{-\infty}^{0} \int_{-\tau}^{\infty} e^{\mathbf{J}k} \, \mathbf{L}\mathbf{D}\mathbf{L}^{\top} \, e^{\mathbf{J}^{\top}(\tau+k)} \, e^{-i\omega\tau} \, \mathrm{d}k \, \mathrm{d}\tau \\ &= \int_{0}^{\infty} \int_{-k}^{0} e^{\mathbf{J}k} \, \mathbf{L}\mathbf{D}\mathbf{L}^{\top} \, e^{\mathbf{J}^{\top}(\tau+k)} \, e^{-i\omega\tau} \, \mathrm{d}\tau \, \mathrm{d}k \end{aligned} \tag{D.19}$$

Next, we simplify II by changing the order of integration,

$$\begin{aligned} II &= \int_{0}^{\infty} \int_{0}^{\infty} e^{\mathbf{J}k} \, \mathbf{L}\mathbf{D}\mathbf{L}^{\top} \, e^{\mathbf{J}^{\top}(\tau+k)} \, e^{-i\omega\tau} \, \mathrm{d}k \, \mathrm{d}\tau \\ &= \int_{0}^{\infty} \int_{0}^{\infty} e^{\mathbf{J}k} \, \mathbf{L}\mathbf{D}\mathbf{L}^{\top} \, e^{\mathbf{J}^{\top}(\tau+k)} \, e^{-i\omega\tau} \, \mathrm{d}\tau \, \mathrm{d}k \\ &= \int_{0}^{\infty} e^{\mathbf{J}k} \, \mathbf{L}\mathbf{D}\mathbf{L}^{\top} \int_{0}^{\infty} e^{-i\omega\tau} \, e^{\mathbf{J}^{\top}(\tau+k)} \, \mathrm{d}\tau \, \mathrm{d}k \end{aligned} \tag{D.20}$$

Upon shifting the bounds of the inner integral by k, we get,

$$\begin{aligned}
II &= \int_0^\infty e^{\mathbf{J}k}\,\mathbf{L}\mathbf{D}\mathbf{L}^\top \int_k^\infty e^{-i\omega(\tau-k)}\, e^{\mathbf{J}^\top\tau}\,\mathrm{d}\tau\,\mathrm{d}k \\
&= \int_0^\infty e^{i\omega k} e^{\mathbf{J}k}\,\mathbf{L}\mathbf{D}\mathbf{L}^\top \int_k^\infty e^{-i\omega\tau}\, e^{\mathbf{J}^\top\tau}\,\mathrm{d}\tau\,\mathrm{d}k \\
&= \int_0^\infty e^{i\omega k} e^{\mathbf{J}k}\,\mathbf{L}\mathbf{D}\mathbf{L}^\top \left(\int_0^\infty e^{-i\omega\tau}\, e^{\mathbf{J}^\top\tau}\,\mathrm{d}\tau - \int_0^k e^{-i\omega\tau}\, e^{\mathbf{J}^\top\tau}\,\mathrm{d}\tau\right)\mathrm{d}k \\
&= \int_0^\infty e^{i\omega k} e^{\mathbf{J}k}\,\mathbf{L}\mathbf{D}\mathbf{L}^\top \underbrace{\int_0^\infty e^{-i\omega\tau} e^{\mathbf{J}^\top\tau}\mathrm{d}\tau}_{III}\,\mathrm{d}k - \int_0^\infty e^{i\omega k} e^{\mathbf{J}k}\,\mathbf{L}\mathbf{D}\mathbf{L}^\top \underbrace{\int_0^k e^{-i\omega\tau} e^{\mathbf{J}^\top\tau}\mathrm{d}\tau}_{IV}\,\mathrm{d}k
\end{aligned} \tag{D.21}$$

We now introduce a general property of the Laplace transform of matrix exponentials (also known as the resolvent of a matrix) which we will use in the derivation.

$$\int_0^\infty e^{-\tau s}\, e^{\tau\mathbf{J}}\mathrm{d}\tau = (s\mathbf{I} - \mathbf{J})^{-1} \tag{D.22}$$

Here s can be any complex number. We calculate this integral for 2 different imaginary values, which we will then use directly. First, we make the substitution $s \to i\omega$, this gives us,

$$\int_0^\infty e^{-i\omega\tau}\, e^{\tau\mathbf{J}}\mathrm{d}\tau = (i\omega\mathbf{I} - \mathbf{J})^{-1} \tag{D.23}$$

Next, we make the substitution $s \to -i\omega$, this gives us,

$$\int_0^\infty e^{i\omega\tau}\, e^{\tau\mathbf{J}}\mathrm{d}\tau = -(i\omega\mathbf{I} + \mathbf{J})^{-1} \tag{D.24}$$

Using Eq. (D.23) and Eq. (D.24) to simplify III, we get,

$$\begin{aligned} III &= \int_0^\infty e^{i\omega k} e^{\mathbf{J}k}\, \mathbf{L}\,\mathbf{D}\,\mathbf{L}^\top \int_0^\infty e^{-i\omega\tau}\, e^{\mathbf{J}^\top \tau}\, \mathrm{d}\tau\, \mathrm{d}k \\ &= \int_0^\infty e^{i\omega k} e^{\mathbf{J}k}\, \mathbf{L}\,\mathbf{D}\,\mathbf{L}^\top\, \mathrm{d}k\, (i\omega\mathbf{I} - \mathbf{J}^\top)^{-1} \\ &= \int_0^\infty e^{i\omega k} e^{\mathbf{J}k}\, \mathrm{d}k\, \mathbf{L}\,\mathbf{D}\,\mathbf{L}^\top\, (i\omega\mathbf{I} - \mathbf{J}^\top)^{-1} \\ &= -(i\omega\mathbf{I} + \mathbf{J})^{-1}\, \mathbf{L}\,\mathbf{D}\,\mathbf{L}^\top\, (i\omega\mathbf{I} - \mathbf{J}^\top)^{-1} \\ &= (i\omega\mathbf{I} + \mathbf{J})^{-1}\, \mathbf{L}\,\mathbf{D}\,\mathbf{L}^\top\, (-i\omega\mathbf{I} + \mathbf{J})^{-\top} \end{aligned} \tag{D.25}$$

Now, we simplify the integral IV, we first make the variable change $\tau = -\alpha$,

$$\begin{aligned} IV &= -\int_0^\infty e^{i\omega k} e^{\mathbf{J}k}\, \mathbf{L}\,\mathbf{D}\,\mathbf{L}^\top \int_0^k e^{-i\omega\tau}\, e^{\mathbf{J}^\top \tau}\, \mathrm{d}\tau\, \mathrm{d}k \\ &= -\int_0^\infty e^{i\omega k} e^{\mathbf{J}k}\, \mathbf{L}\,\mathbf{D}\,\mathbf{L}^\top \int_{-k}^0 e^{i\omega\alpha}\, e^{-\mathbf{J}^\top \alpha}\, \mathrm{d}\alpha\, \mathrm{d}k \\ &= -\int_0^\infty \int_{-k}^0 e^{\mathbf{J}k}\, \mathbf{L}\,\mathbf{D}\,\mathbf{L}^\top\, e^{i\omega(\alpha+k)}\, e^{-\mathbf{J}^\top \alpha}\, \mathrm{d}\alpha\, \mathrm{d}k \end{aligned} \tag{D.26}$$

Next, we make the following variable transformation in the inner integral, $\alpha + k = -m$, this gives us:

$$IV = -\int_0^\infty \int_{-k}^0 e^{\mathbf{J}k}\, \mathbf{L}\,\mathbf{D}\,\mathbf{L}^\top\, e^{-i\omega m}\, e^{\mathbf{J}^\top (m+k)}\, \mathrm{d}m\, \mathrm{d}k \tag{D.27}$$

Finally, we change the variable of integration $\tau = m$ in the inner integral,

$$\begin{aligned} IV &= -\int_0^\infty \int_{-k}^0 e^{\mathbf{J}k}\, \mathbf{L}\,\mathbf{D}\,\mathbf{L}^\top\, e^{-i\omega\tau}\, e^{\mathbf{J}^\top (\tau+k)}\, \mathrm{d}\tau\, \mathrm{d}k \\ &= -\int_0^\infty \int_{-k}^0 e^{\mathbf{J}k}\, \mathbf{L}\,\mathbf{D}\,\mathbf{L}^\top\, e^{\mathbf{J}^\top (\tau+k)}\, e^{-i\omega\tau}\, \mathrm{d}\tau\, \mathrm{d}k \end{aligned} \tag{D.28}$$

The final solution is $I + III + IV$,

$$\begin{aligned}\boldsymbol{\mathcal{S}}(\omega) = &\int_0^\infty \int_{-k}^0 e^{\mathbf{J}k}\,\mathbf{L}\,\mathbf{D}\,\mathbf{L}^\top\, e^{\mathbf{J}^\top(\tau+k)}\, e^{-i\omega\tau}\,\mathrm{d}\tau\,\mathrm{d}k \\ &+ (i\omega\mathbf{I}+\mathbf{J})^{-1}\,\mathbf{L}\,\mathbf{D}\,\mathbf{L}^\top\,(-i\omega\mathbf{I}+\mathbf{J})^{-\top} \\ &- \int_0^\infty \int_{-k}^0 e^{\mathbf{J}k}\,\mathbf{L}\,\mathbf{D}\,\mathbf{L}^\top\, e^{\mathbf{J}^\top(\tau+k)}\, e^{-i\omega\tau}\,\mathrm{d}\tau\,\mathrm{d}k\end{aligned}$$

The first and last integrals cancel each other, and we are left with the final solution,

$$\boldsymbol{\mathcal{S}}(\omega) = (i\omega\mathbf{I}+\mathbf{J})^{-1}\,\mathbf{L}\,\mathbf{D}\,\mathbf{L}^\top\,(-i\omega\mathbf{I}+\mathbf{J})^{-\top} \tag{D.29}$$

We also show that the solution is Hermitian. To do this, take the conjugate transpose of the above expression on both sides, denoted by $*$. Using the properties of conjugate transpose and the fact that $\mathbf{I}, \mathbf{J}, \mathbf{L}, \mathbf{D}$ contain purely real elements, we simplify the expression below to find that the conjugate transpose of the matrix is equal to the matrix itself,

$$\begin{aligned}\boldsymbol{\mathcal{S}}^*(\omega) &= \left[(i\omega\mathbf{I}+\mathbf{J})^{-1}\,\mathbf{L}\,\mathbf{D}\,\mathbf{L}^\top\,(-i\omega\mathbf{I}+\mathbf{J})^{-\top}\right]^* \\ &= ((-i\omega\mathbf{I}+\mathbf{J})^{-\top})^*\,(\mathbf{L}\,\mathbf{D}\,\mathbf{L}^\top)^*\,((i\omega\mathbf{I}+\mathbf{J})^{-1})^* \\ &= ((-i\omega\mathbf{I}+\mathbf{J})^*)^{-\top}\,(\mathbf{L}\,\mathbf{D}\,\mathbf{L}^\top)^*\,((i\omega\mathbf{I}+\mathbf{J})^*)^{-1} \\ &= ((-i\omega\mathbf{I})^*+\mathbf{J}^*)^{-\top}\,(\mathbf{L}^\top)^*\,\mathbf{D}^*\,\mathbf{L}^*\,((i\omega\mathbf{I})^*+\mathbf{J}^*)^{-1} \\ &= (i\omega\mathbf{I}^*+\mathbf{J}^*)^{-\top}\,(\mathbf{L}^*)^\top\,\mathbf{D}\,\mathbf{L}^\top\,(-i\omega\mathbf{I}^*+\mathbf{J}^*)^{-1} \\ &= (i\omega\mathbf{I}+\mathbf{J}^\top)^{-\top}\,(\mathbf{L}^\top)^\top\,\mathbf{D}\,\mathbf{L}^\top\,(-i\omega\mathbf{I}+\mathbf{J}^\top)^{-1} \\ &= (i\omega\mathbf{I}+\mathbf{J})^{-1}\,\mathbf{L}\,\mathbf{D}\,\mathbf{L}^\top\,(-i\omega\mathbf{I}+\mathbf{J})^{-\top} \\ &= \boldsymbol{\mathcal{S}}(\omega)\end{aligned} \tag{D.30}$$

Additionally, if the inverse of the input covariance matrix $\mathbf{C} = \mathbf{L}\,\mathbf{D}\,\mathbf{L}^\top$ exists, i.e., it is positive

definite ($\mathbf{C} \succ 0$), we can write the solution as,

$$\begin{aligned}
\boldsymbol{\mathcal{S}}(\omega) &= (i\omega\mathbf{I}+\mathbf{J})^{-1}\,\mathbf{C}\,(-i\omega\mathbf{I}+\mathbf{J})^{-\top} \\
&= (i\omega\mathbf{I}+\mathbf{J})^{-1}\,\mathbf{C}\,(-i\omega\mathbf{I}+\mathbf{J}^{\top})^{-1} \\
&= \left[(-i\omega\mathbf{I}+\mathbf{J}^{\top})\,\mathbf{C}^{-1}\,(i\omega\mathbf{I}+\mathbf{J})\right]^{-1} \\
&= \left[\mathbf{J}^{\top}\mathbf{C}^{-1}\mathbf{J}+\omega^2\mathbf{C}^{-1}+i\omega(\mathbf{J}^{\top}\mathbf{C}^{-1}-\mathbf{C}^{-1}\mathbf{J})\right]^{-1}
\end{aligned} \tag{D.31}$$

where the matrix $\left[\mathbf{J}^{\top}\mathbf{C}^{-1}\mathbf{J}+\omega^2\mathbf{C}^{-1}+i\omega(\mathbf{J}^{\top}\mathbf{C}^{-1}-\mathbf{C}^{-1}\mathbf{J})\right]$ is Hermitian and positive definite which allows us to use algorithms optimized for the inversion of Hermitian positive definite matrices such as the Cholesky decomposition.

To show that the matrix $\left[\mathbf{J}^{\top}\mathbf{C}^{-1}\mathbf{J}+\omega^2\mathbf{C}^{-1}+i\omega(\mathbf{J}^{\top}\mathbf{C}^{-1}-\mathbf{C}^{-1}\mathbf{J})\right]$ is positive definite, we have to show that the matrix is Hermitian and prove the following,

$$\mathbf{x}^{*}\left[\mathbf{J}^{\top}\mathbf{C}^{-1}\mathbf{J}+\omega^2\mathbf{C}^{-1}+i\omega(\mathbf{J}^{\top}\mathbf{C}^{-1}-\mathbf{C}^{-1}\mathbf{J})\right]\mathbf{x} > 0; \quad \forall\ \mathbf{x}\in\mathbb{C}^{n}\backslash\{\mathbf{0}\} \tag{D.32}$$

The fact that the matrix is Hermitian is easily seen from Eq. (D.30). To prove the second part, consider any non-zero complex vector $\mathbf{x}\in\mathbb{C}^{n}\backslash\{\mathbf{0}\}$. Since, $\mathbf{C}$ is positive definite, $\mathbf{C}^{-1}$ is also positive definite, therefore, $\mathbf{x}^{*}\mathbf{C}^{-1}\mathbf{x} > 0$. Since, $(i\omega\mathbf{I}+\mathbf{J})$ is invertible for any $\omega\in\mathbb{R}$, we can write a transformation $\mathbf{y} = (i\omega\mathbf{I}+\mathbf{J})\,\mathbf{x}$. The complex vector $\mathbf{y}$ must satisfy $\mathbf{y}^{*}\mathbf{C}^{-1}\mathbf{y} > 0$. Upon substitution, we get,

$$\begin{aligned}
\mathbf{y}^{*}\mathbf{C}^{-1}\mathbf{y} &> 0 \\
[(i\omega\mathbf{I}+\mathbf{J})\,\mathbf{x}]^{*}\,\mathbf{C}^{-1}(i\omega\mathbf{I}+\mathbf{J})\,\mathbf{x} &> 0 \\
\mathbf{x}^{*}\left[(i\omega\mathbf{I}+\mathbf{J})^{*}\,\mathbf{C}^{-1}(i\omega\mathbf{I}+\mathbf{J})\right]\mathbf{x} &> 0 \\
\mathbf{x}^{*}\left[(-i\omega\mathbf{I}+\mathbf{J}^{\top})\,\mathbf{C}^{-1}(i\omega\mathbf{I}+\mathbf{J})\right]\mathbf{x} &> 0 \\
\mathbf{x}^{*}\left[\mathbf{J}^{\top}\mathbf{C}^{-1}\mathbf{J}+\omega^2\mathbf{C}^{-1}+i\omega(\mathbf{J}^{\top}\mathbf{C}^{-1}-\mathbf{C}^{-1}\mathbf{J})\right]\mathbf{x} &> 0
\end{aligned} \tag{D.33}$$

Therefore, $\left[\mathbf{J}^\top \mathbf{C}^{-1}\mathbf{J} + \omega^2 \mathbf{C}^{-1} + i\omega(\mathbf{J}^\top \mathbf{C}^{-1} - \mathbf{C}^{-1}\mathbf{J})\right]$ is positive definite.

Now, we proceed with the determination of rational functions for the auto-spectrum (diagonal elements) and the cross-spectrum (off-diagonal elements) using the general matrix solution, as described by Eq. (D.29). In the following sections, we present two distinct approaches to obtaining the rational function solution for $\boldsymbol{\mathcal{S}}(\omega)$. The first approach utilizes a recursive algorithm that calculates the coefficient matrices for the numerator and denominator polynomial coefficients. By employing this method, we can obtain the coefficients for both the auto and cross-spectrum of all variables simultaneously. The second approach involves an element-wise solution, which expresses the auto and cross-spectrum in terms of elementary trace operations applied to the submatrices of $\mathbf{J}$.

D.2 Recursive Algorithm Solutions

D.2.1 Spectral Density Solution

First, we describe the recursive algorithm to calculate the rational function solution for $\boldsymbol{\mathcal{S}}(\omega)$. To make our solution compact, we replace the noise covariance matrix $\mathbf{L}\,\mathbf{D}\,\mathbf{L}^\top$ with $\mathbf{C} \succcurlyeq 0 \in \mathbb{R}^{n\times n}$. Now, we write the inverse of complex matrices in terms of the corresponding determinants, $\det(\mathbf{X})$, and adjugate matrices, $\mathrm{adj}(\mathbf{X})$,

$$\begin{aligned}\boldsymbol{\mathcal{S}}(\omega) &= (i\omega\mathbf{I} + \mathbf{J})^{-1}\,\mathbf{C}\,(-i\omega\mathbf{I} + \mathbf{J})^{-\top} \\ &= \frac{\mathrm{adj}(\mathbf{J} + i\omega\mathbf{I})\,\mathbf{C}\,\mathrm{adj}^\top(\mathbf{J} - i\omega\mathbf{I})}{\det(\mathbf{J} + i\omega\mathbf{I})\,\det(\mathbf{J} - i\omega\mathbf{I})} \\ &= \frac{\mathbf{Z}(\omega)}{Q(\omega)}\end{aligned} \tag{D.34}$$

Here, $\mathbf{Z}(\omega)$ is a complex polynomial matrix representing the numerator of the solution, and $Q(\omega)$ is an even-powered polynomial of degree $2n$ representing the denominator of the solution. When we express the adjugate of the matrices in terms of the corresponding cofactor matrices, it is

evident that $\mathbf{Z}(\omega)$ contains complex polynomials of degree $2n-2$ with even powers of ω being real and odd powers of ω being imaginary. For the denominator, we have,

$$Q(\omega) = |\mathbf{J} + i\omega\mathbf{I}||\mathbf{J} - i\omega\mathbf{I}| \tag{D.35}$$

If λ_i are the eigenvalues of the matrix $\mathbf{J}$, using Eq. (D.233), we have,

$$|\mathbf{J} \pm i\omega| = \prod_{j=1}^{n}(\lambda_j \pm i\omega) \tag{D.36}$$

Therefore,

$$\begin{aligned} Q(\omega) &= \prod_{j=1}^{n}(\lambda_j + i\omega)(\lambda_j - i\omega) \\ &= \prod_{j=1}^{n}(\lambda_j^2 + \omega^2) \end{aligned} \tag{D.37}$$

Therefore, we can write the equation as follows,

$$\begin{aligned} \boldsymbol{\mathcal{S}}(\omega) &= \frac{\mathbf{P}(\omega) + i\omega\mathbf{P}'(\omega)}{Q(\omega)} \\ &= \frac{\mathbf{P}_0 + \mathbf{P}_1\omega^2 + \ldots + \mathbf{P}_{n-1}\omega^{2n-2} + i\omega\left(\mathbf{P}'_0 + \mathbf{P}'_1\omega^2 + \ldots + \mathbf{P}'_{n-2}\omega^{2n-4}\right)}{q_0 + q_1\omega^2 + \ldots + q_n\omega^{2n}} \end{aligned} \tag{D.38}$$

Theorem D.1. *The noise power spectral density matrix of an LTI system is a complex-valued rational function of the form*

$$\begin{aligned} \boldsymbol{\mathcal{S}}(\omega) &= (i\omega\mathbf{I} + \mathbf{J})^{-1}\,\mathbf{C}\,(-i\omega\mathbf{I} + \mathbf{J})^{-\top} \\ &= \frac{\sum_{\alpha=0}^{n-1}\mathbf{P}_\alpha\omega^{2\alpha} + i\omega\sum_{\alpha=0}^{n-2}\mathbf{P}'_\alpha\omega^{2\alpha}}{\sum_{\alpha=0}^{n} q_\alpha\omega^{2\alpha}} \end{aligned} \tag{D.39}$$

The numerator's matrix coefficients are given by the recursive equations,

$$\begin{aligned}\mathbf{P}'_{\alpha-1} &= \mathbf{J}\mathbf{P}_\alpha - \mathbf{P}_\alpha\mathbf{J}^\top - \mathbf{J}\mathbf{P}'_\alpha\mathbf{J}^\top \\ \mathbf{P}_{\alpha-1} &= q_\alpha\mathbf{C} + \mathbf{P}'_{\alpha-1}\mathbf{J}^\top - \mathbf{J}\mathbf{P}'_{\alpha-1} - \mathbf{J}\mathbf{P}_\alpha\mathbf{J}^\top\end{aligned} \tag{D.40}$$

for $\alpha \in \{1, \ldots, n\}$*, starting from* $\alpha = n$ *with* $\mathbf{P}_n = \mathbf{P}'_n = \mathbf{0}$*. The scalar coefficients of the denominator can be recursively calculated using,*

$$q_\alpha = \frac{1}{n-\alpha}\left[\mathrm{Tr}\left(\mathbf{J}\mathbf{Q}'_{\alpha-1}\right) + \mathrm{Tr}\left(\mathbf{J}\mathbf{Q}_\alpha\mathbf{J}^\top\right)\right] \tag{D.41}$$

if $\alpha < n$*, and* $q_n = 1$*. The coefficients* $\mathbf{Q}'_{\alpha-1}$ *and* $\mathbf{Q}_\alpha$ *are given in turn by the recursive equations,*

$$\begin{aligned}\mathbf{Q}'_{\alpha-1} &= \mathbf{J}\mathbf{Q}_\alpha - \mathbf{Q}_\alpha\mathbf{J}^\top - \mathbf{J}\mathbf{Q}'_\alpha\mathbf{J}^\top \\ \mathbf{Q}_{\alpha-1} &= q_\alpha\mathbf{I} + \mathbf{Q}'_{\alpha-1}\mathbf{J}^\top - \mathbf{J}\mathbf{Q}'_{\alpha-1} - \mathbf{J}\mathbf{Q}_\alpha\mathbf{J}^\top\end{aligned} \tag{D.42}$$

for $\alpha \in \{0, 1, \ldots, n\}$*, starting from* $\alpha = n$ *with* $\mathbf{Q}_n = \mathbf{Q}'_n = \mathbf{0}$ *and* $\mathbf{Q}_{-1} = \mathbf{Q}'_{-1} = \mathbf{0}$*.*

Proof. First, we establish a recursive solution for the coefficient matrices of the numerator. Subsequently, we derive the second part of the theorem, presenting a set of recursive equations to calculate the coefficients of the polynomial in the denominator.

D.2.1.1 Coefficient Matrices of the Numerator

Consider Eq. (D.39),

$$\left(i\omega\mathbf{I} + \mathbf{J}\right)^{-1}\mathbf{C}\left(-i\omega\mathbf{I} + \mathbf{J}\right)^{-\top} = \frac{\sum_{\alpha=0}^{n-1}\mathbf{P}_\alpha\omega^{2\alpha} + i\omega\sum_{\alpha=0}^{n-2}\mathbf{P}'_\alpha\omega^{2\alpha}}{\sum_{\alpha=0}^{n}q_\alpha\omega^{2\alpha}} \tag{D.43}$$

Upon rearrangement and left multiplying both sides with $(\mathbf{J} + i\omega\mathbf{I})$ and right multiplying with $(\mathbf{J} - i\omega\mathbf{I})^\top$, we get,

$$
\begin{aligned}
\left(q_0 + q_1\omega^2 + \ldots + q_n\omega^{2n}\right)\mathbf{C} =& \left(\mathbf{J} + i\omega\mathbf{I}\right)\Big(\mathbf{P}_0 + \mathbf{P}_1\omega^2 + \ldots + \mathbf{P}_{n-1}\omega^{2n-2} \\
&+ i\omega\left(\mathbf{P}'_0 + \mathbf{P}'_1\omega^2 + \ldots + \mathbf{P}'_{n-2}\omega^{2n-4}\right)\Big)\left(\mathbf{J} - i\omega\mathbf{I}\right)^\top \\
=& \mathbf{J}\mathbf{P}_0\mathbf{J}^\top + \mathbf{J}\mathbf{P}_1\mathbf{J}^\top\omega^2 + \ldots + \mathbf{J}\mathbf{P}_{n-1}\mathbf{J}^\top\omega^{2n-2} \\
&- \left(\mathbf{P}'_0\mathbf{J}^\top\omega^2 + \mathbf{P}'_1\mathbf{J}^\top\omega^4 + \ldots + \mathbf{P}'_{n-2}\mathbf{J}^\top\omega^{2n-2}\right) \\
&+ \left(\mathbf{J}\mathbf{P}'_0\omega^2 + \mathbf{J}\mathbf{P}'_1\omega^4 + \ldots + \mathbf{J}\mathbf{P}'_{n-2}\omega^{2n-2}\right) \\
&+ \left(\mathbf{P}_0\omega^2 + \mathbf{P}_1\omega^4 + \ldots + \mathbf{P}_{n-1}\omega^{2n}\right) \\
&+ i\left(\mathbf{J}\mathbf{P}'_0\mathbf{J}^\top\omega + \mathbf{J}\mathbf{P}'_1\mathbf{J}^\top\omega^3 + \ldots + \mathbf{J}\mathbf{P}'_{n-2}\mathbf{J}^\top\omega^{2n-3}\right) \\
&+ i\left(\mathbf{P}_0\mathbf{J}^\top\omega + \mathbf{P}_1\mathbf{J}^\top\omega^3 + \ldots + \mathbf{P}_{n-1}\mathbf{J}^\top\omega^{2n-1}\right) \\
&- i\left(\mathbf{J}\mathbf{P}_0\omega + \mathbf{J}\mathbf{P}_1\omega^3 + \ldots + \mathbf{J}\mathbf{P}_{n-1}\omega^{2n-1}\right) \\
&+ i\left(\mathbf{P}'_0\omega^3 + \mathbf{P}'_1\omega^5 + \ldots + \mathbf{P}'_{n-2}\omega^{2n-1}\right)
\end{aligned}
\tag{D.44}
$$

To arrive at the recursive formula for $\mathbf{P}_\alpha$ and $\mathbf{P}'_\alpha$, we compare the like powers of ω on both sides of the equation, starting from the largest power of ω.

$$\begin{aligned}
\mathbf{P}_{n-1} &= q_n \mathbf{C} \\
\mathbf{P}'_{n-2} &= \mathbf{J}\mathbf{P}_{n-1} - \mathbf{P}_{n-1}\mathbf{J}^\top \\
\mathbf{P}_{n-2} &= q_{n-1}\mathbf{C} + \mathbf{P}'_{n-2}\mathbf{J}^\top - \mathbf{J}\mathbf{P}'_{n-2} - \mathbf{J}\mathbf{P}_{n-1}\mathbf{J}^\top \\
\mathbf{P}'_{n-3} &= \mathbf{J}\mathbf{P}_{n-2} - \mathbf{P}_{n-2}\mathbf{J}^\top - \mathbf{J}\mathbf{P}'_{n-2}\mathbf{J}^\top \\
&\ldots, \\
\mathbf{P}'_0 &= \mathbf{J}\mathbf{P}_1 - \mathbf{P}_1\mathbf{J}^\top - \mathbf{J}\mathbf{P}'_1\mathbf{J}^\top \\
\mathbf{P}_0 &= q_1\mathbf{C} + \mathbf{P}'_0\mathbf{J}^\top - \mathbf{J}\mathbf{P}'_0 - \mathbf{J}\mathbf{P}_1\mathbf{J}^\top \\
\mathbf{0} &= \mathbf{J}\mathbf{P}_0 - \mathbf{P}_0\mathbf{J}^\top - \mathbf{J}\mathbf{P}'_0\mathbf{J}^\top \\
\mathbf{0} &= q_0\mathbf{C} - \mathbf{J}\mathbf{P}_0\mathbf{J}^\top
\end{aligned} \tag{D.45}$$

We also verify from these expressions that $\mathbf{P}'_\alpha$ matrices are anti-symmetric, whereas, $\mathbf{P}_\alpha$ matrices are symmetric. Here, the last two equations are redundant and can be used to check the accuracy of the numerical computation. In general for even powers of ω, the coefficients of $\omega^{2\alpha}$ for $0 \leq \alpha \leq n$ are given by,

$$\mathbf{P}_{\alpha-1} = q_\alpha \mathbf{C} + \mathbf{P}'_{\alpha-1}\mathbf{J}^\top - \mathbf{J}\mathbf{P}'_{\alpha-1} - \mathbf{J}\mathbf{P}_\alpha\mathbf{J}^\top \tag{D.46}$$

Note that $\mathbf{P}_n = \mathbf{0}$ and $\mathbf{P}_{-1} = \mathbf{0}$, therefore the above equation is valid for $\alpha \in \{0, n\}$. Similarly, in general for odd powers of ω, the coefficients of $\omega^{2\alpha+1}$ for $0 \leq \alpha \leq n-1$ are given by,

$$\mathbf{P}'_{\alpha-1} = \mathbf{J}\mathbf{P}_\alpha - \mathbf{P}_\alpha\mathbf{J}^\top - \mathbf{J}\mathbf{P}'_\alpha\mathbf{J}^\top \tag{D.47}$$

Note that $\mathbf{P}'_{n-1} = \mathbf{0}$ and $\mathbf{P}'_{-1} = \mathbf{0}$, therefore the above equation is still valid for $\alpha \in \{0, n\}$.

D.2.1.2 Coefficients of the Denominator

Now, onto the second part of the theorem to recursively calculate q_α. Note that $q_n = 1$ can be easily deduced from Eq. (D.37). Consider the Laplace transform, $\mathcal{L}\{f(t)\}(s)$, of the derivative of the exponential of the matrix $e^{it\mathbf{J}}$. For notational convenience, we replace the complex frequency, s, in the Laplace transform with ω and denote $\mathcal{L}\{f(t)\}(\omega)$ as $\mathcal{L}\{f(t)\}$.

$$\mathcal{L}\left\{\frac{\mathrm{d}}{\mathrm{d}t}e^{it\mathbf{J}}\right\} = \mathcal{L}\left\{i\mathbf{J}e^{it\mathbf{J}}\right\} = i\mathbf{J}(\omega\mathbf{I} - i\mathbf{J})^{-1} \tag{D.48}$$

Note that we have used the property of the resolvent of a matrix (Eq. (D.236)). Similarly, we have,

$$\mathcal{L}\left\{\frac{\mathrm{d}}{\mathrm{d}t}e^{-it\mathbf{J}}\right\} = \mathcal{L}\left\{-i\mathbf{J}e^{-it\mathbf{J}}\right\} = -i\mathbf{J}(\omega\mathbf{I} + i\mathbf{J})^{-1} \tag{D.49}$$

Now using the property of the Laplace transform of a derivative of a function, the LHS of the equations above becomes,

$$\omega\mathcal{L}\left\{e^{it\mathbf{J}}\right\} - \mathbf{I} = i\mathbf{J}(\omega\mathbf{I} - i\mathbf{J})^{-1} \tag{D.50}$$

and,

$$\omega\mathcal{L}\left\{e^{-it\mathbf{J}}\right\} - \mathbf{I} = -i\mathbf{J}(\omega\mathbf{I} + i\mathbf{J})^{-1}. \tag{D.51}$$

Now consider the following matrix product,

$$\left(\omega\mathcal{L}\left\{e^{it\mathbf{J}}\right\} - \mathbf{I}\right)\mathbf{C}\left(\omega\mathcal{L}\left\{e^{-it\mathbf{J}}\right\} - \mathbf{I}\right)^\top \tag{D.52}$$

Using Eq. (D.50) & (D.51), we can also write this product as,

$$\left(\omega\mathcal{L}\left\{e^{it\mathbf{J}}\right\} - \mathbf{I}\right)\mathbf{C}\left(\omega\mathcal{L}\left\{e^{-it\mathbf{J}}\right\} - \mathbf{I}\right)^\top = \left(i\mathbf{J}(\omega\mathbf{I} - i\mathbf{J})^{-1}\right)\mathbf{C}\left(-i\mathbf{J}(\omega\mathbf{I} + i\mathbf{J})^{-1}\right)^\top \tag{D.53}$$

We first consider and simplify the RHS of the equation.

$$\begin{aligned}\text{RHS} &= \left(i\mathbf{J}(\omega\mathbf{I} - i\mathbf{J})^{-1}\right)\mathbf{C}\left(-i\mathbf{J}(\omega\mathbf{I} + i\mathbf{J})^{-1}\right)^{\top} \\ &= \mathbf{J}\left[\,(i\omega\mathbf{I} + \mathbf{J})^{-1}\,\mathbf{C}\,(-i\omega\mathbf{I} + \mathbf{J})^{-\top}\right]\mathbf{J}^{\top}\end{aligned} \tag{D.54}$$

Identifying the matrix product in the rectangular brackets from Eq. (D.39), we can write the RHS as,

$$\text{RHS} = \frac{1}{Q(\omega)}\mathbf{J}\left[\sum_{\alpha=0}^{n-1}\mathbf{P}_\alpha\omega^{2\alpha} + i\omega\sum_{\alpha=0}^{n-2}\mathbf{P}'_\alpha\omega^{2\alpha}\right]\mathbf{J}^{\top} \tag{D.55}$$

Now we simplify the LHS by first expanding the product and then using the properties of the Laplace transform,

$$\begin{aligned}\text{LHS} &= \left(\omega\mathcal{L}\left\{e^{it\mathbf{J}}\right\} - \mathbf{I}\right)\mathbf{C}\left(\omega\mathcal{L}\left\{e^{-it\mathbf{J}}\right\} - \mathbf{I}\right)^{\top} \\ &= \omega^2\mathcal{L}\left\{e^{it\mathbf{J}}\right\}\,\mathbf{C}\,\mathcal{L}\left\{e^{-it\mathbf{J}}\right\}^{\top} - \omega\mathcal{L}\left\{e^{it\mathbf{J}}\right\}\mathbf{C} - \omega\,\mathbf{C}\,\mathcal{L}\left\{e^{-it\mathbf{J}}\right\}^{\top} + \mathbf{C} \\ &= \omega^2(\omega\mathbf{I} - i\mathbf{J})^{-1}\,\mathbf{C}\,(\omega\mathbf{I} + i\mathbf{J})^{-\top} - \omega\mathcal{L}\left\{e^{it\mathbf{J}}\right\}\mathbf{C} - \omega\,\mathbf{C}\,\mathcal{L}\left\{e^{-it\mathbf{J}}\right\}^{\top} + \mathbf{C} \\ &= \omega^2\left[(i\omega\mathbf{I} + \mathbf{J})^{-1}\,\mathbf{C}\,(-i\omega\mathbf{I} + \mathbf{J})^{-\top}\right] - \omega\mathcal{L}\left\{e^{it\mathbf{J}}\right\}\mathbf{C} - \omega\,\mathbf{C}\,\mathcal{L}\left\{e^{-it\mathbf{J}}\right\}^{\top} + \mathbf{C}\end{aligned} \tag{D.56}$$

Identifying the matrix product in the rectangular brackets from Eq. (D.39), we can write the LHS as,

$$\text{LHS} = \frac{\omega^2}{Q(\omega)}\left[\sum_{\alpha=0}^{n-1}\mathbf{P}_\alpha\omega^{2\alpha} + i\omega\sum_{\alpha=0}^{n-2}\mathbf{P}'_\alpha\omega^{2\alpha}\right] - \omega\mathcal{L}\left\{e^{it\mathbf{J}}\right\}\mathbf{C} - \omega\,\mathbf{C}\,\mathcal{L}\left\{e^{-it\mathbf{J}}\right\}^{\top} + \mathbf{C} \tag{D.57}$$

Therefore, using Eq. (D.55) & (D.57), we arrive at the following equality,

$$\begin{aligned}\frac{1}{Q(\omega)}\mathbf{J}\left[\sum_{\alpha=0}^{n-1}\mathbf{P}_\alpha\omega^{2\alpha} + i\omega\sum_{\alpha=0}^{n-2}\mathbf{P}'_\alpha\omega^{2\alpha}\right]\mathbf{J}^{\top} =& \frac{\omega^2}{Q(\omega)}\left[\sum_{\alpha=0}^{n-1}\mathbf{P}_\alpha\omega^{2\alpha} + i\omega\sum_{\alpha=0}^{n-2}\mathbf{P}'_\alpha\omega^{2\alpha}\right] \\ &- \omega\mathcal{L}\left\{e^{it\mathbf{J}}\right\}\mathbf{C} - \omega\,\mathbf{C}\,\mathcal{L}\left\{e^{-it\mathbf{J}}\right\}^{\top} + \mathbf{C}\end{aligned} \tag{D.58}$$

Since $\mathbf{C}$ is a covariance matrix, it is positive semi-definite. As we know that the coefficients of the denominator depend only on the matrix $\mathbf{J}$ and not on the covariance matrix $\mathbf{C}$, as seen in Eq. (D.37), the recursive solution of q is valid for any semi-positive definite matrix $\mathbf{C}$. We first derive the recursive solution for q by making the assumption that $\mathbf{C} \succ 0$, and therefore $\mathbf{C}^{-1}$ exists. Multiplying both sides by $\mathbf{C}^{-1}$ in Eq. (D.58), and taking the trace, we get,

$$\begin{aligned}\operatorname{Tr}\left(\frac{\mathbf{C}^{-1}\mathbf{J}}{Q(\omega)}\left[\sum_{\alpha=0}^{n-1}\mathbf{P}_\alpha\omega^{2\alpha}+i\omega\sum_{\alpha=0}^{n-2}\mathbf{P}'_\alpha\omega^{2\alpha}\right]\mathbf{J}^\top\right)=\operatorname{Tr}\left(\frac{\omega^2\mathbf{C}^{-1}}{Q(\omega)}\left[\sum_{\alpha=0}^{n-1}\mathbf{P}_\alpha\omega^{2\alpha}+i\omega\sum_{\alpha=0}^{n-2}\mathbf{P}'_\alpha\omega^{2\alpha}\right]\right)\\ -\omega\operatorname{Tr}\left(\mathbf{C}^{-1}\mathcal{L}\left\{e^{it\mathbf{J}}\right\}\mathbf{C}+\mathcal{L}\left\{e^{-it\mathbf{J}}\right\}^\top\right)+\operatorname{Tr}(\mathbf{I})\end{aligned} \tag{D.59}$$

Using the properties of trace, $\operatorname{Tr}(\mathbf{A}^\top) = \operatorname{Tr}(\mathbf{A})$ and $\operatorname{Tr}(\mathbf{C}^{-1}\mathbf{A}\mathbf{C}) = \operatorname{Tr}(\mathbf{A})$, we can simplify the equation above to,

$$\begin{aligned}\operatorname{Tr}\left(\mathbf{C}^{-1}\mathbf{J}\left[\sum_{\alpha=0}^{n-1}\mathbf{P}_\alpha\omega^{2\alpha}+i\sum_{\alpha=0}^{n-2}\mathbf{P}'_\alpha\omega^{2\alpha+1}\right]\mathbf{J}^\top\right)=\operatorname{Tr}\left(\mathbf{C}^{-1}\left[\sum_{\alpha=0}^{n-1}\mathbf{P}_\alpha\omega^{2\alpha+2}+i\sum_{\alpha=0}^{n-2}\mathbf{P}'_\alpha\omega^{2\alpha+3}\right]\right)\\ -\omega Q(\omega)\operatorname{Tr}\left(\mathcal{L}\left\{e^{it\mathbf{J}}\right\}+\mathcal{L}\left\{e^{-it\mathbf{J}}\right\}\right)+Q(\omega)n\end{aligned} \tag{D.60}$$

Using Theorem D.2, we find,

$$\begin{aligned}\operatorname{Tr}\left(\mathbf{C}^{-1}\mathbf{J}\left[\sum_{\alpha=0}^{n-1}\mathbf{P}_\alpha\omega^{2\alpha}+i\sum_{\alpha=0}^{n-2}\mathbf{P}'_\alpha\omega^{2\alpha+1}\right]\mathbf{J}^\top\right)=\operatorname{Tr}\left(\mathbf{C}^{-1}\left[\sum_{\alpha=0}^{n-1}\mathbf{P}_\alpha\omega^{2\alpha+2}+i\sum_{\alpha=0}^{n-2}\mathbf{P}'_\alpha\omega^{2\alpha+3}\right]\right)\\ -\omega Q'(\omega)+Q(\omega)n\end{aligned} \tag{D.61}$$

Finally, expanding the polynomial corresponding to the denominator, we get,

$$\begin{aligned}\operatorname{Tr}\left(\mathbf{C}^{-1}\mathbf{J}\left[\sum_{\alpha=0}^{n-1}\mathbf{P}_\alpha\omega^{2\alpha}+i\sum_{\alpha=0}^{n-2}\mathbf{P}'_\alpha\omega^{2\alpha+1}\right]\mathbf{J}^\top\right)=\operatorname{Tr}\left(\mathbf{C}^{-1}\left[\sum_{\alpha=0}^{n-1}\mathbf{P}_\alpha\omega^{2\alpha+2}+i\sum_{\alpha=0}^{n-2}\mathbf{P}'_\alpha\omega^{2\alpha+3}\right]\right)\\ +\sum_{\alpha=0}^{n}(n-2\alpha)q_\alpha\omega^{2\alpha}\end{aligned} \tag{D.62}$$

Now, we compare the coefficients of different powers of ω. First, for odd powers of ω, we consider the coefficient of $\omega^{2\alpha+1}$ for $0 \leq \alpha \leq n-1$. We get the following equations,

$$\mathrm{Tr}\left(\mathbf{C}^{-1}\mathbf{P}'_{\alpha-1}\right) = \mathrm{Tr}\left(\mathbf{C}^{-1}\mathbf{J}\mathbf{P}'_{\alpha}\mathbf{J}^{\top}\right) \tag{D.63}$$

Note that $\mathbf{P}'_{n-1} = \mathbf{0}$ and $\mathbf{P}'_{-1} = \mathbf{0}$, therefore the above equation is still valid for $\alpha \in \{0, n-1\}$. Consider the LHS of the equation above,

$$\begin{aligned}
\text{LHS} &= \mathrm{Tr}\left(\mathbf{C}^{-1}\mathbf{P}'_{\alpha-1}\right) \\
&= \mathrm{Tr}\left(\left(\mathbf{C}^{-1}\mathbf{P}'_{\alpha-1}\right)^{\top}\right) \\
&= \mathrm{Tr}\left(\left(\mathbf{P}'_{\alpha-1}\right)^{\top}\left(\mathbf{C}^{-1}\right)^{\top}\right) \\
&= \mathrm{Tr}\left(-\mathbf{P}'_{\alpha-1}\mathbf{C}^{-1}\right) \\
&= -\mathrm{Tr}\left(\mathbf{C}^{-1}\mathbf{P}'_{\alpha-1}\right) \\
&= -\text{LHS}
\end{aligned} \tag{D.64}$$

Therefore, LHS = 0. Note that we have used the following facts: $\mathbf{P}'_{\alpha-1}$ is antisymmetric, and $\mathbf{C}^{-1}$ is symmetric. Similarly, we can prove that RHS = 0. The odd powers of ω in Eq. (D.62) don't give us an insight into the coefficients of the denominator. Therefore, we compare coefficients of even powers of ω. Upon comparing the coefficients of $\omega^{2\alpha}$ for $0 \leq \alpha < n$, we get the following equation,

$$0 = \mathrm{Tr}\left(\mathbf{C}^{-1}\mathbf{P}_{\alpha-1}\right) + (n-2\alpha)q_{\alpha} - \mathrm{Tr}\left(\mathbf{C}^{-1}\mathbf{J}\mathbf{P}_{\alpha}\mathbf{J}^{\top}\right) \tag{D.65}$$

From Eq. (D.46), we know that $\mathbf{P}_{\alpha-1}$ depends on q_{α}, therefore, solving Eq. (D.65) directly for q_{α} does not lead to a recursive solution. Thus, we substitute the expression for $\mathbf{P}_{\alpha-1}$ from Eq. (D.46)

to get,

$$
\begin{aligned}
0 &= \operatorname{Tr}\left(\mathbf{C}^{-1}\left(q_\alpha \mathbf{C} + \mathbf{P}'_{\alpha-1}\mathbf{J}^\top - \mathbf{J}\mathbf{P}'_{\alpha-1} - \mathbf{J}\mathbf{P}_\alpha\mathbf{J}^\top\right)\right) + (n-2\alpha)q_\alpha - \operatorname{Tr}\left(\mathbf{C}^{-1}\mathbf{J}\mathbf{P}_\alpha\mathbf{J}^\top\right) \\
0 &= nq_\alpha + \operatorname{Tr}\left(\mathbf{C}^{-1}\mathbf{P}'_{\alpha-1}\mathbf{J}^\top\right) - \operatorname{Tr}\left(\mathbf{C}^{-1}\mathbf{J}\mathbf{P}'_{\alpha-1}\right) + (n-2\alpha)q_\alpha - 2\operatorname{Tr}\left(\mathbf{C}^{-1}\mathbf{J}\mathbf{P}_\alpha\mathbf{J}^\top\right)
\end{aligned}
\tag{D.66}
$$

Solving the equation for q_α,

$$
\begin{aligned}
q_\alpha &= \frac{1}{n-\alpha}\left[\frac{\operatorname{Tr}\left(\mathbf{C}^{-1}\mathbf{J}\mathbf{P}'_{\alpha-1}\right) - \operatorname{Tr}\left(\mathbf{C}^{-1}\mathbf{P}'_{\alpha-1}\mathbf{J}^\top\right)}{2} + \operatorname{Tr}\left(\mathbf{C}^{-1}\mathbf{J}\mathbf{P}_\alpha\mathbf{J}^\top\right)\right] \\
&= \frac{1}{n-\alpha}\left[\frac{\operatorname{Tr}\left(\mathbf{C}^{-1}\mathbf{J}\mathbf{P}'_{\alpha-1}\right) - \operatorname{Tr}\left(\mathbf{J}\left(\mathbf{P}'_{\alpha-1}\right)^\top\left(\mathbf{C}^{-1}\right)^\top\right)}{2} + \operatorname{Tr}\left(\mathbf{C}^{-1}\mathbf{J}\mathbf{P}_\alpha\mathbf{J}^\top\right)\right] \\
&= \frac{1}{n-\alpha}\left[\frac{\operatorname{Tr}\left(\mathbf{C}^{-1}\mathbf{J}\mathbf{P}'_{\alpha-1}\right) - \operatorname{Tr}\left(-\mathbf{C}^{-1}\mathbf{J}\mathbf{P}'_{\alpha-1}\right)}{2} + \operatorname{Tr}\left(\mathbf{C}^{-1}\mathbf{J}\mathbf{P}_\alpha\mathbf{J}^\top\right)\right] \\
&= \frac{1}{n-\alpha}\left[\operatorname{Tr}\left(\mathbf{C}^{-1}\mathbf{J}\mathbf{P}'_{\alpha-1}\right) + \operatorname{Tr}\left(\mathbf{C}^{-1}\mathbf{J}\mathbf{P}_\alpha\mathbf{J}^\top\right)\right]
\end{aligned}
\tag{D.67}
$$

Since the solution relies on the inverse of the noise covariance matrix $\mathbf{C}$, it might lead to the accumulation of errors in the recursive solution, especially when the dimensionality of the system is large. We also made the assumption that $\mathbf{C}$ was positive definite to be able to calculate the inverse, but that might not be the case for any general stochastic system. Since the solution is valid for any positive semi-definite matrix $\mathbf{C}$, to circumvent the problems above, we choose $\mathbf{C} = \mathbf{I}$, such that we have,

$$
q_\alpha = \frac{1}{n-\alpha}\left[\operatorname{Tr}\left(\mathbf{J}\mathbf{Q}'_{\alpha-1}\right) + \operatorname{Tr}\left(\mathbf{J}\mathbf{Q}_\alpha\mathbf{J}^\top\right)\right] \tag{D.68}
$$

for $0 \leq \alpha < n$ and $\mathbf{Q}'_{-1} = \mathbf{0}$. Here, the matrices $\mathbf{Q}'_{\alpha-1}$ and $\mathbf{Q}_\alpha$ can be interpreted as the coefficient matrices of the numerator of the twin problem given by,

$$\begin{aligned}\boldsymbol{\mathcal{S}}(\omega) &= (i\omega\mathbf{I} + \mathbf{J})^{-1} (-i\omega\mathbf{I} + \mathbf{J})^{-\top} \\ &= \frac{\mathbf{Q}(\omega) + i\omega\mathbf{Q}'(\omega)}{Q(\omega)} \\ &= \frac{\mathbf{Q}_0 + \mathbf{Q}_1\omega^2 + \ldots + \mathbf{Q}_{n-1}\omega^{2n-2} + i\omega\left(\mathbf{Q}'_0 + \mathbf{Q}'_1\omega^2 + \ldots + \mathbf{Q}'_{n-2}\omega^{2n-4}\right)}{q_0 + q_1\omega^2 + \ldots + q_n\omega^{2n}}\end{aligned} \tag{D.69}$$

Therefore, using Eq. (D.46) & (D.47), we can compute the coefficient matrices $\mathbf{Q}'_{\alpha-1}$ and $\mathbf{Q}_\alpha$ recursively,

$$\begin{aligned}\mathbf{Q}'_{\alpha-1} &= \mathbf{J}\mathbf{Q}_\alpha - \mathbf{Q}_\alpha\mathbf{J}^\top - \mathbf{J}\mathbf{Q}'_\alpha\mathbf{J}^\top \\ \mathbf{Q}_{\alpha-1} &= q_\alpha\mathbf{I} + \mathbf{Q}'_{\alpha-1}\mathbf{J}^\top - \mathbf{J}\mathbf{Q}'_{\alpha-1} - \mathbf{J}\mathbf{Q}_\alpha\mathbf{J}^\top\end{aligned} \tag{D.70}$$

by initiating the recursion at $\alpha = n$ and iteratively working backwards until $\alpha = 1$. □

Theorem D.2. *Let* $\mathrm{Tr}(\mathbf{J})$ *denote the trace of the matrix* $\mathbf{J}$, $\mathcal{L}\{f(t)\}$ *denote the Laplace transform of* $f(t)$ *with the complex variable* ω *and* $Q'(\omega)$ *be the derivative of the denominator* $Q(\omega)$ *with respect to* ω, *then we have,*

$$\mathrm{Tr}\left(\mathcal{L}\left\{e^{it\mathbf{J}} + e^{-it\mathbf{J}}\right\}\right) = \frac{Q'(\omega)}{Q(\omega)}. \tag{D.71}$$

Proof. Consider LHS,

$$\begin{aligned}\mathrm{Tr}\left(\mathcal{L}\left\{e^{it\mathbf{J}} + e^{-it\mathbf{J}}\right\}\right) &= \mathcal{L}\left\{\mathrm{Tr}\left(e^{it\mathbf{J}} + e^{-it\mathbf{J}}\right)\right\} \\ &= \mathcal{L}\left\{\mathrm{Tr}\left(\sum_{r=0}^{\infty}\frac{t^r(i\mathbf{J})^r}{r!} + \sum_{r=0}^{\infty}\frac{t^r(-i\mathbf{J})^r}{r!}\right)\right\} \\ &= \mathcal{L}\left\{\sum_{r=0}^{\infty}\mathrm{Tr}\left(\frac{t^r(i\mathbf{J})^r}{r!}\right) + \sum_{r=0}^{\infty}\mathrm{Tr}\left(\frac{t^r(-i\mathbf{J})^r}{r!}\right)\right\}\end{aligned} \tag{D.72}$$

If λ_j are the eigenvalues of $\mathbf{J}$, using Lemma D.3 we can write the equation above as,

$$\begin{aligned}
\mathrm{Tr}\left(\mathcal{L}\left\{e^{it\mathbf{J}} + e^{-it\mathbf{J}}\right\}\right) &= \mathcal{L}\left\{\sum_{r=0}^{\infty}\sum_{j=1}^{n}\frac{t^r(i\lambda_j)^r}{r!} + \sum_{r=0}^{\infty}\sum_{j=1}^{n}\frac{t^r(-i\lambda_j)^r}{r!}\right\} \\
&= \mathcal{L}\left\{\sum_{j=1}^{n} e^{it\lambda_j} + \sum_{j=1}^{n} e^{-it\lambda_j}\right\} \\
&= \sum_{j=1}^{n}\frac{1}{\omega - i\lambda_j} + \sum_{j=1}^{n}\frac{1}{\omega + i\lambda_j} \\
&= \sum_{j=1}^{n}\frac{2\omega}{\omega^2 + \lambda_j^2}
\end{aligned} \tag{D.73}$$

Finally using Lemma D.4, we have,

$$\begin{aligned}
\mathrm{Tr}\left(\mathcal{L}\left\{e^{it\mathbf{J}} + e^{-it\mathbf{J}}\right\}\right) &= \frac{Q'(\omega)}{Q(\omega)} \\
&= \mathrm{RHS}
\end{aligned} \tag{D.74}$$

□

Lemma D.3. *For $\beta \in \mathbb{C}$, $k \in \mathbb{W}$ and $\mathbf{A} \in \mathbb{R}^{n\times n}$ with eigenvalues λ_i*

$$\mathrm{Tr}\left((\beta\mathbf{A})^k\right) = \sum_{i=1}^{n}(\beta\lambda_i)^k \tag{D.75}$$

Proof. Let $\mathbf{A}$ be a square matrix of size $n \times n$ with eigenvalues $\lambda_1, \lambda_2, \ldots, \lambda_n$. The eigenvalues of $\beta\mathbf{A}$ are $\beta\lambda_1, \beta\lambda_2, \ldots, \beta\lambda_n$. Therefore, the eigenvalues of $(\beta\mathbf{A})^k$ are, $(\beta\lambda_1)^k, (\beta\lambda_2)^k, \ldots, (\beta\lambda_n)^k$. Finally, we use the fact that the trace of a given matrix is the sum of its eigenvalues, therefore, we have,

$$\mathrm{Tr}\left((\beta\mathbf{A})^k\right) = \sum_{i=1}^{n}(\beta\lambda_i)^k \tag{D.76}$$

□

Lemma D.4. *If* $Q(\omega) = \prod_{j=1}^{n}(\lambda_j^2 + \omega^2)$, *then*

$$\sum_{j=1}^{n} \frac{2\omega}{\omega^2 + \lambda_j^2} = \frac{Q'(\omega)}{Q(\omega)} \tag{D.77}$$

Proof. Consider $\log Q(\omega)$,

$$\begin{aligned} \log Q(\omega) &= \log \prod_{j=1}^{n} (\lambda_j^2 + \omega^2) \\ &= \sum_{j=1}^{n} \log(\lambda_j^2 + \omega^2) \end{aligned} \tag{D.78}$$

Taking the derivative w.r.t. ω on both sides to get,

$$\frac{Q'(\omega)}{Q(\omega)} = \sum_{j=1}^{n} \frac{2\omega}{\omega^2 + \lambda_j^2} \tag{D.79}$$

□

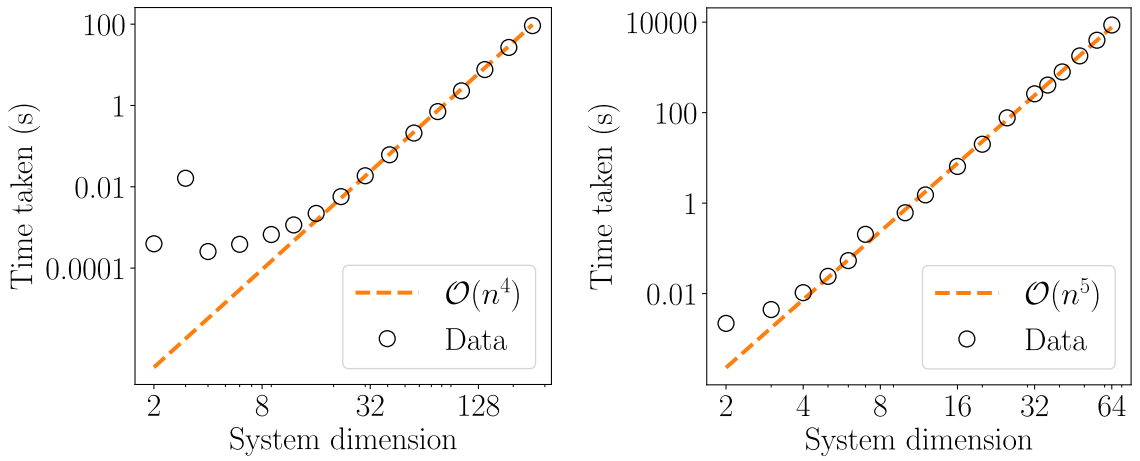


Figure D.1: Time complexity of the recursive algorithm. The time complexity of finding the coefficient matrices of the numerator and the coefficients of the polynomials in the denominator using, **Left:** Fixed precision computations ($O(n^4)$) and **Right:** Rational computations ($O(n^5)$).

D.2.2 Auxiliary Spectral Matrix

Theorem D.5. *Let* $\mathbf{G}$ *be a real square matrix,* $\mathbf{Y}$ *be a positive definite matrix, and* $\boldsymbol{\mathcal{T}}(\omega)$ *be defined as follows,*

$$\begin{aligned}\boldsymbol{\mathcal{T}}(\omega) &= (\omega\mathbf{I}-\mathbf{G})^{-1}\,\mathbf{Y}\,(\omega\mathbf{I}-\mathbf{G}^{\top})^{-1}\\ &= \frac{\sum_{\alpha=0}^{2n-2}\mathbf{P}_{\alpha}\omega^{\alpha}}{\sum_{\alpha=0}^{2n}q_{\alpha}\omega^{\alpha}}\end{aligned} \tag{D.80}$$

The numerator's matrix coefficients are given by the recursive equations,

$$\mathbf{P}_{\alpha-1} = q_{\alpha+1}\mathbf{Y} + \mathbf{G}\mathbf{P}_{\alpha} + \mathbf{P}_{\alpha}\mathbf{G}^{\top} - \mathbf{G}\mathbf{P}_{\alpha+1}\mathbf{G}^{\top} \tag{D.81}$$

for $\alpha \in \{1,\dots,2n-1\}$*, starting from* $\alpha = 2n-1$ *with* $\mathbf{P}_{2n} = \mathbf{P}_{2n-1} = \mathbf{0}$*. The scalar coefficients of the denominator can be recursively calculated using,*

$$q_{\alpha} = \frac{2}{2n-\alpha}\left[\mathrm{Tr}\left(\mathbf{Y}^{-1}\mathbf{G}\mathbf{P}_{\alpha}\mathbf{G}^{\top}\right) - \mathrm{Tr}\left(\mathbf{Y}^{-1}\mathbf{G}\mathbf{P}_{\alpha-1}\right)\right] \tag{D.82}$$

for $\alpha \in \{1,\dots,2n-1\}$*, and* $q_{2n} = 1$*.*

Proof. We follow an approach similar to the one presented in Section D.2. We can write the spectrum as the following rational function,

$$\begin{aligned}\boldsymbol{\mathcal{T}}(\omega) &= (\omega\mathbf{I}-\mathbf{G})^{-1}\,\mathbf{Y}\,(\omega\mathbf{I}-\mathbf{G}^{\top})^{-1}\\ &= \frac{\mathrm{adj}(\omega\mathbf{I}-\mathbf{G})\,\mathbf{Y}\,\mathrm{adj}(\omega\mathbf{I}-\mathbf{G}^{\top})}{\det(\omega\mathbf{I}-\mathbf{G})\det(\omega\mathbf{I}-\mathbf{G}^{\top})}\\ &= \frac{\sum_{\alpha=0}^{2n-2}\mathbf{P}_{\alpha}\omega^{\alpha}}{\sum_{\alpha=0}^{2n}q_{\alpha}\omega^{\alpha}}\end{aligned} \tag{D.83}$$

Upon rearrangement and left multiplying both sides with $(\omega\mathbf{I}-\mathbf{G})$ and right multiplying with $(\omega\mathbf{I}-\mathbf{G}^\top)$, we get,

$$\sum_{\alpha=0}^{2n} q_\alpha \omega^\alpha \mathbf{Y} = (\omega\mathbf{I}-\mathbf{G})\left(\sum_{\alpha=0}^{2n-2}\mathbf{P}_\alpha\omega^\alpha\right)\left(\omega\mathbf{I}-\mathbf{G}^\top\right) \tag{D.84}$$

Expanding the series on the left and right gives us,

$$\begin{aligned}\left(q_0+q_1\omega+q_2\omega^2+\ldots+q_{2n}\omega^{2n}\right)\mathbf{Y} = (\omega\mathbf{I}-\mathbf{G})&\left(\mathbf{P}_0+\mathbf{P}_1\omega+\ldots+\mathbf{P}_{2n-2}\omega^{2n-2}\right)\left(\omega\mathbf{I}-\mathbf{G}^\top\right)\\ =&\mathbf{G}\mathbf{P}_0\mathbf{G}^\top+\mathbf{G}\mathbf{P}_1\mathbf{G}^\top\omega+\ldots+\mathbf{G}\mathbf{P}_{2n-2}\mathbf{G}^\top\omega^{2n-2}\\ &-\left(\mathbf{P}_0\mathbf{G}^\top\omega+\mathbf{P}_1\mathbf{G}^\top\omega^2+\ldots+\mathbf{P}_{2n-2}\mathbf{G}^\top\omega^{2n-1}\right)\\ &-\left(\mathbf{G}\mathbf{P}_0\omega+\mathbf{G}\mathbf{P}_1\omega^2+\ldots+\mathbf{G}\mathbf{P}_{2n-2}\omega^{2n-1}\right)\\ &+\mathbf{P}_0\omega^2+\mathbf{P}_1\omega^3+\ldots+\mathbf{P}_{2n-2}\omega^{2n}\end{aligned} \tag{D.85}$$

Comparing the coefficients of $\omega^{\alpha+1}$ gives us the following recursive solution for $\mathbf{P}_\alpha$ (the matrix with the coefficients of the numerator),

$$\mathbf{P}_{\alpha-1} = q_{\alpha+1}\mathbf{Y}+\mathbf{G}\mathbf{P}_\alpha+\mathbf{P}_\alpha\mathbf{G}^\top-\mathbf{G}\mathbf{P}_{\alpha+1}\mathbf{G}^\top \tag{D.86}$$

To find a recursive solution for the coefficients of the denominator, we consider the Laplace transform of the following matrix and use the property of the resolvent of a matrix (Eq. (D.236)) to find,

$$\begin{aligned}\mathcal{L}\left\{\frac{\mathrm{d}}{\mathrm{d}t}e^{t\mathbf{G}}\right\} &= \mathcal{L}\left\{\mathbf{G}e^{t\mathbf{G}}\right\}\\ &= \mathbf{G}(\omega\mathbf{I}-\mathbf{G})^{-1}\end{aligned} \tag{D.87}$$

Then, using the property of the Laplace transform of the derivative of a function, we can write

the LHS of the equation above as,

$$\omega \mathcal{L}\left\{e^{t\mathbf{G}}\right\} - \mathbf{I} = \mathbf{G}(\omega\mathbf{I} - \mathbf{G})^{-1} \tag{D.88}$$

Now, consider the following matrix product,

$$\text{LHS} \coloneqq \left(\omega \mathcal{L}\left\{e^{t\mathbf{G}}\right\} - \mathbf{I}\right) \mathbf{Y} \left(\omega \mathcal{L}\left\{e^{t\mathbf{G}}\right\} - \mathbf{I}\right)^{\top} = \mathbf{G}\left[(\omega\mathbf{I} - \mathbf{G})^{-1}\, \mathbf{Y}\, (\omega\mathbf{I} - \mathbf{G}^{\top})^{-1}\right] \mathbf{G}^{\top} \coloneqq \text{RHS} \tag{D.89}$$

Further simplification of the LHS gives us,

$$\begin{aligned}
\text{LHS} &= \left(\omega \mathcal{L}\left\{e^{t\mathbf{G}}\right\} - \mathbf{I}\right) \mathbf{Y} \left(\omega \mathcal{L}\left\{e^{t\mathbf{G}}\right\} - \mathbf{I}\right)^{\top} \\
&= \omega^2 \mathcal{L}\left\{e^{t\mathbf{G}}\right\}\, \mathbf{Y}\, \mathcal{L}\left\{e^{t\mathbf{G}}\right\}^{\top} - \omega \mathcal{L}\left\{e^{t\mathbf{G}}\right\} \mathbf{Y} - \omega\, \mathbf{Y}\, \mathcal{L}\left\{e^{t\mathbf{G}}\right\}^{\top} + \mathbf{Y} \\
&= \omega^2 (\omega\mathbf{I} - \mathbf{G})^{-1}\, \mathbf{Y}\, (\omega\mathbf{I} - \mathbf{G})^{-\top} - \omega \mathcal{L}\left\{e^{t\mathbf{G}}\right\} \mathbf{Y} - \omega\, \mathbf{Y}\, \mathcal{L}\left\{e^{t\mathbf{G}}\right\}^{\top} + \mathbf{Y} \\
&= \omega^2 \left[(\omega\mathbf{I} - \mathbf{G})^{-1}\, \mathbf{Y}\, (\omega\mathbf{I} - \mathbf{G}^{\top})^{-1}\right] - \omega \mathcal{L}\left\{e^{t\mathbf{G}}\right\} \mathbf{Y} - \omega\, \mathbf{Y}\, \mathcal{L}\left\{e^{t\mathbf{G}}\right\}^{\top} + \mathbf{Y}
\end{aligned} \tag{D.90}$$

Since, from Eq. (D.83) we know the rational function form of $(\omega\mathbf{I} - \mathbf{G})^{-1}\, \mathbf{Y}\, (\omega\mathbf{I} - \mathbf{G}^{\top})^{-1}$, we substitute it in the LHS and the RHS. We further assume that $\mathbf{Y}$ is positive definite, therefore, its inverse exists, and multiply LHS and RHS with $\mathbf{Y}^{-1}$ on the left, which gives us the following equation,

$$\omega^2\, \mathbf{Y}^{-1} \left[\frac{\sum_{\alpha=0}^{2n-2} \mathbf{P}_\alpha \omega^\alpha}{\sum_{\alpha=0}^{2n} q_\alpha \omega^\alpha}\right] - \omega \left(\mathbf{Y}^{-1} \mathcal{L}\left\{e^{t\mathbf{G}}\right\} \mathbf{Y} + \mathcal{L}\left\{e^{t\mathbf{G}}\right\}^{\top}\right) + \mathbf{I} = \mathbf{Y}^{-1}\mathbf{G} \left[\frac{\sum_{\alpha=0}^{2n-2} \mathbf{P}_\alpha \omega^\alpha}{\sum_{\alpha=0}^{2n} q_\alpha \omega^\alpha}\right] \mathbf{G}^{\top} \tag{D.91}$$

Multiplying both sides with $\sum_{\alpha=0}^{2n} q_\alpha \omega^\alpha$ and taking the trace of both sides yields,

$$\begin{aligned}\omega^2 \operatorname{Tr}\left(\mathbf{Y}^{-1} \sum_{\alpha=0}^{2n-2} \mathbf{P}_\alpha \omega^\alpha\right) - \omega \sum_{\alpha=0}^{2n} q_\alpha \omega^\alpha \operatorname{Tr}\left(\mathbf{Y}^{-1} \mathcal{L}\left\{e^{t\mathbf{G}}\right\} \mathbf{Y} + \mathcal{L}\left\{e^{t\mathbf{G}}\right\}^\top\right) \\ + n \sum_{\alpha=0}^{2n} q_\alpha \omega^\alpha = \operatorname{Tr}\left(\mathbf{Y}^{-1}\mathbf{G}\left(\sum_{\alpha=0}^{2n-2} \mathbf{P}_\alpha \omega^\alpha\right)\mathbf{G}^\top\right)\end{aligned} \tag{D.92}$$

Since $\operatorname{Tr}\left(\mathbf{Y}^{-1}\mathcal{L}\left\{e^{t\mathbf{G}}\right\}\mathbf{Y}\right) = \operatorname{Tr}\left(\mathcal{L}\left\{e^{t\mathbf{G}}\right\}\right)$ and from Lemma D.6 we have that $\operatorname{Tr}\left(\mathcal{L}\left\{e^{t\mathbf{G}}\right\} + \mathcal{L}\left\{e^{t\mathbf{G}}\right\}^\top\right) = Q'(\omega)/Q(\omega)$, where $Q(\omega) = \sum_{\alpha=0}^{2n} q_\alpha \omega^\alpha$ and $Q'(\omega) = \sum_{\alpha=1}^{2n} \alpha q_\alpha \omega^{\alpha-1}$, the equation above simplifies to the following equation,

$$\operatorname{Tr}\left(\mathbf{Y}^{-1} \sum_{\alpha=0}^{2n-2} \mathbf{P}_\alpha \omega^{\alpha+2}\right) + \sum_{\alpha=0}^{2n} (n-\alpha)\, q_\alpha \omega^\alpha = \operatorname{Tr}\left(\mathbf{Y}^{-1}\mathbf{G}\left(\sum_{\alpha=0}^{2n-2} \mathbf{P}_\alpha \omega^\alpha\right)\mathbf{G}^\top\right) \tag{D.93}$$

Now we compare the coefficients of ω^α and find the following recurrent relation,

$$\operatorname{Tr}\left(\mathbf{Y}^{-1}\mathbf{P}_{\alpha-2}\right) + (n-\alpha)\, q_\alpha = \operatorname{Tr}\left(\mathbf{Y}^{-1}\mathbf{G}\mathbf{P}_\alpha\mathbf{G}^\top\right) \tag{D.94}$$

Substituting $\mathbf{P}_{\alpha-2} \longrightarrow q_\alpha \mathbf{Y} + \mathbf{G}\mathbf{P}_{\alpha-1} + \mathbf{P}_{\alpha-1}\mathbf{G}^\top - \mathbf{G}\mathbf{P}_\alpha\mathbf{G}^\top$ using Eq. (D.86), we get the following equation satisfied by q_α,

$$\begin{aligned}\operatorname{Tr}\left(\mathbf{Y}^{-1}\left(q_\alpha\mathbf{Y} + \mathbf{G}\mathbf{P}_{\alpha-1} + \mathbf{P}_{\alpha-1}\mathbf{G}^\top - \mathbf{G}\mathbf{P}_\alpha\mathbf{G}^\top\right)\right) + (n-\alpha)\, q_\alpha = \operatorname{Tr}\left(\mathbf{Y}^{-1}\mathbf{G}\mathbf{P}_\alpha\mathbf{G}^\top\right) \\ n q_\alpha + 2\operatorname{Tr}\left(\mathbf{Y}^{-1}\mathbf{G}\mathbf{P}_{\alpha-1}\right) - \operatorname{Tr}\left(\mathbf{Y}^{-1}\mathbf{G}\mathbf{P}_\alpha\mathbf{G}^\top\right) + (n-\alpha)\, q_\alpha = \operatorname{Tr}\left(\mathbf{Y}^{-1}\mathbf{G}\mathbf{P}_\alpha\mathbf{G}^\top\right)\end{aligned} \tag{D.95}$$

We have used the fact that $\operatorname{Tr}\left(\mathbf{Y}^{-1}\mathbf{G}\mathbf{P}_{\alpha-1}\right) = \operatorname{Tr}\left(\mathbf{P}_{\alpha-1}\mathbf{G}^\top\mathbf{Y}^{-1}\right) = \operatorname{Tr}\left(\mathbf{Y}^{-1}\mathbf{P}_{\alpha-1}\mathbf{G}^\top\right)$ which is true because $\mathbf{P}_{\alpha-1}$ and $\mathbf{Y}^{-1}$ are symmetric matrices. Solving for q_α gives us,

$$q_\alpha = \frac{2}{2n-\alpha}\left[\operatorname{Tr}\left(\mathbf{Y}^{-1}\mathbf{G}\mathbf{P}_\alpha\mathbf{G}^\top\right) - \operatorname{Tr}\left(\mathbf{Y}^{-1}\mathbf{G}\mathbf{P}_{\alpha-1}\right)\right] \tag{D.96}$$

□

Lemma D.6. *Let* $\mathrm{Tr}(\mathbf{G})$ *denote the trace of the matrix* $\mathbf{G}$, $\mathcal{L}\{f(t)\}$ *denote the Laplace transform of* $f(t)$ *with the complex variable* ω *and* $Q'(\omega)$ *be the derivative of the denominator of the rational function in Eq. (D.83),* $Q(\omega) = \sum_{\alpha=0}^{2n} q_\alpha \omega^\alpha$ *with respect to* ω*, then we have,*

$$\mathrm{Tr}\left(\mathcal{L}\left\{e^{t\mathbf{G}}\right\} + \mathcal{L}\left\{e^{t\mathbf{G}}\right\}^\top\right) = \frac{Q'(\omega)}{Q(\omega)}. \tag{D.97}$$

Proof. Consider the LHS,

$$\begin{aligned}
\mathrm{Tr}\left(\mathcal{L}\left\{e^{t\mathbf{G}}\right\} + \mathcal{L}\left\{e^{t\mathbf{G}}\right\}^\top\right) &= \mathcal{L}\left\{\mathrm{Tr}\left(e^{t\mathbf{G}} + e^{t\mathbf{G}^\top}\right)\right\} \\
&= \mathcal{L}\left\{\mathrm{Tr}\left(\sum_{r=0}^{\infty}\frac{t^r(\mathbf{G})^r}{r!} + \sum_{r=0}^{\infty}\frac{t^r(\mathbf{G}^\top)^r}{r!}\right)\right\} \\
&= \mathcal{L}\left\{\sum_{r=0}^{\infty}\mathrm{Tr}\left(\frac{t^r(\mathbf{G})^r}{r!}\right) + \sum_{r=0}^{\infty}\mathrm{Tr}\left(\frac{t^r(\mathbf{G}^\top)^r}{r!}\right)\right\}
\end{aligned} \tag{D.98}$$

If λ_j are the eigenvalues of $\mathbf{G}$ and $\mathbf{G}^\top$, we have,

$$\begin{aligned}
\mathrm{Tr}\left(\mathcal{L}\left\{e^{t\mathbf{G}}\right\} + \mathcal{L}\left\{e^{t\mathbf{G}}\right\}^\top\right) &= \mathcal{L}\left\{\sum_{r=0}^{\infty}\sum_{j=1}^{n}\frac{t^r(\lambda_j)^r}{r!} + \sum_{r=0}^{\infty}\sum_{j=1}^{n}\frac{t^r(\lambda_j)^r}{r!}\right\} \\
&= \mathcal{L}\left\{2\sum_{j=1}^{n}e^{t\lambda_j}\right\} \\
&= 2\sum_{j=1}^{n}\frac{1}{\omega-\lambda_j}
\end{aligned} \tag{D.99}$$

From Eq. (D.239), we have,

$$\begin{aligned}
Q(\omega) &= \det(\omega\mathbf{I}-\mathbf{G})\det(\omega\mathbf{I}-\mathbf{G}^\top) \\
&= \prod_{j=1}^{n}(\omega-\lambda_j)^2
\end{aligned} \tag{D.100}$$

Taking log on both sides and the derivative with respect to ω, we get,

$$\begin{aligned} \log Q(\omega) &= 2 \sum_{j=1}^{n} \log(\omega - \lambda_j) \\ \frac{Q'(\omega)}{Q(\omega)} &= 2 \sum_{j=1}^{n} \frac{1}{\omega - \lambda_j} \end{aligned} \tag{D.101}$$

Therefore,

$$\operatorname{Tr}\left(\mathcal{L}\left\{e^{t\mathbf{G}}\right\} + \mathcal{L}\left\{e^{t\mathbf{G}}\right\}^{\top}\right) = \frac{Q'(\omega)}{Q(\omega)}. \tag{D.102}$$

□

D.2.3 Integrated Covariance Matrix

Theorem D.7. *Let* $\mathbf{G}$ *be a convergent matrix, i.e., with a spectral radius less than 1,* $\mathbf{Y}$ *be a positive definite matrix, and* $\mathbf{R}$ *be a matrix with the following series expansion:*

$$\begin{aligned} \mathbf{R} &= (\mathbf{I} - \mathbf{G})^{-1} \mathbf{Y} \left(\mathbf{I} - \mathbf{G}^{\top}\right)^{-1} \\ &= \sum_{m=0}^{\infty} \sum_{\substack{j+k=m \\ j\geq 0,\, k\geq 0}} \mathbf{G}^j \mathbf{Y} \left(\mathbf{G}^{\top}\right)^k \\ &= \sum_{m=0}^{\infty} \mathbf{S}_m \end{aligned} \tag{D.103}$$

where $\mathbf{S}_m \coloneqq \sum_{\substack{j+k=m \\ j\geq 0,\, k\geq 0}} \mathbf{G}^j \mathbf{Y} \left(\mathbf{G}^{\top}\right)^k$*. The following algorithm provides a recursive method to compute* $\mathbf{S}_m$*,*

$$\begin{aligned} t_m &= \frac{2}{m}\left[\operatorname{Tr}\left(\mathbf{Y}^{-1}\mathbf{G}\mathbf{U}_{m-2}\mathbf{G}^{\top}\right) - \operatorname{Tr}\left(\mathbf{Y}^{-1}\mathbf{G}\mathbf{U}_{m-1}\right)\right] \\ \mathbf{U}_m &= t_m \mathbf{Y} + \mathbf{G}\mathbf{U}_{m-1} + \mathbf{U}_{m-1}\mathbf{G}^{\top} - \mathbf{G}\mathbf{U}_{m-2}\mathbf{G}^{\top} \\ \mathbf{S}_m &= \mathbf{U}_m - \sum_{k=0}^{m-1} t_{m-k}\, \mathbf{S}_k \end{aligned} \tag{D.104}$$

starting with $m = 0$ *until* $m = 2n$ *and the initial values* $t_0 = 1$ *and* $\mathbf{U}_{-2} = \mathbf{U}_{-1} = \mathbf{0}$.

Proof. Consider a matrix defined as follows,

$$\begin{aligned}\boldsymbol{\mathcal{T}}(\omega) &= (\omega\mathbf{I} - \mathbf{G})^{-1}\,\mathbf{Y}\,(\omega\mathbf{I} - \mathbf{G}^\top)^{-1} \\ &= \frac{1}{\omega^2}\left(\mathbf{I} - \frac{1}{\omega}\mathbf{G}\right)^{-1}\,\mathbf{Y}\,\left(\mathbf{I} - \frac{1}{\omega}\mathbf{G}^\top\right)^{-1}\end{aligned} \tag{D.105}$$

Since there always exists a value of ω such that $(\mathbf{I} - \mathbf{G}/\omega)$ and $(\mathbf{I} - \mathbf{G}^\top/\omega)$ are convergent, we can write the inverses as a convergent power series,

$$\begin{aligned}\boldsymbol{\mathcal{T}}(\omega) &= \frac{1}{\omega^2}\left(\sum_{j=0}^{\infty}\frac{1}{\omega^j}\mathbf{G}^j\right)\,\mathbf{Y}\,\left(\sum_{k=0}^{\infty}\frac{1}{\omega^k}\left(\mathbf{G}^\top\right)^k\right) \\ &= \frac{1}{\omega^2}\sum_{j,k=0}^{\infty}\frac{1}{\omega^{j+k}}\mathbf{G}^j\,\mathbf{Y}\,\left(\mathbf{G}^\top\right)^k \\ &= \frac{1}{\omega^2}\sum_{m=0}^{\infty}\frac{1}{\omega^m}\left(\sum_{\substack{j+k=m\\ j\geq 0,\,k\geq 0}}\mathbf{G}^j\,\mathbf{Y}\,\left(\mathbf{G}^\top\right)^k\right) \\ &= \frac{1}{\omega^2}\sum_{m=0}^{\infty}\frac{1}{\omega^m}\mathbf{S}_m\end{aligned} \tag{D.106}$$

where $\mathbf{S}_m$ represents the sum of the contribution of the paths of order (length) m. We now find $\mathbf{S}_m$ recursively. Using Theorem D.5, we get the following equation,

$$\frac{1}{\omega^2}\sum_{m=0}^{\infty}\frac{1}{\omega^m}\mathbf{S}_m = \frac{\sum_{\alpha=0}^{2n-2}\mathbf{P}_\alpha\omega^\alpha}{\sum_{\alpha=0}^{2n}q_\alpha\omega^\alpha} \tag{D.107}$$

alternatively, we have,

$$\left(\sum_{\alpha=0}^{2n}q_\alpha\omega^\alpha\right)\left(\sum_{m=0}^{\infty}\frac{1}{\omega^m}\mathbf{S}_m\right) = \sum_{\alpha=0}^{2n-2}\mathbf{P}_\alpha\omega^{\alpha+2} \tag{D.108}$$

Expanding the product gives us,

$$\sum_{\alpha=0}^{2n}\sum_{m=0}^{\infty} q_\alpha \omega^{\alpha-m}\mathbf{S}_m = \mathbf{P}_0\omega^2 + \mathbf{P}_1\omega^3 + \ldots + \mathbf{P}_{2n-2}\omega^{2n} \tag{D.109}$$

Now we compare the coefficients of ω^{2n-j} on both sides. To find the coefficient of ω^{2n-j} on the LHS of the equation above, we first set $\alpha - m = 2n - j$, which gives us $\alpha = 2n - j + m$ and then we find the values of α for $0 \leq m \leq j$ to ensure that $0 \leq \alpha \leq 2n$. This gives us the following relation,

$$\mathbf{S}_j = \mathbf{P}_{2n-2-j} - \sum_{k=0}^{j-1} q_{2n-j+k}\,\mathbf{S}_k \tag{D.110}$$

Making the following change of index, $j \longrightarrow 2n - 1 - \alpha$, gives us

$$\mathbf{S}_{2n-1-\alpha} = \mathbf{P}_{\alpha-1} - \sum_{k=0}^{2n-2-\alpha} q_{\alpha+k+1}\,\mathbf{S}_k \tag{D.111}$$

with $\mathbf{P}_\alpha$ and q_α given by the recursive algorithm in Theorem D.5. Therefore, the algorithm to recursively find $\mathbf{S}_0, \mathbf{S}_1, \ldots, \mathbf{S}_{2n}$ is given by,

$$\begin{aligned}
\mathbf{P}_{\alpha-1} &= q_{\alpha+1}\mathbf{Y} + \mathbf{G}\mathbf{P}_\alpha + \mathbf{P}_\alpha\mathbf{G}^\top - \mathbf{G}\mathbf{P}_{\alpha+1}\mathbf{G}^\top \\
\mathbf{S}_{2n-1-\alpha} &= \mathbf{P}_{\alpha-1} - \sum_{k=0}^{2n-2-\alpha} q_{\alpha+k+1}\,\mathbf{S}_k \\
q_\alpha &= \frac{2}{2n-\alpha}\left[\mathrm{Tr}\left(\mathbf{Y}^{-1}\mathbf{G}\mathbf{P}_\alpha\mathbf{G}^\top\right) - \mathrm{Tr}\left(\mathbf{Y}^{-1}\mathbf{G}\mathbf{P}_{\alpha-1}\right)\right]
\end{aligned} \tag{D.112}$$

starting with $\alpha = 2n - 1$ until $\alpha = -1$. Note that $\mathbf{P}_{2n} = \mathbf{P}_{2n-1} = \mathbf{P}_{-1} = \mathbf{P}_{-2} = \mathbf{0}$, $q_{2n} = 1$ and $q_{-1} = 0$. Now, we first simplify this algorithm by first making the following substitution: $q_\alpha = t_{2n-\alpha}$ and

$\mathbf{P}_\alpha = \mathbf{U}_{2n-2-\alpha}$. This gives us the following recurrence relation,

$$\begin{aligned} t_{2n-1-\alpha} &= \frac{2}{2n-1-\alpha}\left[\mathrm{Tr}\left(\mathbf{Y}^{-1}\mathbf{G}\mathbf{U}_{2n-3-\alpha}\mathbf{G}^\top\right) - \mathrm{Tr}\left(\mathbf{Y}^{-1}\mathbf{G}\mathbf{U}_{2n-2-\alpha}\right)\right] \\ \mathbf{U}_{2n-1-\alpha} &= t_{2n-1-\alpha}\mathbf{Y} + \mathbf{G}\mathbf{U}_{2n-2-\alpha} + \mathbf{U}_{2n-2-\alpha}\mathbf{G}^\top - \mathbf{G}\mathbf{U}_{2n-3-\alpha}\mathbf{G}^\top \\ \mathbf{S}_{2n-1-\alpha} &= \mathbf{U}_{2n-1-\alpha} - \sum_{k=0}^{2n-2-\alpha} t_{2n-1-\alpha-k}\,\mathbf{S}_k \end{aligned} \tag{D.113}$$

Finally, we make the following index change: $m = 2n-1-\alpha$ which gives us the recursive relation,

$$\begin{aligned} t_m &= \frac{2}{m}\left[\mathrm{Tr}\left(\mathbf{Y}^{-1}\mathbf{G}\mathbf{U}_{m-2}\mathbf{G}^\top\right) - \mathrm{Tr}\left(\mathbf{Y}^{-1}\mathbf{G}\mathbf{U}_{m-1}\right)\right] \\ \mathbf{U}_m &= t_m\mathbf{Y} + \mathbf{G}\mathbf{U}_{m-1} + \mathbf{U}_{m-1}\mathbf{G}^\top - \mathbf{G}\mathbf{U}_{m-2}\mathbf{G}^\top \\ \mathbf{S}_m &= \mathbf{U}_m - \sum_{k=0}^{m-1} t_{m-k}\,\mathbf{S}_k \end{aligned} \tag{D.114}$$

starting with $m = 0$ until $m = 2n$ and the following initial values given: $t_0 = 1$ and $\mathbf{U}_{-2} = \mathbf{U}_{-1} = \mathbf{0}$.

□

D.3 Element-wise Solution

In this section, we describe an element-wise solution for the rational functions of the auto- and cross-spectrum for a general N-dimensional system. We first assume that the matrix $\mathbf{L}$ is square, i.e., $\mathbf{L} \in \mathbb{R}^{n\times n}$ and therefore, $\mathbf{D} \in \mathbb{R}^{n\times n}$. The result can easily be extended to a rectangular $\mathbf{L} \in \mathbb{R}^{n\times m}$ matrix by defining the positive semidefinite matrix $\mathbf{C} = \mathbf{L}\,\mathbf{D}\,\mathbf{L}^\top$ and then computing a new set of $\mathbf{L}$ and $\mathbf{D}$ matrices by LDL decomposition, such that $\mathbf{L}, \mathbf{D} \in \mathbb{R}^{n\times n}$.

We start by rewriting the matrix inverse in Eq. (D.34) in terms of the corresponding adjoints and determinants of the matrices denoted by adj(.) and |.|, respectively. From Eq. (D.5), we know

that the diffusion matrix $\mathbf{D}$ can be written as,

$$\mathbf{D} = \mathbf{S}\,\mathbf{S}^\top \tag{D.115}$$

Substituting in Eq. (D.34),

$$\begin{aligned}\boldsymbol{\mathcal{S}}(\omega) &= \frac{\text{adj}(\mathbf{J} + i\omega\mathbf{I})\,\mathbf{L}\,\mathbf{S}\,\mathbf{S}^\top\,\mathbf{L}^\top\,\text{adj}^\top(\mathbf{J} - i\omega\mathbf{I})}{|\mathbf{J} + i\omega\mathbf{I}|\,|\mathbf{J} - i\omega\mathbf{I}|} \\ &= \frac{\text{adj}(\mathbf{J} + i\omega\mathbf{I})\,\mathbf{L}\,\mathbf{S}\;\;(\text{adj}(\mathbf{J} + i\omega\mathbf{I})\,\mathbf{L}\,\mathbf{S})^*}{|\mathbf{J} + i\omega\mathbf{I}|\,|\mathbf{J} - i\omega\mathbf{I}|} \\ &= \frac{\mathbf{Z}(\omega)}{Q(\omega)}\end{aligned} \tag{D.116}$$

Where $\mathbf{Z}(\omega)$ is a matrix containing the polynomial expansion for the numerators of both auto and cross spectrums, in terms of ω; and $Q(\omega)$ is the polynomial expansion of the denominator.

D.3.1 Denominator and Newton's Identities

We derive the coefficients of the polynomial expansion of the denominator, $Q(\omega)$. First, we will introduce elementary symmetric polynomials, a common tool used throughout this text, which shows how we can express various terms in the numerator and denominator as polynomials of ω. To demonstrate the analysis, which uses elementary symmetric polynomials, we show how we can expand the denominator into a polynomial in ω, and find its coefficients. First, we show a brute force method of calculating the said coefficients and then demonstrate that we get the same expressions using elementary symmetric polynomials, and finally use the function definitions from Section D.4 to write a compact expression for the polynomial. We know from Eq. (D.116) that the denominator $Q(\omega)$ can be written as the product of the determinants,

$$Q(\omega) = |\mathbf{J} + i\omega\mathbf{I}||\mathbf{J} - i\omega\mathbf{I}| \tag{D.117}$$

where $\mathbf{J} \in \mathbb{R}^{n\times n}$. If λ_i are the eigenvalues of the matrix $\mathbf{J}$, using Eq. (D.233), we have,

$$|\mathbf{J} \pm i\omega| = \prod_{i=1}^{n} (\lambda_i \pm i\omega) \tag{D.118}$$

Therefore, we can express the denominator as an even-powered polynomial,

$$\begin{aligned} Q(\omega) &= \prod_{i=1}^{n} (\lambda_i + i\omega)(\lambda_i - i\omega) \\ &= \prod_{i=1}^{n} (\lambda_i^2 + \omega^2) \\ &= q_0 + q_1\omega^2 + q_2\omega^4 + \cdots + q_n\omega^{2n} \end{aligned} \tag{D.119}$$

We also note that the property above is true even if λ is complex. We show this by dividing the product into two parts: first, when the eigenvalues are purely real (cardinality of $n - 2m$) and second, when they are complex (m pairs of conjugate complex pairs). Since the matrix $\mathbf{J}$ is real, its complex eigenvalues occur as complex conjugate pairs. Therefore, we can write,

$$Q(\omega) = \prod_{i=1}^{n-2m} (\lambda_i + i\omega)(\lambda_i - i\omega) \prod_{j=1}^{m} (\lambda_j + i\omega)(\lambda_j - i\omega)(\overline{\lambda}_j + i\omega)(\overline{\lambda}_j - i\omega) \tag{D.120}$$

On further simplification, we can write the equation as,

$$\begin{aligned} Q(\omega) &= \prod_{i=1}^{n-2m} (\lambda_i^2 + \omega^2) \prod_{j=1}^{m} (\lambda_j^2 + \omega^2)(\overline{\lambda}_j^2 + \omega^2) \\ &= \prod_{i=1}^{n} (\lambda_i^2 + \omega^2) \end{aligned} \tag{D.121}$$

Now we demonstrate how we can calculate the coefficients of the polynomials using brute force for a 4-dimensional system. The expansion of Eq. (D.121) can be written as,

$$Q(\omega) = q_0 + q_1\omega^2 + q_2\omega^4 + q_3\omega^6 + q^4\omega^8 \tag{D.122}$$

We find the different coefficients q_k using the properties of matrices, specifically we use the properties from Eq. (D.233) and Eq. (D.234) to find,

$$q_0 = \lambda_1^2\lambda_2^2\lambda_3^2\lambda_4^2 = \prod_{i=1}^{n} \lambda_i = \det^2(\mathbf{J}) \tag{D.123}$$

$$\begin{aligned} q_1 &= \lambda_1^2\lambda_2^2\lambda_3^2 + \lambda_1^2\lambda_2^2\lambda_4^2 + \lambda_1^2\lambda_3^2\lambda_4^2 + \lambda_2^2\lambda_3^2\lambda_4^2 \\ &= \frac{(\sum_{i=1}^{n} \lambda_i^2)^3 + 2\sum_{i=1}^{n} \lambda_i^6 - 3\sum_{i=1}^{n} \lambda_i^4 \sum_{i=1}^{n} \lambda_i^2}{6} \\ &= \frac{(\mathrm{Tr}(\mathbf{J}^2))^3 + 2\,\mathrm{Tr}(\mathbf{J}^6) - 3\,\mathrm{Tr}(\mathbf{J}^4)\,\mathrm{Tr}(\mathbf{J}^2)}{6} \end{aligned} \tag{D.124}$$

$$q_2 = \lambda_1^2\lambda_2^2 + \lambda_1^2\lambda_3^2 + \lambda_1^2\lambda_4^2 + \lambda_2^2\lambda_3^2 + \lambda_2^2\lambda_4^2 + \lambda_3^2\lambda_4^2 = \frac{(\sum_{i=1}^{n} \lambda_i^2)^2 - \sum_{i=1}^{n} \lambda_i^4}{2} = \frac{(\mathrm{Tr}(\mathbf{J}^2))^2 - \mathrm{Tr}(\mathbf{J}^4)}{2} \tag{D.125}$$

$$q_3 = \lambda_1^2 + \lambda_2^2 + \lambda_3^2 + \lambda_4^2 = \sum_{i=1}^{n} \lambda_i^2 = \mathrm{Tr}(\mathbf{J}^2) \tag{D.126}$$

$$q_4 = 1 \tag{D.127}$$

Therefore for a 4-D system, we can write the denominator as,

$$Q(\omega) = \det^2(\mathbf{J}) + \frac{\mathrm{Tr}(\mathbf{J}^2)^3 + 2\,\mathrm{Tr}(\mathbf{J}^6) - 3\,\mathrm{Tr}(\mathbf{J}^4)\,\mathrm{Tr}(\mathbf{J}^2)}{6}\omega^2 + \frac{\mathrm{Tr}(\mathbf{J}^2)^2 - \mathrm{Tr}(\mathbf{J}^4)}{2}\omega^4 + \mathrm{Tr}(\mathbf{J}^2)\omega^6 + \omega^8 \tag{D.128}$$

Alternatively, we can find the general solution for any dimensional system using Newton's identities and thereby write the coefficients of different powers of ω in the denominator. To use this method, we first need to introduce Newton's identities. We give a brief primer on Newton's identities and show how we can express the various orders of elementary symmetric polynomials in terms of Bell polynomials, then continue with our analysis. Let $x_1, x_2, ..., x_n$ be the variables, we define $r^k(x_1, x_2, ..., x_n)$ to be the k^{th} power sum (for $k \geq 1$),

$$r^k(x_1, x_2, ..., x_n) = \sum_{i=1}^{n} x_i^k \tag{D.129}$$

and the elementary symmetric polynomial $e^l(x_1, x_2, ..., x_n)$ (for $l \geq 0$),

$$\begin{aligned}
e^0(x_1, x_2, ..., x_n) &= 1 \\
e^1(x_1, x_2, ..., x_n) &= x_1 + x_2 + ... + x_n \\
e^2(x_1, x_2, ..., x_n) &= \sum\nolimits_{1<i<j<n} x_i x_j \\
&\vdots \\
e^k(x_1, x_2, ..., x_n) &= \sum\nolimits_{1<i<j<...<t<n} \underbrace{x_i x_j ... x_t}_{\text{k vars}} \\
e^n(x_1, x_2, ..., x_n) &= x_1 x_2 ... x_n
\end{aligned} \tag{D.130}$$

that obey the so-called Newton's identities, expressed concisely as,

$$k e^k(x_1, x_2, ..., x_n) = \sum_{i=1}^{k} (-1)^{i-1} e^{k-i}(x_1, x_2, ..., x_n) r^i(x_1, x_2, ..., x_n) \tag{D.131}$$

We note that we can write the coefficients of the polynomial in ω, q_k, in terms of elementary symmetric polynomials of various orders, $e^i(\lambda_1^2, \lambda_2^2, ..., \lambda_n^2)$,

$$Q(\omega) = \prod_{i=1}^{n} (\lambda_i^2 + \omega^2) = \sum_{i=0}^{n} e^i(\lambda_1^2, \lambda_2^2, ..., \lambda_n^2) \omega^{2(n-i)} \tag{D.132}$$

Noting that $e^0(\lambda_1^2, \lambda_2^2, ..., \lambda_n^2) = q_4 = 1$ by definition, and $e^1(\lambda_1^2, \lambda_2^2, ..., \lambda_n^2) = q_3 = \sum_{i=1}^{n} \lambda_i^2 = \text{Tr}(\mathbf{J}^2)$ and that r^k can be written as follows,

$$r^k(\lambda_1^2, \lambda_2^2, ..., \lambda_n^2) = \sum_{j=1}^{n} \lambda_j^{2k} = \text{Tr}(\mathbf{J}^{2k}) \tag{D.133}$$

we can find $e^i(\lambda_1^2, \lambda_2^2, ..., \lambda_n^2)$ recursively for any dimension using Eq. (D.131).

$$\begin{aligned}
e^2(\lambda_1^2, \lambda_2^2, ..., \lambda_n^2) &= q_2 \\
&= \frac{e^1 r^1 - e^0 r^2}{2} \\
&= \frac{\mathrm{Tr}(\mathbf{J}^2)\,\mathrm{Tr}(\mathbf{J}^2) - \mathrm{Tr}(\mathbf{J}^4)}{2} \\
&= \frac{\mathrm{Tr}(\mathbf{J}^2)^2 - \mathrm{Tr}\,(\mathbf{J}^4)}{2} \\
e^3(\lambda_1^2, \lambda_2^2, ..., \lambda_n^2) &= q_1 \\
&= \frac{e^2 r^1 - e^1 r^2 + e^0 r^3}{3} \\
&= \frac{(\mathrm{Tr}(\mathbf{J}^2)^2 - \mathrm{Tr}(\mathbf{J}^4))\,\mathrm{Tr}(\mathbf{J}^2)/2 - \mathrm{Tr}(\mathbf{J}^2)\,\mathrm{Tr}(\mathbf{J}^4) + \mathrm{Tr}(\mathbf{J}^6)}{3} \\
&= \frac{\mathrm{Tr}(\mathbf{J}^2)^3 + 2\,\mathrm{Tr}(\mathbf{J}^6) - 3\,\mathrm{Tr}(\mathbf{J}^4)\,\mathrm{Tr}(\mathbf{J}^2)}{6} \\
e^4(\lambda_1^2, \lambda_2^2, ..., \lambda_n^2) &= q_0 \\
&= \prod_{i=1}^{n} \lambda_i^2 \\
&= \det{}^2(\mathbf{J})
\end{aligned} \tag{D.134}$$

We thus confirm that we find the same expressions for the coefficients (Eq. (D.123)-(D.127)) using the brute force method and using Newton's identities.

We can also express the elementary symmetric polynomial, e^k, in terms of Bell polynomial as follows,

$$e^k = \frac{(-1)^k}{k!} B(-r^1, -1!r^2, ..., -(k-1)!r^k) \tag{D.135}$$

where B is the complete exponential Bell polynomial and can be calculated using the determinant of the upper Hessenberg matrix, $\mathbb{B}^k$, with determinant evaluation in $\mathbb{O}(n^2)$. In general, for a Bell polynomial defined on the set of inputs $(x_1, x_2, ..., x_k)$, we have,

$$B(x_1, x_2, ..., x_k) = \det(\mathbb{B}^k(x_1, x_2, ..., x_k)) \tag{D.136}$$

where the matrix $\mathbb{B}^k(x_1, x_2, ..., x_k)$ is,

$$\mathbb{B}^k(x_1, x_2, ..., x_k) = \begin{bmatrix} \frac{x_1}{0!} & \frac{x_2}{1!} & \frac{x_3}{2!} & \cdots & \frac{x_{k-1}}{(k-2)!} & \frac{x_k}{(k-1)!} \\ -1 & \frac{x_1}{0!} & \frac{x_2}{1!} & \cdots & \frac{x_{k-2}}{(k-3)!} & \frac{x_{k-1}}{(k-2)!} \\ 0 & -2 & \frac{x_1}{0!} & \dots & \frac{x_{k-3}}{(k-4)!} & \frac{x_{k-2}}{(k-3)!} \\ \vdots & & \ddots & & \vdots & \vdots \\ 0 & 0 & 0 & \dots & -(k-1) & \frac{x_1}{0!} \end{bmatrix}. \tag{D.137}$$

Now, for the input $\mathbf{r}^k = (-r^1, -1!r^2, ..., -(k-1)!r^k)$ to the Bell polynomial, we have the simplified $\mathbb{B}^k(\mathbf{r}^k)$ matrix,

$$\mathbb{B}^k(\mathbf{r}^k) = \begin{bmatrix} -r^1 & -r^2 & -r^3 & \dots & -r^{k-1} & -r^k \\ -1 & -r^1 & -r^2 & \dots & -r^{k-2} & -r^{k-1} \\ 0 & -2 & -r^1 & \dots & -r^{k-3} & -r^{k-2} \\ \vdots & & \ddots & & \vdots & \vdots \\ 0 & 0 & 0 & \dots & -(k-1) & -r^1 \end{bmatrix} \tag{D.138}$$

such that,

$$B(\mathbf{r}^k) = \det(\mathbb{B}^k(\mathbf{r}^k)) \tag{D.139}$$

Recall from Eq. (D.133) that $r^k(\lambda_1, \lambda_2, \dots, \lambda_n) = \mathrm{Tr}(\mathbf{X}^k)$. Therefore, we define,

$$\mathbf{r}^k(\mathbf{X}) = (-\mathrm{Tr}(\mathbf{X}), -1!\,\mathrm{Tr}(\mathbf{X}^2), -2!\,\mathrm{Tr}(\mathbf{X}^3), ..., -(k-1)!\,\mathrm{Tr}(\mathbf{X}^k)) \tag{D.140}$$

and,

$$e^k = \frac{(-1)^k}{k!} B(\mathbf{r}^k(\mathbf{X})) \tag{D.141}$$

where,

$$B(\mathbf{r}^k(\mathbf{X})) = \det \begin{bmatrix} -\operatorname{Tr}(\mathbf{X}) & -\operatorname{Tr}(\mathbf{X}^2) & -\operatorname{Tr}(\mathbf{X}^3) & \dots & -\operatorname{Tr}(\mathbf{X}^{k-1}) & -\operatorname{Tr}(\mathbf{X}^k) \\ -1 & -\operatorname{Tr}(\mathbf{X}) & -\operatorname{Tr}(\mathbf{X}^2) & \dots & -\operatorname{Tr}(\mathbf{X}^{k-2}) & -\operatorname{Tr}(\mathbf{X}^{k-1}) \\ 0 & -2 & -\operatorname{Tr}(\mathbf{X}) & \dots & -\operatorname{Tr}(\mathbf{X}^{k-3}) & -\operatorname{Tr}(\mathbf{X}^{k-2}) \\ \vdots & & \ddots & & \vdots & \vdots \\ 0 & 0 & 0 & \dots & -(k-1) & -\operatorname{Tr}(\mathbf{X}) \end{bmatrix} \tag{D.142}$$

We can then express q_α, the coefficient of $\omega^{2\alpha}$ in the expansion of Eq. (D.122), as

$$q_\alpha = \frac{(-1)^{n-\alpha}}{(n-\alpha)!} B(\mathbf{r}^{n-\alpha}(\mathbf{J}^2)) \tag{D.143}$$

This equation forms the basis of our "canonical functions" definitions in Section D.4. Thus, we express the expansion of the polynomial in the denominator as,

$$\begin{aligned} Q(\omega) &= q_0 + q_1\omega^2 + q_2\omega^4 + \cdots + q_n\omega^{2n} \\ &= d(\omega; \mathbf{J}) \end{aligned} \tag{D.144}$$

and q_α can be defined in terms of the canonical function $d^\alpha(\mathbf{J})$ as,

$$q_\alpha = d^\alpha(\mathbf{J}). \tag{D.145}$$

D.3.2 Numerator

Now, we move on to finding the rational function solution for the numerator. This corresponds to finding the polynomial expansion (in ω) of the diagonal (off-diagonal) elements of the numerator

for auto(cross)-spectrum $\mathbf{Z}(\omega)$, of $\boldsymbol{\mathcal{S}}(\omega)$. Following Eq. (D.116), we have,

$$\begin{aligned}\mathbf{Z}(\omega) =& \text{adj}(\mathbf{J} + i\omega\mathbf{I})\,\mathbf{L}\,\mathbf{S}\;\left(\text{adj}(\mathbf{J} + i\omega\mathbf{I})\,\mathbf{L}\,\mathbf{S}\right)^{*} \\ =& \mathbf{P}(\omega) + i\omega\mathbf{P}'(\omega)\end{aligned} \tag{D.146}$$

If a_{ij} are the (i, j) elements of the matrix $\mathbf{J}$, the matrix $\mathbf{J} + i\omega\mathbf{I}$ is given by,

$$\mathbf{J} + i\omega\mathbf{I} = \begin{bmatrix} a_{11} + i\omega & \dots & a_{1n} \\ \vdots & \ddots & \vdots \\ a_{n1} & \dots & a_{nn} + i\omega \end{bmatrix} \tag{D.147}$$

Put simply, the numerator is obtained by multiplying the matrix $\text{adj}(\mathbf{J} + i\omega\mathbf{I})\,\mathbf{L}\,\mathbf{S}$ with its conjugate transpose. Note that from Eq. (D.146), we have that the elements of $\mathbf{Z}(\omega)$ take the form

$$\begin{aligned} Z^{ij}(\omega) &= P^{ij}(\omega) + i\omega P^{ij\prime}(\omega) \\ &= \sum_{\alpha=0}^{n-1} p_{\alpha}^{ij}\omega^{2\alpha} + i\omega\sum_{\alpha=0}^{n-2} p_{\alpha}^{ij\prime}\omega^{2\alpha} \end{aligned} \tag{D.148}$$

We can write the matrix $\text{adj}(\mathbf{J} + i\omega\mathbf{I})\,\mathbf{L}\,\mathbf{S}$ in terms of the corresponding cofactor matrix as,

$$\text{adj}(\mathbf{J} + i\omega\mathbf{I})\,\mathbf{L}\,\mathbf{S} = \begin{bmatrix} M_{11} & \dots & (-1)^{1+n}M_{1n} \\ -M_{21} & . & (-1)^{2+n}M_{2n} \\ \vdots & \ddots & \vdots \\ (-1)^{n+1}M_{n1} & \dots & (-1)^{n+n}M_{nn} \end{bmatrix}^{\top} \begin{bmatrix} \sigma_1 l_{11} & \sigma_2 l_{12} & \dots & \sigma_n l_{1n} \\ \sigma_1 l_{21} & \sigma_2 l_{22} & \dots & \sigma_n l_{2n} \\ \vdots & & \ddots & \vdots \\ \sigma_1 l_{n1} & \sigma_2 l_{n2} & \dots & \sigma_n l_{nn} \end{bmatrix} \tag{D.149}$$

Here the minor M_{ij} is the determinant of the submatrix $\mathbf{M}_{ij} \in \mathbb{C}^{n-1\times n-1}$, formed by excluding the i^{th} row and j^{th} column of the matrix $\mathbf{J} + i\omega\mathbf{I}$. Now, the (a, b) element of the resulting matrix product can be written as $\sum_{o=1}^{n}(-1)^{a+o}M_{oa}(\sigma_b l_{ob})$. Similarly, the (x, y) element of the matrix $\overline{\text{adj}(\mathbf{J} + i\omega\mathbf{I})\,\mathbf{L}\,\mathbf{S}}$ can be written as $\sum_{p=1}^{n}(-1)^{y+p}\overline{M}_{py}(\sigma_x l_{px})$. To extract the (i, j) element of $\mathbf{Z}(\omega)$,

we expand the expression above to find,

$$\begin{aligned} Z^{ij}(\omega) &= \sum_{m=1}^{n}\left(\sum_{o=1}^{n}(-1)^{i+o}M_{oi}\sigma_m l_{om}\right)\left(\sum_{p=1}^{n}(-1)^{j+p}\overline{M}_{pj}\sigma_m l_{pm}\right) \\ &= \sum_{m=1}^{n}\sigma_m^2\sum_{o=1}^{n}\sum_{p=1}^{n}(-1)^{i+j+o+p}l_{om}l_{pm}M_{oi}\overline{M}_{pj} \end{aligned} \tag{D.150}$$

In the following sections, we consider $Z^{ij}(\omega)$ in 2 distinct settings: $i = j$ and $i \neq j$ to find the real and complex rational functions for auto-spectrum and cross-spectrum, respectively.

D.3.2.1 Auto-spectrum

We first find the analytical expressions for the numerator of the auto-spectrum, that correspond to the diagonal elements of $\mathbf{Z}(\omega)$. To facilitate our calculations, we split the expression into 4 parts,

$$\begin{aligned} Z^{ii}(\omega) = \sum_{m=1}^{n}\sigma_m^2\Bigg(& l_{im}^2 M_{ii}\overline{M}_{ii} + \sum_{\substack{j=1\\ j\neq i}}^{n} l_{jm}^2 M_{ji}\overline{M}_{ji} + 2\sum_{\substack{j=1\\ j\neq i}}^{n}(-1)^{i+j}l_{im}l_{jm}\mathrm{Re}[M_{ii}\overline{M}_{ji}] \\ &+ 2\sum_{\substack{j=1\\ j\neq i}}^{n}\sum_{\substack{k=1\\ k\neq i}}^{j-1}(-1)^{j+k}l_{jm}l_{km}\mathrm{Re}[M_{ji}\overline{M}_{ki}]\Bigg) \end{aligned} \tag{D.151}$$

Note that the expression above is purely real, therefore, $\mathbf{Z}(\omega) = \mathbf{P}(\omega)$ and, $Z^{ii}(\omega) = P^{ii}(\omega)$. The minor matrices, $\mathbf{M}_{ij}$, contain some entries with $i\omega$ added to them. Since exchanging the rows and columns of a matrix only changes the sign of the determinant, we systematically define the transformations on the $\mathbf{M}_{ij}$ such that the entries with $i\omega$ appear on the diagonals only. But before defining the transformation, we define the matrices $\mathbf{N}_{ij} \in \mathbb{R}^{n-1\times n-1}$ (with associated minors $N_{ij} \in \mathbb{R}$), which are formed simply by removing the terms $i\omega$ from the corresponding $\mathbf{M}_{ij}$ matrix. Then, by applying a transformation, summarized as an algorithm in Fig. 5.3 of the main text, to $\mathbf{N}_{ij}$, we get the matrices $\mathbf{O}_{ij} \in \mathbb{R}^{n-1\times n-1}$, in terms of which the solution is defined. Therefore, the

$\mathbf{O}_{ij}$ matrices can be calculated directly from the Jacobian matrix $\mathbf{J}$. We show how to construct the matrices for 2, 3, and 4D systems in Fig. 5.3 of the main text.

Note that for $i = j$, the transformation is an identity and all the elements of $\mathbf{M}_{ij}$ containing $\iota\omega$ appear on the diagonal of the matrix. Therefore, we can write $M_{ii} = |\mathbf{O}_{ii} + i\omega\mathbf{I}|$. When $i \neq j$, the exchange of rows and columns in this transformation yields the following relation between the determinants,

$$O_{ij} = (-1)^{\gamma} N_{ij} \tag{D.152}$$

where $\gamma = |i - j| - \delta_{ij}$ are the number of row/column exchanges performed in the transformation, and δ_{ij} is the Kronecker delta. Additionally, we introduce the standard unit matrix $\mathbf{E}_\beta = \mathbf{e}_\beta \mathbf{e}_\beta{}^\top$ associated with the matrix $\mathbf{O}_{ij}$, where $\mathbf{e}_\beta \in \{0, 1\}^{n-1\times 1}$ is the standard unit vector equal to 1 only at index β and 0 everywhere else. The parameter β (for $i \neq j$) is found to be $\beta = \min(i, j)$, which allows us to express the minors as

$$M_{ij} = (-1)^{|i-j|-\delta_{ij}} |\mathbf{O}_{ij} + i\omega\mathbf{I} - i\omega\mathbf{E}_\beta| \tag{D.153}$$

The purpose of this decomposition is that it allows us to write

$$|\mathbf{O}_{ij} + i\omega\mathbf{I} - i\omega\mathbf{E}_\beta| = |\mathbf{O}_{ij} + i\omega\mathbf{I}| - i\omega \mathbf{e}_\beta{}^\top \mathrm{adj}(\mathbf{O}_{ij} + i\omega\mathbf{I})\mathbf{e}_\beta \tag{D.154}$$

Since the non-zero element of $\mathbf{e}_\beta$ lies at the index β, we can simplify the determinant above by defining a submatrix ($\mathbf{O}'_{ij} \in \mathbb{R}^{n-2\times n-2}$) of $\mathbf{O}_{ij}$ formed by removing the row and column at the index β. The equation then simplifies to,

$$|\mathbf{O}_{ij} + i\omega\mathbf{I} - i\omega\mathbf{E}_\beta| = |\mathbf{O}_{ij} + i\omega\mathbf{I}| - i\omega|\mathbf{O}'_{ij} + i\omega\mathbf{I}| \tag{D.155}$$

This property forms the basis for constructing the canonical functions defined in Section D.4.

Upon replacing the matrices in Eq. (D.151) with matrices $\mathbf{O}_{ij}$, we get,

$$\begin{aligned}
P^{ii}(\omega) = \sum_{m=1}^{n} \sigma_m^2 \Bigg(& l_{im}^2 |\mathbf{O}_{ii} + i\omega\mathbf{I}| \overline{|\mathbf{O}_{ii} + i\omega\mathbf{I}|} \\
& + 2 \sum_{\substack{j=1 \\ j\neq i}}^{n} (-1)^{i+j} l_{im} l_{jm} \mathrm{Re}\Big[|\mathbf{O}_{ii} + i\omega\mathbf{I}| (-1)^{|i-j|-1} \overline{|\mathbf{O}_{ji} + i\omega\mathbf{I} - i\omega\mathbf{E}_{\min(i,j)}|} \Big] \\
& + \sum_{\substack{j=1 \\ j\neq i}}^{n} l_{jm}^2 (-1)^{|i-j|-1} |\mathbf{O}_{ji} + i\omega\mathbf{I} - i\omega\mathbf{E}_{\min(i,j)}| (-1)^{|i-j|-1} \overline{|\mathbf{O}_{ji} + i\omega\mathbf{I} - i\omega\mathbf{E}_{\min(i,j)}|} \\
& + 2 \sum_{\substack{j=1 \\ j\neq i}}^{n} \sum_{\substack{k=1 \\ k\neq i}}^{j-1} (-1)^{j+k} l_{jm} l_{km} \mathrm{Re}\Bigg[(-1)^{|j-i|-1} |\mathbf{O}_{ji} + i\omega\mathbf{I} - i\omega\mathbf{E}_{\min(i,j)}| \\
& \qquad \times (-1)^{|k-i|-1} \overline{|\mathbf{O}_{ki} + i\omega\mathbf{I} - i\omega\mathbf{E}_{\min(i,k)}|} \Bigg] \Bigg)
\end{aligned} \tag{D.156}$$

On simplifying this equation, we get,

$$\begin{aligned}
P^{ii}(\omega) = \sum_{m=1}^{n} \sigma_m^2 \Bigg(& l_{im}^2 |\mathbf{O}_{ii} + i\omega\mathbf{I}| \overline{|\mathbf{O}_{ii} + i\omega\mathbf{I}|} - 2 \sum_{\substack{j=1 \\ j\neq i}}^{n} l_{im} l_{jm} \mathrm{Re}\Big[|\mathbf{O}_{ii} + i\omega\mathbf{I}| \overline{|\mathbf{O}_{ji} + i\omega\mathbf{I} - i\omega\mathbf{E}_{\min(i,j)}|} \Big] \\
& + \sum_{\substack{j=1 \\ j\neq i}}^{n} l_{jm}^2 |\mathbf{O}_{ji} + i\omega\mathbf{I} - i\omega\mathbf{E}_{\min(i,j)}| \overline{|\mathbf{O}_{ji} + i\omega\mathbf{I} - i\omega\mathbf{E}_{\min(i,j)}|} \\
& + 2 \sum_{\substack{j=1 \\ j\neq i}}^{n} \sum_{\substack{k=1 \\ k\neq i}}^{j-1} l_{jm} l_{km} \mathrm{Re}\Big[|\mathbf{O}_{ji} + i\omega\mathbf{I} - i\omega\mathbf{E}_{\min(i,j)}| \overline{|\mathbf{O}_{ki} + i\omega\mathbf{I} - i\omega\mathbf{E}_{\min(i,k)}|} \Big] \Bigg)
\end{aligned} \tag{D.157}$$

Using the definitions of the functions above, we can write Eq. (D.157) as,

$$\begin{aligned}
P^{ii}(\omega) = \sum_{m=1}^{n} \sigma_m^2 \Bigg(& l_{im}^2 d(\omega; \mathbf{O}_{ii}) + \sum_{\substack{j=1 \\ j\neq i}}^{n} \sum_{\substack{k=1 \\ k\neq i}}^{j-1} l_{jm} l_{km} t_1(\omega; \mathbf{O}_{ji}, \mathbf{O}_{ki}, \mathbf{e}_{\min(i,j)}, \mathbf{e}_{\min(i,k)}) \\
& + \sum_{\substack{j=1 \\ j\neq i}}^{n} l_{jm}^2 f(\omega; \mathbf{O}_{ji}, \mathbf{e}_{\min(i,j)}) - \sum_{\substack{j=1 \\ j\neq i}}^{n} l_{im} l_{jm} s_1(\omega; \mathbf{O}_{ii}, \mathbf{O}_{ji}, \mathbf{e}_{\min(i,j)}) \Bigg)
\end{aligned} \tag{D.158}$$

Eq. (D.158) defines the closed form polynomial expansion of $P_{ii}(\omega)$ in terms of ω. We can use the corresponding functions to find the coefficient of $\omega^{2\alpha}$. In general, we can write the auto-spectrum for the i^{th} variable as the following polynomial expansion,

$$\mathcal{S}^{ii}(\omega) = \frac{P^{ii}(\omega)}{Q(\omega)} = \frac{p_0^{ii} + p_1^{ii}\omega^2 + p_2^{ii}\omega^4 + \ldots + p_\alpha^{ii}\omega^{2\alpha} + \ldots + p_{n-1}^{ii}\omega^{2n-2}}{q_0 + q_1\omega^2 + q_2\omega^4 + \ldots + q_\alpha\omega^{2\alpha} + \ldots + q_n\omega^{2n}} \tag{D.159}$$

Such that,

$$P^{ii}(\omega) = p_0^{ii} + p_1^{ii}\omega^2 + p_2^{ii}\omega^4 + \ldots + p_\alpha^{ii}\omega^{2\alpha} + \ldots + p_{n-1}^{ii}\omega^{2n-2} \tag{D.160}$$

Where p_α and q_α are coefficients of different even powers of ω in the numerator and the denominator, respectively. In general for the i^{th} variable, using the Eq. (D.158), we can write p_α as,

$$\begin{aligned} p_\alpha^{ii} = \sum_{m=1}^{n} \sigma_m^2 \Bigg(& l_{im}^2 d^\alpha(\mathbf{O}_{ii}) + \sum_{\substack{j=1 \\ j\neq i}}^{n} l_{jm}^2 f^\alpha(\mathbf{O}_{ji}, \mathbf{e}_{\min(i,j)}) - \sum_{\substack{j=1 \\ j\neq i}}^{n} l_{im} l_{jm} s_1^\alpha(\mathbf{O}_{ii}, \mathbf{O}_{ji}, \mathbf{e}_{\min(i,j)}) \\ & + \sum_{\substack{j=1 \\ j\neq i}}^{n} \sum_{\substack{k=1 \\ k\neq i}}^{j-1} l_{jm} l_{km} t_1^\alpha(\mathbf{O}_{ji}, \mathbf{O}_{ki}, \mathbf{e}_{\min(i,j)}, \mathbf{e}_{\min(i,k)}) \Bigg) \end{aligned} \tag{D.161}$$

Special case of independent noise: Now, since the denominator for the auto-spectrum is the same for all the variables and only depends on the Jacobian of the system, we focus on the numerator in the following analysis. We consider special cases of noise correlations and show how the expression for the coefficients of ω in the numerator simplifies. The dynamical system with uncorrelated noise can be analytically realized by constraining the matrix $\mathbf{L}$ to be diagonal such that $l_{ij} = 0$ when $i \neq j$. Using this fact Eq. (D.161) simplifies to,

$$p_\alpha^{ii} = \sigma_i^2\, l_{ii}^2\, d^\alpha(\mathbf{O}_{ii}) + \sum_{\substack{j=1 \\ j\neq i}}^{n} \sigma_j^2\, l_{jj}^2\, f^\alpha(\mathbf{O}_{ji}, \mathbf{e}_{\min\{i,j\}}) \tag{D.162}$$

D.3.2.2 Cross-spectrum

We proceed similarly to calculate the polynomial expansion of the cross-power spectral density (cross-spectrum), i.e., the off-diagonal elements of $\mathbf{Z}(\omega)$. Now when $i \neq j$ Eq. (D.150) can be split into four parts as,

$$\begin{aligned} Z^{ij}(\omega) = \sum_{m=1}^{n} \sigma_m^2 \Bigg(& (-1)^{2(i+j)} l_{im} l_{jm} M_{ii} \overline{M}_{jj} + \sum_{\substack{k=1 \\ k\neq j}}^{n} (-1)^{i+j+i+k} l_{im} l_{km} M_{ii} \overline{M}_{kj} \\ & + \sum_{\substack{k=1 \\ k\neq i}}^{n} (-1)^{i+j+k+j} l_{km} l_{jm} M_{ki} \overline{M}_{jj} + \sum_{\substack{k=1 \\ k\neq i}}^{n} \sum_{\substack{q=1 \\ q\neq j}}^{n} (-1)^{i+j+k+q} l_{km} l_{qm} M_{ki} \overline{M}_{qj} \Bigg) \end{aligned} \tag{D.163}$$

Since the solution is complex, $Z^{ij}(\omega) = P^{ij}(\omega) + i\omega P^{ij\prime}(\omega)$. After replacing the minors with the determinants of the matrices $\mathbf{O}_{ij}$, we find,

$$\begin{aligned} Z^{ij}(\omega) = \sum_{m=1}^{n} \sigma_m^2 \Bigg(& l_{im} l_{jm} |\mathbf{O}_{ii} + i\omega\mathbf{I}| \overline{|\mathbf{O}_{jj} + i\omega\mathbf{I}|} \\ & + \sum_{\substack{k=1 \\ k\neq j}}^{n} (-1)^{j+k} l_{im} l_{km} |\mathbf{O}_{ii} + i\omega\mathbf{I}| (-1)^{|k-j|-1} \overline{|\mathbf{O}_{kj} + i\omega\mathbf{I} - i\omega\mathbf{E}_{\min(k,j)}|} \\ & + \sum_{\substack{k=1 \\ k\neq i}}^{n} (-1)^{i+k} l_{km} l_{jm} (-1)^{|k-i|-1} |\mathbf{O}_{ki} + i\omega\mathbf{I} - i\omega\mathbf{E}_{\min(k,i)}| \overline{|\mathbf{O}_{jj} + i\omega\mathbf{I}|} \\ & + \sum_{\substack{k=1 \\ k\neq i}}^{n} \sum_{\substack{q=1 \\ q\neq j}}^{n} (-1)^{i+j+k+q} l_{km} l_{qm} (-1)^{|k-i|-1} |\mathbf{O}_{ki} + i\omega\mathbf{I} - i\omega\mathbf{E}_{\min(k,i)}| \\ & \qquad \times (-1)^{|q-j|-1} \overline{|\mathbf{O}_{qj} + i\omega\mathbf{I} - i\omega\mathbf{E}_{\min(q,j)}|} \Bigg) \end{aligned} \tag{D.164}$$

Upon further simplification, we get,

$$
\begin{aligned}
Z^{ij}(\omega) = \sum_{m=1}^{n} \sigma_m^2 \Bigg(& l_{im} l_{jm} |\mathbf{O}_{ii} + i\omega\mathbf{I}| \overline{|\mathbf{O}_{jj} + i\omega\mathbf{I}|} \\
& + \sum_{\substack{k=1 \\ k\neq i}}^{n} \sum_{\substack{q=1 \\ q\neq j}}^{n} l_{km} l_{qm} |\mathbf{O}_{ki} + i\omega\mathbf{I} - i\omega\mathbf{E}_{\min(k,i)}| \overline{|\mathbf{O}_{qj} + i\omega\mathbf{I} - i\omega\mathbf{E}_{\min(q,j)}|} \\
& - \sum_{\substack{k=1 \\ k\neq j}}^{n} l_{im} l_{km} |\mathbf{O}_{ii} + i\omega\mathbf{I}| \overline{|\mathbf{O}_{kj} + i\omega\mathbf{I} - i\omega\mathbf{E}_{\min(k,j)}|} \\
& - \sum_{\substack{k=1 \\ k\neq i}}^{n} l_{km} l_{jm} |\mathbf{O}_{ki} + i\omega\mathbf{I} - i\omega\mathbf{E}_{\min(k,i)}| \overline{|\mathbf{O}_{jj} + i\omega\mathbf{I}|} \Bigg)
\end{aligned}
\tag{D.165}
$$

Since we know that the cross-spectrum is a complex expression, we calculate the real and imaginary parts separately. Using the expansion in Eq. (D.38), we can write the complex rational function for the cross-spectrum as,

$$
\begin{aligned}
\mathcal{S}^{ij}(\omega) &= \frac{P^{ij}(\omega) + i\omega P^{ij\prime}(\omega)}{Q(\omega)} \\
&= \frac{(p_0^{ij} + \ldots + p_\alpha^{ij}\omega^{2\alpha} + \ldots + p_{n-1}^{ij}\omega^{2n-2}) + i\omega(p_0^{ij\prime} + \ldots + p_\alpha^{ij\prime}\omega^{2\alpha} + \ldots + p_{n-2}^{ij\prime}\omega^{2n-4})}{q_0 + q_1\omega^2 + q_2\omega^4 + \ldots + q_\alpha\omega^{2\alpha} + \ldots + q_n\omega^{2n}}
\end{aligned}
\tag{D.166}
$$

Where p_α^{ij} and $p_\alpha^{ij\prime}$ are coefficients of different even (real) and odd (imaginary) powers of ω in the numerator, respectively.

Real part of the numerator: We first find the real part of Eq. (D.165). Using the function definitions from Section. D.4, we can write the real part of Eq. (D.165) as,

$$P^{ij}(\omega) = \sum_{m=1}^{n} \frac{\sigma_m^2}{2} \Bigg(l_{im} l_{jm} h_1(\omega; \mathbf{O}_{ii}, \mathbf{O}_{jj}) - \sum_{\substack{k=1 \\ k \neq j}}^{n} l_{im} l_{km} s_1(\omega; \mathbf{O}_{ii}, \mathbf{O}_{kj}, \mathbf{e}_{\min(k,j)}) \\ - \sum_{\substack{k=1 \\ k \neq i}}^{n} l_{km} l_{jm} s_1(\omega; \mathbf{O}_{jj}, \mathbf{O}_{ki}, \mathbf{e}_{\min(k,i)}) \\ + \sum_{\substack{k=1 \\ k \neq i}}^{n} \sum_{\substack{q=1 \\ q \neq j}}^{n} l_{km} l_{qm} t_1(\omega; \mathbf{O}_{ki}, \mathbf{O}_{qj}, \mathbf{e}_{\min(i,k)}, \mathbf{e}_{\min(j,q)}) \Bigg) \tag{D.167}$$

Eq. (D.167) represents a closed-form polynomial expansion (in terms of ω) of the real part of the cross-spectrum between x_i and x_j. Using Eq. (D.167), we can thus write p_α as,

$$p_\alpha^{ij} = \sum_{m=1}^{n} \frac{\sigma_m^2}{2} \Bigg(l_{im} l_{jm} h_1^\alpha(\mathbf{O}_{ii}, \mathbf{O}_{jj}) + \sum_{\substack{k=1 \\ k \neq i}}^{n} \sum_{\substack{q=1 \\ q \neq j}}^{n} l_{km} l_{qm} t_1^\alpha(\mathbf{O}_{ki}, \mathbf{O}_{qj}, \mathbf{e}_{\min(i,k)}, \mathbf{e}_{\min(j,q)}) \\ - \sum_{\substack{k=1 \\ k \neq j}}^{n} l_{im} l_{km} s_1^\alpha(\mathbf{O}_{ii}, \mathbf{O}_{kj}, \mathbf{e}_{\min(k,j)}) - \sum_{\substack{k=1 \\ k \neq i}}^{n} l_{km} l_{jm} s_1^\alpha(\mathbf{O}_{jj}, \mathbf{O}_{ki}, \mathbf{e}_{\min(k,i)}) \Bigg) \tag{D.168}$$

Imaginary part of the numerator: Next, we find the imaginary part of Eq. (D.165). Using the function definitions from Section. D.4, we can write the imaginary part of Eq. (D.165) as,

$$\omega P^{ij\prime}(\omega) = \sum_{m=1}^{n} \frac{\sigma_m^2}{2} \Bigg(-l_{im} l_{jm} h_2(\omega; \mathbf{O}_{ii}, \mathbf{O}_{jj}) + \sum_{\substack{k=1 \\ k \neq i}}^{n} \sum_{\substack{q=1 \\ q \neq j}}^{n} l_{km} l_{qm} t_2(\omega; \mathbf{O}_{ki}, \mathbf{O}_{qj}, \mathbf{e}_{\min(i,k)}, \mathbf{e}_{\min(j,q)}) \\ - \sum_{\substack{k=1 \\ k \neq j}}^{n} l_{im} l_{km} s_2(\omega; \mathbf{O}_{ii}, \mathbf{O}_{kj}, \mathbf{e}_{\min(k,j)}) + \sum_{\substack{k=1 \\ k \neq i}}^{n} l_{km} l_{jm} s_2(\omega; \mathbf{O}_{jj}, \mathbf{O}_{ki}, \mathbf{e}_{\min(k,i)}) \Bigg) \tag{D.169}$$

Eq. (D.169) represents a closed-form polynomial expansion (in terms of ω) of the imaginary part

of the cross-spectrum between x_i and x_j. Using Eq. (D.169), we can thus write $p_\alpha^{ij\prime}$ as,

$$p_\alpha^{ij\prime} = \sum_{m=1}^{n} \frac{\sigma_m^2}{2} \Bigg(- l_{im} l_{jm} h_2^\alpha(\mathbf{O}_{ii}, \mathbf{O}_{jj}) + \sum_{\substack{k=1 \\ k\neq i}}^{n} \sum_{\substack{q=1 \\ q\neq j}}^{n} l_{km} l_{qm} t_2^\alpha(\mathbf{O}_{ki}, \mathbf{O}_{qj}, \mathbf{e}_{\min(i,k)}, \mathbf{e}_{\min(j,q)}) \\ - \sum_{\substack{k=1 \\ k\neq j}}^{n} l_{im} l_{km} s_2^\alpha(\mathbf{O}_{ii}, \mathbf{O}_{kj}, \mathbf{e}_{\min(k,j)}) + \sum_{\substack{k=1 \\ k\neq i}}^{n} l_{km} l_{jm} s_2^\alpha(\mathbf{O}_{jj}, \mathbf{O}_{ki}, \mathbf{e}_{\min(k,i)}) \Bigg) \tag{D.170}$$

Special case of independent noise: Now, since the denominator for the cross-spectrum is the same for all the variables and is equal to the auto-spectrum, we focus on the numerator in the following analysis. Along lines similar to the auto-spectrum, we consider the special case of independent (across variables) Gaussian noise and show how the expression for the coefficients of ω in the numerator simplifies. The dynamical system with uncorrelated noise can be analytically realized by constraining the matrix $\mathbf{L}$ to be diagonal such that $l_{ij} = 0$, when $i \neq j$. Using this fact Eq. (D.168) simplifies to,

$$p_\alpha^{ij\prime} = \sum_{\substack{m=1 \\ m\neq(i,j)}}^{n} \frac{\sigma_m^2}{2} l_{mm}^2 t_1^\alpha(\mathbf{O}_{mi}, \mathbf{O}_{mj}, \mathbf{e}_{\min(i,m)}, \mathbf{e}_{\min(j,m)}) \\ - \frac{\sigma_i^2}{2} l_{ii}^2 s_1^\alpha(\mathbf{O}_{ii}, \mathbf{O}_{ij}, \mathbf{e}_{\min(i,j)}) - \frac{\sigma_j^2}{2} l_{jj}^2 s_1^\alpha(\mathbf{O}_{jj}, \mathbf{O}_{ji}, \mathbf{e}_{\min(j,i)}). \tag{D.171}$$

Similarly, Eq. (D.170) simplifies to,

$$p_\alpha^{ij\prime} = \sum_{\substack{m=1 \\ m\neq(i,j)}}^{n} \frac{\sigma_m^2}{2} l_{mm}^2 t_2^\alpha(\mathbf{O}_{mi}, \mathbf{O}_{mj}, \mathbf{e}_{\min(i,m)}, \mathbf{e}_{\min(j,m)}) \\ - \frac{\sigma_i^2}{2} l_{ii}^2 s_2^\alpha(\mathbf{O}_{ii}, \mathbf{O}_{ij}, \mathbf{e}_{\min(i,j)}) + \frac{\sigma_j^2}{2} l_{jj}^2 s_2^\alpha(\mathbf{O}_{jj}, \mathbf{O}_{ji}, \mathbf{e}_{\min(j,i)}). \tag{D.172}$$

D.3.2.3 Coherence as a Rational Function

Coherence is a measure of the similarity of two signals as a function of frequency. Mathematically, coherence (κ_{ij}) between two variables x_i and x_j is defined as the ratio of the squared magnitude of the cross-power spectral density and their individual power spectral densities. Given the representation of the cross-spectrum and auto-spectrum in terms of numerator and denominator, using Eq. (D.159) and (D.166), we can write coherence as a rational function,

$$\kappa^{ij} = \frac{|\mathcal{S}^{ij}(\omega)|^2}{\mathcal{S}^{ii}(\omega)\mathcal{S}^{jj}(\omega)} = \frac{|P^{ij}(\omega) + i\omega P^{ij\prime}(\omega)|^2}{P^{ii}(\omega)P^{jj}(\omega)} = \frac{\left(\sum_{\alpha=0}^{n-1} p_\alpha^{ij}\omega^{2\alpha}\right)^2 + \omega^2\left(\sum_{\alpha=0}^{n-2} p_\alpha^{ij\prime}\omega^{2\alpha}\right)^2}{\left(\sum_{\alpha=0}^{n-1} p_\alpha^{ii}\omega^{2\alpha}\right)\left(\sum_{\alpha=0}^{n-1} p_\alpha^{jj}\omega^{2\alpha}\right)}, \tag{D.173}$$

where the superscript of p represents that the coefficient comes from the numerator of the polynomial for cross-spectrum (ij) or the auto-spectrum (ii or jj).

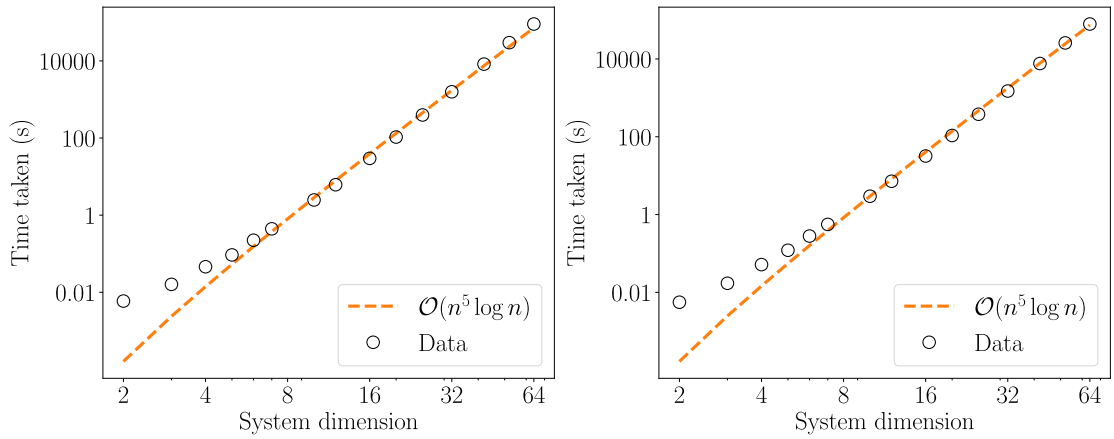


Figure D.2: Time complexity of the element-wise algorithm. The time complexity of finding the auto-spectrum (left) of a given variable and cross-spectrum (right) between any two variables for a non-sparse SDE with additive Gaussian white noise with random correlations using *rational computations*. The algorithms run with time complexity of $O(n^5 \log n)$.

D.4 Detailed Function Definitions

In what follows, we define the set of functions that facilitates the derivation of expressions for auto and cross spectrums.

D.4.1 $d(\omega; \mathbf{A})$

The function $d(\omega; \mathbf{A} \in \mathbb{R}^{n\times n})$ expands the following determinant product into the corresponding polynomial in ω. Here, $\mathbf{A} \in \mathbb{R}^{n\times n}$.

$$\begin{aligned} d(\omega; \mathbf{A}) &= |\mathbf{A} + i\omega\mathbf{I}|\,|\mathbf{A} - i\omega\mathbf{I}| \\ &= |\mathbf{A} + i\omega\mathbf{I}|\,\overline{|\mathbf{A} + i\omega\mathbf{I}|} \\ &= ||\mathbf{A} + i\omega\mathbf{I}||^2 \end{aligned} \tag{D.174}$$

Denoting $\lambda_i \in \mathbb{C}$ to be the eigenvalues of the matrix $\mathbf{A}$, using Eq. (D.238), we can write the modulus of the determinant of the complex matrix as,

$$\begin{aligned} d(\omega; \mathbf{A}) &= \prod_{i=1}^{n} |\lambda_i + i\omega|^2 \\ &= \prod_{i=1}^{n} (\lambda_i^2 + \omega^2) \end{aligned} \tag{D.175}$$

Writing this product as a function of elementary symmetric polynomials (Eq. (D.242)), we find,

$$d(\omega; \mathbf{A}) = \sum_{j=0}^{n} e^{n-j}\omega^{2j} \tag{D.176}$$

Where, e^j is the j^{th} elementary symmetric polynomial with $x_k = {\lambda_k}^2$, and can be calculated recursively using the Newton's identities Eq. (D.131). We can also express them as Bell polynomials

(Eq. (D.135)),

$$d(\omega; \mathbf{A}) = \sum_{j=0}^{n} \frac{(-1)^{n-j}}{(n-j)!} B(\mathbf{r}^{n-j}(\mathbf{A}^2))\omega^{2j} \tag{D.177}$$

Here, $\mathbf{r}^j(\mathbf{X})$ is defined in Eq. (D.140) and $B(\mathbf{r}^{n-j})$ can be computed using Eq. (D.139). Now we define $d^\alpha(\mathbf{A})$, where $\alpha \in \{0, \ldots, n\}$, to be the coefficient of $\omega^{2\alpha}$ from the polynomial expansion of $d(\omega; \mathbf{A})$, namely,

$$d^\alpha(\mathbf{A}) = \frac{(-1)^{n-\alpha}}{(n-\alpha)!} B(\mathbf{r}^{n-\alpha}(\mathbf{A}^2)) \tag{D.178}$$

D.4.2 $g(\omega; \mathbf{A}, \mathbf{B})$

The function $g(\omega; \mathbf{A} \in \mathbb{R}^{n\times n}, \mathbf{B} \in \mathbb{R}^{n-1\times n-1})$ is defined as the product of the following determinants,

$$g(\omega; \mathbf{A}, \mathbf{B}) = 2\omega \overline{|\mathbf{A} + i\omega\mathbf{I}|}\, |\mathbf{B} + i\omega\mathbf{I}| \tag{D.179}$$

If $\lambda_k \in \mathbb{C}$ are the eigenvalues of matrix $\mathbf{A}$ and $\beta_k \in \mathbb{C}$ are the eigenvalues of matrix $\mathbf{B}$, using Eq. (D.238), we can write the equation above as,

$$g(\omega; \mathbf{A}, \mathbf{B}) = 2\omega \prod_{j=1}^{n} (\lambda_j - i\omega) \prod_{k=1}^{n-1} (\beta_k + i\omega) \tag{D.180}$$

Expanding the polynomial into a sum containing elementary symmetric polynomials (Eq. (D.242)), we find,

$$g(\omega; \mathbf{A}, \mathbf{B}) = 2\omega \left(\sum_{j=0}^{n} (-1)^j (i)^j e_1^{n-j} \omega^j \right) \left(\sum_{k=0}^{n-1} (i)^k e_2^{n-k-1} \omega^k \right) \tag{D.181}$$

where, e_1^i and e_2^i are the elementary symmetric polynomials with $x_k = \lambda_k$ and $x_k = \beta_k$, respectively. Using the property of product of polynomials in Eq. (D.241), we expand Eq. (D.181) in ω and find

the coefficients of the powers of ω,

$$\begin{aligned} g(\omega;\mathbf{A},\mathbf{B}) &= 2\omega \sum_{p=0}^{2n-1} \sum_{j+k=p} (-1)^j (i)^{j+k} e_1^{n-j} e_2^{n-k-1} \omega^p \\ &= 2\omega \sum_{p=0}^{2n-1} \sum_{j+k=p} (-1)^j (i)^{p} e_1^{n-j} e_2^{n-k-1} \omega^p \end{aligned} \tag{D.182}$$

subject to the condition,

$$0 \leq j \leq n, \quad 0 \leq k \leq n-1 \tag{D.183}$$

We can divide Eq. (D.182) into real and complex parts by dividing the iterator (p) into even and odd components,

$$g(\omega;\mathbf{A},\mathbf{B}) = 2\omega \sum_{p=0}^{n-1} \sum_{j+k=2p} (-1)^j (i)^{2p} e_1^{n-j} e_2^{n-k-1} \omega^{2p} + 2\omega \sum_{p=0}^{n-1} \sum_{j+k=2p+1} (-1)^j (i)^{2p+1} e_1^{n-j} e_2^{n-k-1} \omega^{2p+1} \tag{D.184}$$

Upon further simplification, we obtain,

$$g(\omega;\mathbf{A},\mathbf{B}) = 2\omega \sum_{p=0}^{n-1} \sum_{j+k=2p} (-1)^{j+p} e_1^{n-j} e_2^{n-k-1} \omega^{2p} + 2i\omega \sum_{p=0}^{n-1} \sum_{j+k=2p+1} (-1)^{j+p} e_1^{n-j} e_2^{n-k-1} \omega^{2p+1} \tag{D.185}$$

We split $g(\omega;\mathbf{A},\mathbf{B})$ into its real and imaginary parts as follows,

$$\begin{aligned} g_1(\omega;\mathbf{A},\mathbf{B}) &= 2\omega \,\mathrm{Re}\left[\overline{|\mathbf{A}+i\omega\mathbf{I}|}\,|\mathbf{B}+i\omega\mathbf{I}|\right] \\ &= 2\omega \sum_{p=0}^{n-1} \sum_{j+k=2p} (-1)^{j+p} e_1^{n-j} e_2^{n-k-1} \omega^{2p} \end{aligned} \tag{D.186}$$

$$\begin{aligned} g_2(\omega;\mathbf{A},\mathbf{B}) &= 2\omega \,\mathrm{Im}\left[\overline{|\mathbf{A}+i\omega\mathbf{I}|}\,|\mathbf{B}+i\omega\mathbf{I}|\right] \\ &= 2\omega \sum_{p=0}^{n-1} \sum_{j+k=2p+1} (-1)^{j+p} e_1^{n-j} e_2^{n-k-1} \omega^{2p+1} \end{aligned} \tag{D.187}$$

such that,

$$g(\omega;\mathbf{A},\mathbf{B}) = g_1(\omega;\mathbf{A},\mathbf{B}) + ig_2(\omega;\mathbf{A},\mathbf{B}) \tag{D.188}$$

Replacing the elementary symmetric polynomials by Bell polynomials (using Eq. (D.135)) we obtain,

$$\begin{aligned} g_1(\omega;\mathbf{A},\mathbf{B}) &= 2\sum_{p=0}^{n-1}\sum_{j+k=2p}\frac{(-1)^{p-k-1}}{(n-j)!(n-k-1)!}B(\mathbf{r}^{n-j}(\mathbf{A}))B(\mathbf{r}^{n-k-1}(\mathbf{B}))\omega^{2p+1} \\ g_2(\omega;\mathbf{A},\mathbf{B}) &= 2\sum_{p=0}^{n-1}\sum_{j+k=2p+1}\frac{(-1)^{p-k-1}}{(n-j)!(n-k-1)!}B(\mathbf{r}^{n-j}(\mathbf{A}))B(\mathbf{r}^{n-k-1}(\mathbf{B}))\omega^{2p+2} \end{aligned} \tag{D.189}$$

Finally, $g_1^\alpha(\mathbf{A},\mathbf{B})$, for $\alpha \in \{0,\dots,n-1\}$, and $g_2^\alpha(\mathbf{A},\mathbf{B})$, for $\alpha \in \{0,\dots,n\}$, can be defined as the coefficients of $\omega^{2\alpha+1}$ and $\omega^{2\alpha}$ for $g_1(\omega;\mathbf{A},\mathbf{B})$ and $g_2(\omega;\mathbf{A},\mathbf{B})$, respectively,

$$g_1^\alpha(\mathbf{A},\mathbf{B}) = 2\sum_{j+k=2\alpha}\frac{(-1)^{\alpha-j-1}}{(n-j)!(n-k-1)!}B(\mathbf{r}^{n-j}(\mathbf{A}))B(\mathbf{r}^{n-k-1}(\mathbf{B})) \tag{D.190}$$

$$g_2^\alpha(\mathbf{A},\mathbf{B}) = 2\sum_{j+k=2\alpha-1}\frac{(-1)^{\alpha-j-1}}{(n-j)!(n-k-1)!}B(\mathbf{r}^{n-j}(\mathbf{A}))B(\mathbf{r}^{n-k-1}(\mathbf{B})) \tag{D.191}$$

D.4.3 $h(\omega;\mathbf{A},\mathbf{B})$

The function $h(\omega;\mathbf{A}\in\mathbb{R}^{n\times n},\mathbf{B}\in\mathbb{R}^{n\times n})$ is defined as the product of the following determinants,

$$h(\omega;\mathbf{A},\mathbf{B}) = 2\,\overline{|\mathbf{A}+i\omega\mathbf{I}|}\,|\mathbf{B}+i\omega\mathbf{I}| \tag{D.192}$$

If $\lambda_k \in \mathbb{C}$ are the eigenvalues of matrix $\mathbf{A}$ and $\beta_k \in \mathbb{C}$ are the eigenvalues of matrix $\mathbf{B}$, using Eq. (D.238), we can write the equation above as,

$$h(\omega;\mathbf{A},\mathbf{B}) = 2\prod_{j=1}^{n}(\lambda_j - i\omega)\prod_{k=1}^{n}(\beta_k + i\omega) \tag{D.193}$$

Expanding the polynomial into a sum containing elementary symmetric polynomials (Eq. (D.242)), we find,

$$h(\omega;\mathbf{A},\mathbf{B}) = 2\left(\sum_{j=0}^{n}(-1)^j(i)^j e_1^{n-j}\omega^j\right)\left(\sum_{k=0}^{n}(i)^k e_2^{n-k}\omega^k\right) \tag{D.194}$$

where, e_1^i and e_2^i are the elementary symmetric polynomials with $x_k = \lambda_k$ and $x_k = \beta_k$, respectively. Using the property of product of polynomials in Eq. (D.241), we expand Eq. (D.194) in ω and find the coefficients of the powers of ω,

$$h(\omega;\mathbf{A},\mathbf{B}) = 2\sum_{p=0}^{2n}\sum_{j+k=p}(-1)^j(i)^{j+k}e_1^{n-j}e_2^{n-k}\omega^p = 2\sum_{p=0}^{2n}\sum_{j+k=p}(-1)^j(i)^p e_1^{n-j}e_2^{n-k-1}\omega^p \tag{D.195}$$

subject to the condition,

$$0 \le j \le n, \quad 0 \le k \le n \tag{D.196}$$

We can divide Eq. (D.195) into real and complex parts by dividing the iterator (p) into even and odd components,

$$h(\omega;\mathbf{A},\mathbf{B}) = 2\sum_{p=0}^{n}\sum_{j+k=2p}(-1)^j(i)^{2p}e_1^{n-j}e_2^{n-k}\omega^{2p} + 2\sum_{p=0}^{n-1}\sum_{j+k=2p+1}(-1)^j(i)^{2p+1}e_1^{n-j}e_2^{n-k}\omega^{2p+1} \tag{D.197}$$

Upon further simplification, we obtain,

$$h(\omega;\mathbf{A},\mathbf{B}) = 2\sum_{p=0}^{n}\sum_{j+k=2p}(-1)^{j+p}e_1^{n-j}e_2^{n-k}\omega^{2p} + 2i\sum_{p=0}^{n-1}\sum_{j+k=2p+1}(-1)^{j+p}e_1^{n-j}e_2^{n-k}\omega^{2p+1} \tag{D.198}$$

We split $h(\omega;\mathbf{A},\mathbf{B})$ into its real and imaginary parts as follows,

$$\begin{aligned} h_1(\omega;\mathbf{A},\mathbf{B}) &= 2\,\mathrm{Re}\left[\overline{|\mathbf{A}+i\omega\mathbf{I}|}\,|\mathbf{B}+i\omega\mathbf{I}|\right] \\ &= 2\sum_{p=0}^{n}\sum_{j+k=2p}(-1)^{j+p}e_1^{n-j}e_2^{n-k}\omega^{2p} \end{aligned} \tag{D.199}$$

$$
\begin{aligned}
h_2(\omega;\mathbf{A},\mathbf{B}) &= 2\,\mathrm{Im}\left[\overline{|\mathbf{A}+i\omega\mathbf{I}|}\,|\mathbf{B}+i\omega\mathbf{I}|\right] \\
&= 2\sum_{p=0}^{n-1}\sum_{j+k=2p+1}(-1)^{j+p}e_1^{n-j}e_2^{n-k}\omega^{2p+1}
\end{aligned}
\tag{D.200}
$$

such that,

$$
h(\omega;\mathbf{A},\mathbf{B}) = h_1(\omega;\mathbf{A},\mathbf{B}) + ih_2(\omega;\mathbf{A},\mathbf{B}) \tag{D.201}
$$

Replacing the elementary symmetric polynomials by Bell polynomials (using Eq. (D.135)) we find,

$$
\begin{aligned}
h_1(\omega;\mathbf{A},\mathbf{B}) &= 2\sum_{p=0}^{n}\sum_{j+k=2p}\frac{(-1)^{p-k}}{(n-j)!(n-k)!}B(\mathbf{r}^{n-j}(\mathbf{A}))B(\mathbf{r}^{n-k}(\mathbf{B}))\omega^{2p} \\
h_2(\omega;\mathbf{A},\mathbf{B}) &= 2\sum_{p=0}^{n-1}\sum_{j+k=2p+1}\frac{(-1)^{p-k}}{(n-j)!(n-k)!}B(\mathbf{r}^{n-j}(\mathbf{A}))B(\mathbf{r}^{n-k}(\mathbf{B}))\omega^{2p+1}
\end{aligned}
\tag{D.202}
$$

Finally, $h_1^\alpha(\mathbf{A},\mathbf{B})$, for $\alpha \in \{0,\ldots,n\}$, and $h_2^\alpha(\mathbf{A},\mathbf{B})$, for $\alpha \in \{0,\ldots,n-1\}$, can be defined as the coefficients of $\omega^{2\alpha}$ and $\omega^{2\alpha+1}$ for $h_1(\omega;\mathbf{A},\mathbf{B})$ and $h_2(\omega;\mathbf{A},\mathbf{B})$, respectively,

$$
h_1^\alpha(\mathbf{A},\mathbf{B}) = 2\sum_{j+k=2\alpha}\frac{(-1)^{\alpha-k}}{(n-j)!(n-k)!}B(\mathbf{r}^{n-j}(\mathbf{A}))B(\mathbf{r}^{n-k}(\mathbf{B})) \tag{D.203}
$$

$$
h_2^\alpha(\mathbf{A},\mathbf{B}) = 2\sum_{j+k=2\alpha+1}\frac{(-1)^{\alpha-k}}{(n-j)!(n-k)!}B(\mathbf{r}^{n-j}(\mathbf{A}))B(\mathbf{r}^{n-k}(\mathbf{B})) \tag{D.204}
$$

D.4.4 $f(\omega;\mathbf{A},\mathbf{e}_\beta)$

The function $f(\omega;\mathbf{A}\in\mathbb{R}^{n\times n},\mathbf{e}_\beta\in\{0,1\}^{n\times 1})$ is defined as the expansion of the following determinant,

$$
f(\omega;\mathbf{A},\mathbf{e}_\beta) = |\mathbf{A}+i\omega\mathbf{I}-i\omega\,\mathbf{e}_\beta\mathbf{e}_\beta{}^\top|\,|\mathbf{A}-i\omega\mathbf{I}+i\omega\,\mathbf{e}_\beta\mathbf{e}_\beta{}^\top| \tag{D.205}
$$

The elements of the vector $\mathbf{e}_\beta$, the standard unit vector, are equal to 1 only at the index β and zero everywhere else. Eq. (D.205) is just the modulus-squared of one of the determinants, therefore,

$$f(\omega; \mathbf{A}, \mathbf{e}_\beta) = ||\mathbf{A} + i\omega\,\mathbf{I} - i\omega\,\mathbf{e}_\beta\mathbf{e}_\beta{}^\top||^2 \tag{D.206}$$

We use the property from Eq. (D.237), to write Eq. (D.206) as,

$$f(\omega; \mathbf{A}, \mathbf{e}_\beta) = \left|\,||\mathbf{A} + i\omega\,\mathbf{I}| - i\omega\,\mathbf{e}_\beta{}^\top \mathrm{adj}(\mathbf{A} + i\omega\mathbf{I})\mathbf{e}_\beta\right| \tag{D.207}$$

Since only one of the entries in the vector $\mathbf{e}_\beta$ is 1, we can simplify $f(\omega; \mathbf{A}, \mathbf{e}_\beta)$ by defining a submatrix ($\mathbf{B} \in \mathbb{R}^{n-1\times n-1}$) of $\mathbf{A}$, by excluding the row and column of $\mathbf{A}$ at the index β. Eq. (D.207) then becomes,

$$f(\omega; \mathbf{A}, \mathbf{e}_\beta) = ||\mathbf{A} + i\omega\mathbf{I}| - i\omega\,|\mathbf{B} + i\omega\mathbf{I}||^2 \tag{D.208}$$

Expanding the complex expression, we get,

$$f(\omega; \mathbf{A}, \mathbf{e}_\beta) = ||\mathbf{A} + i\omega\mathbf{I}||^2 + \omega^2\,||\mathbf{B} + i\omega\mathbf{I}||^2 - i\omega\left[\overline{|\mathbf{A} + i\omega\mathbf{I}|}\,|\mathbf{B} + i\omega\mathbf{I}| - |\mathbf{A} + i\omega\mathbf{I}|\,\overline{|\mathbf{B} + i\omega\mathbf{I}|}\right] \tag{D.209}$$

We can also write Eq. (D.209) as,

$$f(\omega; \mathbf{A}, \mathbf{e}_\beta) = ||\mathbf{A} + i\omega\mathbf{I}||^2 + \omega^2\,||\mathbf{B} + i\omega\mathbf{I}||^2 + 2\,\omega\,\mathrm{Imag}\left[\overline{|\mathbf{A} + i\omega\mathbf{I}|}\,|\mathbf{B} + i\omega\mathbf{I}|\right] \tag{D.210}$$

Using the definition of the functions, $d(\omega; \mathbf{A})$ (Eq. (D.174)) and $g_2(\omega; \mathbf{A}, \mathbf{B})$ (Eq. (D.187)), we can write,

$$f(\omega; \mathbf{A}, \mathbf{e}_\beta) = d(\omega; \mathbf{A}) + \omega^2 d(\omega; \mathbf{B}) + g_2(\omega; \mathbf{A}, \mathbf{B}) \tag{D.211}$$

Now we denote $f^{\alpha}(\mathbf{A}, \mathbf{e}_{\beta})$, for $\alpha \in \{0, \ldots, n\}$, to be the coefficient of $\omega^{2\alpha}$ from the polynomial expansion of $f(\omega; \mathbf{A}, \mathbf{e}_{\beta})$,

$$f^{\alpha}(\mathbf{A}, \mathbf{e}_{\beta}) = d^{\alpha}(\mathbf{A}) + d^{\alpha-1}(\mathbf{B}) + g_2^{\alpha}(\mathbf{A}, \mathbf{B}) \tag{D.212}$$

D.4.5 $s(\omega; \mathbf{A}, \mathbf{B}, \mathbf{e}_{\beta})$

The function $s(\omega; \mathbf{A} \in \mathbb{R}^{n\times n}, \mathbf{B} \in \mathbb{R}^{n\times n}, \mathbf{e}_{\beta} \in \{0, 1\}^{n\times 1})$ is defined as follows,

$$s(\omega; \mathbf{A}, \mathbf{B}, \mathbf{e}_{\beta}) = 2\,|\mathbf{A} + i\omega\mathbf{I}|\,\overline{|\mathbf{B} + i\omega\mathbf{I} - i\omega\,\mathbf{e}_{\beta}\mathbf{e}_{\beta}{}^{\top}|} \tag{D.213}$$

Since all the matrices and vectors are purely real, we can write,

$$s(\omega; \mathbf{A}, \mathbf{B}, \mathbf{e}_{\beta}) = 2\,|\mathbf{A} + i\omega\mathbf{I}|\,|\mathbf{B} - i\omega\mathbf{I} + i\omega\,\mathbf{e}_{\beta}\mathbf{e}_{\beta}{}^{\top}| \tag{D.214}$$

We use the property from Eq. (D.237), to write Eq. (D.214) as,

$$s(\omega; \mathbf{A}, \mathbf{B}, \mathbf{e}_{\beta}) = 2\,|\mathbf{A} + i\omega\mathbf{I}|\,\left(|\mathbf{B} - i\omega\mathbf{I}| + i\omega\,\mathbf{e}_{\beta}{}^{\top}\mathrm{adj}(\mathbf{B} - i\omega\mathbf{I})\mathbf{e}_{\beta}\right) \tag{D.215}$$

Since only one of the entries in the vector $\mathbf{e}_{\beta}$ is 1, and the index is the same for both vectors (row or column), we can simplify $s(\omega; \mathbf{A}, \mathbf{B}, \mathbf{e}_{\beta})$ by defining a submatrix ($\mathbf{C} \in \mathbb{R}^{n-1\times n-1}$) of $\mathbf{B}$, by excluding the row and column of $\mathbf{B}$ at the index β. Eq. (D.215) then becomes,

$$s(\omega; \mathbf{A}, \mathbf{B}, \mathbf{e}_{\beta}) = 2\,|\mathbf{A} + i\omega\mathbf{I}|\,\left(|\mathbf{B} - i\omega\mathbf{I}| + i\omega|\mathbf{C} - i\omega\mathbf{I}|\right) \tag{D.216}$$

On expanding the product, we get,

$$\begin{aligned} s(\omega; \mathbf{A}, \mathbf{B}, \mathbf{e}_\beta) &= 2\,|\mathbf{A} + i\omega\mathbf{I}|\,|\mathbf{B} - i\omega\mathbf{I}| + i\omega|\mathbf{A} + i\omega\mathbf{I}||\mathbf{C} - i\omega\mathbf{I}| \\ &= 2\,|\mathbf{A} + i\omega\mathbf{I}|\,|\mathbf{B} - i\omega\mathbf{I}| + 2\,i\omega|\mathbf{A} + i\omega\mathbf{I}||\mathbf{C} - i\omega\mathbf{I}| \\ &= 2\,|\mathbf{A} + i\omega\mathbf{I}|\,\overline{|\mathbf{B} + i\omega\mathbf{I}|} + 2\,i\omega|\mathbf{A} + i\omega\mathbf{I}||\mathbf{C} - i\omega\mathbf{I}| \end{aligned} \tag{D.217}$$

We split $s(\omega; \mathbf{A}, \mathbf{B}, \mathbf{e}_\beta)$ into its real and imaginary parts as follows,

$$\begin{aligned} s_1(\omega; \mathbf{A}, \mathbf{B}, \mathbf{e}_\beta) &= 2\,\mathrm{Re}\left[|\mathbf{A} + i\omega\mathbf{I}|\,\overline{|\mathbf{B} + i\omega\mathbf{I} - i\omega\,\mathbf{e}_\beta\mathbf{e}_\beta{}^\top|}\right] \\ &= 2\,\mathrm{Re}\left[|\mathbf{A} + i\omega\mathbf{I}|\,\overline{|\mathbf{B} + i\omega\mathbf{I}|}\right] + 2\,\mathrm{Re}\left[i\omega|\mathbf{A} + i\omega\mathbf{I}||\mathbf{C} - i\omega\mathbf{I}|\right] \\ &= 2\,\mathrm{Re}\left[\overline{|\mathbf{A} + i\omega\mathbf{I}|}\,|\mathbf{B} + i\omega\mathbf{I}|\right] - 2\,\omega\mathrm{Im}\left[|\mathbf{A} + i\omega\mathbf{I}||\mathbf{C} - i\omega\mathbf{I}|\right] \\ &= 2\,\mathrm{Re}\left[\overline{|\mathbf{A} + i\omega\mathbf{I}|}\,|\mathbf{B} + i\omega\mathbf{I}|\right] + 2\,\omega\mathrm{Im}\left[\overline{|\mathbf{A} + i\omega\mathbf{I}|}|\mathbf{C} + i\omega\mathbf{I}|\right] \end{aligned} \tag{D.218}$$

$$\begin{aligned} s_2(\omega; \mathbf{A}, \mathbf{B}, \mathbf{e}_\beta) &= 2\,\mathrm{Im}\left[|\mathbf{A} + i\omega\mathbf{I}|\,\overline{|\mathbf{B} + i\omega\mathbf{I} - i\omega\,\mathbf{e}_\beta\mathbf{e}_\beta{}^\top|}\right] \\ &= 2\,\mathrm{Im}\left[|\mathbf{A} + i\omega\mathbf{I}|\,\overline{|\mathbf{B} + i\omega\mathbf{I}|}\right] + 2\,\mathrm{Im}\left[i\omega|\mathbf{A} + i\omega\mathbf{I}||\mathbf{C} - i\omega\mathbf{I}|\right] \\ &= 2\,\mathrm{Im}\left[|\mathbf{A} + i\omega\mathbf{I}|\,\overline{|\mathbf{B} + i\omega\mathbf{I}|}\right] + 2\,\omega\mathrm{Re}\left[\overline{|\mathbf{A} + i\omega\mathbf{I}|}|\mathbf{C} + i\omega\mathbf{I}|\right] \end{aligned} \tag{D.219}$$

so that,

$$s(\omega; \mathbf{A}, \mathbf{B}, \mathbf{e}_\beta) = s_1(\omega; \mathbf{A}, \mathbf{B}, \mathbf{e}_\beta) + is_2(\omega; \mathbf{A}, \mathbf{B}, \mathbf{e}_\beta) \tag{D.220}$$

Using the definitions of functions $g(\omega; \mathbf{A}, \mathbf{C})$ (Eq. (D.188)) and $h(\omega; \mathbf{A}, \mathbf{B})$ (Eq. (D.201)), we can write,

$$\begin{aligned} s_1(\omega; \mathbf{A}, \mathbf{B}, \mathbf{e}_\beta) &= h_1(\omega; \mathbf{A}, \mathbf{B}) + g_2(\omega; \mathbf{A}, \mathbf{C}) \\ s_2(\omega; \mathbf{A}, \mathbf{B}, \mathbf{e}_\beta) &= -h_2(\omega; \mathbf{A}, \mathbf{B}) + g_1(\omega; \mathbf{A}, \mathbf{C}) \end{aligned} \tag{D.221}$$

Finally, $s_1^\alpha(\mathbf{A}, \mathbf{B}, \mathbf{e}_\beta)$, for $\alpha \in \{0, \ldots, n\}$, and $s_2^\alpha(\mathbf{A}, \mathbf{B}, \mathbf{e}_\beta)$, for $\alpha \in \{0, \ldots, n-1\}$, are defined to be the coefficients of $\omega^{2\alpha}$ and $\omega^{2\alpha+1}$ from the polynomial expansion of $s_1(\omega; \mathbf{A}, \mathbf{B}, \mathbf{e}_\beta)$ and $s_2(\omega; \mathbf{A}, \mathbf{B}, \mathbf{e}_\beta)$, respectively.

$$\begin{aligned} s_1^\alpha(\mathbf{A}, \mathbf{B}, \mathbf{e}_\beta) &= h_1^\alpha(\mathbf{A}, \mathbf{B}) + g_2^\alpha(\mathbf{A}, \mathbf{C}) \\ s_2^\alpha(\mathbf{A}, \mathbf{B}, \mathbf{e}_\beta) &= -h_2^\alpha(\mathbf{A}, \mathbf{B}) + g_1^\alpha(\mathbf{A}, \mathbf{C}) \end{aligned} \tag{D.222}$$

D.4.6 $t(\omega; \mathbf{A}, \mathbf{B}, \mathbf{e}_{\beta_1}, \mathbf{e}_{\beta_2})$

The function $t(\omega; \mathbf{A} \in \mathbb{R}^{n\times n}, \mathbf{B} \in \mathbb{R}^{n\times n}, \mathbf{e}_{\beta_1} \in \{0,1\}^{n\times 1}, \mathbf{e}_{\beta_2} \in \{0,1\}^{n\times 1})$ is defined as follows,

$$t(\omega; \mathbf{A}, \mathbf{B}, \mathbf{e}_{\beta_1}, \mathbf{e}_{\beta_2}) = 2\,|\mathbf{A} + i\omega\mathbf{I} - i\omega\,\mathbf{e}_{\beta_1}\mathbf{e}_{\beta_1}{}^\top|\,\overline{|\mathbf{B} + i\omega\mathbf{I} - i\omega\,\mathbf{e}_{\beta_2}\mathbf{e}_{\beta_2}{}^\top|} \tag{D.223}$$

Since all the matrices and vectors are purely real, we can write,

$$t(\omega; \mathbf{A}, \mathbf{B}, \mathbf{e}_{\beta_1}, \mathbf{e}_{\beta_2}) = 2\,|\mathbf{A} + i\omega\mathbf{I} - i\omega\,\mathbf{e}_{\beta_2}\mathbf{e}_{\beta_2}{}^\top|\,|\mathbf{B} - i\omega\mathbf{I} + i\omega\,\mathbf{e}_{\beta_2}\mathbf{e}_{\beta_2}{}^\top| \tag{D.224}$$

We use the property from Eq. (D.237), to write Eq. (D.224) as,

$$t(\omega; \mathbf{A}, \mathbf{B}, \mathbf{e}_{\beta_1}, \mathbf{e}_{\beta_2}) = 2\left(|\mathbf{A}+i\omega\mathbf{I}|-i\omega\mathbf{e}_{\beta_1}{}^\top\mathrm{adj}(\mathbf{A}+i\omega\mathbf{I})\mathbf{e}_{\beta_1}\right)\left(|\mathbf{B}-i\omega\mathbf{I}|+i\omega\,\mathbf{e}_{\beta_2}{}^\top\mathrm{adj}(\mathbf{B}-i\omega\mathbf{I})\mathbf{e}_{\beta_2}\right) \tag{D.225}$$

Since only one of the entries in the vectors $\mathbf{e}_{\beta_1}$ and $\mathbf{e}_{\beta_2}$ are 1, and the index is the same for both vectors (row or column), we can simplify $t(\omega; \mathbf{A}, \mathbf{B}, \mathbf{e}_{\beta_1}, \mathbf{e}_{\beta_2})$ by defining submatrices $\mathbf{C} \in \mathbb{R}^{n-1\times n-1}$ and $\mathbf{D} \in \mathbb{R}^{n-1\times n-1}$, by excluding the β_1 and β_2 row and column of the matrices $\mathbf{A}$ and $\mathbf{B}$, respectively. Eq. (D.225) then becomes,

$$t(\omega; \mathbf{A}, \mathbf{B}, \mathbf{e}_{\beta_1}, \mathbf{e}_{\beta_2}) = 2\left(|\mathbf{A} + i\omega\mathbf{I}| - i\omega|\mathbf{C} + i\omega\mathbf{I}|\right)\left(|\mathbf{B} - i\omega\mathbf{I}| + i\omega|\mathbf{D} - i\omega\mathbf{I}|\right) \tag{D.226}$$

On expanding the product, we get,

$$\begin{aligned} t(\omega; \mathbf{A}, \mathbf{B}, \mathbf{e}_{\beta_1}, \mathbf{e}_{\beta_2}) =& 2\,|\mathbf{A} + i\omega\mathbf{I}||\mathbf{B} - i\omega\mathbf{I}| + 2\,\omega^2|\mathbf{C} + i\omega\mathbf{I}||\mathbf{D} - i\omega\mathbf{I}| \\ & - 2\,i\omega|\mathbf{C} + i\omega\mathbf{I}||\mathbf{B} - i\omega\mathbf{I}| + 2\,i\omega|\mathbf{A} + i\omega\mathbf{I}||\mathbf{D} - i\omega\mathbf{I}|\Big] \end{aligned} \tag{D.227}$$

We split $t(\omega; \mathbf{A}, \mathbf{B}, \mathbf{e}_{\beta_1}, \mathbf{e}_{\beta_2})$ into its real and imaginary parts as follows,

$$\begin{aligned} t_1(\omega; \mathbf{A}, \mathbf{B}, \mathbf{e}_{\beta_1}, \mathbf{e}_{\beta_2}) =&\ 2\,\mathrm{Re}\left[|\mathbf{A} + i\omega\mathbf{I} - i\omega\,\mathbf{e}_{\beta_1}\mathbf{e}_{\beta_1}{}^{\top}|\,\overline{|\mathbf{B} + i\omega\mathbf{I} - i\omega\,\mathbf{e}_{\beta_2}\mathbf{e}_{\beta_2}{}^{\top}|}\right] \\ =&\ 2\,\mathrm{Re}\Big[|\mathbf{A} + i\omega\mathbf{I}||\mathbf{B} - i\omega\mathbf{I}|\Big] + 2\,\mathrm{Re}\Big[\omega^2|\mathbf{C} + i\omega\mathbf{I}||\mathbf{D} - i\omega\mathbf{I}|\Big] \\ &+ 2\,\mathrm{Re}\Big[-i\omega|\mathbf{C} + i\omega\mathbf{I}||\mathbf{B} - i\omega\mathbf{I}|\Big] + 2\,\mathrm{Re}\Big[i\omega|\mathbf{A} + i\omega\mathbf{I}||\mathbf{D} - i\omega\mathbf{I}|\Big]\Big] \\ =&\ 2\,\mathrm{Re}\Big[\overline{|\mathbf{A} + i\omega\mathbf{I}|}|\mathbf{B} + i\omega\mathbf{I}|\Big] + 2\,\omega^2\mathrm{Re}\Big[\overline{|\mathbf{C} + i\omega\mathbf{I}|}|\mathbf{D} + i\omega\mathbf{I}|\Big] \\ &+ 2\,\omega\mathrm{Im}\Big[\overline{|\mathbf{B} + i\omega\mathbf{I}|}|\mathbf{C} + i\omega\mathbf{I}|\Big] + 2\,\omega\mathrm{Im}\Big[\overline{|\mathbf{A} + i\omega\mathbf{I}|}|\mathbf{D} + i\omega\mathbf{I}|\Big]\Big] \end{aligned} \tag{D.228}$$

$$\begin{aligned} t_2(\omega; \mathbf{A}, \mathbf{B}, \mathbf{e}_{\beta_1}, \mathbf{e}_{\beta_2}) =&\ 2\,\mathrm{Im}\left[|\mathbf{A} + i\omega\mathbf{I} - i\omega\,\mathbf{e}_{\beta_1}\mathbf{e}_{\beta_1}{}^{\top}|\,\overline{|\mathbf{B} + i\omega\mathbf{I} - i\omega\,\mathbf{e}_{\beta_2}\mathbf{e}_{\beta_2}{}^{\top}|}\right] \\ =&\ 2\,\mathrm{Im}\Big[|\mathbf{A} + i\omega\mathbf{I}||\mathbf{B} - i\omega\mathbf{I}|\Big] + 2\,\mathrm{Im}\Big[\omega^2|\mathbf{C} + i\omega\mathbf{I}||\mathbf{D} - i\omega\mathbf{I}|\Big] \\ &+ 2\,\mathrm{Im}\Big[-i\omega|\mathbf{C} + i\omega\mathbf{I}||\mathbf{B} - i\omega\mathbf{I}|\Big] + 2\,\mathrm{Im}\Big[i\omega|\mathbf{A} + i\omega\mathbf{I}||\mathbf{D} - i\omega\mathbf{I}|\Big]\Big] \\ =&\ -2\,\mathrm{Im}\Big[\overline{|\mathbf{A} + i\omega\mathbf{I}|}|\mathbf{B} + i\omega\mathbf{I}|\Big] - 2\,\omega^2\mathrm{Im}\Big[\overline{|\mathbf{C} + i\omega\mathbf{I}|}|\mathbf{D} + i\omega\mathbf{I}|\Big] \\ &- 2\,\omega\mathrm{Re}\Big[\overline{|\mathbf{B} + i\omega\mathbf{I}|}|\mathbf{C} + i\omega\mathbf{I}|\Big] + 2\,\omega\mathrm{Re}\Big[\overline{|\mathbf{A} + i\omega\mathbf{I}|}|\mathbf{D} + i\omega\mathbf{I}|\Big]\Big] \end{aligned} \tag{D.229}$$

so that,

$$t(\omega; \mathbf{A}, \mathbf{B}, \mathbf{e}_{\beta_1}, \mathbf{e}_{\beta_2}) = t_1(\omega; \mathbf{A}, \mathbf{B}, \mathbf{e}_{\beta_1}, \mathbf{e}_{\beta_2}) + it_2(\omega; \mathbf{A}, \mathbf{B}, \mathbf{e}_{\beta_1}, \mathbf{e}_{\beta_2}) \tag{D.230}$$

Using the definitions of functions $g(\omega; \mathbf{A}, \mathbf{C})$ (Eq. (D.188)) and $h(\omega; \mathbf{A}, \mathbf{B})$ (Eq. (D.201)), we can write,

$$\begin{aligned} t_1(\omega; \mathbf{A}, \mathbf{B}, \mathbf{e}_{\beta_1}, \mathbf{e}_{\beta_2}) &= h_1(\omega; \mathbf{A}, \mathbf{B}) + \omega^2 h_1(\omega; \mathbf{C}, \mathbf{D}) + g_2(\omega; \mathbf{B}, \mathbf{C}) + g_2(\omega; \mathbf{A}, \mathbf{D}) \\ t_2(\omega; \mathbf{A}, \mathbf{B}, \mathbf{e}_{\beta_1}, \mathbf{e}_{\beta_2}) &= -h_2(\omega; \mathbf{A}, \mathbf{B}) - \omega^2 h_2(\omega; \mathbf{C}, \mathbf{D}) - g_1(\omega; \mathbf{B}, \mathbf{C}) + g_1(\omega; \mathbf{A}, \mathbf{D}) \end{aligned} \tag{D.231}$$

Finally, $t_1^\alpha(\mathbf{A}, \mathbf{B}, \mathbf{e}_{\beta_1}, \mathbf{e}_{\beta_2})$, for $\alpha \in \{0, \ldots, n\}$, and $t_2(\mathbf{A}, \mathbf{B}, \mathbf{e}_{\beta_1}, \mathbf{e}_{\beta_2})$, for $\alpha \in \{0, \ldots, n-1\}$, are defined to be the coefficients of $\omega^{2\alpha}$ and $\omega^{2\alpha+1}$ from the polynomial expansion of $t_1(\omega; \mathbf{A}, \mathbf{B}, \mathbf{e}_{\beta_1}, \mathbf{e}_{\beta_2})$ and $t_2(\omega; \mathbf{A}, \mathbf{B}, \mathbf{e}_{\beta_1}, \mathbf{e}_{\beta_2})$, respectively.

$$\begin{aligned} t_1^\alpha(\mathbf{A}, \mathbf{B}, \mathbf{e}_{\beta_1}, \mathbf{e}_{\beta_2}) &= h_1^\alpha(\mathbf{A}, \mathbf{B}) + h_1^{\alpha-1}(\mathbf{C}, \mathbf{D}) + g_2^\alpha(\mathbf{B}, \mathbf{C}) + g_2^\alpha(\mathbf{A}, \mathbf{D}) \\ t_2^\alpha(\mathbf{A}, \mathbf{B}, \mathbf{e}_{\beta_1}, \mathbf{e}_{\beta_2}) &= -h_2^\alpha(\mathbf{A}, \mathbf{B}) - h_2^{\alpha-1}(\mathbf{C}, \mathbf{D}) - g_1^\alpha(\mathbf{B}, \mathbf{C}) + g_1^\alpha(\mathbf{A}, \mathbf{D}) \end{aligned} \tag{D.232}$$

D.5 Basic Identities

In this section, we outline basic matrix identities and definitions that we utilize.

- If λ are the eigenvalues of matrix $\mathbf{A} \in \mathbb{R}^{n \times n}$, then λ^k are the eigenvalues of $\mathbf{A}^k$, where $k \in \mathbb{N}$.
- If λ are the eigenvalues of matrix $\mathbf{A} \in \mathbb{R}^{n \times n}$, then $\lambda + \alpha$, where $\alpha \in \mathbb{C}$, are the eigenvalues of the matrix $\mathbf{A} + \alpha \mathbf{I}$.
- If λ_i are the eigenvalues of matrix $\mathbf{A} \in \mathbb{R}^{n \times n}$, then we have,

$$\det(\mathbf{A}) = \prod_{k=1}^{n} \lambda_k \tag{D.233}$$

$$\mathrm{Tr}(\mathbf{A}) = \sum_{k=1}^{n} \lambda_k \tag{D.234}$$

- Properties of the adjugate of a matrix $\mathbf{A} \in \mathbb{R}^{n \times n}$,

$$\text{adj}(\mathbf{A})^\top = \text{adj}(\mathbf{A}^\top) \quad \text{and} \quad \text{adj}(\overline{\mathbf{A}}) = \overline{\text{adj}(\mathbf{A})} \tag{D.235}$$

- Laplace transform of a matrix exponential amounts to the resolvent of the matrix ($\mathbf{A} \in \mathbb{R}^{n \times n}$),

$$\mathcal{L}(e^{t\mathbf{A}}) = (s\mathbf{I} - \mathbf{A})^{-1} \tag{D.236}$$

- For a matrix $\mathbf{A} \in \mathbb{R}^{n \times n}$, vectors $\mathbf{u} \in \mathbb{R}^{n \times 1}$ and $\mathbf{v} \in \mathbb{R}^{n \times 1}$, and scalar $\alpha \in \mathbb{C}$, we have,

$$\det(\mathbf{A} + \alpha\, \mathbf{u}\mathbf{v}^\top) = \det(\mathbf{A}) + \alpha\, \mathbf{v}^\top \text{adj}(\mathbf{A})\mathbf{u} \tag{D.237}$$

- For a matrix $\mathbf{A} \in \mathbb{R}^{n \times n}$ with eigenvalues λ_k, the square modulus of the determinant of matrix $\mathbf{A} + i\omega\mathbf{I}$ can be written as,

$$||\mathbf{A} + i\omega\mathbf{I}||^2 = \prod_{k=1}^{n} |\lambda_k + i\omega|^2 = \prod_{k=1}^{n} (\lambda_k^2 + \omega^2) \tag{D.238}$$

- For a matrix $\mathbf{A} \in \mathbb{R}^{n \times n}$ with eigenvalues λ_k, we have,

$$\det(\omega\mathbf{I} - \mathbf{A}) \det(\omega\mathbf{I} - \mathbf{A}^\top) = \left(\prod_{j=1}^{n} (\omega - \lambda_j) \right) \left(\prod_{k=1}^{n} (\omega - \lambda_k) \right) = \prod_{j=1}^{n} (\omega - \lambda_j)^2 \tag{D.239}$$

- Given two polynomials $a(x) = a_0 + a_1 x + a_2 x^2 + \ldots + a_n x^n$ and $b(x) = b_0 + b_1 x + b_2 x^2 + \ldots + b_m x^m$, the product $a(x)b(x)$ yields a new polynomial of degree $m + n$,

$$a(x)b(x) = \sum_{k=0}^{m+n} c_k x^k \tag{D.240}$$

where c_k can be written as,

$$c_k = \sum_{i+j=k} a_i b_j \tag{D.241}$$

- We can express a monic polynomial in ω, in terms of elementary symmetric polynomials $e^i(\lambda_1, \lambda_2, \ldots, \lambda_n)$ as,

$$\prod_{i=1}^{n} (\lambda_i + \omega) = \sum_{i=0}^{n} e^i \omega^{n-i} \tag{D.242}$$

E | Upcrossings

E.1 Theory for the Upcrossing Process

We assume that all the properties of the autocorrelation function $r(t)$ described in Section 6.3 are followed. The upcrossing counting process $N_u^{\uparrow}(T)$ can be written as the integral of the underlying generator stochastic process X_t,

$$N_u^{\uparrow}(T) = \int_0^T \delta\left(X_{t_1} - u\right) \mathrm{H}\left(\dot{X}_{t_1}\right) \mathrm{d}X_{t_1} \tag{E.1}$$

where, $\dot{X}_t$ is the derivative stochastic process, $\delta(x)$ is the Dirac delta function and $\mathrm{H}(x)$ is the Heaviside step function. The condition $\delta\left(X_{t_1} - u\right)$ ensures that only the crossings of level u are counted and the condition $\mathrm{H}(\dot{X}_{t_1})$ ensures that only upcrossings are counted. Writing the expression above as an integral in time, we get,

$$N_u^{\uparrow}(T) = \int_0^T \delta\left(X_{t_1} - u\right) \mathrm{H}\left(\dot{X}_{t_1}\right) \dot{X}_{t_1} \, \mathrm{d}t_1 \tag{E.2}$$

E.1.1 Mean Number of Upcrossings

We take the expectation of $N_u^{\uparrow}(T)$ to get the mean number of upcrossings of X_t in time T,

$$\begin{aligned}\mathbb{E}\left[N_u^{\uparrow}(T)\right] &= \mathbb{E}\left[\int_0^T \delta\left(X_{t_1}-u\right)\ \mathrm{H}\left(\dot{X}_{t_1}\right)\dot{X}_{t_1}\,\mathrm{d}t_1\right] \\ &= \int_0^T \mathbb{E}\left[\delta\left(X_{t_1}-u\right)\ \mathrm{H}\left(\dot{X}_{t_1}\right)\dot{X}_{t_1}\right]\,\mathrm{d}t_1\end{aligned} \tag{E.3}$$

We define the random vector $\mathbf{P} = [X_{t_1},\, \dot{X}_{t_1}]^\top$ with probability density function (p.d.f.) given by $f_{\mathbf{P}}(x,\, y)$. Since X_t is stationary process, the distribution of $\mathbf{P}$ does not depend on t_1, implying that we can write $\mathbf{P} = [X_0,\, \dot{X}_0]^\top$. Therefore, $f_{\mathbf{P}}(u,\, y)$ is independent of time t_1 and we can rewrite Eq. (E.3) as,

$$\begin{aligned}\mathbb{E}\left[N_u^{\uparrow}(T)\right] &= \int_0^T \mathbb{E}\left[\delta\left(X_{t_1}-u\right)\ \mathrm{H}\left(\dot{X}_{t_1}\right)\dot{X}_{t_1}\right]\,\mathrm{d}t_1 \\ &= \int_0^T \int_{-\infty}^{\infty}\int_{-\infty}^{\infty} \delta\left(x-u\right)\ \mathrm{H}\left(y\right)\, y\, f_{\mathbf{P}}(x,\, y)\,\mathrm{d}x\,\mathrm{d}y\,\mathrm{d}t_1 \\ &= \int_0^T \int_{-\infty}^{\infty} \mathrm{H}\left(y\right)\, y\, f_{\mathbf{P}}(u,\, y)\,\mathrm{d}y\,\mathrm{d}t_1 \\ &= \int_0^T \int_{0}^{\infty} y\, f_{\mathbf{P}}(u,\, y)\,\mathrm{d}y\,\mathrm{d}t_1\end{aligned} \tag{E.4}$$

Since $f_{\mathbf{P}}(u,\, y)$ does not depend on time, t_1, we have,

$$\boxed{\mathbb{E}\left[N_u^{\uparrow}(T)\right] = T\int_0^{\infty} y\, f_{\mathbf{P}}(u,\, y)\,\mathrm{d}y} \tag{E.5}$$

If we further assume that X_t is zero-mean and Gaussian distributed, this implies that $\mathbf{P}$ is a zero-mean multivariate Gaussian stationary process with the correlation matrix defined as,

$$\Sigma_{\mathbf{P}} = \begin{bmatrix} \mathbb{E}\left[X_0 X_0\right] & \mathbb{E}\left[X_0 \dot{X}_0\right] \\ \mathbb{E}\left[\dot{X}_0 X_0\right] & \mathbb{E}\left[\dot{X}_0 \dot{X}_0\right] \end{bmatrix} = \begin{bmatrix} r(0) & 0 \\ 0 & -r''(0) \end{bmatrix} \tag{E.6}$$

We have calculated the entries of this matrix as follows:

- $\mathbb{E}\left[X_0 X_0\right] = r(0)$ by definition.
- $\mathbb{E}[X_0 \dot{X}_0] = \mathbb{E}[X_{t_1} \dot{X}_{t_2}]_{t_2=t_1}$. Taking the derivative outside of the expectation, we get, $\mathbb{E}[X_0 \dot{X}_0] = \frac{\partial \mathbb{E}[X_{t_1} X_{t_2}]}{\partial t_2}\Big|_{t_2=t_1} = \frac{\partial r(t_2 - t_1)}{\partial t_2}\Big|_{t_2=t_1} = r'(t_2 - t_1)|_{t_2=t_1} = r'(0) = 0.$
- $\mathbb{E}\left[\dot{X}_0 X_0\right] = \mathbb{E}[X_0 \dot{X}_0] = 0.$
- $\mathbb{E}[\dot{X}_0 \dot{X}_0] = \mathbb{E}[\dot{X}_{t_1} \dot{X}_{t_2}]_{t_2=t_1}$. Taking the derivatives outside of the expectation, we get, $\mathbb{E}[\dot{X}_0 \dot{X}_0] = \frac{\partial^2 \mathbb{E}[X_{t_1} X_{t_2}]}{\partial t_1 \partial t_2}\Big|_{t_2=t_1} = \frac{\partial^2 r(t_2 - t_1)}{\partial t_1 \partial t_2}\Big|_{t_2=t_1} = -r''(t_2 - t_1)|_{t_2=t_1} = -r''(0).$

Using this covariance matrix, we can define the p.d.f. $f_{\mathbf{P}}(x, y)$ as,

$$\begin{aligned} f_{\mathbf{P}}(x, y) &= \frac{1}{2\pi\sqrt{|\Sigma_{\mathbf{P}}|}} \exp\left(-\frac{1}{2}[x, y]\, \Sigma_{\mathbf{P}}^{-1}\, [x, y]^\top\right) \\ &= \frac{1}{2\pi\sqrt{r(0)\,(-r''(0))}} \exp\left(-\frac{1}{2}\left(\frac{x^2}{r(0)} + \frac{y^2}{(-r''(0))}\right)\right). \end{aligned} \tag{E.7}$$

Substituting the expression for $f_{\mathbf{P}}(x,\, y)$ into the integral in Eq. (E.5) yields

$$\mathbb{E}\left[N_u^{\uparrow}(T)\right] = T\, \frac{1}{2\pi} \sqrt{\frac{-r''(0)}{r(0)}}\, e^{-\frac{u^2}{2r(0)}}. \tag{E.8}$$

E.1.2 Variance of Upcrossings

The variance of $N_u^{\uparrow}(T)$ is given by,

$$\mathrm{Var}\left[N_u^{\uparrow}(T)\right] = \mathbb{E}\left[N_u^{\uparrow}(T)^2\right] - \mathbb{E}\left[N_u^{\uparrow}(T)\right]^2 \tag{E.9}$$

$\mathbb{E}\left[N_u^{\uparrow}(T)\right]$ is known from the previous section, therefore, we focus on $\mathbb{E}\left[N_u^{\uparrow}(T)^2\right]$. Consider the counting process $N_u^{\uparrow}(T)$ as the integral over time of the differential process, i.e.,

$$N_u^{\uparrow}(T) = \int_0^T \mathrm{d}N_u^{\uparrow}(t_1) \tag{E.10}$$

Therefore, we can write $\mathbb{E}\left[N_u^{\uparrow}(T)^2\right]$ as,

$$\begin{aligned}
\mathbb{E}\left[N_u^{\uparrow}(T)^2\right] &= \mathbb{E}\left[\int_0^T \mathrm{d}N_u^{\uparrow}(t_1) \int_0^T \mathrm{d}N_u^{\uparrow}(t_2)\right] \\
&= \mathbb{E}\left[\int_0^T \int_0^T \mathrm{d}N_u^{\uparrow}(t_1)\, \mathrm{d}N_u^{\uparrow}(t_2)\right] \\
&= \mathbb{E}\left[\int_0^T \int_0^T \mathbf{1}_{t_1=t_2}\, \mathrm{d}N_u^{\uparrow}(t_1)\, \mathrm{d}N_u^{\uparrow}(t_2) + \int_0^T \int_0^T \mathbf{1}_{t_1\neq t_2}\, \mathrm{d}N_u^{\uparrow}(t_1)\, \mathrm{d}N_u^{\uparrow}(t_2)\right] \\
&= \mathbb{E}\left[\int_0^T \mathrm{d}N_u^{\uparrow}(t_1)^2 + \int_0^T \int_0^T \mathbf{1}_{t_1\neq t_2}\, \mathrm{d}N_u^{\uparrow}(t_1)\, \mathrm{d}N_u^{\uparrow}(t_2)\right]
\end{aligned} \tag{E.11}$$

Now since there can only be either zero or one crossing at any given time, or $\mathrm{d}N_u^{\uparrow}(t_1)$ can either be 0 or 1, we have the following relation $\mathrm{d}N_u^{\uparrow}(t_1)^2 = \mathrm{d}N_u^{\uparrow}(t_1)$. Substituting this in the expression above, we get,

$$\begin{aligned}
\mathbb{E}\left[N_u^{\uparrow}(T)^2\right] &= \mathbb{E}\left[\int_0^T \mathrm{d}N_u^{\uparrow}(t_1)\right] + \mathbb{E}\left[\int_0^T \int_0^T \mathbf{1}_{t_1\neq t_2}\, \mathrm{d}N_u^{\uparrow}(t_1)\, \mathrm{d}N_u^{\uparrow}(t_2)\right] \\
&= \mathbb{E}\left[N_u^{\uparrow}(T)\right] + \underbrace{\mathbb{E}\left[\int_0^T \int_0^T \mathbf{1}_{t_1\neq t_2}\, \mathrm{d}N_u^{\uparrow}(t_1)\, \mathrm{d}N_u^{\uparrow}(t_2)\right]}_{M_2}
\end{aligned} \tag{E.12}$$

Hence, $\mathbb{E}\left[N_u^{\uparrow}(T)^2\right] = \mathbb{E}\left[N_u^{\uparrow}(T)\right] + M_2$, where M_2 is the second factorial moment of $N_u^{\uparrow}(T)$. Now, we use the definition of $N_u^{\uparrow}(T)$ from Eq. (E.2) to get the following expression for M_2,

$$M_2 = \int_0^T \int_0^T \mathbb{E}\left[\mathbf{1}_{t_1\neq t_2}\, \mathrm{H}\left(\dot{X}_{t_1}\right) \mathrm{H}\left(\dot{X}_{t_2}\right) \delta\left(X_{t_1} - u\right)\, \delta\left(X_{t_2} - u\right)\, \dot{X}_{t_1}\, \dot{X}_{t_2}\right] \mathrm{d}t_1\, \mathrm{d}t_2 \tag{E.13}$$

We define the random vector $\mathbf{Q} = [X_{t_1},\, X_{t_2},\, \dot{X}_{t_1},\, \dot{X}_{t_2}]^\top$ with p.d.f. given by $f_{\mathbf{Q}}(x_1,\, x_2,\, y_1,\, y_2;\, t_1,\, t_2)$. Since X_t is a stationary process, $\mathbf{Q}$ only depends on t_1 and t_2 through their difference $(t_2 - t_1)$ or $f_{\mathbf{Q}}(x_1,\, x_2,\, y_1,\, y_2;\, t_2 - t_1)$. Further, since X_t is zero-mean and Gaussian distributed, $\mathbf{Q}$ is a zero-mean multivariate Gaussian stationary process with the correlation matrix defined as,

$$\Sigma_{\mathbf{Q}}(t) = \begin{bmatrix} \mathbb{E}\left[X_{t_1}X_{t_1}\right] & \mathbb{E}\left[X_{t_1}X_{t_2}\right] & \mathbb{E}\left[X_{t_1}\dot{X}_{t_1}\right] & \mathbb{E}\left[X_{t_1}\dot{X}_{t_2}\right] \\ \mathbb{E}\left[X_{t_2}X_{t_1}\right] & \mathbb{E}\left[X_{t_2}X_{t_2}\right] & \mathbb{E}\left[X_{t_2}\dot{X}_{t_1}\right] & \mathbb{E}\left[X_{t_2}\dot{X}_{t_2}\right] \\ \mathbb{E}\left[\dot{X}_{t_1}X_{t_1}\right] & \mathbb{E}\left[\dot{X}_{t_1}X_{t_2}\right] & \mathbb{E}\left[\dot{X}_{t_1}\dot{X}_{t_1}\right] & \mathbb{E}\left[\dot{X}_{t_1}\dot{X}_{t_2}\right] \\ \mathbb{E}\left[\dot{X}_{t_2}X_{t_1}\right] & \mathbb{E}\left[\dot{X}_{t_2}X_{t_2}\right] & \mathbb{E}\left[\dot{X}_{t_2}\dot{X}_{t_1}\right] & \mathbb{E}\left[\dot{X}_{t_2}\dot{X}_{t_2}\right] \end{bmatrix} = \begin{bmatrix} r(0) & r(t) & 0 & r'(t) \\ r(t) & r(0) & -r'(t) & 0 \\ 0 & -r'(t) & -r''(0) & -r''(t) \\ r'(t) & 0 & -r''(t) & -r''(0) \end{bmatrix}, \tag{E.14}$$

where $t = t_2 - t_1$. The following properties emerge from the fact that $r(t)$ is a symmetric function about origin: $r(-t) = r(t)$, $r'(-t) = -r'(t)$ and $r''(-t) = r''(t)$. We used these properties to simplify the covariance matrix above. Using the p.d.f., we can write M_2 from Eq. (E.13) as,

$$\begin{aligned} M_2 &= \int_0^T \int_0^T \mathbb{E}\left[\mathbf{1}_{t_1 \neq t_2}\, \mathrm{H}\left(\dot{X}_{t_1}\right) \mathrm{H}\left(\dot{X}_{t_2}\right) \delta\left(X_{t_1} - u\right)\, \delta\left(X_{t_2} - u\right)\, \dot{X}_{t_1}\, \dot{X}_{t_2}\right] \mathrm{d}t_1\, \mathrm{d}t_2 \\ &= \int_0^T \int_0^T \int_{-\infty}^{\infty} \int_{-\infty}^{\infty} \int_{-\infty}^{\infty} \int_{-\infty}^{\infty} \Big(\mathbf{1}_{t_1 \neq t_2}\, \mathrm{H}\left(y_1\right) \mathrm{H}\left(y_2\right) \delta\left(x_1 - u\right)\, \delta\left(x_2 - u\right) \\ &\qquad\qquad y_1 y_2\, f_{\mathbf{Q}}(x_1,\, x_2,\, y_1,\, y_2;\, t_2 - t_1) \Big) \mathrm{d}x_1\, \mathrm{d}x_2\, \mathrm{d}y_1\, \mathrm{d}y_2\, \mathrm{d}t_1\, \mathrm{d}t_2 \\ &= \int_0^T \int_0^T \int_{-\infty}^{\infty} \int_{-\infty}^{\infty} \mathbf{1}_{t_1 \neq t_2}\, \mathrm{H}\left(y_1\right) \mathrm{H}\left(y_2\right) y_1 y_2\, f_{\mathbf{Q}}(u,\, u,\, y_1,\, y_2;\, t_2 - t_1)\, \mathrm{d}y_1\, \mathrm{d}y_2\, \mathrm{d}t_1\, \mathrm{d}t_2 \\ &= \int_0^T \int_0^T \int_0^{\infty} \int_0^{\infty} y_1 y_2\, f_{\mathbf{Q}}(u,\, u,\, y_1,\, y_2;\, t_2 - t_1)\, \mathrm{d}y_1\, \mathrm{d}y_2\, \mathrm{d}t_1\, \mathrm{d}t_2 \end{aligned} \tag{E.15}$$

Note that we neglected the condition $\mathbf{1}_{t_1 \neq t_2}$ in the integrand above because the only time-dependent term is the p.d.f., and it has no singularities; therefore, its contribution to the final integral is infinitesimally small. Consider $\mathbb{E}\left[N_u^{\uparrow}(T)\right]^2$, using Eq. (E.4), we get,

$$\begin{aligned} \mathbb{E}\left[N_u^{\uparrow}(T)\right]^2 &= \left(\int_0^T \int_0^{\infty} y_1\, f_{\mathrm{P}}(u,\, y_1)\, \mathrm{d}y_1\, \mathrm{d}t_1 \right) \left(\int_0^T \int_0^{\infty} y_2\, f_{\mathrm{P}}(u,\, y_2)\, \mathrm{d}y_2\, \mathrm{d}t_2 \right) \\ &= \int_0^T \int_0^T \int_0^{\infty} \int_0^{\infty} y_1 y_2\, f_{\mathrm{P}}(u,\, y_1)\, f_{\mathrm{P}}(u,\, y_2)\, \mathrm{d}y_1\, \mathrm{d}y_2\, \mathrm{d}t_1\, \mathrm{d}t_2 \end{aligned} \tag{E.16}$$

The variance of $N_u^{\uparrow}(T)$ is given by,

$$\begin{aligned}\operatorname{Var}\left[N_u^{\uparrow}(T)\right] =& \mathbb{E}\left[N_u^{\uparrow}(T)^2\right] - \mathbb{E}\left[N_u^{\uparrow}(T)\right]^2 \\ =& \mathbb{E}\left[N_u^{\uparrow}(T)\right] + M_2 - \mathbb{E}\left[N_u^{\uparrow}(T)\right]^2 \\ =& \mathbb{E}\left[N_u^{\uparrow}(T)\right] + \int_0^T \int_0^T \int_0^\infty \int_0^\infty y_1 y_2 \left(f_{\mathrm{Q}}(u,\, u,\, y_1,\, y_2;\, t_2 - t_1)\right. \\ & \left. - f_{\mathrm{P}}(u,\, y_1)\, f_{\mathrm{P}}(u,\, y_2)\right) \mathrm{d}y_1\, \mathrm{d}y_2\, \mathrm{d}t_1\, \mathrm{d}t_2\end{aligned} \tag{E.17}$$

We define I' as follows:

$$I' = \int_0^T \int_0^T \int_0^\infty \int_0^\infty y_1 y_2 \left(f_{\mathrm{Q}}(u, u, y_1, y_2; t_2 - t_1) - f_{\mathrm{P}}(u, y_1)\, f_{\mathrm{P}}(u, y_2)\right)\, \mathrm{d}y_1\, \mathrm{d}y_2\, \mathrm{d}t_1\, \mathrm{d}t_2. \tag{E.18}$$

We make the following variable change in I': $t = t_2 - t_1$ and $s = t_2$. The integral over t_1 and t_2 is calculated on the positive quadrant (Fig. E.1a), and this transforms to the area in Fig. E.1b when done in the new coordinates, t and s. We write the new integral separately over the regions I and II (Fig. E.1b),

$$\begin{aligned}I' =& \int_{-T}^0 \int_0^{t+T} \int_0^\infty \int_0^\infty y_1 y_2 \left(f_{\mathrm{Q}}(u,\, u,\, y_1,\, y_2;\, t) - f_{\mathrm{P}}(u,\, y_1)\, f_{\mathrm{P}}(u,\, y_2)\right)\, \mathrm{d}y_1\, \mathrm{d}y_2\, \mathrm{d}s\, \mathrm{d}t \\ &+ \int_0^T \int_t^T \int_0^\infty \int_0^\infty y_1 y_2 \left(f_{\mathrm{Q}}(u,\, u,\, y_1,\, y_2;\, t) - f_{\mathrm{P}}(u,\, y_1)\, f_{\mathrm{P}}(u,\, y_2)\right)\, \mathrm{d}y_1\, \mathrm{d}y_2\, \mathrm{d}s\, \mathrm{d}t\end{aligned} \tag{E.19}$$

Transforming the sign of t in the first integral, we get,

$$\begin{aligned}I' =& \int_0^T \int_0^{-t+T} \int_0^\infty \int_0^\infty y_1 y_2 \left(f_{\mathrm{Q}}(u,\, u,\, y_1,\, y_2;\, -t) - f_{\mathrm{P}}(u,\, y_1)\, f_{\mathrm{P}}(u,\, y_2)\right)\, \mathrm{d}y_1\, \mathrm{d}y_2\, \mathrm{d}s\, \mathrm{d}t \\ &+ \int_0^T \int_t^T \int_0^\infty \int_0^\infty y_1 y_2 \left(f_{\mathrm{Q}}(u,\, u,\, y_1,\, y_2;\, t) - f_{\mathrm{P}}(u,\, y_1)\, f_{\mathrm{P}}(u,\, y_2)\right)\, \mathrm{d}y_1\, \mathrm{d}y_2\, \mathrm{d}s\, \mathrm{d}t\end{aligned} \tag{E.20}$$

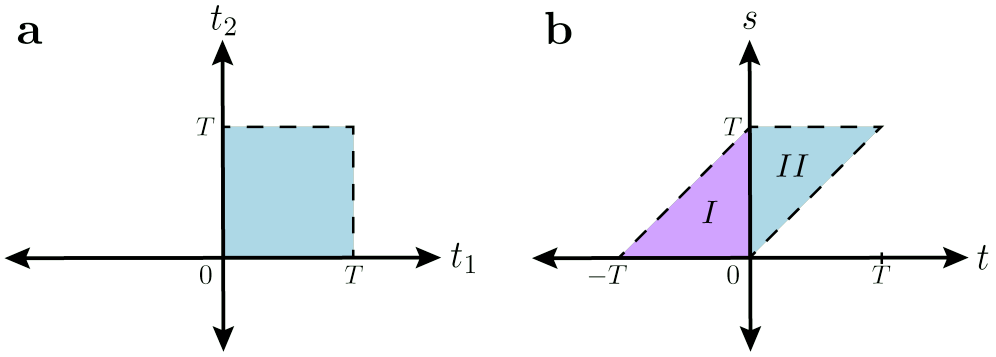


Figure E.1: Variable transform visualized. (a) The area under which the integral is performed for t_1 and t_2. (b) The area under which the integral should be performed upon variable transformation given by $t = t_2 - t_1$ and $s = t_2$. I and II represent further partitioning of this region.

Since the integrand does not depend on s, we integrate in s and get,

$$\begin{aligned} I' = &\int_0^T \int_0^\infty \int_0^\infty (T-t)\, y_1 y_2 \, \left(f_{\mathbf{Q}}(u,\, u,\, y_1,\, y_2;\, -t) - f_{\mathbf{P}}(u,\, y_1)\, f_{\mathbf{P}}(u,\, y_2) \right) \, \mathrm{d}y_1 \, \mathrm{d}y_2 \, \mathrm{d}t \\ &+ \int_0^T \int_0^\infty \int_0^\infty (T-t)\, y_1 y_2 \, \left(f_{\mathbf{Q}}(u,\, u,\, y_1,\, y_2;\, t) - f_{\mathbf{P}}(u,\, y_1)\, f_{\mathbf{P}}(u,\, y_2) \right) \, \mathrm{d}y_1 \, \mathrm{d}y_2 \, \mathrm{d}t \end{aligned} \tag{E.21}$$

The two integrals are done over the same volume and have the same integrands except for the sign of t in the p.d.f. Consider the p.d.f. in the first integrand $f_{\mathbf{Q}}(u,\, u,\, y_1,\, y_2;\, -t)$. Since $\mathbf{Q}$ is a multivariate Gaussian, we have,

$$f_{\mathbf{Q}}(u,\, u,\, y_1,\, y_2;\, -t) = \frac{1}{4\pi^2 \sqrt{\left|\Sigma_{\mathbf{Q}}(-t)\right|}} \exp\left(-\frac{1}{2} [u, u, y_1, y_2]\, \Sigma_{\mathbf{Q}}(-t)^{-1}\, [u, u, y_1, y_2]^\top \right) \tag{E.22}$$

Using the definition of $\Sigma_{\mathbf{Q}}(-t)$ in Eq. (E.14) and the properties of $r(t)$, $r'(t)$ and $r''(t)$, we have,

$$\Sigma_{\mathbf{Q}}(-t) = \begin{bmatrix} r(0) & r(t) & 0 & -r'(t) \\ r(t) & r(0) & r'(t) & 0 \\ 0 & r'(t) & -r''(0) & -r''(t) \\ -r'(t) & 0 & -r''(t) & -r''(0) \end{bmatrix}. \tag{E.23}$$

Notice that $\Sigma_{\mathbf{Q}}(-t)$ is related to the $\Sigma_{\mathbf{Q}}(t)$ by just a change of sign on the antidiagonal. It can

be easily verified that $\left|\Sigma_{\mathrm{Q}}(-t)\right| = \left|\Sigma_{\mathrm{Q}}(t)\right|$ and $f_{\mathrm{Q}}(u,\, u,\, y_1,\, y_2;\, -t) = f_{\mathrm{Q}}(u,\, u,\, y_2,\, y_1;\, t)$. Therefore, Eq. (E.21) becomes,

$$\begin{aligned} I' = &\int_0^T \int_0^\infty \int_0^\infty (T-t)\, y_1 y_2 \, \left(f_{\mathrm{Q}}(u,\, u,\, y_2,\, y_1;\, t) - f_{\mathrm{P}}(u,\, y_1)\, f_{\mathrm{P}}(u,\, y_2)\right) \, \mathrm{d}y_1 \, \mathrm{d}y_2 \, \mathrm{d}t \\ &+ \int_0^T \int_0^\infty \int_0^\infty (T-t)\, y_1 y_2 \, \left(f_{\mathrm{Q}}(u,\, u,\, y_1,\, y_2;\, t) - f_{\mathrm{P}}(u,\, y_1)\, f_{\mathrm{P}}(u,\, y_2)\right) \, \mathrm{d}y_1 \, \mathrm{d}y_2 \, \mathrm{d}t \end{aligned} \tag{E.24}$$

In the first integral, we interchange the variables y_1 and y_2 to get,

$$\begin{aligned} &\int_0^T \int_0^\infty \int_0^\infty (T-t)\, y_1 y_2 \, \left(f_{\mathrm{Q}}(u,\, u,\, y_2,\, y_1;\, t) - f_{\mathrm{P}}(u,\, y_1)\, f_{\mathrm{P}}(u,\, y_2)\right) \, \mathrm{d}y_1 \, \mathrm{d}y_2 \, \mathrm{d}t \\ &\quad = \int_0^T \int_0^\infty \int_0^\infty (T-t)\, y_1 y_2 \, \left(f_{\mathrm{Q}}(u,\, u,\, y_1,\, y_2;\, t) - f_{\mathrm{P}}(u,\, y_1)\, f_{\mathrm{P}}(u,\, y_2)\right) \, \mathrm{d}y_1 \, \mathrm{d}y_2 \, \mathrm{d}t \end{aligned} \tag{E.25}$$

Therefore, I' is given by,

$$I' = 2\,T \int_0^T \int_0^\infty \int_0^\infty \left(1 - \frac{t}{T}\right) y_1 y_2 \, \left(f_{\mathrm{Q}}(u,\, u,\, y_1,\, y_2;\, t) - f_{\mathrm{P}}(u,\, y_1)\, f_{\mathrm{P}}(u,\, y_2)\right) \, \mathrm{d}y_1 \, \mathrm{d}y_2 \, \mathrm{d}t \tag{E.26}$$

Therefore, the variance of $N_u^{\uparrow}(T)$ is given by,

$$\boxed{\begin{aligned} \mathrm{Var}\left[N_u^{\uparrow}(T)\right] = \mathbb{E}\left[N_u^{\uparrow}(T)\right] + 2\,T \int_0^T \int_0^\infty \int_0^\infty \left(1 - \frac{t}{T}\right) y_1 y_2 \big(f_{\mathrm{Q}}(u,\, u,\, y_1,\, y_2;\, t) \\ - f_{\mathrm{P}}(u,\, y_1)\, f_{\mathrm{P}}(u,\, y_2)\big) \, \mathrm{d}y_1 \, \mathrm{d}y_2 \, \mathrm{d}t. \end{aligned}} \tag{E.27}$$

E.1.2.1 Central Limit Theorem for Variance

We consider the infinite time limit for the variance per unit time, i.e., $\lim_{T\to\infty} \frac{\mathrm{Var}[N_u^{\uparrow}(T)]}{T}$. We can split the integral in Eq. (E.27) as follows,

$$\begin{aligned}
&\lim_{T\to\infty} \frac{\mathrm{Var}\left[N_u^{\uparrow}(T)\right]}{T} = \lim_{T\to\infty} \frac{\mathbb{E}\left[N_u^{\uparrow}(T)\right]}{T} \\
&+ 2\int_0^\infty \int_0^\infty \int_0^\infty y_1 y_2 \big(f_{\mathrm{Q}}(u,\, u,\, y_1,\, y_2;\, t) - f_{\mathrm{P}}(u,\, y_1)\, f_{\mathrm{P}}(u,\, y_2)\big) \mathrm{d}y_1\, \mathrm{d}y_2\, \mathrm{d}t \\
&- \lim_{T\to\infty} \frac{2}{T} \underbrace{\int_0^\infty \int_0^\infty \int_0^\infty t\, y_1 y_2\, \left(f_{\mathrm{Q}}(u,\, u,\, y_1,\, y_2;\, t) - f_{\mathrm{P}}(u,\, y_1)\, f_{\mathrm{P}}(u,\, y_2)\right)\, \mathrm{d}y_1\, \mathrm{d}y_2\, \mathrm{d}t}_{I''}
\end{aligned} \tag{E.28}$$

Consider the second integral in the expression above: $2\lim_{T\to\infty} I''/T$. If I'' is finite then $2\lim_{T\to\infty} I''/T = 0$. In fact, if the following condition is satisfied, then I'' is finite [170], pg. 60.

$$\int_0^\infty t\, \left(|r(t)| + |r'(t)| + |r''(t)|\right)\, \mathrm{d}t < \infty\,. \tag{E.29}$$

Assuming this condition is satisfied, the variance in the long time limit is given by,

$$\boxed{\begin{aligned}
\lim_{T\to\infty} \frac{\mathrm{Var}\left[N_u^{\uparrow}(T)\right]}{T} = \lim_{T\to\infty} \frac{\mathbb{E}\left[N_u^{\uparrow}(T)\right]}{T} + 2\int_0^\infty \int_0^\infty \int_0^\infty y_1 y_2 \big(f_{\mathrm{Q}}(u,\, u,\, y_1,\, y_2;\, t) \\
- f_{\mathrm{P}}(u,\, y_1)\, f_{\mathrm{P}}(u,\, y_2)\big) \mathrm{d}y_1\, \mathrm{d}y_2\, \mathrm{d}t.
\end{aligned}} \tag{E.30}$$

E.1.3 Fano Factor

The Fano factor is defined as the ratio of variance and mean of $N_u^{\uparrow}(T)$ in the infinite time limit,

$$\mathrm{F}^{\uparrow} = \lim_{T\to\infty} \frac{\mathrm{Var}[N_u^{\uparrow}(T)]}{\mathbb{E}[N_u^{\uparrow}(T)]} \tag{E.31}$$

Taking the formula for variance from Eq. (E.30), we get,

$$\begin{aligned} \mathrm{F}^{\uparrow} &= \frac{\mathbb{E}\left[N_u^{\uparrow}(T)\right] + 2\,T \int_0^{\infty}\int_0^{\infty}\int_0^{\infty} y_1 y_2 \,\left(f_{\mathrm{Q}}(u,\,u,\,y_1,\,y_2;\,t) - f_{\mathrm{P}}(u,\,y_1)\,f_{\mathrm{P}}(u,\,y_2)\right)\,\mathrm{d}y_1\,\mathrm{d}y_2\,\mathrm{d}t}{\mathbb{E}[N_u^{\uparrow}(T)]} \\ &= 1 + \frac{2\,T \int_0^{\infty}\int_0^{\infty}\int_0^{\infty} y_1 y_2 \,\left(f_{\mathrm{Q}}(u,\,u,\,y_1,\,y_2;\,t) - f_{\mathrm{P}}(u,\,y_1)\,f_{\mathrm{P}}(u,\,y_2)\right)\,\mathrm{d}y_1\,\mathrm{d}y_2\,\mathrm{d}t}{\mathbb{E}[N_u^{\uparrow}(T)]} \end{aligned} \tag{E.32}$$

Substituting the mean formula from Eq. (E.5), we get the final expression for the Fano factor,

$$\boxed{\mathrm{F}^{\uparrow} = 1 + \frac{2\int_0^{\infty}\int_0^{\infty}\int_0^{\infty} y_1 y_2 \,\left(f_{\mathrm{Q}}(u,\,u,\,y_1,\,y_2;\,t) - f_{\mathrm{P}}(u,\,y_1)\,f_{\mathrm{P}}(u,\,y_2)\right)\,\mathrm{d}y_1\,\mathrm{d}y_2\,\mathrm{d}t}{\int_0^{\infty} y\, f_{\mathrm{P}}(u,\,y)\,\mathrm{d}y}.} \tag{E.33}$$

E.2 Theory for the Crossing Process

In this section, we derive the formulae for the mean, variance, and Fano factor for the crossing process, i.e., including both *up* and *down* crossings. The steps involved in deriving these formulae are similar to the ones we used for the upcrossing process in Section E.1, therefore, we offer a brief discussion of the proof. The counting process for the total number of crossings can be written as,

$$N_u(T) = \int_0^T \delta\left(X_{t_1} - u\right)\left|\dot{X}_{t_1}\right|\,\mathrm{d}t_1 \tag{E.34}$$

E.2.1 Mean Number of Crossings

Taking the expectation of the equation above, we get,

$$\begin{aligned} \mathbb{E}\left[N_u(T)\right] &= \int_0^T \mathbb{E}\left[\delta\left(X_{t_1} - u\right)\left|\dot{X}_{t_1}\right|\right]\,\mathrm{d}t_1 \\ &= \int_0^T \int_{-\infty}^{\infty} |y|\, f_{\mathrm{P}}(u,\,y)\,\mathrm{d}y\,\mathrm{d}t_1 \end{aligned} \tag{E.35}$$

where, $f_{\mathbf{P}}(x,\, y)$ is the p.d.f. of the random vector $\mathbf{P} = [X_{t_1},\, \dot{X}_{t_1}]^\top$.

E.2.2 Variance and Fano Factor of Crossings

Using an argument similar to that in Section E.1.2 we can write $\mathbb{E}\left[N_u(T)^2\right]$ as the following integral,

$$\mathbb{E}\left[N_u(T)^2\right] = \mathbb{E}\left[N_u(T)\right] + \underbrace{\mathbb{E}\left[\int_0^T \int_0^T \mathbf{1}_{t_1 \neq t_2}\, \mathrm{d}N_u(t_1)\, \mathrm{d}N_u(t_2)\right]}_{M_2} \tag{E.36}$$

Now using Eq. (E.34), M_2 can be written as,

$$\begin{aligned} M_2 &= \int_0^T \int_0^T \mathbb{E}\left[\mathbf{1}_{t_1 \neq t_2}\, \delta\left(X_{t_1} - u\right)\, \delta\left(X_{t_2} - u\right) \left|\dot{X}_{t_1}\right| \left|\dot{X}_{t_2}\right|\right] \mathrm{d}t_1\, \mathrm{d}t_2 \\ &= \int_0^T \int_0^T \int_{-\infty}^{\infty} \int_{-\infty}^{\infty} |y_1 y_2|\; f_{\mathbf{Q}}(u,\, u,\, y_1,\, y_2;\, t_2 - t_1)\, \mathrm{d}y_1\, \mathrm{d}y_2\, \mathrm{d}t_1\, \mathrm{d}t_2 \end{aligned} \tag{E.37}$$

where, $f_{\mathbf{Q}}(u,\, u,\, y_1,\, y_2;\, t_2 - t_1)$ is the p.d.f. of the random vector $\mathbf{Q} = [X_{t_1},\, X_{t_2},\, \dot{X}_{t_1},\, \dot{X}_{t_2}]^\top$. The variance of $N_u(T)$ is given by,

$$\begin{aligned} \mathrm{Var}\left[N_u(T)\right] &= \mathbb{E}\left[N_u(T)^2\right] - \mathbb{E}\left[N_u(T)\right]^2 \\ &= \int_0^T \int_0^T \int_{-\infty}^{\infty} \int_{-\infty}^{\infty} |y_1 y_2|\; f_{\mathbf{Q}}(u,\, u,\, y_1,\, y_2;\, t_2 - t_1)\, \mathrm{d}y_1\, \mathrm{d}y_2\, \mathrm{d}t_1\, \mathrm{d}t_2 \\ &\quad + \mathbb{E}\left[N_u(T)\right] - \mathbb{E}\left[N_u(T)\right]^2 \end{aligned} \tag{E.38}$$

We use Eq. (E.35) to write $\mathbb{E}\left[N_u(T)\right]^2$ as a double integral, which gives us,

$$\begin{aligned} \mathrm{Var}\left[N_u(T)\right] &= \mathbb{E}\left[N_u(T)^2\right] - \mathbb{E}\left[N_u(T)\right]^2 \\ &= \mathbb{E}\left[N_u(T)\right] + \int_0^T \int_0^T \int_{-\infty}^{\infty} \int_{-\infty}^{\infty} |y_1 y_2| \left(f_{\mathbf{Q}}(u,\, u,\, y_1,\, y_2;\, t_2 - t_1)\right. \\ &\qquad \left. - f_{\mathbf{P}}(u,\, y_1)\, f_{\mathbf{P}}(u,\, y_2)\right) \mathrm{d}y_1\, \mathrm{d}y_2\, \mathrm{d}t_1\, \mathrm{d}t_2 \end{aligned} \tag{E.39}$$

We define:

$$I' = \int_0^T \int_0^T \int_{-\infty}^{\infty} \int_{-\infty}^{\infty} |y_1 y_2| \left(f_{\mathrm{Q}}(u, u, y_1, y_2; t_2 - t_1) - f_{\mathrm{P}}(u, y_1)\, f_{\mathrm{P}}(u, y_2) \right) \mathrm{d}y_1\, \mathrm{d}y_2\, \mathrm{d}t_1\, \mathrm{d}t_2 \quad \text{(E.40)}$$

Making the variable transformation $t_2 - t_2 = t$, $t_2 = s$ and using the arguments about the integral from Section E.1.2, we can write I' as,

$$I' = 2\,T \int_0^T \int_{-\infty}^{\infty} \int_{-\infty}^{\infty} \left(1 - \frac{t}{T}\right) |y_1 y_2| \left(f_{\mathrm{Q}}(u,\, u,\, y_1,\, y_2;\, t) - f_{\mathrm{P}}(u,\, y_1)\, f_{\mathrm{P}}(u,\, y_2) \right) \mathrm{d}y_1\, \mathrm{d}y_2\, \mathrm{d}t \quad \text{(E.41)}$$

Therefore, the variance is given by,

$$\boxed{\begin{aligned} \mathrm{Var}\left[N_u(T)\right] = \mathbb{E}\left[N_u(T)\right] + 2\,T \int_0^T \int_{-\infty}^{\infty} \int_{-\infty}^{\infty} \left(1 - \frac{t}{T}\right) |y_1 y_2| \left(f_{\mathrm{Q}}(u,\, u,\, y_1,\, y_2;\, t) \right. \\ \left. - f_{\mathrm{P}}(u,\, y_1)\, f_{\mathrm{P}}(u,\, y_2) \right) \mathrm{d}y_1\, \mathrm{d}y_2\, \mathrm{d}t. \end{aligned}} \quad \text{(E.42)}$$

And in the long time limit if the condition in Eq. (E.29) is satisfied, we have,

$$\boxed{\begin{aligned} \lim_{T\to\infty} \frac{\mathrm{Var}\left[N_u(T)\right]}{T} = \lim_{T\to\infty} \frac{\mathbb{E}\left[N_u(T)\right]}{T} + 2 \int_0^{\infty} \int_{-\infty}^{\infty} \int_{-\infty}^{\infty} |y_1 y_2| \left(f_{\mathrm{Q}}(u,\, u,\, y_1,\, y_2;\, t) \right. \\ \left. - f_{\mathrm{P}}(u,\, y_1)\, f_{\mathrm{P}}(u,\, y_2) \right) \mathrm{d}y_1\, \mathrm{d}y_2\, \mathrm{d}t. \end{aligned}} \quad \text{(E.43)}$$

Finally, the Fano factor is given by,

$$\boxed{\mathrm{F} = 1 + \frac{2 \int_0^{\infty} \int_{-\infty}^{\infty} \int_{-\infty}^{\infty} |y_1 y_2| \left(f_{\mathrm{Q}}(u,\, u,\, y_1,\, y_2;\, t) - f_{\mathrm{P}}(u,\, y_1)\, f_{\mathrm{P}}(u,\, y_2) \right) \mathrm{d}y_1\, \mathrm{d}y_2\, \mathrm{d}t}{\int_{-\infty}^{\infty} |y|\, f_{\mathrm{P}}(u,\, y)\, \mathrm{d}y}.} \quad \text{(E.44)}$$

E.3 Explicit Formulae for Level Crossings

We employ an approach similar to that outlined in the proof of Theorem 6.1. First, we use the variance formula from Eq. (E.42) to calculate the double integral in y_1 and y_2,

$$I = \underbrace{\int_{-\infty}^{\infty}\int_{-\infty}^{\infty} |y_1 y_2|\, f_{\mathrm{Q}}(u,u,y_1,y_2;t)\,\mathrm{d}y_1\,\mathrm{d}y_2}_{I_1} - \underbrace{\int_{-\infty}^{\infty}\int_{-\infty}^{\infty} |y_1 y_2|\, f_{\mathrm{P}}(u,y_1)\, f_{\mathrm{P}}(u,y_2)\,\mathrm{d}y_1\,\mathrm{d}y_2}_{I_2} \tag{E.45}$$

I_2 can be evaluated as,

$$\begin{aligned} I_2 &= \frac{e^{-u^2/r_0}}{4\pi^2\, r_0 q_0}\int_{-\infty}^{\infty}\int_{-\infty}^{\infty} |y_1 y_2| \exp\left(-\frac{1}{2q_0}\left(y_1^2+y_2^2\right)\right)\mathrm{d}y_1\,\mathrm{d}y_2 \\ &= \frac{1}{\pi^2}\left(\frac{q_0}{r_0}\right) e^{-u^2/r_0} \end{aligned} \tag{E.46}$$

To evaluate the expression for I_1, we make the variable transform $(y_1,\, y_2) \longrightarrow (z_1, z_2)$, which gives us,

$$I_1 = \frac{1}{2}\int_{-\infty}^{\infty}\int_{-\infty}^{\infty} \left|z_2^2 - z_1^2\right|\, f_{\mathrm{Q}}(u,\, u,\, z_1,\, z_2;\, t)\,\mathrm{d}z_2\,\mathrm{d}z_1 \tag{E.47}$$

Using the expression for $f_{\mathrm{Q}}(u,\, u,\, z_1,\, z_2;\, t)$ from the main text (Eq. (6.50)), we get,

$$\begin{aligned} I_1 &= \frac{1}{2}\int_{-\infty}^{\infty}\int_{-\infty}^{\infty} \left|z_2^2 - z_1^2\right| \left(\frac{1}{2\pi^2}\sqrt{\frac{\alpha\beta}{r_0^2 - r^2}}\, \exp\left(-\delta\, u^2 - \alpha\,(z_1-\gamma)^2 - \beta\, z_2^2\right)\right)\mathrm{d}z_2\,\mathrm{d}z_1 \\ &= \frac{e^{-\delta\, u^2}}{4\pi^2}\sqrt{\frac{\alpha\beta}{r_0^2 - r^2}}\int_{-\infty}^{\infty}\int_{-\infty}^{\infty} \left|z_2^2 - z_1^2\right| \exp\left(-\alpha\,(z_1-\gamma)^2 - \beta\, z_2^2\right)\mathrm{d}z_2\,\mathrm{d}z_1 \end{aligned} \tag{E.48}$$

We derive the result for this double integral in Theorem E.4, which gives us,

$$I_1 = \frac{e^{-\delta u^2}}{4\pi^2\sqrt{r_0^2 - r^2}}\left[\frac{2e^{-\alpha\gamma^2}}{\sqrt{\alpha\beta}}\left(1 + \sqrt{\pi}\,\gamma\sqrt{\alpha+\beta}\,e^{\frac{\alpha^2\gamma^2}{\alpha+\beta}}\,\operatorname{Erf}\left(\frac{\alpha\gamma}{\sqrt{\alpha+\beta}}\right)\right)\right. \\ \left. + 4\pi\left(\frac{\alpha - \beta - 2\alpha\beta\gamma^2}{\alpha\beta}\right)\left(\mathcal{T}\left(\gamma\sqrt{\frac{2\alpha\beta}{\alpha+\beta}}, \sqrt{\frac{\alpha}{\beta}}\right) - \frac{1}{8}\right)\right], \tag{E.49}$$

and the final expression for I is,

$$\boxed{I = \frac{e^{-\delta u^2}}{4\pi^2\sqrt{r_0^2 - r^2}}\left[\frac{2e^{-\alpha\gamma^2}}{\sqrt{\alpha\beta}}\left(1 + \sqrt{\pi}\,\gamma\sqrt{\alpha+\beta}\,e^{\frac{\alpha^2\gamma^2}{\alpha+\beta}}\,\operatorname{Erf}\left(\frac{\alpha\gamma}{\sqrt{\alpha+\beta}}\right)\right)\right. \\ \left. + 4\pi\left(\frac{\alpha - \beta - 2\alpha\beta\gamma^2}{\alpha\beta}\right)\left(\mathcal{T}\left(\gamma\sqrt{\frac{2\alpha\beta}{\alpha+\beta}}, \sqrt{\frac{\alpha}{\beta}}\right) - \frac{1}{8}\right)\right] - \frac{1}{\pi^2}\left(\frac{q_0}{r_0}\right)e^{-u^2/r_0}.} \tag{E.50}$$

Plugging in the p.d.f. of $\mathbf{P}$ into Eq. (E.35), gives us,

$$\boxed{\mathbb{E}\left[N_u(T)\right] = T\,\frac{1}{\pi}\sqrt{\frac{q_0}{r_0}}\,e^{-u^2/(2r_0)}} \tag{E.51}$$

Using the result from Eq. (E.42) and the expression for I found in Eq. (E.50), for a finite time T, we have,

$$\boxed{\operatorname{Var}\left[N_u(T)\right] = T\left(\frac{1}{\pi}\sqrt{\frac{q_0}{r_0}}\,e^{-u^2/(2r_0)} + 2\int_0^T\left(1 - \frac{t}{T}\right)I\,\mathrm{d}t\right),} \tag{E.52}$$

and in the long time limit, we have,

$$\boxed{\lim_{T\to\infty}\frac{\operatorname{Var}\left[N_u(T)\right]}{T} = \frac{1}{\pi}\sqrt{\frac{q_0}{r_0}}\,e^{-u^2/(2r_0)} + 2\int_0^\infty I\,\mathrm{d}t.} \tag{E.53}$$

$$\boxed{\mathrm{F} = 1 + 2\pi\sqrt{\frac{r_0}{q_0}}\,e^{u^2/(2r_0)}\int_0^\infty I\,\mathrm{d}t.} \tag{E.54}$$

E.4 Special Formulae for Zero Level Upcrossings and Crossings

E.4.1 Upcrossings

We present the simplified formula for mean and variance for mean level upcrossings, i.e., when $u = 0$. First, we substitute $u = 0$ in Eq. (6.24) to get the result for $\mathbb{E}\left[N_0^{\uparrow}(T)\right]$,

$$\boxed{\mathbb{E}\left[N_0^{\uparrow}(T)\right] = T\frac{1}{2\pi}\sqrt{\frac{q_0}{r_0}}.} \tag{E.55}$$

Similarly, substituting $u = 0$ in Eq. (6.56), we get,

$$\begin{aligned} I_0 =& \frac{1}{4\pi^2\sqrt{r_0^2 - r^2}}\left[\frac{1}{2\sqrt{\alpha\beta}} + \pi\left(\frac{\alpha-\beta}{\alpha\beta}\right)\mathcal{T}\left(0, \sqrt{\frac{\alpha}{\beta}}\right)\right] - \frac{1}{4\pi^2}\left(\frac{q_0}{r_0}\right) \\ =& \frac{1}{4\pi^2\sqrt{r_0^2 - r^2}}\left[\frac{1}{2\sqrt{\alpha\beta}} + \pi\left(\frac{\alpha-\beta}{\alpha\beta}\right)\left(\frac{1}{2\pi}\arctan\left(\sqrt{\frac{\alpha}{\beta}}\right)\right)\right] - \frac{1}{4\pi^2}\left(\frac{q_0}{r_0}\right) \\ =& \frac{1}{8\pi^2\sqrt{r_0^2 - r^2}}\left[\frac{1}{\sqrt{\alpha\beta}} + \left(\frac{\alpha-\beta}{\alpha\beta}\right)\arctan\left(\sqrt{\frac{\alpha}{\beta}}\right)\right] - \frac{1}{4\pi^2}\left(\frac{q_0}{r_0}\right) \end{aligned} \tag{E.56}$$

Note that in the simplification above, we have used the fact that $\gamma = 0$ when $u = 0$, and $\mathcal{T}(0, a) = \arctan(a)/(2\pi)$. The variance and Fano factor are found by substituting $u = 0$ in Eq. (6.25), (6.59) and (6.60).

$$\begin{aligned} \boxed{\mathrm{Var}\left[N_u^{\uparrow}(T)\right] = T\Bigg(&\frac{1}{2\pi}\sqrt{\frac{q_0}{r_0}} \\ &+ \frac{1}{4\pi^2}\int_0^T \left(1 - \frac{t}{T}\right)\left[\frac{1}{\sqrt{r_0^2 - r^2}}\left[\frac{1}{\sqrt{\alpha\beta}} + \left(\frac{\alpha-\beta}{\alpha\beta}\right)\arctan\left(\sqrt{\frac{\alpha}{\beta}}\right)\right] - \frac{q_0}{r_0}\right]\mathrm{d}t\Bigg).} \end{aligned} \tag{E.57}$$

This formula has been reported by Steinberg [163] and Leadbetter [173]. In the long time limit, we have,

$$\boxed{\frac{\text{Var}\left[N_u^{\uparrow}(T)\right]}{T} = \frac{1}{2\pi}\sqrt{\frac{q_0}{r_0}} + \frac{1}{4\pi^2}\int_0^{\infty} \frac{1}{\sqrt{r_0^2 - r^2}}\left[\frac{1}{\sqrt{\alpha\beta}} + \left(\frac{\alpha-\beta}{\alpha\beta}\right)\arctan\left(\sqrt{\frac{\alpha}{\beta}}\right)\right] - \frac{q_0}{r_0}\,\mathrm{d}t} \tag{E.58}$$

$$\boxed{\mathrm{F}^{\uparrow} = 1 + \frac{1}{\pi}\sqrt{\frac{r_0}{q_0}}\, e^{u^2/(2r_0)} \int_0^{\infty} \frac{1}{2\sqrt{r_0^2 - r^2}}\left[\frac{1}{\sqrt{\alpha\beta}} + \left(\frac{\alpha-\beta}{\alpha\beta}\right)\arctan\left(\sqrt{\frac{\alpha}{\beta}}\right)\right] - \frac{q_0}{r_0}\,\mathrm{d}t} \tag{E.59}$$

E.4.2 Crossings

We find the simplified formulae for mean and variance for mean level crossings by substituting $u = 0$ in the results reported in Section E.3. We first substitute $u = 0$ in Eq. (E.51) to get the formula for the mean,

$$\boxed{\mathbb{E}\left[N_u(T)\right] = T\,\frac{1}{\pi}\sqrt{\frac{q_0}{r_0}}} \tag{E.60}$$

Next, to find the formula for variance, we evaluate I from Eq. (E.50) at $u = 0$,

$$\begin{aligned}
I_0 =& \frac{1}{4\pi^2\sqrt{r_0^2 - r^2}}\left[\frac{2}{\sqrt{\alpha\beta}} + 4\pi\left(\frac{\alpha-\beta}{\alpha\beta}\right)\left(\mathcal{T}\left(0, \sqrt{\frac{\alpha}{\beta}}\right) - \frac{1}{8}\right)\right] - \frac{1}{\pi^2}\left(\frac{q_0}{r_0}\right) \\
=& \frac{1}{4\pi^2\sqrt{r_0^2 - r^2}}\left[\frac{2}{\sqrt{\alpha\beta}} + 4\pi\left(\frac{\alpha-\beta}{\alpha\beta}\right)\left(\frac{1}{2\pi}\arctan\left(\sqrt{\frac{\alpha}{\beta}}\right) - \frac{1}{8}\right)\right] - \frac{1}{\pi^2}\left(\frac{q_0}{r_0}\right) \\
=& \frac{1}{4\pi^2\sqrt{r_0^2 - r^2}}\left[\frac{2}{\sqrt{\alpha\beta}} + 2\left(\frac{\alpha-\beta}{\alpha\beta}\right)\left(\arctan\left(\sqrt{\frac{\alpha}{\beta}}\right) - \frac{\pi}{4}\right)\right] - \frac{1}{\pi^2}\left(\frac{q_0}{r_0}\right) \\
=& \frac{1}{2\pi^2\sqrt{r_0^2 - r^2}}\left[\frac{1}{\sqrt{\alpha\beta}} + \left(\frac{\alpha-\beta}{\alpha\beta}\right)\arctan\left(\frac{\sqrt{\alpha/\beta} - 1}{\sqrt{\alpha/\beta} + 1}\right)\right] - \frac{1}{\pi^2}\left(\frac{q_0}{r_0}\right)
\end{aligned} \tag{E.61}$$

Therefore, we have the following expression for the variance,

$$\boxed{\begin{aligned}\text{Var}\left[N_u(T)\right] = T\Bigg(\frac{1}{\pi}\sqrt{\frac{q_0}{r_0}}+\frac{2}{\pi^2}\int_0^T\left(1-\frac{t}{T}\right)\Bigg[\frac{1}{2\sqrt{r_0^2-r^2}}\Bigg[\frac{1}{\sqrt{\alpha\beta}}\\ +\left(\frac{\alpha-\beta}{\alpha\beta}\right)\arctan\left(\frac{\sqrt{\alpha/\beta}-1}{\sqrt{\alpha/\beta}+1}\right)\Bigg]-\frac{q_0}{r_0}\Bigg]\mathrm{d}t\Bigg).\end{aligned}} \tag{E.62}$$

In the long time limit, we have,

$$\boxed{\frac{\text{Var}\left[N_u(T)\right]}{T} = \frac{1}{\pi}\sqrt{\frac{q_0}{r_0}}+\frac{1}{\pi^2}\int_0^\infty\frac{1}{\sqrt{r_0^2-r^2}}\Bigg[\frac{1}{\sqrt{\alpha\beta}}+\left(\frac{\alpha-\beta}{\alpha\beta}\right)\arctan\left(\frac{\sqrt{\alpha/\beta}-1}{\sqrt{\alpha/\beta}+1}\right)\Bigg]-\frac{q_0}{r_0}\,\mathrm{d}t} \tag{E.63}$$

$$\boxed{\mathrm{F} = 1+\frac{2}{\pi}\sqrt{\frac{r_0}{q_0}}\,e^{u^2/(2r_0)}\int_0^\infty\frac{1}{2\sqrt{r_0^2-r^2}}\Bigg[\frac{1}{\sqrt{\alpha\beta}}+\left(\frac{\alpha-\beta}{\alpha\beta}\right)\arctan\left(\frac{\sqrt{\alpha/\beta}-1}{\sqrt{\alpha/\beta}+1}\right)\Bigg]-\frac{q_0}{r_0}\,\mathrm{d}t} \tag{E.64}$$

E.5 Note About the Dimensionality

In this section, we note the units of various variables $(\alpha, \beta, \gamma, \delta)$ and expressions $(I^{\uparrow}, I)$ used to define our main results. We note that the autocorrelation function $r(t)$ will be of the form,

$$r \coloneqq r(t) = \sigma^2\, g\left(t/\tau;\, \boldsymbol{\theta}\right) \tag{E.65}$$

where σ defines the dimension of the stochastic process, τ defines the timescales of the process and $\boldsymbol{\theta}$ denotes dimensionless variables associated with the correlation function. Therefore, $g\left(t/\tau;\, \boldsymbol{\theta}\right)$ is a dimensionless function. Taking the derivatives with respect to time on both sides, we get,

$$p = r'(t) = \frac{\sigma^2}{\tau}\, g'\left(t/\tau;\, \boldsymbol{\theta}\right) \qquad \text{and} \qquad q = -r''(t) = -\frac{\sigma^2}{\tau^2}\, g''\left(t/\tau;\, \boldsymbol{\theta}\right) \tag{E.66}$$

Substituting $t = 0$ in these expressions,

$$r_0 = \sigma^2 \, g\,(0;\, \boldsymbol{\theta}) \qquad \text{and} \qquad q_0 = -\frac{\sigma^2}{\tau^2} \, g''\,(0;\, \boldsymbol{\theta}) \tag{E.67}$$

Consider the mean, variance, and Fano factor results for level up/down crossing and crossings. All of the results depend on α, β, γ and δ. Therefore, first, we determine the dimensionality of these variables by plugging in the expressions above. First, consider α,

$$\begin{aligned} \alpha &= -\frac{r + r_0}{2\,(p^2 + (q - q_0)(r + r_0))} \\ &= -\frac{\tau^2}{\sigma^2} \left(\frac{g\,(t/\tau;\, \boldsymbol{\theta}) + g\,(0;\, \boldsymbol{\theta})}{2\,((g'\,(t/\tau;\, \boldsymbol{\theta}))^2 - (g''\,(t/\tau;\, \boldsymbol{\theta}) - g''\,(0;\, \boldsymbol{\theta}))(g\,(t/\tau;\, \boldsymbol{\theta}) + g\,(0;\, \boldsymbol{\theta})))} \right) \end{aligned} \tag{E.68}$$

where the expression in the bracket is dimensionless; therefore,

$$\alpha = \frac{\tau^2}{\sigma^2} \, h_\alpha \left(\tilde{t};\, \boldsymbol{\theta} \right) \tag{E.69}$$

where, $\tilde{t} = t/\tau$ is a dimensionless time and $h_\alpha \left(\tilde{t};\, \boldsymbol{\theta} \right)$ is the dimensionless expression. A similar analysis reveals,

$$\beta = \frac{\tau^2}{\sigma^2} \, h_\beta \left(\tilde{t};\, \boldsymbol{\theta} \right), \qquad \gamma = \frac{u}{\tau} \, h_\gamma \left(\tilde{t};\, \boldsymbol{\theta} \right) \qquad \text{and} \qquad \delta = \frac{1}{\sigma^2} \, h_\delta \left(\tilde{t};\, \boldsymbol{\theta} \right) \tag{E.70}$$

where $h_\beta \left(\tilde{t};\, \boldsymbol{\theta} \right)$, $h_\gamma \left(\tilde{t};\, \boldsymbol{\theta} \right)$ and $h_\delta \left(\tilde{t};\, \boldsymbol{\theta} \right)$ are dimensionless functions. Using these expressions, it can be shown that $I^\uparrow$ and I can be separated into the following dimensional and dimensionless parts,

$$I^\uparrow = \frac{1}{\tau^2} \, h_{I^\uparrow} \left(\tilde{t};\, \psi,\, \boldsymbol{\theta} \right) \qquad \text{and} \qquad I = \frac{1}{\tau^2} \, h_I \left(\tilde{t};\, \psi,\, \boldsymbol{\theta} \right) \tag{E.71}$$

where we additionally define the dimensionless parameter $\psi = u/\sigma$. Separating the dimensional and dimensionless expression for mean of upcrossings, we get,

$$\mathbb{E}\left[N_u^{\uparrow}(T)\right] = T\,\frac{1}{2\pi}\sqrt{\frac{q_0}{r_0}}\,e^{-u^2/(2r_0)} = \frac{T}{\tau}\left(\frac{1}{2\pi}\sqrt{\frac{-g''\left(0;\,\boldsymbol{\theta}\right)}{g\left(0;\,\boldsymbol{\theta}\right)}}\,e^{-\psi^2/(2g(0;\boldsymbol{\theta}))}\right). \tag{E.72}$$

Similarly, for variance in finite time, we have,

$$\begin{aligned}\mathrm{Var}\left[N_u^{\uparrow}(T)\right] &= T\left(\frac{1}{2\pi}\sqrt{\frac{q_0}{r_0}}\,e^{-u^2/(2r_0)} + 2\int_0^T\left(1-\frac{t}{T}\right)\,I^{\uparrow}\,\mathrm{d}t\right)\\ &= \frac{T}{\tau}\left(\frac{1}{2\pi}\sqrt{\frac{-g''\left(0;\,\boldsymbol{\theta}\right)}{g\left(0;\,\boldsymbol{\theta}\right)}}\,e^{-\psi^2/(2g(0;\boldsymbol{\theta}))} + 2\int_0^{T/\tau}\left(1-\frac{\tau}{T}\,\tilde{t}\right)\,h_{I^{\uparrow}}\left(\tilde{t};\,\psi,\,\boldsymbol{\theta}\right)\,\mathrm{d}\tilde{t}\right),\end{aligned} \tag{E.73}$$

and in the long time limit,

$$\mathrm{Var}\left[N_u^{\uparrow}(T)\right] = \frac{T}{\tau}\left(\frac{1}{2\pi}\sqrt{\frac{-g''\left(0;\,\boldsymbol{\theta}\right)}{g\left(0;\,\boldsymbol{\theta}\right)}}\,e^{-\psi^2/(2g(0;\boldsymbol{\theta}))} + 2\int_0^{\infty} h_{I^{\uparrow}}\left(\tilde{t};\,\psi,\,\boldsymbol{\theta}\right)\,\mathrm{d}\tilde{t}\right). \tag{E.74}$$

Finally, the Fano factor (Eq. (E.33)) can be shown to be independent of τ,

$$\mathrm{F}^{\uparrow} = 1 + 4\pi\sqrt{\frac{r_0}{q_0}}\,e^{u^2/(2r_0)}\int_0^{\infty} I^{\uparrow}\,\mathrm{d}t = 1 + 4\pi\sqrt{\frac{g\left(0;\,\boldsymbol{\theta}\right)}{-g''\left(0;\,\boldsymbol{\theta}\right)}}\,e^{\psi^2/(2g(0;\boldsymbol{\theta}))}\int_0^{\infty} h_{I^{\uparrow}}\left(\tilde{t};\,\psi,\,\boldsymbol{\theta}\right)\,\mathrm{d}\tilde{t} \tag{E.75}$$

Similar results can be found for the mean, variance, and Fano factor of the level crossing process.

E.6 Additional Theorems

Theorem E.1. *Let $r(t)$ be the autocorrelation function of a one-dimensional real Gaussian stationary process. For brevity, we introduce the following notations: $r(t) \to r$, $r(0) \to r_0$, $r'(t) \to p$, $r'(0) \to p_0$, $-r''(t) \to q$, and $-r''(0) \to q_0$. Then, for all $t \geq 0$ the following expressions are strictly*

positive,

$$\begin{aligned} -\frac{r + r_0}{2\left(p^2 + (q - q_0)(r + r_0)\right)} &> 0 \\ -\frac{r_0 - r}{2\left(p^2 + (q + q_0)(r - r_0)\right)} &> 0 \end{aligned} \tag{E.76}$$

Proof. Since $r(t)$ is the autocorrelation function of a real stationary process, it has the spectral representation

$$r(t) = \int_{-\infty}^{\infty} \cos(\omega t)\, dF(\omega), \tag{E.77}$$

where F is a nonnegative measure. Differentiating w.r.t. time, we obtain

$$r'(t) = -\int_{-\infty}^{\infty} \omega \sin(\omega t)\, dF(\omega) \quad \text{and} \quad r''(t) = -\int_{-\infty}^{\infty} \omega^2 \cos(\omega t)\, dF(\omega). \tag{E.78}$$

In the notation defined in the theorem and using the integral formulae above, we have,

$$\begin{aligned} r &= \int_{-\infty}^{\infty} \cos(\omega t)\, dF(\omega) \\ p &= -\int_{-\infty}^{\infty} \omega \sin(\omega t)\, dF(\omega) \\ q &= \int_{-\infty}^{\infty} \omega^2 \cos(\omega t)\, dF(\omega) \\ r_0 &= \int_{-\infty}^{\infty} dF(\omega) \\ p_0 &= 0 \\ q_0 &= \int_{-\infty}^{\infty} \omega^2\, dF(\omega) \end{aligned} \tag{E.79}$$

Using these relations, we have the following integral expressions for the relevant quantities,

$$r + r_0 = \int_{-\infty}^{\infty} \big(1 + \cos(\omega t)\big)\, dF(\omega) \quad \text{and} \quad r_0 - r = \int_{-\infty}^{\infty} \big(1 - \cos(\omega t)\big)\, dF(\omega), \tag{E.80}$$

and,

$$q_0 - q = \int_{-\infty}^{\infty} \omega^2 \Big(1 - \cos(\omega t)\Big) dF(\omega) \quad \text{and} \quad q_0 + q = \int_{-\infty}^{\infty} \omega^2 \Big(1 + \cos(\omega t)\Big) dF(\omega). \tag{E.81}$$

Now, writing

$$p^2 = \left(\int_{-\infty}^{\infty} \omega \sin(\omega t)\, dF(\omega)\right)^2, \tag{E.82}$$

and applying Cauchy-Schwarz inequality,

$$\left(\int_S f(x) g(x)\, d\mu(x)\right)^2 \leqslant \left(\int_S f(x)^2\, d\mu(x)\right)\left(\int_S g(x)^2\, d\mu(x)\right), \tag{E.83}$$

gives us,

$$p^2 \leqslant \left(\int_{-\infty}^{\infty} \omega^2 \frac{\sin^2(\omega t)}{1 + \cos(\omega t)}\, dF(\omega)\right)\left(\int_{-\infty}^{\infty} (1 + \cos(\omega t))\, dF(\omega)\right). \tag{E.84}$$

A short calculation shows that

$$\frac{\sin^2(\omega t)}{1 + \cos(\omega t)} = \frac{4 \sin^2\left(\frac{\omega t}{2}\right) \cos^2\left(\frac{\omega t}{2}\right)}{2 \cos^2\left(\frac{\omega t}{2}\right)} = 2 \sin^2\left(\frac{\omega t}{2}\right) = 1 - \cos(\omega t). \tag{E.85}$$

Therefore,

$$p^2 \leqslant \left(\int_{-\infty}^{\infty} \omega^2 (1 - \cos(\omega t))\, dF(\omega)\right)\left(\int_{-\infty}^{\infty} (1 + \cos(\omega t))\, dF(\omega)\right), \tag{E.86}$$

or,

$$p^2 \leq (q_0 - q)(r_0 + r). \tag{E.87}$$

Since equality in the Cauchy-Schwarz inequality can occur only if the integrands are proportional, which is excluded for a nondegenerate spectral measure, i.e., a spectral measure not concentrated on just a finite set of points, we have,

$$p^2 - (q_0 - q)(r + r_0) < 0. \tag{E.88}$$

Further, since $r + r_0 > 0 \; \forall \; t \geq 0$, we have,

$$-\frac{r + r_0}{2\left(p^2 + (q - q_0)(r + r_0)\right)} > 0 \tag{E.89}$$

Applying Cauchy-Schwarz, we can also write,

$$\begin{aligned} p^2 &\leq \left(\int_{-\infty}^{\infty} \omega^2 \frac{\sin^2(\omega t)}{1 - \cos(\omega t)}\, dF(\omega)\right)\left(\int_{-\infty}^{\infty} (1 - \cos(\omega t))\, dF(\omega)\right) \\ p^2 &\leq \left(\int_{-\infty}^{\infty} \omega^2 \left(1 + \cos(\omega t)\right)\, dF(\omega)\right)\left(\int_{-\infty}^{\infty} (1 - \cos(\omega t))\, dF(\omega)\right) \\ p^2 &\leq (q_0 + q)\,(r_0 - r) \end{aligned} \tag{E.90}$$

Since the spectral measure is nondegenerate, strict inequality is followed,

$$p^2 - (q_0 + q)\,(r_0 - r) < 0 \tag{E.91}$$

Further, since $r_0 - r > 0 \; \forall \; t \geq 0$, we have,

$$-\frac{r_0 - r}{2\left(p^2 + (q + q_0)(r - r_0)\right)} > 0 \tag{E.92}$$

□

Theorem E.2. *Let $\alpha > 0$, $\beta > 0$, and $\gamma \in \mathbb{R}$. The following result holds:*

$$\begin{aligned} \int_{-\infty}^{\infty} \int_{|x|}^{\infty} (y^2 - x^2)\, e^{-\alpha(x-\gamma)^2 - \beta y^2} \mathrm{d}y\, \mathrm{d}x = &\frac{e^{-\alpha\gamma^2}}{2\alpha\beta}\left(1 + \sqrt{\pi}\,\gamma\sqrt{\alpha + \beta}\, e^{\frac{\alpha^2\gamma^2}{\alpha+\beta}}\, \operatorname{Erf}\left(\frac{\alpha\gamma}{\sqrt{\alpha + \beta}}\right)\right) \\ &+ \pi\left(\frac{\alpha - \beta - 2\alpha\beta\gamma^2}{(\alpha\beta)^{3/2}}\right)\mathcal{T}\left(\gamma\sqrt{\frac{2\alpha\beta}{\alpha + \beta}}, \sqrt{\frac{\alpha}{\beta}}\right) \end{aligned} \tag{E.93}$$

where $\mathrm{Erf}(z)$ *is the error function defined as*

$$\mathrm{Erf}(z) = \frac{2}{\sqrt{\pi}} \int_0^z e^{-t^2} \mathrm{d}t, \tag{E.94}$$

and $\mathcal{T}(h, a)$ *is Owen's T function [172] defined as*

$$\mathcal{T}(h, a) = \frac{1}{2\pi} \int_0^a \frac{e^{-\frac{1}{2}h^2(1+t^2)}}{1+t^2} \mathrm{d}t. \tag{E.95}$$

Proof. Denoting the integral that we have to evaluate by,

$$I = \int_{-\infty}^{\infty} \int_{|x|}^{\infty} (y^2 - x^2)\, e^{-\alpha(x-\gamma)^2 - \beta y^2} \mathrm{d}y\, \mathrm{d}x \tag{E.96}$$

Integrating the inner integral in y and using the result from Lemma E.6, we have,

$$\begin{aligned} I &= \int_{-\infty}^{\infty} \frac{1}{2\beta} |x|\, e^{-\alpha(x-\gamma)^2 - \beta x^2} - \frac{\sqrt{\pi}}{4\beta^{3/2}} \left(2\beta x^2 - 1\right) e^{-\alpha(x-\gamma)^2} \mathrm{Erfc}\left(\sqrt{\beta}|x|\right) \mathrm{d}x \\ &= \frac{1}{2\beta} \underbrace{\int_{-\infty}^{\infty} |x|\, e^{-\alpha(x-\gamma)^2 - \beta x^2} \mathrm{d}x}_{I_1} - \frac{\sqrt{\pi}}{4\beta^{3/2}} \underbrace{\int_{-\infty}^{\infty} \left(2\beta x^2 - 1\right) e^{-\alpha(x-\gamma)^2} \mathrm{Erfc}\left(\sqrt{\beta}|x|\right) \mathrm{d}x}_{I_2} \end{aligned} \tag{E.97}$$

I_1 is shown to be given by the following expression in Lemma E.7,

$$I_1 = \frac{e^{-\alpha\gamma^2}}{(\alpha+\beta)^{3/2}} \left(\sqrt{\alpha+\beta} + \sqrt{\pi}\, \alpha\gamma\, e^{\frac{\alpha^2\gamma^2}{\alpha+\beta}} \mathrm{Erf}\left(\frac{\alpha\gamma}{\sqrt{\alpha+\beta}} \right) \right) \tag{E.98}$$

We make the variable change of $\sqrt{\beta}\, x = k$ in the integral I_2 which gives us,

$$\begin{aligned} I_2 &= \frac{1}{\sqrt{\beta}} \int_{-\infty}^{\infty} \left(2k^2 - 1\right) e^{-\frac{\alpha}{\beta}(k - \gamma\sqrt{\beta})^2} \mathrm{Erfc}\left(|k|\right) \mathrm{d}k \\ &= \frac{1}{\sqrt{\beta}} \underbrace{\int_{-\infty}^{\infty} \left(2k^2 - 1\right) e^{-\frac{\alpha}{\beta}(k - \gamma\sqrt{\beta})^2} \mathrm{d}k}_{I_{21}} - \frac{1}{\sqrt{\beta}} \underbrace{\int_{-\infty}^{\infty} \left(2k^2 - 1\right) e^{-\frac{\alpha}{\beta}(k - \gamma\sqrt{\beta})^2} \mathrm{Erf}\left(|k|\right) \mathrm{d}k}_{I_{22}} \end{aligned} \tag{E.99}$$

The integral in I_{21} is given by Lemma E.8, upon simplification, we get,

$$I_{21} = \sqrt{\pi}\sqrt{\frac{\beta}{\alpha}}\left(\frac{\beta}{\alpha} + 2\beta\gamma^2 - 1\right) \tag{E.100}$$

and I_{22} can be written as,

$$\begin{aligned}
I_{22} &= \int_{-\infty}^{\infty} \left(2k^2 - 1\right) e^{-\frac{\alpha}{\beta}(k-\gamma\sqrt{\beta})^2} \operatorname{Erf}\left(|k|\right) \mathrm{d}k \\
&= \int_{0}^{\infty} e^{-\frac{\alpha}{\beta}(k-\gamma\sqrt{\beta})^2} \left(2k^2 - 1\right) \operatorname{Erf}\left(k\right) \mathrm{d}k + \int_{-\infty}^{0} e^{-\frac{\alpha}{\beta}(k-\gamma\sqrt{\beta})^2} \left(2k^2 - 1\right) \operatorname{Erf}\left(-k\right) \mathrm{d}k \\
&= \int_{0}^{\infty} e^{-\frac{\alpha}{\beta}(k-\gamma\sqrt{\beta})^2} \left(2k^2 - 1\right) \operatorname{Erf}\left(k\right) \mathrm{d}k + \int_{0}^{\infty} e^{-\frac{\alpha}{\beta}(k+\gamma\sqrt{\beta})^2} \left(2k^2 - 1\right) \operatorname{Erf}\left(k\right) \mathrm{d}k \\
&= \int_{0}^{\infty} \left(e^{-\frac{\alpha}{\beta}(k-\gamma\sqrt{\beta})^2} + e^{-\frac{\alpha}{\beta}(k+\gamma\sqrt{\beta})^2}\right) \left(2k^2 - 1\right) \operatorname{Erf}\left(k\right) \mathrm{d}k
\end{aligned} \tag{E.101}$$

Applying integration by parts, we get

$$\begin{aligned}
I_{22} &= \int_{0}^{\infty} \underbrace{\left(e^{-\frac{\alpha}{\beta}(k-\gamma\sqrt{\beta})^2} + e^{-\frac{\alpha}{\beta}(k+\gamma\sqrt{\beta})^2}\right) \left(2k^2 - 1\right)}_{\text{second part}} \underbrace{\operatorname{Erf}\left(k\right)}_{\text{first part}} \mathrm{d}k \\
&= \underbrace{\left[\operatorname{Erf}\left(k\right) \int \left(e^{-\frac{\alpha}{\beta}(k-\gamma\sqrt{\beta})^2} + e^{-\frac{\alpha}{\beta}(k+\gamma\sqrt{\beta})^2}\right) \left(2k^2 - 1\right) \mathrm{d}k\right]_{0}^{\infty}}_{I_{221}} \\
&\quad \underbrace{- \int_{0}^{\infty} \left(\frac{2}{\sqrt{\pi}} e^{-k^2}\right) \left(\int \left(e^{-\frac{\alpha}{\beta}(k-\gamma\sqrt{\beta})^2} + e^{-\frac{\alpha}{\beta}(k+\gamma\sqrt{\beta})^2}\right) \left(2k^2 - 1\right) \mathrm{d}k\right) \mathrm{d}k}_{I_{222}}
\end{aligned} \tag{E.102}$$

First, the indefinite integral can be evaluated using the standard results on the normal integrals [172],

$$\begin{aligned}
\int \left(e^{-\frac{\alpha}{\beta}(k-\gamma\sqrt{\beta})^2} + e^{-\frac{\alpha}{\beta}(k+\gamma\sqrt{\beta})^2}\right) \left(2k^2 - 1\right) \mathrm{d}k &= \frac{\beta}{\alpha} e^{-\frac{\alpha}{\beta}\left(k+\gamma\sqrt{\beta}\right)^2} \left(\gamma\sqrt{\beta} - \left(k + \gamma\sqrt{\beta}\right) e^{\frac{4\alpha\gamma}{\sqrt{\beta}}k} - k\right) \\
&\quad + \frac{\sqrt{\pi}}{2\alpha}\sqrt{\frac{\beta}{\alpha}} \left(\beta - \alpha + 2\alpha\beta\gamma^2\right) \left(\operatorname{Erf}\left(\sqrt{\frac{\alpha}{\beta}}\left(k + \gamma\sqrt{\beta}\right)\right) + \operatorname{Erf}\left(\sqrt{\frac{\alpha}{\beta}}\left(k - \gamma\sqrt{\beta}\right)\right)\right)
\end{aligned} \tag{E.103}$$

Let's denote the integral above by $v(k)$, we have the following,

$$\left[\operatorname{Erf}(k)\int\left(e^{-\frac{\alpha}{\beta}(k-\gamma\sqrt{\beta})^2}+e^{-\frac{\alpha}{\beta}(k+\gamma\sqrt{\beta})^2}\right)\left(2k^2-1\right)\mathrm{d}k\right]_0^\infty=\lim_{k\to\infty}\operatorname{Erf}(k)\,v(k)-\lim_{k\to 0}\operatorname{Erf}(k)\,v(k) \tag{E.104}$$

Using the fact that $\lim_{k\to\infty}\operatorname{Erf}(k)=1$ and $\lim_{k\to\infty}\left(k\,e^{-a\,k}\right)=0$, we have,

$$\lim_{k\to\infty}\operatorname{Erf}(k)\,v(k)=\frac{\sqrt{\pi}}{\alpha}\sqrt{\frac{\beta}{\alpha}}\left(\beta-\alpha+2\alpha\beta\gamma^2\right), \tag{E.105}$$

and using the fact that $\lim_{k\to 0}\operatorname{Erf}(k)=0$, we have,

$$\lim_{k\to 0}\operatorname{Erf}(k)\,v(k)=0. \tag{E.106}$$

Therefore, the first term of I_{22} in Eq. (E.102) is,

$$I_{221}=\operatorname{Erf}(k)\int\left(e^{-\frac{\alpha}{\beta}(k-\gamma\sqrt{\beta})^2}+e^{-\frac{\alpha}{\beta}(k+\gamma\sqrt{\beta})^2}\right)\left(2k^2-1\right)\mathrm{d}k\Bigg]_0^\infty=\frac{\sqrt{\pi}}{\alpha}\sqrt{\frac{\beta}{\alpha}}\left(\beta-\alpha+2\alpha\beta\gamma^2\right) \tag{E.107}$$

Using the integral in Eq. (E.103), we can write I_{222} as the following definite integral,

$$\begin{aligned}I_{222}=\int_0^\infty&\left(\frac{2}{\sqrt{\pi}}e^{-k^2}\right)\left(\frac{\beta}{\alpha}e^{-\frac{\alpha}{\beta}\left(k+\gamma\sqrt{\beta}\right)^2}\left(\gamma\sqrt{\beta}-\left(k+\gamma\sqrt{\beta}\right)e^{\frac{4\alpha\gamma}{\sqrt{\beta}}k}-k\right)\right.\\&\left.+\frac{\sqrt{\pi}}{2\alpha}\sqrt{\frac{\beta}{\alpha}}\left(\beta-\alpha+2\alpha\beta\gamma^2\right)\left(\operatorname{Erf}\left(\sqrt{\frac{\alpha}{\beta}}\left(k+\gamma\sqrt{\beta}\right)\right)+\operatorname{Erf}\left(\sqrt{\frac{\alpha}{\beta}}\left(k-\gamma\sqrt{\beta}\right)\right)\right)\right)\mathrm{d}k\end{aligned} \tag{E.108}$$

Upon expanding, we get,

$$I_{222} = \frac{2}{\sqrt{\pi}}\frac{\beta}{\alpha}\underbrace{\int_0^\infty e^{-\frac{\alpha}{\beta}\left(k+\gamma\sqrt{\beta}\right)^2-k^2}\left(\gamma\sqrt{\beta}-\left(k+\gamma\sqrt{\beta}\right)e^{\frac{4\alpha\gamma}{\sqrt{\beta}}k}-k\right)\mathrm{d}k}_{I_{2221}}$$
$$+\frac{1}{\alpha}\sqrt{\frac{\beta}{\alpha}}\left(\beta-\alpha+2\alpha\beta\gamma^2\right)\underbrace{\int_0^\infty e^{-k^2}\left(\mathrm{Erf}\left(\sqrt{\frac{\alpha}{\beta}}\left(k+\gamma\sqrt{\beta}\right)\right)+\mathrm{Erf}\left(\sqrt{\frac{\alpha}{\beta}}\left(k-\gamma\sqrt{\beta}\right)\right)\right)\mathrm{d}k}_{I_{2222}} \tag{E.109}$$

Using Lemma E.9, we have the following expression for I_{2221},

$$I_{2221} = -\frac{\beta\, e^{-\alpha\gamma^2}}{(\alpha+\beta)^{3/2}}\left(\sqrt{\alpha+\beta}+\sqrt{\pi}\,\gamma\,(2\alpha+\beta)\,e^{\frac{\alpha^2\gamma^2}{\alpha+\beta}}\,\mathrm{Erf}\left(\frac{\alpha\gamma}{\sqrt{\alpha+\beta}}\right)\right). \tag{E.110}$$

Finally, using Lemma E.10, we have the following expression for I_{2222},

$$I_{2222} = 4\sqrt{\pi}\,\mathcal{T}\left(\sqrt{\frac{2\alpha\beta}{\alpha+\beta}}\,\gamma, \sqrt{\frac{\alpha}{\beta}}\right) \tag{E.111}$$

Now, we go backward to find a simplified expression for I. First, we find I_{222} using the definition in Eq. (E.109),

$$\begin{aligned} I_{222} =& \frac{2}{\sqrt{\pi}}\frac{\beta}{\alpha}I_{2221}+\frac{1}{\alpha}\sqrt{\frac{\beta}{\alpha}}\left(\beta-\alpha+2\alpha\beta\gamma^2\right)I_{2222} \\ =& -\frac{2\beta^2\,e^{-\alpha\gamma^2}}{\sqrt{\pi}\,\alpha\,(\alpha+\beta)^{3/2}}\left(\sqrt{\alpha+\beta}+\sqrt{\pi}\,\gamma\,(2\alpha+\beta)\,e^{\frac{\alpha^2\gamma^2}{\alpha+\beta}}\,\mathrm{Erf}\left(\frac{\alpha\gamma}{\sqrt{\alpha+\beta}}\right)\right) \\ &+\frac{4\sqrt{\pi}}{\alpha}\sqrt{\frac{\beta}{\alpha}}\left(\beta-\alpha+2\alpha\beta\gamma^2\right)\mathcal{T}\left(\sqrt{\frac{2\alpha\beta}{\alpha+\beta}}\,\gamma, \sqrt{\frac{\alpha}{\beta}}\right) \end{aligned} \tag{E.112}$$

Next, we find I_{22} using the definition in Eq. (E.102),

$$\begin{aligned}
I_{22} =& I_{221} - I_{222} \\
=& \frac{\sqrt{\pi}}{\alpha}\sqrt{\frac{\beta}{\alpha}}\left(\beta - \alpha + 2\alpha\beta\gamma^2\right) + \frac{2\beta^2\, e^{-\alpha\gamma^2}}{\sqrt{\pi}\,\alpha\,(\alpha+\beta)^{3/2}}\left(\sqrt{\alpha+\beta} + \sqrt{\pi}\,\gamma\,(2\alpha+\beta)\, e^{\frac{\alpha^2\gamma^2}{\alpha+\beta}}\,\mathrm{Erf}\left(\frac{\alpha\gamma}{\sqrt{\alpha+\beta}}\right)\right) \\
& - \frac{4\sqrt{\pi}}{\alpha}\sqrt{\frac{\beta}{\alpha}}\left(\beta - \alpha + 2\alpha\beta\gamma^2\right)\mathcal{T}\left(\sqrt{\frac{2\alpha\beta}{\alpha+\beta}}\,\gamma, \sqrt{\frac{\alpha}{\beta}}\right)
\end{aligned} \tag{E.113}$$

Using the definition in Eq. (E.99), I_2 is given by,

$$\begin{aligned}
I_2 =& \frac{1}{\sqrt{\beta}}\left(I_{21} - I_{22}\right) \\
=& \cancel{\sqrt{\frac{\pi}{\alpha}}\left(\frac{\beta}{\alpha} + 2\beta\gamma^2 - 1\right)} - \cancel{\frac{\sqrt{\pi}}{\alpha^{3/2}}\left(\beta - \alpha + 2\alpha\beta\gamma^2\right)} + \frac{4\sqrt{\pi}}{\alpha^{3/2}}\left(\beta - \alpha + 2\alpha\beta\gamma^2\right)\mathcal{T}\left(\sqrt{\frac{2\alpha\beta}{\alpha+\beta}}\,\gamma, \sqrt{\frac{\alpha}{\beta}}\right) \\
& - \frac{2\beta^{3/2}\, e^{-\alpha\gamma^2}}{\sqrt{\pi}\,\alpha\,(\alpha+\beta)^{3/2}}\left(\sqrt{\alpha+\beta} + \sqrt{\pi}\,\gamma\,(2\alpha+\beta)\, e^{\frac{\alpha^2\gamma^2}{\alpha+\beta}}\,\mathrm{Erf}\left(\frac{\alpha\gamma}{\sqrt{\alpha+\beta}}\right)\right)
\end{aligned} \tag{E.114}$$

Finally, using the definition in Eq. (E.97), we get the expression for I,

$$\begin{aligned}
I =& \frac{1}{2\beta}I_1 - \frac{\sqrt{\pi}}{4\beta^{3/2}}I_2 \\
=& \frac{e^{-\alpha\gamma^2}}{2\beta\,(\alpha+\beta)^{3/2}}\left(\sqrt{\alpha+\beta} + \sqrt{\pi}\,\alpha\gamma\, e^{\frac{\alpha^2\gamma^2}{\alpha+\beta}}\,\mathrm{Erf}\left(\frac{\alpha\gamma}{\sqrt{\alpha+\beta}}\right)\right) \\
& - \frac{\pi}{(\alpha\beta)^{3/2}}\left(\beta - \alpha + 2\alpha\beta\gamma^2\right)\mathcal{T}\left(\sqrt{\frac{2\alpha\beta}{\alpha+\beta}}\,\gamma, \sqrt{\frac{\alpha}{\beta}}\right) \\
& + \frac{e^{-\alpha\gamma^2}}{2\alpha\,(\alpha+\beta)^{3/2}}\left(\sqrt{\alpha+\beta} + \sqrt{\pi}\,\gamma\,(2\alpha+\beta)\, e^{\frac{\alpha^2\gamma^2}{\alpha+\beta}}\,\mathrm{Erf}\left(\frac{\alpha\gamma}{\sqrt{\alpha+\beta}}\right)\right)
\end{aligned} \tag{E.115}$$

Simplifying the expression above gives us the final result,

$$I = \frac{e^{-\alpha\gamma^2}}{2\alpha\beta}\left(1 + \sqrt{\pi}\gamma\sqrt{\alpha+\beta}e^{\frac{\alpha^2\gamma^2}{\alpha+\beta}}\,\mathrm{Erf}\left(\frac{\alpha\gamma}{\sqrt{\alpha+\beta}}\right)\right) + \pi\left(\frac{\alpha-\beta-2\alpha\beta\gamma^2}{(\alpha\beta)^{3/2}}\right)\mathcal{T}\left(\gamma\sqrt{\frac{2\alpha\beta}{\alpha+\beta}}, \sqrt{\frac{\alpha}{\beta}}\right) \tag{E.116}$$

□

Corollary E.3 (to Theorem. E.2)**.** *Let $\alpha > 0$ and $\beta > 0$. The following result holds:*

$$\int_{-\infty}^{\infty}\int_{|x|}^{\infty}(y^2-x^2)\,e^{-\alpha x^2-\beta y^2}\,\mathrm{d}y\,\mathrm{d}x = \frac{\sqrt{\alpha\beta}+(\alpha-\beta)\,\arctan\left(\sqrt{\alpha/\beta}\right)}{2(\alpha\beta)^{3/2}} \tag{E.117}$$

Proof. The integral is a special case of the integral in Theorem E.2 with the parameter $\gamma = 0$. Eq. (E.93) states that,

$$\begin{aligned}\int_{-\infty}^{\infty}\int_{|x|}^{\infty}(y^2-x^2)\,e^{-\alpha(x-\gamma)^2-\beta y^2}\,\mathrm{d}y\,\mathrm{d}x =& \frac{e^{-\alpha\gamma^2}}{2\alpha\beta}\left(1+\sqrt{\pi}\,\gamma\sqrt{\alpha+\beta}\,e^{\frac{\alpha^2\gamma^2}{\alpha+\beta}}\,\operatorname{Erf}\left(\frac{\alpha\gamma}{\sqrt{\alpha+\beta}}\right)\right)\\ &+\pi\left(\frac{\alpha-\beta-2\alpha\beta\gamma^2}{(\alpha\beta)^{3/2}}\right)\mathcal{T}\left(\gamma\sqrt{\frac{2\alpha\beta}{\alpha+\beta}},\sqrt{\frac{\alpha}{\beta}}\right).\end{aligned} \tag{E.118}$$

Upon substituting $\gamma = 0$ on both sides, we get,

$$\int_{-\infty}^{\infty}\int_{|x|}^{\infty}(y^2-x^2)\,e^{-\alpha x^2-\beta y^2}\,\mathrm{d}y\,\mathrm{d}x = \frac{1}{2\alpha\beta}+\pi\left(\frac{\alpha-\beta}{(\alpha\beta)^{3/2}}\right)\mathcal{T}\left(0,\sqrt{\frac{\alpha}{\beta}}\right). \tag{E.119}$$

Since $\mathcal{T}(0,a) = \arctan(a)/(2\pi)$ [172], the integral becomes,

$$\begin{aligned}\int_{-\infty}^{\infty}\int_{|x|}^{\infty}(y^2-x^2)\,e^{-\alpha x^2-\beta y^2}\,\mathrm{d}y\,\mathrm{d}x &= \frac{1}{2\alpha\beta}+\left(\frac{\alpha-\beta}{2(\alpha\beta)^{3/2}}\right)\arctan\left(\sqrt{\frac{\alpha}{\beta}}\right)\\ &= \frac{\sqrt{\alpha\beta}+(\alpha-\beta)\,\arctan\left(\sqrt{\alpha/\beta}\right)}{2(\alpha\beta)^{3/2}}.\end{aligned} \tag{E.120}$$

□

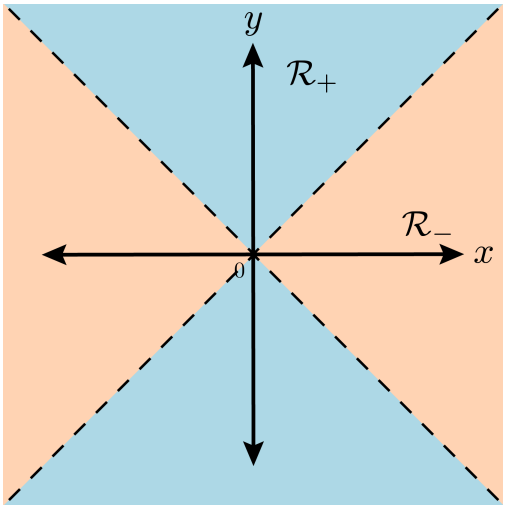


Figure E.2: Splitting of $\mathbb{R}^2$ into two disjoint regions. $\mathcal{R}_+$ is the region in blue satisfying $|y| \geq |x|$ and $\mathcal{R}_-$ is the region in orange satisfying $|x| > |y|$.

Theorem E.4. *Let $\alpha > 0$, $\beta > 0$, and $\gamma \in \mathbb{R}$. The following result holds:*

$$\int_{-\infty}^{\infty}\int_{-\infty}^{\infty} \left|y^2 - x^2\right| e^{-\alpha(x-\gamma)^2-\beta y^2}\,\mathrm{d}y\,\mathrm{d}x = \frac{2e^{-\alpha\gamma^2}}{\alpha\beta}\left(1 + \sqrt{\pi}\,\gamma\sqrt{\alpha+\beta}\,e^{\frac{\alpha^2\gamma^2}{\alpha+\beta}}\,\mathrm{Erf}\left(\frac{\alpha\gamma}{\sqrt{\alpha+\beta}}\right)\right) + 4\pi\left(\frac{\alpha-\beta-2\alpha\beta\gamma^2}{(\alpha\beta)^{3/2}}\right)\left(\mathcal{T}\left(\gamma\sqrt{\frac{2\alpha\beta}{\alpha+\beta}}, \sqrt{\frac{\alpha}{\beta}}\right) - \frac{1}{8}\right) \tag{E.121}$$

Proof. Let's denote the integral we have to evaluate by I.

$$I = \int\int_{\mathbb{R}^2} \left|y^2 - x^2\right| e^{-\alpha(x-\gamma)^2-\beta y^2}\,\mathrm{d}y\,\mathrm{d}x \tag{E.122}$$

The integral is evaluated over $(x, y) \in \mathbb{R}^2$. We split $\mathbb{R}^2$ into two disjoint regions (Fig. E.2), defined as follows:

- $\mathcal{R}_+ : \{(x, y) : |y| \geq |x|\}$, i.e., $y^2 \geq x^2$, and
- $\mathcal{R}_- : \{(x, y) : |x| > |y|\}$, i.e., $x^2 > y^2$.

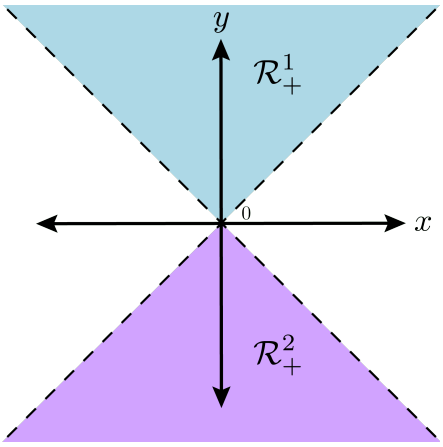


Figure E.3: Splitting of $\mathcal{R}_+$ into two disjoint regions. $\mathcal{R}_+^1$ is the region in blue satisfying $y \geq |x|$ and $\mathcal{R}_+^2$ is the region in purple satisfying $y \leq -|x|$.

Writing the integral over these disjoint regions gives us,

$$\begin{aligned} I &= \int\int_{\mathcal{R}_+} \left|y^2 - x^2\right| \, e^{-\alpha(x-\gamma)^2-\beta y^2} \mathrm{d}y \, \mathrm{d}x + \int\int_{\mathcal{R}_-} \left|y^2 - x^2\right| \, e^{-\alpha(x-\gamma)^2-\beta y^2} \mathrm{d}y \, \mathrm{d}x \\ &= \underbrace{\int\int_{\mathcal{R}_+} \left(y^2 - x^2\right) \, e^{-\alpha(x-\gamma)^2-\beta y^2} \mathrm{d}y \, \mathrm{d}x}_{I_1} - \underbrace{\int\int_{\mathcal{R}_-} \left(y^2 - x^2\right) \, e^{-\alpha(x-\gamma)^2-\beta y^2} \mathrm{d}y \, \mathrm{d}x}_{I_2} \end{aligned} \tag{E.123}$$

Therefore, $I = I_1 - I_2$. For evaluating the integral I_1, we split $\mathcal{R}_+$ into two disjoint subregions (Fig. E.3) defined as follows:

- $\mathcal{R}_+^1 : \{(x, y) : y \geq |x|\}$, and
- $\mathcal{R}_+^2 : \{(x, y) : y \leq -|x|\}$.

Therefore, I_1 can be written as,

$$\begin{aligned} I_1 &= \int\int_{\mathcal{R}_+} \left(y^2 - x^2\right) \, e^{-\alpha(x-\gamma)^2-\beta y^2} \mathrm{d}y \, \mathrm{d}x \\ &= \int\int_{\mathcal{R}_+^1} \left(y^2 - x^2\right) \, e^{-\alpha(x-\gamma)^2-\beta y^2} \mathrm{d}y \, \mathrm{d}x + \int\int_{\mathcal{R}_+^2} \left(y^2 - x^2\right) \, e^{-\alpha(x-\gamma)^2-\beta y^2} \mathrm{d}y \, \mathrm{d}x \\ &= \int_{-\infty}^{\infty} \int_{|x|}^{\infty} \left(y^2 - x^2\right) \, e^{-\alpha(x-\gamma)^2-\beta y^2} \mathrm{d}y \, \mathrm{d}x + \int_{-\infty}^{\infty} \int_{-\infty}^{-|x|} \left(y^2 - x^2\right) \, e^{-\alpha(x-\gamma)^2-\beta y^2} \mathrm{d}y \, \mathrm{d}x \end{aligned} \tag{E.124}$$

Since the integrand in the second integral is independent of the sign of y, we have,

$$\begin{aligned} I_1 &= \int_{-\infty}^{\infty} \int_{|x|}^{\infty} \left(y^2 - x^2\right)\, e^{-\alpha(x-\gamma)^2-\beta y^2} \mathrm{d}y\, \mathrm{d}x + \int_{-\infty}^{\infty} \int_{|x|}^{\infty} \left(y^2 - x^2\right)\, e^{-\alpha(x-\gamma)^2-\beta y^2} \mathrm{d}y\, \mathrm{d}x \\ &= 2 \underbrace{\int_{-\infty}^{\infty} \int_{|x|}^{\infty} \left(y^2 - x^2\right)\, e^{-\alpha(x-\gamma)^2-\beta y^2} \mathrm{d}y\, \mathrm{d}x}_{I_0} \end{aligned} \tag{E.125}$$

We know the result of I_0 from Theorem E.2. Therefore, we have $I_1 = 2I_0$. Now consider the following integral, the result of which is known (Lemma E.11),

$$\begin{aligned} I' &= \int \int_{\mathbb{R}^2} \left(y^2 - x^2\right)\, e^{-\alpha(x-\gamma)^2-\beta y^2} \mathrm{d}y\, \mathrm{d}x \\ &= \int \int_{\mathcal{R}_+} \left(y^2 - x^2\right)\, e^{-\alpha(x-\gamma)^2-\beta y^2} \mathrm{d}y\, \mathrm{d}x + \int \int_{\mathcal{R}_-} \left(y^2 - x^2\right)\, e^{-\alpha(x-\gamma)^2-\beta y^2} \mathrm{d}y\, \mathrm{d}x \end{aligned} \tag{E.126}$$

We recognize these integrals from Eq. (E.123) and have the following relation,

$$I' = I_1 + I_2 \quad \text{or} \quad I_2 = I' - I_1 \tag{E.127}$$

Therefore, I can be expressed in terms of the known integrals as follows,

$$
\begin{aligned}
I =& I_1 - I_2 \\
=& I_1 - (I' - I_1) \\
=& 2I_1 - I' \\
=& 4I_0 - I' \\
=& 4\left(\frac{e^{-\alpha\gamma^2}}{2\alpha\beta}\left(1 + \sqrt{\pi}\,\gamma\sqrt{\alpha+\beta}\,e^{\frac{\alpha^2\gamma^2}{\alpha+\beta}}\ \mathrm{Erf}\left(\frac{\alpha\gamma}{\sqrt{\alpha+\beta}}\right)\right) + \pi\left(\frac{\alpha-\beta-2\alpha\beta\gamma^2}{(\alpha\beta)^{3/2}}\right)\mathcal{T}\left(\gamma\sqrt{\frac{2\alpha\beta}{\alpha+\beta}}, \sqrt{\frac{\alpha}{\beta}}\right)\right) \\
& - \frac{\pi}{2}\left(\frac{\alpha-\beta-2\alpha\beta\gamma^2}{(\alpha\beta)^{3/2}}\right) \\
=& \frac{2e^{-\alpha\gamma^2}}{\alpha\beta}\left(1 + \sqrt{\pi}\,\gamma\sqrt{\alpha+\beta}\,e^{\frac{\alpha^2\gamma^2}{\alpha+\beta}}\ \mathrm{Erf}\left(\frac{\alpha\gamma}{\sqrt{\alpha+\beta}}\right)\right) + 4\pi\left(\frac{\alpha-\beta-2\alpha\beta\gamma^2}{(\alpha\beta)^{3/2}}\right)\left(\mathcal{T}\left(\gamma\sqrt{\frac{2\alpha\beta}{\alpha+\beta}}, \sqrt{\frac{\alpha}{\beta}}\right) - \frac{1}{8}\right)
\end{aligned}
\tag{E.128}
$$

□

Corollary E.5 (to Theorem. E.4)**.** *Let $\alpha > 0$ and $\beta > 0$. The following result holds:*

$$
\int_{-\infty}^{\infty}\int_{-\infty}^{\infty}\left|y^2 - x^2\right| e^{-\alpha x^2 - \beta y^2}\,\mathrm{d}y\,\mathrm{d}x = \frac{2}{(\alpha\beta)^{3/2}}\left(\sqrt{\alpha\beta} + (\alpha-\beta)\left(\arctan\left(\sqrt{\frac{\alpha}{\beta}}\right) - \frac{\pi}{4}\right)\right) \tag{E.129}
$$

Proof. The integral is a special case of the integral in Theorem E.4 with the parameter $\gamma = 0$. Eq. (E.121) states that,

$$
\begin{aligned}
\int_{-\infty}^{\infty}\int_{-\infty}^{\infty}\left|y^2 - x^2\right| e^{-\alpha(x-\gamma)^2 - \beta y^2}\,\mathrm{d}y\,\mathrm{d}x =& \frac{2e^{-\alpha\gamma^2}}{\alpha\beta}\left(1 + \sqrt{\pi}\,\gamma\sqrt{\alpha+\beta}\,e^{\frac{\alpha^2\gamma^2}{\alpha+\beta}}\ \mathrm{Erf}\left(\frac{\alpha\gamma}{\sqrt{\alpha+\beta}}\right)\right) \\
& + 4\pi\left(\frac{\alpha-\beta-2\alpha\beta\gamma^2}{(\alpha\beta)^{3/2}}\right)\left(\mathcal{T}\left(\gamma\sqrt{\frac{2\alpha\beta}{\alpha+\beta}}, \sqrt{\frac{\alpha}{\beta}}\right) - \frac{1}{8}\right)
\end{aligned}
\tag{E.130}
$$

Upon substituting $\gamma = 0$ on both sides, we get,

$$
\int_{-\infty}^{\infty}\int_{-\infty}^{\infty}\left|y^2 - x^2\right| e^{-\alpha x^2 - \beta y^2}\,\mathrm{d}y\,\mathrm{d}x = \frac{2}{\alpha\beta} + 4\pi\left(\frac{\alpha-\beta}{(\alpha\beta)^{3/2}}\right)\left(\mathcal{T}\left(0, \sqrt{\frac{\alpha}{\beta}}\right) - \frac{1}{8}\right). \tag{E.131}
$$

Since $\mathcal{T}(0,a) = \arctan(a)/(2\pi)$ [172], the integral becomes,

$$\begin{aligned}\int_{-\infty}^{\infty}\int_{-\infty}^{\infty}\left|y^2-x^2\right| e^{-\alpha x^2-\beta y^2}\,\mathrm{d}y\,\mathrm{d}x &= \frac{2}{\alpha\beta}+2\left(\frac{\alpha-\beta}{(\alpha\beta)^{3/2}}\right)\left(\arctan\left(\sqrt{\frac{\alpha}{\beta}}\right)-\frac{\pi}{4}\right)\\ &= \frac{2}{(\alpha\beta)^{3/2}}\left(\sqrt{\alpha\beta}+(\alpha-\beta)\left(\arctan\left(\sqrt{\frac{\alpha}{\beta}}\right)-\frac{\pi}{4}\right)\right).\end{aligned} \tag{E.132}$$

□

Lemma E.6. *Let $\alpha > 0$, $\beta > 0$, and $\gamma \in \mathbb{R}$. The following result holds:*

$$\begin{aligned}\int_{|x|}^{\infty}\left(y^2-x^2\right)e^{-\alpha(x-\gamma)^2-\beta y^2}\,\mathrm{d}y =& \frac{1}{2\beta}|x|e^{-\alpha(x-\gamma)^2-\beta x^2}\\ &-\frac{\sqrt{\pi}}{4\beta^{3/2}}\left(2\beta x^2-1\right)e^{-\alpha(x-\gamma)^2}\operatorname{Erfc}\left(\sqrt{\beta}|x|\right)\end{aligned} \tag{E.133}$$

Proof. We begin by evaluating the integral

$$I = \int_{|x|}^{\infty}\left(y^2-x^2\right)e^{-\alpha(x-\gamma)^2-\beta y^2}\,\mathrm{d}y. \tag{E.134}$$

Since x is treated as a constant with respect to the integration variable y, we can factor out the constant exponential term,

$$I = e^{-\alpha(x-\gamma)^2}\left(\int_{|x|}^{\infty} y^2 e^{-\beta y^2}\,\mathrm{d}y - x^2\int_{|x|}^{\infty} e^{-\beta y^2}\,\mathrm{d}y\right). \tag{E.135}$$

These integrals are standard and can be evaluated in terms of the complementary error functions $\operatorname{Erfc}(z) = 1-\operatorname{Erf}(z)$,

$$\int_{|x|}^{\infty} e^{-\beta y^2}\,\mathrm{d}y = \frac{1}{2}\sqrt{\frac{\pi}{\beta}}\operatorname{Erfc}\left(\sqrt{\beta}|x|\right) \tag{E.136}$$

and

$$\int_{|x|}^{\infty} y^2 e^{-\beta y^2}\,\mathrm{d}y = \frac{|x|}{2\beta}e^{-\beta x^2}+\frac{\sqrt{\pi}}{4\beta^{3/2}}\operatorname{Erfc}\left(\sqrt{\beta}|x|\right). \tag{E.137}$$

Substituting these results back into the expression for I, we get,

$$I = \frac{1}{2\beta}|x|e^{-\alpha(x-\gamma)^2-\beta x^2} - \frac{\sqrt{\pi}}{4\beta^{3/2}}\left(2\beta x^2 - 1\right)e^{-\alpha(x-\gamma)^2}\,\mathrm{Erfc}\left(\sqrt{\beta}|x|\right) \tag{E.138}$$

□

Lemma E.7. *Let $\alpha > 0$, $\beta > 0$, and $\gamma \in \mathbb{R}$. The following result holds:*

$$\int_{-\infty}^{\infty} |x|e^{-\alpha(x-\gamma)^2-\beta x^2}\mathrm{d}x = \frac{e^{-\alpha\gamma^2}}{(\alpha+\beta)^{3/2}}\left(\sqrt{\alpha+\beta} + \sqrt{\pi}\,\alpha\gamma\, e^{\frac{\alpha^2\gamma^2}{\alpha+\beta}}\,\mathrm{Erf}\left(\frac{\alpha\gamma}{\sqrt{\alpha+\beta}}\right)\right) \tag{E.139}$$

Proof. We denote the integral by I and split it at 0 to get,

$$\begin{aligned} I &= \int_{-\infty}^{0} (-x)\, e^{-\beta x^2-\alpha(x-\gamma)^2}\mathrm{d}x + \int_{0}^{\infty} x\, e^{-\beta x^2-\alpha(x-\gamma)^2}\mathrm{d}x \\ &= \underbrace{\int_{0}^{\infty} x\, e^{-\beta x^2-\alpha(x+\gamma)^2}\mathrm{d}x}_{I_1} + \underbrace{\int_{0}^{\infty} x\, e^{-\beta x^2-\alpha(x-\gamma)^2}\mathrm{d}x}_{I_2}. \end{aligned} \tag{E.140}$$

We complete the square in x for both I_1 and I_2, which gives us,

$$I_1 = e^{-\frac{\alpha\beta\gamma^2}{\alpha+\beta}}\int_{0}^{\infty} x\, e^{-\left(\sqrt{\alpha+\beta}\,x+\frac{\alpha\gamma}{\sqrt{\alpha+\beta}}\right)^2}\mathrm{d}x \quad \text{and} \quad I_2 = e^{-\frac{\alpha\beta\gamma^2}{\alpha+\beta}}\int_{0}^{\infty} x\, e^{-\left(\sqrt{\alpha+\beta}\,x-\frac{\alpha\gamma}{\sqrt{\alpha+\beta}}\right)^2}\mathrm{d}x \tag{E.141}$$

These are well known integrals [172] and are given by,

$$I_1 = \frac{e^{-\alpha\gamma^2}}{2(\alpha+\beta)^{3/2}}\left(\sqrt{\alpha+\beta} - \sqrt{\pi}\,\alpha\gamma\, e^{\frac{\alpha^2\gamma^2}{\alpha+\beta}}\,\mathrm{Erfc}\left(\frac{\alpha\gamma}{\sqrt{\alpha+\beta}}\right)\right) \tag{E.142}$$

$$I_2 = \frac{e^{-\alpha\gamma^2}}{2(\alpha+\beta)^{3/2}}\left(\sqrt{\alpha+\beta} + \sqrt{\pi}\,\alpha\gamma\, e^{\frac{\alpha^2\gamma^2}{\alpha+\beta}}\,\mathrm{Erfc}\left(-\frac{\alpha\gamma}{\sqrt{\alpha+\beta}}\right)\right) \tag{E.143}$$

Substituting $\mathrm{Erfc}(z) = 1 - \mathrm{Erf}(z)$ and noting that $\mathrm{Erf}(-z) = -\mathrm{Erf}(z)$, we get the following

expresssion for I,

$$\begin{aligned} I &= I_1 + I_2 \\ &= \frac{e^{-\alpha\gamma^2}}{(\alpha+\beta)^{3/2}} \left(\sqrt{\alpha+\beta} + \sqrt{\pi}\, \alpha\gamma\, e^{\frac{\alpha^2\gamma^2}{\alpha+\beta}} \operatorname{Erf}\left(\frac{\alpha\gamma}{\sqrt{\alpha+\beta}} \right) \right) \end{aligned} \tag{E.144}$$

□

Lemma E.8. *Let $\alpha > 0$, $\beta > 0$, and $\gamma \in \mathbb{R}$. The following result holds:*

$$\int_{-\infty}^{\infty} \left(2x^2 - 1\right) e^{-\frac{\alpha}{\beta}(x-\gamma\sqrt{\beta})^2} \mathrm{d}x = \sqrt{\pi}\sqrt{\frac{\beta}{\alpha}} \left(\frac{\beta}{\alpha} + 2\beta\gamma^2 - 1 \right) \tag{E.145}$$

Proof. We denote the integral under consideration by I and make the following variable transformation, $x = k + \gamma\sqrt{\beta}$. This gives us

$$\begin{aligned} I &= \int_{-\infty}^{\infty} \left(2\left(k + \gamma\sqrt{\beta}\right)^2 - 1 \right) e^{-\frac{\alpha}{\beta}k^2} \mathrm{d}k \\ &= \int_{-\infty}^{\infty} \left(2k^2 + 4\gamma\sqrt{\beta}\, k + 2\beta\gamma^2 - 1 \right) e^{-\frac{\alpha}{\beta}k^2} \mathrm{d}k \\ &= 2 \underbrace{\int_{-\infty}^{\infty} k^2 e^{-\frac{\alpha}{\beta}k^2} \mathrm{d}k}_{I_1} + 4\gamma\sqrt{\beta} \underbrace{\int_{-\infty}^{\infty} k\, e^{-\frac{\alpha}{\beta}k^2} \mathrm{d}k}_{I_2} + \left(2\beta\gamma^2 - 1\right) \underbrace{\int_{-\infty}^{\infty} e^{-\frac{\alpha}{\beta}k^2} \mathrm{d}k}_{I_3} \end{aligned} \tag{E.146}$$

The integrand of I_2 is an odd function; therefore, $I_2 = 0$. I_1 and I_3 are standard integrals given by,

$$I_1 = \frac{\sqrt{\pi}}{2} \left(\frac{\beta}{\alpha} \right)^{3/2} \quad \text{and} \quad I_3 = \sqrt{\pi}\sqrt{\frac{\beta}{\alpha}} \tag{E.147}$$

Therefore, I is given by,

$$\begin{aligned} I &= \sqrt{\pi} \left(\frac{\beta}{\alpha} \right)^{3/2} + \left(2\beta\gamma^2 - 1\right) \sqrt{\pi}\sqrt{\frac{\beta}{\alpha}} \\ &= \sqrt{\pi}\sqrt{\frac{\beta}{\alpha}} \left(\frac{\beta}{\alpha} + 2\beta\gamma^2 - 1 \right) \end{aligned} \tag{E.148}$$

□

Lemma E.9. *Let $\alpha > 0$, $\beta > 0$, and $\gamma \in \mathbb{R}$. The following result holds:*

$$\begin{aligned}\int_0^\infty e^{-\frac{\alpha}{\beta}\left(x+\gamma\sqrt{\beta}\right)^2-x^2}\left(\gamma\sqrt{\beta}-\left(x+\gamma\sqrt{\beta}\right)e^{\frac{4\alpha\gamma}{\sqrt{\beta}}x}-x\right)\mathrm{d}x = \\ -\frac{\beta\, e^{-\alpha\gamma^2}}{(\alpha+\beta)^{3/2}}\left(\sqrt{\alpha+\beta}+\sqrt{\pi}\,\gamma\,(2\alpha+\beta)\,e^{\frac{\alpha^2\gamma^2}{\alpha+\beta}}\,\mathrm{Erf}\left(\frac{\alpha\gamma}{\sqrt{\alpha+\beta}}\right)\right)\end{aligned} \tag{E.149}$$

Proof. We denote the integral by I and expand to get the following four integrals,

$$\begin{aligned}I =&\gamma\sqrt{\beta}\int_0^\infty e^{-\frac{\alpha}{\beta}\left(x+\gamma\sqrt{\beta}\right)^2-x^2}\,\mathrm{d}x-\gamma\sqrt{\beta}\int_0^\infty e^{-\frac{\alpha}{\beta}\left(x+\gamma\sqrt{\beta}\right)^2-x^2+\frac{4\alpha\gamma}{\sqrt{\beta}}x}\,\mathrm{d}x\\ &-\int_0^\infty x\,e^{-\frac{\alpha}{\beta}\left(x+\gamma\sqrt{\beta}\right)^2-x^2}\,\mathrm{d}x-\int_0^\infty x\,e^{-\frac{\alpha}{\beta}\left(x+\gamma\sqrt{\beta}\right)^2-x^2+\frac{4\alpha\gamma}{\sqrt{\beta}}x}\,\mathrm{d}x\end{aligned} \tag{E.150}$$

Forming a square in x in the exponential terms, we get,

$$\begin{aligned}I =&\gamma\sqrt{\beta}\,e^{-\frac{\alpha\beta\gamma^2}{\alpha+\beta}}\int_0^\infty e^{-\left(\sqrt{\frac{\alpha+\beta}{\beta}}x+\frac{\alpha\gamma}{\sqrt{\alpha+\beta}}\right)^2}\,\mathrm{d}x-\gamma\sqrt{\beta}\,e^{-\frac{\alpha\beta\gamma^2}{\alpha+\beta}}\int_0^\infty e^{-\left(\sqrt{\frac{\alpha+\beta}{\beta}}x-\frac{\alpha\gamma}{\sqrt{\alpha+\beta}}\right)^2}\,\mathrm{d}x\\ &-e^{-\frac{\alpha\beta\gamma^2}{\alpha+\beta}}\int_0^\infty x\,e^{-\left(\sqrt{\frac{\alpha+\beta}{\beta}}x+\frac{\alpha\gamma}{\sqrt{\alpha+\beta}}\right)^2}\,\mathrm{d}x-e^{-\frac{\alpha\beta\gamma^2}{\alpha+\beta}}\int_0^\infty x\,e^{-\left(\sqrt{\frac{\alpha+\beta}{\beta}}x-\frac{\alpha\gamma}{\sqrt{\alpha+\beta}}\right)^2}\,\mathrm{d}x\end{aligned} \tag{E.151}$$

These are standard integrals of normal functions. Using the results in [172], we get,

$$\int_0^\infty e^{-\left(\sqrt{\frac{\alpha+\beta}{\beta}}x+\frac{\alpha\gamma}{\sqrt{\alpha+\beta}}\right)^2}\,\mathrm{d}x=\frac{\sqrt{\pi}}{2}\sqrt{\frac{\beta}{\alpha+\beta}}\left(1-\mathrm{Erf}\left(\frac{\alpha\gamma}{\sqrt{\alpha+\beta}}\right)\right) \tag{E.152}$$

$$\int_0^\infty e^{-\left(\sqrt{\frac{\alpha+\beta}{\beta}}x-\frac{\alpha\gamma}{\sqrt{\alpha+\beta}}\right)^2}\,\mathrm{d}x=\frac{\sqrt{\pi}}{2}\sqrt{\frac{\beta}{\alpha+\beta}}\left(1+\mathrm{Erf}\left(\frac{\alpha\gamma}{\sqrt{\alpha+\beta}}\right)\right) \tag{E.153}$$

$$\int_0^\infty x\,e^{-\left(\sqrt{\frac{\alpha+\beta}{\beta}}x+\frac{\alpha\gamma}{\sqrt{\alpha+\beta}}\right)^2}\,\mathrm{d}x=\frac{\beta}{2(\alpha+\beta)^{3/2}}\left(\sqrt{\alpha+\beta}\,e^{-\frac{\alpha^2\gamma^2}{\alpha+\beta}}-\sqrt{\pi}\,\alpha\gamma\left(1-\mathrm{Erf}\left(\frac{\alpha\gamma}{\sqrt{\alpha+\beta}}\right)\right)\right) \tag{E.154}$$

$$\int_0^\infty x\, e^{-\left(\sqrt{\frac{\alpha+\beta}{\beta}}\, x - \frac{\alpha\gamma}{\sqrt{\alpha+\beta}}\right)^2} \mathrm{d}x = \frac{\beta}{2(\alpha+\beta)^{3/2}} \left(\sqrt{\alpha+\beta}\, e^{-\frac{\alpha^2\gamma^2}{\alpha+\beta}} + \sqrt{\pi}\, \alpha\gamma \left(1 + \mathrm{Erf}\left(\frac{\alpha\gamma}{\sqrt{\alpha+\beta}} \right) \right) \right) \tag{E.155}$$

Substituting these expressions in Eq. (E.151) and simplifying, we get,

$$I = -\frac{\beta\, e^{-\alpha\gamma^2}}{(\alpha+\beta)^{3/2}} \left(\sqrt{\alpha+\beta} + \sqrt{\pi}\, \gamma\, (2\alpha+\beta)\, e^{\frac{\alpha^2\gamma^2}{\alpha+\beta}}\, \mathrm{Erf}\left(\frac{\alpha\gamma}{\sqrt{\alpha+\beta}} \right) \right) \tag{E.156}$$

□

Lemma E.10. *Let $\alpha > 0$, $\beta > 0$, and $\gamma \in \mathbb{R}$. The following result holds:*

$$\int_0^\infty e^{-x^2} \left(\mathrm{Erf}\left(\sqrt{\frac{\alpha}{\beta}} \left(x + \gamma\sqrt{\beta} \right) \right) + \mathrm{Erf}\left(\sqrt{\frac{\alpha}{\beta}} \left(x - \gamma\sqrt{\beta} \right) \right) \right) \mathrm{d}x = 4\sqrt{\pi}\, \mathcal{T}\left(\sqrt{\frac{2\alpha\beta}{\alpha+\beta}}\, \gamma, \sqrt{\frac{\alpha}{\beta}} \right) \tag{E.157}$$

Proof. Consider the result "10, 016.6" from Owen's table of normal integrals [172]. It states that,

$$\int_0^\infty G'(x)\, G(a+bx)\, \mathrm{d}x = \frac{1}{2} G\left(\frac{a}{\sqrt{1+b^2}} \right) + \mathcal{T}\left(\frac{a}{\sqrt{1+b^2}}, b \right) \tag{E.158}$$

where $G(z)$ is the cumulative density function of a standard normal Gaussian random variable and $G'(z)$ is its derivative, i.e.,

$$G(z) = \frac{1}{\sqrt{2\pi}} \int_{-\infty}^{z} e^{-t^2/2}\, \mathrm{d}t \quad \text{and} \quad G'(z) = \frac{1}{\sqrt{2\pi}} e^{-z^2/2}, \tag{E.159}$$

and $\mathcal{T}(h, a)$ is the Owen's T function defined as,

$$\mathcal{T}(h, a) = \frac{1}{2\pi} \int_0^a \frac{e^{-\frac{1}{2}h^2(1+t^2)}}{1+t^2}\, \mathrm{d}t. \tag{E.160}$$

First, we note the following relation,

$$G(z) = \frac{1}{2} \left(1 + \mathrm{Erf}\left(\frac{z}{\sqrt{2}} \right) \right) \tag{E.161}$$

We plug in this expression on the LHS of Eq. (E.158),

$$\begin{aligned}
\text{LHS} &= \int_0^\infty G'(x)\, G(a+bx)\, \mathrm{d}x \\
&= \int_0^\infty \left(\frac{1}{\sqrt{2\pi}} e^{-x^2/2}\right) \left(\frac{1}{2}\left(1 + \text{Erf}\left(\frac{a+bx}{\sqrt{2}}\right)\right)\right) \mathrm{d}x \\
&= \frac{1}{2\sqrt{2\pi}} \int_0^\infty e^{-x^2/2}\, \mathrm{d}x + \frac{1}{2\sqrt{2\pi}} \int_0^\infty e^{-x^2/2}\, \text{Erf}\left(\frac{a+bx}{\sqrt{2}}\right) \mathrm{d}x \\
&= \frac{1}{4} + \frac{1}{2\sqrt{2\pi}} \int_0^\infty e^{-x^2/2}\, \text{Erf}\left(\frac{a+bx}{\sqrt{2}}\right) \mathrm{d}x
\end{aligned} \tag{E.162}$$

Making the variable change $k = x/\sqrt{2}$ gives us,

$$\text{LHS} = \frac{1}{4} + \frac{1}{2\sqrt{\pi}} \int_0^\infty e^{-k^2}\, \text{Erf}\left(bk + \frac{a}{\sqrt{2}}\right) \mathrm{d}k \tag{E.163}$$

Now, RHS of Eq. (E.158) can be written as,

$$\begin{aligned}
\text{RHS} &= \frac{1}{2} G\left(\frac{a}{\sqrt{1+b^2}}\right) + \mathcal{T}\left(\frac{a}{\sqrt{1+b^2}}, b\right) \\
&= \frac{1}{4}\left(1 + \text{Erf}\left(\frac{a}{\sqrt{2(1+b^2)}}\right)\right) + \mathcal{T}\left(\frac{a}{\sqrt{1+b^2}}, b\right)
\end{aligned} \tag{E.164}$$

Equating LHS = RHS gives us the following relation,

$$\int_0^\infty e^{-k^2}\, \text{Erf}\left(bk + \frac{a}{\sqrt{2}}\right) \mathrm{d}k = \sqrt{\pi}\left(\frac{1}{2}\, \text{Erf}\left(\frac{a}{\sqrt{2(1+b^2)}}\right) + 2\,\mathcal{T}\left(\frac{a}{\sqrt{1+b^2}}, b\right)\right) \tag{E.165}$$

Finally, we replace $a/\sqrt{2}$ by c on both sides to get the relation,

$$\boxed{\int_0^\infty e^{-k^2}\, \text{Erf}\,(bk + c)\, \mathrm{d}k = \sqrt{\pi}\left(\frac{1}{2}\, \text{Erf}\left(\frac{c}{\sqrt{1+b^2}}\right) + 2\,\mathcal{T}\left(\sqrt{\frac{2}{1+b^2}}\, c, b\right)\right)} \tag{E.166}$$

Replacing $c \longrightarrow -c$ and using the properties that $\text{Erf}(-z) = -\text{Erf}(z)$ and $\mathcal{T}(-h, a) = \mathcal{T}(h, a)$, we

also have the relation,

$$\boxed{\int_0^\infty e^{-k^2}\,\mathrm{Erf}\,(bk-c)\;\mathrm{d}k = \sqrt{\pi}\left(-\frac{1}{2}\,\mathrm{Erf}\left(\frac{c}{\sqrt{1+b^2}}\right) + 2\,\mathcal{T}\left(\sqrt{\frac{2}{1+b^2}}\,c, b\right)\right)} \tag{E.167}$$

Adding these two equations gives the following result,

$$\boxed{\int_0^\infty e^{-k^2}\left(\mathrm{Erf}\,(bk+c) + \mathrm{Erf}\,(bk-c)\right)\;\mathrm{d}k = 4\sqrt{\pi}\,\mathcal{T}\left(\sqrt{\frac{2}{1+b^2}}\,c, b\right)} \tag{E.168}$$

Substituting $b \to \sqrt{\alpha/\beta}$ and $c \to \gamma\sqrt{\alpha}$ in the equation above gives us,

$$\int_0^\infty e^{-k^2}\left(\mathrm{Erf}\left(\sqrt{\frac{\alpha}{\beta}}\,k + \gamma\sqrt{\alpha}\right) + \mathrm{Erf}\left(\sqrt{\frac{\alpha}{\beta}}\,k - \gamma\sqrt{\alpha}\right)\right)\;\mathrm{d}k = 4\sqrt{\pi}\,\mathcal{T}\left(\sqrt{\frac{2\alpha\beta}{\alpha+\beta}}\,\gamma, \sqrt{\frac{\alpha}{\beta}}\right) \tag{E.169}$$

□

Lemma E.11. *Let $\alpha > 0$, $\beta > 0$, and $\gamma \in \mathbb{R}$. The following result holds:*

$$\int_{-\infty}^\infty \int_{-\infty}^\infty \left(y^2 - x^2\right)\; e^{-\alpha(x-\gamma)^2-\beta y^2}\mathrm{d}y\,\mathrm{d}x = \frac{\pi}{2}\left(\frac{\alpha-\beta-2\alpha\beta\gamma^2}{(\alpha\beta)^{3/2}}\right) \tag{E.170}$$

Proof. Let the integral we need to evaluate be denoted by I. First we integrate in y assuming x constant,

$$\begin{aligned} I &= \int_{-\infty}^\infty e^{-\alpha(x-\gamma)^2}\left(\int_{-\infty}^\infty y^2\,e^{-\beta y^2}\mathrm{d}y - x^2\int_{-\infty}^\infty e^{-\beta y^2}\mathrm{d}y\right)\mathrm{d}x \\ &= \int_{-\infty}^\infty e^{-\alpha(x-\gamma)^2}\left(\frac{\sqrt{\pi}}{2\beta^{3/2}} - \sqrt{\frac{\pi}{\beta}}\,x^2\right)\mathrm{d}x \\ &= \frac{\sqrt{\pi}}{2\beta^{3/2}}\int_{-\infty}^\infty e^{-\alpha(x-\gamma)^2}\,\mathrm{d}x - \sqrt{\frac{\pi}{\beta}}\int_{-\infty}^\infty x^2 e^{-\alpha(x-\gamma)^2}\,\mathrm{d}x \end{aligned} \tag{E.171}$$

Evaluating the integral in x and simplifying the expressions, we get the final expression for I,

$$\begin{aligned} I &= \frac{\sqrt{\pi}}{2\beta^{3/2}} \int_{-\infty}^{\infty} e^{-\alpha(x-\gamma)^2} \, \mathrm{d}x - \sqrt{\frac{\pi}{\beta}} \int_{-\infty}^{\infty} x^2 e^{-\alpha(x-\gamma)^2} \, \mathrm{d}x \\ &= \frac{\sqrt{\pi}}{2\beta^{3/2}} \sqrt{\frac{\pi}{\alpha}} - \sqrt{\frac{\pi}{\beta}} \left(\frac{\sqrt{\pi}}{2\alpha^{3/2}} \left(1 + 2\alpha\gamma^2\right) \right) \\ &= \frac{\pi}{2\sqrt{\alpha\beta}} \left(\frac{1}{\beta} - \frac{1}{\alpha} - 2\gamma^2 \right) \\ &= \frac{\pi}{2} \left(\frac{\alpha - \beta - 2\alpha\beta\gamma^2}{(\alpha\beta)^{3/2}} \right) \end{aligned} \tag{E.172}$$

□

Bibliography

[1] Wulfram Gerstner and Werner M Kistler. *Spiking neuron models: Single neurons, populations, plasticity*. Cambridge university press, 2002.

[2] Rodney J Douglas and KA Martin. "A functional microcircuit for cat visual cortex." In: *The Journal of physiology* 440.1 (1991), pp. 735–769.

[3] Rodney J Douglas et al. "Recurrent excitation in neocortical circuits". In: *Science* 269.5226 (1995), pp. 981–985.

[4] Rodney J Douglas, Kevan AC Martin, and David Whitteridge. "A canonical microcircuit for neocortex". In: *Neural computation* 1.4 (1989), pp. 480–488.

[5] Matteo Carandini and David J Heeger. "Normalization as a canonical neural computation". In: *Nature reviews neuroscience* 13.1 (2012), pp. 51–62.

[6] Randy L Buckner and Fenna M Krienen. "The evolution of distributed association networks in the human brain". In: *Trends in cognitive sciences* 17.12 (2013), pp. 648–665.

[7] Kenneth D Miller. "Canonical computations of cerebral cortex". In: *Current opinion in neurobiology* 37 (2016), pp. 75–84.

[8] Peter Dayan and Laurence F Abbott. *Theoretical neuroscience: computational and mathematical modeling of neural systems*. MIT press, 2005.

[9] David J Heeger. "Normalization of cell responses in cat striate cortex". In: *Visual neuroscience* 9.2 (1992), pp. 181–197.

[10] Ruben Coen-Cagli, Adam Kohn, and Odelia Schwartz. “Flexible gating of contextual influences in natural vision”. In: *Nature neuroscience* 18.11 (2015), pp. 1648–1655.

[11] Odelia Schwartz and Eero Simoncelli. “Natural sound statistics and divisive normalization in the auditory system”. In: *Advances in neural information processing systems* 13 (2000).

[12] Hugh R Wilson and Jack D Cowan. “Excitatory and inhibitory interactions in localized populations of model neurons”. In: *Biophysical journal* 12.1 (1972), pp. 1–24.

[13] Daniel B Rubin, Stephen D Van Hooser, and Kenneth D Miller. “The stabilized supralinear network: a unifying circuit motif underlying multi-input integration in sensory cortex”. In: *Neuron* 85.2 (2015), pp. 402–417.

[14] Jesús Malo, José Juan Esteve-Taboada, and Marcelo Bertalmío. “Cortical Divisive Normalization from Wilson–Cowan Neural Dynamics”. In: *Journal of Nonlinear Science* 34.2 (2024), pp. 1–36.

[15] David J Heeger and Wayne E Mackey. “Oscillatory recurrent gated neural integrator circuits (ORGaNICs), a unifying theoretical framework for neural dynamics”. In: *Proceedings of the National Academy of Sciences* 116.45 (2019), pp. 22783–22794.

[16] David J Heeger and Klavdia O Zemlianova. “A recurrent circuit implements normalization, simulating the dynamics of V1 activity”. In: *Proceedings of the National Academy of Sciences* 117.36 (2020), pp. 22494–22505.

[17] Wilson S Geisler and Duane G Albrecht. “Visual cortex neurons in monkeys and cats: detection, discrimination, and identification”. In: *Visual neuroscience* 14.5 (1997), pp. 897–919.

[18] Matteo Carandini and David J Heeger. “Summation and division by neurons in primate visual cortex”. In: *Science* 264.5163 (1994), pp. 1333–1336.

[19] Duane G Albrecht and Wilson S Geisler. "Motion selectivity and the contrast-response function of simple cells in the visual cortex". In: *Visual neuroscience* 7.6 (1991), pp. 531–546.

[20] David J Heeger. "Modeling simple-cell direction selectivity with normalized, half-squared, linear operators". In: *Journal of neurophysiology* 70.5 (1993), pp. 1885–1898.

[21] Shawn R Olsen, Vikas Bhandawat, and Rachel I Wilson. "Divisive normalization in olfactory population codes". In: *Neuron* 66.2 (2010), pp. 287–299.

[22] John H Reynolds and David J Heeger. "The normalization model of attention". In: *Neuron* 61.2 (2009), pp. 168–185.

[23] Wei Ji Ma, Masud Husain, and Paul M Bays. "Changing concepts of working memory". In: *Nature neuroscience* 17.3 (2014), pp. 347–356.

[24] Kenway Louie, Lauren E Grattan, and Paul W Glimcher. "Reward value-based gain control: divisive normalization in parietal cortex". In: *Journal of Neuroscience* 31.29 (2011), pp. 10627–10639.

[25] Eero P Simoncelli and David J Heeger. "A model of neuronal responses in visual area MT". In: *Vision research* 38.5 (1998), pp. 743–761.

[26] John H Reynolds, Leonardo Chelazzi, and Robert Desimone. "Competitive mechanisms subserve attention in macaque areas V2 and V4". In: *Journal of Neuroscience* 19.5 (1999), pp. 1736–1753.

[27] Davide Zoccolan, David D Cox, and James J DiCarlo. "Multiple object response normalization in monkey inferotemporal cortex". In: *Journal of Neuroscience* 25.36 (2005), pp. 8150–8164.

[28] Geoffrey M Boynton. "A framework for describing the effects of attention on visual responses". In: *Vision research* 49.10 (2009), pp. 1129–1143.

[29] Joonyeol Lee and John HR Maunsell. “A normalization model of attentional modulation of single unit responses”. In: *PloS one* 4.2 (2009), e4651.

[30] Paul M Bays. “Noise in neural populations accounts for errors in working memory”. In: *Journal of Neuroscience* 34.10 (2014), pp. 3632–3645.

[31] Barbara Zenger-Landolt and David J Heeger. “Response suppression in V1 agrees with psychophysics of surround masking”. In: *Journal of Neuroscience* 23.17 (2003), pp. 6884–6893.

[32] John M Foley. “Human luminance pattern-vision mechanisms: masking experiments require a new model”. In: *JOSA A* 11.6 (1994), pp. 1710–1719.

[33] Martin J Wainwright, Odelia Schwartz, and Eero P Simoncelli. “Natural Image Statistics and Divisive Normalization”. In: *Probabilistic Models of the Brain* (), p. 203.

[34] Zachary M Westrick, David J Heeger, and Michael S Landy. “Pattern adaptation and normalization reweighting”. In: *Journal of Neuroscience* 36.38 (2016), pp. 9805–9816.

[35] David J Heeger, Eero P Simoncelli, and J Anthony Movshon. “Computational models of cortical visual processing.” In: *Proceedings of the National Academy of Sciences* 93.2 (1996), pp. 623–627.

[36] Siwei Lyu and Eero P Simoncelli. “Nonlinear extraction of independent components of natural images using radial gaussianization”. In: *Neural computation* 21.6 (2009), pp. 1485–1519.

[37] Gijs Joost Brouwer and David J Heeger. “Cross-orientation suppression in human visual cortex”. In: *Journal of neurophysiology* 106.5 (2011), pp. 2108–2119.

[38] James R Cavanaugh, Wyeth Bair, and J Anthony Movshon. “Nature and interaction of signals from the receptive field center and surround in macaque V1 neurons”. In: *Journal of neurophysiology* 88.5 (2002), pp. 2530–2546.

[39] Jing Xing and David J Heeger. "Center-surround interactions in foveal and peripheral vision". In: *Vision research* 40.22 (2000), pp. 3065–3072.

[40] Alexander A Petrov, Barbara Anne Dosher, and Zhong-Lin Lu. "The dynamics of perceptual learning: an incremental reweighting model." In: *Psychological review* 112.4 (2005), p. 715.

[41] Frances S Chance, L.F Abbott, and Alex D Reyes. "Gain Modulation from Background Synaptic Input". In: *Neuron* 35.4 (2002), pp. 773–782. ISSN: 0896-6273. DOI: https://doi.org/10.1016/S0896-6273(02)00820-6.

[42] Matteo Carandini, David J Heeger, and Walter Senn. "A synaptic explanation of suppression in visual cortex". In: *Journal of Neuroscience* 22.22 (2002), pp. 10053–10065.

[43] Hirofumi Ozeki et al. "Inhibitory stabilization of the cortical network underlies visual surround suppression". In: *Neuron* 62.4 (2009), pp. 578–592.

[44] Hillel Adesnik and Massimo Scanziani. "Lateral competition for cortical space by layer-specific horizontal circuits". In: *Nature* 464.7292 (2010), pp. 1155–1160.

[45] Tatsuo K Sato et al. "An excitatory basis for divisive normalization in visual cortex". In: *Nature neuroscience* 19.4 (2016), pp. 568–570.

[46] Hillel Adesnik. "Synaptic mechanisms of feature coding in the visual cortex of awake mice". In: *Neuron* 95.5 (2017), pp. 1147–1159.

[47] Kevin A Bolding and Kevin M Franks. "Recurrent cortical circuits implement concentration-invariant odor coding". In: *Science* 361.6407 (2018), eaat6904.

[48] Matteo Carandini, David J Heeger, and J Anthony Movshon. "Linearity and normalization in simple cells of the macaque primary visual cortex". In: *Journal of Neuroscience* 17.21 (1997), pp. 8621–8644.

[49] Hirofumi Ozeki et al. "Inhibitory stabilization of the cortical network underlies visual surround suppression". In: *Neuron* 62.4 (2009), pp. 578–592.

[50] Tobias Brosch and Heiko Neumann. “Interaction of feedforward and feedback streams in visual cortex in a firing-rate model of columnar computations”. In: *Neural Networks* 54 (2014), pp. 11–16.

[51] Shivang Rawat, David Heeger, and Stefano Martiniani. “Unconditional stability of a recurrent neural circuit implementing divisive normalization”. In: *Advances in Neural Information Processing Systems* 37 (2024), pp. 14712–14750.

[52] S.C. Cannon, D.A. Robinson, and S. Shamma. “A proposed neural network for the integrator of the oculomotor system”. In: *Biol. Cybernetics* 49 (1983), pp. 127–136. DOI: https://doi.org/10.1007/BF00320393.

[53] Matteo Carandini. “Amplification of trial-to-trial response variability by neurons in visual cortex”. In: *PLoS biology* 2.9 (2004), e264.

[54] Jeffrey S Anderson et al. “The contribution of noise to contrast invariance of orientation tuning in cat visual cortex”. In: *Science* 290.5498 (2000), pp. 1968–1972.

[55] Nicholas J Priebe and David Ferster. “Inhibition, spike threshold, and stimulus selectivity in primary visual cortex”. In: *Neuron* 57.4 (2008), pp. 482–497.

[56] AB Bonds. “Role of inhibition in the specification of orientation selectivity of cells in the cat striate cortex”. In: *Visual neuroscience* 2.1 (1989), pp. 41–55.

[57] GC DeAngelis et al. “Organization of suppression in receptive fields of neurons in cat visual cortex”. In: *Journal of Neurophysiology* 68.1 (1992), pp. 144–163.

[58] Gregory C DeAngelis, RALPH D Freeman, and IZUMI Ohzawa. “Length and width tuning of neurons in the cat’s primary visual cortex”. In: *Journal of neurophysiology* 71.1 (1994), pp. 347–374.

[59] Wyeth Bair, James R Cavanaugh, and J Anthony Movshon. “Time course and time-distance relationships for surround suppression in macaque V1 neurons”. In: *Journal of Neuroscience* 23.20 (2003), pp. 7690–7701.

[60] Nicole C Rust et al. “How MT cells analyze the motion of visual patterns”. In: *Nature neuroscience* 9.11 (2006), pp. 1421–1431.

[61] James R Cavanaugh, Wyeth Bair, and J Anthony Movshon. “Selectivity and spatial distribution of signals from the receptive field surround in macaque V1 neurons”. In: *Journal of neurophysiology* 88.5 (2002), pp. 2547–2556.

[62] Zheng Liu et al. “Interneuronal interaction between members of quadrature phase and anti-phase pairs in the cat’s visual cortex”. In: *Vision research* 32.7 (1992), pp. 1193–1198.

[63] Hassan K Khalil. *Control of nonlinear systems*. Prentice Hall, New York, NY, 2002.

[64] John R Silvester. “Determinants of block matrices”. In: *The Mathematical Gazette* 84.501 (2000), pp. 460–467.

[65] Peter Lancaster. *Lambda-matrices and vibrating systems*. Courier Corporation, 2002.

[66] Françoise Tisseur and Karl Meerbergen. “The quadratic eigenvalue problem”. In: *SIAM review* 43.2 (2001), pp. 235–286.

[67] Peter Lancaster. “Stability of linear gyroscopic systems: a review”. In: *Linear Algebra and its Applications* 439.3 (2013), pp. 686–706.

[68] Oleg N Kirillov. *Nonconservative stability problems of modern physics*. Vol. 14. Walter de Gruyter GmbH & Co KG, 2021.

[69] Wolfhard Kliem and Christian Pommer. “Indefinite damping in mechanical systems and gyroscopic stabilization”. In: *Zeitschrift für angewandte Mathematik und Physik* 60 (2009), pp. 785–795.

[70] Abraham Berman and Robert J Plemmons. *Nonnegative matrices in the mathematical sciences*. SIAM, 1994.

[71] Flaviano Morone et al. "Stabilization of recurrent neural networks through divisive normalization". In: *bioRxiv* (2025), pp. 2025–05.

[72] Lei Dai et al. "Generic indicators for loss of resilience before a tipping point leading to population collapse". In: *Science* 336.6085 (2012), pp. 1175–1177.

[73] Marten Scheffer et al. "Anticipating critical transitions". In: *science* 338.6105 (2012), pp. 344–348.

[74] EP Wigner. "Statistical properties of real symmetric matrices with many dimensions Can". In: *Math. Congr. Proc., University of Toronto Press, Toronto* (1957), p. 174.

[75] R. M. May. "Will a Large Complex System be Stable?" In: *Nature* 238 (1972), pp. 413–414. DOI: https://doi.org/10.1038/238413a0.

[76] Stefano Allesina and Si Tang. "Stability criteria for complex ecosystems". In: *Nature* 483.7388 (2012), pp. 205–208.

[77] Flaviano Morone, Gino Del Ferraro, and Hernán A Makse. "The k-core as a predictor of structural collapse in mutualistic ecosystems". In: *Nature physics* 15.1 (2019), pp. 95–102.

[78] K. S. McCann. "The diversity–stability debate". In: *Nature* 405 (2000), pp. 228–233. DOI: https://doi.org/10.1038/35012234.

[79] Francesca Arese Lucini et al. "Diversity increases the stability of ecosystems". In: *PloS one* 15.4 (2020), e0228692.

[80] Ian A Hatton et al. "Diversity begets stability: Sublinear growth and competitive coexistence across ecosystems". In: *Science* 383.6688 (2024), eadg8488.

[81] C. van Vreeswijk and H. Sompolinsky. “Chaos in Neuronal Networks with Balanced Excitatory and Inhibitory Activity”. In: *Science* 274.5293 (1996), pp. 1724–1726. DOI: 10.1126/science.274.5293.1724.

[82] Shivang Rawat and Stefano Martiniani. “Element-wise and recursive solutions for the power spectral density of biological stochastic dynamical systems at fixed points”. In: *Physical Review Research* 6.4 (2024), p. 043179.

[83] Marten Scheffer et al. “Early-warning signals for critical transitions”. In: *Nature* 461.7260 (2009), pp. 53–59.

[84] Jean-Paul Noel and Dora E Angelaki. “A theory of autism bridging across levels of description”. In: *Trends in Cognitive Sciences* 27.7 (2023), pp. 631–641.

[85] Ari Rosenberg, Jaclyn Sky Patterson, and Dora E Angelaki. “A computational perspective on autism”. In: *Proceedings of the National Academy of Sciences* 112.30 (2015), pp. 9158–9165.

[86] Ilan Dinstein et al. “Unreliable evoked responses in autism”. In: *Neuron* 75.6 (2012), pp. 981–991.

[87] Ilan Dinstein, David J Heeger, and Marlene Behrmann. “Neural variability: friend or foe?” In: *Trends in cognitive sciences* 19.6 (2015), pp. 322–328.

[88] Xiaowen Chen and William Bialek. “Searching for long timescales without fine tuning”. In: *Physical Review E* 110.3 (2024), p. 034407.

[89] Alex Krizhevsky, Ilya Sutskever, and Geoffrey E Hinton. “Imagenet classification with deep convolutional neural networks”. In: *Advances in neural information processing systems* 25 (2012).

[90] Ashish Vaswani et al. “Attention is all you need”. In: *Advances in neural information processing systems* 30 (2017).

[91] Sepp Hochreiter and Jürgen Schmidhuber. "Long short-term memory". In: *Neural computation* 9.8 (1997), pp. 1735–1780.

[92] Jack D Cowan, Jeremy Neuman, and Wim van Drongelen. "Wilson–Cowan equations for neocortical dynamics". In: *The Journal of Mathematical Neuroscience* 6 (2016), pp. 1–24.

[93] Yashar Ahmadian, Daniel B Rubin, and Kenneth D Miller. "Analysis of the stabilized supralinear network". In: *Neural computation* 25.8 (2013), pp. 1994–2037.

[94] James Kotary et al. "End-to-end constrained optimization learning: A survey". In: *arXiv preprint arXiv:2103.16378* (2021).

[95] Priya L Donti, David Rolnick, and J Zico Kolter. "DC3: A learning method for optimization with hard constraints". In: *arXiv preprint arXiv:2104.12225* (2021).

[96] Eldad Haber and Lars Ruthotto. "Stable architectures for deep neural networks". In: *Inverse problems* 34.1 (2017), p. 014004.

[97] Sergey Ioffe and Christian Szegedy. "Batch normalization: Accelerating deep network training by reducing internal covariate shift". In: *International conference on machine learning*. pmlr. 2015, pp. 448–456.

[98] Jimmy Lei Ba, Jamie Ryan Kiros, and Geoffrey E Hinton. "Layer normalization". In: *arXiv preprint arXiv:1607.06450* (2016).

[99] Lei Huang et al. "Normalization techniques in training dnns: Methodology, analysis and application". In: *IEEE transactions on pattern analysis and machine intelligence* 45.8 (2023), pp. 10173–10196.

[100] Mengye Ren et al. "Normalizing the normalizers: Comparing and extending network normalization schemes". In: *arXiv preprint arXiv:1611.04520* (2016).

[101] Yuxin Wu and Kaiming He. "Group normalization". In: *Proceedings of the European conference on computer vision (ECCV)*. 2018, pp. 3–19.

[102] Michelle Miller, SueYeon Chung, and Kenneth D Miller. "Divisive feature normalization improves image recognition performance in AlexNet". In: *International Conference on Learning Representations*. 2021.

[103] Saurabh Singh and Shankar Krishnan. "Filter response normalization layer: Eliminating batch dependence in the training of deep neural networks". In: *Proceedings of the IEEE/CVF conference on computer vision and pattern recognition*. 2020, pp. 11237–11246.

[104] Junyoung Chung et al. "Empirical evaluation of gated recurrent neural networks on sequence modeling". In: *arXiv preprint arXiv:1412.3555* (2014).

[105] Ilya Sutskever, Oriol Vinyals, and Quoc V Le. "Sequence to sequence learning with neural networks". In: *Advances in neural information processing systems* 27 (2014).

[106] Kyunghyun Cho et al. "Learning phrase representations using RNN encoder-decoder for statistical machine translation". In: *arXiv preprint arXiv:1406.1078* (2014).

[107] Alex Graves, Abdel-rahman Mohamed, and Geoffrey Hinton. "Speech recognition with deep recurrent neural networks". In: *2013 IEEE international conference on acoustics, speech and signal processing*. Ieee. 2013, pp. 6645–6649.

[108] Alex Graves. "Generating sequences with recurrent neural networks". In: *arXiv preprint arXiv:1308.0850* (2013).

[109] Wayne Soo and Máté Lengyel. "Training stochastic stabilized supralinear networks by dynamics-neutral growth". In: *Advances in Neural Information Processing Systems* 35 (2022), pp. 29278–29291.

[110] H Francis Song, Guangyu R Yang, and Xiao-Jing Wang. "Training excitatory-inhibitory recurrent neural networks for cognitive tasks: a simple and flexible framework". In: *PLoS computational biology* 12.2 (2016), e1004792.

[111] Wayne Soo, Vishwa Goudar, and Xiao-Jing Wang. "Training biologically plausible recurrent neural networks on cognitive tasks with long-term dependencies". In: *Advances in Neural Information Processing Systems* 36 (2024).

[112] Huaguang Zhang, Zhanshan Wang, and Derong Liu. "A comprehensive review of stability analysis of continuous-time recurrent neural networks". In: *IEEE Transactions on Neural Networks and Learning Systems* 25.7 (2014), pp. 1229–1262.

[113] Bo Chang et al. "AntisymmetricRNN: A dynamical system view on recurrent neural networks". In: *arXiv preprint arXiv:1902.09689* (2019).

[114] N Benjamin Erichson et al. "Lipschitz recurrent neural networks". In: *arXiv preprint arXiv:2006.12070* (2020).

[115] T Konstantin Rusch and Siddhartha Mishra. "Coupled Oscillatory Recurrent Neural Network (coRNN): An accurate and (gradient) stable architecture for learning long time dependencies". In: *arXiv preprint arXiv:2010.00951* (2020).

[116] T Konstantin Rusch and Siddhartha Mishra. "Unicornn: A recurrent model for learning very long time dependencies". In: *International Conference on Machine Learning*. PMLR. 2021, pp. 9168–9178.

[117] Li Deng. "The mnist database of handwritten digit images for machine learning research [best of the web]". In: *IEEE signal processing magazine* 29.6 (2012), pp. 141–142.

[118] Shaojie Bai, J Zico Kolter, and Vladlen Koltun. "Deep equilibrium models". In: *Advances in neural information processing systems* 32 (2019).

[119] Kaiming He et al. "Delving deep into rectifiers: Surpassing human-level performance on imagenet classification". In: *Proceedings of the IEEE international conference on computer vision*. 2015, pp. 1026–1034.

[120] Quoc V Le, Navdeep Jaitly, and Geoffrey E Hinton. “A simple way to initialize recurrent networks of rectified linear units”. In: *arXiv preprint arXiv:1504.00941* (2015).

[121] Martin Arjovsky, Amar Shah, and Yoshua Bengio. “Unitary evolution recurrent neural networks”. In: *International conference on machine learning*. PMLR. 2016, pp. 1120–1128.

[122] Piet Mondrian. *Broadway Boogie Woogie*. Museum of Modern Art, New York, 1943.

[123] Albert Einstein. “Über die von der molekularkinetischen Theorie der Wärme geforderte Bewegung von in ruhenden Flüssigkeiten suspendierten Teilchen”. In: *Annalen der physik* 4 (1905).

[124] Paul Langevin. “Sur la théorie du mouvement brownien”. In: *Compt. Rendus* 146 (1908), pp. 530–533.

[125] Simo Särkkä and Arno Solin. *Applied stochastic differential equations*. Vol. 10. Cambridge University Press, 2019.

[126] Crispin W Gardiner et al. *Handbook of stochastic methods*. Vol. 3. springer Berlin, 1985.

[127] Thomas Kailath. “A view of three decades of linear filtering theory”. In: *IEEE Transactions on information theory* 20.2 (1974), pp. 146–181.

[128] Ali H Sayed and Thomas Kailath. “A survey of spectral factorization methods”. In: *Numerical linear algebra with applications* 8.6-7 (2001), pp. 467–496.

[129] Shui-Hung Hou. “Classroom Note: A Simple Proof of the Leverrier–Faddeev Characteristic Polynomial Algorithm”. In: *SIAM review* 40.3 (1998), pp. 706–709.

[130] Dmitrii Konstantinovich Faddeev, Vera Nikolaevna Faddeeva, and Robert C Williams. “Computational methods of linear algebra”. In: (1963).

[131] Dennis S Bernstein. “Matrix mathematics”. In: *Matrix Mathematics*. Princeton university press, 2009.

[132] Alan G Hawkes. “Point spectra of some mutually exciting point processes”. In: *Journal of the Royal Statistical Society Series B: Statistical Methodology* 33.3 (1971), pp. 438–443.

[133] Richard FitzHugh. “Impulses and physiological states in theoretical models of nerve membrane”. In: *Biophysical journal* 1.6 (1961), pp. 445–466.

[134] Jinichi Nagumo, Suguru Arimoto, and Shuji Yoshizawa. “An active pulse transmission line simulating nerve axon”. In: *Proceedings of the IRE* 50.10 (1962), pp. 2061–2070.

[135] Marius E Yamakou et al. “The stochastic Fitzhugh–Nagumo neuron model in the excitable regime embeds a leaky integrate-and-fire model”. In: *Journal of mathematical biology* 79 (2019), pp. 509–532.

[136] James L Hindmarsh and RM Rose. “A model of neuronal bursting using three coupled first order differential equations”. In: *Proceedings of the Royal society of London. Series B. Biological sciences* 221.1222 (1984), pp. 87–102.

[137] Alan L Hodgkin and Andrew F Huxley. “A quantitative description of membrane current and its application to conduction and excitation in nerve”. In: *The Journal of physiology* 117.4 (1952), p. 500.

[138] Eric Temple Bell. “Exponential polynomials”. In: *Annals of Mathematics* (1934), pp. 258–277.

[139] Stephen Barnett. “Leverrier’s algorithm: a new proof and extensions”. In: *SIAM Journal on Matrix Analysis and Applications* 10.4 (1989), pp. 551–556.

[140] Marco Storace, Daniele Linaro, and Enno de Lange. “The Hindmarsh–Rose neuron model: bifurcation analysis and piecewise-linear approximations”. In: *Chaos: An Interdisciplinary Journal of Nonlinear Science* 18.3 (2008), p. 033128.

[141] Stephen Keeley et al. “Firing rate models for gamma oscillations”. In: *Journal of neurophysiology* 121.6 (2019), pp. 2181–2190.

[142] Danielle FP Toupo and Steven H Strogatz. “Nonlinear dynamics of the rock-paper-scissors game with mutations”. In: *Physical Review E* 91.5 (2015), p. 052907.

[143] Peter Welch. “The use of fast Fourier transform for the estimation of power spectra: a method based on time averaging over short, modified periodograms”. In: *IEEE Transactions on audio and electroacoustics* 15.2 (1967), pp. 70–73.

[144] Guillaume Hennequin et al. “The dynamical regime of sensory cortex: stable dynamics around a single stimulus-tuned attractor account for patterns of noise variability”. In: *Neuron* 98.4 (2018), pp. 846–860.

[145] Nataliya Kraynyukova and Tatjana Tchumatchenko. “Stabilized supralinear network can give rise to bistable, oscillatory, and persistent activity”. In: *Proceedings of the National Academy of Sciences* 115.13 (2018), pp. 3464–3469.

[146] Caleb J Holt, Kenneth D Miller, and Yashar Ahmadian. “The stabilized supralinear network accounts for the contrast dependence of visual cortical gamma oscillations”. In: *bioRxiv* (2023), pp. 2023–05.

[147] Eric R Kandel et al. *Principles of neural science*. Vol. 4. McGraw-hill New York, 2000.

[148] Immanuel M Bomze. “Lotka-Volterra equation and replicator dynamics: a two-dimensional classification”. In: *Biological cybernetics* 48.3 (1983), pp. 201–211.

[149] Josef Hofbauer and Karl Sigmund. “Evolutionary game dynamics”. In: *Bulletin of the American mathematical society* 40.4 (2003), pp. 479–519.

[150] Mauro Mobilia. “Oscillatory dynamics in rock–paper–scissors games with mutations”. In: *Journal of Theoretical Biology* 264.1 (2010), pp. 1–10.

[151] Volker Pernice et al. “How structure determines correlations in neuronal networks”. In: *PLoS computational biology* 7.5 (2011), e1002059.

[152] Srdjan Ostojic, Nicolas Brunel, and Vincent Hakim. “How connectivity, background activity, and synaptic properties shape the cross-correlation between spike trains”. In: *Journal of Neuroscience* 29.33 (2009), pp. 10234–10253.

[153] James Trousdale et al. “Impact of network structure and cellular response on spike time correlations”. In: *PLoS computational biology* 8.3 (2012), e1002408.

[154] Tatiana Verechtchaguina, Igor M Sokolov, and Lutz Schimansky-Geier. “First passage time densities in resonate-and-fire models”. In: *Physical Review E—Statistical, Nonlinear, and Soft Matter Physics* 73.3 (2006), p. 031108.

[155] Tatjana Tchumatchenko et al. “Correlations and synchrony in threshold neuron models”. In: *Physical review letters* 104.5 (2010), p. 058102.

[156] Laurent Badel. “Firing statistics and correlations in spiking neurons: A level-crossing approach”. In: *Nature Precedings* (2011), pp. 1–1.

[157] Robert P Gowers and Magnus JE Richardson. “Upcrossing-rate dynamics for a minimal neuron model receiving spatially distributed synaptic drive”. In: *Physical Review Research* 5.2 (2023), p. 023095.

[158] GR Jafari et al. “Level crossing analysis of the stock markets”. In: *Journal of Statistical Mechanics: Theory and Experiment* 2006.06 (2006), P06008.

[159] Farzaneh Shayeganfar et al. “The level crossing and inverse statistic analysis of German stock market index (DAX) and daily oil price time series”. In: *Physica A: Statistical Mechanics and its Applications* 391.1-2 (2012), pp. 209–216.

[160] M. Kac. “On the average number of real roots of a random algebraic equation”. In: *Bulletin of the American Mathematical Society* 49.4 (1943), pp. 314–320.

[161] Stephen O Rice. “Mathematical analysis of random noise”. In: *The Bell System Technical Journal* 23.3 (1944), pp. 282–332.

[162] Marie F. Kratz. “Level crossings and other level functionals of stationary Gaussian processes”. In: *Probability Surveys* 3 (2006), pp. 230–288.

[163] Herbert Steinberg et al. “Short-Time Frequency Measurement of Narrow-Band Random Signals by Means of a Zero Counting Process”. In: *Journal of Applied Physics* 26.2 (1955), pp. 195–201.

[164] Jean-Marc Azaıs, Christine Cierco-Ayrolles, and Alain Croquette. “Bounds and asymptotic expansions for the distributionof the Maximum of a smooth stationary Gaussian process”. In: *ESAIM: Probability and Statistics* 3 (1999), pp. 107–129.

[165] Christine Cierco-Ayrolles, Alain Croquette, and Céline Delmas. “Computing the distribution of the maximum of Gaussian random processes”. In: *Methodology and Computing in Applied Probability* 5 (2003), pp. 427–438.

[166] Kiyosi Ito. “The expected number of zeros of continuous stationary Gaussian processes”. In: *Journal of Mathematics of Kyoto University* 3.2 (1963), pp. 207–216.

[167] N Donald Ylvisaker. “The expected number of zeros of a stationary Gaussian process”. In: *The Annals of Mathematical Statistics* 36.3 (1965), pp. 1043–1046.

[168] Donald Geman. “On the variance of the number of zeros of a stationary Gaussian process”. In: *The Annals of Mathematical Statistics* (1972), pp. 977–982.

[169] Marie F. Kratz and José R. León. “On the second moment of the number of crossings by a stationary Gaussian process”. In: *The Annals of Probability* 34.4 (2006), pp. 1601–1607. DOI: 10.1214/009117906000000142.

[170] Vladimir Ilich Piterbarg. *Asymptotic methods in the theory of Gaussian processes and fields*. Vol. 148. American Mathematical Soc., 1996.

[171] Harald Cramér and M. R. Leadbetter. *Stationary and related stochastic processes. Sample function properties and their applications*. John Wiley & Sons, Inc., New York-London-Sydney, 1967, pp. xii+348.

[172] Donald Bruce Owen. "A table of normal integrals: A table". In: *Communications in Statistics-Simulation and Computation* 9.4 (1980), pp. 389–419.

[173] M. R. Leadbetter and J. D. Cryer. "The variance of the number of zeros of a stationary normal process". In: *Bulletin of the American Mathematical Society* 71.3.P1 (1965), pp. 561–563.

[174] Robert Pawula. "Analysis of an estimator of the center frequency of a power spectrum". In: *IEEE Transactions on Information Theory* 14.5 (1968), pp. 669–676.

[175] Georg Lindgren. "Spectral moment estimation by means of level crossings". In: *Biometrika* 61.2 (1974), pp. 401–418.

[176] Lorna RM Wilson and Keith I Hopcraft. "Periodicity in the autocorrelation function as a mechanism for regularly occurring zero crossings or extreme values of a Gaussian process". In: *Physical Review E* 96.6 (2017), p. 062129.

[177] Joseph L Doob. "The Brownian movement and stochastic equations". In: *Annals of Mathematics* 43.2 (1942), pp. 351–369.

[178] Bruce J West and V Seshadri. "Linear systems with Lévy fluctuations". In: *Physica A: Statistical Mechanics and its Applications* 113.1-2 (1982), pp. 203–216.

[179] AV Chechkin and V Yu Gonchar. "Linear relaxation processes governed by fractional symmetric kinetic equations". In: *Journal of Experimental and Theoretical Physics* 91 (2000), pp. 635–651.

[180] N Lin and SV Lototsky. "Undamped harmonic oscillator driven by additive Gaussian white noise: a statistical analysis". In: *Communications on Stochastic Analysis* 5.1 (2011), p. 13.

[181] Bartłomiej Dybiec, Ewa Gudowska-Nowak, and Igor M Sokolov. "Underdamped stochastic harmonic oscillator driven by Lévy noise". In: *Physical Review E* 96.4 (2017), p. 042118.

[182] Jaume Masoliver and Matteo Palassini. "Counting of level crossings for inertial random processes: Generalization of the Rice formula". In: *Physical Review E* 107.2 (2023), p. 024111.

[183] Jaume Masoliver. "Level-crossing counting for generalized Langevin equations". In: *Physical Review E* 111.1 (2025), p. 014113.

[184] Rubén Moreno et al. "Response of spiking neurons to correlated inputs". In: *Physical Review Letters* 89.28 (2002), p. 288101.

[185] Christopher KI Williams and Carl Edward Rasmussen. *Gaussian processes for machine learning*. Vol. 2. 3. MIT press Cambridge, MA, 2006.

[186] Eran Assaf, Jeremiah Buckley, and Naomi Feldheim. "An asymptotic formula for the variance of the number of zeroes of a stationary Gaussian process". In: *Probability Theory and Related Fields* 187.3 (2023), pp. 999–1036.

[187] Shivang Rawat, David Heeger, and Stefano Martiniani. "A comprehensive large-scale model of primary visual cortex (V1)". In: *Bulletin of the American Physical Society* (2024).

[188] Eero P Simoncelli and William T Freeman. "The steerable pyramid: A flexible architecture for multi-scale derivative computation". In: *Proceedings., international conference on image processing*. Vol. 3. IEEE. 1995, pp. 444–447.

[189] Christina Allen and Charles F Stevens. "An evaluation of causes for unreliability of synaptic transmission." In: *Proceedings of the National Academy of Sciences* 91.22 (1994), pp. 10380–10383.

[190] Zachary F Mainen and Terrence J Sejnowski. "Reliability of spike timing in neocortical neurons". In: *Science* 268.5216 (1995), pp. 1503–1506.

[191] Xiaoxuan Jia, Dajun Xing, and Adam Kohn. “No consistent relationship between gamma power and peak frequency in macaque primary visual cortex”. In: *Journal of Neuroscience* 33.1 (2013), pp. 17–25.

[192] Dora Hermes et al. “Stimulus dependence of gamma oscillations in human visual cortex”. In: *Cerebral cortex* 25.9 (2015), pp. 2951–2959.

[193] Bruss Lima et al. “Synchronization dynamics in response to plaid stimuli in monkey V1”. In: *Cerebral cortex* 20.7 (2010), pp. 1556–1573.

[194] Mark M Churchland et al. “Stimulus onset quenches neural variability: a widespread cortical phenomenon”. In: *Nature neuroscience* 13.3 (2010), pp. 369–378.

[195] Ruben Coen-Cagli and Selina S Solomon. “Relating divisive normalization to neuronal response variability”. In: *Journal of Neuroscience* 39.37 (2019), pp. 7344–7356.

[196] Asit Pal et al. “Hierarchical Neural Circuit Theory of Normalization and Inter-areal Communication”. In: *bioRxiv* (2025), pp. 2025–07.

[197] Robbe LT Goris, J Anthony Movshon, and Eero P Simoncelli. “Partitioning neuronal variability”. In: *Nature neuroscience* 17.6 (2014), pp. 858–865.

[198] Fuzhen Zhang. *The Schur complement and its applications*. Vol. 4. Springer Science & Business Media, 2006.

[199] Roger A Horn and Charles R Johnson. *Matrix analysis*. Cambridge university press, 2012.